AN INTEGRATED STUDY OF MAGMATISM, MAGMATIC Ni-Cu SULPHIDE MINERALIZATION AND METALLOGENY IN THE UMIAKOVIARUSEK LAKE REGION, LABRADOR, CANADA

STEPHEN JOHN PIERCEY

An Integrated Study of Magmatism, Magmatic Ni-Cu Sulphide Mineralization and Metallogeny in the Umiakoviarusek Lake Region, Labrador, Canada.

by

©Stephen John Piercey, B.Sc. (Hons.)

A Thesis Submitted to the School of Graduate Studies in Partial Fulfilment of the Requirements for the Degree of Master of Science

Department of Earth Sciences
Memorial University of Newfoundland

May 1998

St. John's *Newfoundland*

Abstract

The OKG prospect in the Umiakoviarusek Lake region of Labrador provides an excellent laboratory to study anorthosite-mangeric-charnockite-granite (AMCG) magmatism, pyroxenite-leucotroctolite hosted magmatic Ni-Cu sulphide mineralization and metallogeny. This thesis has used a combined field, geochemical and isotopic approach to assess the following problems: 1) what is the geology and nature of mineralization at the OKG prospect; 2) what are the isotopic and geochemical attributes of the anorthositic and granitoid rocks, and do they display any similarities to the Nain Plutonic Suite (NPS); 3) what is the nature and style of magmatic Ni-Cu sulphide mineralization; and 4) what are the chemical and isotopic controls on the genesis of the OKG Ni-Cu sulphide mineralization.

The geology of the OKG prospect consists largely of anorthositic (*sensu lato*) and granitoid rocks, with lesser Archean gneisses and mineralized pyroxenitic (*sensu lato*) rocks. The Archean gneisses are predominantly amphibolitic/mafic granulite and subequal metatonalitic to quartzofeldspathic gneisses. The anorthositic and granitoid rocks of the property are predominantly anorthositic and leuconoritic and occur both north and south of Umiakoviarusek Lake and as a northwesterly trending body in the eastern portion of the property. Granitoid rocks are in roughly subequal proportions to the anorthositic rocks and range from mozonite, quartz monzonite, syenite, quartz syenite, alkali feldspar granite and granite. Traditionally these anorthositic and granitoid rocks have been assigned to the Nain Plutonic Suite (NPS); however, recent work in this region has shown that much of the rocks in this region actually, and likely Paleoproterozoic and exhibit evidence of deformation and metamorphic influence from the ca. 1.86-1.74 Ga Torngat Orogen. These features include: 1) localized sinistral strike-slip and ductile (mylonitic) faulting and related folding; 2) the presence of foliations within the granitoid rocks that mirror the grain of the Archean gneisses and the Torngat Orogen; 3) prevalent secondary, metamorphic replacement and recrystallization of primary igneous mineralogy with secondary greenschist facies assemblages; and 4) intrusion by metabasic dykes that have widespread replacement of primary igneous mineralogy by secondary greenschist facies assemblages.

In contrast, the mineralized pyroxenitic-leuctroctolitic rocks of the OKG prospect do not show the secondary deformation and metamorphic features common in the anorthositic and granitoid rocks. Furthermore, even in proximity to ductile faulting they retain pristine igneous textures without secondary replacement of igneous mineral assemblages. The apparent lack of influence from the Torngat Orogen suggests a likely Mesoproterozoic age for the dykes and related mineralization. The mineralization within the OKG is always spatially, and genetically, associated with these pyroxenitic dykes. Commonly on surface the massive sulphide mineralization is podiform in nature and is localized near the dykes, within the anorthositic rocks. Disseminated mineralization is typically found within the pyroxenitic intrusives occurring as intercumulus disseminations, that locally grade to semi-massive in nature and exhibiting "net textures". In drill core the pyroxenitic intrusives show sharp contacts with the surrounding

anorthositic rocks and have gradational assemblages from disseminated (≈5%) near their tops, through to semi-massive (≈30%), to massive sulphide near their basal contacts with the anorthositic rocks. Sulphide assemblages for both the massive and disseminated sulphides have a high temperature assemblage of magnetite and pyrrhotite, with successively lower temperature exsolved grains of pyrite, chalcopyrite and pentlandite, in this order.

Geochemically the anorthositic and granitoid rocks have similar attributes to the younger Nain Plutonic Suite. On primitive mantle normalized multi-element plots the anorthositic rocks have variably positive Sr, Eu, and Ti anomalies, and flat to negative Th and Nb anomalies. The granitoid rocks also show relatively flat to negative Th and Nb anomalies, but have higher total REE, in particular LREE, have negative Sr and Ti anomalies, relatively flat to slightly positive Eu anomalies, and very pronounced positive Zr anomalies. Isotopically the anorthositic rocks have ISr (@2050Ma) ranging from 0.7048-0.7082, εNd (@2050Ma) = -4.1 to –11.8, $f_{Sm/Nd}$ from –0.30 to -0.68, and T_{DM} ages from 2.54 to 3.64Ma (average 3.16Ga). The granitoids have ISr (@2050Ma) ranging from 0.7036 to 0.7598, εNd (@2050Ma) = -5.1 to -9.7, $f_{Sm/Nd}$ from –0.35 to –0.50, and T_{DM} ages from 2.82 to 3.26 Ga (average 3.03 Ga). The presence of negative Th and Nb, coupled with the isotopic data, suggest that the anorthositic and granitoid rocks have significant contribution from a source with negative Th and Nb, coupled with a long crustal residence time. This is consistent with incorporation and influence from Archean source materials, most likely the Nain Province gneiss. Furthermore, although older than the NPS, the similarities in geochemistry and isotope behaviour suggest that these Paleoproterozoic anorthositic and granitoid rocks formed in a manner petrogenetically similar to the NPS.

An integrated geochemical and isotopic approach to the pyroxenite hosted mineralization has been undertaken using trace and REE geochemistry, PGE geochemistry, sulphur isotopes, and Nd isotopes. Using the trace and REE chemistry there are two distinctive chemical subdivisions of the dykes including those from surface and those from the subsurface. Pyroxenitic rocks from the surface zones of mineralization are characterized by variably depleted LREE relative to the MREE and HREE (La_N/Yb_N=0.18-0.31, Ce_N/Yb_N=0.22-0.36, La_N/Sm_N= 0.28-0.52), and have variably flat to negative Eu anomalies (Eu/Eu* = 0.08-0.14). In contrast, the subsurface dykes from one drill hole have marked increases in the LREE relative to the surface dykes (La_N/Yb_N=1.23-3.33, Ce_N/Yb_N=1.16-3.50, La_N/Sm_N= 1.47-1.99), but retain similar Eu concentrations (Eu/Eu* = 0.04-0.21). The extended plots for the dykes also show varying behaviour with the surface dykes having lesser enrichments in the LFSE and Zr (Zr/Y = 0.6-1.4) relative to the subsurface dykes (Zr/Y = 0.6-2.3); while both groups of dykes show well developed negative Th anomalies. Neodymium isotopes also show the same distribution with the surface samples containing εNd (@1300Ma) = -1.1 to –4.8, and $f_{Sm/Nd}$ = +0.39 to +0.75; while the subsurface dykes have εNd (@1300Ma) = -3.9 to –13.6, $f_{Sm/Nd}$ = -0.30 to –0.47, and T_{DM} ages from 2.39 to 3.40 Ga (average 2.74 Ga). The marked differences in trace, REE, and Nd isotope geochemistry of the surface and

subsurface dykes suggest that the subsurface dykes underwent significant degrees of crustal contamination relative to the surface dykes.

The PGE patterns for the OKG surface pyroxenites and the massive sulphides show very distinctive patterns. The PGE patterns for the pyroxenitic rocks with disseminated (2-20%) sulphide show trough shapes with depleted PGE relative to Ni and Cu (Ni/Ir_{MN} (average) = 17.47, Cu/Pd_{MN} (average) = 14.12). The massive sulphides have a similar trough pattern (Ni/Ir_{MN} (average) = 7.85, Cu/Pd_{MN} (average) = 4.96) with the exception of total concentration of the PGE, and the development of a negative Pt anomaly; suggesting a common genetic relationship between the pyroxenitic intrusives and sulphide mineralization. However, all are depleted in PGE relative to Ni and Cu suggest PGE loss due to a prior sulphide removal event. Sulphur isotope data for the OKG sulphides are very restricted and range from $\delta^{34}S = +1.0$ to $+1.8‰$. The overwhelming homogeneity of the sulphides and location within magmatic sulphur ranges ($\delta^{34}S = 0\pm3‰$) suggests that magmatic sulphur, rather than external sulphurization was the major source of sulphur in the sulphides.

The combination of field, geochemical and isotopic geochemistry allows a model for the OKG sulphides to be proposed. The REE chemistry of the surface pyroxenitic and leucotrocolitic rocks have similarities to compiled values for spinel lherzolites and peridotites from the subcontinental lithospheric mantle (SCLM). It is suggested that the pyroxenitic-leucotroctolitic dykes evolved and equilibrated with source liquids that were Eu and LREE depleted and derived from a depleted mantle (SCLM) source. The presumed Mesoproterozoic age for the pyroxenitic dykes suggests that melting was likely initiated by basaltic underplating associated with plumes associated with NPS magmatism. It is interpreted that early melts, that comprised the subsurface occurrences, rose along preexisting faults and structures that were both associated with the remnants of the Torngat Orogen, and those accompanying extension and emplacement of the NPS. While rising along these faults the pyroxenitic magmas underwent both fractionation and assimilation of Nain Province crustal material (ca. 35% as deduced from neodymium crustal index (NCI) calculations) resulting in LREE, Ba, Rb, and K enrichments, retention of low Th and Nb, and obtaining low εNd (@1300Ma) signatures. This crustal contamination resulted in an increase in silica to the pyroxenitic magmas inducing sulphide saturation and with continued rising into the crust were emplaced with some degree of turbulence into their anorthositic hosts. Upon emplacement sulphide segregation occurred resulting in the subsurface base-metal sulphide occurrences.

Surface pyroxenitic rocks also show Nain Province influence, including negative Th anomalies and εNd (@1300Ma) signatures. It is likely that crustal contamination (ca. 5% as deduced from NCI calculations), coupled with natural silicate fractionation resulted in sulphur saturation and segregation upon emplacement on surface. The lower degrees of contamination in the surface pulses may be explained if they are actually younger than the subsurface pulses and followed chemically insulated paths that were previously taken by the subsurface pulses.

Acknowledgements

The production and completion of this thesis would not have been possible without the help of many. To my supervisor Derek Wilton I extend my sincere thanks for suggesting and supervising this project. Derek's constant academic support, good humour, guidance and the willingness to discuss anything and everything are the true measures of an excellent mentor; I thank you dearly for a great learning experience. Funding for this project was provided by a grant from Castle Rock Exploration Corporation and an NSERC operating grant to Derek Wilton. I wish to thank the kind and gracious support of the Natural Sciences and Engineering Research Council for providing me with an NSERC PGS-A award; while the Buchans' Scholarship of ASARCO Incorporated from Memorial University is also gratefully acknowledged.

I wish to thank Castle Rock Exploration Corporation for providing funding, employment and logistical support for this project; in particular, Nelson Baker, Terry Ryan, John O'Sullivan, Don Sheldon, and Eugene Beukman. I extend a special thanks to Nelson for having the confidence and foresight to see the importance of this research and for "teaching me the ropes" of the mineral exploration world. Nelson's influence on my current and future career path has been invaluable. Thanks are extended to my capable and good humoured field assistants Jeff Morgan and Mike Rees. This work and the fun in Labrador would not have been the same without your help. Other fellow employees of Castle Rock are also thanked for serious and not so serious discussions during the summer of 1996, including: Mike Regular, Harry Lucci, Mike Parsons, Sean Ryan, and the late David Spencer.

The technical staff of the Department of Earth Sciences are thanked for their contributions to this project, including Lakmali Hewa (ICP-MS), Pat Horan (TI-MS), Pam King (XRF/ICP-MS), Mike Tubrett (XRF/ICP-MS), and Alison Weick (IR-MS). Their assistance, or preparation and completion of analyses are gratefully appreciated; while expedient sample cutting and preparation from Corey Fitzgerald and Ken Smith are thanked as well. Rick Soper is thanked for speedy preparation of my thin sections, while Gerry Ford and Maureen Moore are thanked for their administrative contributions to this project. Darren Smith and the staff at technical services are thanked for sorting out the computer problems and getting them fixed as soon as possible. Richard Taylor and Gilles St. Jean are thanked for preparation and sulphur isotope analyses of some samples at the Ottawa-Carleton Geoscience Centre.

I wish to thank Mark Wilson (MUN) for numerous discussions during the tenure of this project. His knowledge of geochemical and isotopic processes and mineral deposits has been an invaluable source of information and guidance. George Jenner (MUN) is thanked for his knowledge of trace element and radiogenic isotope geochemistry, and his insistence and instilling the importance of data validation and quality control. Discussions on the geology of the Umiakoviarusek Lake region with Bruce Ryan (NDME) have been invaluable, and for converting me to the Paleoproterozoic side. Likewise discussions with Andy Kerr (NDME) on the nature and style of mineralization at the OKG prospect are also acknowledged.

I wish to extend thanks to my fellow students who have shared in the fruits of this project, particularly Lawrence Winter, Rod Smith, Lori Dwyer, Joy Reid and Richard Cox. Richard is especially thanked for the numerous discussions near the completion of this thesis. To my friends Ed Davis, Pablo Gosse, Des Janes, Dan Mulrooney, Dave Myrden, and John Ogg, thanks for the good times over the last few years. I extend special thanks to my mother, father and sister, their emotional, financial and academic support during my university career, without their constant support I would not be where I am today. My Aunt Gwen and Uncle Dave are thanked for the many meals and for open ears. Finally, I would like to thank Michelle Delahunty, her emotional support and companionship, both here and over the miles, have been a constant source of inspiration and guidance.

Table of Contents

Chapter 3: Geology, Structure, Mineralization, and Silicate and Sulphide Petrography

Chapter 4: Major, Trace, and Rare-Earth Element Geochemistry

Chapter 5: Metal and Platinum Group Element Geochemistry

Chapter 6: Radiogenic Isotope Geochemistry

Chapter 7: Sulphur Isotope Geochemistry

Chapter 8: Discussion and Conclusions

Appendix A: Analytical Methods

List of Figures

List of Tables

List of Plates

Chapter 1: Introduction

1.1 Introduction

The discovery of the Ni-Cu-Co deposit at Voisey's Bay, Labrador in November 1994 led to a frenzy of claim staking and exploration for similar sulphide occurrences elsewhere in northern Labrador. Although studies of similar deposits have been carried out in other parts of the world (e.g. Sudbury, Ontario; Kambalda, Australia; Noril'sk, Siberia; and others), minimal research has been carried out on the Ni-Cu-Co accumulations in northern Labrador (Ryan *et al.*, 1995; Naldrett *et al.*, 1996a; Ryan, 1996; Naldrett, 1997), and hence, the genesis of such deposits is poorly known.

Through preliminary grass roots prospecting and exploration during the spring and summer of 1995, Castle Rock Exploration Corporation geologists delineated numerous prospects in the Nain, Webb Bay and Okak Bay regions of Labrador which may have similar economic potential to the Voisey's Bay discovery; including the OKG prospect. Grab sample assays from a surface pyroxenite-anorthosite hosted gossan at the OKG prospect yielded Ni values with economic to subeconomic grades with a best sample containing 1.78% Ni, 1.44% Cu, and 0.212% Co (Castle Rock Exploration Press Release, September 21, 1995; Kerr and Smith, 1997). Following initial prospecting, ground

geophysical surveys, further prospecting and diamond drilling have yielded promising results with variable intersections of pyroxenite and anorthosite hosted sulphides containing economic to subeconomic grades of Ni, Cu and Co (see review by Kerr and Smith, 1997).

During the 1996 field season intense prospecting, geologic mapping, geophysical surveys and diamond drilling were carried out. As part of this integrated exploration program, detailed field mapping, lithogeochemical and sulphide sampling were undertaken for this study. The results of field work completed during this time will be combined with detailed sulphide and silicate petrography, trace and rare earth element (REE) geochemistry, stable (S-isotope) and radiogenic isotope geochemistry (Rb-Sr, Sm-Nd), and platinum group element (PGE) geochemistry to formulate an integrated petrologic-metallogenic model of sulphide formation. A detailed description of the purpose and scope of the above is presented at the end of this chapter. The remainder of this chapter will discuss the location and access, controls on magmatic Ni-Cu sulphide occurrences, petro-tectonic aspects of Ni-Cu sulphide deposits and genetic models for magmatic Ni-Cu sulphide genesis.

1.2 Location and Access

The OKG prospect consists of 352 contiguous mineral land claims located approximately 10 kilometers south of Okak Bay, 100 kilometers north-northwest of the coastal community of Nain, approximately 350 kilometers north of Goose Bay, Labrador, and is roughly centered on UTM coordinates 538000E/6356000N in UTM Zone 21 (Figure 1.1). Topographically, the property consists of a central valley containing

significant glacial drift (up to 350m thick) bounded by two steep walled bluffs flanking the valley on the western and eastern sides of the property. Outcrop exposure on the tops of the bluffs is up to 90% in places; in valley areas, outcrop is notably absent due to a thick veneer of glacial drift; while on the steep walls of the valleys outcrop is present, but access is limited to the lower parts of these walls due to their steepness.

Vegetation is typical of a sub-arctic climate consisting of small shrubs and trees and swamp/marsh in the low lying valley areas. Topographically higher hilltops and valley walls are virtually devoid of vegetation with the exception of small shrubs. The sub-arctic climate and remoteness of the property require helicopter-based fieldwork, which is limited to the months of June through September.

1.3 A Review of Ni-Cu-Co-(±PGE) Sulphide Deposits

Magmatic Ni-Cu-Co-(±PGE) sulphide deposits occur in a variety of petro-tectonic settings throughout the world including cratonic, orogenic, rifted margins, ophiolites, and synvolcanic settings (Naldrett and Macdonald, 1980; Naldrett, 1989a; Eckstrand, 1996; Naldrett, 1997; Figure 1.2). Although present in many settings, a number of characteristics are consistent to all. All magmatic Ni-Cu sulphide occurrences are associated with mafic to ultramafic igneous rocks and distributed primarily in the Precambrian with only a few important exceptions (e.g. Noril'sk-Talnakh; Naldrett, 1989a; Barley and Groves, 1991; Eckstrand, 1996; Naldrett, 1997). Another common feature associated with Ni-Cu-Co deposits is the presumed segregation of an immiscible sulphide liquid from a silicate liquid due to sulphur saturation of the mafic-ultramafic

silicate melt (Naldrett, 1973; Rajamani and Naldrett, 1978; Naldrett and MacDonald, 1980; Naldrett, 1989a, 1997; and others; Figure 1.3). These characteristics hold for most (if not all) primary Ni-Cu sulphide accumulations; however, why are such similar characteristics common to such varied petro-tectonic conditions?

This question and the common characteristics are discussed in the following subsections. However, a brief overview of the types of settings in which these deposits occur is warranted and the following sub-sections give specific examples with models for Ni-Cu sulphide genesis.

All Ni-Cu sulphide occurrences are generally classified petro-tectonically. Naldrett (1989a), Eckstrand (1996), and Naldrett (1997) all provide subdivisions and classifications that vary in fine detail, but have consistent grand scale classifications. This review provides a fivefold classification, including:

1) ***Greenstone Belt Associated***

Since greenstone belts and komatiites are temporally restricted (predominantly Archean), and odd when compared to modern day tectonics, they are placed in a separate subdivision (Naldrett, 1997). Two subdivisions of the greenstone belt category include: a) *komatiite hosted deposits*, (e.g. Kambalda in western Australia; Lesher *et al.*, 1984; Groves *et al.*, 1986; Lesher, 1989; Figure 1.2); and b) *tholeiite related deposits*, including picritic tholeiite associated (e.g. Munni-Munni Complex in western Australia; Hoatson and Keays, 1989; Figure 1.2) and anorthositic gabbro tholeiite associated (e.g. Montcalm deposit in Ontario; Barrie and Naldrett, 1988; Figure 1.2).

2) Rifted Continental Environments

Rifted margin environments include deposits which are floored by, or closely associated with, continental crust, and those not associated with continental crust (Naldrett, 1989a; Naldrett, 1997). Deposits floored by continental crust include those in the Circum-Superior rift zone, including the Thompson Ni-bodies (Peredery *et al.*, 1982), Fox River Sill (Naldrett, 1997) and Cape Smith Fold Belt (Barnes *et al.*, 1992; Barnes and Picard, 1993; Barnes *et al.*, 1997a; Figure 1.2). Those not associated with continental crust are ophiolite hosted types (e.g. Zambaldes Ophiolite in the Philippines; Abrajano and Pasteris, 1989; Abrajano *et al.*, 1989; Figure 1.2). The major Ni-Cu deposit of Jinchuan, China is a possible member of the rift environment sub-class (cf. Chai and Naldrett, 1992a,b; Figure 1.2).

3) Cratonic Environments

Three sub-types of this group exist including those related to picritic-tholeiitic flood basalt magmatism (e.g. Noril'sk-Talnakh; Naldrett, 1989c ; Naldrett *et al.*, 1992,1995,1996b), anorthositic magmatism (e.g. Voisey's Bay; Ryan *et al.*, 1995; Naldrett *et al.*, 1996a; Naldrett, 1997), and large stratiform complexes (e.g. Bushveld Complex; Campbell *et al.*, 1983; Naldrett and von Gruenewaldt, 1989; Naldrett, *1989d*, 1993; Figure 1.2)

4) Active Orogenic Belts

Deposits associated with active orogenic belts have yet to be defined as significant resources of Ni, Cu, and PGE. Examples of this group include synorogenic intrusions

such as the Moxie Intrusion and Katahadin Gabbro, Maine (Thompson and Naldrett, 1984), and those in the Scandinavian Caledonides (Barnes, 1987; Barnes *et al.*, 1988), and late orogenic or Alaskan-type intrusions such as the Tulameen Complex, British Columbia (St. Louis *et al.*, 1986) or Salt Chuck, Alaska (Loney and Himmelberg, 1992; Figure 1.2).

5) Astrobleme Related

Although it could be argued that the Sudbury sulphide deposit host is a sheet-like intrusion related to a cratonic zone (Naldrett, 1989a, 1997), it is defined here as a separate subgroup (Eckstrand, 1996) because of the critical importance that a meteorite impact had on ore genesis at Sudbury (Naldrett and MacDonald, 1980; Naldrett, 1984a,c, 1989d; Naldrett, 1997; and others; Figure 1.2).

The simple five-fold classification above illustrates the varied petro-tectonic environments in which Ni-Cu-Co-(±PGE) sulphide deposits occur. The remainder of this review will discuss the controls on the precipitation of magmatic sulphides in mafic-ultramafic systems, followed by an overview of genetic models associated with magmatic Ni-Cu sulphide deposits.

1.3.1 Controls on the Precipitation of Magmatic Sulphides in Mafic-Ultramafic Magmas.

The precipitation and segregation of magmatic Ni-Cu-Co sulphides from mafic to ultramafic silicate magmas occurs when the silicate melt becomes saturated in sulphur, such that a sulphide liquid segregates from the silicate liquid creating two immiscible liquids: a sulphide liquid and a silicate liquid (Maclean, 1969; Naldrett, 1973; Rajamani and Naldrett, 1978; Naldrett and MacDonald, 1980; Naldrett, 1989b, 1997; and others;

Figure 1.3). With the segregation of a sulphide liquid from a silicate magma elemental partitioning between the two liquids occurs; *chalcophile elements* (i.e.. sulphide loving; Ni, Cu, Co, PGE) partition into the sulphide liquid, while *lithophile elements* (i.e. silicate loving; Na, Mg, Ca, etc.) remain in the silicate magma (Figure 1.3).

The question that arises from this is: how does a mafic-ultramafic magma become saturated in sulphide? Work by authors such as Maclean (1969), Naldrett (1973), Irvine (1975), Rajamani and Naldrett (1978), Campbell *et al.* (1983), Naldrett (1989b) and others, suggest that a number of factors can control the sulphur saturation of a mafic-ultramafic melt, including:

1) temperature and pressure;

2) the activity of FeO (a_{FeO}) and TiO_2 (a_{TiO2});

3) the fugacity of O_2 in the melt;

4) increases in the activity of SiO_2 (a_{SiO2}) and S;

5) *and/or the influx of a more primitive mantle melt into a melt at a more evolved crystallization/fractionation state. This includes a combination of some (or all) of the factors 1-4.*

Factors 1 through 4 are typically associated with most Ni-Cu dominated deposits, while factor 5 is predominantly associated with PGE accumulations. Since the OKG project is not PGE enriched (e.g. Chapter 5), this section will not discuss this factor but readers are guided towards papers by Irvine (1975), Campbell *et al.* (1983), Campbell and Barnes (1984), Barnes and Naldrett (1985, 1986), Naldrett (1989e), Naldrett *et al.* (1990) and Naldrett (1993).

The effect of temperature on sulphur solubility in a silicate melt has not been the subject of exhaustive experimental study; however, it is generally accepted that sulphur solubility in a silicate melt decreases with decreasing temperature (Naldrett, 1989b). In contrast to temperature, pressure decreases generally enhance the solubility of sulphur in a silicate melt. In a study of the Fe-Si-S-O system at 32kbar, Huang and Williams (1980) showed that with increasing pressure an increasing misciblity gap between sulphide and silicate liquids occurred. However, Naldrett (1989a) and Naldrett (1997) suggest that pressure has minimal effects on sulphide segregation and in most cases can be considered to have a negligible role in magmatic Ni-Cu–Co sulphide genesis.

The role of Fe (and to a lesser extent Ti) activity in the formation of sulphide liquids is based on the nature of 2+ valence cations (and 4+ in the case of Ti) within the silicate-sulphide system. In a study of the Fe-S-O-SiO_2 system, Maclean (1969) noticed that the ability of S to dissolve in a silicate melt is related to it being able to displace O^{2-} radicals bonded to Fe^{2+}. In the instance where Fe^{2+} is decreased in the melt (e.g. magnetite and/or ilmeno-magnetite crystallization) the melt cannot carry as much S, leading to the formation of two liquids (Maclean, 1969). Closely related to this, but to a lesser extent, is the role of Ti^{4+} (Naldrett, 1989b).

The role of oxygen fugacity in the melt is quite similar to that of Fe^{2+} but in the opposite direction. Considering that S-solubility related to the ability of the S to displace O^{2-} bonded to Fe^{2+}, increases in the oxygen fugacity in the melt result in an oxidation of Fe^{2+} to the Fe^{3+} state decreasing S-solubility in the silicate melt (Maclean, 1969).

The role of SiO_2 assimilation has been explored in the experimental studies of Maclean (1969) on the FeO-FeS-SiO_2 system, and subsequent examinations on natural systems by Irvine (1975) and Naldrett and Macdonald (1980) and others. Considering the apices of the system (Figure 1.4), with the FeO-SiO_2 side representing silicate melts (with fayalitic olivine), while the FeS apex represents the sulphide liquid. Taking any liquid, for instance from point A, and keeping all other factors constant, the addition of SiO_2 drives the system from A to B (Figure 1.4). At B the system will be driven into the two liquid field and the formation of silicate and sulphide liquids occurs (Figure 1.4). The addition of sulphur achieves the same end as the addition of silica. Adding sulphur to a silicate magma at A will drive the system towards the FeS axis and point C, at this point the segregation of two separate silicate and sulphide liquids will also occur (Figure 1.4).

1.3.2 Genetic Models for Magmatic Ni-Cu Sulphide Deposits

When considering how a Ni-Cu sulphide deposit forms there are three major criteria that are integral to their formation, including (cf. Naldrett, 1981, 1989a, 1997): 1) a host magma (mafic or ultramafic) that is saturated in sulphide and segregates immiscible sulphides; 2) sulphides are spatially restricted to a small area and with enough abundance to constitute ore; and 3) the sulphides have reacted and equilibrated with a sufficient amount of silicate magma to concentrate chalcophile elements to an economic level within the sulphide liquid (e.g. R-factor; Campbell and Naldrett, 1979; Naldrett, 1997).

Most mafic (or ultramafic) magmas contain dissolved sulphide upon emplacement, and typically the mafic/ultramafic magmas which host the sulphide are at, or close to, the sulphide liquidus temperature upon emplacement (Naldrett, 1997). With small drops in

temperature the sulphide becomes immiscible; however, temperature drops also lead to silicate crystallization and the formation of cumulus silicate and sulphides (Naldrett, 1997); this is problematic because then large masses of sulphide liquid cannot form. Similar cumulus textures and small sulphide occurrences form with FeO and TiO_2 changes during crystallization; while oxidation can induce immisciblity without decreasing temperatures (Naldrett, 1997).

A corollary to the above is that to form significant sulphide accumulations, sulphide saturation must occur without significant temperature decrease, effectively preventing silicate mineral crystallization. To achieve such state, sulphide saturation must be induced by either felsification (SiO_2 addition) or sulphurization (Naldrett, 1997); however, neither method is mutually exclusive and there is often overlap with both processes occurring simultaneously (e.g Noril'sk-Talnakh, Voisey's Bay?). The following subsections discuss sulphur assimilation dominated (e.g. Duluth, Kambalda, Noril'sk-Talnakh), silica assimilation dominated (e.g. Sudbury) and debated genetic models (e.g. Voisey's Bay) for magmatic Ni-Cu sulphide occurrences.

1.3.2.1 Sulphur Assimilation Dominated Models

Genetic models involving the assimilation of sulphur from surrounding country rocks dominate many descriptions of Ni-Cu sulphide genesis. Although this method of achieving sulphide saturation is therefore widely accepted, it is often coupled with other processes, some of which overlap with the silica assimilation models (e.g. Noril'sk-Talnakh). This subsection discusses genetic models which are dominated by sulphur

assimilation with specific examples from the Duluth Complex, the Kambalda deposits, and the Noril'sk-Talnakh deposits.

The Duluth Complex of Minnesota contains approximately $4x10^9$ of Ni-Cu sulphide ore with grades of 0.66 wt% Cu and 0.2% Ni (Listerud and Meineke, 1977) occurring as disseminations and locally massive sulphide zones and PGE rich horizons, hosted by troctolitic and noritic rocks (Mainwaring and Naldrett, 1977; Ripley, 1981, 1986, 1990a,b; Thériault *et al.*, 1997). The intrusive rocks of the complex are underlain by and in intrusive contact with the Virginia Formation sulphidic argillites, greywackes, siltstones, graphitic slates and sulphide bearing iron formation (Ripley, 1981; Naldrett, 1989c, 1997; Thériault *et al.*, 1997).

By using predominantly sulphur isotope and S/Se geochemical data, a number of workers have shown that external sulphurization has been important in the genesis of the Duluth deposits. Mainwaring and Naldrett (1977) first noticed that the sulphur isotope composition of sulphides within the Waterhen Intrusion of the Duluth Complex had $\delta^{34}S$ values ranging from +11.0‰ to +18.8‰, closely overlapping those of the sulphur-rich Virginia Formation rocks which it intrudes ($\delta^{34}S$= +11.0‰ to +16.0‰). This led the latter authors to suggest that up to 75% of the sulphur within the Waterhen sulphides was contributed from the external Virginia Formation sulphidic metasedimentary rocks. Further support for a sulphurization origin was also proposed by Ripley (1981) for the Dunka Road sulphides who noticed that the $\delta^{34}S$ signatures ($\delta^{34}S$= +0.2‰ to +15.3‰) were very close to the Virginia Formation sulphides and suggested that the mechanism of

sulphide saturation involved pyrite breakdown and volatilization into the mafic magma inducing saturation.

Ripley (1986, 1990b) noticed that both the $\delta^{34}S$ and Se/S signatures were locally variable and suggested that bulk (equilibrium) sulphide saturation did not occur in the Dunka Road sulphides and rather that assimilation and saturation were localized in proximity to the sulphidic rock of the Virginia Formation. Recent work by Thériault *et al.* (1997) on the Dunka Road Deposit adds further support to localized sulphurization. They suggested that sulphides in the Dunka Road occur as three types, formed by three mechanisms, including: 1) norite-hosted sulphides formed at low silicate to sulphide mass ratios (R factor) by assimilation of a granitic partial melt and S-bearing hydrous fluid, both derived from the Virginia Formation; 2) troctolite hosted sulphides formed at moderate R factors with moderate degrees of contamination, as illustrated by mantle-like Cu/Pd ratios and moderate Se/S ratios; and 3) PGE enriched horizons are uncontaminated, formed from mixing of a primitive magma influx and a fractionated resident magma at high R factors.

Sulphide deposits of the Norseman-Wiluna Greenstone Belt formed by sulphur assimilation processes similar to those of the Duluth Complex; however, unlike the Duluth deposits, bulk assimilation of sulphidic metasediments and fluid dynamic properties in the komatiitic lavas played an integral role in sulphide saturation/genesis. The geology of the Norseman-Wiluna Greenstone belt is highly variable containing a plethora of komatiitic lavas, basaltic lavas, epiclastic sedimentary rocks, felsic volcanics, sulphidic metasedimentary rocks and iron formations (Groves *et al.*, 1979; Naldrett, 1981; Gresham

and Loftus-Hills, 1981; Lesher *et al.*, 1984; Lesher, 1989; Hill *et al.*, 1995; Lesher and Arndt, 1995).

The komatiite-hosted deposits of the Norseman-Wiluna belt have common descriptive and genetic features with most deposits located within channel-flow facies komatiitic lavas and topographic depressions in footwall rocks (Lesher *et al.*, 1984; Huppert and Sparks 1985; Groves *et al.*, 1986; Lesher, 1989; Hill *et al.*, 1995; Lesher and Arndt, 1995; Naldrett, 1997). This association has been proposed to be a result of turbulently flowing lavas assimilating and incorporating sulphide from footwall sulphidic sedimentary rocks (Huppert *et al.*, 1984; Lesher *et al.*, 1984; Huppert and Sparks 1985; Groves *et al.*, 1986; Lesher, 1989; Hill *et al.*, 1995; Lesher and Arndt, 1995; Naldrett, 1997).

A diagnostic sulphur source for the deposits is not readily supported by S-isotope data (Lesher and Groves, 1986), and it is likely that the genesis of the Norseman-Wiluna ores overlaps with felsification models. Arndt and Jenner (1986) presented trace element and Sm-Nd data to suggest that the Kambalda komatiitic rocks had assimilated up to 8% sulphidic metasedimetary and basaltic footwall rock; while Lesher and Arndt's (1995) REE and Nd isotope geochemistry favour assimilation of between 2-30% crustal material in some of the Kambalda komatiites, suggesting that felsification may be important. However, in the case of the Kambalda ores, there is generally a ubiquitous presence of sulphidic metasedimentary rocks underlying the channelized, Ni-Cu sulphide bearing flows and suggests that any crustal contamination would likely also incorporate sulphur from this material (Lesher and Groves, 1986; Groves *et al.*, 1986; Naldrett, 1997).

The Noril'sk-Talnakh region of Siberia hosts the world's largest magmatically formed Cu accumulation, and second largest PGE and Ni accumulations (Naldrett *et al.*, 1996b). Geologically the Noril'sk-Talnakh deposits are associated with subvolcanic intrusions which were feeders to a 3.5km thick succession of flood basalt and tuff of the Permo-Triassic Siberian Flood Basalt Province (Naldrett, 1989c). Underlying the flood basalts and tuff rocks is a basement of Proterozoic crystalline rocks and an assemblage of Lower Paleozoic marine argillite, dolomite and sandstone; Devonian evaporates and marls; Lower Carboniferous shallow water limestones; and Mid-Carboniferous lagoonal and continental gravels, congiomerates and coal measures (Naldrett and MacDonald, 1980; Naldrett, 1989c). The Ni-Cu-PGE deposits of the region are located at two major ore junctions between the trans-crustal Noril'sk-Kharayelakh Fault and axis of a major regional anticline (Naldrett and MacDonald, 1980; Naldrett, 1989c; Naldrett *et al.*, 1992; Naldrett *et al.*, 1996b; Naldrett, 1997; and others; Figure 1.5a).

Volcanic and intrusive rocks of the Noril'sk-Talnakh region have been subject to intensive scrutiny over the past decade, leading to 11 petrographic and geochemical divisions of the volcanic formations (Lightfoot *et al.*, 1990,1994; Naldrett *et al.*, 1992; Federenko, 1994). Similarly, the intrusive phases are subdivided into five geochemical groups, in which the intrusives at the ore junctions are associated with differentiated bodies (Lightfoot *et al.*, 1990,1994; Naldrett *et al.*, 1992; Federenko, 1994).
The geochemistry of the volcanic formations show a progressive variation in both chemistry and PGE content. The lowermost suites consist of normal chalcophile element abundance (Ivakinsky, Syverminsky, Gudchinsky, and Tuklonsky Formations (*tk*);

Lightfoot *et al.*, 1990,1994; Federenko, 1994; Naldrett *et al.*, 1992, 1995, 1996b). Overlying the lower section of lavas are a chalcophile element depleted (75% Ni and Cu and up to 90% PGE depletions) suite of lavas (Lower Nadezhdinsky, *nd1* and *nd2*; Lightfoot *et al.*, 1990, 1994; Brughman *et al.*, 1993; Naldrett *et al.*, 1992, 1995; Federenko, 1994). The chalcophile-depleted suite is then overlain by lavas with transitional chemistry (Nadezhdinsky, *nd3*), and normal chalcophile abundance (Morongovsky, *mr*, and Mokulaevsky, *mk*; Lightfoot *et al.*, 1990, 1994; Brughman *et al.*, 1993; Naldrett *et al.*, 1992, 1995; Federenko, 1994). Chemically correlative with the volcanic formations are two ore-bearing intrusion types, including: 1) the Noril'sk-type intrusions, that are correlable to the *mr* lavas; and 2) the Lower Talnakh-type intrusions that are correlable with the *nd2* and *nd3* lavas (Naldrett *et al.*, 1992, 1995; Federenko, 1994; Likhachev, 1994). Typical petrographic and ore relationships to the intrusions are shown in Figure 1.5b.

The geological model for the Noril'sk-Talnakh ore deposits must account for the observed chemostratigraphic variations and the high $\delta^{34}S$ values (+8 to +12‰; Godlevsky and Grinecko, 1963; Grinecko, 1985) of the sulphide ores. The models proposed by Lightfoot *et al.* (1994) and Naldrett *et al.* (1995) suggested that the ore bearing intrusions, and the *nd* suite magmas were initially *tk* magmas that underwent crustal contamination and fractionation at mid-crustal levels, resulting in sulphide saturation and chalcophile element depletion (Figure 1.5c). These sulphide bearing magmas continued to flow along the trans-crustal Noril'sk-Kharayelakh Fault, ponding at the base of a regional syncline were they ingested evaporitic sediments and coal measures, followed by

subsequent segregation of sulphides (Naldrett *et al.*, 1995; Figure 1.5c). The high PGE content in the ores is believed to be a result of a zone-refining effect by subsequent magma pulses that interacted with previously segregated sulphides resulting in PGE upgrading (Naldrett *et al.*, 1996b; Figure 1.5c). This model shows both effects of sulphurization and felsification and provides a logical continuum into the next section on felsification dominated models.

1.3.2.2 Silica Assimilation Dominated Models

The deposits of the Sudbury Igneous Complex (SIC) typify the influence of silica assimilation (felsification) on the genesis of magmatic Ni-Cu sulphide formation (SIC). The 1.85 Ga SIC represents the largest single concentration of Ni in the world with over 1548 million metric tonnes grading ~1.2 % Ni (Lightfoot, 1996). The SIC is a composite plutonic suite which is in contact with Archean (>2.5Ga) tonalitic gneisses (Levack Gneiss) and intrusive quartz-monzonites (Cartier Granite) along the north margin of the complex; while along the south margin the contact is with Proterozoic Southern Province rocks (Naldrett, 1984a, 1989d, 1997; Figure 1.8a).

Overlying the SIC is the Early Proterozoic Whitewater Group consisting of the Onaping, Onwatin and Chelmsford Formations (Rousell, 1984a,b; Muir and Peredery, 1984; Figure 1.6a). The lowermost, Onaping Formation is a heterolithic breccia of fragments and shards of country rock set in a recrystallized, glassy matrix, interpreted to be an ignimbrite or "fall-back" breccia from a meteorite impact (Peredery and Morrison, 1984; Muir, 1984). The geological elements associated with the SIC event include (after Naldrett, 1984a, 1989d; 1997): 1) Sudbury Breccia consisting of country rock fragments

in dykes and irregular masses; 2) Footwall Breccia (FWB) consisting of shattered or crushed country rocks between the SIC and the footwall gneisses and monzonites of the North Range; 3) the Onaping Formation, as above; and 4) the SIC proper.

The SIC intruded between the Footwall Breccia and the Onaping Formation and consists of: 1) the Sublayer; 2) quartz-rich norite of the South Range and mafic norite of the North Range; 3) South Range felsic norite and norite; 4) quartz gabbro; and 5) granophyre and plagioclase rich granophyre (Naldrett and Hewins, 1984; Naldrett *et al.*, 1984a; Naldrett, *1989d*, 1997; Lightfoot *et al.*, 1997a,b,c; and others). All of the units, except the Sublayer, constitute the Main Mass of the SIC (cf. Naldrett *et al.*, 1984a; Naldrett, *1989d*, 1997; Lightfoot *et al.*, 1997a,b,c; and others).

Ore deposits of the SIC are of five types (after Naldrett 1984a, 1989d, 1997), including: 1) South Range deposits; 2) North Range deposits; 3) Offset deposits; 4) Fault Related; and 5) a miscellaneous group. Features common to all of the Sudbury ore deposits at Sudbury, include: 1) *embayments and other irregularities at the base of the SIC* where embayments or terraces are present and the thickness of sulphide increases and becomes sufficient to constitute ore (Naldrett, *1989d*; Naldrett, 1997; Lightfoot *et al.*, 1997a,b,c); 2) *the presence of the Sublayer* where sulphides are spatially related, and appear to have settled out of bodies of Sublayer magma (Naldrett *et al.*, 1984a; Naldrett, *1989d*; Naldrett, 1997); and 3) *ultramafic and mafic inclusions within Sublayer host rocks* are found in regions that contain ore and are absent in regions that are barren (Scribbins *et al.*, 1984; Grant and Bite, 1984; Naldrett *1989d*; Naldrett, 1997; Lightfoot *et al.*, 1997a,b,c; Zhou *et al.*, 1997).

The origins of the SIC and it's ores have been subject to debate for significant time; however, it is generally accepted that the SIC was generated due to a meteorite impact (Naldrett, 1997). The origin of the ore deposits at Sudbury has been also subject to debate, but is largely associated with felsification of a mafic-ultramafic magma. Early work by Kuo and Crocket (1977), Naldrett and Hewins (1984) and Naldrett *et al.* (1984a, 1986) showed that the Sublayer rocks of the SIC underwent significant crustal influence, based on REE and Nd-Sr isotope geochemistry (Figure 1.6b); while Naldrett *et al.* (1986) suggested equivalent amounts of basaltic magma mixed with impact melt (derived from crustal melting during meteorite impact). Walker *et al.* (1991, 1994), using Re-Os isotope data, suggested that at least 75%, and up to 90%, of the Os in the ores was crustally derived, advocating mixing of basaltic magma with upper crustal material. In contrast, Lightfoot *et al.* (1997a,b,c) have suggested that most of the Sublayer was derived from the meteorite-melt derived sheet, mixed with up to 20% picritic mantle material.

The relationship of the Sublayer to the remainder of the SIC is also problematic. Chai *et al.* (1993) and Chai and Eckstrand (1994) proposed that the SIC formed from two separate magmas, a granophyric magma and a different mafic magma for the remainder of the SIC. In contrast, Lightfoot *et al.* (1997a,b,c) suggests that the Main Mass and Offsets were generated from a similar parental magma; while the Sublayer is geochemically distinct from the Main Mass, but chemically variable from embayment to embayment. Although geochemically distinct, the mafic and ultramafic inclusions in the Sublayer have U-Pb zircon ages of 1.85 Ga (Corfu and Lightfoot, 1996), overlapping the SIC ages of

Krogh *et al.* (1982, 1984); suggesting that the Sublayer is related to the genesis of the Main Mass of the SIC.

The present model for the SIC origin involves impact melting of the continental crust and pressure decreases associated with removal of 50% of overlying crust following meteorite impact (Naldrett, 1997). Fracturing in the surrounding host rocks, impact melt generation, and mantle melting caused the formation of a largely felsic dominated melt sheet and picritic mantle melts (Lightfoot *et al.*, 1997a,b,c; Naldrett, 1997; Zhou *et al.*, 1997). Mixing of these picritic melts (up to 20% picritic) and the felsic dominated impact melt resulted in felsification (cf. Irvine, 1975) of the picritic melts, sulphide saturation and subsequent segregation and downwelling of the sulphide magmas (Lightfoot *et al.*, 1997a,b,c; Naldrett, 1997; Zhou *et al.*, 1997). Upon settling out from the Sublayer the sulphide magmas, and associated Sublayer silicate magmas, mixed with preexisting mafic-ultramafic material forming the observed inclusions (*op cit*).

1.3.2.3 Debated Models

The close spatial association, and likely similar petro-tectonic setting, of the OKG prospect to that of the Voisey's Bay deposits warrant a discussion on the origin and genesis of the Voisey's Bay deposits. The research on the Voisey's Bay deposits is clearly in the early stages, and to date a definitive model for their genesis has yet to be proposed; however, preliminary models have been formulated (Ryan *et al.*, 1995; Naldrett *et al.*, 1996a; Ryan, 1996, 1997; Naldrett, 1997; Lightfoot, 1998; Li and Naldrett, 1997). The Voisey's Bay deposit, discovered in November 1994, is the most significant Canadian Ni-Cu sulphide occurrence defined in the last 25 years, and to date has in excess of 31.8

million metric tonnes (reserves) grading 2.83% Ni, 1.74% Cu and 0.12% Co, with an estimated total tonnage of 150 million metric tonnes (Naldrett *et al.*, 1996a; Naldrett, 1997). The Voisey's Bay deposits are hosted by troctolitic rocks of the Reid Brook Intrusion (RBI), a troctolitic member of the 1.34-1.29 Ga Nain Plutonic Suite (Ryan, 1990a; Ryan and Emslie, 1994; Emslie *et al.*, 1994; Ryan *et al.*, 1995; Naldrett *et al.*, 1996a; Figure 1.7).

The deposit contains four similar, yet different ore horizons within a single troctolitic intrusion, including: 1) the Ovoid; 2) the mini-Ovoid, west of the Ovoid; 3) the Western Extension, west of the mini-Ovoid; and 4) the Eastern Deeps, to the east of the Ovoid (Naldrett *et al.*, 1996a; Naldrett, 1997; Figure 1.8). The Western Extension is characterized by a well developed stratigraphy, containing and upper unmineralized troctolite either chilled against, or mixed with overlying Nain and Churchill Province gneisses (Naldrett *et al.*, 1996a; Naldrett, 1997; Figure 1.8b). In the upper troctolite sulphides rarely exceed 2%, but increase up to 50% at depth, and some areas contain 20-25% disseminated sulphides associated with oikocrysts of olivine or augite; the latter termed a leopard textured troctolite (Naldrett *et al.*, 1996a; Naldrett, 1997). At greater depths, disseminated sulphide gives way to massive sulphide lenses, underlain by troctolite with brecciated gneiss fragments termed the basal breccia sequence (BBS; Naldrett *et al.*, 1996a; Naldrett, 1997; Li and Naldrett, 1998; Figure 1.18b).

The Ovoid and mini-Ovoid have a similar stratigraphy consisting of an upper sequence troctolite, underlain by a thick zone of massive sulphide and a variably thick BBS grading into basement gneiss at depth (Naldrett *et al.*, 1996a; Naldrett, 1997; Figure

1.8c). The troctolitic sheet that hosts the Western Extension and Ovoid thickens towards the southeast and becomes a larger intrusion, common to the Eastern Deeps (Naldrett *et al.*, 1996a; Naldrett, 1997; Figure 1.8d). The troctolitic body in the Eastern Deeps has an upper, medium grained, uniformly textured troctolite (Normal Troctolite; NT), underlain by medium grained to pegmatoidal troctolite (Varied Textured Troctolite; VTT) with trace (10-15%) to leopard textured ore; while massive sulphide lenses are common near the BBS (Varied Textured Troctolite; VTT; Naldrett *et al.*, 1996a; Naldrett, 1997; Figure 1.8d).

The earliest geological model for the Voisey's Bay proposed by Ryan *et al.* (1995) involved wedging of the Tasiuyak Gneiss between the Nain and Rae Cratons during the ca. 1860 Torngat orogen (Wardle *et al.*, 1990a; Bertrand *et al.*, 1993; Ryan *et al.*, 1995; Figure 1.9a). The collisional boundary remained active along sub-vertical faults until ca. 1740 providing a through going structure for the uprising of troctolitic magmas associated with Reid Brook Intrusion during NPS magmatism (Bertrand *et al.*, 1993; Ryan *et al.*, 1995; Figure 1.9b). Troctolitic magmas of the RBI assimilated sulphide from the Tasiuyak gneiss, inducing sulphide saturation (Figure 1.9c), and upon emplacement into their respective magma chambers segregated sulphides that gravitationally settled out to form the Voisey's Bay deposits (Ryan *et al.*, 1995; Figure 1.9d).

A subsequent model by Naldrett *et al.* (1996a) suggested that the four settings of the Voisey's Bay deposit are related to a single mineralized horizontal feeder intrusion (troctolite sheet) of the RBI (Figure 1.10). In Naldrett *et al.*'s (op cit) model they suggested that a turbulently flowing (sulphide saturated?) magma entered into the feeder

system and upon reaching the mouth of the intrusion rapid decreases in the flow velocity resulted in a change in flow from turbulent to laminar conditions. The changing flow conditions at this point resulted in the deposition of the sulphide magmas and the BBS forming a berm whereby subsequent intrusive pulses deposited their denser sulphide and BBS material near the mouth of the intrusion (Naldrett *et al.* 1996a; Figure 1.10). The leopard textured troctolites are believed to represent the feeder intrusion proper and have a disseminated nature because the high turbulence did not allow the accumulation of massive sulphide lenses (Naldrett *et al.*, 1996a; Figure 1.10).

Although explaining the mechanism of emplacement and occurrence, Naldrett *et al.* (1996a) do not discuss a mechanism for sulphide saturation and quote that their model is similar to the Ryan *et al.* (1995) model. Sulphur saturation by the Tasiuyak gneiss (e.g. Ryan *et al.*, 1995) has been shown to be of lesser importance in the formation of the Voisey's Bay ores based on recent work (Ripley *et al.*, 1997; Lightfoot, 1998; Li and Naldrett, 1998). Ripley *et al.* (1997) have shown that a maximum of 30% Tasiuyak gneiss sulphur has been contributed to the sulphur isotope signatures of the Voisey's Bay ores. Furthermore, Lightfoot (1998) and Lambert *et al.* (1997) have shown that crustal contamination by the Nain Province gneisses were likely important in the genesis of the ores; while Li and Naldrett (1998) have suggested that crustal contamination by the Tasiuyak gneiss was likely important. Likewise, based on olivine compositions, and Ni-Cu-PGE tenor in the ores led Naldrett *et al.* (1998) suggested that the ores were a result of a reaction of olivine gabbros with Tasiuyak paragneiss with subsequent recharge and upgrading of the metal tenor by a second phase troctolitic magma. It is clear that from

this work that the understanding of the genesis of the Voisey's Bay deposits is in the early stages and modification will occur in time.

1.4 Purpose and Scope

Preliminary geological and metallogenic work on the OKG prospect has resulted in the discovery of numerous showings and drill core intersections of massive, semi-massive to disseminated base-metal sulphides that are spatially, and likely genetically, associated with pyroxenitic intrusives of presumed Mesoproterozoic age (Wilton and Baker, 1996; Kerr, 1998; *this study*). The geology of the prospect is an apparent contrast to the mineralization and consists of Archean gneisses, and likely Paleoproterozoic anorthositic, granitoid, and basic dyke rocks (Ryan *et al.*, 1998; Hamilton *et al.*, 1998). These magmatic and metallogenic events in the Umiakoviarusek Lake region have yet to be readily explained, and numerous questions remain. The underlying problem associated with the OKG prospect (and many other Labrador Ni-Cu-Co prospects) is that there is a very poor understanding of the nature and controls on the mineralization; as well as the nature of Paleoproterozoic anorthositic and granitoid magmatism. In particular little is known about petrographic character of the host rocks and sulphides, geochemical attributes of the host rocks and sulphides (e.g. major, trace, REE, and PGE character), as well as the stable and radiogenic isotope attributes of the host rocks and sulphides. Similar, geologic, geochemical and isotopic uncertainties exist with respect to the Paleoproterozoic magmatism as well and these problems constitute the major focus of this thesis.

Preliminary work carried out during the summer of 1996 has resulted in the production of a 1: 25 000 scale map for the property (see Figure 2.1) and the collection of approximately 130 lithologic samples for petrographic and geochemical analyses. With this preliminary work in hand, numerous questions remain unanswered and constitute the major purpose and scope of this thesis, including:

1) To provide a detailed petrographic and field documentation of the lithologic elements of the OKG prospect such that there is an adequate descriptive understanding of both sulphide mineralization, host pyroxenitic rocks and other rock types of the property.
2) Very little geochemical and minimal radiogenic isotope data have been collected from the likely Paleoproterozoic anorthositic and granitoid rocks of the Umiakoviarusek Lake region. This study will attempt to use trace and rare earth elements (REE), and radiogenic isotopes (Rb-Sr and Nd-Sm systems) to geochemically characterize the anorthositic-granitoid rocks and to see if there is a relationship between magmatism, crustal contamination and petrogenesis. Furthermore, to see if the petrogenetic processes that are common to Nain Plutonic Suite (Emslie *et al.*, 1994) hold true for this likely older suite of Paleoproterozoic anorthositic and granitoid rocks.
3) To use a combined trace element, rare-earth element (REE), platinum-group element (PGE), sulphur isotopes, and radiogenic isotopes to geochemically characterize the mineralized pyroxenitic intrusives and to decipher the geochemical controls on sulphide genesis. In particular, to decipher the relationship between mantle magmatism and sulphide saturation and sulphide genesis.

4) By combining field observations, petrography, and geochemical and isotopic data to provide a physio-chemical model for the genesis of the OKG sulphide occurrences.

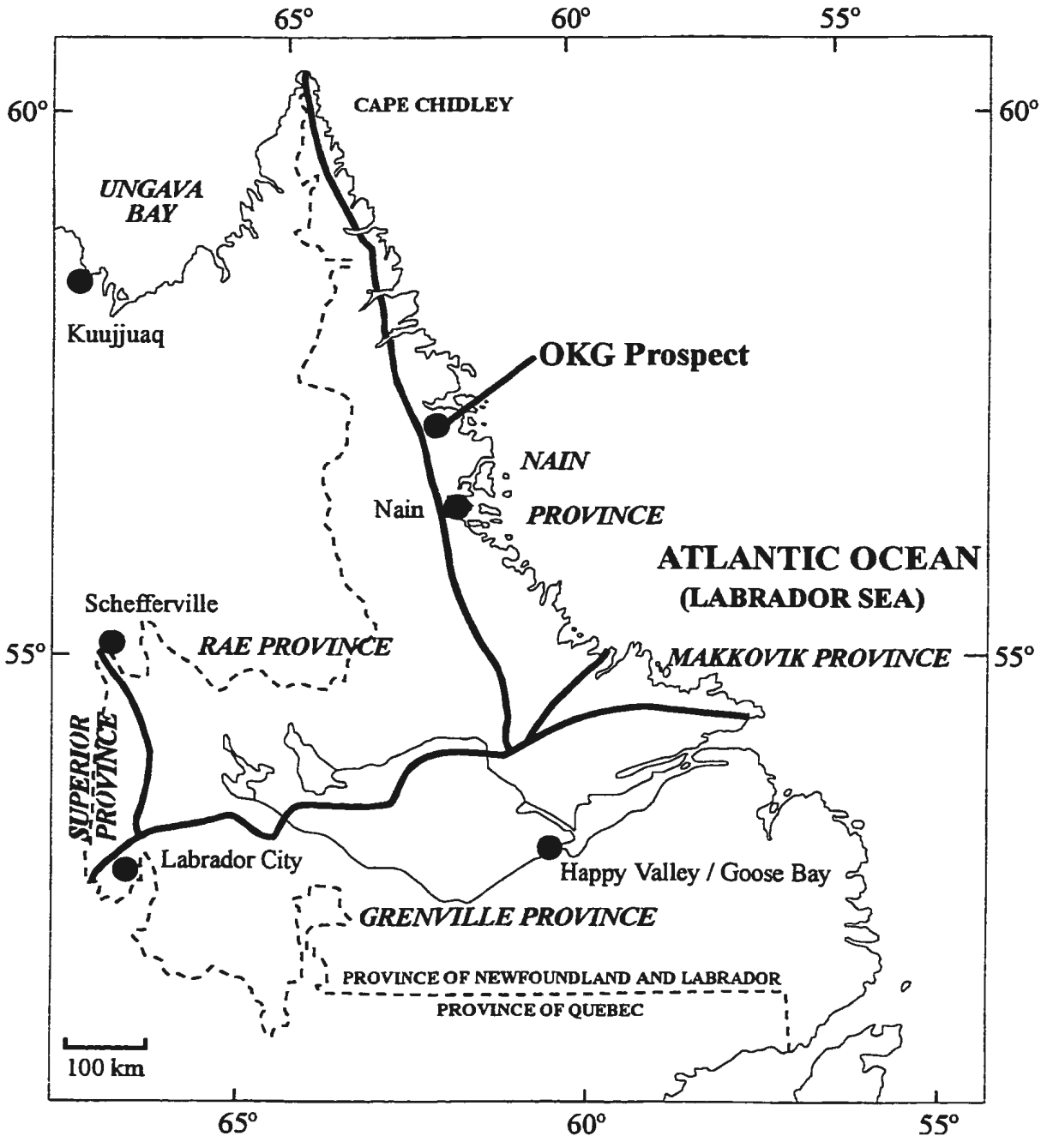

Figure 1.1. Location of OKG prospect and the simplified geology of the Precambrian structural provinces of Labrador (after Greene, 1972).

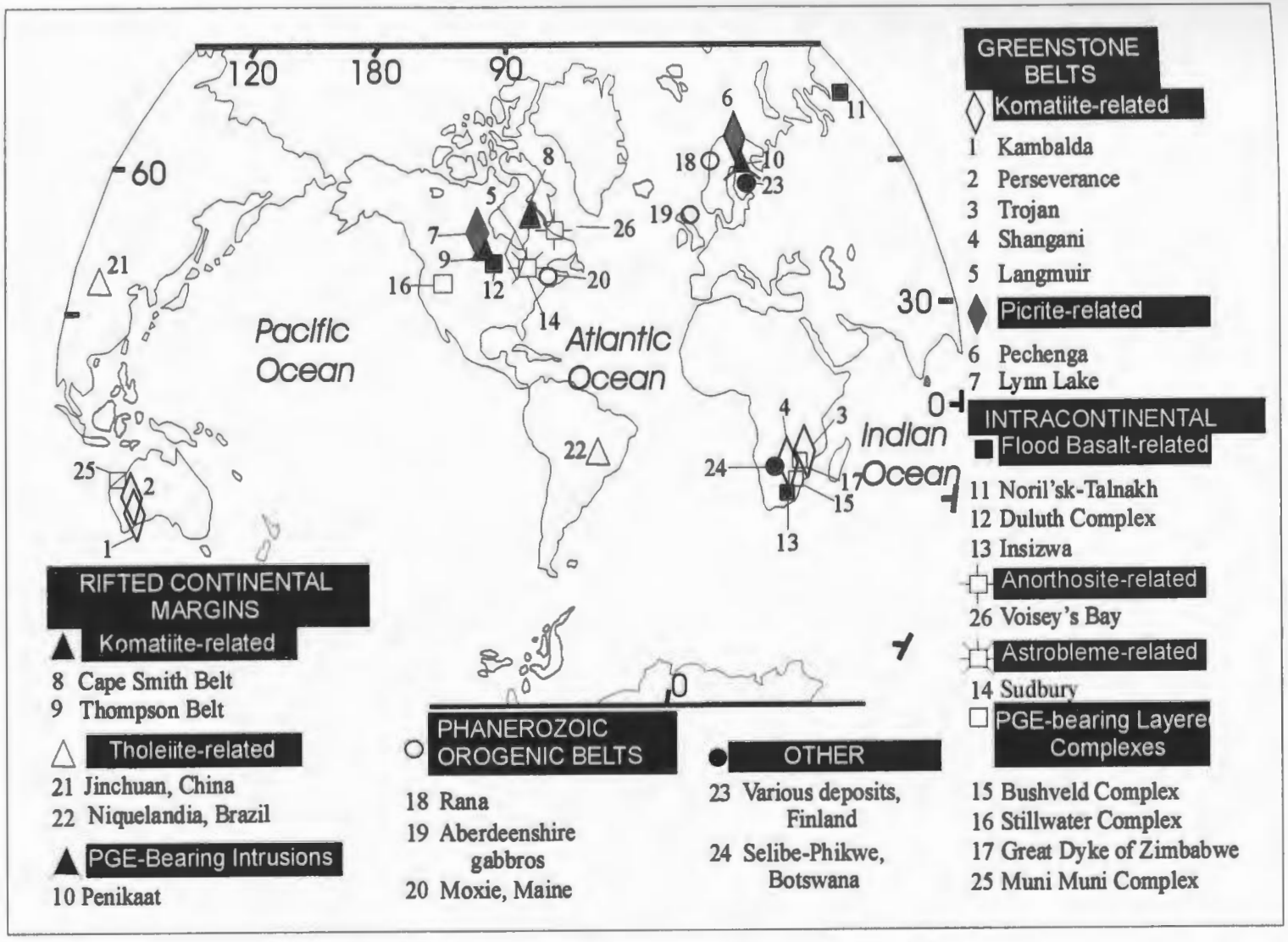

Figure 1.2. Worldwide distribution of magmatic Ni-Cu-PGE deposits and their respective petro-tectonic settings (modified after Naldrett, 1997).

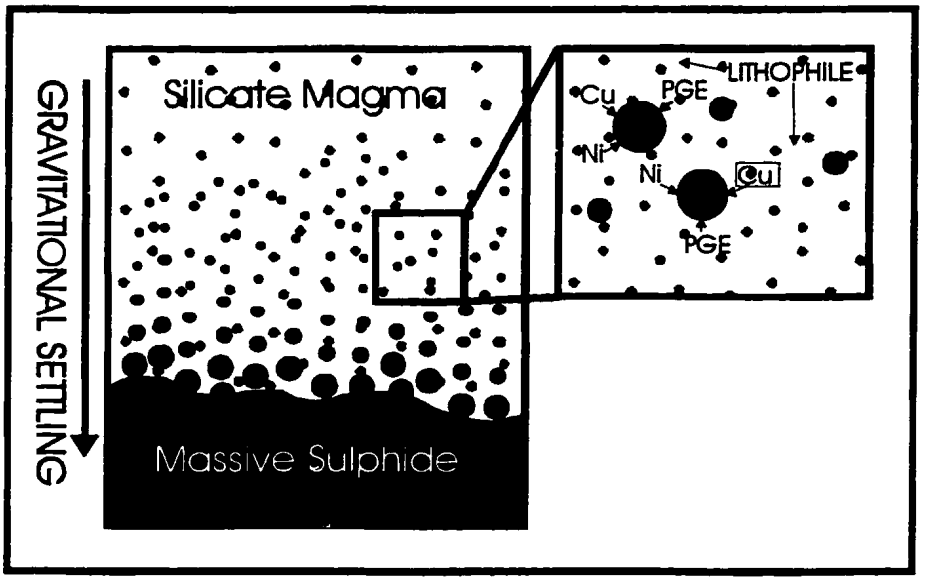

Figure 1. 3. Schematic model of sulphide segregation from a silicate magma and partitioning of chalcophile elements into sulphide liquid and lithophile elements into silicate magma (modified after Naldrett, 1973).

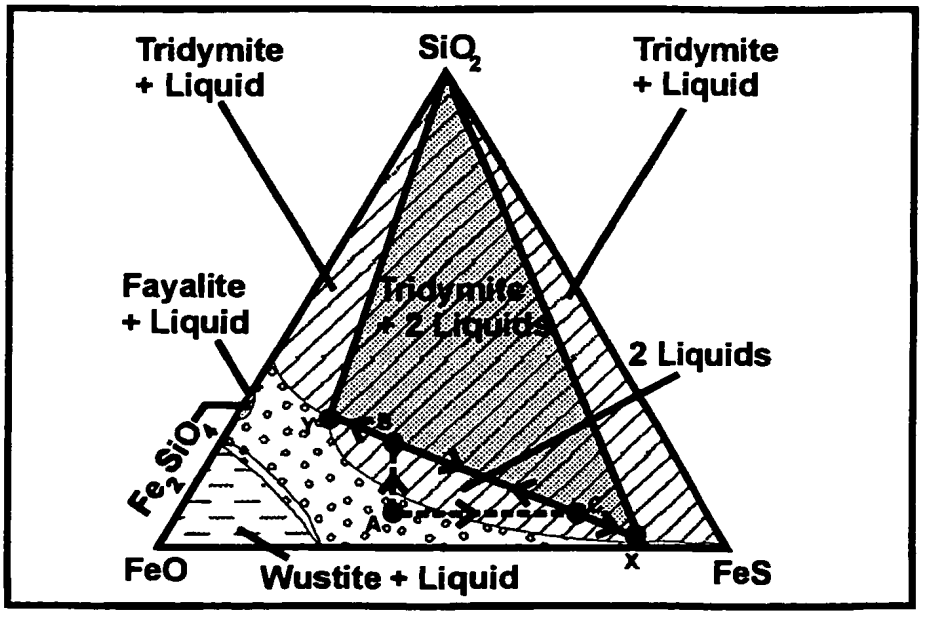

Figure 1.4. Schematic illustrating the effects of adding silica (felsification), or sulphur (sulphurization) to a mafic-ultramafic magma and the induction of sulphide imiscibility. Details on the mechanisms involved are provided in the text. Diagram modified after MacLean (1969) and Irvine (1975).

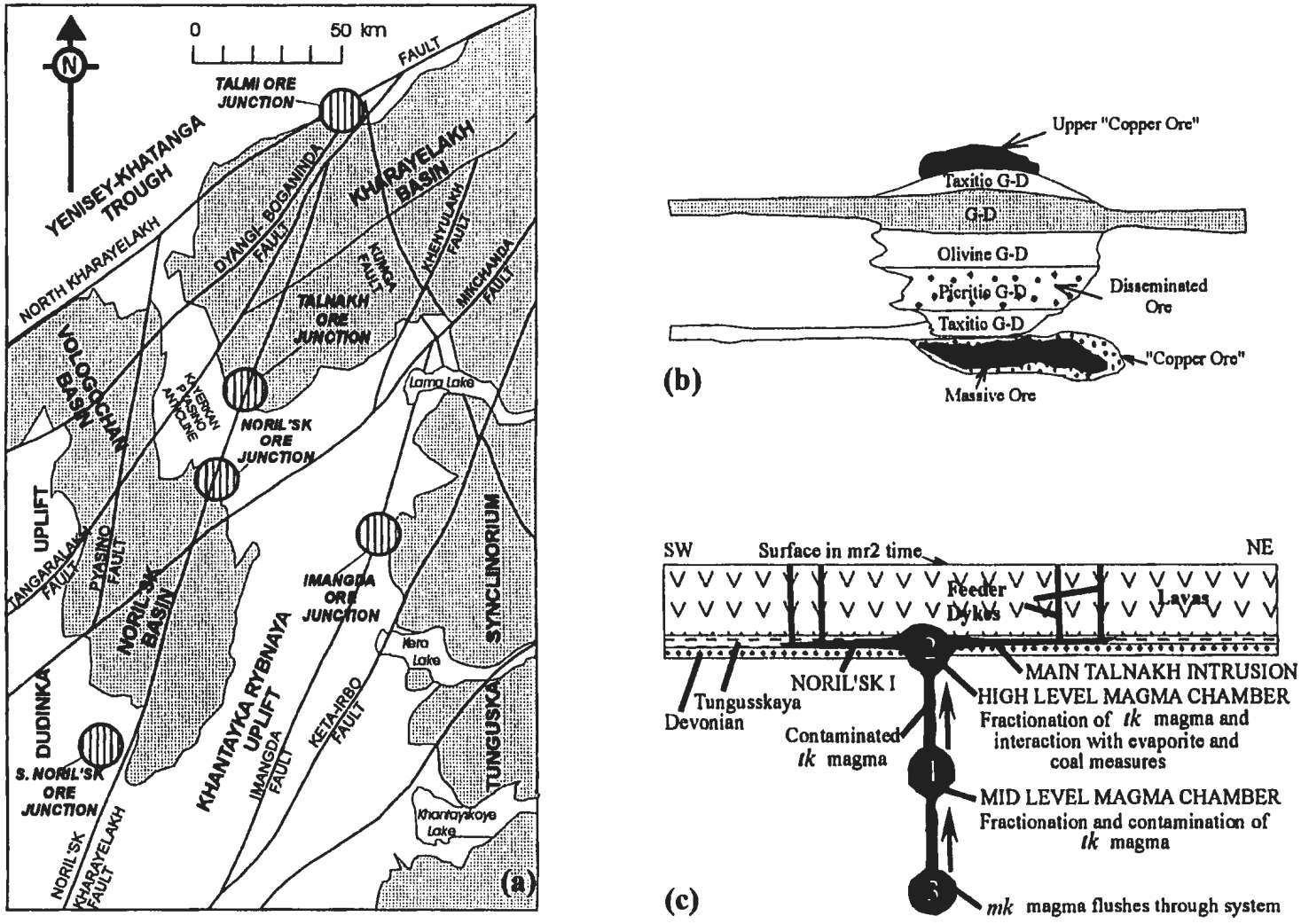

Figure 1.5. Tectonic map of the Noril'sk-Talnakh region, Siberia (a), typical ore-bearing intrusion stratigraphy (b) and geological model for the genesis of the Noril'sk-Talnakh ore bearing intrusions (modified after Naldrett et al., 1995).

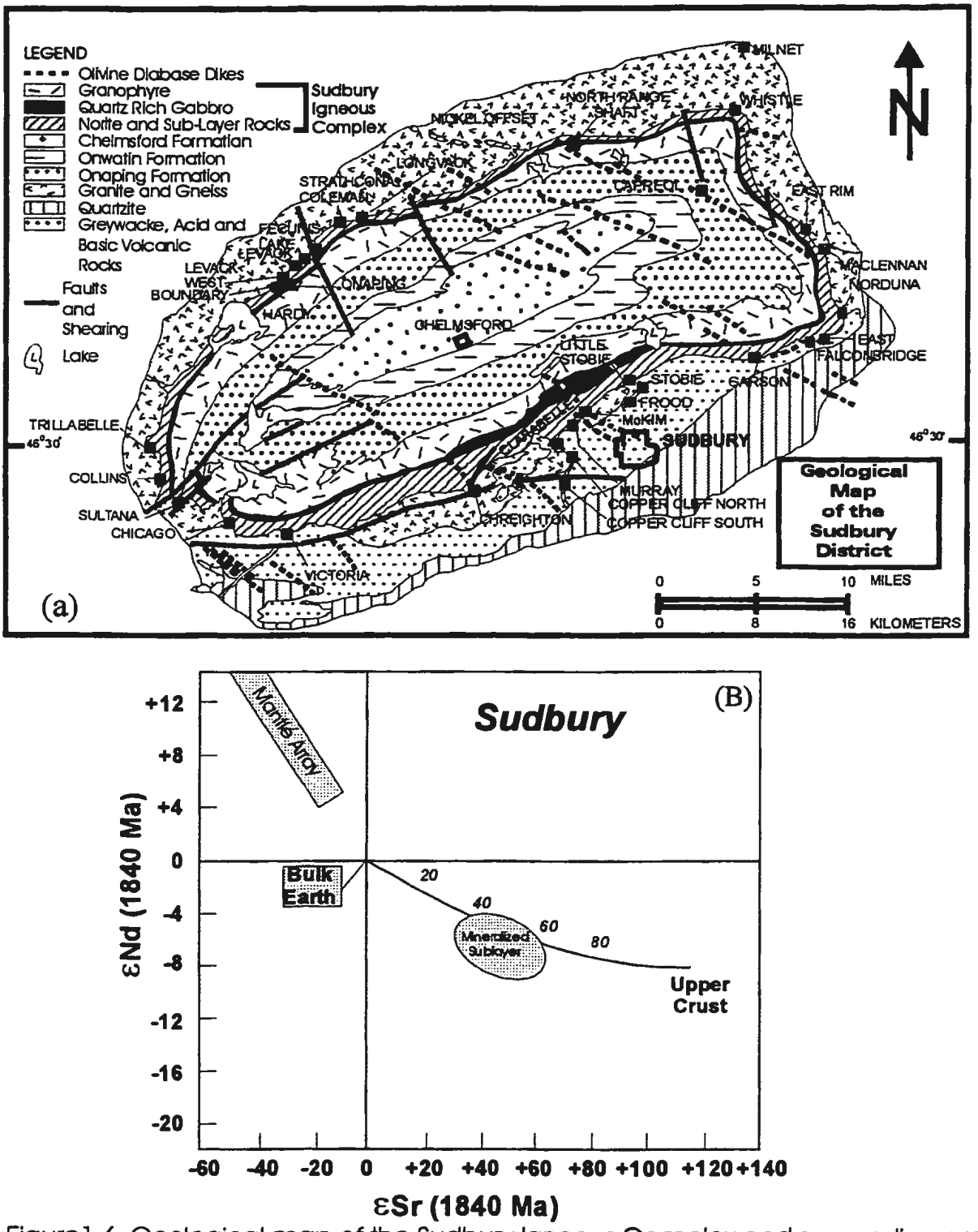

Figure1.6. Geological map of the Sudbury Igneous Complex and surrounding area (a), and radiogenic isotope geochemistry of the SIC showing extensive evidence of crustal contamination (b). Modified after Naldrett and MacDonald (1980) and Naldrett et al. (1984a, 1986).

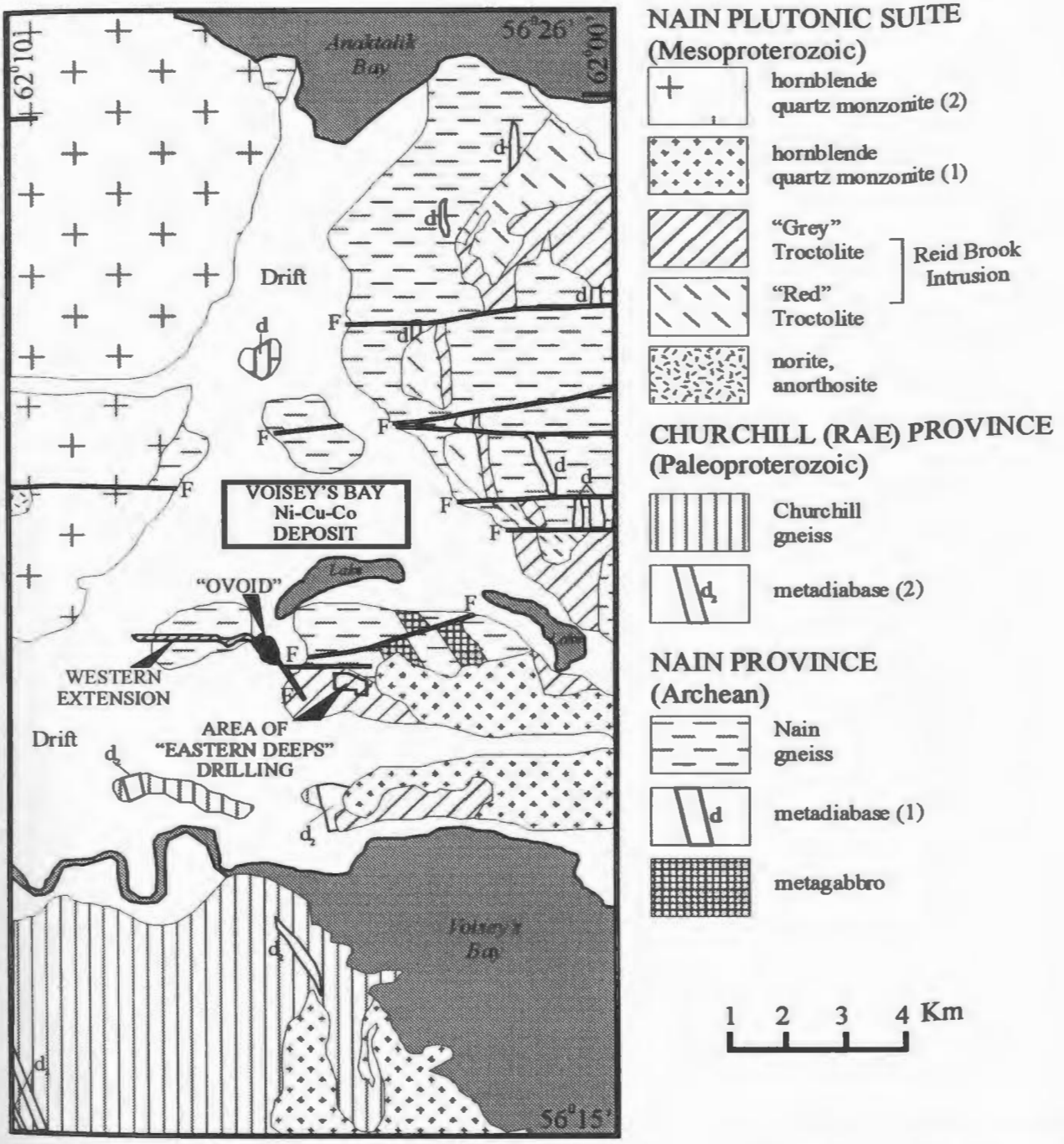

Figure 1.7. Geology of the Voisey's Bay area, Labrador and outline of the settings of the Voisey's Bay deposit. Modified after Ryan et al. (1995), Naldrett et al. (1996), and Naldrett (1997).

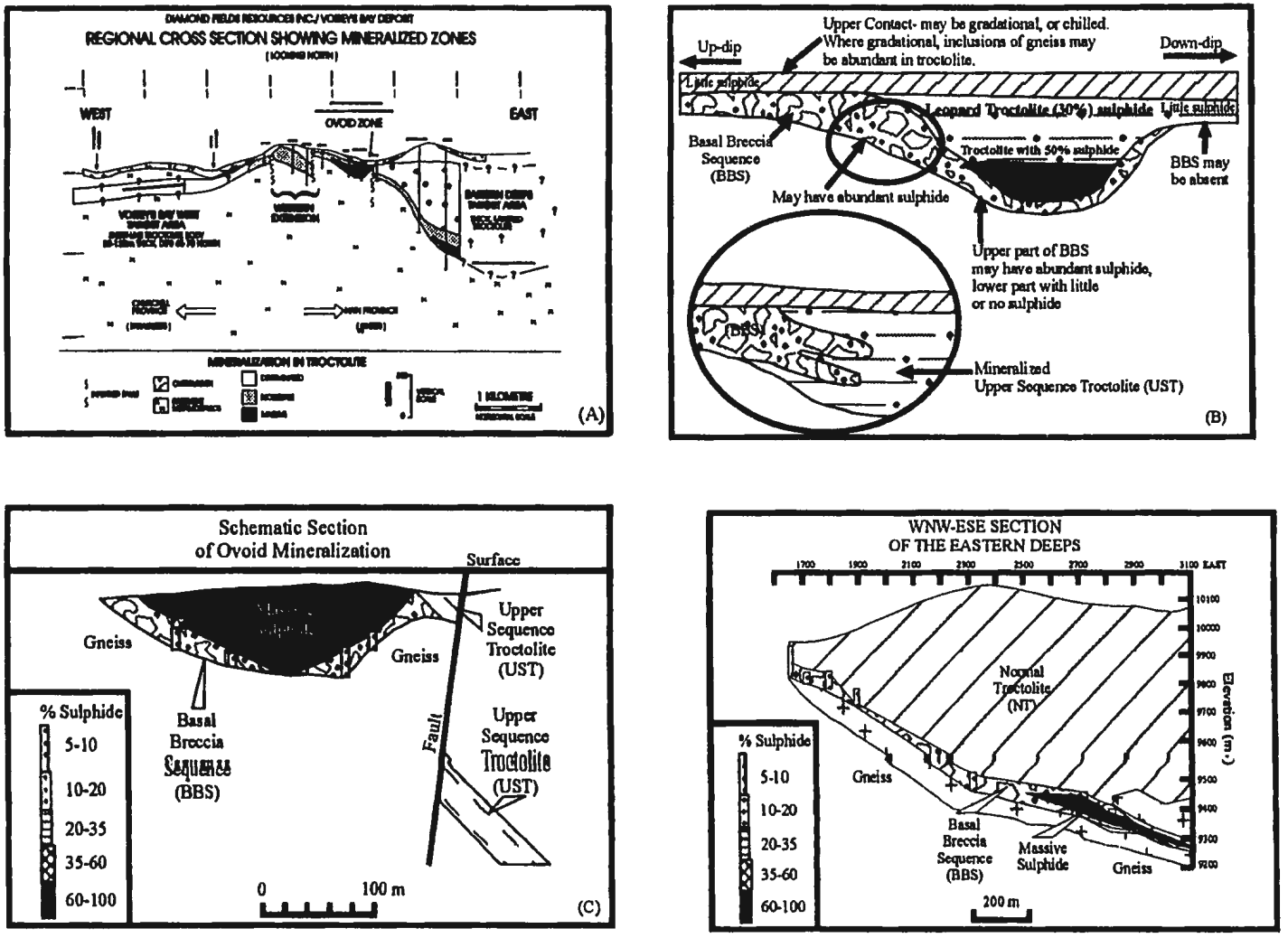

Figure 1.8. Cross section of the Volsey's Bay deposit and the respective ore horizons (after Diamond Fields Resources press release, January 6th, 1996 (a); and cross sections of the Western Extension (b), Ovoid (c), and the Eastern Deeps (d) (after Naldrett et al., 1996).

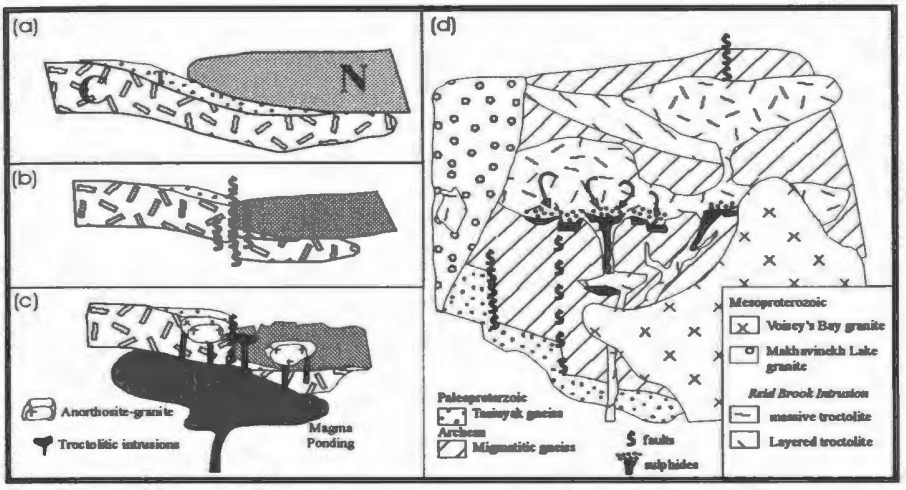

Figure 1.9. Geologicl model for the genesis of the Voisey's Bay deposit after Ryan et al. (1995). Collision of the Nain and Churchill (Rae) provinces at ca. 1860 Ma associated with the Torngat orogen resulted in wedging of the sulphide-bearing Tasiuyak paragneiss. Uplift along the boundary between 1790-1740 Ma resulted in large scale crustal faults and the end of orogenic activiety (b). At ca. 1350-1290 Ma there was a large scale mantle plume and crust-mantle melting and the genesis of the Nain Plutonic Suite, including the troctolitic rocks of the Reid Brook Intrusion (c). The upwelling of the metal rich troctolitic magmas scavenged sulphur from the Tasiuyak gneiss which led to sulphide saturation and subsequent segregation of a metal-rich sulphide liquid that settled to the base of the magma chamber associated with the Reid Brook Intrusion.

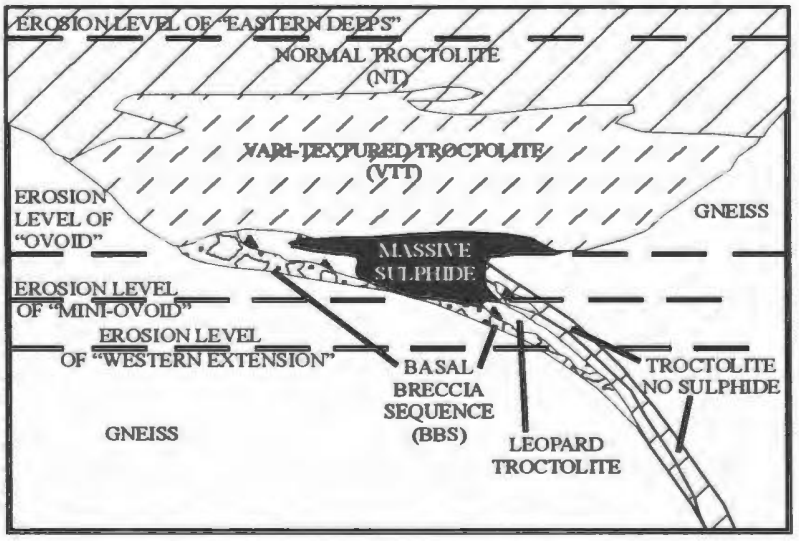

Figure 1.10. Schematic model of the Voisey's Bay deposit and it's genesis (after Naldrett et al., 1996a). Details of the model are provided in the text.

Chapter 2. Regional Setting of the OKG Prospect with Emphasis on the Tectono-Magmatic Evolution of the Nain Province

2.1 Introduction

The geology of Labrador is a diverse collage of rocks representing widespread magmatism and tectonism over 3.5 billion years of Earth's history. This chapter contains an overview of the geology of Labrador, the pre-Torngat Orogen evolution of the Nain Province, the evolution of the Torngat Orogen, descriptive and genetic aspects of the Nain Plutonic Suite, and the significance of Paleoproterozoic anorthosite-granitoid plutonism in the north-central portion of the Nain Province. This chapter provides the tectono-magmatic framework from which all further work in this thesis is developed.

2.2 Geologic Framework of Labrador

The geology of Labrador represents a variety of rock units ranging in age from Archean to Cretaceous, with most rocks between 3.9-1.2 Ga (Wardle, 1995; Wilton, 1996a). This section will concentrate on the broad scale geologic elements of Labrador, and the following sections will discuss those of significance to the OKG and Voisey's Bay sulphide occurrences.

The oldest rocks of Labrador are manifested in the Archean Nain and Superior Provinces in northeastern and western Labrador, respectively (Figure 1.1). The western Superior Province represents only a minor portion of Labrador geology and consists

predominantly of metasedimentary gneiss, orthogneiss, mafic intrusions and granitoid diatextite plutons of the Ashuanipi Complex (James, 1993; James and Mahoney, 1993; James, 1995).

In contrast to the Superior, the Nain Province (Taylor, 1971) comprises a significant portion of north-central Labrador and geologically is much more complex (Figure 2.1). The Nain Province is subdivided into two blocks: 1) the Saglek block in the north (ca. >3.9 to 2.5 Ga), and 2) the Hopedale block in the south (ca. 3.2-2.8 Ga; Ermanovics, 1993; Figure 2.1). The Saglek Block consists of a variety of largely granulite facies rocks including high grade metasedimentary and mafic gneiss, meta-igneous complexes and migmatized tonalitic gneiss (Taylor, 1971; Schiøtte *et al.*, 1989a,b; Ryan, 1990a,b; Collerson, 1991; Wardle and Wilton, 1995). Overlying portions of the Saglek Block are a series of relatively undeformed ca. 2.0 Ga supracrustal shelf-foredeep sequences including the Snyder, Mugford and Ramah Groups (Morgan, 1975; Speer, 1978; Smyth and Knight, 1978; Knight and Morgan, 1981; Hamilton, 1994; Wilton *et al.*, 1993, 1994; Wilton, 1994; Archibald, 1995; Figure 2.2).

The southern Hopedale block is less complex than the northern Saglek block and is younger (ca. 3.2-3.1 Ga) and is preserved at amphibolite facies rather than granulite facies, consisting predominantly of metasedimetary gneiss amphibolite enclaves and two greenstone belts, the Florence Lake and Hunt River greenstone belts (Brace and Wilton, 1989; Brace, 1991; Ermanovics and Raudsepp, 1979; Ermanovics, 1993; Wardle and Wilton, 1995; Wasteneys *et al.*, 1995; Wilton, 1996a; Figure 2.1 and 2.3).

Wedged between the Nain and Superior Provinces is the southeastern Churchill Province (SECP) containing a central Archean core, the Rae Province, bounded on both sides by the western New Quebec Orogen, and the eastern Torngat Orogen (Hoffman, 1988; Wardle *et al.*, 1990a,b; Wardle *et al.*, 1995a; James *et al.*, 1996a; Figure 2.4). The Rae Province consists predominantly of reworked Archean gneisses, Early Proterozoic supracrustal rocks, and variably deformed 1.83-1.81 Ga granitic plutons (Wardle *et al.*, 1995a; James *et al.*, 1996a; Figure 2.4). The western New Quebec Orogen (Hoffman, 1988) consists of a variety of low grade, sedimentary and volcanic rock sequences disposed in a westerly verging fold and thrust belt, intruded by mafic to ultramafic sills (Wardle *et al.*, 1990b; Wardle *et al.*, 1995a; Figure 2.4); while the Torngat Orogen consists predominantly of Archean granitoid gneisses, Early Proterozoic supracrustal gneisses, and deformed to relatively undeformed granitoid gneisses (Bertrand *et al.*, 1993; Wardle *et al.*, 1995a; and others; Figures 2.4 and 2.5).

Located in east-central Labrador, and wedged against the Hopedale block of the Nain Province, is the triangular shaped Paleoproterozoic Makkovik Province, consisting of a northern margin of reworked Nain Province rocks, Early Proterozoic volcanic and plutonic rocks and ca. 2.0 Ga supracrustal sequences (Ryan, 1984; Gower and Ryan, 1986; Kerr, 1994; Wardle *et al.*, 1995b; Wilton, 1996a,b; Figures 2.1-2.4).

Truncating the Makkovik, Churchill and Superior Provinces is the southernmost Precambrian structural province, the Grenville Province of southern Labrador (Rivers *et al.*, 1989; Gower *et al.*, 1995; Rivers, 1997; Figures 2.3-2.4). The Grenville Province contains metasedimentary gneiss, migmatized to unmigmatized granitoid gneiss, felsic

volcanics, granitoid plutons, anorthosite-mangerite-charnockite-granite suites (see below), mafic dyke swarms, and silicaclastic and carbonaceous sedimentary rocks (Kamo *et al.*, 1989; Rivers *et al.*, 1989; Gower *et al.*, 1995; Rivers, 1997).

Intruding much of the Nain, Churchill and Grenville Provinces are suites of Mesoproterozoic anorthositic-mangerite-charnockite-rapikivi granite complexes (AMCG; Emslie, 1978, 1980, 1985; Emslie *et al.*, 1994; Ryan *et al.*, 1995; Figure 2.6).

2.3 Magmatic and Tectonic Evolution of North-Central Labrador

The tectonic and magmatic evolution of the north-central regions of Labrador plays a significant role in the genesis of the Voisey's Bay deposit, and possibly many other Ni-Cu-Co sulphide occurrences within this region of Labrador. Hence, in order to place any credibility on genetic models proposed in this thesis an overview of the tectonic and magmatic evolution of this regime is warranted. The following subsections provide an overview of the evolution of the Nain Province, in particular the northern Nain Province, the eastern portions of the Churchill Province and Torngat Orogen, and the genesis of the Nain Plutonic Suite (NPS). Although there is a paucity of data on the Paleoproterozoic AMCG suites in Labrador, a brief discussion of their occurrence, and their significance is also discussed at the end of this chapter.

2.3.1 Tectonomagmatic Evolution of the Nain Province Prior to the Torngat Orogen

The Nain Province (Taylor, 1971) represents a diverse collage of geological elements that record a series of magmatic, metamorphic, sedimentary and tectonic events. This section discusses the evolution of the Nain Province in a pre-Torngat (ca. 1880 Ma; Bertrand *et al.*, 1990, 1993) context prior to deformation and metamorphism associated

with the Torngat Orogen. The Nain Province itself is divided into two structural blocks, which have similar, yet different geological evolutions, *viz*: 1) the northern Saglek Block; and 2) and a southern Hopedale Block (Ermanovics, 1993; Figure 2.1). The Saglek Block is generally older (ca. >3.9-2.5 Ga; Schiøtte *et al.*, 1989a,b; Connelly and Ryan, 1992,1994; Figure 2.1) and preserved at upper amphibolite to granulite facies, while the Hopedale Block is younger (ca. 3.3-2.8 Ga; Ermanovics, 1993) and is preserved at amphibolite facies (cf. Wardle and Wilton, 1995; Wilton, 1996a; Figures 2.1 and 2.3).

The Saglek Block records a much more prolonged geological history than the Hopedale block and consists of rocks of pre-3.9 Ga affinity, including zircon cores in the Nanok Gneisses (Schiøtte *et al.*, 1989a; Collerson, 1991; Table 2.1). These are succeeded by the ca. 3.8 Ga Nulliak Supracrustal rocks, (Nutman *et al.*, 1989; Nutman and Collerson, 1991; Table 2.1), the igneous precursors to the Uivak I gneisses (3732±6 (Schiøtte *et al.*, 1989a,b, 1990; Nutman and Collerson, 1991; Table 2.1); and metamorphism and migmatization of the Uivak I and formation of the Uivak II gneisses ca. 3620 Ma (Schiøtte *et al.*, 1989a,b, 1990; Table 2.1). All of the above units underwent regional scale granulite metamorphism at ca. 2.8-2.7 Ga (Schiøtte *et al.*, 1989a,b, 1990; Table 2.1).

The Hopedale Block is characterized by rocks ranging from ca. 3.3-2.8 Ga. The oldest rocks of the block include the Hunt River Group (3105±2 Ma), Weekes Amphibolite (3258±24 Ma) and the Maggo Gneiss (ca. 3105 Ma; Ryan, 1984; Loveridge *et al.*, 1987; Schiøtte *et al.*, 1990; Ermanovics, 1993; Wasteneys *et al.*, 1995; James *et al.*, 1996b, 1997; James, 1997; Table 2.1). Intruding rocks of the Maggo Gneiss are sheets of

amphibolite interpreted as dykes, called the Hopedale Dykes (Ermanovics, 1993). All of the aforementioned units underwent metamorphism, deformation and migmatization during the ca. 3.1-3.0 Ga, in the Hopedalian structural event (Finn, 1989; Ermanovics, 1993; Table 2.1). Following the Hopedalian event uplift, erosion, and deposition of the Florence Lake greenstone belt occurred between 3002±2 Ma and 2979 Ma (Ermanovics and Raudsepp, 1979; Wasteneys *et al.*, 1995; James *et al.*, 1996b, 1997; Table 2.1); followed by the 2858 +4/-3 Ma to 2838 Ma emplacement of tonalite-trondjhemite-granodiorite rocks of the Kanairiktok Intrusive Suite (Loveridge *et al.*, 1987; Ermanovics and Raudsepp, 1979; Ermanovics, 1993; Table 2.1). Most of the rocks of the Hopedale Block were deformed and metamorphosed during the 2825±20 to ca. 2550 Ma Fiordian deformation and metamorphic event (Finn, 1989; Ermanovics, 1993; Wasteneys *et al.*, 1995; Table 2.1).

The continental collision between the Saglek and Hopedale Blocks occurred between 2578±3 to 2549±3 Ma and is marked by widespread deformation, metamorphism, basic dyke emplacement and mylonitization (locally granulite facies), (Connelly and Ryan, 1992, 1994; Table 2.1). Post-collisional activity in the two blocks was marked by mafic dyke emplacement, including the ca. 2450-2200 Ma Napaktok and Domes dykes in the Saglek Block, and the 2235±2 Ma Kikkertevak dyke swarm in the Hopedale Block (Ermanovics et al, 1989, Ermanovics and Van Kranendonk, 1990; Ryan, 1990b; Cadman *et al.*, 1993; Ryan *et al.*, 1995; Table 2.1). Following basic dyke emplacement in the Saglek Block was the intrusion of ca. 2.1-2.0 Ma fluorite bearing granites (Emslie and Loveridge, 1992). Recently ca. 2135-2045 Ma anorthositic,

granitoid, and basic dyke magmatism has been documented (Ryan *et al.*, 1997, 1998; Hamilton, 1997; Hamilton *et al.*, 1998; Table 2.1).

At ca. 2.0 Ga both blocks of the Nain Province were characterized by extensive Lower Proterozoic supracrustal sequence development. In the northern Saglek Block the Ramah, Mugford, and Snyder Groups were deposited upon the northern Nain Craton (Figure 2.2; Morgan, 1975; Smyth, 1976; Smyth and Knight, 1978; Speer, 1978; Knight and Morgan, 1981; Hamilton, 1994; Wilton *et al.*, 1993, 1994; Wilton, 1994, 1996c; Archibald, 1995; Rogers, 1997). Concurrently, the Moran Lake, Lower Aillik, and Ingrid Groups were deposited upon the Hopedale Block (Smyth *et al.*, 1978; Wardle and Bailey, 1981; Gower *et al.*, 1982; Ryan, 1984; Wardle *et al.*, 1986; Ermanovics, 1993; Wardle and Wilton, 1995; Wilton, 1996b).

2.3.2 Evolution of the Eastern Churchill Province and Torngat Orogen

The evolution of the Eastern Churchill Province and the Torngat Orogen are of fundamental importance in the genesis of the NPS (section 2.3.5), and possibly the genesis of the Voisey's Bay deposit (Emslie *et al.*, 1994; Ryan *et al.*, 1995; Ryan, 1996; Naldrett *et al.*, 1996). Hence, a description of the evolution of this orogenic system is presented.

The Torngat Orogen (TO) represents a complex structural, metamorphic and plutonic domain marking the structural suture between the Archean and Paleoproterozoic rocks of the Nain and Churchill structural provinces (Hoffman, 1988; Figure 2.5). The orogen consists of four domains including the Lac Lomier Complex (LLC), Tasiuyak

Gneiss Complex (TGC), Burwell Domain (BD), and reworked rocks of the Nain Province in the Torngat foreland (Wardle and Wilton, 1995; Van Kranendonk, 1996; and others).

The Lac Lomier Complex consists of an assemblage of Archean granulite facies gneisses similar to the Rae Province with infolded Early Proterozoic shelf and turbiditic supracrustal gneisses of the Lake Harbour Group (Figure 2.5), intruded by deformed orthopyroxene-bearing tonalite and granodiorite plutons likely correlative to those in the TGC (Van Kranendonk and Ermanovics, 1990; Ermanovics and Van Kranendonk, 1990; Van Kranendonk *et al.*, 1992; Wardle and Wilton, 1995; Van Kranendonk, 1996).

The Tasiuyak Gneiss Complex is dominated by the sulphide rich garnet-silimanite-biotite-graphite bearing Tasiuyak Gneiss (TG; Figure 2.5; Wardle, 1983), which extends the length of the Torngat Orogen in Labrador (Wardle and Wilton, 1995). The TG was originally believed to represent continental rise-shelf sediments, which were a continuation of the Lake Harbour Group (Van Kranendonk *et al.*, 1992). Feininger and Ermanovics (1994) have suggested that it represents a flyschoid sequence marking the Nain-Rae boundary; while Nd and trace element work has suggested that the TG has been derived from a Late Archean, or mixed Late Archean-Early Proterozoic unidentified source (Thériault *et al.*, 1994; Thériault and Ermanovics, 1997). From these isotopic results, Thériault *et al.* (1994), Thériault and Ermanovics (1997) and Van Kranendonk and Wardle (1994) have suggested that the TG represents an accretionary prism, possibly formed on both the Rae and Nain cratonic margins. Age dating by Scott and Machado (1994) have shown that ca. 2.0-1.94 Ga detrital zircons exist in the Tasiuyak Gneiss and support the latter interpretations. Intrusive rocks in the TGC consist of linear, strongly

deformed bodies of orthopyroxene-bearing tonalite with ages that range from 1877±1 Ma (Bertrand *et al.*, 1993) to 1839±2 Ma (Scott and Machado, 1994; Table 2.1).

The most northerly expression of the Torngat Orogen is exemplified by the pelitic gneisses, mafic granulite and orthogneiss, orthopyroxene-bearing charnockite, granulite facies diorite, tonalite and granodiorite of the Burwell Domain (BD; Figure 2.5; Wardle and Wilton, 1995). Amphibolite facies plutonic rocks from the BD have yielded ages of 1910-1885 Ma; while younger metatonalitic and granitoid rocks have yielded ages of 1869+3/-2 and 1864±2 Ma, respectively (Scott and Machado, 1995; Table 2.1). The western Nain Province within the Torngat Orogen consists of Archean, migmatitic and granulite facies orthogneiss, similar to others in the Nain Province, which are deformed by the Komaktorvik shear zone and infolded with the Early Proterozoic or Archean, Hutton anorthosite body (Van Kranendonk *et al.*, 1992; Wardle and Wilton, 1995).

The tectonic evolution of the Torngat Orogen (TO) occurred over approximately 100 million years, and in approximately five stages. The earliest stages of the TO occurred at ca. 1880-1840 Ma, marked by the emplacement of calc-alkaline enderbite-charnockite plutonic bodies into the TGC and LLC, likely representing arc-magmatism in the early stages of the orogen (Bertrand *et al.*, 1993; Scott and Machado, 1994; Table 2.1). The determination of subduction polarity in this arc has been somewhat problematic due to the complex geological history of this area and has been variably suggested to have been westward (Bertrand *et al.*, 1993), or possibly westward and eastward (Van Kranendonk and Wardle, 1994); and recently it has been proposed to have been predominantly eastward (Ryan *et al.*, 1995; Ellis *et al.*, 1997).

The initial arc-magmatic stages of the TO were followed by widespread crustal thickening and nappe tectonism between ca. 1860-1853 Ma (Bertrand *et al.*, 1993; Table 2.1). Related to this crustal thickening was the widespread development of an east-verging foreland fold and thrust belt within the Ramah Group and related Nain Province Basement (Calon and Jamison, 1992, 1994; Jamison and Calon, 1995). The latter workers have suggested this stage preceded transpressional tectonism associated with the TO.

Easterly verging foreland fold and thrust tectonism was followed by granulite facies sinistral transpressional tectonism ca. 1845-1820 Ma which involved the development of the Abloviak shear zone (ASZ); the present day suture between the Nain and Churchill cratons (Bertrand *et al.*, 1993;Van Kranendonk and Wardle, 1994, 1997; Van Kranendonk, 1996; Table 2.1). Reworked Nain Province gneisses in the ASZ-foreland zone boundary were then intruded by post-tectonic granitoid stocks at ca. 1806 Ma (Bertrand *et al.*, 1993; Table 2.1); while at ca. 1795-1740 Ma uplift and thrust faulting and the formation of widespread sub-vertical crustal faults marked the latter stages of the Torngat Orogen (Mengel *et al.*, 1991; Bertrand *et al.*, 1993; Table 2.1).

2.3.3 Magmatic Evolution and Genesis of the Nain Plutonic Suite

The Nain Plutonic Suite (Ryan, 1990a) is spatially, and possibly genetically, associated with many of the Ni-Cu sulphide occurrences in north-central Labrador, and NPS genesis is likely to have been important in the genesis of some of the sulphide occurrences in north-central Labrador (Ryan *et al.*, 1995; Naldrett *et al.*, 1996a; Lightfoot, 1998). The NPS is a composite suite of anorthosite (*sensu lato*), granitoid,

ferrodiorite and troctolite plutons, emplaced between ca. 1350-1290 Ma (Ryan and Emslie, 1994; Emslie *et al.*, 1994; Hamilton *et al.*, 1994; Ryan *et al.*, 1995; Hamilton, 1997; Figure 2.6; Table 2.2). Unlike the prior sections of this chapter, this section is subdivided into a number of portions to describe the different lithologic elements, chemical and isotopic characteristics, and genesis of the Nain Plutonic Suite. This is done primarily because: 1) the OKG prospect may contain rocks of this suite (e.g. pyroxenites); and 2) if the OKG prospect is not part of this suite (e.g. Ryan *et al.*, 1998) it may have similar geological and geochemical attributes, and may have formed by similar mechanisms.

2.3.3.1 Descriptive Aspects of the Nain Plutonic Suite

The Nain Plutonic Suite provides one of the best exposed anorogenic AMCG terrains in the world, and much of our present understanding relies on the early descriptive geological work carried out by a number of authors. Early research on the suite was carried out in the landmark work of E.P. Wheeler II (Wheeler, 1942, 1960) which subdivided the many phases of the NPS and provided an excellent groundwork of descriptive geology and observation. The work of Wheeler was added upon to by that of S.A. Morse (e.g. Morse, 1969) and the Nain Anorthosite Project associated with the University of Massachusetts, as well as contributions from J.Berg., R.A. Wiebe, R.F. Emslie, and more recently B. Ryan, and M.A. Hamilton (cf. Emslie *et al.*, 1994). All of this descriptive work over the decades has provided general descriptive subdivisions of the rock types associated with the NPS, in particular, those of Emslie *et al.* (1994), Ryan *et al.* (1995), and Ryan (1995). In terms of descriptive units, the work of Ryan *et al.*

(1995) and Ryan (1995) is most applicable and they have divided the NPS into: 1) anorthositic rocks (*sensu lato*); 2) granitoid rocks; 3) ferrodioritic rocks; and 4) troctolitic rocks (Figure 2.6). The classification of Emslie *et al.* (1994) includes: 1) mafic and anorthositic rocks; 2) granitoid rocks; and 3) ferrodioritic rocks (Figure 2.6). The Emslie *et al.* (1994) subdivisions are better for discussing the geochemical and isotopic attributes of the Nain Plutonic Suite; however, for descriptive purposes the subdivisions of Ryan *et al.* (1995) and Ryan (1995) are used below.

The anorthositic rocks comprise a significant volume of the magmatic rocks associated with the NPS and have a variety of emplacement styles ranging from solid state diapirs with foliated margins, to in-situ bodies with well preserved sub-ophitic textures (Ryan *et al.*, 1995; Ryan, 1995). The rocks of this group are generally plagioclase rich, medium to coarse grained, and consist predominantly of anorthosite (*sensu stricto*), leuconorite and norite, with subordinate gabbro, troctolite and their leucocratic variants (Emslie, 1978, 1980; Ryan *et al.*, 1995; Ryan, 1990a, 1991a,b, 1993, 1995; and others; Figure 2.6). This suite is further subdivided into anorthosite-leuconorite-norite types, and troctolitic members (see difference in these versus troctolitic plutons below); examples from the first category include the Bird Lake massif (Morse, 1983), Mount Lister intrusion (Ryan, 1993), Pearly Gates intrusion (Ryan, 1993), while those of the troctolite subgroup include the Port Manvers Run and Kikkertevak intrusions (Xue and Morse, 1993; Figure 2.6).

The granitoid rocks of the NPS have volumetrically similar abundance to the anorthositic rocks and likely form a cap on the anorthositic rocks (Ryan, 1991a,b, 1993,

1995; Emslie *et al.*, 1994; Ryan *et al.*, 1995). The granitoids are largely medium to coarse grained, compositionally range from early fayalite and hornblende bearing monzonites and quartz monzonites (or mangerites), to later stage hornblende-biotite bearing granitic rocks (or charnockites), and are believed to have formed from high temperature, water poor magmas (Ryan, 1991b, 1993, 1995; Emslie and Loveridge, 1992; Emslie and Stirling, 1993; Emslie *et al.*, 1994; Ryan *et al.*, 1995). Examples of this group include the Makhavinekh Lake pluton (Ryan, 1991b), the Umiakovik Batholith (Emslie and Russell, 1988; Emslie and Loveridge, 1992; Emslie and Stirling, 1993), and the Voisey's Bay-Notakwanon granite (Emslie and Stirling, 1993; Figure 2.6).

The ferrodiorite and troctolite plutons of the NPS are volumetrically small, yet significant, when compared to the anorthositic and granitoid rocks of the NPS. Ferrodioritic rocks are generally found in small plutons or as small medium to fine grained dykes, and are believed to be the residual liquids from anorthosite crystallization (Wiebe, 1990; Emslie *et al.*, 1994; Hamilton, 1997). Some ferrodiorites are characterized by cumulate textures, while others are fine grained, approaching liquid compositions (Wiebe, 1990; Emslie *et al.*, 1994). Well documented ferrodioritic occurrences in the NPS include the Tigalak intrusion (Wiebe, 1980; Ryan *et al.*, 1995), the Cabot Lake Sheet, and the Ukpaume (Akpaume) intrusion (Emslie *et al.*, 1994; Ryan *et al.*, 1995; Ryan, 1995; Figure 2.6).

The troctolitic plutons of the NPS are also volumetrically small, and may be considered part of a continuum with the anorthositic grouping; however, they are marked by olivine as a significant cumulus phase, in contrast to the anorthositic group (Ryan *et*

al., 1995; Ryan, 1995). Most of the troctolitic intrusions of the NPS are characterized by well developed layering and indications of both cumulus crystallization and chilled crystallization (Ryan *et al.*, 1995; Ryan, 1995). The classic NPS troctolite intrusion is the Kiglapait intrusion (Morse, 1969) which consists of a basinal shaped intrusion with olivine tholeiite parentage, that has largely undergone closed system fractional crystallization (Morse, 1969; DePaolo, 1985; Ryan *et al.*, 1995; Ryan, 1995; Figure 2.6). Other examples of troctolite intrusions include the Hettasch intrusion, Newark Island layered intrusion (Wiebe, 1988), Barth Island intrusion, Jonathan Island intrusion, and the host of the Voisey's Bay deposit, the Reid Brook intrusion (Wiebe, 1988; Ryan and Lee, 1989; Ryan *et al.*, 1995; Ryan, 1995; Lightfoot, 1998; Figure 2.6).

2.3.3.2 The Timing and Emplacement of the Nain Plutonic Suite

The NPS provides a testament to the premise that AMCG suites are a function of multiple pulses of magma, which have been emplaced over discrete time intervals (Ryan *et al.*, 1991; Emslie and Loveridge, 1992; Connelly and Ryan, 1994; Ryan and Emslie, 1994; Hamilton *et al.*, 1994, 1998; Hamilton, 1997; and others). Early work by Wheeler (1960) showed that the granitoid rocks often intruded the anorthositic rocks of the suites; while Emslie *et al.* (1994) stated that the mafic rocks intrude the anorthositic rocks, ferrodiorites and granitoids intrude the anorthositic and mafic groups; while rarely do the ferrodiorites intrude the granitoids. Bearing this in mind, it has been shown by detailed geochronology (predominantly U-Pb) that much of the older rocks of the NPS are actually the granitoids (Ryan *et al.*, 1991; Emslie and Loveridge, 1992; Connelly and Ryan, 1994; Hamilton et al., 1994; Table 2.2); and that magmatism in the NPS likely

began (and ceased?) in the western part of the suite, prior to commencement in the eastern part of the suite (Emslie *et al.*, 1994; Hamilton in Berg *et al.*, 1994). Furthermore, the entire NPS has been emplaced roughly between 1350-1290 Ma (Ryan and Emslie, 1994; Emslie *et al.*, 1994; Hamilton *et al.*, 1994, 1998; Hamilton, 1997; Table 2.2).

In contrast to the idea that magmatism began and ceased in the west is the presence of foliated monzonite, marginal to the Mount Lister anorthosite, near Webb Bay (Figure 2.6). At this location Connelly and Ryan (1994) obtained a U-Pb zircon age of 1343 ± 3 Ma and stated that it probably represents the earliest crystallization of NPS rocks; providing a possible upper limit on magmatism (Figure 2.6; Table 2.2). The Makhavinekh pluton (Ryan, 1991b) in the western part of the NPS has yielded U-Pb ages of 1322±1 Ma (Ryan *et al.*, 1991) representing one of the earliest NPS granitoid batholiths (Figure 2.6; Table 2.2). Other dated intrusions include the Umiakovik batholith (Emslie and Russell, 1988) with ages of 1319±2 and 1316±3 Ma (Emslie and Loveridge, 1992), the Dog Island intrusion (ca. 1295 Ma; Krogh and Davis, 1973), the northern margin of the Voisey's Bay-Notakwanon batholith (1292±4 Ma; Ryan *et al.*, 1991), while some peralkaline plutons are as young as ca. 1287 Ma (Emslie and Hamilton *in* Hamilton, 1997; Figure 2.6; Table 2.2). This range of dates puts a minimum of 50-55 Ma of granitoid magmatism associated with the NPS (Ryan and Connelly, 1994; Hamilton, 1997).

The anorthositic and mafic plutons of the NPS are much harder to date because they do not have the correct mineralogy for U-Pb geochronology (e.g. Ryan *et al.*, 1995;

Hamilton, 1997; and others). Detailed work by many workers, however, has shown that some zircons and baddelleyite are present in the anorthositic rocks; while in other cases ^{40}Ar-^{39}Ar systematics have been employed (Yu and Morse, 1993; Connelly and Ryan, 1994; Hamilton *et al.*, 1994; Hamilton, 1997; Amelin *et al.*, 1997; and others). Numerous results have been published from these studies for both the anorthositic and mafic members of the NPS; all quoted ages in the following paragraphs are from U-Pb geochronology unless otherwise stated (Table 2.2).

The Mount Lister intrusion produced the earliest date for the anorthositic rocks of the NPS with an age of ca. 1331 Ma (Hamilton *in* Berg *et al.*, 1994); however, Ryan *et al.* (1995) suggested that this age may actually be in excess of 1340 Ma, and Ryan (1997) suggests it may be nearly 1350 Ma based on the age of ca 1343 Ma foliated mozonite that cuts the Mount Lister intrusion (Connelly and Ryan, 1994; Figure 2.6; Table 2.2). Other older plutons of the NPS include rocks from the Eastern Deeps and Reddog bodies of the Reid Brook intrusion (1333.7±1.7 Ma; Amelin *et al.*, 1997); Ukpaume (Akpaume) intrusion leuconorite (1330±2 Ma; Hamilton, 1997); Bird Lake massif (ca. 1328 Ma ^{40}Ar-^{39}Ar; Yu and Morse, 1993); the Paul Island intrusion (1322±1 Ma; Hamilton in Berg *et al.*, 1994; Hamilton, 1997); leuconorite from the Makhavinekh Lake area (1322±1 Ma; Hamilton, 1997); and troctolitic pillows from the Barth Island intrusion (ca. 1320 Ma; Hamilton, 1997; Figure 2.6; Table 2.2). Younger anorthositic members include the Asina intrusion near Voisey's Bay (1317.2±1.4 Ma; Amelin *et al.*, 1997); Kikkertevak and Tabor Island intrusions (ca. 1311 Ma; Hamilton in Berg *et al.*, 1994; Hamilton, 1997); Jonathan Island intrusion (ca. 1312-1311 Ma; Hamilton *et al.*, 1994; Hamilton, 1997);

gabbro pegmatite from the Lower Zone of the Kiglapait intrusion (1307±1 Ma; Hamilton, 1997); Kolikatik Island anorthosite (1305±2 Ma; Hamilton, 1997); Newark Island intrusion (ca. 1305 Ma; Simmons *et al.*, 1986); and leucotroctolites from Sango Bay area (1294±2 Ma; Hamilton, 1997; Figure 2.6; Table 2.2). These dates suggest that anorthositic magmatism in the NPS spanned at least 35 Ma, and is more likely closer to 55 Ma (Hamilton, 1997).

Ferrodioritic rocks of the NPS span a similar time frame to the anorthositic rocks (minimum 34 Ma), consistent with the interpretation that they have formed from residual liquids after anorthosite formation (Emslie *et al.*, 1994; Hamilton, 1997). Dated intrusions include the Ukpaume (Akpaume) intrusion ferrodiorites (1332±3 Ma; Hamilton *et al.*, 1994; Hamilton, 1997); marginal ferrodiorites at Barth Island (1322 Ma; Hamilton, 1997; Satosuakuluk ferrodiorite dyke (1315±2 Ma; Hamilton, 1997); isolated diorites at Jonathan Island (1311 Ma; Hamilton, 1997); Tigalik intrusion (1306±3 Ma; Hamilton *et al.*, 1994; Hamilton, 1997); and the Cabot Lake Sheet (1298±2 Ma; Hamilton *et al.*, 1994; Hamilton, 1997; Figure 2.6; Table 2.2).

2.3.3.3 Geochemical and Isotopic Characteristics of the Nain Plutonic Suite

The anorthositic rocks of the Nain Plutonic Suite, by virtue of their mineralogy, are quite elevated in plagioclase compatible elements, and to a lesser extent the mafic minerals associated with these rocks (e.g. orthopyroxene, clinopyroxene, olivine). The anorthositic rocks are typically elevated in Al_2O_3, to a lesser extent CaO, and to an even lesser extent Na_2O and K_2O (Emslie, 1980; Xue and Morse, 1993; Emslie *et al.*, 1994; and others). Granitoid rocks of the NPS are characterized by elevated K_2O, Rb, and have

high K/Ti and Fe/Fe+Mg ratios, the latter usually greater than 0.4 (Emslie and Stirling, 1993; Emslie *et al.*, 1994); while ferrodioritic rocks are typically elevated in Al_2O_3, CaO, total Fe, Fe / (Fe+Mg) ratios and are notably enriched Ti and P (Emslie *et al.*, 1994).

Multi-element, primitive mantle normalized plots provide an adequate means for illustrating the geochemical characteristics of the different NPS groups (Figure 2.7). On these plots Ba, La, Ce, Sm, and Yb are approximately collinear in all of the groups (Emslie *et al.*, 1994; Figure 2.7). The granitoid rocks are notably depleted in Nb, Sr, P, Eu, and Ti, while Zr and Rb are enriched relative to the other groupings (Emslie and Stirling, 1993; Emslie *et al.*, 1994; Figure 2.7). The ferrodiorites have depletions in Rb, K, Nb, Sr, and Zr and have no marked enrichments; while the anorthositic rocks are depleted in Rb and Nb, and strongly enriched in Sr and Eu (Emslie *et al.*, 1994; Figure 2.7). Those elements enriched in the anorthosites, notably Sr and Eu, are variably depleted in the granitoids, suggesting a possible genetic link with the anorthosites (Emslie and Stirling, 1993; Emslie *et al.*, 1994). Furthermore, the geochemistry of the anorthositic rocks are similar to xenolithic lower crustal feldspathic granulites; this combined with the chemical attributes of the granitoids relative to the anorthosites has important implications when discussing genetic models for AMCG genesis (see section 2.3.3.4; Emslie *et al.*, 1994).

Although the major and trace element geochemical data provide some inferences about the petrological characteristics of AMCG suites, the cumulate mineralogy of the AMCG rocks are far removed from liquid compositions and the elemental geochemistry is strongly controlled by the cumulus mineralogy. To combat such problems, workers in

the NPS (and elsewhere) have used isotope geochemistry to further assess petrological aspects and petrogenesis of NPS rocks (e.g. Emslie and Loveridge, 1992; Emslie and Thériault, 1991; Hamilton and Shirey, 1992; Hamilton *et al.*, 1994; Emslie *et al.*, 1994; Hamilton, 1997).

Using primarily Nd and Sr isotope geochemistry Emslie *et al.* (1994) and Hamilton (*in* Berg *et al.*, 1994) noticed that certain isotopic characteristics are found throughout the NPS. From their work, in tandem with Emslie and Thériault (1991), Emslie and Loveridge (1992), Hamilton and Shirey (1992), Emslie *et al.* (1994) and Hamilton (1997) it was noticed there was a strong geographic influence on the isotope geochemistry of the NPS, particularly Nd, and it was controlled by the postulated Nain-Churchill suture (Figure 2.8). With the discovery of Paleoproterozoic anorthositic suites, this may not be as strong an argument as it was at the time of writing, as some of these rocks may in fact be older with abnormally high values.

Other isotopic conclusions of Emslie *et al.* (1994) include: 1) the Nd isotope geochemistry of the NPS is controlled by geographic position relative to the Nain-Churchill boundary, regardless of rock type, with εNd (@1300 Ma) < -10 in rocks east of the boundary, that intrude Nain Province crust, and those west of the boundary that intrude Churchill Province crust have εNd (@1300 Ma) > -10; 2) Sr isotopes (ISr @ 1300 Ma), are largely controlled by compositional group, with the highest values in the granitoid rocks (0.7047-0.7124), intermediate values in the anorthositic and mafic rocks (0.7034-0.7718), and the ferrodiorites near the most contaminated anorthositic and mafic

rocks (0.7054-0.7090); and 3) the basement was a major contributor to the source materials for granites and to a lesser extent the anorthositic and ferrodioritic rocks.

Using Nd isotope data, Emslie *et al.* (1994) showed that the anorthositic and mafic rocks have the lowest Nd crustal input, but are still strongly influenced with up to 65% basement input; while the ferrodiorites have slightly higher crustal influence than the anorthositic and mafic rocks and have slightly lesser crustal input than the granitoids. The variable signatures in the anorthositic and mafic rocks likely represent variable, yet progressive contamination during assimilation of crustal material and generation of plagioclase cumulates (Emslie *et al.*, 1994). The isotopic similarities between the ferrodioritic and most-contaminated anorthositic rocks suggest that the ferrodiorites form from the residual liquids following plagioclase flotation and anorthosite massif genesis (Emslie *et al.*, 1994). As expected, Emslie *et al.*'s (1994) Nd data show that the granitoids have the highest crustal input; however, some of the granitoids have up to 50% mantle Nd, suggesting a significant mantle component in their genesis (Emslie *et al.*, 1994). The mantle influence in the granitoids can be explained if the granitoids were formed by the combination of highly fractionated basalt from basaltic underplating, and melted crustal material resulting from the underplating event (Emslie *et al.*, 1994).

2.3.3.4 A Genetic Model for the Nain Plutonic Suite

Genetic models for AMCG complexes like the NPS and others (e.g. Laramie Complex, Wyoming; Scoates and Frost, 1996 and others), must answer a number of questions including: 1) the observed voluminous essentially bimodal suite of granitoids and anorthositic-mafic bodies; 2) the relatively minor volume of ferrodioritic rocks; 3)

the observed chemical and isotopic signatures associated with these units; and 4) their largely anorogenic characteristics. This discussion will emphasize the Nain Plutonic Suite, however, it will document past and present models for anorthositic rocks elsewhere in Labrador as well (e.g. Emslie, 1978, 1980).

Early models for the genesis of anorthositic rocks in Labrador proposed by Emslie (1978) suggested that the "Elsonian" anorthosite massifs were generated by the fractionation of plagioclase-rich materials from multiple intrusions of high-Al gabbroic material in an anorogenic setting. Granitoids related to the anorthositic rocks were likely later stage magmas resulting from partial fusion of deep crustal granulites by the parental basic magmas of the anorthositic rocks (Emslie, 1978). Modifications by Emslie (1980), for the Harp Lake Complex rocks, suggested that anorthositic rocks were generated by underplating of the crust by olivine tholeiitic magmas which fractionated orthopyroxene and minor olivine resulting in residual magmas of high-Al gabbroic composition (Figure 2.9). Subsequently, these upwelling high-Al magmas crystallized plagioclase that accumulated in intracrustal chambers while the low-Al magmas extruded as fissure-fed flows at the surface (Emslie, 1980; Figure 2.9). With continued underplating and multiple injections of high-Al gabbro, the large scale anorthosite massif formed like that observed at Harp Lake; while penecontemporaneous partial fusion of the lower crust resulted in the genesis of magmas and subsequent adamellite plutons (Figure 2.9). As the supply of olivine tholeiite magma wanes, late stage crystallization of residual ferrodioritic liquids rise upward into the complex (Emslie, 1980; Figure 2.9).

This model, though attractive, did not consider the relative densities of magmas (e.g. ferrodioritic liquids); furthermore, the absence of detailed chemistry on the complex did not allow for the formulation of a well constrained petrologic model for the AMCG suite. From a general perspective Taylor *et al.* (1984) suggested that the lower crust was the probable area of origin for massif anorthosites, suggesting that the Eu- and Al-rich crust (after extraction of granitoid magmas for the upper crust) when partially melted could give rise to massif type anorthositic magmas. Although quite simplistic it helped formulate the ideas for the new breed of model for the AMCG suite.

Ashwal (1993) suggested that a mafic magma of unspecified composition forms from partial melting of the depleted upper mantle ascending and ponding at the crust-mantle interface (MOHO) forming a large pancake structure. In this model early crystallization of olivine and perhaps high-Al pyroxene lead to the formation of mafic silicates which sink forming ultramafic cumulates in the lower part of the basaltic magma chamber (Ashwal, 1993). Following this a residual high-Al (17-18wt% Al_2O_3) tholeiitic magma that would have plagioclase as the primary liquidus phase, and will slowly crystallize plagioclase in large homogenous crystals at elevated pressures followed by subsequent flotation of plagioclase (Ashwal, 1993).

Pressure contrasts between the ultramafic cumulates and the plagioclase result in gravitational instability leading to a diapiric rise of a plagioclase-liquid mush (±pyroxene megacrysts) that rise and are emplaced forming the plagioclase-rich massifs (Ashwal, 1993). The latent heat of crystallization of these massifs produces enough heat to

produce crustal anatexis and the generation of silicic magmas parental to the granitoids (Ashwal, *op cit*).

The relative timing and integration of a full dataset of field, geochemical, and isotopic data led to Emslie *et al.*'s (1994) revised model for the NPS, the model that is the most coherent and most probable for AMCG genesis (Figure 2.10). In their model they suggest that the genesis of AMCG suites occurs in an anorgenic setting in an upper mantle-lower crustal region associated with basaltic mantle plumes or "hot spots". (Figure 2.10). They suggest that the earliest members of the suite are the granitoids based on the fact that many of the oldest rocks of the NPS are granitoids (Ryan *et al.*, 1991; Emslie and Loveridge, 1992; Connelly and Ryan, 1994; Hamilton *et al.*, 1994; Hamilton, 1997). Basaltic underplating of a fairly undepleted lower crustal material would result in the genesis of granitoids that would be enriched in SiO_2, K, Rb, Ba, Zr, Pb, U and REE; and leave a lower crustal residue depleted in these elements and enriched in Ca, Al, Mg, Sr, Eu, and Ti (Emslie and Hegner, 1993; Emslie and Stirling, 1993; Emslie *et al.*, 1994; Figure 2.10). Furthermore, granitoid extraction would leave a hot, pyroxene-plagioclase rich crustal residue that is close to the plagioclase liquidus, which would have prime potential for contaminating basaltic magmas (*op cit*; Figure 2.10). Assimilation of this residue by basaltic magma would be very efficient, since the residue is probably at temperatures in excess of $900^{o}C$, and would be readily assimilated by the basaltic magma (Emslie *et al.*, 1994; Figure 2.10).

Assimilation of this residue would place plagioclase on the liquidus for extended periods of time and would allow for the genesis of plagioclase-rich crystal mushes

(anorthositic magmas) which most likely would float upwards due to gravitational instability (Emslie *et al.*, 1994; Figure 2.10). Furthermore, fractionation of the anorthositic magmas would result in the formation of Fe-enriched residual liquids, which would have a greater density than the surrounding anorthositic magma (Emslie *et al.*, 1994; Figure 2.10). This residual ferrodioritic liquid would sink below the anorthositic material forming the ferrodioritic rocks associated with AMCG suites (Emslie *et al.*, 1994; Figure 2.10).

Although the anorthositic-granitoid rocks of the OKG prospect may not be members of the NPS (cf. Ryan *et al.*, 1998), their genesis may be similar and the model of the NPS may provide a gauge from which the OKG anorthosite-granitoid can be compared.

2.3.4 Paleoproterozoic AMCG Suites and their Importance

Recent field and geochronological work in the northern Nain Plutonic Suite and surrounding cover rocks have shown that many anorthositic and granitoid rocks of this area, classically grouped with the NPS, may in fact be much older with Paleoproterozoic ages (cf. Connelly and Ryan, 1994; Ryan and Connelly, 1996; Emslie *et al.*, 1997; Hamilton, 1997; Hamilton *et al.*, 1998; Ryan *et al.*, 1997, 1998). The presence of widespread magmatism of this age has not yet been widely proven (cf. Ryan *et al.*, 1998); however, there is significant evidence to suggest that anorthositic magmatism did occur at this time, thus there may have been a similar NPS-like event nearly 800 million years earlier (Ryan and Connelly, 1996; Hamilton, 1997; Hamilton *et al.*, 1998). This is quite

important when considering petrogenetic models, conventional ideas on the genesis of AMCG complexes, and the genesis of magmatic Ni-Cu-Co mineralization in Labrador.

The presence of variably foliated anorthositic (*s.l.*)-granitoid rocks in the Nain region and farther north near Umiakoviarusek Lake and Okak Bay led Ryan (1993) to surmise that some of the rocks traditionally assigned to the NPS may in fact be older in age, and their observed fabrics may be a function of deformation during the ca. 1.8 Ga Torngat Orogen (cf. Bertrand *et al.*, 1993; Van Kranendonk, 1996; and others). Most of the early geochronological work concentrated on the granitoid rocks in the region from Nain to Okak Bay, and yielded some very interesting results. Emslie and Loveridge (1992) dated a granitoid pluton in the region of Okak Bay, the Wheeler Mountain granite, and obtained an age of ca. 2135 Ma (2134 +3/-1 and 2137 ± 2 Ma). At the point of writing, this was the first evidence of plutonism in this region of Paleoproterozoic age, and Emslie and Loveridge (1992) were not really sure of its significance.

With the acquisition of more data, coupled with regional mapping it was noticed that there was a swath of Paleoproterozoic intrusions. Connelly and Ryan (1994) and Ryan and Connelly (1996) found that there were a number of granitoids in the region around Nain and Webb Bay of Paleoproterozoic age including: 1) the Sheet Hill granite (2110 +5/-1 Ma), 2) Loon Island potassic granite (2047 +14/-11 Ma), and 3) the Satok Island monzonite (2032 +17/-12 Ma). Further regional mapping, in the Alliger Lake area, and the Illuiluk Ridge-Umiakoviarusek Lake region, led Ryan *et al.* (1997, 1998) to suggest that there is considerable field evidence for Paleoproterozoic anorthositic-granitoid magmatism, and that these rocks show metamorphic and deformation features

consistent with influence from the Torngat Orogen. Ryan *et al.*'s field subdivision of Paleoproterozoic from Mesoproterozoic rocks includes: 1) Paleoproterozoic rocks are intruded by melanocratic-granular "granulite" dykes; 2) they are intruded by altered and deformed mafic dykes with predominant 140° trends; 3) they are intruded by foliated pink aplite dykes that have a similar trend to the diabase dykes; 4) they show evidence of high temperature subsolidus hydration; 5) they exhibit regional, though not evenly, alteration (greenschist facies) similar to the diabase dykes; and 6) they are regionally, yet heterogeneously, foliated.

Geochronological studies by Hamilton (1997) and Hamilton *et al.* (1998) have provided U-Pb data to augment these field-based hypotheses, and suggest that magmatism ranges from ca. 2135-2045 Ma. Specific dated intrusions include anorthositic rocks from the Aupalukitak Mountain (2112 +5/-4 Ma), variable foliated granitic-monzonitic-dioritic rocks (Halbach, 2128 Ma; Illulik, 2124 Ma; Alliger Lake, 2109 Ma), and metamorphosed basic dykes with ages of 2121±1.5 Ma and ca. 2045 Ma (Hamilton, 1997; Hamilton *et al.*, 1998). The latter ages for anorthositic, granitoid and basic dyke rocks of this region illustrate the supposed uniqueness and Mesoproterozoic restriction of the NPS, and other AMCG complexes (cf. Ashwal, 1993), may not be so and that similar magmatism occurred at an earlier time in the Nain-Okak region (e.g. Paleoproterozoic).

The recognition of Paleoproterozoic AMCG plutonism opens a pandora's box of questions, including: 1) does this magmatism represent a truly anorogenic petro-tectonic setting as the NPS (and other AMCG complexes); and 2) if there is NPS-like magmatism,

is there potential for Reid Brook-like intrusions that may host significant Ni-Cu sulphide mineralization?

To tackle the first question, one must consider the geological history of the Nain Province during the late-Archean and Paleoproterozoic. The earliest preceding tectonic event within the Nain craton prior to the emplacement of these Paleoproterozoic massifs was the collision of the Saglek and Hopedale Blocks at ca. 2.5 Ga (Connelly and Ryan, 1992, 1994), followed by basic dyke emplacement at ca. 2450-2200 Ma (Ermanovics *et al.*, 1989; Ermanovics and Van Kranendonk, 1990; Ryan, 1990b; Ryan *et al.*, 1995). Post-emplacement events would include ca. 2.0 Ga rifting and passive margin sedimentation in the Mugford, Ramah, and Snyder Groups (e.g. Hamilton *in* Wilton (1996c)), followed by the Torngat Orogen at ca. 1.86-1.74 Ga (Bertrand *et al.*, 1993; Van Kranendonk and Wardle, 1994, 1997; Van Kranendonk, 1996; and others). The emplacement of these suites between major orogenic events, accompanied by preceding basic dyke emplacement suggest that the regime of intrusion for these anorthositic-granitoid-basic dyke rocks was that of extension possibly similar to the conditions during NPS formation.

Answering the second question is much more problematic, since to date a second Voisey's Bay has yet to be discovered, and the discussions about Ni-Cu-Co sulphide potential are purely speculative based solely on the possibility that the petro-tectonic setting of the Paleoproterozoic rocks is similar to the NPS. If they do form in similar petro-tectonic settings then it is highly probable that other troctolitic plutons, like the RBI, and mafic-ultramafic rocks may exist in this older suite. If these mafic-ultramafic

rocks could be of sufficient size, have undergone sulphurization or felsification, and be emplaced in favorable traps, then Paleoproterozoic Ni-Cu sulphide mineralization could be just as likely in this older suite (Ryan *et al.*, 1998; Kerr, 1998).

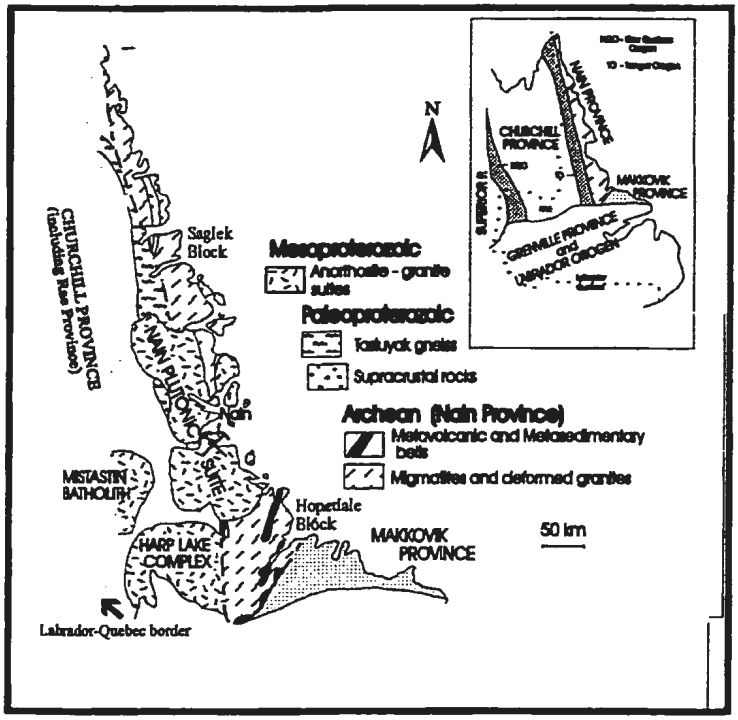

Figure 2.1. Simplified geology of the Nain Province, including the Hopedale and Saglek Blocks, and Nain Plutonic Suite. Modified after Ryan et al. (1995)

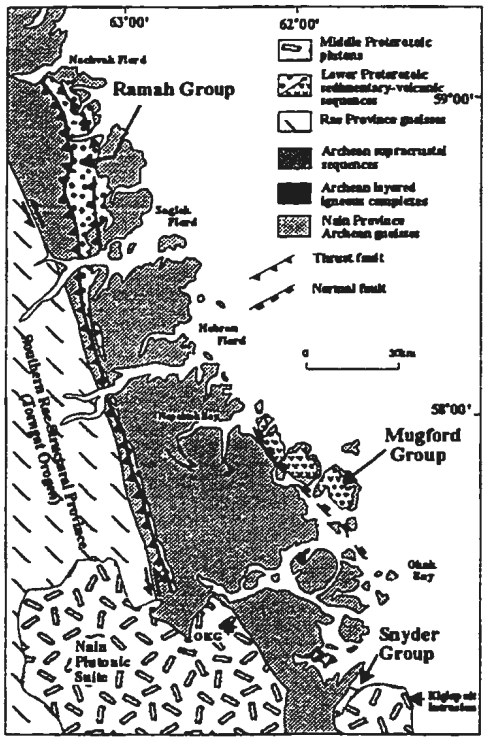

Figure 2.2. Geology of the northern Nain Province and related rocks, including the Ramah, Mugford and Snyder Group supracrustal sequences. Modified after Swinden et al. (1991)

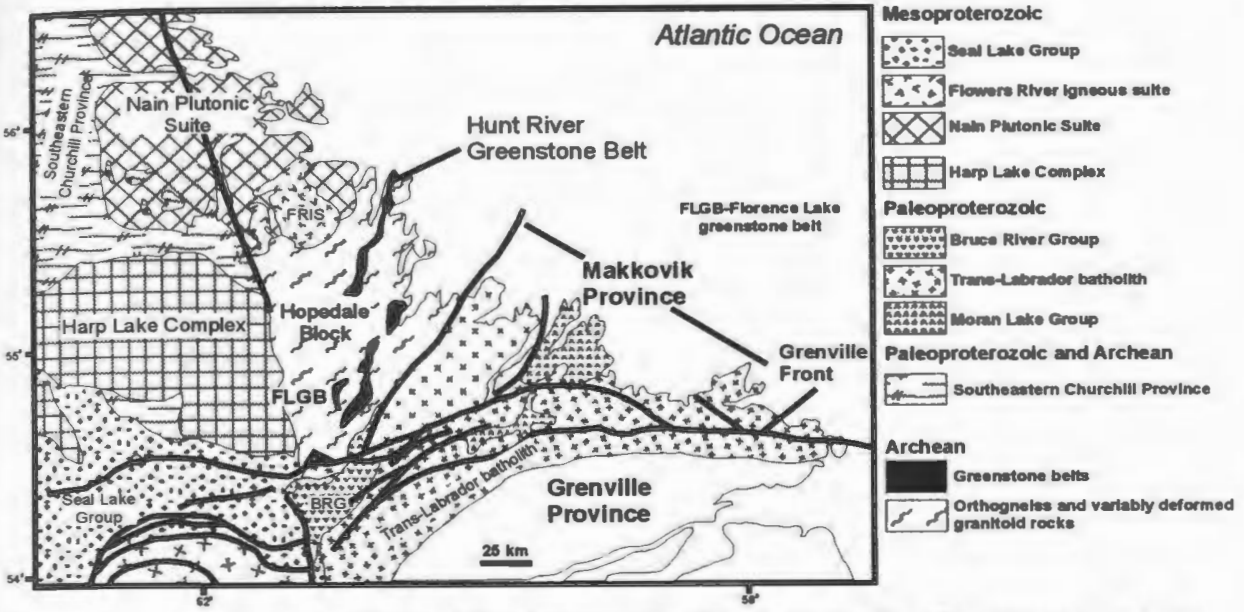

Figure 2.3. Regional setting of the Hopedale Block, including the Florence Lake and Hunt River greenstone belts. Modified after James et al. (1997)

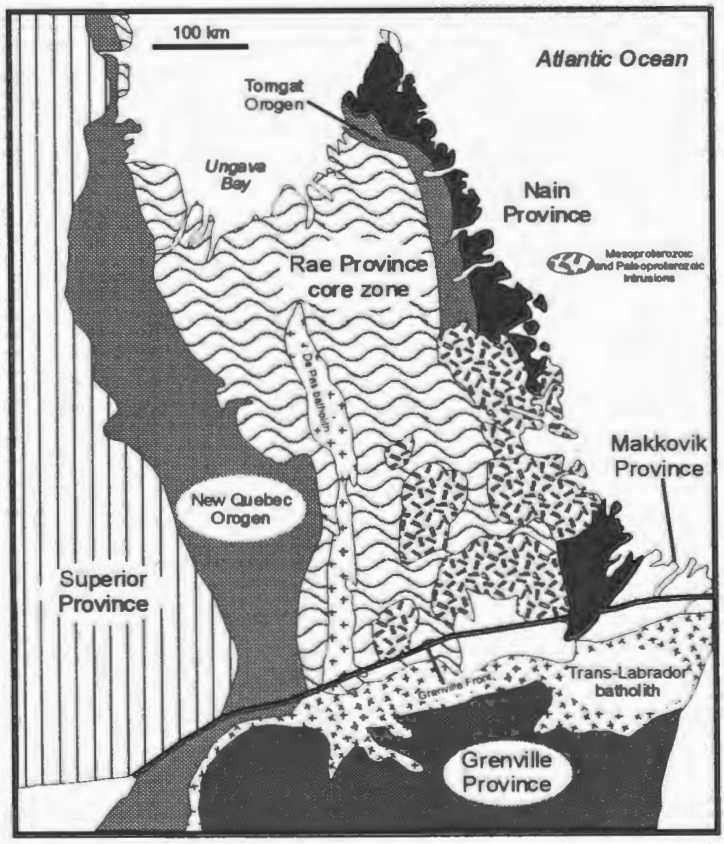

Figure 2.4. Geologic setting of the Southeastern Churchill Province, including the Rae Province, New Quebec and Torngat Orogens. Modified after James et al. (1996a).

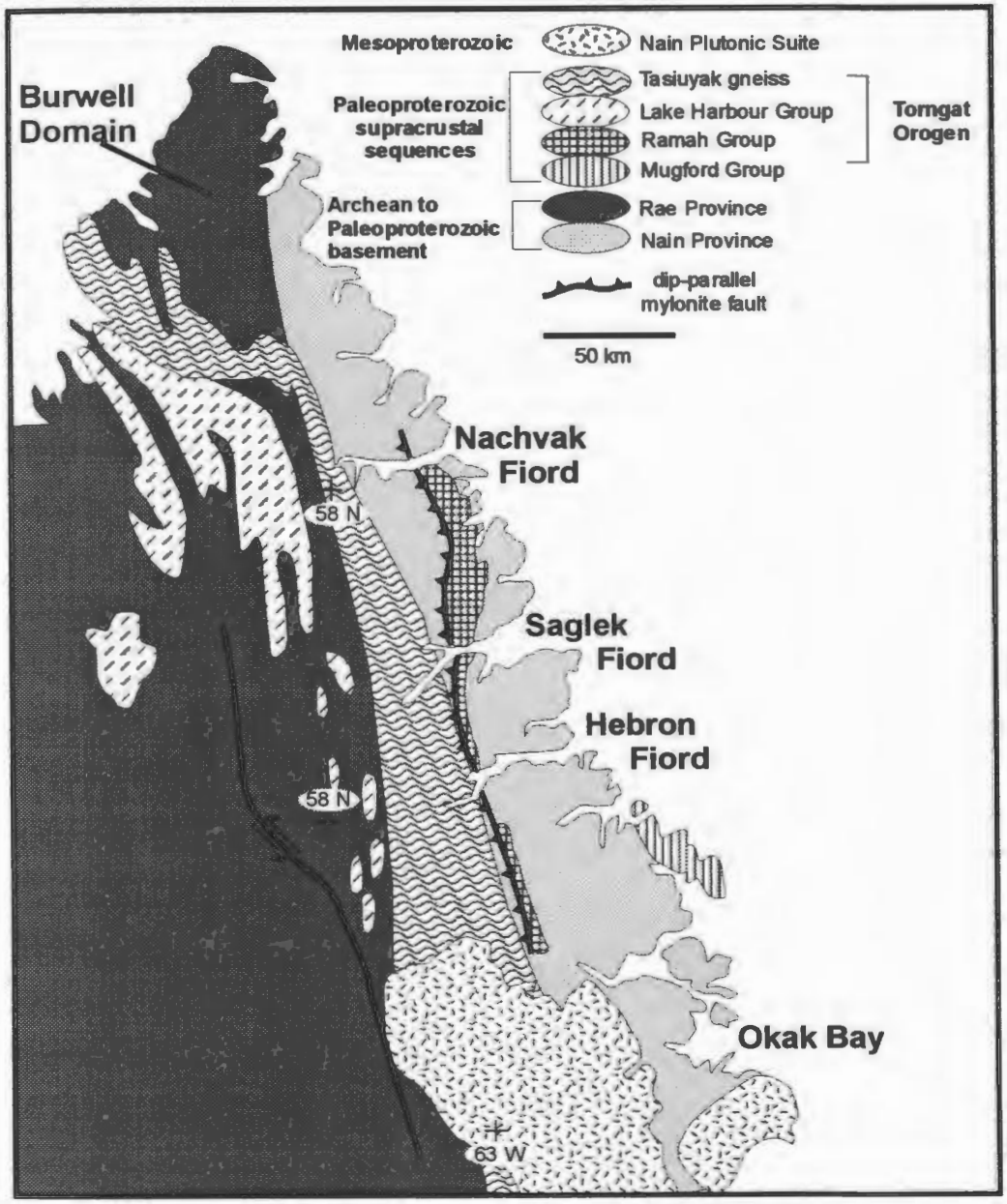

Figure 2.5. Simplified lithotectonic elements of the Torngat Orogen. Modified after Ermanovics and Van Kranendonk (1990) and Theriault and Ermanovics (1997).

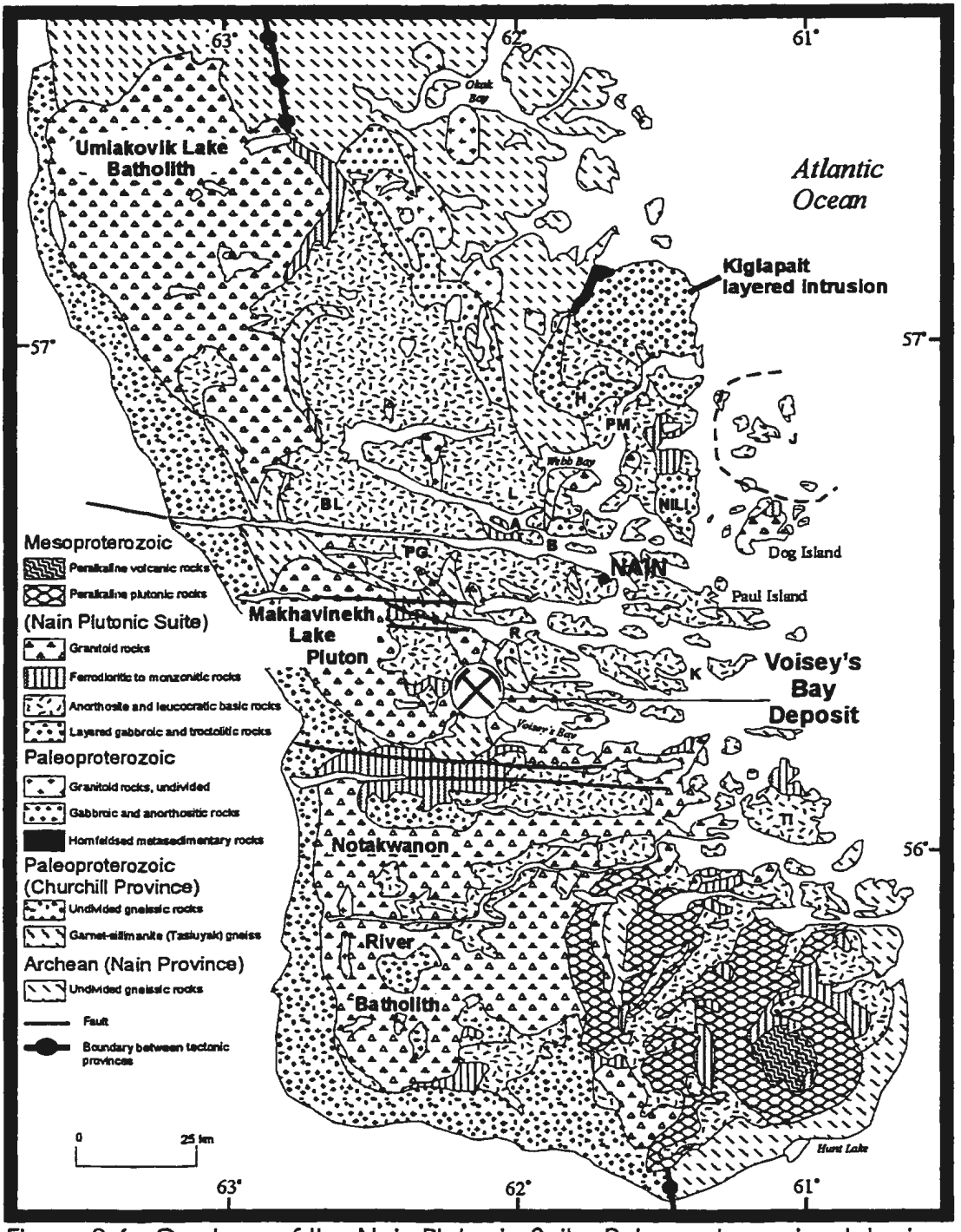

Figure 2.6. Geology of the Nain Plutonic Suite, Paleoproterozoic plutonic rocks and related cover rocks. Intrusions include: H: Hettasch, PM: Port Manvers Run, L: Lister, NILI: Newark Island, J: Jonathan Island, A: Akpaume (Ukpaume), B: Barth Island, BL: Bird Lake, PG: Pearly Gates R: Reid Brook, K: Kikkertevak Island, TI: Tunungayualok Island. Modified after Ryan (1997).

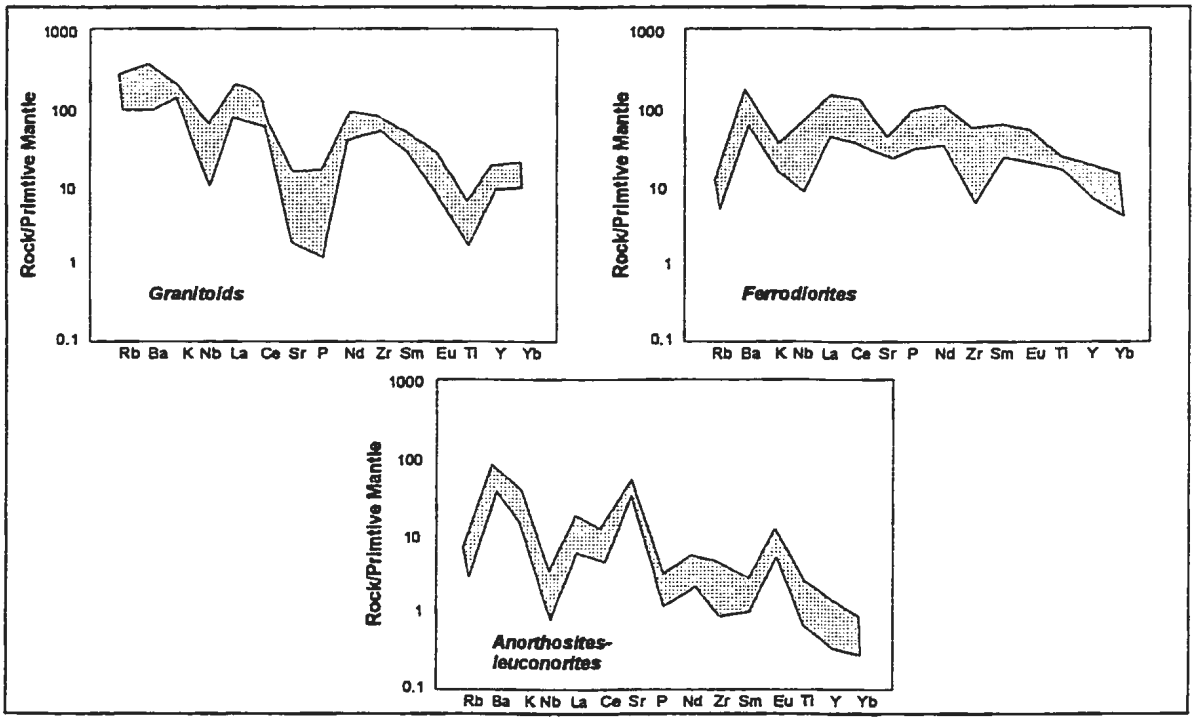

Figure 2.7. Primitive mantle normalized multi-element plots for representative rocks of the Nain Plutonic Suite. Data from Emslie et al. (1994).

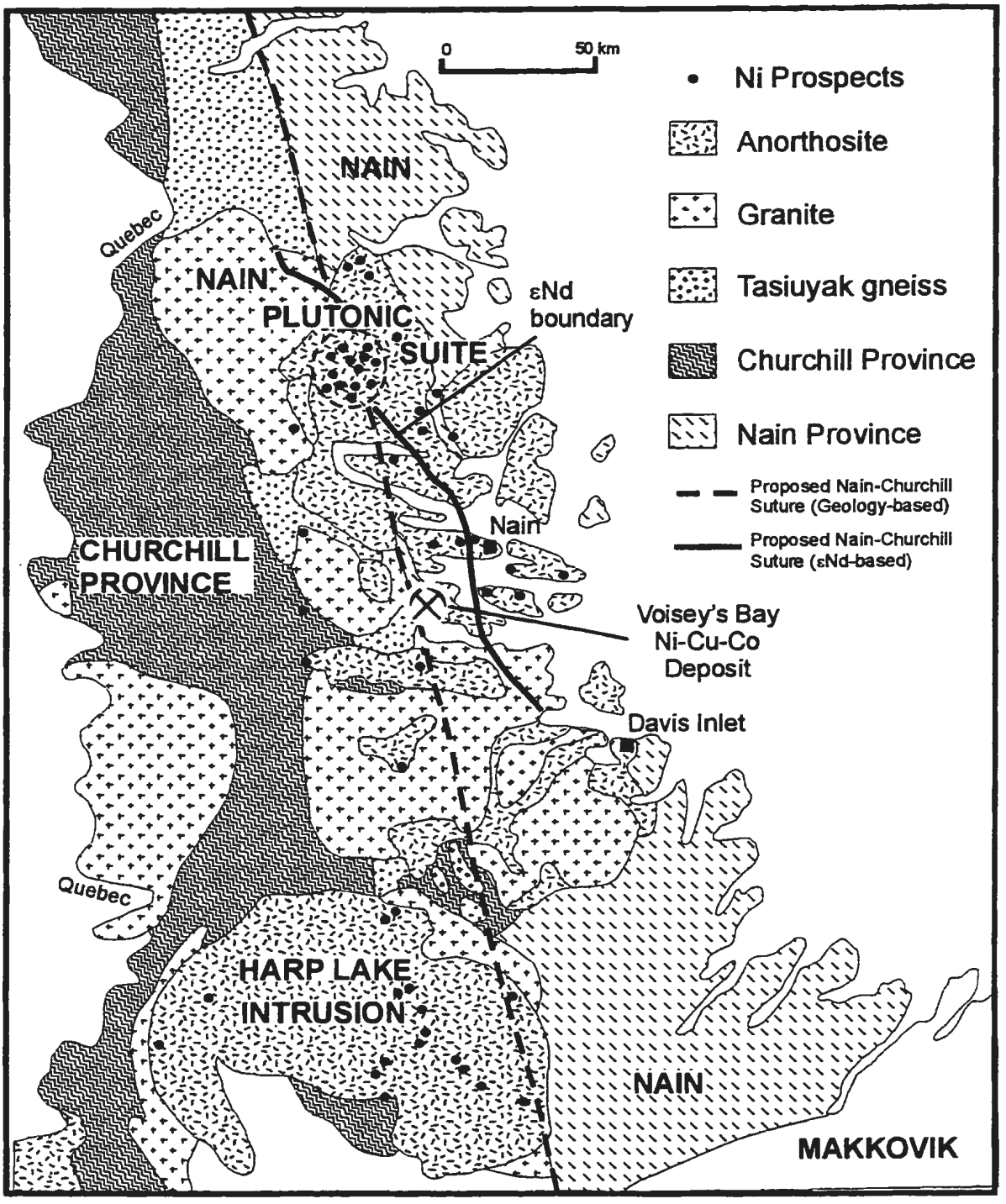

Figure 2.8. Schematic illustrating the proposed εNd boundary for the Nain-Churchill suture underlying the Nain Plutonic Suite. Modified after Emslie et al. (1994) and Ryan (1996a).

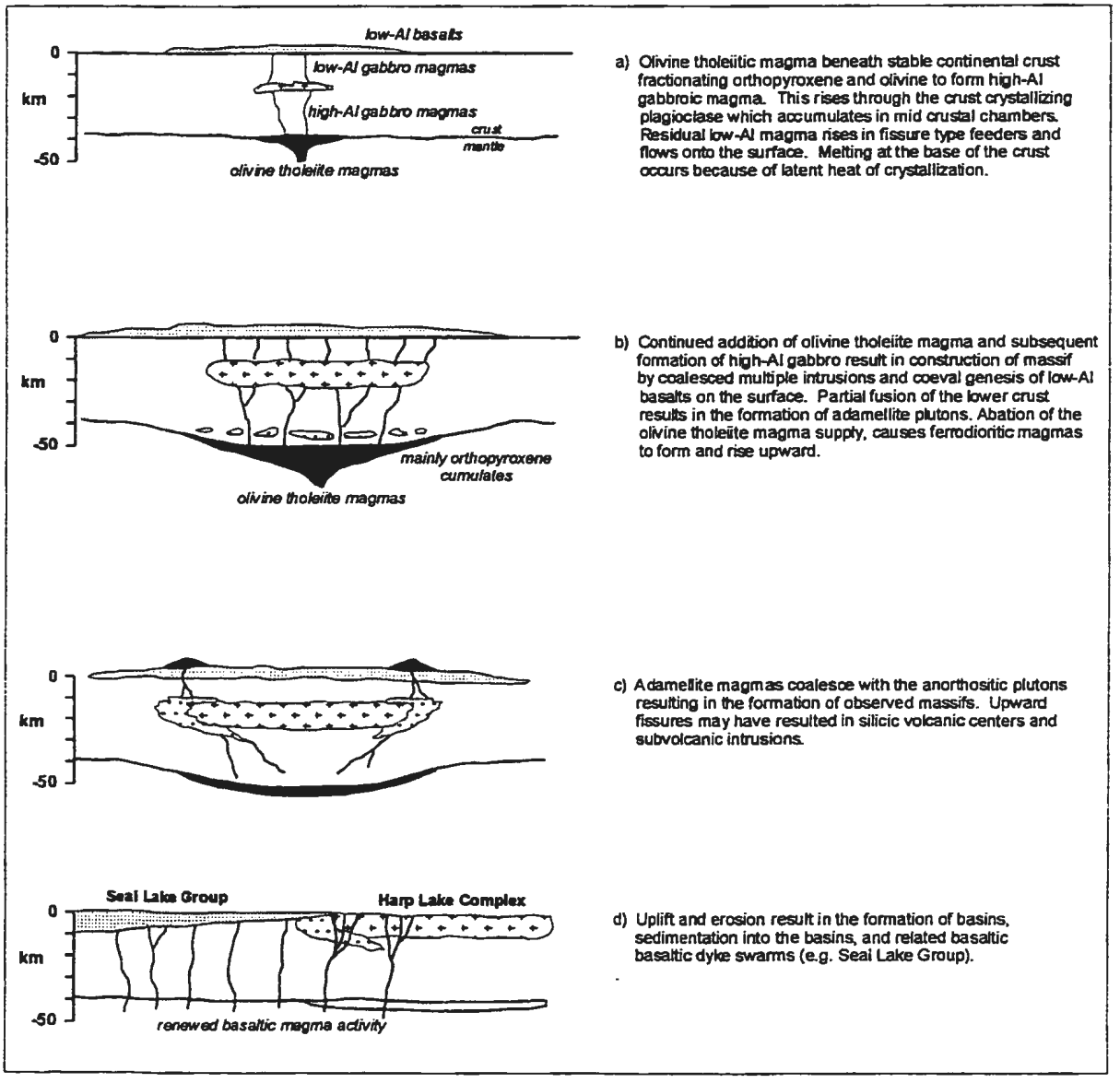

Figure 2.9. Schematic model for the genesis of the Harp Lake Intrusion anorthositic and related rocks in the region. Modified after Emslie (1980).

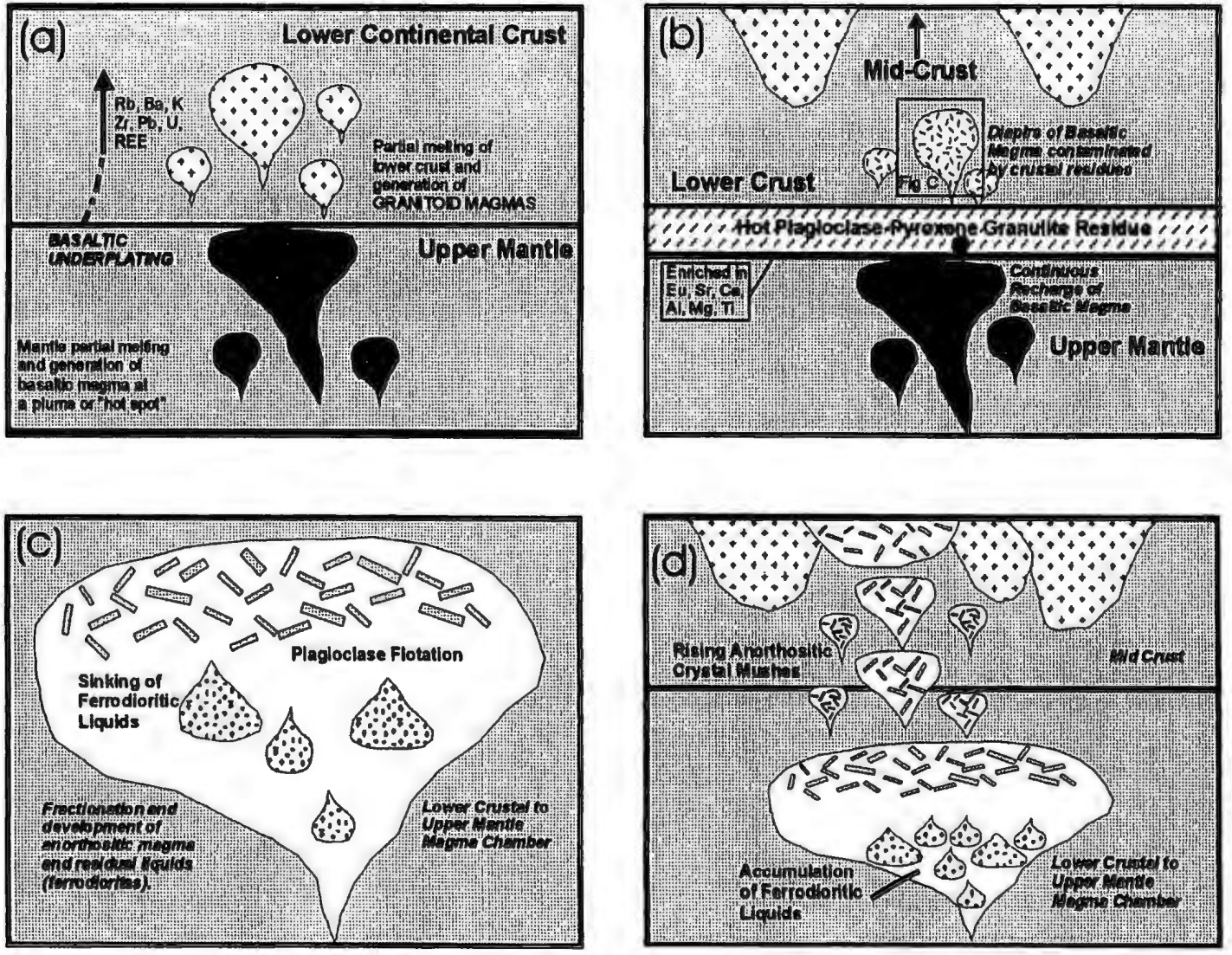

Figure 2.10. Schematic model for the petrogenesis of the Nain Plutonic suite and AMCG suites. Diagram constructed based on the ideas of Emslie et al. (1994).

Table 2.1. Chronology of tectono-magmatic events in the Saglek and Hopedale Blocks of the Nain Province prior to emplacement of the Nain Plutonic Suite. Sources of data are quoted in the text.

Age	Saglek Block	Hopedale Block	Age
Pre 3.9 Ga	Cores in zircons of Nanok gneisses		
ca. 3.8 Ga	Nulliak Supracrustals		
3732 Ma	Igneous precursors of the Uivak I gneiss		
3620 Ma	Metamorphism and migmatization of the Uivak I and formation of Uivak II gneisses		
		Weekes Amphibolite	3258 Ma
		Maggo Gneiss	3105 Ma
		Hunt River Group	3105 +/- 2 Ma
		Hopedale Dykes	?
		Hopedalian Deformation	3.1-3.0Ga
		Florence Lake Group	3002 Ma 2990 Ma 2979 Ma
		Kanairiktok Intrusive Suite	ca. 2858 Ma
		Fiordian metamorphism	2825 Ma to 2550? Ma
2.8-2.7 Ga	Granulite facies metamorphism		
2578-2549 Ma	Collision of the Saglek and Hopedale Blocks (deformation, metamorphism, basic dyke emplacement, mylonitization)		2578-2549 Ma
2450-2200 Ma	Napaktok and Domes Dykes	Kikkertevak Dykes	2235 Ma
2135-2045 Ma	Anorthositic, granitoid and basic dyke emplacement		
2.1-2.0 Ga	Granitoid magmatism		
ca. 2.0 Ga (1969 Ma)	Mugford, Synder and Ramah Group	Moran Lake, Lower Aillik, and Ingrid Group	ca. 2.0 Ga

Table 2.1. (continued)

Age	Saglek Block	Hopedale Block	Age
1880-1840 Ma	Torngat Orogen (TO): granitoid plutonismin the Tasiuyak Gneiss Complex and Lac Lomier Complex		
1860-1853 Ma	TO: crustal thickening and east-vergent fold and thrust tectonism		
1845-1820 Ma	TO: development of Abloviak Shear Zone		
1790-1745 Ma	TO: uplift and thrusting, sub-vertical crustal scale faults	Effects of Makkovikian orogeny on Hopedale Block	1810-1790 Ma
1350-1290 Ma	Nain Plutonic Suite (Table 2.2)		1350-1290 Ma

Table 2.2. Chrononology of dated Nain Plutonic Suite granitoid, ferrodioritic, and anorthositic and basic plutons. All ages are U-Pb determinations unless otherwise stated.

	Age (Ma)	Intrusive	Source
Granitoids	1343 +/- 3 Ma	Foliated monzonite marginal to the Mount Lister anorthosite	Connelly and Ryan (1994)
	1322 +/- 1 Ma	Makhavinekh Lake Intrusion	Ryan et al. (1991)
	1319 +/- 2 Ma 1316 +/- 3 Ma	Umiakovik Lake batholith	Emslie & Loveridge (1992)
	ca. 1295 Ma	Dog Island	Krogh & Davis (1973)
	1292 +/- 4 Ma	Voisey's Bay-Notakwanon intrusion	Ryan et al. (1991)
	ca. 1287 Ma	Peralkaline plutons of NPS	Emslie and Hamilton in Hamilton (1997)

	Age (Ma)	Intrusive	Source
Ferrodiorites	1332 +/- 3 Ma	Akpaume ferrodiorites	Hamilton et al. (1994) Hamilton (1997)
	1322 Ma	Barth Island intrustion marginal ferrodiorites	Hamilton (1997)
	1315 +/- 2 Ma	Satosuakuluk ferrodiorite dyke	Hamilton (1997)
	1311 Ma	Isolated diorites-Jonathan Island	Hamilton (1997)
	1306 +/- 3 Ma	Tigalik intrusion	Hamilton et al. (1994) Hamilton (1997)
	1298 +/- 2ma	Cabot Lake sheet	Hamilton et al. (1994) Hamilton (1997)

Table 2.2. (Continued)

	Age (Ma)	Intrusive	Source
Anorthositic and Basic Rocks	ca. 1331, >1340 Ma?	Mount Lister Intrusion	Ryan et al. (1995);Hamilton in Berg et al. (1994)
	1333.7 +/- 1 Ma	Eastern Deeps and Reddog bodies of RBI	Amelin et al. (1997)
	1330 +/- 2 Ma	Akpaume Intrusion leuconorite	Hamilton (1997)
	ca. 1328 ma (Ar-Ar)	Bird Lake massif	Yu and Morse (1993)
	1322 +/- 1 Ma	Paul Island intrusion	Hamilton in Berg et al. (1994)
	1322 +/- 1Ma	Makhavinekh Lake are leuconorite	Hamilton (1997)
	ca. 1320 Ma	Troctolite pillows, Barth Island Intrusion	Hamilton (1997)
	1317.2 +/- 1 Ma	Asina intrusion, RBI	Amelin et al. (1997)
	ca. 1311 Ma	Kikkertevak and Tabor Island intrusions	Hamilton (1997)
	1312-1311 Ma	Jonathan Island intrusion	Hamilton (1997)
	1307 +/- 1 Ma	Gabbro pegmatite in LZ of Kiglapait intrusion	Hamilton (1997)
	1305 +/- 2 Ma	Kolikatik Island intrusion	Hamilton (1997)
	ca. 1305 Ma	Newark Island intrusion	Simmons et al. (1986)
	1294 +/- 2 Ma	Leuconorite-Sango Bay	Hamilton (1997)

Chapter 3: Geology, Structure, Mineralization, and Silicate and Sulphide Petrography

3.1 Introduction

The OKG prospect contains a variety of rock types ranging from Archean to Mesoproterozoic in age (Quaternary cover non-inclusive). Archean rocks are typified by amphibolitic, mafic granulitic and metatonalitic (quartzofelspathic) gneisses of the Nain Province. Paleoproterozoic units include foliated and non-foliated granitoids, anorthositic rocks, and mafic dykes (Figure 3.1); while Mesoproterozoic rocks appear to be restricted to pyroxenitic rocks and associated Ni-Cu sulphide mineralization (Figures 3.2 and 3.3). This chapter provides a synopsis of the geology, petrography, sulphide mineralization, contact relationships and structural geology of the OKG prospect.

3.2 Geologic Units

3.2.1 Archean Rocks: Nain Province Gneisses

The easternmost lithological unit of the OKG prospect consists of well foliated intercalated and interlayered mafic granulite, amphibolite and metatonalite (quartzofeldspathic) gneiss of the Archean Nain Province (Figure 3.1; Plate 3.1). These gneisses are typically fine to medium grained with centimeter to tens of meter scale layers. Mafic granulite and amphibolitic rocks are black to dark brown, locally rusted

consisting of subhedral orthopyroxene, brown to brown-green hornblende, plagioclase and lesser biotite (Plate 3.1). Metatonalite layers are light coloured (white to grey), fine to medium grained, and locally granular, consisting predominantly of 1-3mm anhedral plagioclase feldspar and quartz (±K-feldspar), and lesser biotite, muscovite, and orthopyroxene (Plate 3.1).

The proportion of metabasic and metatonalite layers is highly variable. In some areas metabasic and metatonalite material have subequal proportions; in others metabasic material comprises 90% of the layers; while in others the metatonalitic material is as abundant as 70%. In the latter case rafts of irregularly shaped amphibolitic material in a sea of metatonalite are common. Localized meter scale folding of the layers is quite common and all layers have a pervasive northwesterly to southeasterly striking subvertical foliation (Plate 3.2; Figure 3.3).

3.2.2 Paleoproterozoic Units

3.2.2.1 Granitoid Rocks

The OKG prospect contains two broad areas of granitoid rocks including those south of Umiakoviarusek Lake, and a northwesterly striking unit in the core of the eastern portion of the property (Figure 3.1). Felsic dykes occur in the Main Showing region (Figure 3.2) and comprise only a minor proportion of the granitoids. South of Umiakoviarusek Lake two phases of granitoids exist, however, this study concentrates only on those within property boundaries, and only a few of the second phase rocks have been observed. The first phase granitoids (Owl River Valley pluton of Ryan *et al.*, 1998) are typified by medium to coarse grained, brown to rusty and variably foliated

hornblende and pyroxene bearing monzonites and lesser syenite (Plate 3.3). In proximity to their eastern boundary with anorthositic rocks the granitoids exhibit a well defined foliation with mineral parallelism on a centimeter to meter scale (Plate 3.3); while towards the west of this boundary the granitoids become more massive and a less pervasive foliation is present (Figure 3.1). Mafic minerals are dominated by 0.5-3cm subhedral hornblende and lesser anhedral pyroxene; while 0.5-1cm subhedral plagioclase and K-feldspar are modally subequal. Quartz is notably absent from the first phase granitoids; while accessory 1-3mm anhedral oxides (magnetite and ilmenite) are present but rarely exceed 5% modally. Locally, 2-3m pegmatoidal (?) patches of coarse grained magnetite, ilmenite and hornblende are found and the grain size of the oxides/hornblende increase to 2-5cm.

Towards the western part of the property, the first phase granitoids are intruded by a second phase of medium grained, granular quartz-bearing monzonites (Figure 3.1; Plate 3.4). In contrast to the phase 1 monzonites, the phase 2 monzonites contain less mafic minerals, are quartz bearing, do not exhibit a pronounced foliation, and intrude the phase 1 granitoids as irregularly shaped plugs and dykes, 2-5m and 30-45cm, respectively (cf. Ryan *et al.*, 1998). Mafic minerals associated with the monzonites are predominantly: 1-2mm flecks of biotite and lesser hornblende, rarely exceeding 10-15% modally. Although the phase 1 rocks have been observed within the property boundaries they are only a minor constituent of the mapped granitoids; however, towards the west, outside the property boundaries, these granitoids form a larger intrusive body consisting of

ovoidal feldspar clinopyroxene bearing quartz monzonite (B. Ryan, pers. comm., 1997; Ryan *et al.*, 1998).

In the eastern part of the property the granitoids form a northeasterly trending belt which exhibits a well developed foliation coincident with that in the Archean gneisses (Figure 3.3). The lithology of this belt ranges from quartz monzonite to quartz syenite, most of which are medium grained and contain between 5-10% modal mafic minerals. Mafic minerals consist predominantly of 0.5-3mm biotite grains which are elongate with the fabric of the rock, and 1-4mm hornblende grains; the latter two are commonly found as anhedral aggregates. Plagioclase and K-feldspar vary in percentage, but have a consistent 0.5mm to 1cm size and are anhedral. Quartz grains are between 0.5-1cm in size and anhedral, and in some places they are rounded, and typically have lustrous surfaces. Outside of the property boundaries, U-Pb zircon dating of this intrusive has yielded a ca. 2124 Ma age (Hamilton *et al.*, 1998; Ryan *et al.*, 1998).

Felsic dykes form only a minor constituent of the granitoids of the property and intrude the anorthositic rocks of the Main Showing area (Figure 3.2). These dykes range in size from 5cm up to 3m in size and have strike lengths of up to 200m. Lithologically, the dykes are predominantly coarse to medium grained monzonite, quartz monzonite, to granite; however, some are aplitic in nature. The coarsest dykes contain subequal percentages of 0.5-1.5cm plagioclase and potassic feldspar with up to 15% subhedral hornblende, lesser biotite, magnetite rosettes and anhedral quartz grains. Aplitic dykes exhibit a sugary texture with 1-2mm grains of plagioclase and potassic feldspar, blue quartz eyes, and lesser biotite, hornblende and magnetite. The aplitic variants of the

felsic dykes are likely recrystallized, as most of the dykes in the Main Showing region show well developed folding, and are offset by up to 5-10m by ductile faults in this region (Figure 3.2).

3.2.2.2 Anorthositic Rocks

Anorthositic (*sensu lato; s.l.*) rocks form a significant proportion of the rocks of the OKG prospect and outcrop in the area near the Main Zone north of Umiakoviarusek Lake, south of the lake, and along the ridges on the eastern part of the property. In each of these three regions the anorthositic rocks have distinctive characteristics and there appear to be geographic subdivisions of the anorthositic rocks (see section 3.3.3.1).

In the region of the Main Showing and North of Umiakoviarusek Lake the anorthositic rocks are dominated by dark grey to black, medium to coarse grained anorthosite with euhedral, 0.25-2.5cm, dark grey to black plagioclase (Plate 3.5). Mafic minerals rarely exceed 10% modally, consisting predominantly of 2-7mm intercumulus (?) clots of orthopyroxene and clinopyroxene and related alteration products, including chlorite and actinolite with minor magnetite.

To the south of Umiakoviarusek Lake the anorthositic rocks are typically lighter in colour (white to light grey), contain greater abundances of mafic minerals (15-25%: leuconoritic), and have a slightly more altered mineralogy. Euhedral plagioclase is similar to those north of the lake, with the exception of a lighter colour and lesser abundance. Mafic minerals consist of orthopyroxene, lesser clinopyroxene, and altered chlorite-tremolite-actinolite assemblages, which are interstitial to the plagioclase crystals. In certain locations small 5-20m outcrops of medium grained, granular recrystallized

anorthosite are present. The rocks both north and south of Umiakoviarusek Lake as described above form part of Ryan *et al.*'s (1998) Goudie Lake pluton.

On the ridges in the eastern part of the property (Figure 3.1), a northwesterly trending unit of anorthositic rocks is present (Pripet Marshes pluton of Ryan *et al.*, 1998); however, due to property boundaries only the northeastern portion of the unit is present within the study area. In this location the anorthositic rocks are distinct, have a rusty, buff coloration, and are extremely crumbly containing ca. 25-35% mafic minerals, with similar grain sizes as those in other areas of the property. Orthopyroxene is the dominant mafic mineral, and occurs as 2-4mm to 5-7cm anhedral grains which are honey to dark brown coloured; while plagioclase is similar in size but is light beige to white in colour.

3.2.2.3 Mafic Dykes

Mafic dykes and sills form only a small proportion of the OKG prospect and are localized in the anorthositic rocks south of Umiakoviarusek Lake, where they intrude anorthositic rocks (*s.l.*). The dykes are fine to medium grained and are black to black-green with strike orientations varying from northwest, east-northeast, to north (Plates 3.6-3.8). The mafic dykes are typically 5-45cm in width but some dykes are over 15m wide and extend for at least 50 meters. The small dykes contain fine grained mineral assemblages with very fine grained laths of plagioclase set in a dark green to black mafic matrix. Larger dykes have an interlocking network of euhedral plagioclase laths and dark green to black matrix material, giving the rock a 'salt and pepper' texture. Terminations and dyke edges are highly variable with some dykes having straight walls (Plate 3.6); other dykes exhibit almost lance-like terminations where their edges protrude into the

anorthosite host in a tentacle like fashion (Plate 3.7); while other samples have bulbous margins which are well rounded, almost like pillows. What is particularly odd about some dykes is the presence of rounded, ball like masses ca. 10-30cm disassociated from the dyke and located within the anorthositic host (Plate 3.8). Although the dykes have highly variable terminations, orientations and textures, the dykes do not exhibit well developed shearing or deformational fabrics; however, all of the dykes show secondary greenschist facies mineral assemblages.

3.2.2.4 Mylonitic Rocks

Two 0.5- 3m wide zones of mylonitic rock exist within the Main Zone region of mineralization and are associated with a series of south-southwesterly verging compressional faults (Figure 3.2; Plate 3.9; see section 3.6.3). The mylonitic rocks have a white to light grey colouration with 1-2mm to 15 cm long chlorite streaks associated with pervasive mylonitic foliation (Plate 3.9). In outcrop the specific mineralogy of the rocks is extremely difficult to distinguish due to their very fine-grained texture. Well developed structural features and kinematic indicators are associated with these mylonite zones (Figure 3.2; see sections 3.3.2.4 and 3.6.3).

3.2.3 Mesoproterozoic Units

3.2.3.1 Pyroxenitic Rocks

Pyroxenitic dykes represent a volumetrically minor, yet highly important lithological component, acting as the source for the observed Ni-Cu mineralization. The dykes are rubbly, characterized by a rusty, gossanous character on weathered surfaces; while on fresher surfaces have a dark brown to black to bronze coloration with dyke

margins that are irregular and bulbous; rarely do they exhibit straight margins (see section 3.4). At all locations on surface, the pyroxenitic rocks are spatially associated with disseminated to massive sulphide mineralization, and the dykes themselves always contain disseminated interstitial sulphides. In one location on surface, gossanous outcroppings of plug-like sulphide bearing leucotroctolite are present (see section 3.3.3.1; Figure 2).

The distribution of the mineralized pyroxenitic rocks are always spatially associated with (within 5m) zones of ductile faulting and mylonitic rocks. Even in proximity to these fault zones the dyke mineralogy is pristine retaining igneous textures with no evidence of secondary alteration that is common to the anorthositic and felsic dyke rocks in this region. Leucotroctolitic rocks are like the pyroxenitic rocks in that they are associated with faulting, but unlike the others mylonitic rocks are not present; however, they also do not exhibit secondary alteration. The relationship between the troctolitic and pyroxenitic rocks is not readily observable in the field; however, their similar spatial location to faults, lack of secondary alteration, and similar geochemical signatures (see Chapter 4) and radiogenic isotope systematics (see Chapter 6) suggest a commonality and genetic relationship between the two types of intrusives. Further details on the relationships between mineralization and the pyroxenite-leucotroctolitic rocks are given in section 3.4.

3.3 Petrographic Characteristics of Geologic Units and Subdivisions

As a second order refinement of the geological units outlined above, detailed petrographic examinations of the OKG rocks have been undertaken. These

classifications and observations of the OKG rocks indicate significant petrographic variations in the rocks when compared to the field observations. All classifications for plutonic rocks outlined follow Streckeisen's (1976) IUGS classification scheme; while metamorphic rocks are discussed based on their metamorphic mineral assemblages according to Bucher and Frey (1994).

3.3.1 Archean Nain Gneisses

3.3.1.1 Amphibolitic and Mafic Granulitic Rocks

Amphibolitic and mafic granulitic rocks are dominated by the ACF phases orthopyroxene (opx), biotite (bio), hornblende (hbl), clinopyroxene (cpx) and plagioclase (pl). The rocks have highly variable assemblages including: opx-pl-hbl-bio, opx-cpx-pl, opx-cpx-hbl-pl, to hbl-bio-pl (Plates 3.10-3.11). All consist of fine to medium grained textures that are dominated by extensive parallelism of minerals, well developed annealed textures, subgrain formation, and in some cases symplectic intergrowth textures (Plates 3.10-3.11).

The mineral assemblages are typically variable in grain size with orthopyroxene and hornblende forming the larger grains. Orthopyroxene grains are typically 0.25-2mm, anhedral, and contain small rods and patches of exsolved rutile; while biotite rims are very common. Subhedral to euhedral hornblende grains, 1-4mm in size, exhibit distinctive brown to olive green coloration, and are often located along the edges of the pyroxene grains, often forming coronas; while in other cases where pyroxenes are absent, hornblende forms symplecitic intergrowths with plagioclase. Clinopyroxene is typically anhedral, 0.25-1mm in size, and in lesser abundance than the orthopyroxene grains.

Plagioclase is highly variable occurring as symplectic intergrowths with the hornblende grains (Plate 3.11), while in other areas occurs as subhedral, 0.25-1mm grains that have extensive subgrain formation with larger grains containing numerous smaller grains along their edges (Plate 3.10-3.11).

Although the latter minerals form the predominant mineral assemblages of the metamafic layers, a few samples have mineralogical evidence of a second metamorphic/fluid alteration event (Plate 3.12). Small, 1-2mm veinlets of polycrystalline quartz, chlorite, sericite, actinolite, epidote and carbonate are present and appear to have altered the higher grade mineral assemblage (Plate 3.12). Although some veinlets contain all of the lower grade minerals, a chlorite-sericite-quartz assemblage is most common and exhibits a zonation, with the vein proper containing the multitude of the lower grade minerals, accompanied by a decrease outwards within 1-2mm from the veinlet.

The predominant metamorphic assemblage associated with the metabasitic layers includes: opx-cpx-hbl-pl-bio, of which the rocks contain some or all of these components (e.g. Plate 3.10). The upper amphibolitic rocks are typified by the cpx-hbl-pl assemblage, while the granulite facies assemblage is manifested in the opx-cpx-pl assemblage. Assemblages that are transitional to these, like the opx-cpx-hbl-pl assemblage, likely represent disequilibrium assemblages transitional between granulite and amphibolite facies, and are likely retrogressed granulites. In contrast, the veinlet assemblages are typical greenschist facies assemblages likely a result of sinistral strike-slip faulting associated with this area (see section 3.6.2; Figure 3.1).

3.3.1.2 Quartzofeldspathic (Metatonalite) Layers

Metatonalite layers consist predominantly of a quartz-plagioclase-(±K-feldspar) assemblage. Quartz is the most abundant mineral phase, with subequal plagioclase, and lesser K-feldspar. Quartz forms the largest grains in the metatonalites, ranging in size from 0.5-1mm, and the grains are very anhedral with extensive elongation, often delineating the fabric of the rock (Plate 3.13). Subgrain formation is quite commonly associated with the quartz grains with larger grains having edges with smaller, rounded to ovoid grains, often forming polycrystalline aggregates with slight dustings of sericite. Plagioclase is very similar to the quartz grains exhibiting an anhedral character with extensive subgrain formation, but is smaller in size (0.25-1mm). Annealing is not as common as the metamafic layers; however, minor annealing is observed in the plagioclase grains of some sections and most sections have plagioclase and K-feldspar containing dustings of sericite.

Potassic feldspar and mafic minerals are present in minor abundance. Potassic feldspar are smaller than the plagioclase crystals, but exhibit well developed myrmekitic textures with worm-like, vermicular intergrowths of quartz. Mafic minerals do not exceed 2% modally and are dominated by small (0.25-0.5mm) grains of orthopyroxene and clinopyroxene (opx>cpx), and lesser biotite, that are interstitial to the plagioclase/quartz grains and elongated with the fabric of the rock (Plate 3.13).

Similar to the metamafic layers, a lower grade metamorphic/fluid derived assemblage is present in some sections as a series of veinlets. Sericite-chlorite-quartz-carbonate veinlets 1-2mm wide cut some of the sections; while in other sections a

complete replacement of all minerals, with the exception of quartz, occurs, leading to a matrix of needle-like sercite and chlorite.

3.3.2 Paleoproterozoic Units

3.3.2.1 Granitoids

Similar to the field classifications of the granitoid rocks, significant petrographic differences exist between the granitoids of the OKG prospect. To the south of Umiakoviarusek Lake only the phase 1 granitoids have been petrographically analyzed, since most of the rocks from the phase 2 granitoids lie outside the property boundaries. The phase 1 granitoids are petrographically classified as monzonitic to syenitic, containing greater variance in mafic minerals than field classifications, with some or all of the following: fayalitic olivine, orthopyroxene, clinopyroxene, hornblende and biotite (Plate 3.14). Fayalite is particularly common in granitoids proximal to the anorthosite-granitoid contact, occurring as 2-4mm anhedral grains with variable alteration and reaction textures (Plate 3.14). In most cases the fayalite contains fracture infillings or coronas of iddingsite and hematite (±other oxides); while to a lesser extent clinopyroxene is observed along the edges of the fayalite grains. Fayalitic olivine rarely exceeds 5% modally.

Orthopyroxene and clinopyroxene are in greater abundance than fayalitic olivine, typically present as anhedral to subhedral grains 1-5mm in size (Plate 3.14). Rarely are the pyroxenes fresh and generally have evidence of significant hydration, often found as cores or crystal remnants within the larger hornblende sheets (Plates 3.14-3.15). Orthopyroxenes often contain exsolved platelets of clinopyroxene in some sections along

with oxides, along their edges and within the grains. Clinopyroxenes, when not significantly hydrated (e.g. core phases), have small patches of hornblende along their predominant cleavage.

Hornblende is by far the most significant mafic mineral associated with the phase 1 granitoids and is present as 2-8mm sheets or as 1-2mm small grains. The grains of hornblende are typically subhedral showing well developed pleochroism in olive greens to dark brown and contain a plethora of inclusions. Excluding the cores of pyroxene in many of the hornblende there is typically abundant apatite inclusions, with lesser titanite and zircon. Biotite flecks and grains are common along the grain edges and rarely biotite are found as isolated 0.5-1mm grains (Plate 3.14).

Feldspars are typically in subequal proportions and have variable grain size ranging from 0.25-7mm. Plagioclase is typically subhedral to anhedral and with increasing size and show extensive evidence of subgrain formation and are more anhedral. Myrmekitic textures are not common, but present in some of the plagioclase. Perthitic K-feldspar is the predominant potassic feldspar type and the K-feldspars are typically larger than the plagioclase feldspars forming anhedral sheets with seriate edges and abundant subgrain formation. In rare cases the potassic feldspar is microcline. Quartz is notably absent from the phase 1 granitoids and alteration of the feldspars is typically in the form of fine sericite and epidote dustings.

In the eastern part of the property, the rocks from the northeasterly foliated unit have extremely variable petrographic character ranging from monzonite, quartz monzonite, syenite, quartz syenite to alkali feldspar granite (e.g. Plate 3.16). Most of the

eastern granitoid rocks are medium grained and contain between 5-20% mafic minerals including, fayalite, orthopyroxene, clinopyroxene, hornblende and biotite (Plate 3.16).

Fayalitic olivine occurs in a few samples from this eastern location, typically in quartz poor variants. When present, it occurs as anhedral grains 0.5-7mm in size and has abundant secondary alteration to iddingsite along grain boundaries and within crystal fractures (Plate 3.16). Rounded plagioclase inclusions are also common in the fayalitic olivine. Orthopyroxene occurs either as orthopyroxene proper or as inverted pigeonite. Most orthopyroxene grains are anhedral, occurring as aggregates with multiple grains of orthopyroxene between 0.5-4mm in size. The grain boundaries of the orthopyroxenes typically contain minor amounts of green-brown hornblende and actinolite; while oxides (ilmenite and magnetite) are commonly found in proximity to the grains. In many cases the orthopyroxene forms cores to the larger hornblende grains, and they often contain inclusions of plagioclase. Clinpyroxene is in lesser abundance than the orthopyroxene but usually forms a core phase to larger hornblende grains.

Hornblende and biotite typically occur as coronas on the orthopyroxene and clinopyroxene, but in rarer cases are found as isolated grains. Most of the hornblende grains are olive green to brown, forming elongate anhedral sheets 2-3mm in size, with individual grains 0.5-1mm. Most of the grains contain inclusions of plagioclase, oxides, apatite and titanite. Biotite is present mostly on the edges of the hornblende grains in 0.5-1mm subhedral, red-brown grains that often contain zircon inclusions.

Quartz, plagioclase and potassic feldspar have variable proportions within the granitoids (Plate 3.17). Quartz, although absent in some rocks, occurs as 3-7mm rounded

grains that show extensive subgrain formation with 0.25-0.5mm grains along the larger grain edges (Plate 3.17); while in some larger grains, small spot-like inclusions of quartz occur within the plagioclase grains. Potassic feldspar occurs as perthite and microcline, with the latter less common; many perthites contain euhedral, exsolved patches of plagioclase feldspar (Plate 3.17). Most grains are subhedral to anhedral and 0.25-7mm in size, with subgrain formation similar to quartz. Plagioclase is variable from being subequal to the plagioclase, to being totally absent in some sections. The plagioclase is typically smaller than the K-feldspar and occurs as 0.5-3mm euhedral to subhedral grains with minor subgrain formation (Plate 3.17); some of which have myrmekitic intergrowths of quartz. All feldspars have light dustings of epidote and sericite.

Felsic dykes from the Main Showing area have fine to medium grained mineral assemblages and are petrographically classified as quartz-monzonite to granite. Quartz is quite abundant in the dykes occurring as irregularly shaped coarse grains 1-5mm grains, along with 0.2-0.5mm aggregates of recrystallized quartz (Plate 3.18). Commonly the larger grains of quartz have a linearity and define a pseudo-fabric. Plagioclase and K-feldspar are less recrystallized and are typically smaller in size (1-2mm) and have evidence of smaller subgrains along their edges; while often containing a partial to full replacement by sericite and epidote (Plate 3.18). Anhedral 0.5-3mm clots of hornblende and biotite with blebby textures are common in the dykes; while rosettes of magnetite are of lesser abundance, but are common to most dykes. Minor biotite, muscovite, chlorite, and apatite are often present within the matrix of some of the finer dykes.

3.3.2.2 Anorthositic Rocks

Similar to the field characteristics of the anorthositic rocks of the OKG prospect, geographical, petrographical and topographical variations exist. The rocks north of Umiakoviarusek Lake consist principally of anorthosite (*senso-stricto*) with most rocks containing greater than 90% modal plagioclase (Plate 3.19; e.g. *an* group rocks); however, a small portion of samples are leuconoritic to leucogabbroic in composition. Plagioclase feldspar is present as 0.25-1.25cm, subhedral to euhedral grains forming the predominant cumulus phase of the rock. In some sections the larger plagioclase have 1-3mm, rounded subgrains along the major grain edges, typical of subsolidus or metamorphic recrystallization. Plagioclase is fairly fresh in some sections (Plate 3.19), while in others dustings of sericite and epidote are common (Plate 3.20), while in others the plagioclase are totally replaced by the other minerals.

Mafic, oxide and sulphide minerals constitute the remainder of the minerals associated with the anorthositic rocks. Orthopyroxene, and lesser clinopyroxene occur as anhedral, 0.1-0.5cm intercumulus clots which show variable degrees of alteration. Many of the orthopyroxene and clinopyroxene grains are characterized by extensive replacement with tremolite-actinolite-chlorite assemblages (Plate 3.21), while often retaining cores of pyroxene. Magnetite, ilmenite and lesser pyrite are associated with intercumulus phases and typically have hematite associated with their margins.

South of Umiakoviarusek Lake the anorthositic rocks the exhibit a continuum into leuconoritic rocks (*lnl* group rocks); however, they retain similar grain size and mineralogy with the exception of modal proportions. In this region mafic mineral

replacement is much more intense with some pyroxenes exhibiting complete replacement by secondary minerals (Plate 3.21). Furthermore, some of the anorthositic rocks contain chlorite-sericite-epidote bearing and lesser dolomite-calcite bearing veinlets approximately 0.5-1mm in width (Plate 3.22). The southernmost occurrence of anorthositic rock on the property contrasts with the moderately altered southern material, consisting of pristine leuconorite with 15-20% modal orthopyroxene (Plate 3.23). In this area the grain sizes of the plagioclase are similar; however, the plagioclase show lesser subgrain formation and some exhibit bent twins (Plate 3.23). Anhedral intercumulus orthopyroxene shows little evidence of alteration and contains clinopyroxene, minor biotite and oxide along grain edges, along with clinopyroxene inclusions and rutile exsolution needles (Plate 3.23).

The hills atop of the Main Showing area, north of Umiakoviarusek Lake region, illustrate a topographic effect on the composition of the anorthositic rocks. In this region the rocks are very fresh and unaltered leuconorite to anorthosite in subequal proportions (*an* to *ln1* group). Leuconoritic rocks are characterized by approximately 35% mafic minerals which are predominantly orthopyroxene and lesser clinopyroxene. Orthopyroxene occurs in a series of polycrystalline aggregates composed of euhedral, subhedral and anhedral orthopyroxene. Smaller grains of orthopyroxene are typically the most euhedral grains; while larger grains are subhedral to anhedral with a variable exsolution lamellae, including: rod and needle-like exsolution lamellae of rutile and lamellar and blebby clinopyroxene exsolution. Clinopyroxene occurs predominantly as an intercumulus phase, filling the interstices between orthopyroxene grains and is

typically anhedral and ca. 0.25mm in size. Plagioclase in the anorthositic and leuconoritic rocks are subhedral to euhedral, form the major cumulus phase, and are larger than the orthopyroxene aggregates ranging in size from 0.5-1.0 cm. Unlike the rocks of lower elevations in this area, very little alteration of the primary mineral assemblages is associated with these rocks.

In the eastern and northeastern part of the property the anorthositic rocks are different than the other parts of the property and are predominantly leuconoritic (opx 25-35% modally; *ln2* group rocks) with very minimal anorthosite (Plate 3.24). Rocks from this eastern anorthositic unit have only been sampled in the northeastern terminus of the property. From this region anorthositic and leuconoritic rocks are present. Leuconoritic rocks typically have between 20-25% modal orthopyroxene that occurs either as 1-3mm, intercumulus clots between the plagioclase grains, or as 0.5-1mm subhedral grains within sheet-like plagioclase grains (Plate 3.24). Orthopyroxene occurs in two forms, either as orthopyroxene proper, or as inverted pigeonite (Plates 3.24-3.25); the latter is very common in rocks from this region and is notably absent in all other anorthositic rocks of the property. Plagioclase grains larger than the orthopyroxene grains and are typically subhedral to euhedral, ranging in size from 1-2mm up to 1cm, with most between 5-7mm. Large plagioclase grains are typically associated with smaller grains along their edges, and some have 5mm wide zones, which appear to have underwent subsolidus recrystallization. It could be argued that the orthopyroxene-plagioclase crystallization sequence and the presence of inverted pigeonite suggest that these rocks may have

formed from a different magma batch than the remainder of the anorthositic rocks of the property.

3.3.2.3 Mafic dykes

Field characteristics of the mafic dykes illustrate that they are highly variable, similarly, the petrography of the dykes is also highly variable. Fine grained mafic dyke samples are characterized by subequal abundances of plagioclase laths set in a dark green to black, mafic groundmass (Plate 3.26). Plagioclase laths are typically 0.5-1mm, subhedral, and set in a matrix of chlorite and actinolite (Plate 3.26) with localized 0.5-1mm rounded grains of olivine, altered to talc and serpentine. Fine grained, 0.25mm rounded magnetite and cubic pyrite grains are also found in the matrices of some samples.

Coarser grained samples contain well developed, euhedral 0.5-2mm plagioclase crystals that constitute the major cumulus phase. Most of the plagioclase grains show some degree of alteration with fine dustings of sericite and epidote; however, some are totally replaced by the latter minerals. Engulfing and totally enclosing the plagioclase crystals are large anhedral 0.5-3mm mats and smaller 0.5-1mm intercumulus grains of orthopyroxene. Rarely are the orthopyroxene grains fresh and most are either partially or totally replaced by chlorite and lesser tremolite. Biotite flakes have much greater abundance in the coarser grained samples and are located along grain boundaries of the fresh or altered pyroxene grains. Magnetite and pyrite form accessory intercumulus phases.

One anomalous dyke was sampled which contained predominantly plagioclase as 0.2-0.5mm grains, exhibiting extensive replacement by secondary sericite and epidote. This dyke is almost granular in texture and contained minor amounts of biotite and magnetite. The fine grained nature and dominance of plagioclase suggests that this dyke may be a chilled anorthositic dyke, or a recrystallized raft of anorthositic material.

3.3.2.4 Mylonitic Rocks

Mylonitic rocks are extremely fine grained with a fabric defined by very fine grained chlorite, polycrystalline quartz and sericite (Plate 3.27). The chloritic material is the predominant mineral defining the fabric and constitutes the majority of the rock as small granular grains in a linear array (Plate 3.27). Polycrystalline quartz layers are larger in width than the chlorite layers and have larger grains of quartz in comparison to the chlorite (Plate 3.27). Closely associated with these later minerals are discontinuous layers of sericite and larger grains of muscovite, which appear to terminate into the chlorite-quartz fabric (Plate 3.27). Porphyroblasts of 0.5-1mm plagioclase are very common and are rounded being wrapped by the chlorite-quartz fabric and often have grains boundaries with minor sericite (Plate 3.27); lack of rotation associated with the porphyroblasts suggests a pre-tectonic origin. A second set of minor veinlets (ca. 1-2mm) cuts the mylonitic foliation and consists of anhedral quartz, chlorite, muscovite and carbonate.

3.3.3 Mesoproterozoic Units

3.3.3.1 Mineralized Pyroxenitic dykes

Detailed petrographic examinations of the pyroxenitic dykes have been undertaken by analyzing samples from both the surface showings and random drill core samples. Unlike field observations, the pyroxenitic (*sensu lato*) dykes are much more variable and have a variety of closely related, yet different petrographic distinctions. From this petrographic analysis a two fold subdivision has been proposed with Type 1 dykes which are predominantly orthopyroxenite and variants; a subtype of this group has been proposed based on exsolution products in orthopyroxene and crystallization history relative to the sulphide phases. The Type 1 dykes and their related subtypes are location in both surface and drill core; while, the Type 2 subdivision is restricted to one location on surface, and consists predominantly of leucotroctolite and olivine gabbro (Figure 3.2). It should be noted that the Type 1 and Type 2 dykes are subdivided *based on petrography* and not on chemical or isotopic grounds (see Chapters 4 and 6).

Type 1 dykes are characterized by a predominantly orthopyroxenitic (*sensu stricto*) character (Plate 3.28); however, minor variations exist with dykes ranging from orthopyroxenite to websterite to gabbronorite, significant overlap exists between all dykes of this type. The primary mineral associated with the dykes is orthopyroxene occurring as euhedral, and lesser anhedral, 2-5mm grains (Plate 3.28). Many of the orthopyroxene grains show minor annealing, which unlike the metamorphosed rocks of the property, is a result of sub-solidus recrystallization. Exsolution is common in the

orthopyroxenes of the type 1 dykes, consisting chiefly of 0.2-0.3 mm rutile laths (Plates 3.28-3.29).

Sulphide grains are interstitial to the orthopyroxene grains and likely represent and intercumulus sulphide liquid (see section 3.5.2), and the sulphide grains are partially to fully enclosed by clinopyroxene grains (Plate 3.28). Clinopyroxene grains have variable texture and size, some exhibit well developed crystal faces, and partially enclose the orthopyroxene and sulphide. The clinopyroxene grains are 2-3mm up to 5mm in size and have high birefringence in violets and blues suggesting they may be Ti-rich. Like the opx, the cpx also have needle-like exsolution lamellae of rutile, supporting a Ti-rich nature.

Plagioclase is low in abundance in most dyke samples, rarely exceeding 5-7% modally. Two plagioclase variants exist, including: 1) a larger 5-7mm variant and 2) a smaller 2-4mm variant. Both variants exhibit similar characteristics and are anhedral to subhedral, enclose orthopyroxene, clinopyroxene and sulphide grains, and are likely of post-cumulus origin.

Type 1A dykes are subdivided from the Type 1 dykes based on the order of crystallization between silicate and sulphide phases and exsolution products within the orthopyroxene grains. Type 1A dykes are characterized by orthopyroxene that is larger than the Type 1 dykes, ranging from 0.5-1.5cm, is subhedral to anhedral containing clinopyroxene exsolution products in contrast to rutile (Plates 3.30-3.31). Clinopyroxene exsolution occurs in two forms, including: 1) 0.3-0.4mm wide rod-like exsolution lamellae, similar to the rutile exsolution in the Type 1 dykes, which extend the length of

the crystal (Plates 3.30-3.31), and 2) 0.1-0.3 blebby, rounded, oval, and worm-like forms (Plate 3.30). The latter exsolution phenomena give the orthopyroxene a 'spotted' texture that appears to be somewhat like a leopard skin. Some clinopyroxene also appear to be irregularly shaped, and are intercumulus to the orthopyroxene (Plate 3.30).

A second criteria for subdividing the Type 1 and Type 1A dykes is the order in which the sulphides crystallize relative to orthopyroxene. In the Type 1 dykes the general order of crystallization includes orthopyroxene -> sulphide-> clinopyroxene (Plate 3.28). In the Type 1A dykes there is evidence for interstitial sulphide; however, many orthopyroxene grains contain inclusions of sulphide, that appears to have crystallized ***before*** the orthopyroxenes (Plate 3.31). For instance, most of the smaller orthopyroxene grains fully to partially enclose the smaller 0.5-1mm sulphide grains; while the larger sulphide grains are partially enclosed in a sub-ophitic fashion (Plate 3.31). The latter textural aspects provide good support for a different order of crystallization.

Type 2 dykes have petrographic characteristics that are unique compared to the Type 1 and Type 1A dykes and are leucotroctolitic to olivine-gabbroic rather than orthopyroxenite dominated (Plate 3.32). The Type 2 dykes are characterized by cumulus olivine and plagioclase with intercumulus sulphide and clinopyroxene. Olivine is the first crystallizing phase, and is approximately 25% of the rock modally, occurring as anhedral, cracked grains, 0.7-1.5 mm in size (Plate 3.32). The olivine grains exhibit both subophitic and ophitic relationships with plagioclase and appear to have both co-crystallized and post-crystallized relative to the olivine grains. Two textural types of

plagioclase are observed within the Type 2 dykes, including: 1) pristine, elongate, euhedral grains of plagioclase, 0.5-2.5mm in size, which are subhedral only near olivine crystals where they conform in co-crystallizing manner; and 2) 0.25-0.5cm post-cumulus sheet-like, anhedral grains which completely surround the olivine crystals. In total both types of plagioclase comprises approximately 40-45% of the rock.

Clinopyroxene grains fully or partially enclose all other mineral grains, including sulphides (e.g. Plate 3.33). Most of the clinopyroxene exhibits very high violet to blue birefringence and has a slight pinkish pleochroism suggesting that it may be Ti-rich. Clinopyroxene composes approximately 10% of the rock and is found in 0.5-4mm post-cumulus grains that are irregular in shape and anhedral (Plate 3.33). Larger accumulations of clinopyroxene are located in the region of sulphide minerals where they mantle the larger sulphide grains and have smaller sulphide grains enclosed within them; however, some of these larger sheets appear to have been thermally eroded by the sulphide grains (Plate 3.33). From the latter relationship it can be assumed that the crystallization order of the dykes was as follows: olivine->olivine+plagioclase-> plagioclase-> clinopyroxene -> sulphide.

Alteration within the dykes is variable and localized. Fine dustings of actinolite±oxides, and minor biotite, are found on some of the orthopyroxene; however, this is very localized and is not pervasive in any thin sections, likely a result of late stage fluids associated with the magmas.

3.4 Mineralization

Mineralization within the OKG prospect occurs within two zones, in a single area approximately 200m long by 40m wide, that includes the Main Zone, and a North-Striking Shear Zone with associated mineralization (Figure 3.2). Both areas are associated with gossanous zones containing massive, semi-massive and disseminated base-metal sulphides spatially (Plates 3.34-3.35), and likely genetically associated with pyroxenitic intrusives. Mineralization in drill core provides unequivocal support for a genetic relationship between the pyroxenitic dykes and Ni-Cu sulphide mineralization as most mineralization is located within and associated with pyroxenitic dykes (Plates 3.36-3.37; Wilton and Baker, 1996; Kerr and Smith, 1997; Piercey, 1997; Piercey and Wilton, 1998; Kerr, 1998).

3.4.1 Main Zone Mineralization

The Main Zone (MZ) of mineralization is characterized by numerous occurrences of massive to disseminated sulphide mineralization spatially and genetically association with ultramafic to mafic dyke-like intrusions (loosely called pyroxenitic; Plate 3.34). The occurrences of mineralization are found in 0.5-1m by 2-3m zones that have a strong spatial association (within 2-3m) with the above dyke like intrusions and to ductile faulting (Figure 3.2). Massive sulphide mineralization is generally found as podiform pockets of massive sulphide that are commonly hosted by anorthositic to leuconoritic rocks but spatially grade from massive to disseminated mineralization into the pyroxenitic rocks over a few meters (Figures 3.2 and 3.4a; Plates 3.34-3.35). The massive sulphide pods typically contain coarse grained (0.5-5cm) euhedral pyrrhotite

with chalcopyrite that forms 1-3mm by 2cm stringers along the pyrrhotite grain boundaries or as individual rounded, and irregularly shaped grains 3-7mm in size interstitial to the pyrrhotite.

The massive sulphide pods also contain fragments of plagioclase and anorthositic wall rock material, and in some samples orthopyroxene grains are present (Figure 3.4b). Spatially associated with these inclusions is chalcopyrite that occurs as stringers along the inclusion edges, as well as along the crystallographic axes or fractures in the plagioclase crystals (Figure 3.4b). These anorthosite fragments are the most abundant inclusion type in the sulphides and are 0.5-5cm in size and contain subhedral edges that appear to be rounded from thermal reactions with the sulphide liquid; or straight where relatively unaffected by the sulphide liquid (Figure 3.4b). In some sulphide samples the plagioclase/anorthositic inclusions are totally replaced by secondary clay minerals.

Disseminated sulphide mineralization of this zone occurs in both anorthositic and pyroxenitic-leucotroctolitic host rocks, with the latter more common. Anorthosite hosted sulphides consist predominantly of fine grained, 1-3mm anhedral pyrrhotite grains that conform to the shape of the plagioclase crystals; while chalcopyrite occurs as 1mm flecks. In some cases semi-massive pockets approximately 5cm in size are found in the anorthositic rocks and contain 1.5-2cm pyrrhotite with stringer chalcopyrite; the latter is a rare occurrence. There appears to be a spatial association of fracturing in the wall rock anorthositic material and the distribution of sulphide mineralization in the wall rock is likely the result of emplacement of sulphide liquid into favourable fracture-related spatial traps.

Disseminated pyroxenite hosted sulphide is the most common type of disseminated mineralization and is associated with discontinuous and irregularly shaped pyroxenitic dykes with variable widths, strike lengths and shape. Some outcrops of the pyroxenitic rocks are almost plug like (ca. 1-2m in size) and irregularly shaped, while most are in the form of dykes 10cm to 1.0m wide with strike lengths ranging from 1.5 to 5m in length (Figure 3.4b). Dyke margins are not easily discernable, but appear to be irregular and bulbous; however, no observed dykes appear to contain fragments of anorthositic material. Sulphide mineralization occurs as disseminated pyrrhotite and chalcopyrite (with minor magnetite) ranging from 5-25% of the total mineralogy. Pyrrhotite is the most common sulphide mineral occurring in 0.25-4mm rounded grains with small amounts of chalcopyrite along grain edges. In contrast to the disseminated anorthosite hosted sulphides, the pyroxenite hosted sulphides are interstitial and appear intercumulus relative to the cumulus orthopyroxene grains (Plate 3.28). These textures are quite similar to classic "net textures" (Naldrett, 1973) and point to a strong syngenetic relationship between the sulphides and the dykes, likely that the sulphides were derived from the melts that formed the pyroxenitic rocks.

Leucotroctolitic-hosted sulphides (Type 2 dykes) are located in one location on surface (Figure 2) and have very similar sulphide-silicate textural relationships as the pyroxenitic rocks (see section 3.5.2). In contrast to the pyroxenitic rocks, however, there are no massive sulphide pods associated with the leucotroctolitic intrusives. Furthermore, the sulphides form similar intercumulus disseminations to the olivine and

plagioclase; but in some cases large, up to 1cm grains of coarse pyrrhotite and chalcopyrite occur interstitial to the silicate minerals (Plate 3.33; see also section 3.5.2).

3.4.2 North-Striking Shear Zone Mineralization

The North-Striking Shear Zone (NSSZ) associated mineralization is located in proximity to a shear zone of ductile faulting and mylonitic rocks, approximately 35m northwest of the Main Zone of mineralization (Figure 3.2). Although this region exhibits shearing, the mineralization appears to be unaffected by the shearing and retains pristine igneous textures and primary igneous mineralogy. Mineralization in this region consists predominantly of disseminated sulphide with lesser massive sulphide, and similar to the Main Zone, mineralization occurs in both anorthositic and pyroxenitic rocks. Anorthosite hosted sulphides are associated with recrystallized and moderately silicified anorthosite containing glassy feldspars that have been recrystallized by faulting. The sulphides constitute 5% of less of the rock and are found as 1-2mm to 1cm disseminations of fleck-like and blebby anhedral pyrrhotite; while chalcopyrite is present to a lesser extent, occurring as isolated blebs and flecks on the edges of pyrrhotite grains. Pyroxenite hosted (Type 1 dykes) disseminated sulphides exhibit similar textural relationships as those of the Main Zone with intercumulus anhedral pyrrhotite blebs with chalcopyrite edges and stringers.

Massive sulphide mineralization associated with the NSSZ is much less abundant than that of the MZ and is found only as a series of irregularly shaped isolated pockets 30-45cm in size. However, like the MZ, the massive sulphides are always in close proximity and likely gradational into the pyroxenitic rocks. The massive sulphides

consist predominantly of coarse grained pyrrhotite with very minimal chalcopyrite; the latter only comprising 1-2% of the total sulphides. Pyrrhotite occurs as 0.5-1cm euhedral grains that have a pinkish hue, unlike the sulphides of the MZ.

3.4.3 Drill Core Mineralization

Approximately 20 diamond drill holes have been drilled on the OKG prospect and have yet to delineate an economic ore body; however, variable intersections ranging from 0.25m up to 9m have yielded geologically interesting, yet subeconomic concentrations of Ni-Cu-Co sulphide mineralization associated with pyroxenitic rocks. Detailed drill core logging was not undertaken as part of this thesis; however, general observations on the style and nature of mineralization from drill core were made for this study (Plates 3.36-3.37; Figure 3.4c). Further details on the nature of core mineralization can be obtained from T.Ryan (1996), Wilton and Baker (1996), and Kerr (1998).

Similar to surface mineralization, drill core mineralization provides unequivocal evidence of the genetic relationship between the pyroxenitic dykes and Ni-Cu sulphide mineralization. Pyroxenitic rocks typically have very sharp intrusive contacts with the surrounding anorthositic rocks and are typically straight walled. Pyroxenites are never barren of sulphide, but typically have gradational assemblages with increasing sulphide content towards their basal contacts (Plates 3.36-3.37; Figure 3.4c); ranging from disseminated near the top, to semi-massive, to massive sulphide towards the basal contact (Figure 3.4c; cf. Wilton and Baker, 1996; Kerr, 1998). Within the basal massive sulphides minor centimeter sized inclusion of host rock anorthositic material are present as inclusions (Figure 3.4c), and these likely are a result of entrainment upon emplacement

of the pyroxenitic dykes and associated sulphide. Sulphide stringers are also commonly emplaced within a few centimeters of the basal contacts with the pyroxenites into the anorthositic rocks underlying the dykes (Figure 3.4). The nature of sulphide mineralization associated with the dykes suggests sulphide saturation prior to emplacement into the anorthositic rocks, and was not likely locally controlled.

3.5 Sulphide Petrography

3.5.1 Massive Sulphides

Massive and semi-massive sulphide mineralogy is dominated by a pyrrhotite-chalcopyrite-pentlandite-pyrite-magnetite assemblage, where pyrrhotite is host or proximal to all other sulphide/oxide minerals (e.g. Plates 3.38-3.48). Pyrrhotite occurs as euhedral, and lesser subhedral grains that are 0.5-2.5cm, comprising 75-85% of the sulphide minerals. In surface samples the pyrrhotite is not always fresh and contains abundant hematite along the basal partings and fractures of the grains; however, in drill core pyrrhotite is very fresh containing no hematite, suggesting the latter is a function of surface weathering.

Chalcopyrite and pentlandite comprise 5-10% of the sulphide mineralogy and are in roughly subequal proportions. Chalcopyrite is present in a variety of forms, occurring along pyrrhotite grain boundaries or as grains radiating inwards from the pyrrhotite grain-boundaries (Plates 3.38). Edge-type chalcopyrite occur as stringers ca. 0.1-1mm wide by 0.5-7mm long, and are very anhedral (Plate 3.38); some of these stringers appear to be remobilized along the fractures and are intergrown with hematite. Inwardly extending chalcopyrite has a variety of shapes including: 0.25-0.5mm wide flame-like grains (Plate

3.38), similar sized rounded and blebby grains (Plate 3.39), and 0.1-0.5mm elongate worm-like grains. In addition to the pyrrhotite associated chalcopyrite, chalcopyrite forms 0.5-2mm anhedral coronas which partially or fully enclose the silicate mineral grains (plagioclase and orthopyroxene; Plate 3.40).

Similar to the chalcopyrite, pentlandite occurs in a wide variety of forms. Flame-like lamellae (<0.1mm) are very common and are associated with all pyrrhotite grains (Plates 3.41-3.42). Closely associated with the flame-like lamellae are 0.25-1mm rounded blebs, worm-like, and irregularly shaped granular exsolved pentlandite (Plate 3.41). Both of the latter are associated with the interiors of the pyrrhotite grains. Pentlandite also occurs along the partings of the pyrrhotite grains and along fractures in the crystals (Plates 3.41-3.43). Along these fractures, similar flame-like occurrences of pentlandite (<0.1mm) which are pseudo-orthogonal to the fracture boundaries occur (Plate 3.42); while anhedral, 0.5-1mm rims of pentlandite occur on many of the pyrrhotite grain edges (Plate 3.43). The latter form is quite common; however, complete enclosure of the pyrrhotite crystals is rare, and in most cases they are only partially enclosed (e.g. loop textures; Plate 3.43). Pentlandite is also closely associated with chalcopyrite forming 0.5-0.75mm anhedral grains intergrown with chalcopyrite forming 1-3mm trains of pentlandite and chalcopyrite (Plate 3.44); and is often found as a partial corona to the chalcopyrite grains.

Pyrite grains are in lesser abundance relative to pyrrhotite, pentlandite and chalcopyrite; however, are present in most sections. Pyrite is generally found as resorbed grains which are very anhedral and are generally found included within the pyrrhotite

grains. Furthermore, all pyrite grains are mantled by a rim of irregularly shaped chalcopyrite (Plate 3.45).

Unlike the sulphide phases, magnetite is not a ubiquitous mineral phase and ranges between 0-5% modally. When present, it occurs as 0.5-7mm grains that show well developed euhedral to subhedral octahedra which are fully and partially enclosed by the pyrrhotite (Plate 3.46). Less commonly magnetite occurs as 0.5-3mm rounded to irregular shaped grains on the edges of the pyrrhotite grains, or as 0.5-1mm isolated grains between crystals with hematite. Similar to the magnetite, silicate inclusions in the sulphides are not present in all sections and appear to be restricted to either orthopyroxene (Plate 3.47) or plagioclase. In both cases, the silicate grains often show embayed rims that appear to have been eroded by the surrouding sulphide liquid (Plate 3.47).

3.5.2 Disseminated Sulphides in Pyroxenite and Leucotroctolite

Pyroxenite and leucotroctolite hosted disseminated sulphides are by far the most common hosts to disseminated sulphide mineralization within the OKG prospect. Sulphide mineralogy is very similar to the massive sulphides consisting of pyrrhotite, chalcopyrite, pentlandite and magnetite in 0.25-4mm rounded to irregularly shaped aggregates that comprise 10-25% of the rock. Most of the grains appear to be interstitial (intercumulus) to the silicate mineral phase, while most of the sulphide phases are hosted by pyrrhotite (Plates 3.48-3.49). Pyrrhotite blebs contain 0.1-0.25mm rims of chalcopyrite which partially enclose the pyrrhotite grains; while solitary chalcopyrite blebs occur as intercumulus material between the silicate grains (Plate 3.49).

Furthermore, flame-like and blebby grains of chalcopyrite extend from the edges to the interiors of many pyrrhotite blebs.

Pentlandite occurs as blebby, irregular and flame-like lamellae within the pyrrhotite grains (Plate 3.48). The pentlandite appear to be lamellar continuations of the chalcopyrite grains or as irregular psuedo-rims to the chalcopyrite. Magnetite is present as rims on the edges of the pyrrhotite grains, as inclusions along the grain boundaries or intercumulus to the orthopyroxene grains (Plate 3.48).

Leucotroctolite hosted sulphides are very similar to the pyroxenite hosted sulphides with the exception that the sulphide grains attain a greater size in some samples (Plate 3.49). Sulphide grains range from 0.25mm up to 1cm in size and have similar sulphide/oxide-silicate relationships.

3.5.3 Disseminated Sulphides in Anorthosite

Disseminated sulphide in anorthosite are much less abundant than pyroxenite hosted sulphide and only a few samples have been observed in both drill core and surface showings. Unlike the pyroxenite hosted sulphides, the disseminated anorthosite-hosted sulphide appears to be spatially, but not genetically related to the massive sulphide mineralization. The predominance of resorbed plagioclase grains and reaction textures along plagioclase-sulphide boundaries, suggests that the sulphide liquid may have infiltrated and thermally eroded the plagioclase grain boundaries.

Similar to massive and disseminated pyroxenite sulphides, the predominant mineral phase is irregularly shaped 0.5-2mm pyrrhotite blebs. Chalcopyrite is intimately associated with the pyrrhotite blebs occurring as 0.5-1mm long by 0.5mm wide stringers

and stripes along the edges of the pyrrhotite blebs. Needle like forms of chalcopyrite are common close to the grain edges, as are coronas of chalcopyrite around subhedral, resorbed pyrite grains; the latter being restricted to pyrrhotite grain boundaries. Pentlandite occurs as flame-like lamellae and less commonly blebby exsolution; while accessory magnetite is present as 0.25-0.5mm anhedral grains

3.5.4 Paragenetic Sequence of Sulphide Minerals

From the observed textures of the massive sulphides there appears to be a distinctive high temperature, followed by successively lower temperature, sulphide-oxide mineral assemblages (Figure 3.5). The presence of well developed euhedral magnetite grains hosted within the pyrrhotite grains (e.g. Plate 3.46) infer that this oxide mineral was the highest temperature mineral associated with mineralization at the OKG prospect. Furthermore, the pseudo-sub-ophitic nature of some magnetite grains with pyrrhotite, also suggest that they may have also co-crystallized together, suggesting that pyrrhotite is the next crystallizing phase within the sulphide-oxide assemblage (Figure 3.5). This is supported by its predominant euhedral nature, and because it hosts all the other sulphide phases.

Monosulphide solid solution (pyrrhotite) and magnetite are likely the higher temperature assemblages associated with the OKG sulphides, as all pyrite, chalcopyrite and pentlandite are characterized by exsolution behaviour (Figure 3.5; Plates 3.38-3.45). It is this subsolidus behaviour that suggests that these sulphide minerals represent a lower temperature origin. The relative relationship between pyrite, chalcopyrite and pentlandite can be readily observed by the nature of intergrowth textures between these three

minerals. The resorbed nature of the pyrites, and consistent mantling by chalcopyrite suggest that the pyrite was the higher temperature phase of the low temperature assemblage, followed by chalcopyrite (Plate 3.45; Figure 3.5),. Similarly, pentlandite is generally found to partially mantle the chalcopyrite (Plates 3.39 and 3.44), suggesting that pentlandite is the lowest temperature sulphide phase in the low temperature assemblage (Figure 3.5).

From the work of Naldrett (1984b), a relative temperature scheme can be proposed for the OKG sulphide assemblages (Figure 3.5). Magnetite and pyrrhotite likely crystallized in the range of 1120°C to 1040°C, these representing the liquidus and solidus, respectively, of the monosulphide solid solution (MSS), typical of the OKG sulphide assemblage. Pyrite exsolution likely occurred at ca. 600°C, with chalcopyrite exsolution between 600-300°C, and pentlandite at temperatures less than 300°C (Figure 3.5).

3.6 Structural Geology and Contact Relationships Between Units

3.6.1 Granitoid-Anorthosite Contact Relationships and Structure of Area South of Umiakoviarusek Lake

In the region south of Umiakoviarusek Lake the outer core of rocks is marked by a group of anorthositic rocks in contact with foliated granitoids; the latter intruded by a quartz-bearing granitoid suite farther west (Figure 3.1). The anorthositic rocks of this region show only minor deformation, yet most show evidence of secondary metamorphic mineral assemblages, typically greenschist facies assemblages. Furthermore, minor compressional faulting has been observed in these rocks along their eastern boundary with Quarternary sediments (Figure 3.1). Although relatively undeformed, some areas, in

particular near mafic dykes, the anorthosites have a very distinctive bleaching and white colouration, with bright green secondary mafic mineral replacement.

In relation to the foliated granitoids, the anorthositic rocks appear to be intruded by the granitoids (cf. Ryan *et al.*, 1998), and within the granitoids there are small 30-45cm granular anorthositic fragments, as well as 2-3m and 10-25m raft like occurrences. The foliation of the granitoids in this area is very odd with both variable strikes and steepness of dip (Figure 3.6). The folations of the granitoids have shallow to moderate dips, striking northwesterly and southeasterly and are best developed along their eastern margin with the anorthositic rocks (Figures 3.1 and 3.6).

The foliation of this group of granitoids decreases in strength or is totally absent towards the western boundary with the quartz-bearing phase 2 granitoids; the latter appear to intrude the phase 1 granitoids as small plugs. An extensive study of the contact relationships and character of these second phase granitoids could not be completed because most of them lie outside of the property boundaries. However, further west of the property this unit forms a major regional ovoidal feldspar quartz monzonite intrusion (Ryan, pers. comm. 1997; Ryan *et al.*, 1998).

3.6.2 Gneiss-Granitoid-Anorthosite Relationships in the Eastern Portion of the Property

In the eastern portion of the property a linearly distributed belt of anorthositic, granitoid and gneissic rocks are present. There appears to be a well defined tectonic contact between the granitoid and gneissic rocks as both units show a well developed, coincident, steeply dipping, northwesterly to southeasterly dipping foliation (Figure 3.3); suggesting a common deformational origin. Furthermore, close to this boundary between

the granitoids and gneiss there is evidence for sinistral strike-slip faulting manifested in well developed topographic variations and development of sinistral C-S kinematic indicators in a few outcrops of forest green chloritic schist (Figure 3.3; Plate 3.50).

The relationship of anorthositic rocks to the granitoid and gneissic rocks is much more ambiguous, since the anorthositic rocks were only observed in the northeastern portion of the property. In this region the anorthositic rocks appear to be younger than the granitoids as they show no pervasive foliation and some have well developed cumulate textures. Although the anorthosite-granitoid contact was not observed by the author, the anorthosites intrude into the granitoids in this region (Ryan, pers. comm., 1997; Ryan *et al.*, 1998).

3.6.3 Faulting and Folding in the Main Zone and North-Striking Shear Zone

Well developed ductile faulting and folding are present within the Main and North Striking Shear Zones of mineralization of the OKG prospect. Within the MZ, a pervasive unit of mylonitic rocks extends from approximately 10m below the Main Showing and to at least the base of the steep cliffs north of the Main Zone (Figure 3.2). The mylonitic rocks are between 0.45-1m in width and show well developed horst and duplex-like structures which are consistent with south-southwesterly verging motion (Figures 3.2 and 3.7). This is also supported from the moderate to shallowly north-northeasterly dipping mylonitic foliation (Figure 3.7), and north-northeasterly plunging slickenside and fault step lineations. Furthermore, felsic dykes which cut the anorthositic rocks show well developed south-southwesterly verging folds, typical of fault-bend-fold relations associated with compressional motion.

In the NSSZ the mylonitic rocks are less developed and are mostly between 30-45cm in width showing similar north-northeasterly dipping foliations. A south-southwesterly verging compression, consistent with the MZ, is also observed from fault slick and step lineations in the NSSZ (Figure 3.2).

3.6.4 Contact Relationship of Mineralized Pyroxenites

The overwhelming presence of Paleoproterozoic anorthositic and granitoid rocks within the OKG prospect and surrounding area suggests that the potential for pyroxenite-leucotroctolite related mineralization to be of Paleoproterozoic origin is probable (cf. Ryan *et al.*, 1998). An unequivocal answer to this problem is not easily discerned; however, a number of arguments can be put forth, based on primarily field and petrographic observations, that argue against a Paleoproterozoic origin.

Considering first the surface pyroxenites (Type 1 dykes) and leucotroctolites (Type 2 dykes). As illustrated on Figure 3.2 all of the mineralized pyroxenitic rocks lie in proximity to either ductile (mylonitic) faulting or zones of shearing. Closely associated with these shear zones is widespread secondary replacement of the igneous mineralogy of the wall rock anorthositic material with greenschist facies assemblages (see sections 3.2.2.2 and 3.3.2.2). In contrast, all of the mineralized dykes retain primary, pristine igneous mineralogy and do not exhibit secondary metamorphic mineral assemblages.

In subsurface drill core, Kerr (1998) noted that widespread shearing, locally mylonitic, is commonly associated with felsic and mafic dykes of likely Paleoproterozoic age. However, in contrast, none of the pyroxenitic dykes in drill core of this study have

shearing associated with their margins, and this is consistent with the interpretations of Kerr (1998). Furthermore, subsurface pyroxenite dykes have pristine igneous textures and do not exhibit secondary metamorphic mineral assemblages typically associated with the bounding anorthositic rocks.

Based on the above arguments it is likely that the dykes at the OKG are of Mesoproterozoic age. For instance, the close spatial association of the surface mineralized dykes with faulting without evidence for metamorphism or deformation suggests that they likely post-date Torngat Orogen deformation and metamorphism. Likewise, the lack of deformation associated with the pyroxenite dykes in drill core that is common to Paleoproterozoic age felsic and mafic dykes, coupled with the retention of primary igneous mineralogy and textures also suggests that they have not been influenced by the Torngat Orogen and are likely Mesoproterozoic in age. Geochronological dating is required to prove or disprove this hypothesis.

3.6.5 Paleoproterozoic or Mesoproterozoic Granitoids and Anorthosites?

Traditionally, massif-type anorthosite-granitoid suites have been assigned and interpreted to be temporally restricted to the Mesoproterozoic (e.g. Emslie, 1978, 1980; Ashwal, 1993). However, recent work by Ryan *et al.* (1997, 1998), Hamilton (1997), and Hamilton *et al.* (1998) provide good evidence for AMCG magmatism occurring during the Paleoproterozoic, in the region of north-central Labrador; the anorthositic and granitoid rocks of the OKG have been placed within this Paleoproterozoic grouping (cf. Ryan *et al.*, 1998). This section discusses the plausibility of this subdivision and the

authors interpretation of the Paleoproterozoic or Mesoproterozoic origin for the anorthositic and granitoid rocks of the OKG prospect.

The presence of Paleoproterozoic granitoids in north-central Labrador has been readily documented in the last few years, particularly within the Nain Province of north-central Labrador (e.g. Emslie and Loveridge, 1992; Ryan and Connelly, 1996; Ryan *et al.*, 1997, 1998; Hamilton, 1997; Hamilton *et al.*, 1998). The granitoid rocks of the OKG prospect are most likely, if not certainly, of Paleoproterozoic age based on several lines of evidence. Firstly, considering the relationship between the gneisses and granitoids in the eastern portion of the property. The overwhelming consistency in foliation strike and sinistral strike slip faulting between the granitoids and gneisses suggests a common deformation origin, and the only natural event that could explain this deformation would be deformation associated with the Torngat Orogen (cf. Wardle *et al.*, 1990a; Van Kranendonk and Ermanovics, 1990; Van Kranendonk and Wardle, 1994, 1997; Van Kranendonk, 1996). Likewise, secondary greenschist facies assemblages and recrystallization associated with the dykes requires a deformational origin, likely linked above. Furthermore, further south of the Umiakoviarusek Lake region, the regional extension of this granitoid unit has yielded a U-Pb zircon age of ca. 2124 Ma, confirming the Paleoproterozoic origin (Hamilton *et al.*, 1998).

The granitoids south of Umiakoviarusek Lake are somewhat more problematic because of their inconsistent foliations, and lack thereof towards the west. Even though the foliations are inconsistent, they exhibit similar recrystallization to the granitoids of the eastern sector; suggesting they have underwent a similar deformation/metamorphic

event. The age of the second phase granitoids in this region cannot be commented on because only minor examinations of these rocks have been undertaken; thus, they may or may not be Paleoproterozoic in age, but a Paleoproterozoic age has been suggested by Ryan *et al.* (1998).

The anorthositic rocks of the property are much more problematic than the granitoids because they do not show readily developed foliations or pervasive metamorphic grade. Regardless, complete replacement of primary mafic minerals with secondary greenschist assemblages, coupled with sericite and epidote dustings on much of the plagioclase of these units, attests to the effects of a regional metamorphic / deformation origin.

Ryan *et al.* (1997,1998) advocate the use of metamorphic grade and orientation of mafic dykes to define a Paleoproterozoic origin for the anorthositic rocks of north-central Labrador. They suggest that the amphibolite and greenschist facies assemblages of some of the mafic dykes in this region are consistent with those of the Paleoproterozoic Kikkertervak and Napaktok dyke swarms (cf. Ermanovics and Ryan, 1990; Ryan, 1990b; Cadman *et al.*, 1993). Mafic dykes from the OKG do not have a consistent orientation, nor do they exhibit well developed shearing or deformation; however, all are characterized by low grade greenschist facies assemblages typically associated with regional deformation and metamorphism.

The most compelling argument for a Paleoproterozoic origin for the anorthositic rocks comes from the Main Showing region. In this area well developed ductile shearing and mylonite zones attest to some regional scale deformation event to explain their

occurrence. No such event occurs in post-NPS time and suggests that the most logical orogenic event to explain these foliations would be the Torngat Orogen, and suggest a pre-Torngat, Paleoproterozoic origin for the anorthositic rocks.

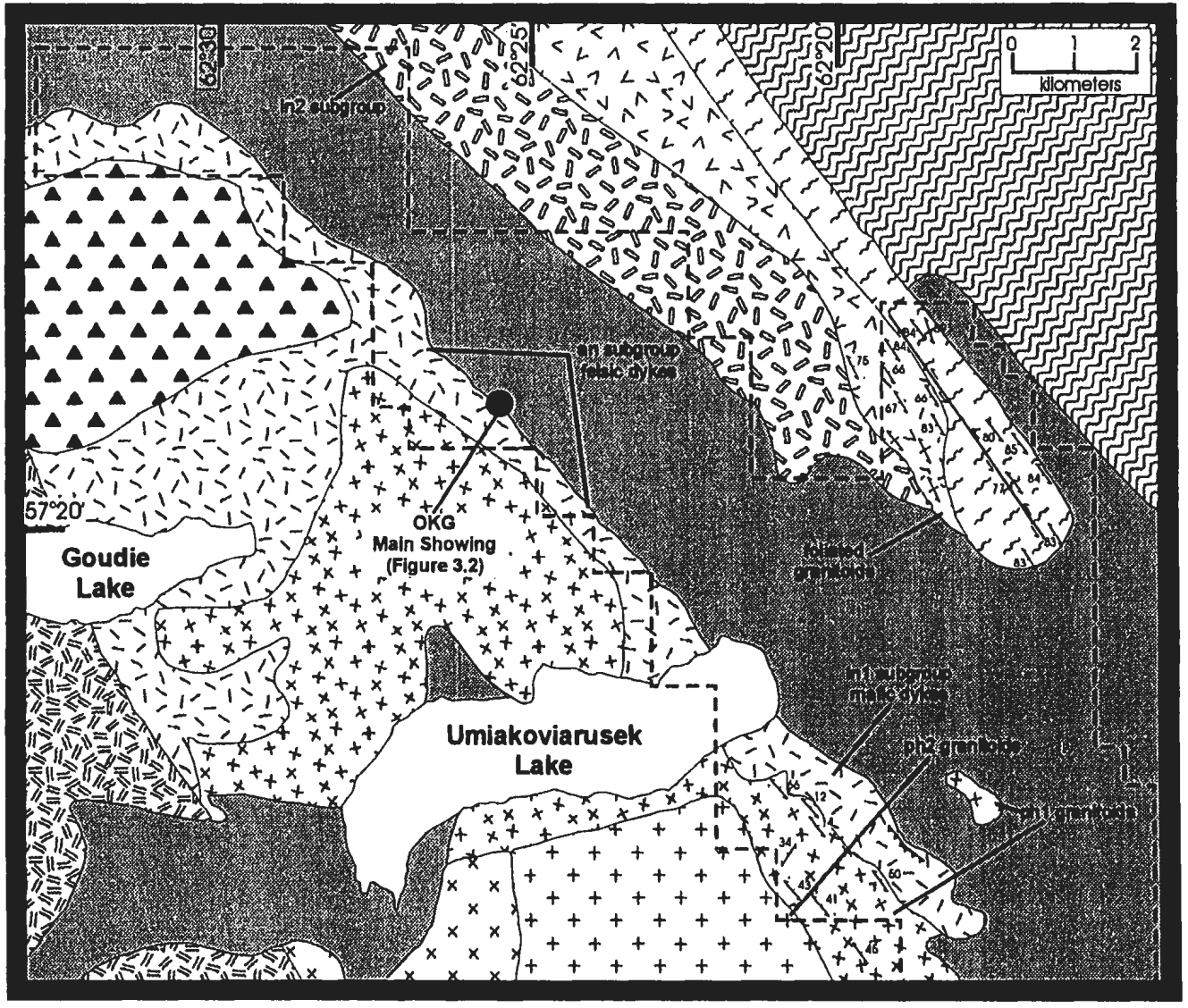

Figure 3.1. Geology of the OKG prospect with location of lithogeochemical groups outlined in chapter 4. Geology outside of property boundaries from Ryan et al. (1997, 1998) and Emslie et al. (1997).

Legend

Quaternary

Overburden and glacial drift

Paleoproterozoic

Granitoid Plutons

Hornblende granite

Quartz monzonites, ovoidal feldspar clinopyroxene quartz monzonite (phase 2 granitoids)

Variably foliated orthopyroxene, fayalite, clinopyroxene, hornblende, biotite-bearing monzonites, syenites (phase 1 granitoids)

Foliated orthopyroxene, fayalite, clinopyroxene, biotite bearing quartz syenites, monzonite, granite

Anorthositic Plutons

Dark grey and black anorthosite

Buff, olivine-bearing leuconorite

Dark black to light grey anorthosite and leuconorite (contains *an* and *ln1* subgroups)

Buff weathering leuconorite and gabbronorite (*ln2* subgroup)

Archean

Amphibolite, mafic granulite, metatonalite, quartzofeldspathic gneiss

Quartzofeldspathic gneiss

Symbols

- Foliation or gneissosity, inclined
- Foliation or gneissosity, vertical
- Compressional fault
- Sinistral strike-slip fault
- Claim boundary

Figure 3.1. (Continued)

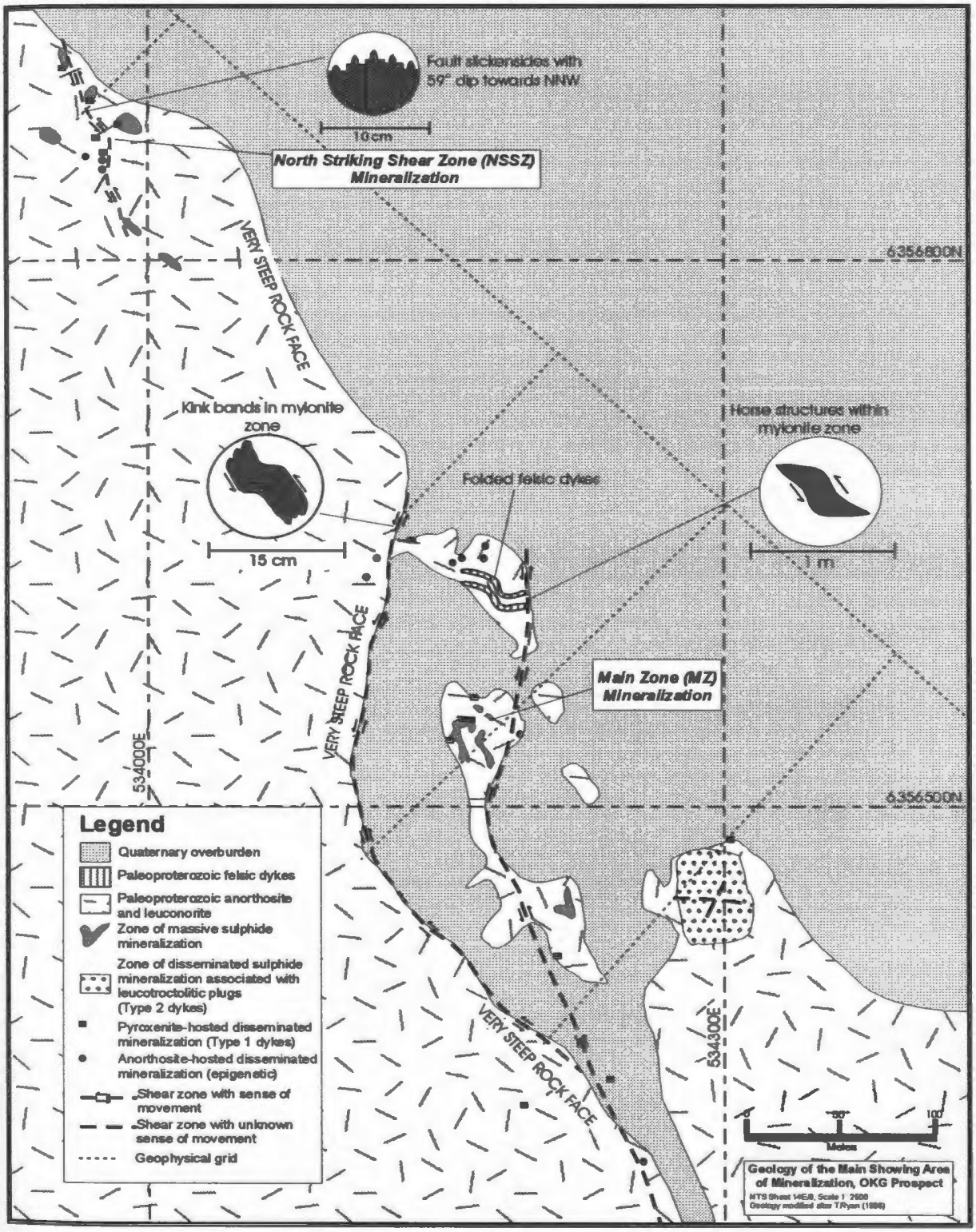

Figure 3.2. Geology of the Main Showing area and related mineralization, additional information from T.Ryan (1996).

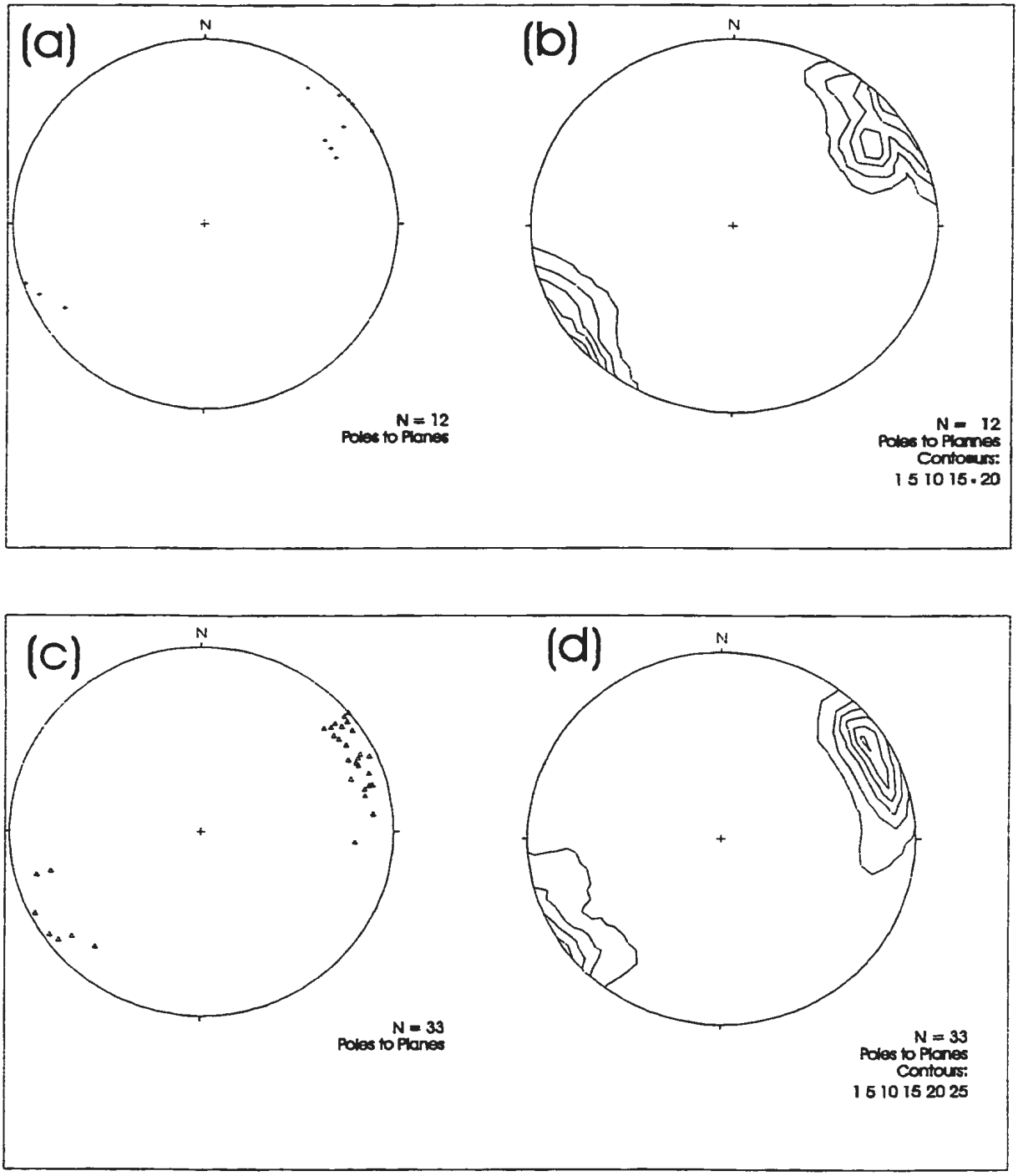

Figure 3.3. Stereoplots and contoured stereoplots of poles to planes of foliation in the foliated granitoids, (a) and (b), and for the Nain Province gneisses, (c) and (d). The close similarity between the distributions of both plots suggest a common deformational origin.

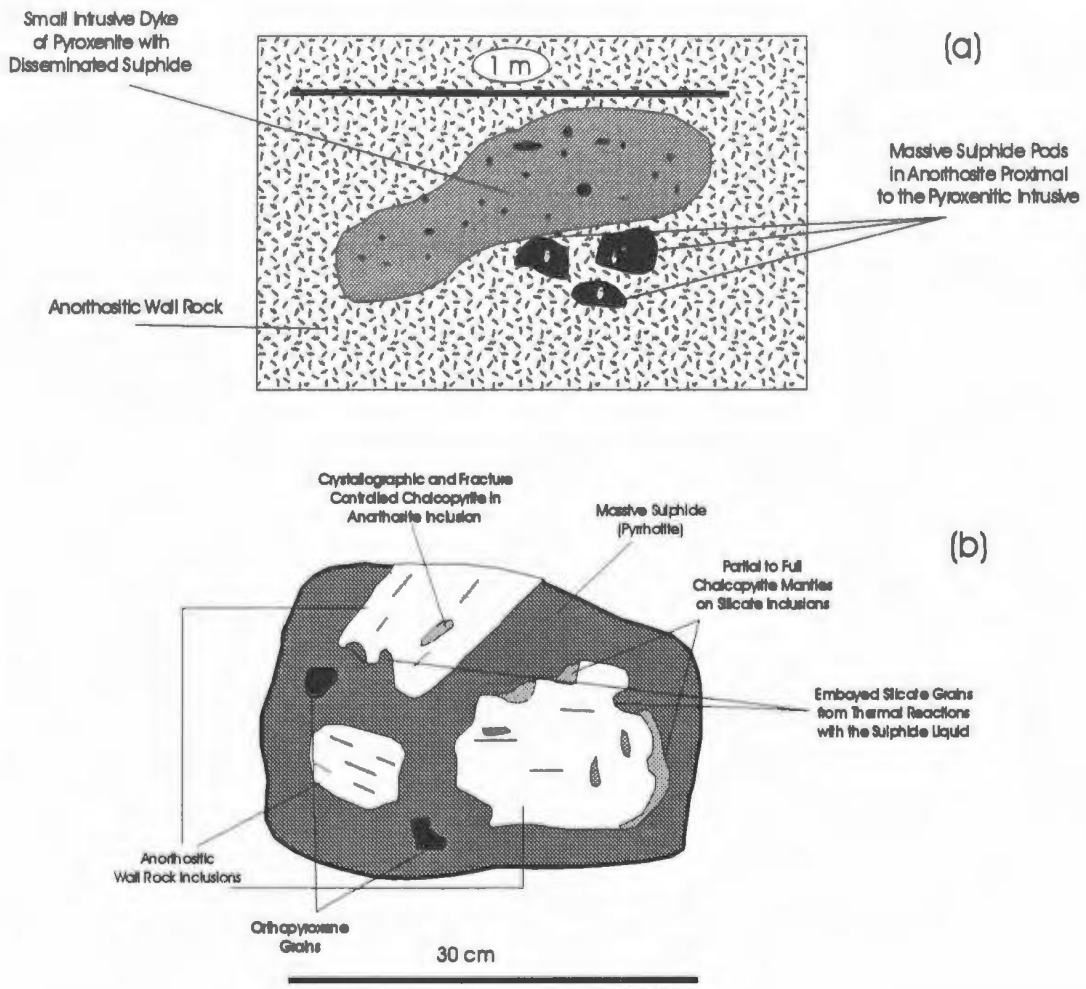

Figure 3.4. Schematic of typical pyroxenite-anorthosite-sulphide relationship from the Main Showing Region (a), typical silicate inclusion-massive sulphide relationships associated with the surface mineralization (b), and a schematic of typical pyroxenite-sulphide-anorthosite relationship from drill core intersections (c) (cf. Wilton and Baker, 1996; Kerr, 1998).

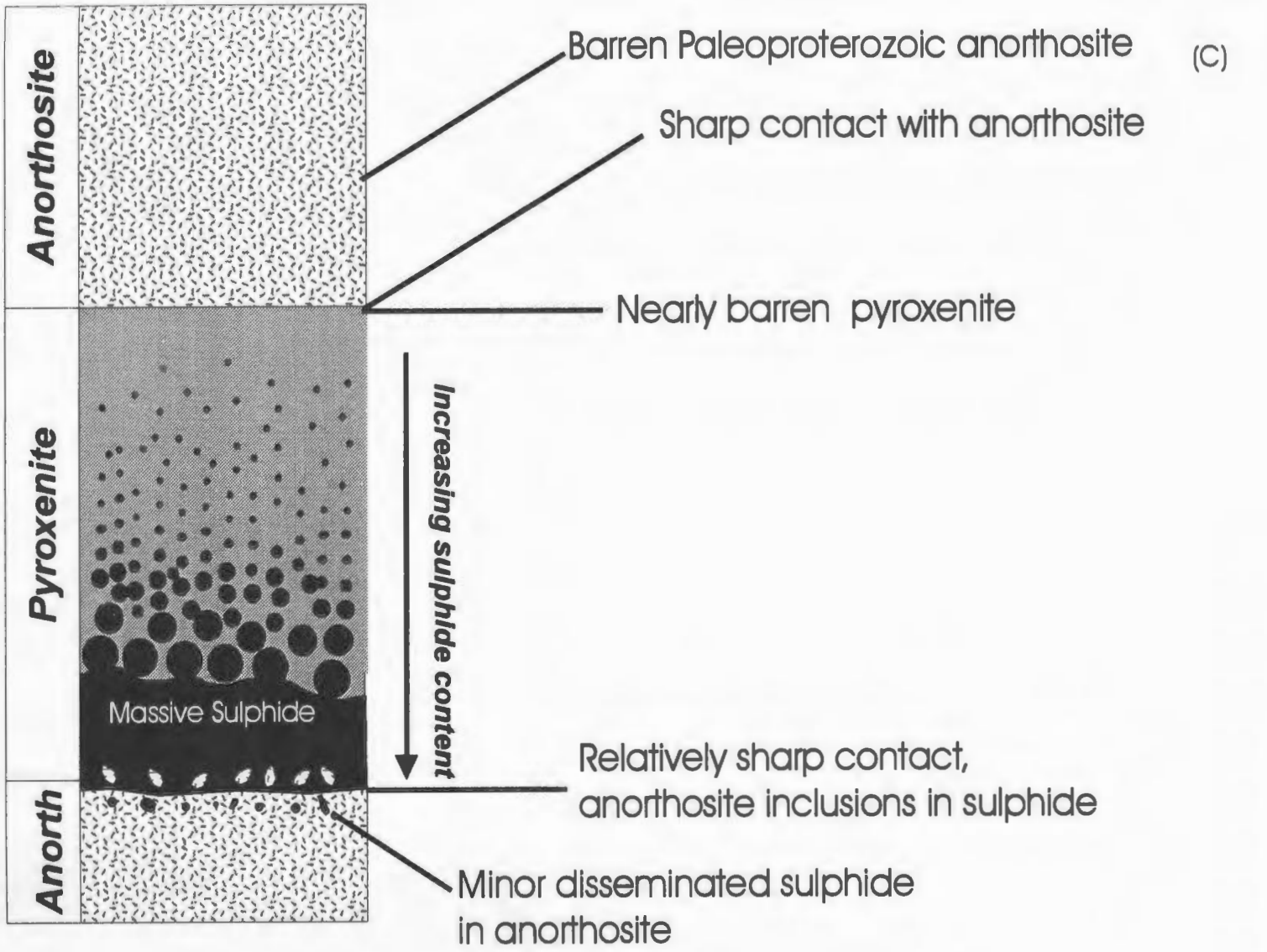

Figure 3.4. (continued)

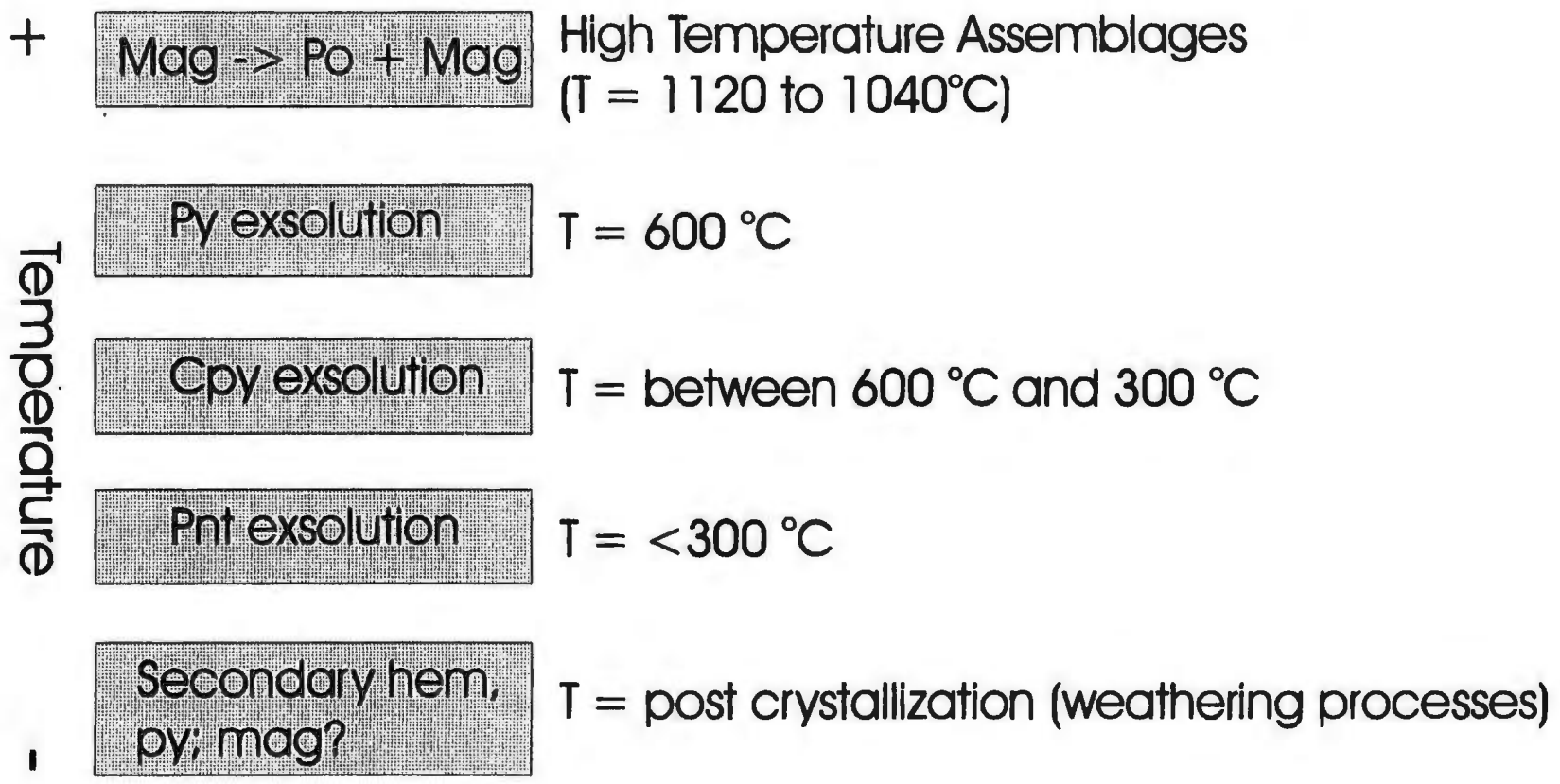

Figure 3.5. Schematic paragenetic sequence for the sulphide-oxide assemblages within the massive and disseminated sulphides of the OKG prospect. Approximate temperatures of formation are from Naldrett (1984a).

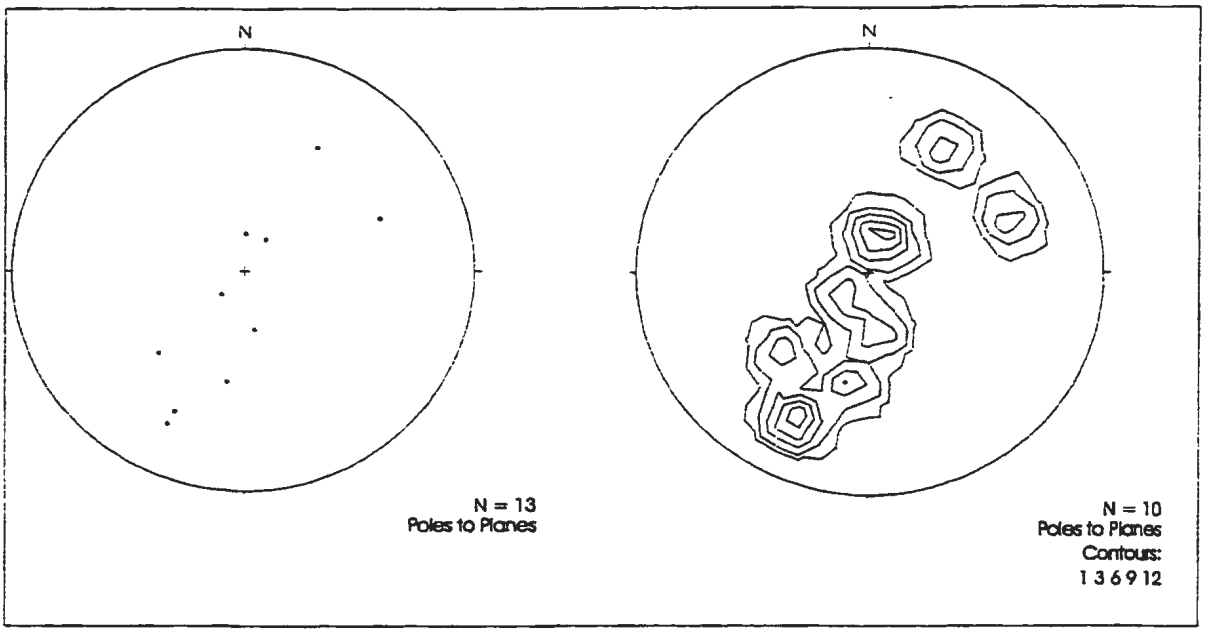

Figure 3.6. Stereplot (a) and countoured stereoplot (b) of poles to planes of foliations within the phase 1 granitoid rocks south of Umiakoviarusek Lake.

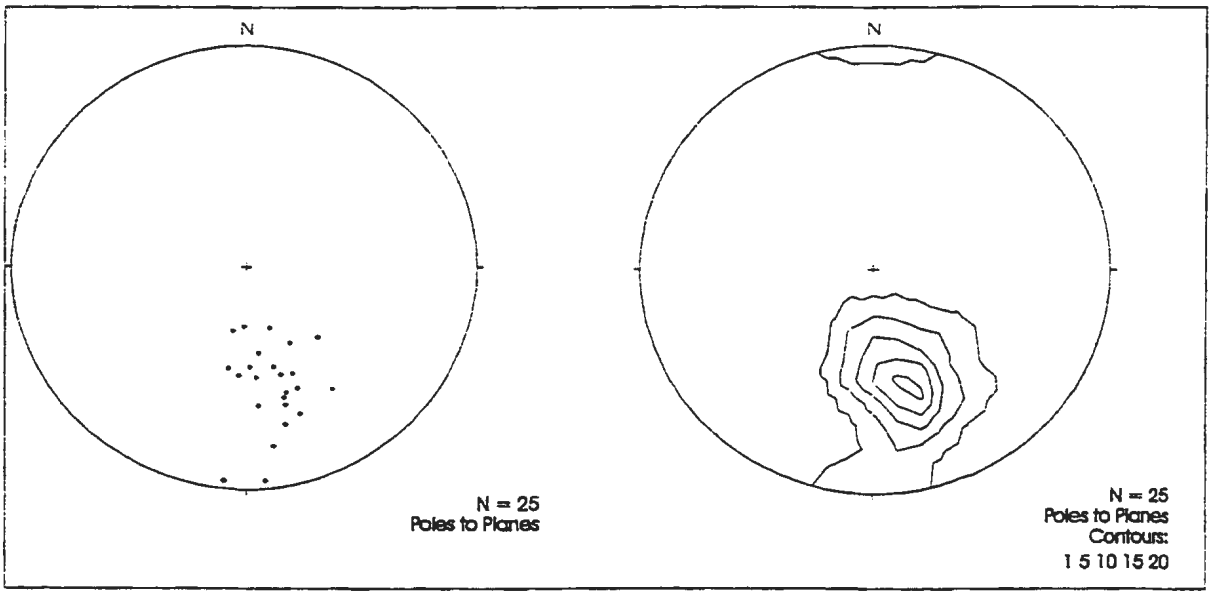

Figure 3.7. Stereplot (a) and countoured stereoplot (b) of poles to planes of mylonitic foliations observed within ductile shear zones of the Main Showing region.

Plate 3.1. Intercalated and interlayered mafic granulitic-amphibolitic and metatonalitic gneiss of the Nain Province.

Plate 3.2. Localized meter scale isoclinal folding associated with mafic granulite and amphibolite

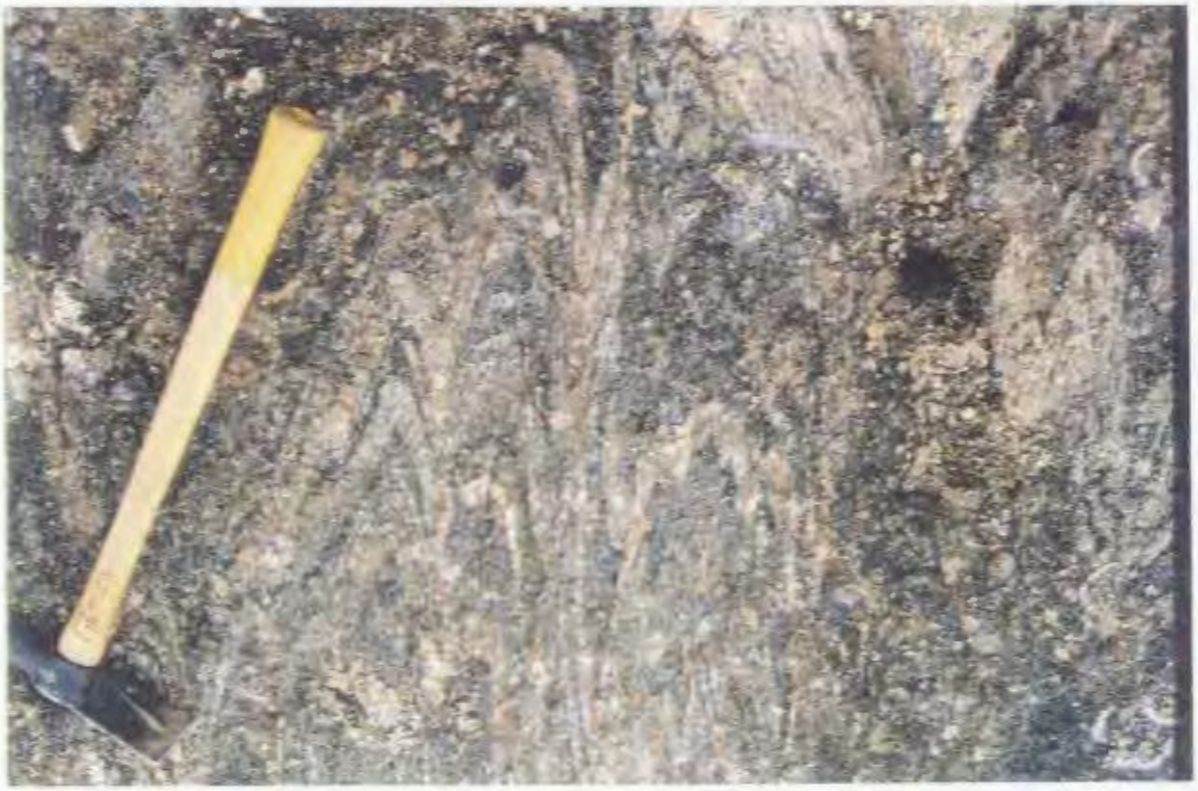

Plate 3.3. Well foliated phase 1 hornblende-orthopyroxene-biotite bearing granitoids that outcrop south of Umiakoviarusek Lake.

Plate 3.4. Unfoliated hornblende and quartz-bearing monzonites, typical of the phase 2 granitoid intrusives south of Umiakoviarusek Lake.


PENTAX

Plate 3.5. Typical outcropping of dark grey to medium grey coloured anorthositic rocks, typical of the Main Showing region and the region north of Umiakoviarusek Lake. Looking closely at the picture, well pronounced folding of felsic dykes is common, and is associated with ductile shearing located at the leftmost portion of the outcrop shown in the photo.

Plate 3.6. Straight walled mafic dyke intruding anorthositic rocks, typical of those located south of Umiakoviarusek Lake region.


Piercey
NCI

Plate 3.7. Mafic dyke intruding anorthositic rocks south of Umiakoviarusek Lake. This dyke exhibits well developed tentacle-like terminations, while the surrouding anorthositic rocks exhibit a distinctive bleaching.

Plate 3.8. Straight walled mafic dyke intruding anorthositic rocks exhibiting ball-like masses disassociated from the dykes proper, within the anorthositic host.


PENTAX

Plate 3.9 Well developed mylonitic foliation and ductile shearing associated with compressional faulting within the Main Zone mineralization.

Plate 3.10. Mafic granulite of the Nain Province gneisses with an assemblage of hornblende, biotite, orthopyroxene (slight pinkish hue), clinopyroxene (similar relief but no pinkish hue), and plagioclase (low relief clear grains; magnification = 2.5x, cross-polarized light).

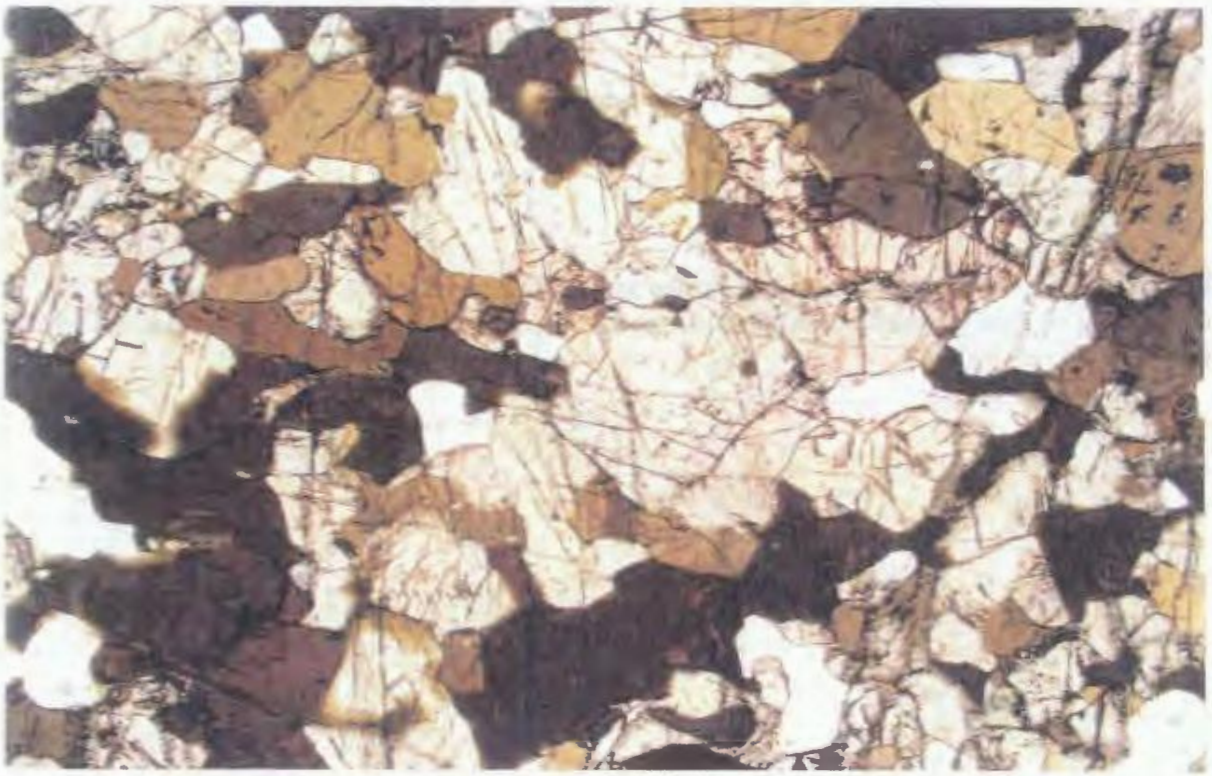

Plate 3.11. Amphibolite from the Nain Province gneisses exhibiting symplectic intergrowths of plagioclase and hornblende, along with minor red-orange biotite (magnification = 2.5x, plane polarized light)

Plate 3.12. Lower grade, greenshist facies assemblage within the mafic granulites, consisting of fine grained sericite, chlorite, carbonate and quartz (magnification = 10x, cross polarized light).

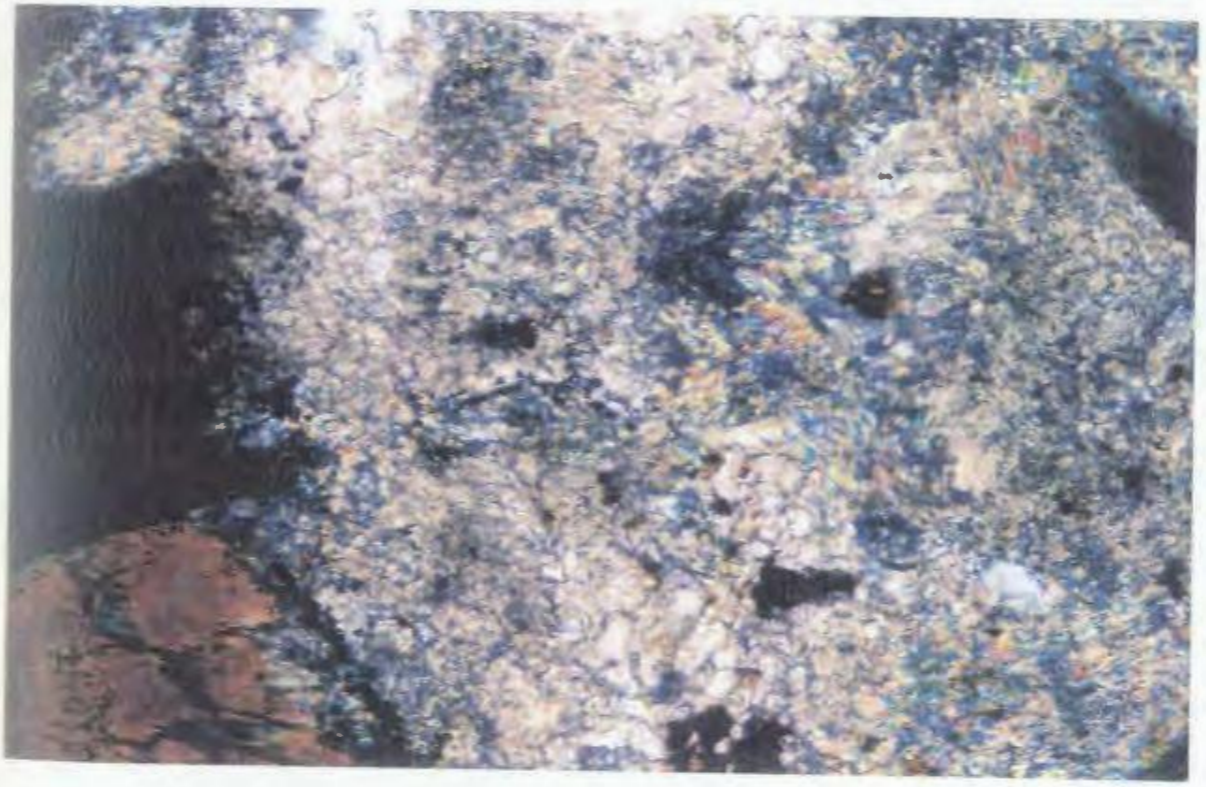

Plate 3.13. Metatonalitic to quartzofeldspathic gneiss of the Nain Province gneisses containing a central portion of low relief and relatively unaltered quartz, low relief and altered feldspar, and greenish hornblende, and high relief, cracked grains of orthopyroxene (magnification = 2.5x, plane polarized light).

Plate 3.14. Phase 1 monzonite with recrystallized feldspars (white) and a variety of mafic minerals, including cracked, pink grains of fayalite; forest green to light brown orthopyroxene forming cores with coronitic overgrowths of dark green hornblende, and overgrowths of brown biotite (magnification = 2.5x, cross polarized light).

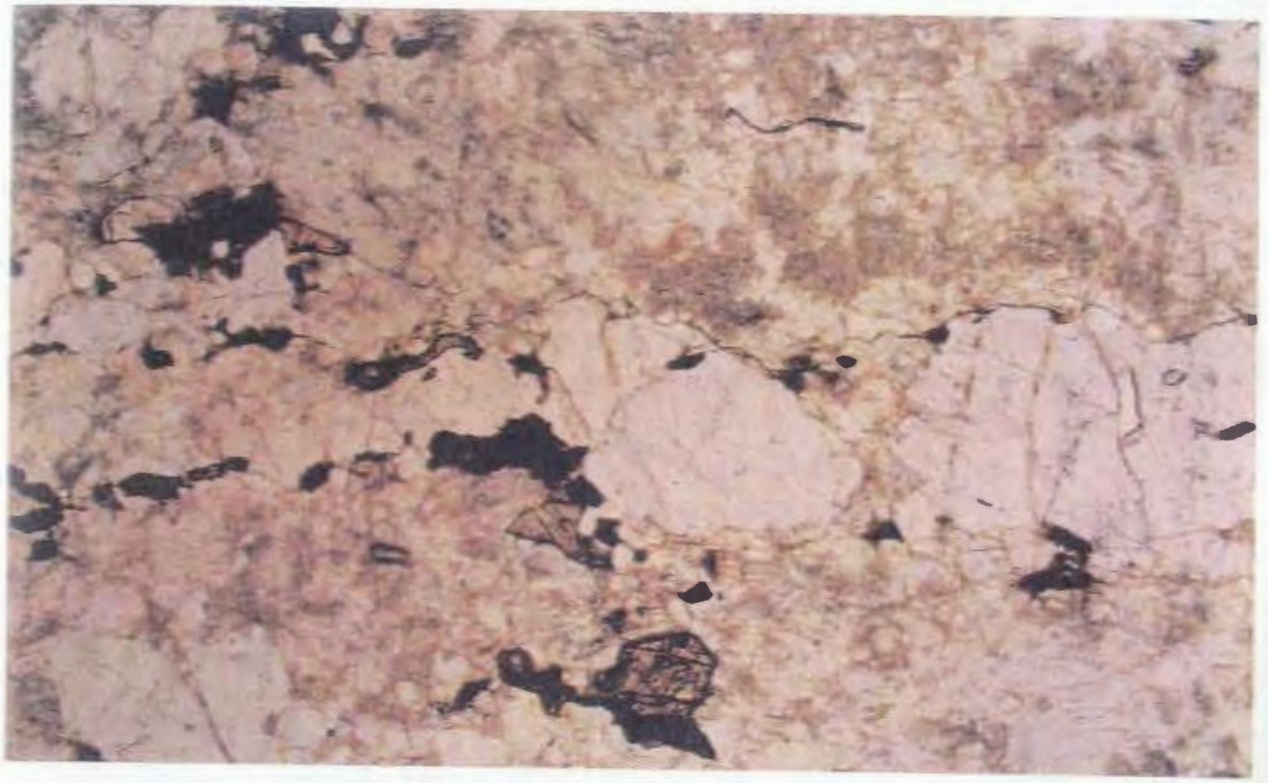

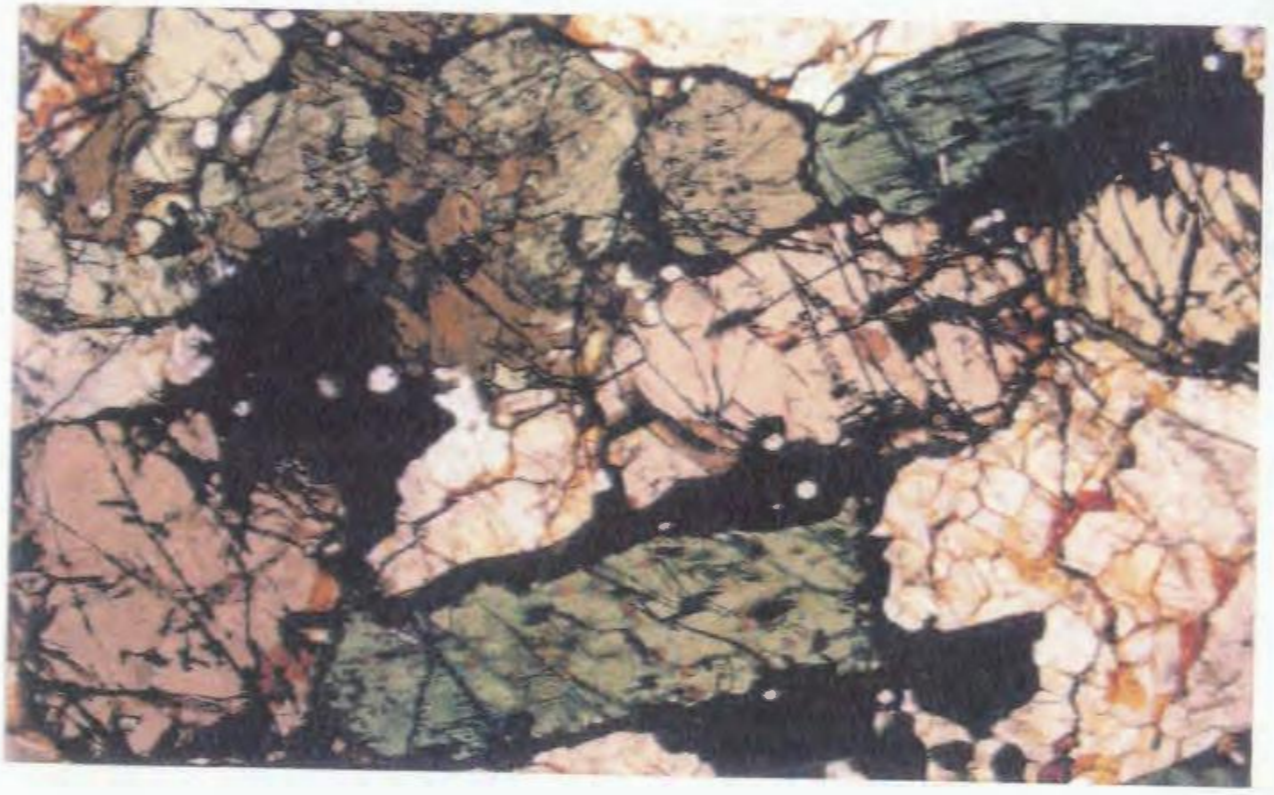

Plate 3.15. Recrystallized plagioclase and perthite, with coronitic overgrowths of hornblende enclosing a core of orthopyoxene, within a typical phase 1 monzonite (magnification = 2.5x, cross polarized light).

Plate 3.16. Typical foliated fayalite-orthopyroxene bearing monzonite associated with the foliated granitoids in the eastern portion of the property.

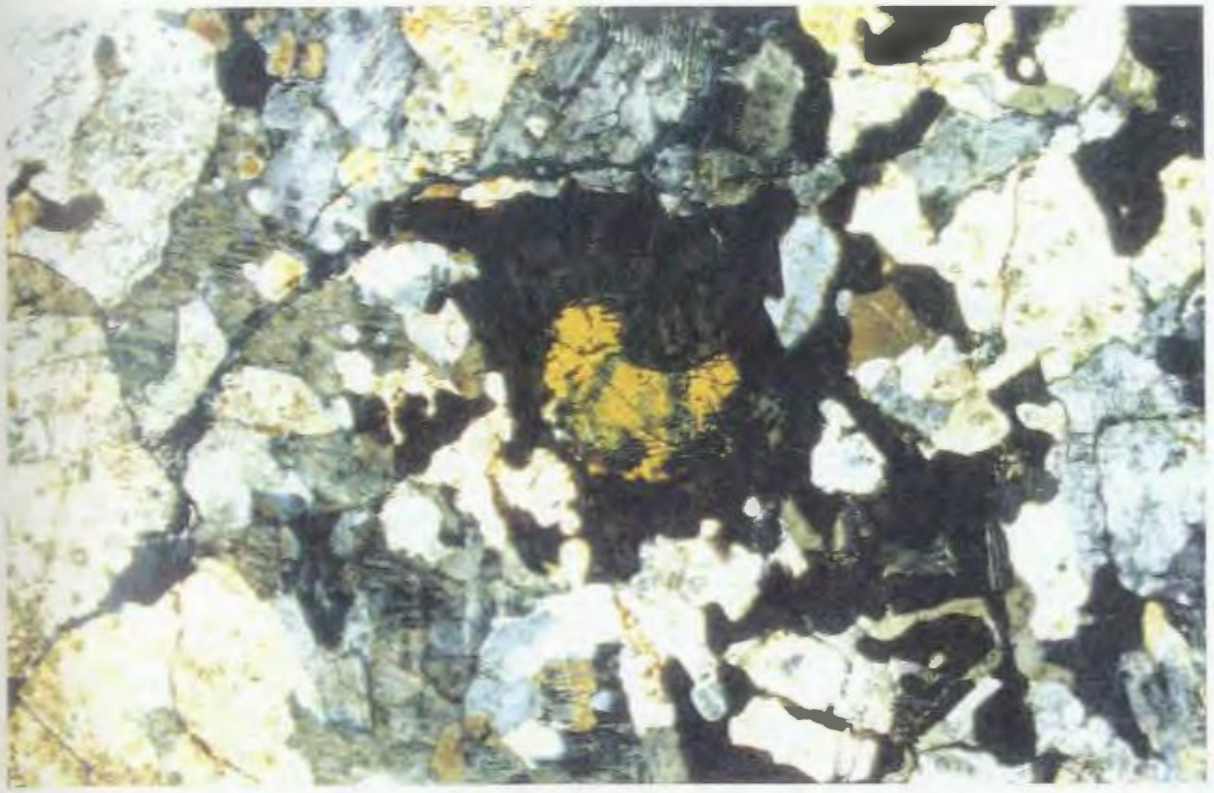

Plate 3.17. Plagioclase, microclinic K-feldspar, and quartz within a fayalite-orthopyroxene bearing granite from the foliated granitoids (magnification = 2.5x, cross polarized light).

Plate 3.18. Perthitic K-feldspar, minor sericite and well developed recrystallized quartz within felsic dykes associated with the Main Zone of mineralization (magnification = 2.5x, cross polarized light).

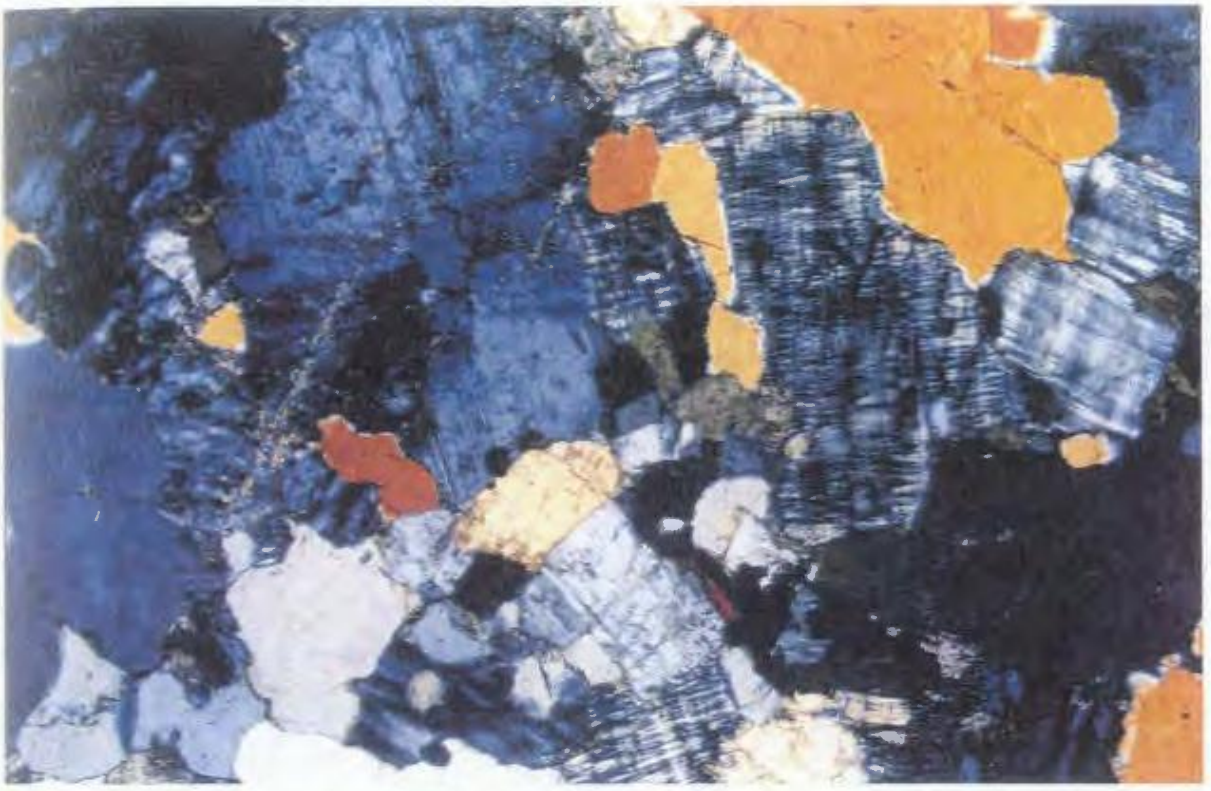

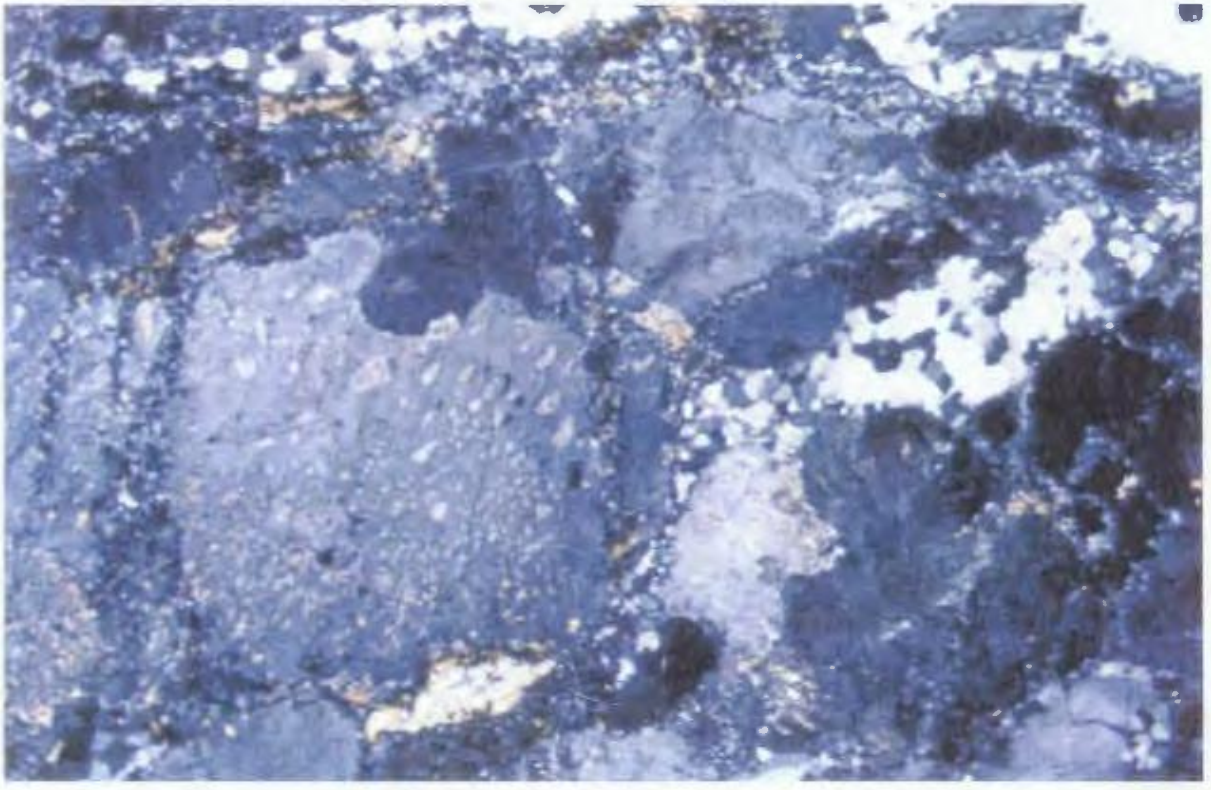

Plate 3.19. Fresh cumulus plagioclase associated with anorthosite from north of Umiakoviarusek Lake (magnification 2.5x, cross polarized light).

Plate 3.20. Plagioclase in anorthosite with dustings of sericite and epidote (magnification = 2.5x, cross polarized light).

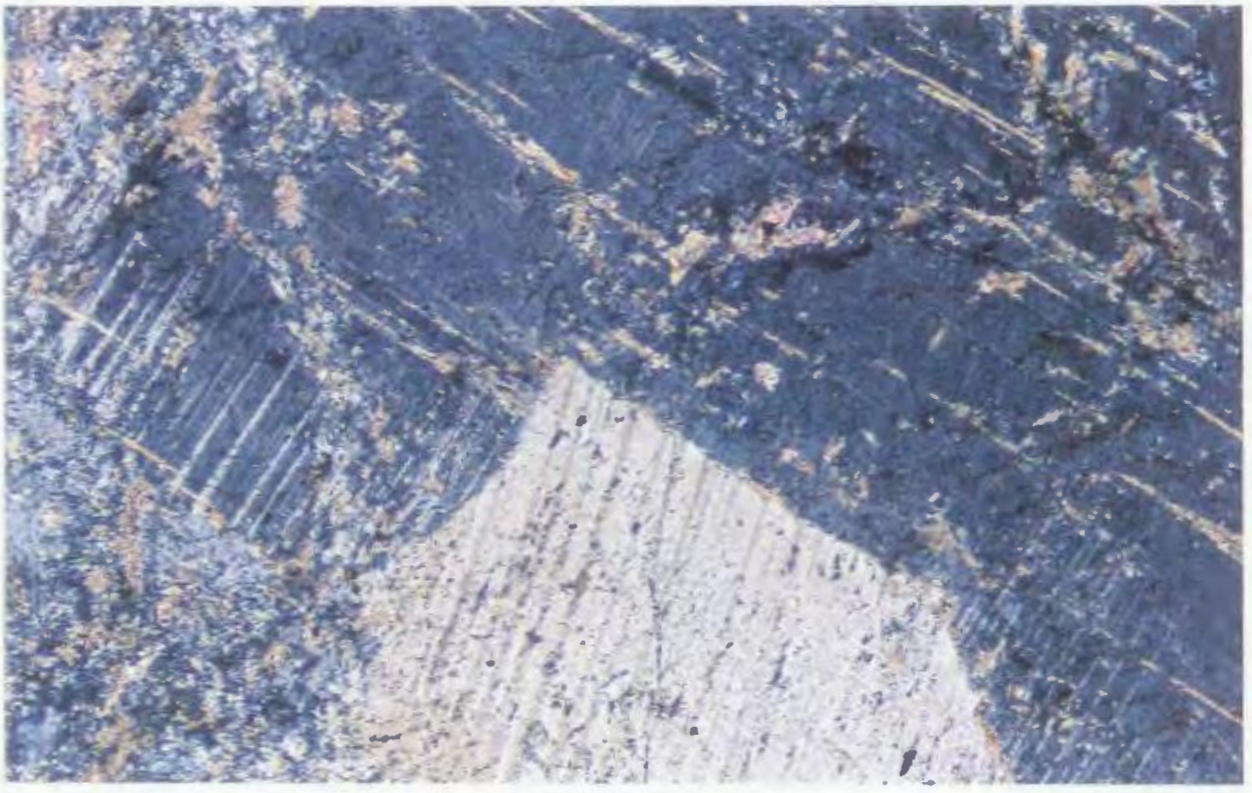

Plate 3.21. Total replacement of pyroxene by secondary actinolite and chlorite within leuconorite, south of Umiakoviarusek Lake (magnification = 2.5x, plane polarized light)

Plate 3.22. Quartz-calcite-dolomite veinlet with associated sericite located on the edges of the veinlet, within leuconorite south of Umiakoviarusek Lake region (magnification = 10x, cross polarized light).

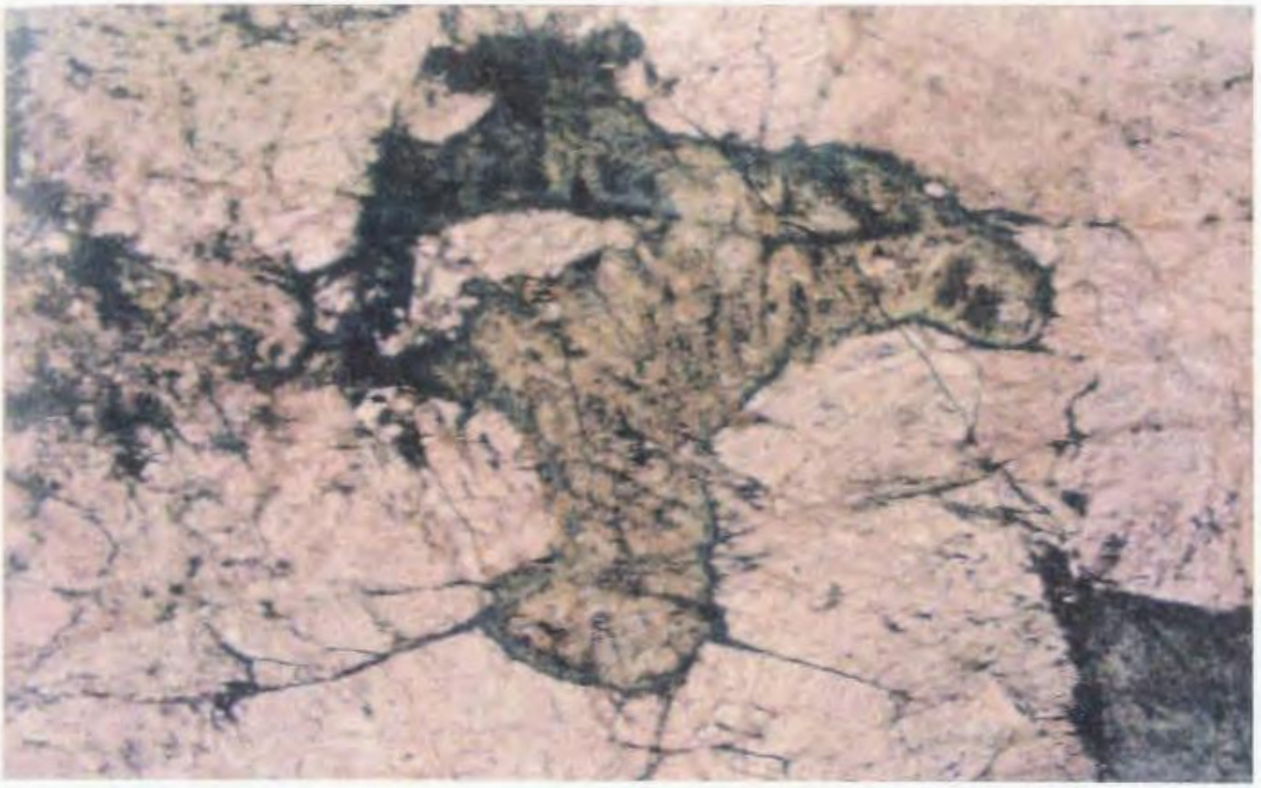

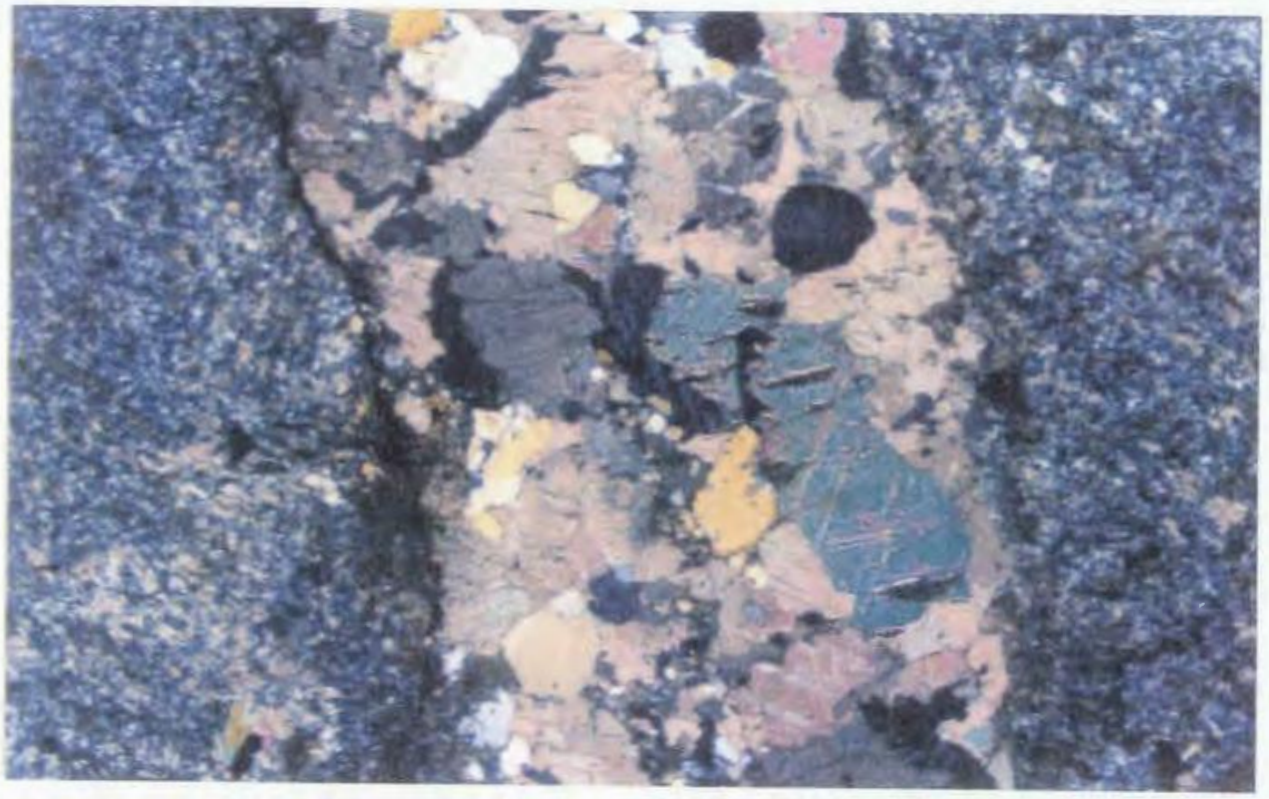

Plate 3.23. Pristine leuconorite from south of Umiakoviarusek Lake, containing cumulus plagioclase, and subhedral, intercumulus orthopyroxene with exsolved needles of rutile and lesser clinopyroxene (magnification = 2.5x, cross polarized light).

Plate 3.24. Buff weathering leuconorite from the northeastern terminus of the property consisting of subhedral plagioclase, inverted pigeonite and intercumulus oxides (magnification = 2.5x, cross polarized light).

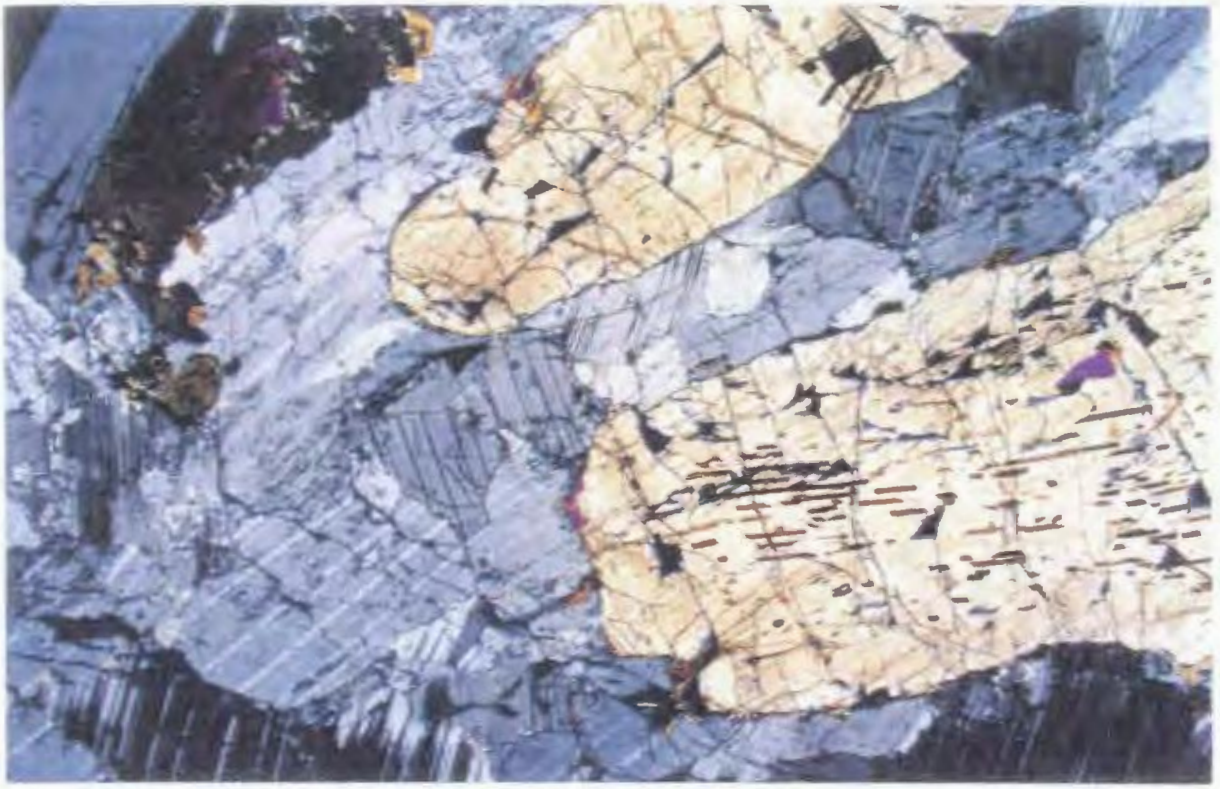

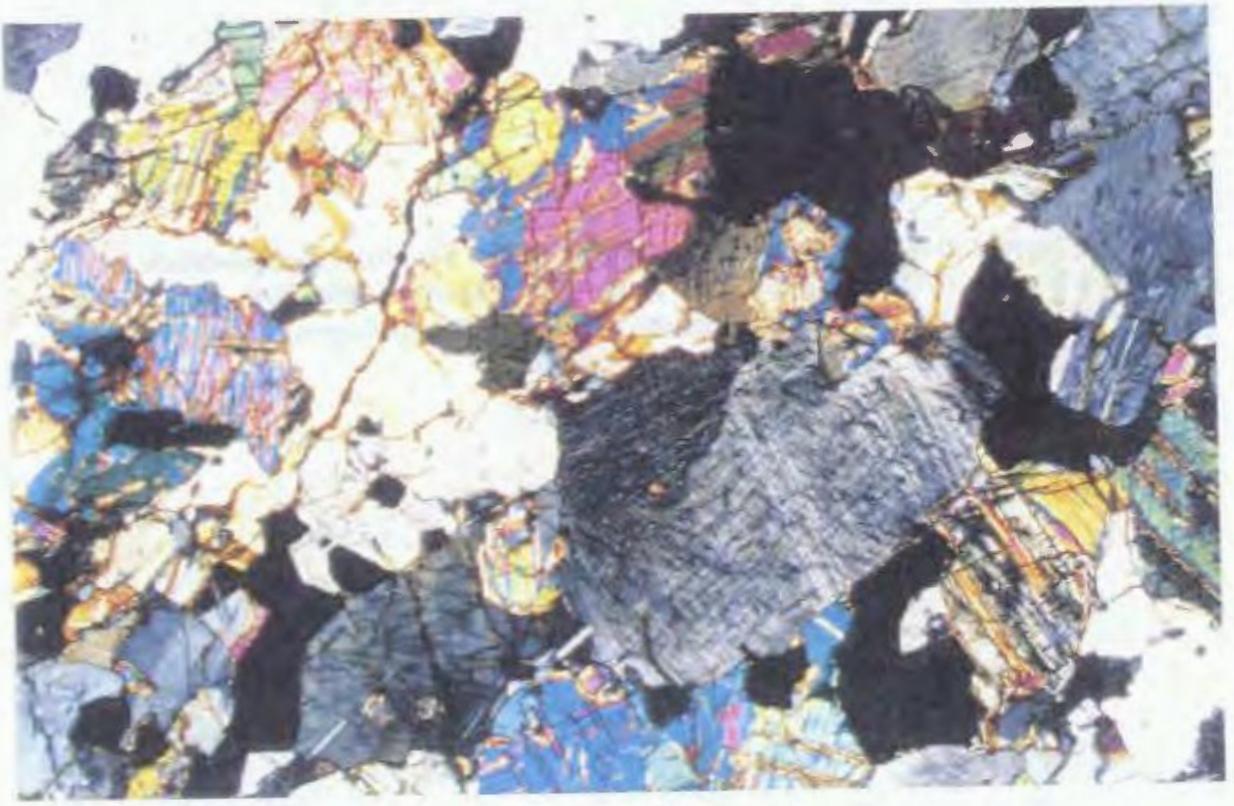

Plate 3.25. Intercumulus inverted pigeonite associated with buff weathering anorthositic rocks in the northeastern terminus of the property (magnification = 10x, cross polarized light).

Plate 3.26. Needle to lath-like plagioclase grains within a matrix of green-black mafic material in a mafic dyke typical of those south of Umiakoviarusek Lake. The distinctive green coloration is the characteristic greenschist facies assemblage associated with the dykes (magnification = 10x, cross polarized light).

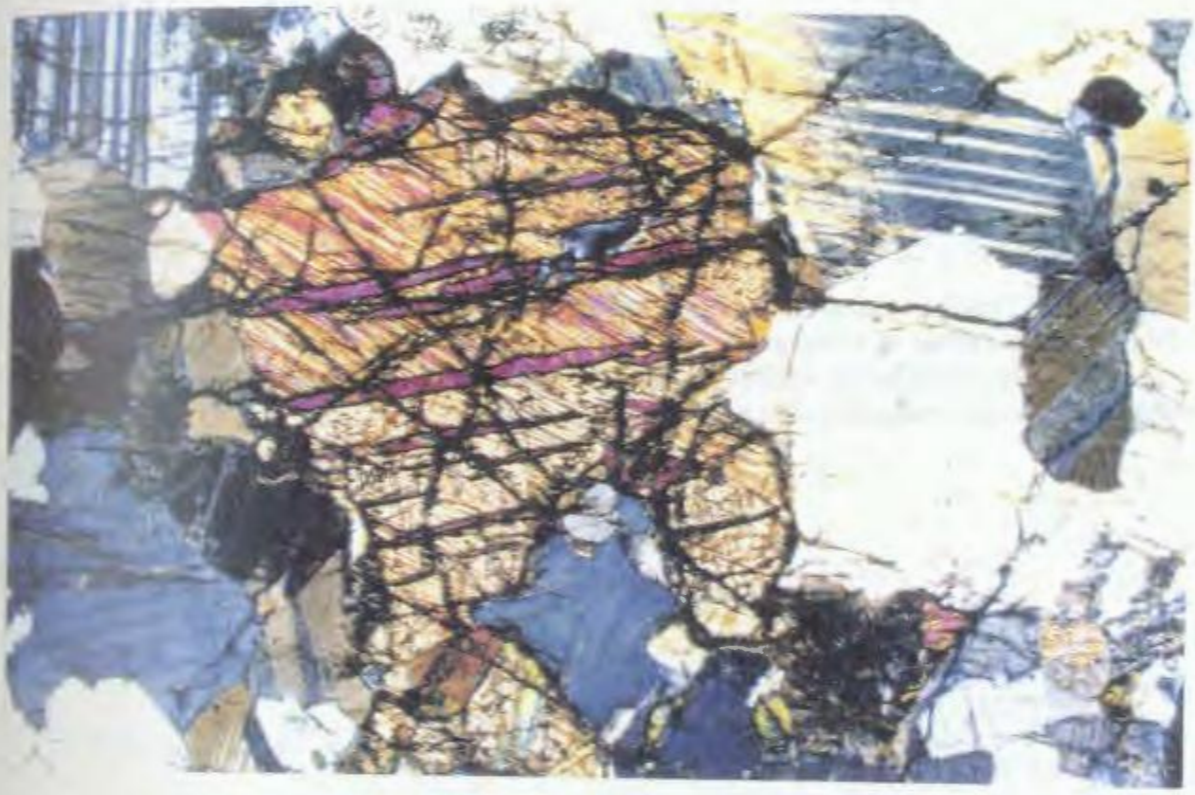

Plate 3.27. Typical quartz-chlorite-sericite assemblage within a well foliated mylonite from the Main Zone of mineralization. Distinct quartz porphyroblasts show a wrapping by muscovite and chlorite; while quartz within the fabric shoes well developed recrystallization (magnification = 10x, cross polarized light).

Plate 3.28. Typical Type 1 orthopyroxenite containing euhedral orthopyroxene and intercumulus sulphide mineralization (black; magnification = 2.5x, plain polarized light).

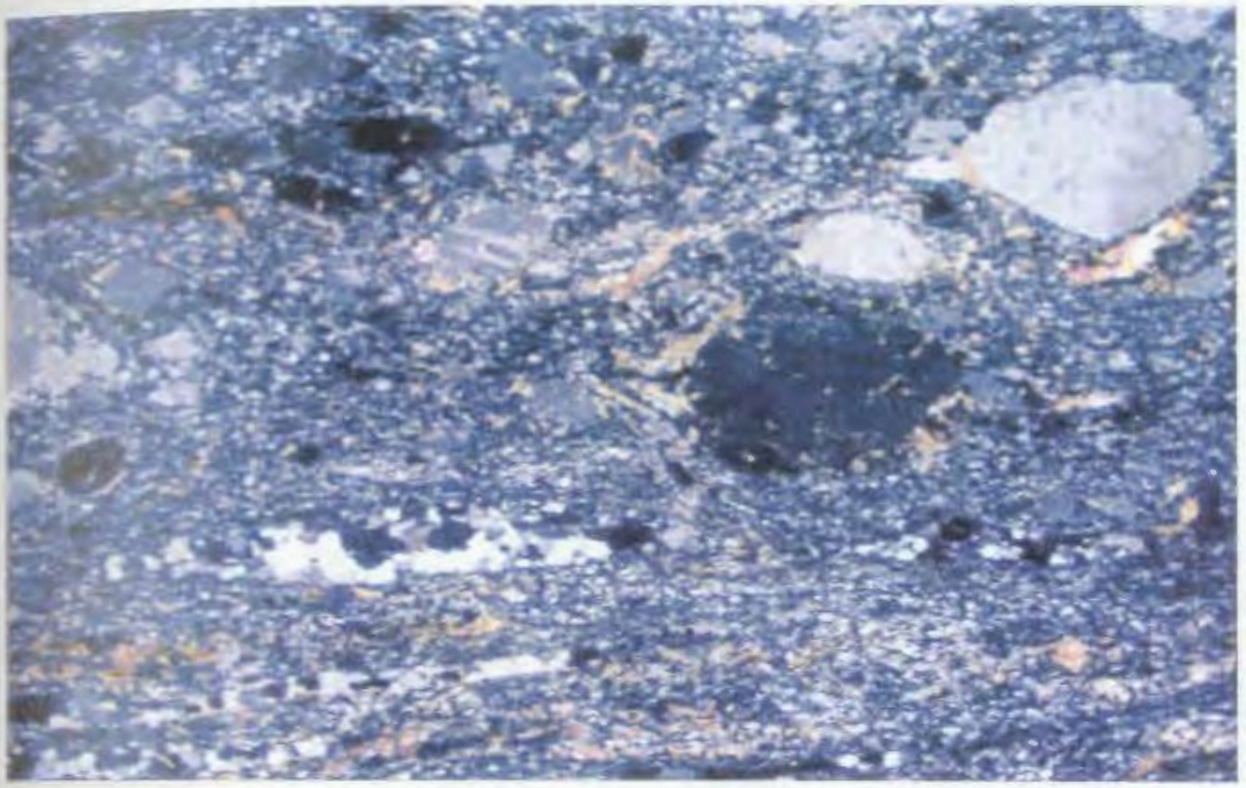

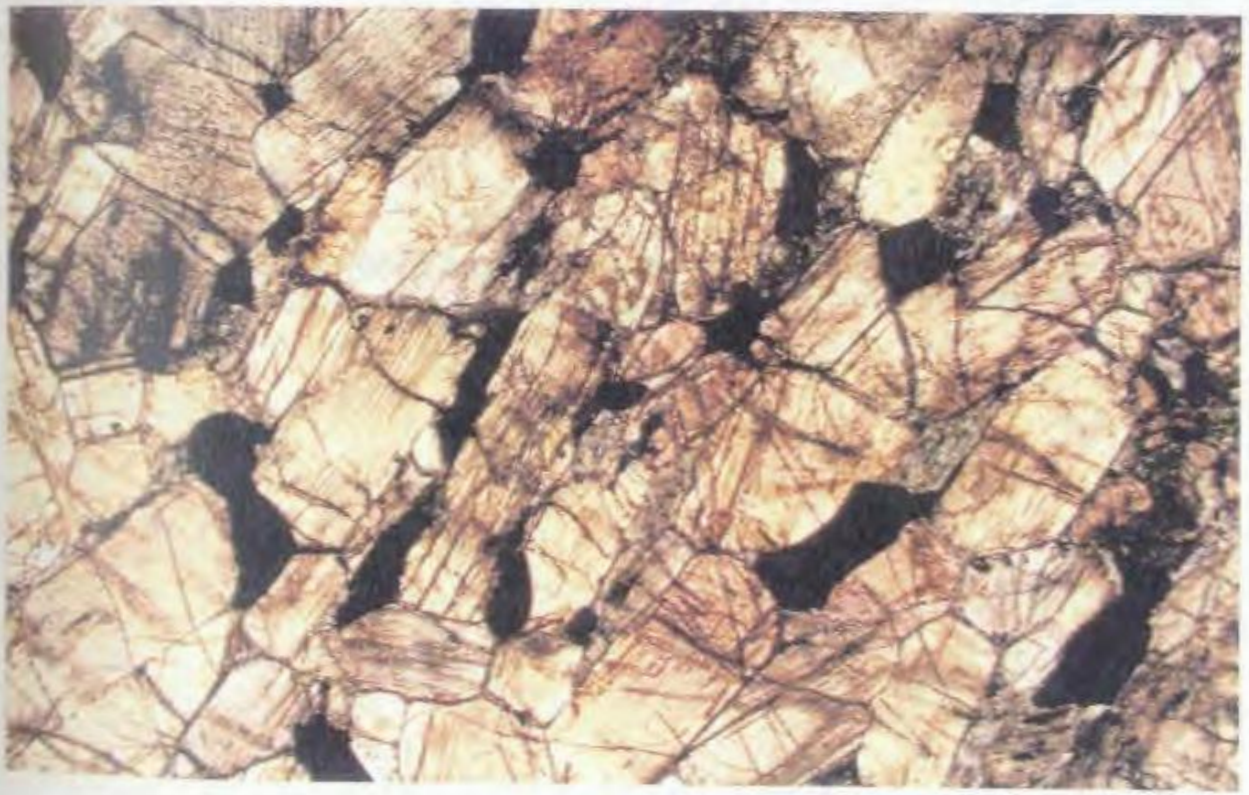

Plate 3.29. Orthopyroxene from a Type 1 pyroxenite containing exsolution lamellae and patches of reddish rutile (magnification = 10x, plane polarized light).

Plate 3.30. Typical Type 1A pyroxenite with lath like and blebby exsolution of clinopyroxene, as well as intercumulus clinopyroxene (magnification = 10x, cross polarized light).

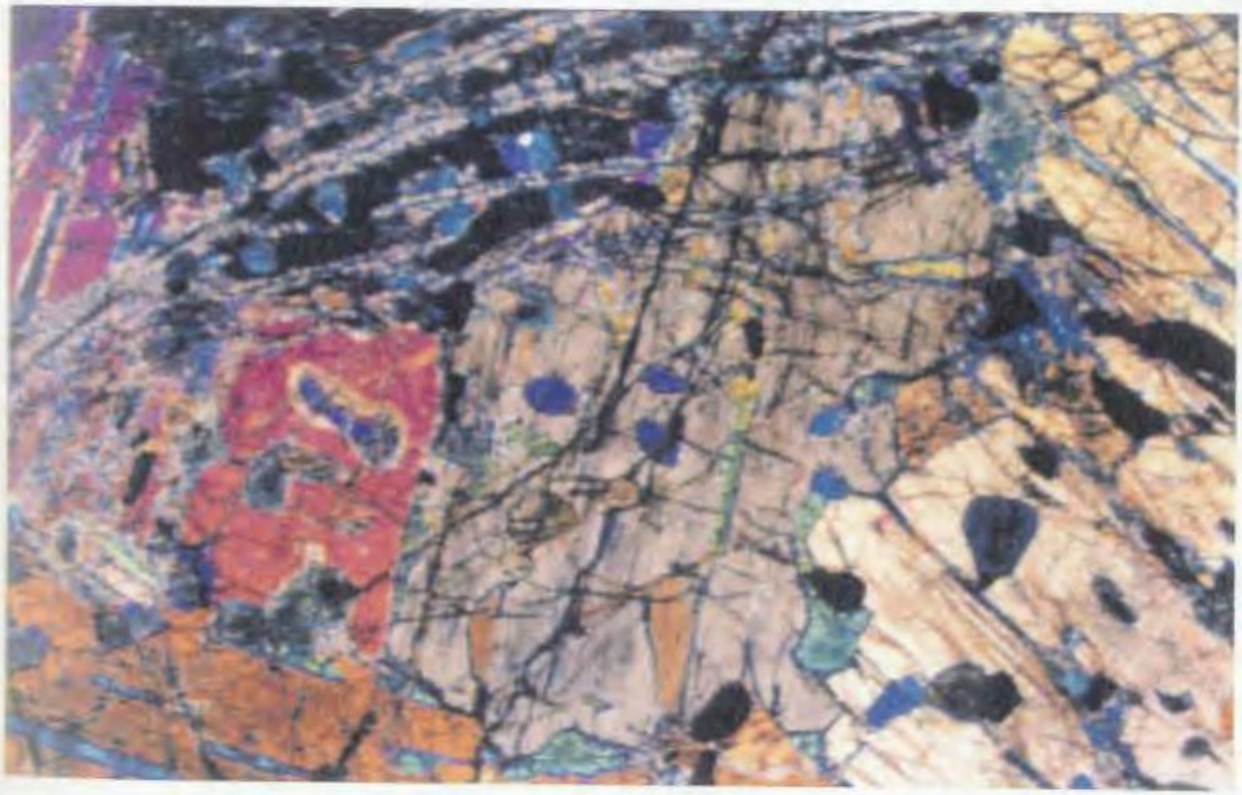

Plate 3.31. Type 1A pyroxenite with orthopyroxene containing crystallographically controlled and blebby exsolution of clinopyroxene as well as included and intercumulus sulphide (magnification = 10x, cross polarized light).

Plate 3.32. Typical Type 2 leucotroctolitic dyke with well developed cracked olivine and euhedral to subhedral plagioclase (magnification = 2.5x, cross polarized light).

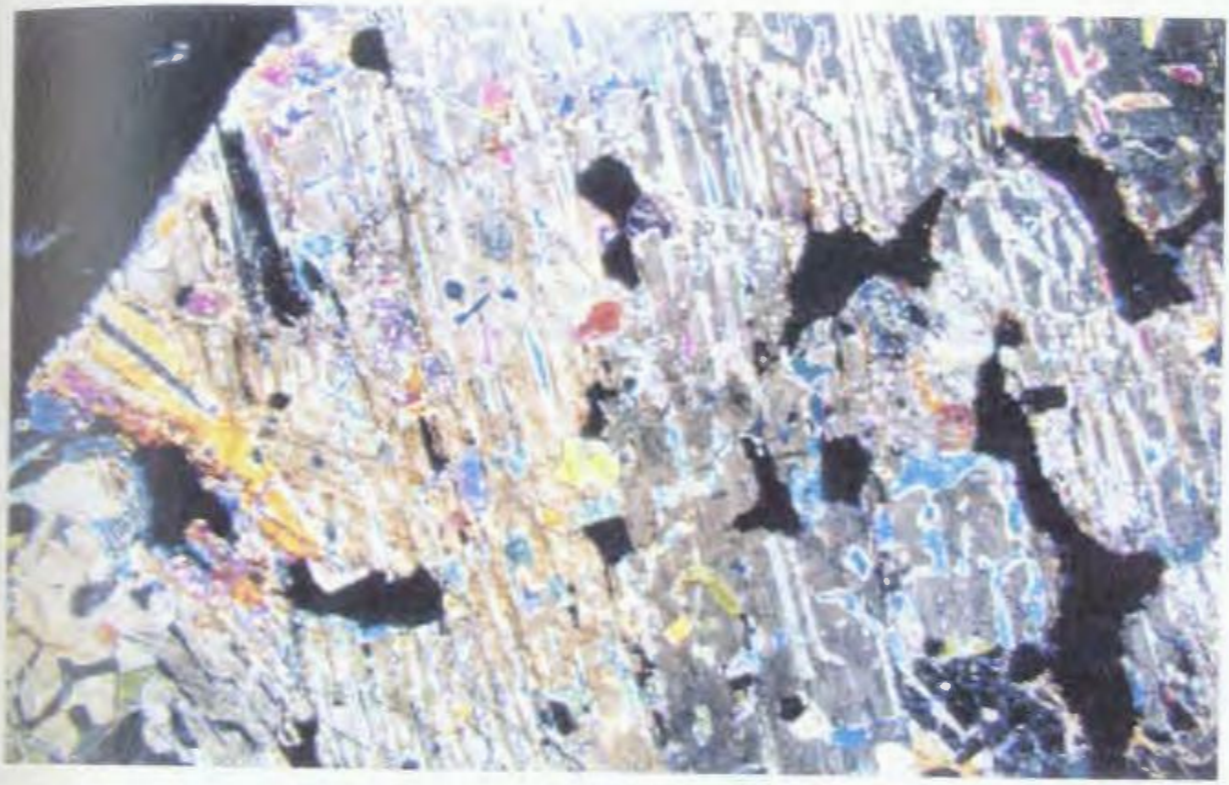

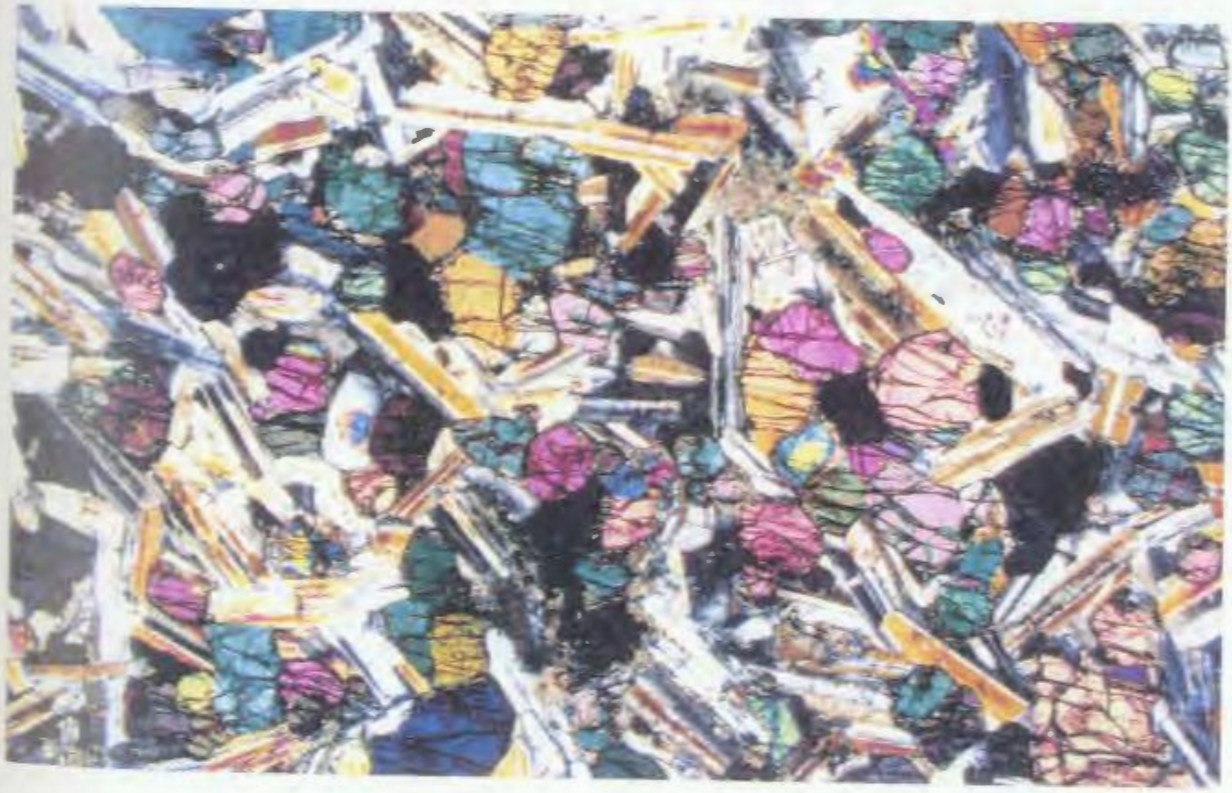

Plate 3.33. Type 2 leucotroctolite with interstitial sulphide, mantled by clinopyroxene. The blue clinopyroxene appear to have been eroded by the sulphide liquid as they show rounded edges in contact with interstitial sulphide (magnification = 2.5x, cross polarized light).

Plate 3.34. Gossanous outcropping of sulphides associated with dark grey anorthositic rocks from the Main Showing proper. Field of view is approximately 5 meters.

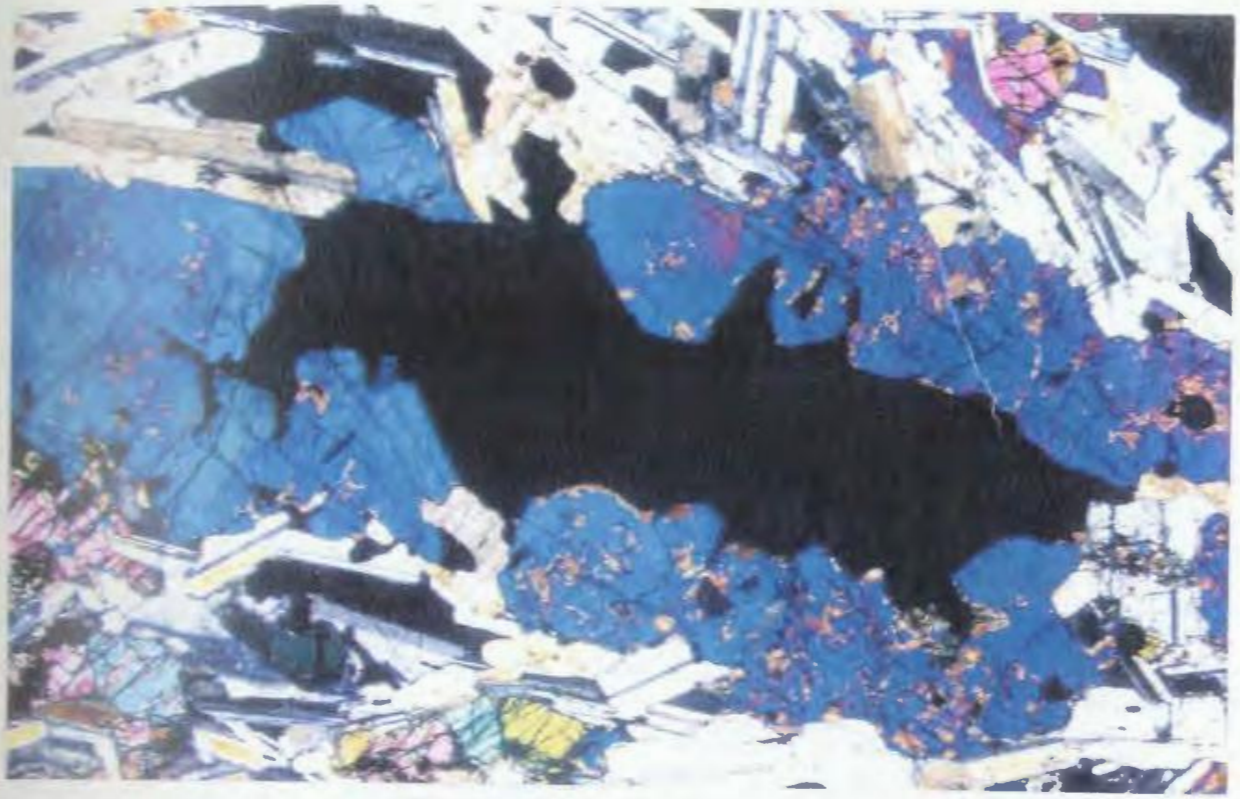

Plate 3.35. Outcroppings of gossanous leucotroctolite containing disseminated sulphide. Field of view is approximately 10 meters, for location see Figure 2.

Plate 3.36. Drill core example of disseminated pyroxenite hosted sulphides, exhibiting a well developed "net texture" of intercumulus sulphides within a pyroxenite host. As evidenced by this section, none of the pyroxenites are barren of sulphide and appear to show gradational habit.

Plate 3.37. Drill core disseminated sulphide within pyroxenites showing a gradational behaviour from disseminated to minor massive sulphide.

Plate 3.38. Photomicrograph of a typical pyrrhotite host and exsolved grains of chalcopyrite in flame and blebby form radiating inward from the pyrrhotite grain boundary. This section also shows a migration of chalcopyrite from the grain edges into the host silicate material (magnification = 10x, transmitted light).


160.32

Plate 3.39. Photomicrograph of pyrrhotite (darker beige) with exsolved blebby chalcopyrite (yellow), and blebby exsolved pentlandite (lighter beige; magnification = 10x, transmitted light).

Plate 3.40. Typical included grain of silicate material (black) within pyrrhotite (light beige) containing a partial corona of exsolved chalcopyrite. Subsurface weathering has resulted in the formation of hematite (grey) along fractures and edges of the pyrrhotite grains (magnification = 10x, transmitted light).

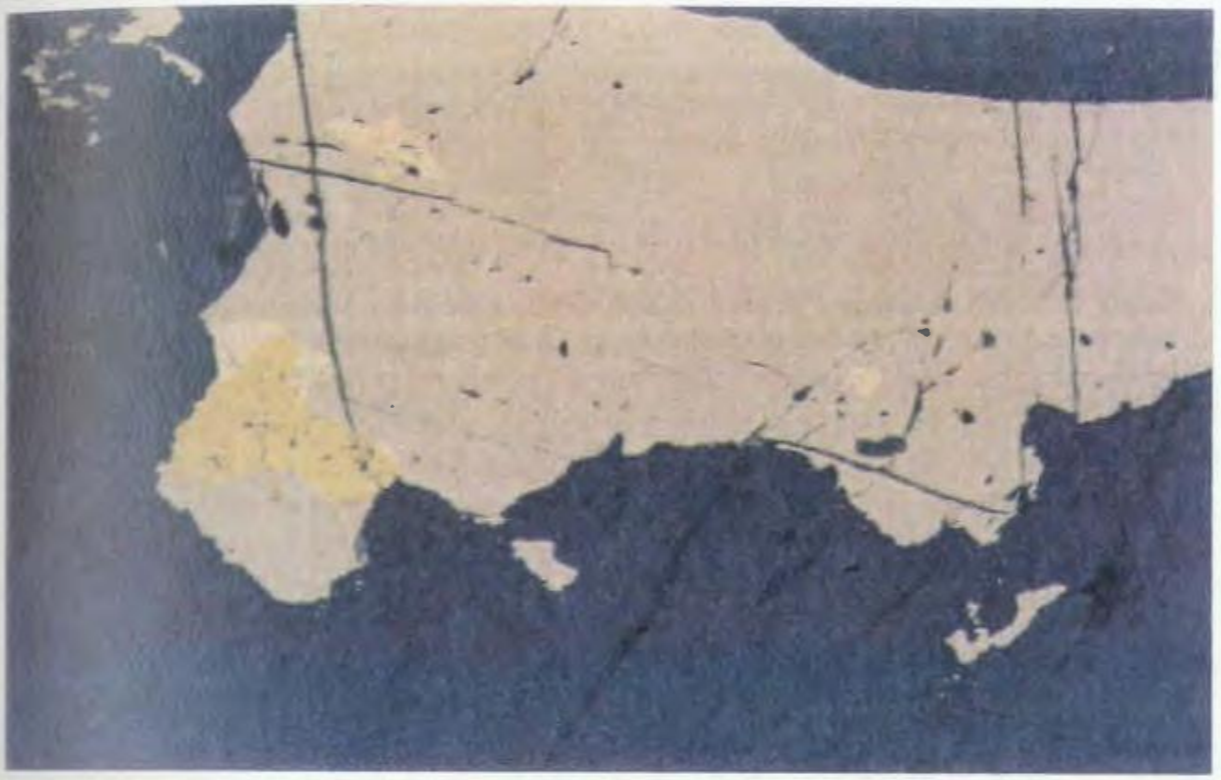

Plate 3.41. Well developed worm-like and blebby exsolution lamellae of pentlandite (light beige) within a pyrrhotite (darker beige) host (magnification = 10x, transmitted light).

Plate 3.42. Flame like exsolution of pentlandite (light beige) within a pyrrhotite host (darker beige). These flames also show a pseudo-orthogonal character relative to the grain boundary of the pyrrhotite (magnfication = 50x, transmitted light).

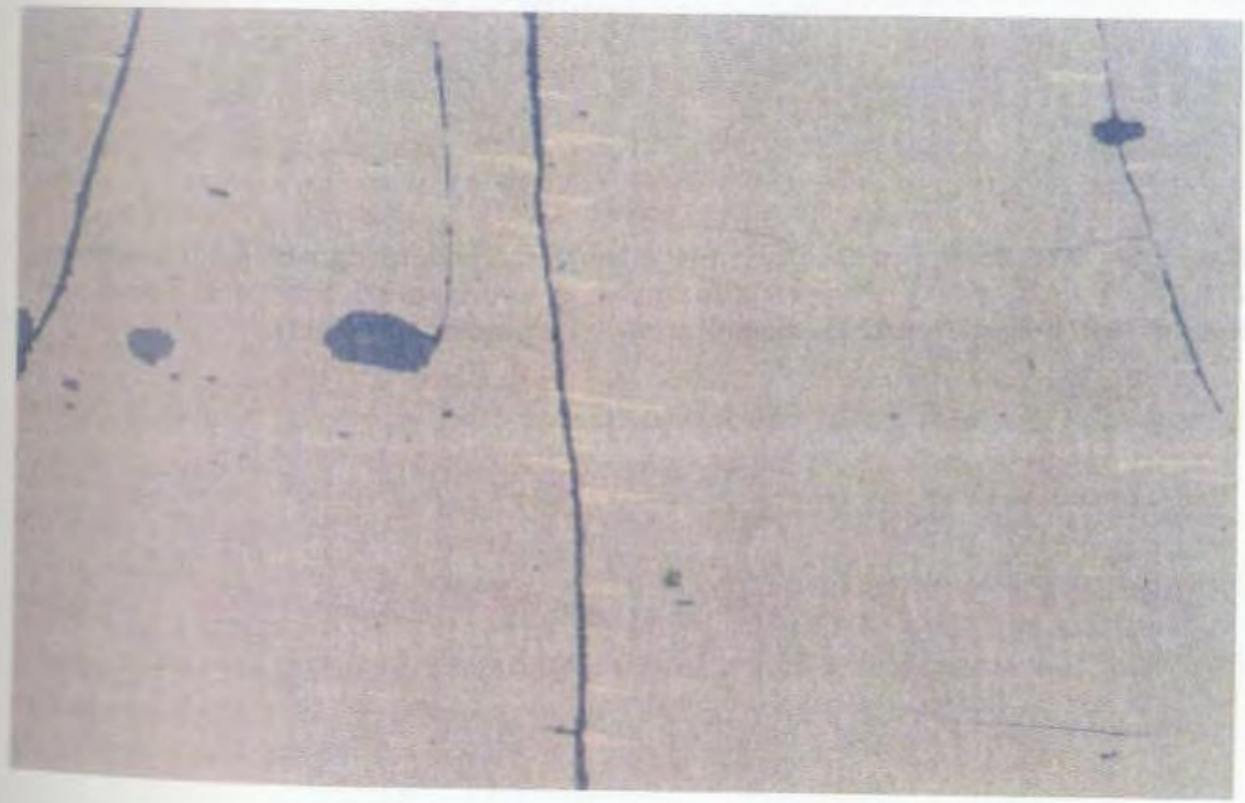

Plate 3.43. Flame like exsolution of pentlandite in pyrrhotite (small light beige flecks), and larger blebby pentlandite exsolution partially enclosing the pyrrhotite grain boundary (magnification = 10x, transmitted light).

Plate 3.44. Well developed chalcopyrite (yellow)-pentdlandite (light beige) intergrowths along the grain boundary of a pyrrhotite crystal. Also present are orthogonal flames and blebs of light beige pentlandite (magnfication = 10x, transmitted light).

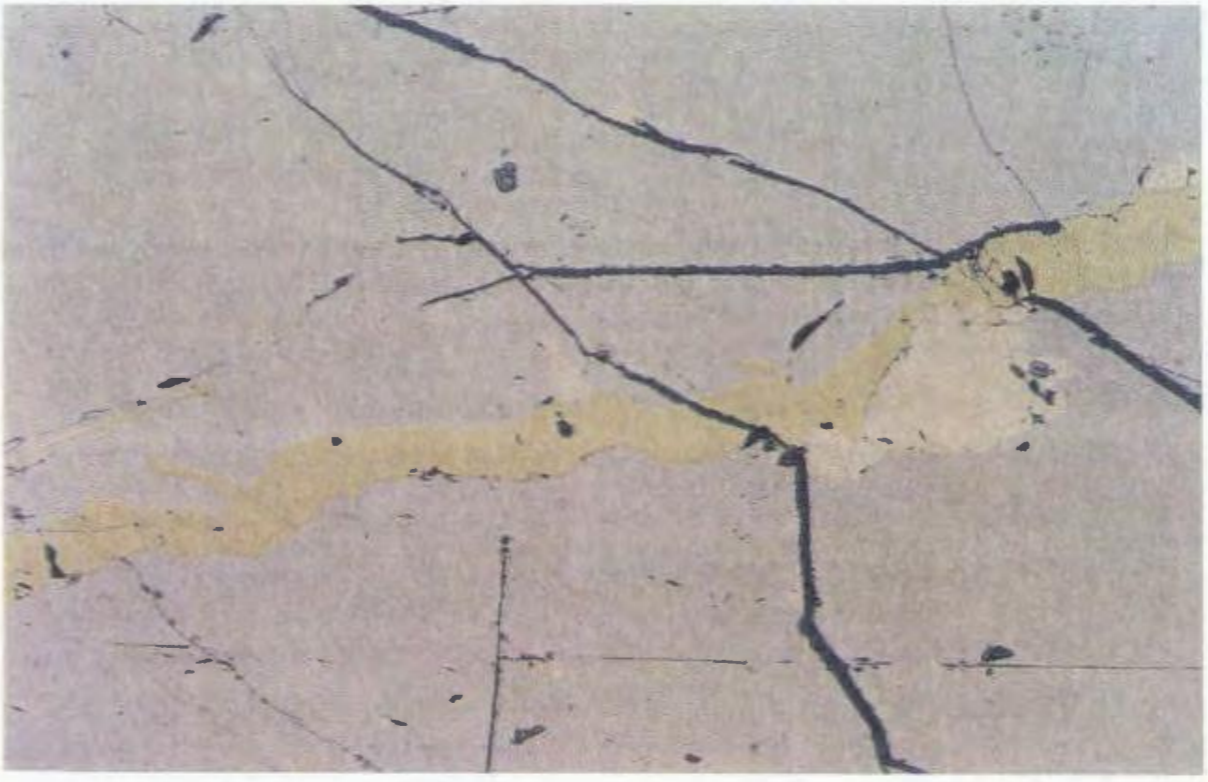

Plate 3.45. Typical resorbed pyrite (beige colored, high relief) enclosed within a corona of chalcopyrite (yellow; magnfication = 10x, transmitted light).

Plate 3.46. Euhedral magnetite (grey) enclosed within pyrrhotite (dark beige), and flame and blebby lamellae of pentlandite (light beige; magnification = 10x, transmitted light).

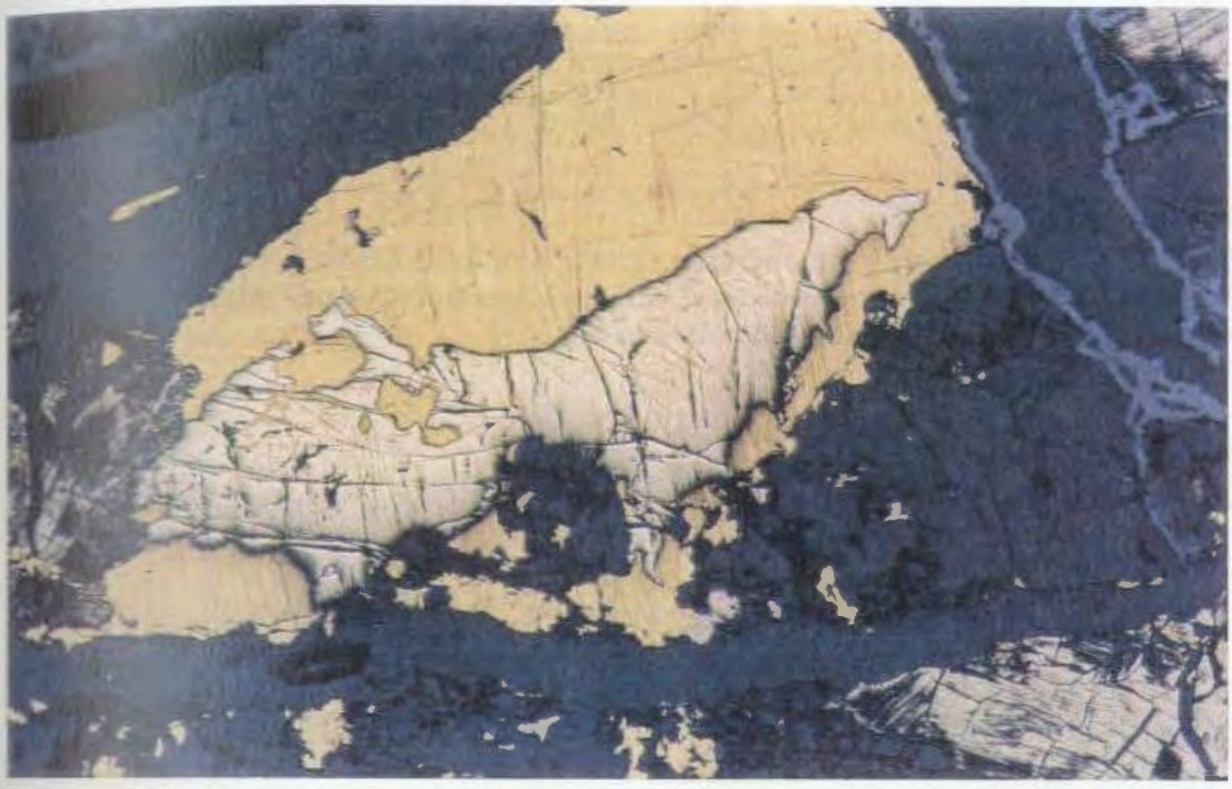

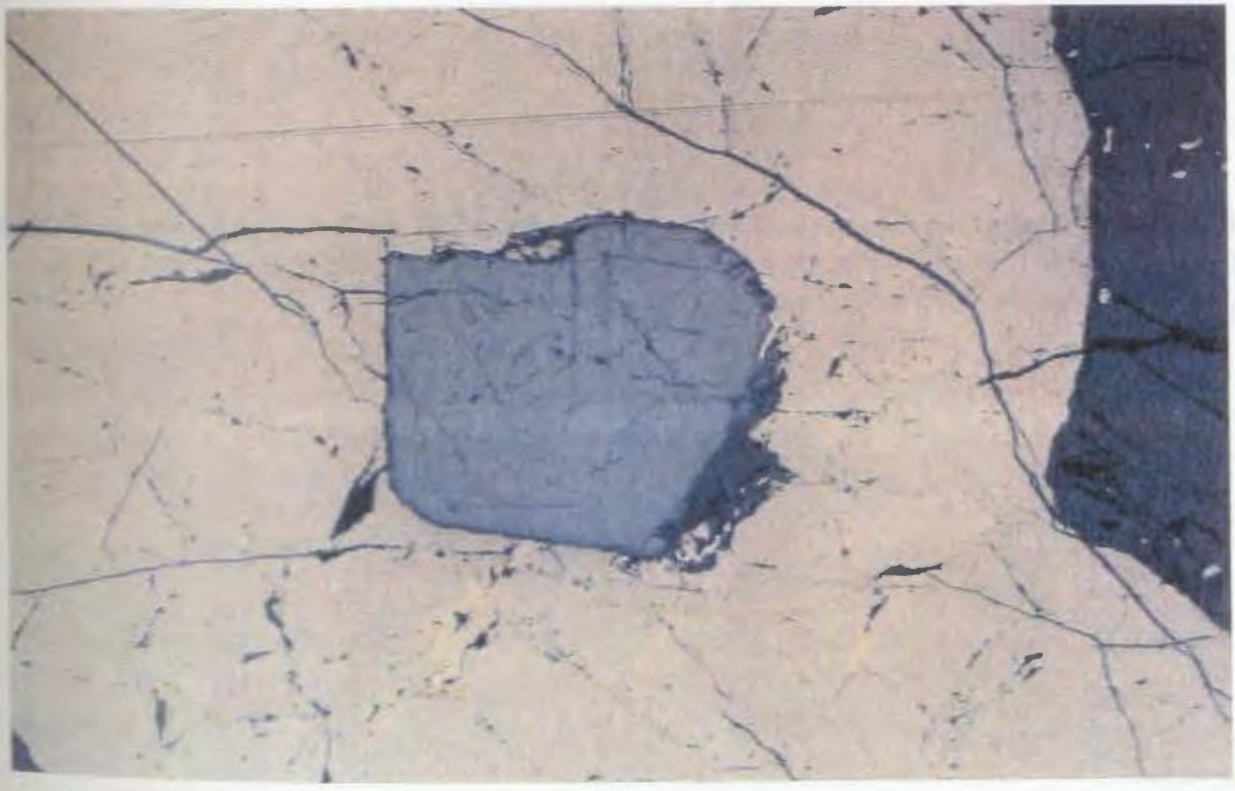

Plate 3.47. Typical Type 1 orthopyroxene grains with rutile exsolution within massive sulphide (black) exhibiting coroded and rounded edges from reaction with the sulphide liquid (magnification = 2.5x, plane polarized light).

Plate 3.48. Typical pyrrhotite (dark beige), magnetite (light grey), and exsolved pentlandite (light beige) within a pyroxenitic matrix (black), typical of sulphides associated with the pyroxenitic dykes (magnification = 10x, transmitted light).

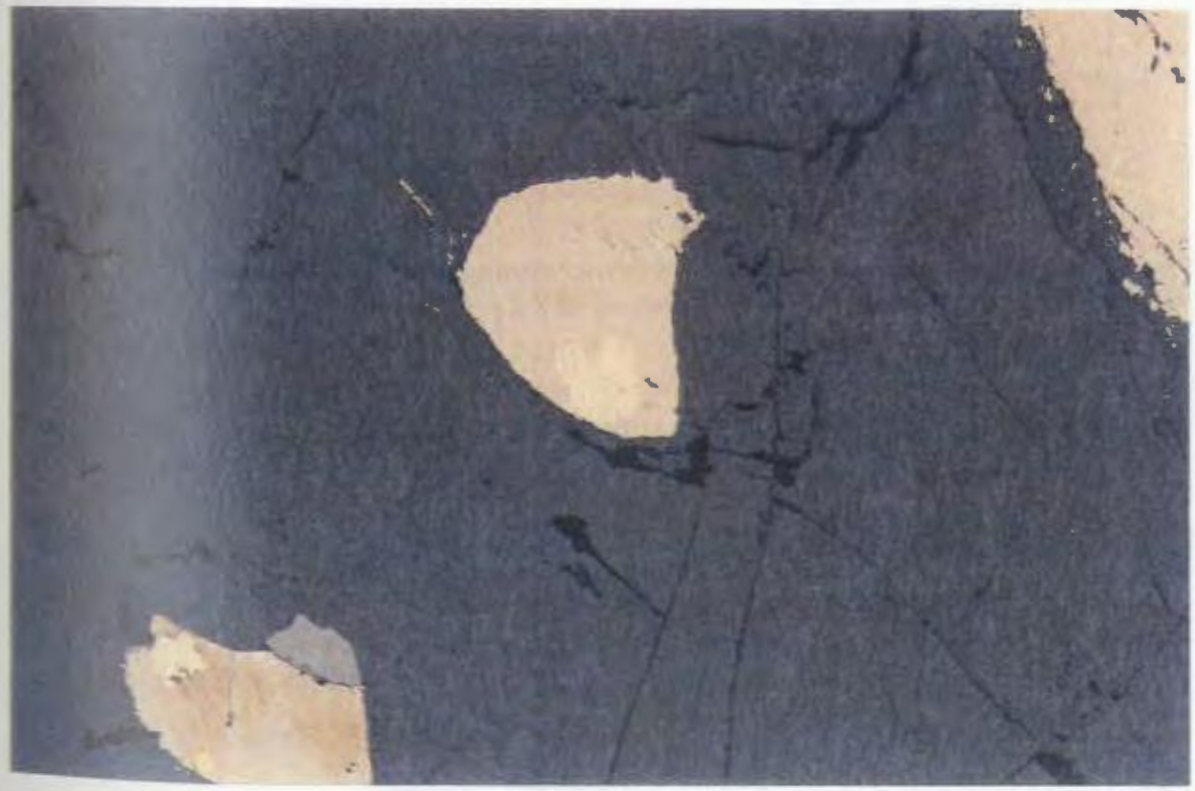

Plate 3.49. Typical disseminated pyrrhotite (beige) and chalcopyrite (yellow) occuring as interstitial material within a Type 2 leucotroctolite (magnification = 2.5x, transmitted light).

Plate 3.50. Well developed sinistral C-S fabric within chloritic schists associated with the Nain Province gneisses in the eastern portion of the property.

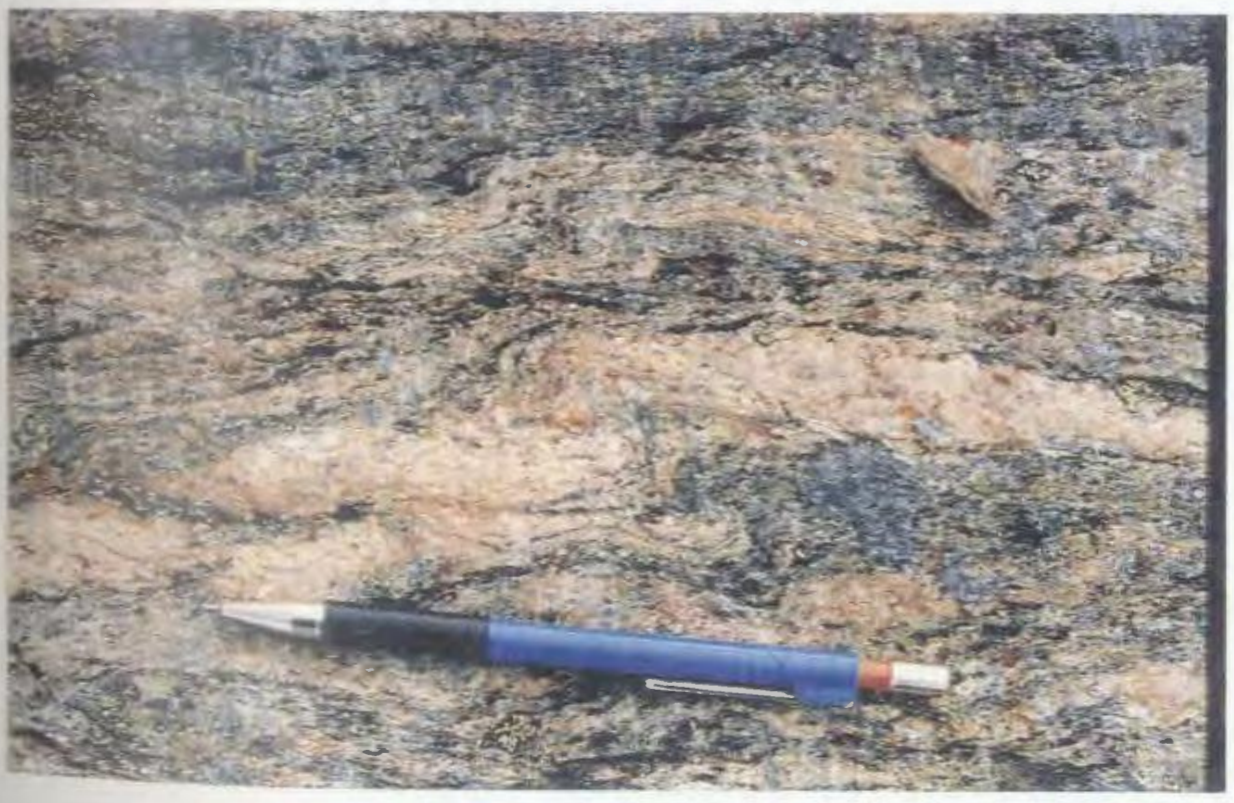

Chapter 4. Major, Trace, and Rare-Earth Element Geochemistry

4.1 Introduction: The Purpose and Scope of Using Geochemical Data

Evaluation of major, trace, and rare earth element geochemical data can provide considerable insight into petrologic and petrogenetic conditions of igneous rock formation. This chapter discusses the major element, trace element, and rare-earth element (REE) geochemistry of the representative lithologies at the OKG prospect, including: 1) the Paleoproterozoic anorthositic rocks; 2) Paleoproterozoic granitoids; 3) Paleoproterozoic mafic-felsic dykes; 4) Mesoproterozoic mineralized pyroxenitic-leucotroctolitic dykes; and 5) Archean Nain Province amphibolites and mafic granulites. The purpose of the geochemical prognostication presented in this chapter is as follows: 1) to provide a documentation of the geochemical characteristics of a poorly known AMCG terrain; 2) to infer the controls that cumulate and accessory mineralogy have on the geochemistry of the respective rocks units; 3) to use the geochemical data to provide insight into the petrogenetic and metallogenic controls on the formation of the OKG lithologies; and 4) to decipher whether contamination has effected the mineralized pyroxenitic rocks of the OKG.

The presentation of this section is subdivided into the lithologic groupings as presented in Chapter 3, with a particular bias towards the anorthositic, pyroxenitic, mafic dyke and granitoid chemistry; where applicable, the chemistry of other units will be discussed in subsequent chapters. It should be noted that with the exception of the mafic dykes all of the rocks in this chapter are cumulate compositions and are likely far removed from liquid compositions. Although this can cause problems for interpreting magma evolution, the chemistry of these units does reflect the cumulate and accessory mineralogy of the rocks, and this is the interpretive approach that is taken. Furthermore, the geochemical data is provided in a descriptive fashion and where applicable is compared to documented examples of petrologically similar rocks, either in this chapter or subsequent ones (e.g. Chapter 8).

All geochemical analyses were carried out at laboratories in the Department of Earth Sciences, Memorial University of Newfoundland. All major and trace element analyses were completed using pressed-powder pellets and analyses by X-ray Fluorescence (XRF) following the methods of Longerich (1995); while the REE were analyzed by inductively-coupled plasma mass-spectrometry (ICP-MS) following the Na_2O_2 sinter preparation method of Longerich *et al.* (1990). Details on sampling protocol, elements analyzed, analytical methods, and precision and accuracy are outlined in Appendix A.

4.2 Paleoproterozoic Anorthositic Rocks

4.2.1 Discrimination Diagrams

As a first pass in understanding the geochemical characteristics of the anorthositic rocks, all samples are plotted on discrimination plots to understand their particular geochemical affinity. Plots used in this section include the total alkalis versus silica (TAS) and AFM plots of Irvine and Baragar (1971) and Jensen's (1976) cation plot. Although these plots were developed for basaltic rocks their application can be extended to the anorthositic rocks for a cursory understanding of their geochemical behaviour; however, it must be noted that their major element affinities are strongly controlled by their cumulate mineralogy and these diagrams are for descriptive purposes only.

On the TAS plot the anorthositic show a very tight clustering, with the exception of one sample, within the subalkaline field and close to the alkaline-subalkaline boundary, typical of most anorthositic rocks (Ashwal, 1993; Figure 4.1a). The AFM and Jensen plots show similar clustering with most samples showing a well defined trend extending from the Al_2O_3 apex towards the MgO and FeO*(+TiO_2) side of the diagrams (Figure 4.1b-c); likely reflecting the varying plagioclase : mafic mineral (orthopyroxene) content of the suite. A group of four samples lie off the main trend of the anorthositic rocks with increased FeO* and FeO*+TiO_2 contents (Figure 4.1b-c), and contain elevated magnetite, ilmenite, and/or sulphide contents.

4.2.2 MgO versus Major Element Plots

Since anorthositic rocks contain mineral assemblages which are predominantly mafic (e.g. plagioclase, orthopyroxene, clinopyroxene and olivine), MgO is chosen as an

index to measure fractionation and mineralogical trends within the OKG suite. Magnesium is plotted against the major elements CaO, Na_2O, K_2O, Al_2O_3, FeO*, TiO_2 and P_2O_5 to measure the effects of cumulus and accessory mineralogy on the suite chemistry.

MgO values for the anorthositic rocks are fairly consistent ranging from 0.31 wt% in the least mafic sample (anorthosite, *s.s.*) to 7.59% in the most mafic sample (leuconorite with 25-35% orthopyroxene). Mg#'s (=[MgO/MgO+FeO*]*100) for the anorthositic rocks are variable and range from 22-67, occurring in three groups: 1) one anomalously low sample with Mg# =22, containing anomalous concentrations of sulphide and oxide minerals (leading to Fe enrichment); 2) a second cluster between 29.88-37.26 which are fairly fractionated but contain oxides; and 3) a cluster between 49.39-67.01 which are not primitive but show variable fractionation.

The elements CaO (7.91-10.61%), Al_2O_3 (16.23-28.13%), Na_2O (3.13-5.56%) and to a lesser extent K_2O (0.29-1.67%) show progressive decreases in their respective concentrations within increasing MgO (Figure 4.2a-d). These elements are enriched in plagioclase, and their decreasing nature reflects increases in orthopyroxene content at the expense of plagioclase (Figure 4.2a-c). Potassium shows a less drastic decrease in comparison to the latter elements (Figure 4.2d); however, the crude decrease is probably related to plagioclase decreases, but plagioclase with antiperthitic inclusions of potassic feldspar. Scatter within the latter diagram may also be a result of K_2O mobility due to greenschist facies metamorphic effects.

Contrasting the behaviour of CaO, Al_2O_3, Na_2O and K_2O is the behavior of FeO* (main trend: 0.93-8.86%; elevated trend: 6.76-9.42%) and MnO (0.01-0.05%) which show progressive increases with MgO (Figure 4.2e-f). In the case of FeO*, the main trend increases with MgO* are attributed to increased amounts of orthopyroxene and decreasing plagioclase; while the elevated FeO* group is explained by increased magnetite and/or sulphides (Figure 4.2e). The MnO increases with MgO is similar to FeO*, and MnO increases are attributed to Mn^{2+} substitution for Fe^{2+} in the orthopyroxene structure; a most probable occurrence (Figure 4.2f).

Plots of MgO versus TiO_2 and P_2O_5 show very little information about the mineralogy or differentiation behaviour of the suite, for the most part. Most anorthositic rocks have very little TiO_2 (0.06-0.53%) and the elevated samples are most likely the result of ilmenite or magnetite accumulation (Figure 4.2g). Similarly, the P_2O_5 values in the anorthositic rocks are quite low (0-0.18%) with a few elevated samples reflecting the occurrence of accessory apatite (Figure 4.2h).

4.2.3 MgO versus Trace Element, and Other Trace Element Plots

Similar to the major element plots, the trace element plots use MgO as an index for suite fractionation and the effect of mineral phases on trace element chemistry. The trace elements Cr, Ni, Sc, V, Y, Rb, Sr, and Ga are used to measure the above effects. The elements Cr, Sc, V and Y are useful in assessing the pyroxene content (in particular orthopyroxene), in main trend rocks, and the accumulation of oxide phases in non-main trend rocks. Nickel is used to assess the effect of sulphide and/or olivine accumulation; while Sr provides a check on the behavior of CaO, and Ga on Al_2O_3 behaviour.

Chromium (main trend: 9-111 ppm; elevated trend: 165-206ppm) and V values (main trend: 7-78 ppm; elevated trend: 103-364 ppm) show fairly well developed increases with MgO reflecting increases in cumulus orthopyroxene (±clinopyroxene) and decreases in cumulus plagioclase (Figure 4.3a,b). Although scattered, Sc (1-24ppm) roughly increases with increasing MgO and scatter of the trend may reflect exsolved clinopyoxene in the orthopyroxenes (Figure 4.3c). Yttrium values are typically low (1.17-6.59 ppm) and show very little increases or decreases with MgO with the exception of three samples which have elevated Y (14.16-32.25ppm) reflecting minor clinopyroxene content (Figure 4.3d).

Nickel abundance is typically low (8-131 ppm) but one sample shows elevated values of Ni (980ppm) reflecting minor either disseminated sulphide or olivine (Figure 4.3e). A plot of Ni versus S (Figure 4.3f) shows illustrates that the elevated Ni sample is also associated with high S values and suggests that the Ni content is controlled by sulphide accumulation rather than olivine. Strontium values are quite elevated between 590-875ppm, reflecting the substitution of Sr^{2+} for Ca^{2+} in the plagioclase lattice; this also explains the virtually identical decrease in Sr with MgO when compared to CaO (Figure 4.3g). Gallium, which should plot similar to Al_2O_3, has a crude decrease with MgO, but is not as pronounced as Al_2O_3 (Figure 4.3h).

4.2.4 Normalized Rare-Earth Element and Multi-Element Plots

All anorthositic samples have been plotted according to their REE and extended trace-element chemistry on primitive mantle normalized plots, normalized to the primitive mantle values of Hofmann (1988) as well as the values for the average

leuconorite from the OKG prospect (e.g. *ln1*). The plots are used to assess the geochemical differences within the suite of anorthositic rocks and to assess the differences between each group of anorthositic rocks (e.g. *an* and *ln2* against *ln1*; Figure 4.4).

4.2.4.1 Primitive Mantle Normalized REE Plots

On primitive mantle normalized plots the anorthositic rocks have a similar, yet variable trend across the diagram, with overall decreases from the LREE to HREE, variable total REE and size of the positive Eu anomaly (Figure 4.5a-d). The *an* group show the greatest decrease in total REE, ranging from 2-10 times primitive mantle for the LREE (La_N/Yb_N = 8.17-155.12; Ce_N/Yb_N = 5.64-94.61; La_N/Sm_N= 3.08-7.96), to 0.04-0.13 times the primitive mantle for the HREE (Gd_N/Yb_N = 1.27-4.61), coupled with the largest positive Eu anomaly (Eu/Eu* = 6.24-12.06; Figure 4.5a; Table 4.1). The *ln1* grouping have moderately higher total REE with LREE approximately 10 times primitive mantle (La_N/Yb_N = 5.93-16.02; Ce_N/Yb_N = 4.93-12.90; La_N/Sm_N= 2.24-4.95), HREE approximately 1 times the primitive mantle (Gd_N/Yb_N = 1.33-3.02) and a moderately positive Eu anomaly (Eu/Eu* = 2.07-3.03; Figure 4.5b; Table 4.1). The *ln2* group have the highest total REE with LREE 20-40 times primitive mantle (La_N/Yb_N = 7.20-9.65; Ce_N/Yb_N = 6.49-8.34; La_N/Sm_N= 2.26-3.02), HREE 3-6 times primitive mantle (Gd_N/Yb_N = 2.03-2.08), and a very minor positive Eu anomaly (Eu/Eu* = 1.62-1.79; Figure 4.5c; Table 4.1).

The changes in total REE and size of the positive Eu anomaly are reflects the control of the relative amounts of orthopyroxene and plagioclase in the anorthositic

rocks. The lowest total REE and largest positive Eu anomaly occurs in highest plagioclase rich samples, the *an* group (Figure 4.5d). The *ln1* group manifests moderate REE and positive Eu anomalies; while the highest total REE and lowest Eu anomaly is represented by the *ln2* group (Figure 4.5d). These characteristics are attributed to the greater amounts of variably REE enriched intercumulus liquids (and orthopyroxene) which are enhanced as the orthopyroxene : plagioclase ratio increases (e.g. Ashwal, 1993). As the plagioclase decreases and mafic minerals increase there is a greater abundance of HREE enriched orthopyroxenes, which combined with the LREE enriched plagioclase cumulates causes a total REE increase and shadow of the positive Eu anomaly.

4.2.4.2 Extended Primitive Mantle Normalized Trace Element Plots

Extended REE and trace element plots are also normalized to the primitive mantle values of Hofmann (1988). These plots display similar characteristics to the REE plots with overall decreases in elements from the less incompatible to the more incompatible. The *an* group is characterized by negative Rb anomalies, and well developed positive Sr Eu and Ti anomalies; (Figure 4.6a). The *ln1* group shows a similar trend, but has higher total abundance of most of the REE, and shows pronounced positive Sr and Eu anomalies, flat to negative Th and Nb, and variably flat to positive Zr and Ti anomalies (Figure 4.6b). The *ln2* group has the highest total element abundance and are characterized by very slight positive Sr and Eu, very pronounced negative Rb and Th anomalies, and flat to negative Zr anomalies, and flat to positive Ti anomalies (Figure 4.6c).

The plots of the three groups are rather similar with the exception of total abundance. Particularly interesting is the decrease in Sr and Eu anomalies, as well as an increase in total abundance of the REE and HFSE (Figure 4.6). The pronounced negative Th anomaly exhibited by the *ln2* and to a lesser extent the *ln1* group are features consistent with that of the Nain Province gneisses (see section 4.6; cf. Schiøtte *et al.*, 1993), and suggest a crustal influence by the latter. Notably, although mobile during metamorphism, Ba, Rb and K behave similarly in all the anorthositic rocks plotted on these diagrams and likely have not been significantly mobilized by metamorphism.

4.2.4.3 Average Leuconorite Normalized REE Plots

Average leuconorite normalized plots are used to further illustrate the effects that plagioclase and orthopyroxene abundance have on the REE chemistry of the OKG anorthosites. The average leuconorite normalization values are taken from the average REE composition of the *ln1* group. When the *ln1* group is plotted against the average leuconorite values, there is some scatter with respect to total REE, but there is a general flat pattern, with an overwhelming agreement with respect to the Eu values (Figure 4.7a). The *an* group has a fairly flat to slightly decreasing pattern from LREE to HREE, with a distinctive positive Eu anomaly, and total REE less than the average leuconorite (Figure 4.7b); while the *ln2* group is elevated in total REE, has an increasing trend from La to Nd, a marked negative Eu anomaly, and fairly flat HREE (Figure 4.7c). These characteristics augment the REE and extended REE plots and show the control of the plagioclase : orthopyroxene ratios have on the REE chemistry.

4.3 Paleoproterozoic Granitoid Rocks

Granitoid rocks have been subdivided into three groupings for the purposes of assessing the geochemical behaviour, *viz*: 1) the phase 1 and phase 2 granitoids from south of Umiakoviarusek Lake; 2) the foliated granitoids in the eastern portion of the property; and 3) felsic dykes of the Main Showing area. Like all the other rock types the data presentation involves discrimination plots, major element versus silica plots (e.g. Harker plots), and rare-earth and extended trace element plots.

4.3.1 Discrimination Diagrams

As a first pass at describing the geochemical attributes of the OKG granitoids, all the samples have been plotted on a series of discrimination diagrams to give a broad scale understanding of their geochemical characteristics. The plots used include Shand's Index (Maniar and Piccoli, 1989) and the Rb-Y+Nb and Nb-Y diagrams of Pearce *et al.* (1984).

On the Shand's Index all the granitoids are characterized by $Al_2O_3/(Na_2O+K_2O)$ >1, with most having a metaluminous character (e.g. $Al_2O_3/(CaO+Na_2O+K_2O) < 1$). The phase 1 intrusives have predominantly metaluminous affinities, with one sample peraluminous field character (Figure 4.8a). Similarly, the phase 2 intrusives are predominantly metaluminous with only a few samples jutting into the peraluminous field (Figure 4.10a). The foliated granitoids are somewhat different and cluster between the metaluminous-peraluminous boundary; while the felsic dykes near the Main Showing cluster solely within the peraluminous field (Figure 4.8a). Most of the rock have a tight clustering except for two samples with elevated $Al_2O_3/(Na_2O+K_2O)$ and have likely had

insignificant element mobility during metamorphism; the latter two samples have likely experienced element mobility and were not used for any REE analyses.

On the Rb-Y+Nb plot most of the phase 1 granitoids lie within the within-plate (A-type)-granite (WPG) field with high Rb and fairly high Y+Nb (Figure 4.8b). The phase 2 granitoids cluster the WPG to volcanic-arc (I-type)-granite (VAG) field, but still have similar Rb values with similar to slightly lower Y+Nb values (Figure 4.8b). The foliated granitoids are extremely odd as some plot in the WPG field, while many plot in the VAG field, with the exception of one within the ORG field (Figure 4.8b). The felsic dykes of the Main Showing area have WPG to VAG affinity, similar to the phase 2 granitoids (Figure 4.8b). It should be noted that Rb can be mobile during metamorphism and that this can cause erroneous results; however, with few exceptions there are close similarities between the granitoid distribution on the Nb-Y plots and the Rb-Y+Nb plots. On the Nb-Y plots the ph1 granitoids solely in the WPG field, the ph2 granitoids close to the WPG-VAG boundary, the foliated granitoids lying in both the VAG and WPG fields, and the felsic dykes within the WPG field (Figure 4.8c).

4.3.2 SiO_2 versus Major Elements (Harker Diagrams)

Unlike the other rocks at the OKG prospect which are largely mafic in composition, the granitoids have a predominant felsic mineralogy and thus SiO_2 is chosen to measure fractionation, and the effects of cumulus and accessory mineralogy have on the geochemistry of the granitoid suite. Although SiO_2 can be mobile during hydrothermal alteration and higher grades of metamorphism, the predominant cumulate

mineralogy, low grade metamorphism, and lack of hydrothermal alteration in the granitoids makes it fairly safe to use SiO_2 as a fractionation index.

Like the anorthositic rocks, the granitoids are separated into groups for geochemical characterization, including: 1) phase 1 granitoids south of Umiakoviarusek Lake (SiO_2 = 55.22-66.74 wt%); 2) phase 2 granitoids (SiO_2 = 57.23-73.87 wt%); 3) foliated granitoids (SiO_2 = 59.27-73.71); and 4) felsic dykes in the Main Showing area (SiO_2 = 72.06-74.04 wt%). The elements plotted against silica are subdivided into three groups, including: 1) those controlled by feldspar (Al_2O_3, CaO, K_2O, Na_2O); 2) mafic mineral (±oxide) controlled (MgO, FeO*, MnO, TiO_2); and 3) those controlled by other minerals (P_2O_5).

The feldspar-controlled group shows variable behavior depending on the granitoid group. The phase 1 rocks show increases in Al_2O_3 (12.37-19.60 wt%) with increasing SiO_2, reflecting increases in total feldspar (Figure 4.9a). At the Al_2O_3 maximum point for the phase 1 rocks, there is a decrease in alumina with increasing silica for the phase 2 rocks (Al_2O_3= 13.15-18.95 wt%), and the foliated granitoids (Al_2O_3= 13.52-17.61 wt%; Figure 4.9a), which is most likely related to the decrease in cumulus plagioclase (±K-feldspar) coupled with increasing quartz in the rocks. At the end of this downward trend are the felsic dykes from the Main Showing area which have relatively low Al_2O_3 (13.93-14.26 wt%), which corresponds to the samples with the lowest feldspar and highest quartz content (Figure 4.9a).

Although there are slight offsets with SiO_2, all of the granitoid groups, with few exceptions, show decreases in CaO with increasing SiO_2 typical of increases in quartz at

the expense of plagioclase (Figure 4.9b). The behaviour of K_2O and Na_2O is much more variable than CaO. The phase 1 granitoids show increases in K_2O (4.09-6.45 wt%) with SiO_2, typical of increased K-feldspar with silica (Figure 4.9c). The phase 2 granitoids have relatively consistent K_2O with silica (K_2O = 4.24-4.75 wt%) suggesting that because of the low content of plagioclase in these samples, the sensitivity of the rocks to K_2O changes are much less than for the anorthositic rocks (Figure 4.9c). Likewise, the foliated granitoids have clustered K_2O (2.84-5.35 wt%) and show no predominant trend with increasing SiO_2 (Figure 4.9c). Both the phase 1 and phase 2 granitoids have little change in Na_2O with increasing SiO_2 (Na_2O = 3.59-5.29 and 3.21-3.71 wt%, respectively); while the foliated granitoids show a slight decrease with SiO_2 (Na_2O = 2.35-4.62 wt%); and the dykes of the Main Showing appear to be at the end of the foliated granitoid trend with Na_2O = 2.35-4.62 wt% (Figure 4.9d). The behaviour of Na_2O versus SiO_2 in the foliated granitoids is likely a function of the percentage of Na_2O in the K-feldspar; the lack of change in the phase 1 and 2 granitoids is likely a function of having subequal plagioclase and K-feldspar, both of which contain Na_2O, thus resulting in a constant content of Na_2O.

All of the elements that are compatible in mafic minerals (MgO, FeO*, MnO, TiO_2) are likely controlled by hornblende, and to a lesser extent pyroxene and olivine. On all of the plots there is a decrease in MgO, FeO*, MnO and TiO_2 with increasing SiO_2, reflecting the decrease in mafic minerals and increase in quartz and feldspar with increasing silica. The concentrations of each element and group can be seen on figures (4.9e-h). Only one element lies within the other group, and this includes P_2O_5 which

have decreases with increasing SiO_2 in the phase 1 rocks and phase 2 rocks with only minor exceptions (Figure 4.9i). The foliated granitoids have a distinct vertical trend, which accompanied by those off the main trend in phases 1 and 2 represent the presence of accessory apatite (Figure 4.9i).

4.3.3 SiO_2 versus Trace Elements (Harker Diagrams)

As a check on the behaviour of the major elements in the granitoids Rb, Sr, Ba and Zr are plotted against SiO_2. The behaviour of these elements is very variable and shows no systematic expression like the major elements (Figure 4.10a-d). With Rb, the phase 1 granitoids form a cluster (Rb = 9.83-185.43 ppm), which has vertical trends, rather than a smooth trend indicative of changing plagioclase, K-feldspar and quartz contents (Figure 4.10a). Likewise the phase 2 granitoids have a distinct horizontal pattern with no change in Rb (99.34-147.11 ppm) with increasing SiO_2 (Figure 4.10a). The foliated granitoids (Rb = 4.58-238.69 ppm) cluster with a vertical trend with increasing SiO_2, indicative of increasing K-feldspar with increased SiO_2 (Figure 4.10a); while the distinctive flat to clustered trends of the phase 1 and 2 granitoids may reflect the higher plagioclase and K-feldspar contents in these rocks versus the quartz-K-feldspar dominant character of the foliated rocks.

Against Sr and Ba, the groups show very similar geochemical behaviour. The phase 1 granitoids show crude Sr and Ba increases with increasing SiO_2, the phase 2 granitoids have flat to slightly decreasing behaviour with Sr and Ba, while the foliated granitoids have distinctive decreases in Sr and relatively clustered to flat Ba chemistry (Figure 4.10b-c). The relative increases in Rb, Sr, and Ba with SiO_2 in the phase 1 rocks

are indicative of increasing total feldspar with increasing silica, at the expense of hornblende and other mafic minerals typical of this suite (Figure 4.10a-c). The relatively flat patterns of the phase 2 granitoids probably reflect the constant plagioclase, K-feldspar and quartz, and minimal mafic mineral content; while the vertical trends with Rb and Sr reflect changes in the plagioclase:K-feldspar ratios with increasing SiO_2 (Figure 4.10a-c). In the foliated granitoids Ba should follow Sr in its geochemical trend; however, it has a distinctive clustering, which does appear to be decreasing with SiO_2 increases, but the trend is not really diagnostic. The significant scatter observed in the Rb, Ba and Sr data may be in part due to some mobility of the elements during metamorphism.

Zirconium behaviour is very odd in the granitoid rocks as it shows a general decreasing trend in the phase 1 rocks (Zr = 68.27-888.04 ppm), and roughly increasing trends in the phase 2 and foliated granitoids (Zr = 343.66-613.92 and 139.13-581.07 ppm, respectively; Figure 4.10d). The general increases and decreases in these rocks probably reflect the increase/decrease of accessory zircon in the samples; while two samples at ca. 55-57% SiO_2 exhibit very high Zr and likely reflect greater accumulations of zircon.

4.3.4 Primitive Mantle Normalized REE and Extended Trace Element Plots

Similar to the mafic rocks, all granitoid samples are normalized to the primitive mantle values of Hofmann (1988). The granitoids chosen for the purposes of this exercise include the phase 1 and phase 2 granitoids south of Umiakoviarusek Lake region, felsic dykes from the Main Showing area, and foliated granitoid samples from the eastern portion of the property.

4.3.4.1 Primitive Mantle Normalized REE Plots

On the REE plots, all of the granitoids are characterized by patterns which are flat or having slight decreases from the LREE to the HREE (Figure 4.11a-d). Most phase 1 rocks have relatively flat patterns with gentle decreases from the LREE to HREE (La_N/Yb_N = 2.83-5.13, Ce_N/Yb_N = 4.99-7.37, Gd_N/Yb_N = 1.43-1.91) and contain very weak negative Eu anomalies (Eu/Eu* = 0.71-0.85), reflecting the greater abundance of plagioclase versus the phase 2 granitoids (Figure 4.11a; Table 4.2).

The phase 2 granitoids have very similar REE patterns to the phase 1 granitoids with the exception of slightly lesser total REE (La_N/Yb_N = 6.20-9.28, Ce_N/Yb_N = 8.74-12.23, Gd_N/Yb_N = 2.12-2.65) and the absence of a weak negative Eu anomaly (Eu/Eu* = 0.37-0.53; Figure 4.11b; Table 4.2). The felsic dykes of the Main Showing area are very different from the other groups of granitoids and are characterized by very high total REE, particularly the LREE (La_N/Yb_N = 4.69-6.43, Ce_N/Yb_N = 5.38-6.94), and very positive Eu anomalies (Eu/Eu* = 1.00-1.26), reflecting greater plagioclase content relative to the granitoids south of Umiakoviarusek Lake (Figure 4.11c; Table 4.2). Foliated granitoids have similar plots to the phase 1 and phase 2 with the exception of slightly negative Eu anomalies (Eu/Eu* = 0.31-0.34; Figure 4.11d; Table 4.2).

4.3.4.2 Extended Primitive Mantle Normalized Trace Element Plots

The extended trace element plots for the OKG granitoids show remarkable consistency with only minor variations between the groups, and generally show overall decreases from the more incompatible to the less incompatible elements (Figure 4.12a-d).

Consistent with all the groups are pronounced negative Th anomalies, with the exception of one foliated granitoid, negative Sr and Ti; as well as variably positive Zr anomalies. Values for Nb are variable, with all granitoids showing a rough flat to negative behaviour (Figure 4.12). Similar to the anorthositic rocks the highly mobile elements Ba, Rb and K behave fairly coherently on these plots, with one foliated granitoid exception (Figure 4.12d), and suggest that the samples chosen for these plots have not had significant changes in their chemistry due to metamorphism.

The pronounced negative Th, and relatively flat to negative Nb are features within the granitoids that are particularly interesting and suggest that they have inherited this signature from some crustal source depleted in these elements. The Nain Province gneisses from this study (section 4.6), those of Schiøtte *et al.* (1993), and Lightfoot (1998), also contain pronounced negative Th and Nb anomalies and suggest a most probable crustal link to the Nain Province. Likewise, the *In1* and *In2* groups of the anorthositic rocks of the property also show this behaviour. Furthermore, the negative Sr and Ti, and positive Zr anomalies associated with the granitoids (Figure 4.12), appear to contrast with the anorthositic rocks of the property, which show positive Sr and Ti, as well as relatively flat to negative Zr (Figure 4.6). This divergent behaviour suggests that there is a common crustal source and a genetic tie to each other; similar results have been observed within the Nain Plutonic Suite (Emslie and Stirling, 1993; Emslie *et al.*, 1994), and suggests that there is a cursory similarity between the Paleoproterozoic anorthositic-granitoid rocks of the property and those of the younger Mesoproterozoic NPS.

4.4 Paleoproterozoic Mafic-Felsic Dykes

Since most of the mafic dykes associated with the OKG prospect are fine to medium grained they either reflect liquid compositions, or are close approximations of the liquid compositions; hence, the effects of cumulus mineralogy on the geochemistry of the dykes is not as pronounced as the anorthositic-granitoid rocks of the property. This section provides major and trace element discrimination diagrams, coupled with REE and extended-REE plots for the mafic dykes of the property. Since only six samples have been collected (5 mafic, 1 felsic), the usage of MgO versus major and trace element plots would not readily represent the fractionation trends associated with the suite, and are not used herein.

4.4.1 Discrimination Diagrams

The discrimination diagrams chosen to geochemically characterize the mafic dykes include Irvine and Baragar's (1971) TAS and AFM plots, and Jensen's (1976) cation plot, for the major elements; and Pearce and Cann's (1973) Ti-Zr-Y plot, Pearce and Norry's (1979) Zr/Y-Zr plot and Meschede's (1986) Zr-Nb-Y plot for the trace elements.

On the TAS plot, most of the mafic dyke samples cluster close along the alkaline-subalkaline boundary with a transitional chemistry between the two geochemical groups (Figure 4.13a). The dykes have a predominant tholeiitic affinity on the AFM plot with most samples having elevated MgO and FeO* with the exception of the felsic dyke (P96-42B) that lies in the left-hand side of the plot (Figure 4.13b). A similar geochemical clustering occurs on the Jensen (1976) cation plot, with most dykes lying within the high-

Fe tholeiite -> high-Mg tholeiite -> basaltic komatiite fields; while the felsic dyke has a tholeiitic dacite character (Figure 4.13c).

Although the major element plots provide a descriptive characterization, they give little information about the petro-tectonic affinity of the dykes. Although the chosen diagrams were created for basaltic rocks, the predominant fine-grained nature of the dykes and mafic character renders the diagrams useful for discrimination purposes. On Pearce and Cann's (1973) Ti-Zr-Y diagram most of the dykes lie in field D, typical of within plate basalts; while the felsic dyke lies outside of all the fields (Figure 4.14a). A similar distribution occurs on the Zr-Zr/Y diagram of Pearce and Norry (1979), with all samples lying within or along the edge of field A, typical of within plate basalts (Figure 4.14b). With the exception of the felsic dyke, the mafic dykes all lie within fields AII and C of Meschede's (1986) Zr-Nb-Y diagram, typical of within-plate tholeiitic basalts; while the felsic dyke lies outside of all fields (Figure 4.14c).

4.4.2 Primitive Mantle Normalized REE and Extended Trace Element Plots

Primitive mantle normalized REE patterns for the mafic dykes have a decreasing pattern from the LREE (10-40x primitive mantle; La_N/Yb_N = 2.71-4.68; Ce_N/Yb_N = 3.98-6.36) to the HREE (4-7x primitive mantle; Gd_N/Yb_N = 1.64-2.13), with no enrichment or depletion in any of the REE (e.g. no + or – Eu anomalies); this pattern is typical of within plate tholeiites (WPT; Figure 4.15a; Table 6.3). The exception to this behaviour is the felsic dyke sample (P96-42B) which shows a decrease from the LREE (100-200x primitive mantle; La_N/Yb_N = 5.49; Ce_N/Yb_N = 7.57) to HREE (20-30x primitive mantle;

Gd_N/Yb_N = 1.72), have higher total REE, and a weakly negative Eu anomaly (Eu/Eu* = 0.63); this pattern is very similar to some of the granitoids (Figure 4.14a; Table 4.3).

Extended elemental plots show decreases from the more incompatible to the less incompatible elements, with an overall decreasing pattern from left to right on the diagram. In particular, all of the mafic dykes appear to have variably flat to negative Rb, Th, and K; variably positive to flat Nb, flat to negative Sr, and distinctly positive Zr and Ti anomalies (Figure 4.15a). This pattern is typical of within plate tholeiitic rocks; however, the relative enrichments in some of the LFSE (e.g. K), and the enrichments in LREE and Zr suggest a crustal influence, or inheritance from the mantle source region. Furthermore, some of the samples show negative Th, consistent with a Nain Province crustal influence; while high Ti within the dykes suggests that these rocks may have some similarities to high-Ti flood basalts (i.e. Michael and Shabogamo gabbros; cf. Emslie *et al.*, 1997).

The sample P96-42B contains higher total REE, and greater enrichments in LREE and LFSE relative to the WPT group (Figure 4.15b). This sample also shows a depletion in Th and K, very pronounced negative Sr and Ti, and a positive Zr anomaly (Figure 4.15b). The pattern of this sample has some similarities to the granitoids of the property.

4.5 Mesoproterozoic Mineralized Pyroxenitic Rocks

4.5.1 Discrimination Diagrams

The pyroxenitic rocks have been plotted on similar discrimination type diagrams as the anorthositic rocks from the OKG prospect. On the TAS plot the pyroxenites are characterized by very low Na_2O+K_2O (0.18-0.23wt%) and low SiO_2 (35.70-48.68wt%)

with most samples in the subalkaline field, and others straddling the alkaline-subalkaline field or just slightly within it (Figure 4.16a). On the AFM plot the pyroxenites are characterized by high MgO (6.10-23.21wt%) and FeO* (19.35-62.78wt%) and show a distinctive clustering within the tholeiitic field hugging the MgO-FeO* side of the diagram (Figure 4.16b).

The Jensen (1976) cation plot shows the greatest evidence for an ultramafic and mantle-derived origin for the OKG pyroxenites. All the pyroxenite samples are intensely clustered with elevated FeO*+TiO_2 and MgO, within the basaltic komatiite to peridotitic komatiite field (Figure 4.16c). Some inkling of elevated Al_2O_3 is observed in some samples, reflects minor plagioclase abundance; however, these samples still have very elevated MgO (Figure 4.16c).

4.5.2 MgO versus Major Element Plots

Similar to the anorthositic rocks, the pyroxenitic rocks have MgO plotted against the major elements CaO, Na_2O, K_2O, Al_2O_3, FeO*, TiO_2 and P_2O_5 to measure the effects that cumulus and accessory mineralogy have on the dykes (Figure 4.17). The MgO content of the dykes is variable occurring in three clusters with most having MgO=13.37-23.21wt%; a moderately sulphide enriched group with MgO=11.87-13.35wt%; and a high sulphide group of two samples with MgO=6.10-7.50wt%. These are closely paralleled by their Mg#'s with the groups having Mg#'s between 39.53-63.51, 28.06-31.76, and 15.41-17.54, respectively. The wide range of the higher Mg# group ranges from relatively unfractionated to moderately fractionated; however, the lower Mg#

groups likely have diluted Mg#'s due to elevated FeO* associated with sulphide mineralization.

The elements plotted against MgO appear to be in three groups, including: 1) those controlled by cumulus plagioclase; 2) those controlled by cumulus pyroxene; and 3) those controlled by sulphides. The plagioclase dependant elements include Na_2O (0.17-1.80wt%), K_2O (0.01-0.57wt%), Al_2O_3 (0.08-8.83wt%), and to a lesser extent CaO (2.04-6.11wt%). With increasing MgO the former three elements either show a decrease with MgO, in the case of plagioclase bearing samples, or are flat in plagioclase absent samples (Figure 4.17a-c). CaO shows a weak drop with MgO, however, the significant scatter suggests that some Ca may have been substituted into the orthopyroxene structure, and is not solely controlled by plagioclase (Figure 4.17d).

Those which are controlled by orthopyroxene accumulation include MnO (0.03-0.54wt%) and TiO_2 (0.25-0.63wt%) which show progressive increases with MgO, reflecting increases in cumulus orthopyroxene; a group of Ti-elevated samples most likely reflect increases in cumulus ilmenite or titanomagnetite (Figure 4.17e-f). In contrast to increases with MgO, the sulphide controlled element(s) show decreases with MgO. Typical fractionation trends for MgO versus FeO* should show progressive increases and positive slope for both elements; however, the replacement of MgO rich orthopyroxene with FeO* rich sulphide accounts for the progressive decrease in the latter with increasing MgO (Figure 4.17g). Phosphorous shows very little important information about the dykes, as most values are quite low (0.01-0.28), elevated samples reflecting accessory apatite inclusions in either the plagioclase or sulphides (Figure 4.9h).

4.5.3 MgO versus Trace Element, and Other Trace Element Plots

Similar to the major element plots the trace element plots show the similar three groups of plagioclase, pyroxene and sulphide controlled elements. The pyroxene-controlled elements include Cr (739-1444ppm), Sc (18-44ppm), V (54-156ppm), and Y (3-12.20ppm). All of these elements increase progressively with MgO; however, there is scatter on many of the plots that indicates a secondary control outside of orthopyroxene. The Cr values are fairly consistent with a few low Cr values (475-684ppm), reflecting lower Cr in orthopyroxene and one high sample (1729ppm) reflecting excess oxide or chromite (?; Figure 4.18a). Although the Sc plot shows significant scatter, there is a rough increase with MgO, and the scatter may reflect variable amounts of clinopyroxene and/or clinopyroxene exsolution in orthopyroxene (Figure 4.18b). Vanadium is very similar to MnO and TiO_2 with the exception of an elevated group with V=159-334ppm, reflective of cumulus oxides (Figure 4.18c). Yttrium has a similar character to V, but is slightly more scattered with a few samples with elevated Y (17-33ppm), most likely reflecting cumulus clinopyroxene instead of clinopyroxene exsolution in orthopyroxene (Figure 4.18d).

Nickel contents show a decrease with increasing with MgO very similar to the behaviour of FeO*, and is found in three groups including a high Ni group (14249-14564 ppm), moderate Ni group (9173-9787 ppm), and low Ni group (564-5295 ppm) (Figure 4.18e). The variations in the Ni content could be reflective of olivine; however, decreasing Ni contents with increasing with MgO is opposite to what would be expected with increasing olivine content in a rock. Furthermore, Figure 4.18f illustrates the strong

positive correlation between Ni and S and shows that the Ni contents are controlled by sulphide accumulation rather than olivine accumulation. The plot of Mg# versus Ni (Figure 4.18g) would be expected to show a positive correlation if Ni was controlled by olivine content and adds support to the other diagrams and the control of Ni content by sulphides.

Copper values (397-5935ppm) show a similar nature to the Ni values with decreases with increasing MgO; however, there is significant scatter in the dataset (Figure 4.18g). A plot of Cu versus S also has scatter but has a general increase in Cu with increasing S content (Figure 4.18i). The scatter in the Cu values also appears to be associated with higher S values and lower MgO values. It is likely that the scatter in the Cu values with higher sulphide content is due to weathering and mobilization of Cu, as is observed along some of the pyrrhotite grain edges in the massive sulphides (higher S content, lower MgO); features that are not readily observed in the disseminated pyroxenitic sulphides (lower S content, higher MgO). It is possible that fractionation of a Cu-rich sulphide liquid could explain the low Cu at high S contents (e.g. Li *et al.*, 1992; Zientek *et al.*, 1994; Barnes *et al.*, 1997a,b; Figure 4.18f), but this does not seem as likely as the above hypothesis.

The elements controlled by plagioclase include Sr (1.30-778.2 ppm), Ba (29.41-282.23 ppm), and Ga (3.99-23.11 ppm) which show progressive decreases with MgO (Figure 4.18g-j); Rb shows no particular trend and is very non-descriptive (Figure 4.18i). The decreases in the former three elements mirror the behaviour of Na_2O, K_2O and Al_2O_3 and represent decreasing plagioclase with increasing MgO.

4.5.4 Primitive Mantle Normalized Plots

4.5.4.1 Primitive Mantle Normalized REE Plots

With REE geochemistry there are two diverging subgroups including the surface pyroxenites and leucotroctolite, and samples from the subsurface drillhole OKG 96-09. Surface examples are relatively refractory having depletions in the LREE (La_N/Yb_N=0.19-0.39; Ce_N/Yb_N=0.21-0.36; La_N/Sm_N=0.28-0.63) and show general increases towards the HREE (Gd_N/Yb_N=0.47-0.66), with variably flat to negative Eu anomalies (Eu/Eu*= 0.08-0.14; Figure 4.19a; Table 4.4). One leucotroctolite sample from surface is grouped into the surface dyke category as it has an identical signature to the pyroxenitic rocks and suggests derivation from a common geochemical reservoir.

The subsurface dykes exhibit some contrasting geochemical behaviour relative to the surface dykes (Figure 4.19b) and are characterized by somewhat similar HREE distributions (Gd_N/Yb_N= 0.65-1.62), and similar negative to slightly positive Eu anomalies (Eu/Eu*=0.04-0.21; Figure 4.19b; Table 4.4). However, in contrast, the subsurface examples have much higher LREE, nearly and order of magnitude higher (La_N/Yb_N = 1.23-3.33; Ce_N/Yb_N = 1.16-3.50; La_N/Sm_N = 1.47-1.99; Figure 4.19b; Table 4.4). It is highly probable that this enrichment in the LREE is a function of greater contributions of LREE-enriched crustal material, likely a function of crustal contamination (see section 4.5.4.2, and 4.5.4.3).

4.5.4.2 Extended Primitive Mantle Normalized Trace Element Plots

Similar to the REE plots, the extended trace element plots also show a distinction between the surface and subsurface pyroxenites. Surface pyroxenites are characterized by an overall increase in elements from the LREE and LFSE to the HREE and HFSE (i.e. left to right in the diagram (Figure 4.19c). The dykes typically have elevated Rb, to a lesser extent K and Ti; and have well developed negative Th and Zr (Zr/Y = 0.6-1.4; Th/Y = 0.003-0.008), and to a lesser extent Eu (Figure 4.19c; Table 4.4). Strontium has variable behaviour and has both negative and positive anomalies that are either related to plagioclase content, or preferential contamination (Figure 4.19c). Although the dykes have refractory REE chemistry, there is some inkling of crustal influence at least in the form of Rb and K and suggests that these dykes may have experienced some contamination, but to a lesser extent than the subsurface dykes (e.g. Figure 4.19d); this is also supported by Nd isotope data (see Chapter 6). The negative Th anomaly associated with the surface dykes also points to at least a minor contribution from a Th depleted source, be this the original mantle source region, or influence from the negative Th Nain Province rocks (cf. Schiøtte *et al.*, 1993; Lightfoot, 1998; section 4.6).

The subsurface dykes are characterized by an overall greater abundance in most elements, and much higher LREE and LFSE (Figure 4.19d). The dykes are also characterized by elevated Ba, Rb and K, flat to very pronounced negative Th anomalies (Th/Y = 0.002-0.114); variably negative to positive Sr; flat to negative Zr (Zr/Y = 0.6-2.3), and flat to negative Ti (Figure 4.19d; Table 4.4). The pronounced increase in the LFSE and LREE, coupled higher Zr/Y ratios suggest that the subsurface dykes have

experienced greater levels of contamination relative to the surface dykes (e.g. Table 4.4). Furthermore, the pronounced negative Th anomaly associated with the dykes is consistent with the surface dykes, most of the granitoid and anorthositic rocks, and was likely inherited from Nain Province crustal contaminant (cf. Lightfoot, 1998).

4.5.4.3 Average Leuconorite and Surface Pyroxenite Normalized Plots

Leuconorite normalized plots of both the surface and subsurface dykes are plotted in figure 4.20a to see if there is geochemical coherence between both the subsurface and surface dykes. On this plot both the surface and subsurface dykes have decreased LREE, pronounced negative Eu, and relatively consistent and coherent HREE (Figure 4.20a). Although the patterns are similar, the subsurface dykes are characterized by greater enrichments in the LREE, a feature consistent with data presented earlier. However, the overall similar abundance with the exception of total abundance suggests that the subsurface and surface dykes have been derived from a common source, but have variable degrees of contamination.

In figures 4.20b and 4.20c, the subsurface pyroxenites are normalized to the average surface pyroxenite in order to distinguish the relative geochemical enrichments and depletions of these dykes relative to the surface dykes. On the normalized REE plot (Figure 4.20b), the subsurface dykes have much greater LREE enrichment and have pseudo-similar behaviour from the Eu to the HREE. These results confirm that the subsurface dykes have had significant LREE-enriched crustal input. On the multi-element plot the dykes are characterized by overall increases in the LREE and LFSE, have variably positive and negative Sr and Eu, but show pronounced increases in Zr (with

the exception of one samples, and a marked depletion in Ti (Figure 4.20c). The increases in LREE, LFSE and Zr, coupled with negative Ti, add further support to greater crustal influence in their genesis relative to the surface dykes.

4.5.4.4 A Subcontinental Lithospheric Mantle Source?

The high MgO, mafic to ultramafic mineralogy, and refractory REE chemistry in the case of the surface pyroxenitic-leucotroctolitic dykes points to a mantle source region for their genesis. In the case of the surface pyroxenites REE geochemistry shows very pronounced depletions in the LREE, variably negative Eu, and relatively enrichments in the HREE relative to the LREE (Figure 4.19a; Table 4.4). Such depletions in the LREE (+some LFSE; Figure 4.19c) are typical of depleted source regions (e.g. Hofmann, 1988); however, this may be in part due to the cumulate nature of these rocks.

Regardless, when the REE data for the OKG surface pyroxenites are compared with compiled values for subcontinental lithospheric mantle (SCLM) spinel peridotites and lherzonlites of Jochum *et al.* (1989), McDonough (1990), and Wilson *et al.* (1996), there is a fairly good compliance between the dykes and the SCLM (Figure 4.21a,b). Exceptions include a slight enrichment in the MREE and HREE, as well as Ti and Y (Figure 4.21a,b). Although there are minor discrepancies, the fairly similar patterns between the pyroxenites and compiled SCLM values suggest that the OKG pyroxenitic rocks may have been derived from such a depleted (spinel peridotite/lherzolite?) source region. However, since these rocks do not represent liquid compositions it is not possible to prove that they are direct partial melts from this source; however, the strong

similarities between compiled SCLM values and the OKG pyroxenites may reflect generation from a depleted source region.

4.6 Archean Nain Province Gneisses

4.6.1 Primitive Mantle Normalized REE and Extended Trace Element Plots

Only four samples of the Nain Province gneisses (3 amphibolite-mafic granulite, 1 metatonalite) have been analyzed for REE and trace elements as part of this study, and the results are plotted on Figure 4.22a and 4.22b. Primitive mantle normalized REE patterns of the samples have two distributions, the three mafic-granulite/amphibolite samples have relative flat patterns with slight enrichments in the LREE and have moderate to slightly negative Eu anomalies (Figure 4.22). The metatonalitic sample is characterized by an order of magnitude enrichment in the LREE has a relatively flat Eu anomaly (Figure 4.22a).

On the extended trace element plots, the amphibolitic samples are characterized by pronounced negative Th and Sr anomalies, as well as relatively flat to negative Nb and Zr and Ti; the latter are much to a lesser extent (Figure 4.22b). Furthermore, the metabasic samples have enrichments in Ba, Rb, K, and relative enrichments in the LREE (Figure 4.22b). The metatonalitic sample is characterized by well developed negative Th and Sr like the metabasic samples, but is also characterized by negative Th, and Ti, coupled with enrichments in Ba, Rb, K, the LREE and Zr (Figure 4.22b). The pronounced negative Th and Nb are features similar to the Nain Province rocks of Schiøtte *et al.* (1993) located approximately 10 kilometers north in Okak Bay, and the

negative Th and Nb of the Nain Province rocks is consistent with the Nain Province near Voisey's Bay (Lightfoot, 1998).

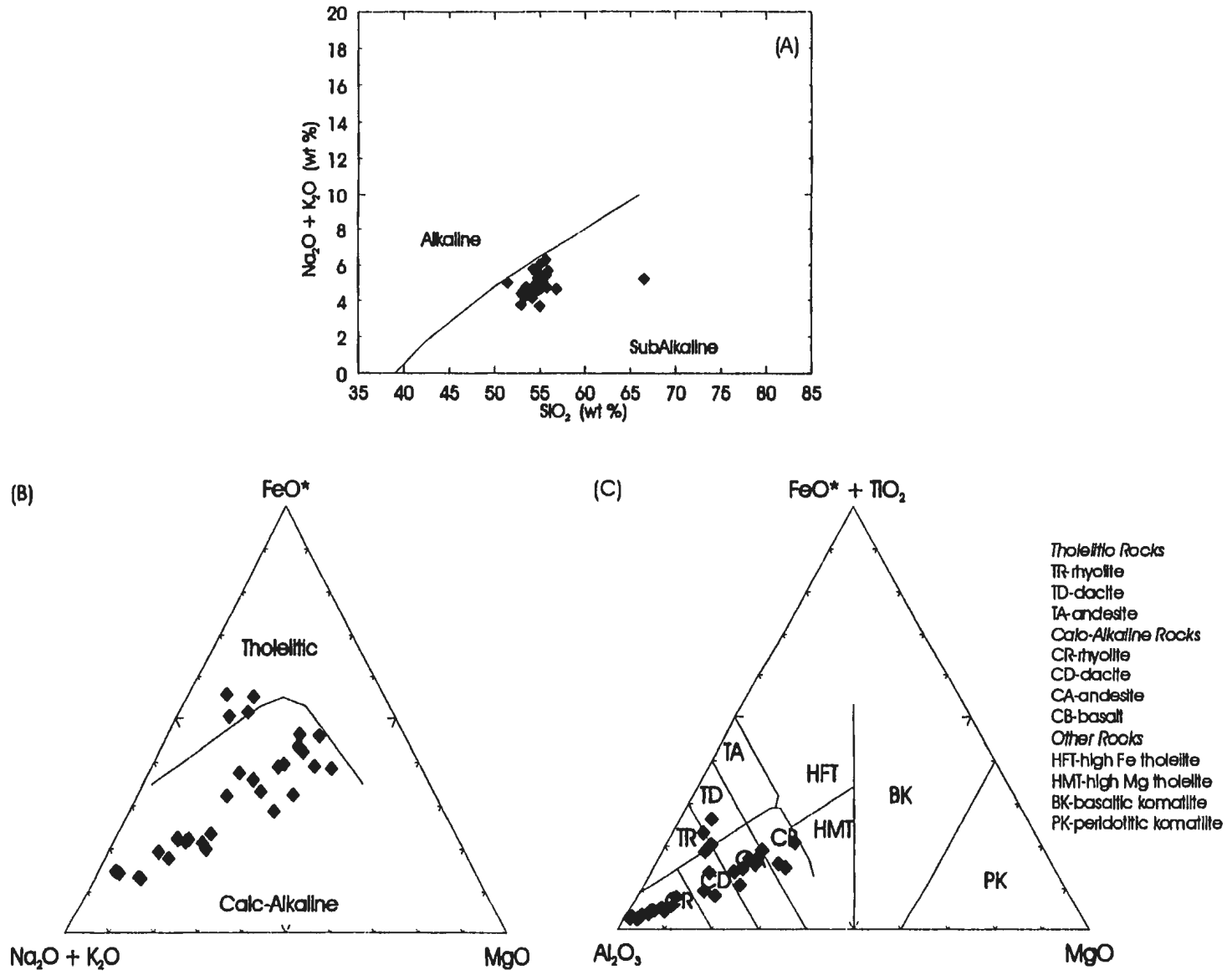

Figure 4.1. Irvine and Baragar's (1971) TAS (a) and AFM (b), and Jensen's (1976) cation plots of the OKG anorthositic rocks.

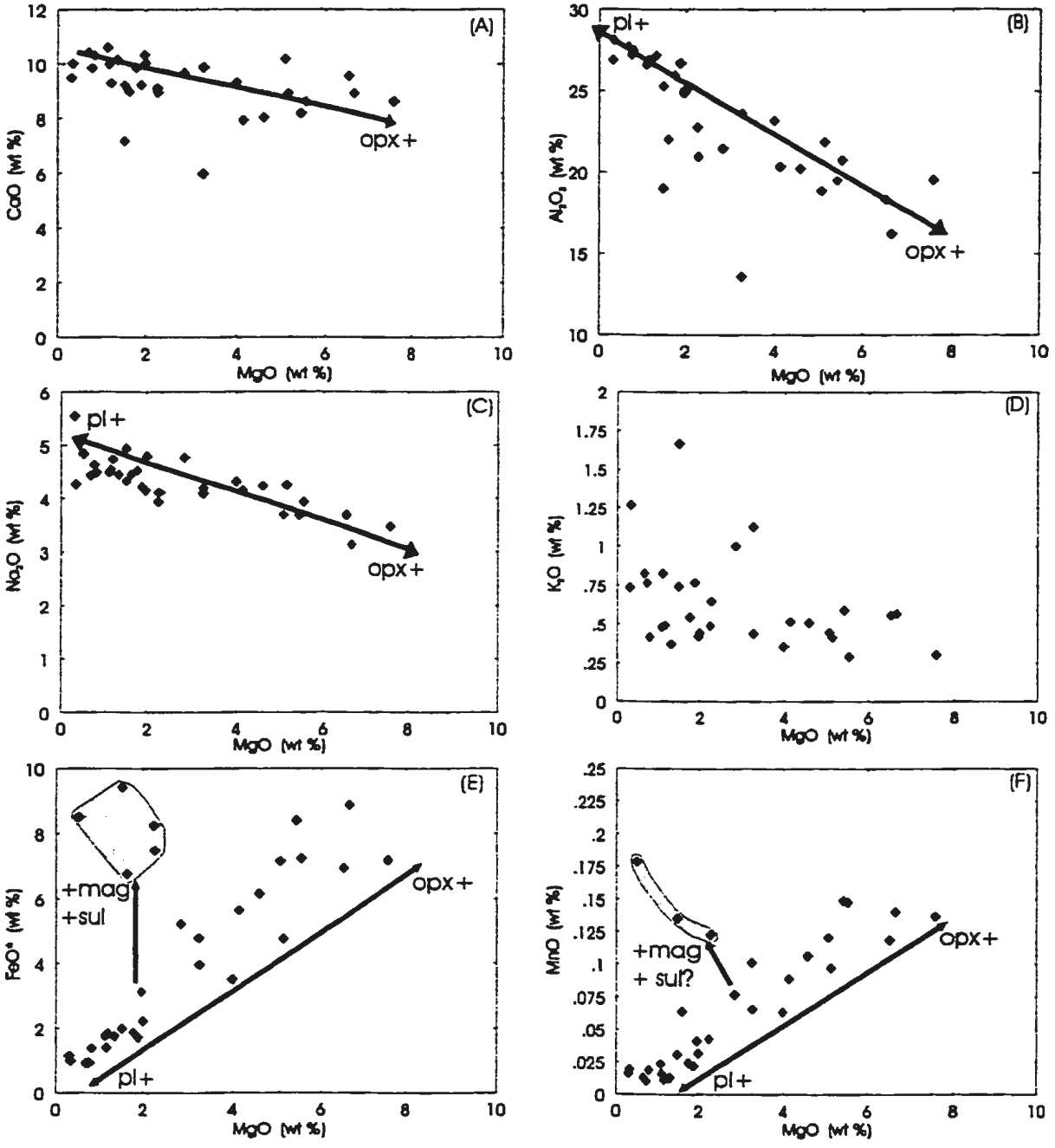

Figure 4.2. MgO versus major element plots of the OKG anorthositic rocks, including (a) CaO, (b) Al_2O_3, (c) Na_2O, (d) K_2O, (d) FeO*, (e) MnO, (f) TiO_2, and (g) P_2O_5.

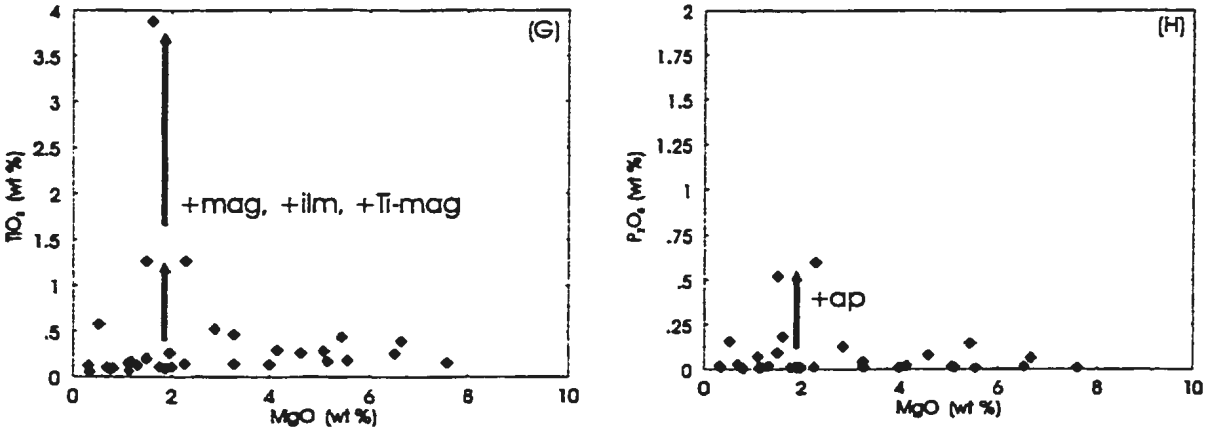

Figure 4.2. (Continued)

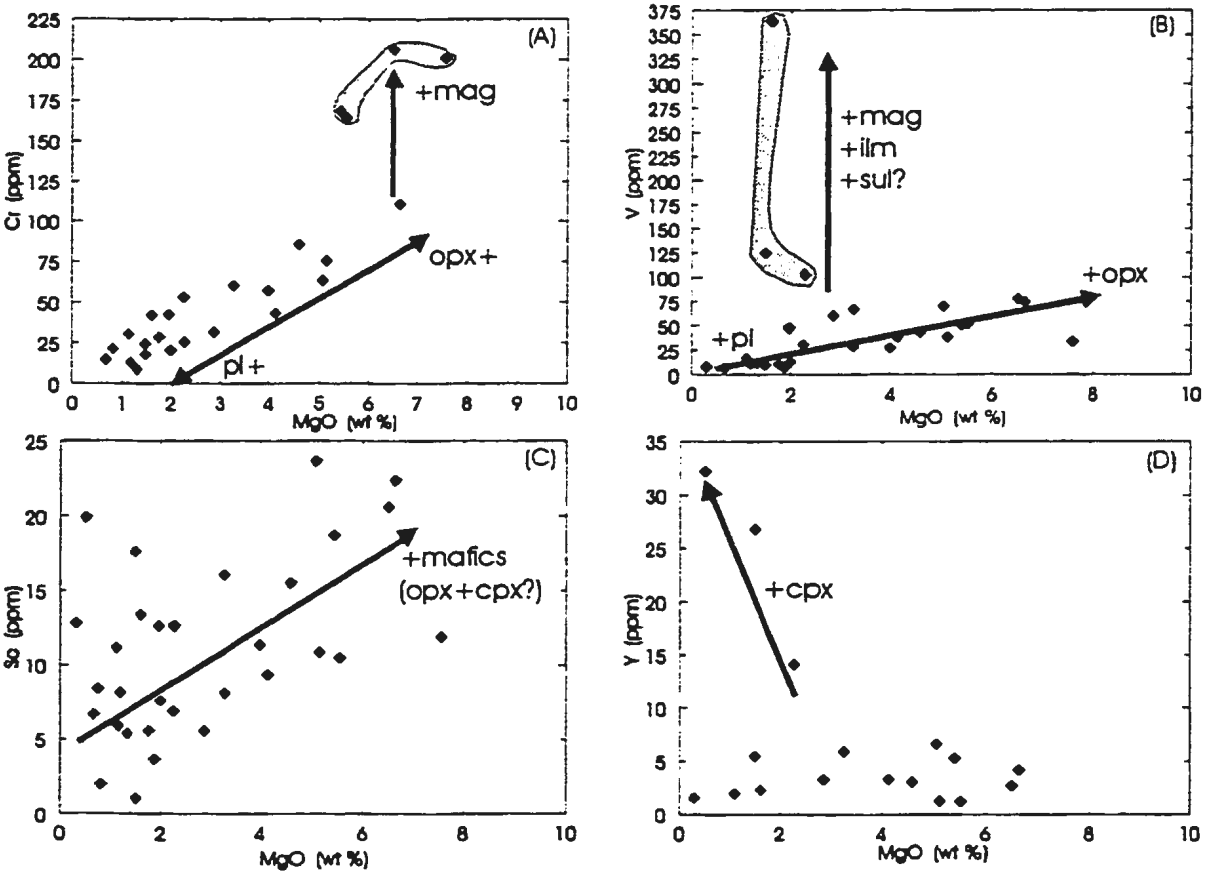

Figure 4.3. MgO versus (a) Cr, (b) V, (c) Sc, (d) Y, (e) Ni, (f) Ni versus S, and MgO versus (g) Sr, and (h) Ga for the OKG anorthositic rocks.

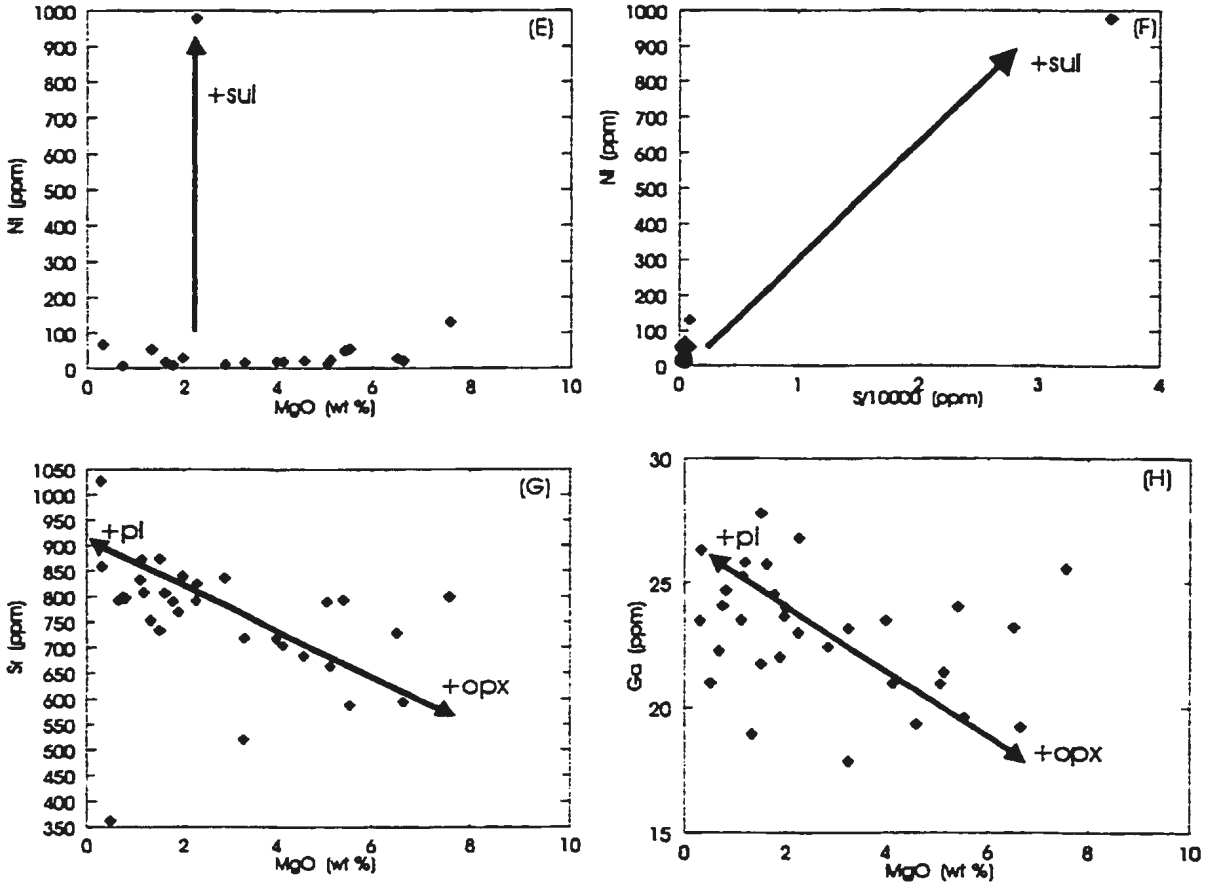

Figure 4.3. (Continued).

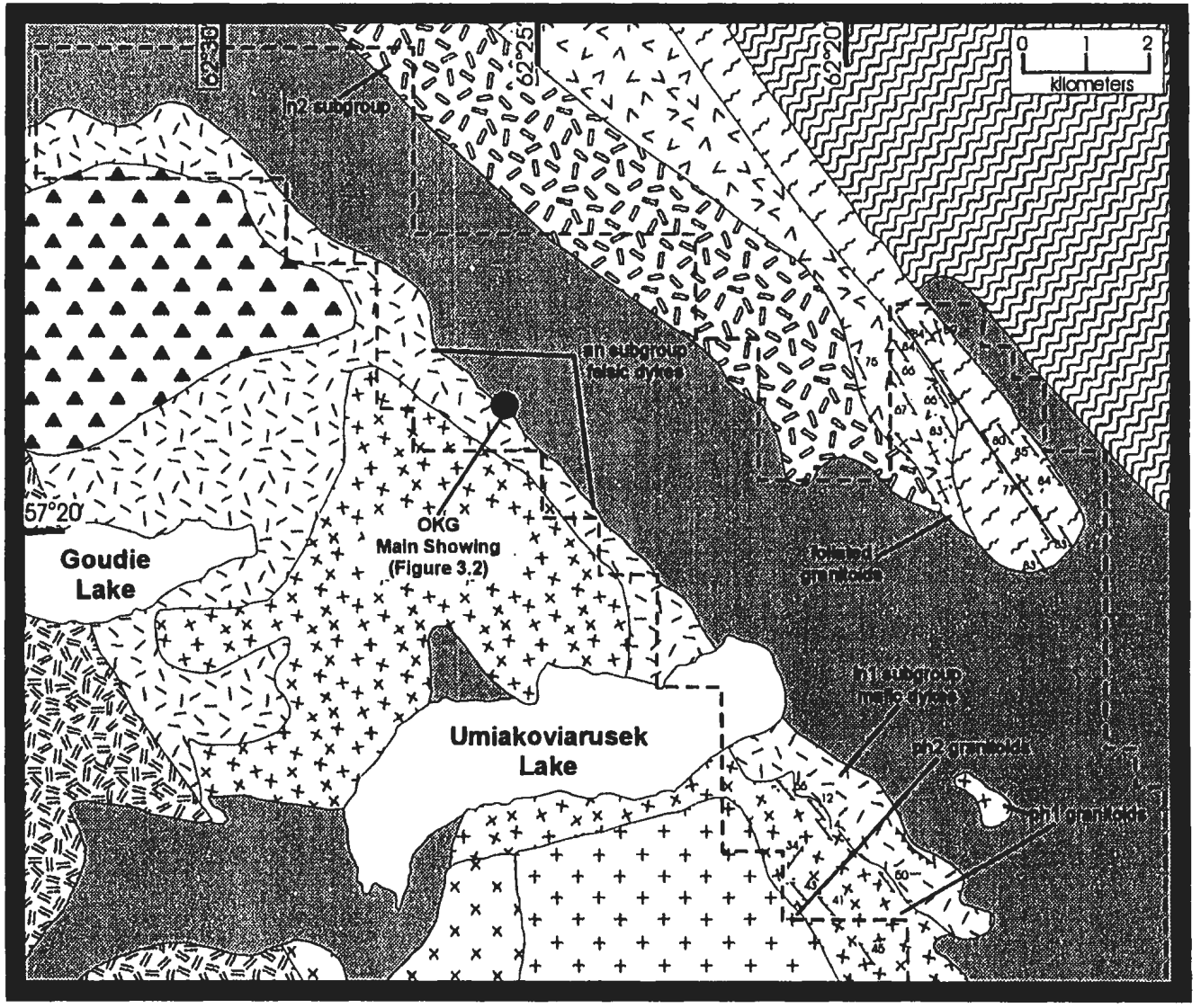

Figure 4.4. Geology of the OKG prospect with location of lithogeochemical groups. Geology outside of property boundaries from Ryan et al. (1997, 1998) and Emslie et al. (1997).

Legend

Quaternary

Overburden and glacial drift

Paleoproterozoic

Granitoid Plutons

Hornblende granite

Quartz monzonites, ovoidal feldspar clinopyroxene quartz monzonite (phase 2 granitoids)

Variably foliated orthopyroxene, fayalite, clinopyroxene, hornblende, biotite-bearing monzonites, syenites (phase 1 granitoids)

Foliated orthopyroxene, fayalite, clinopyroxene, biotite bearing quartz syenites, monzonite, granite

Anorthositic Plutons

Dark grey and black anorthosite

Buff, olivine-bearing leuconorite

Dark black to light grey anorthosite and leuconorite (contains *an* and *ln1* subgroups)

Buff weathering leuconorite and gabbronorite (*ln2* subgroup)

Archean

Amphibolite, mafic granulite, metatonalite, quartzofeldspathic gneiss

Quartzofeldspathic gneiss

Symbols

Foliation or gneissosity, inclined

Foliation or gneissosity, vertical

Compressional fault

Sinistral strike-slip fault

Claim boundary

Figure 4.4. (Continued)

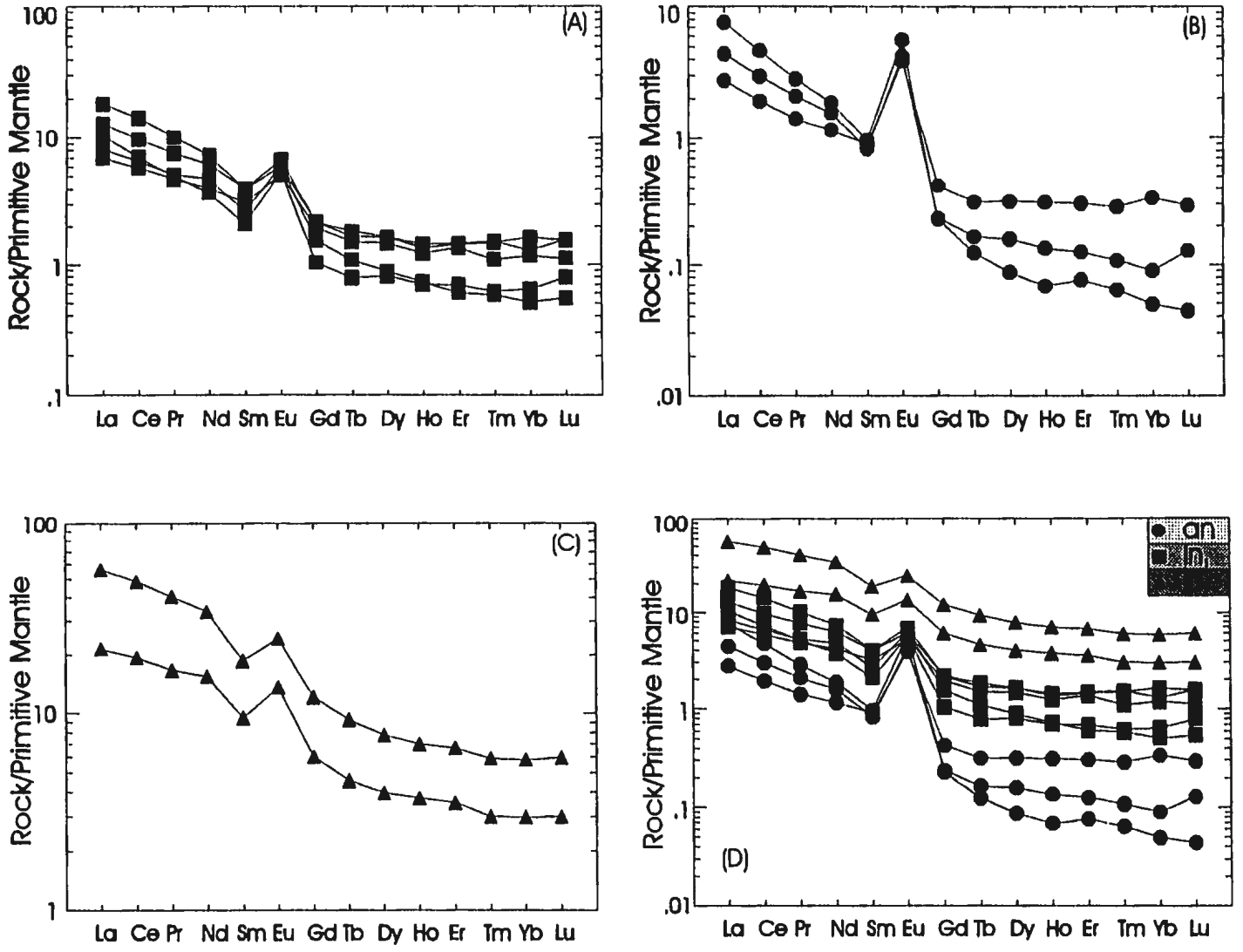

Figure 4.5. Primitive mantle normalized REE plots of the OKG anorthositic rocks, including (a) *an* group, (b) *In1* group, (c) *In2* group, and (d) composite plot of all groups. Primitive mantle normalization factors from Hofmann (1988).

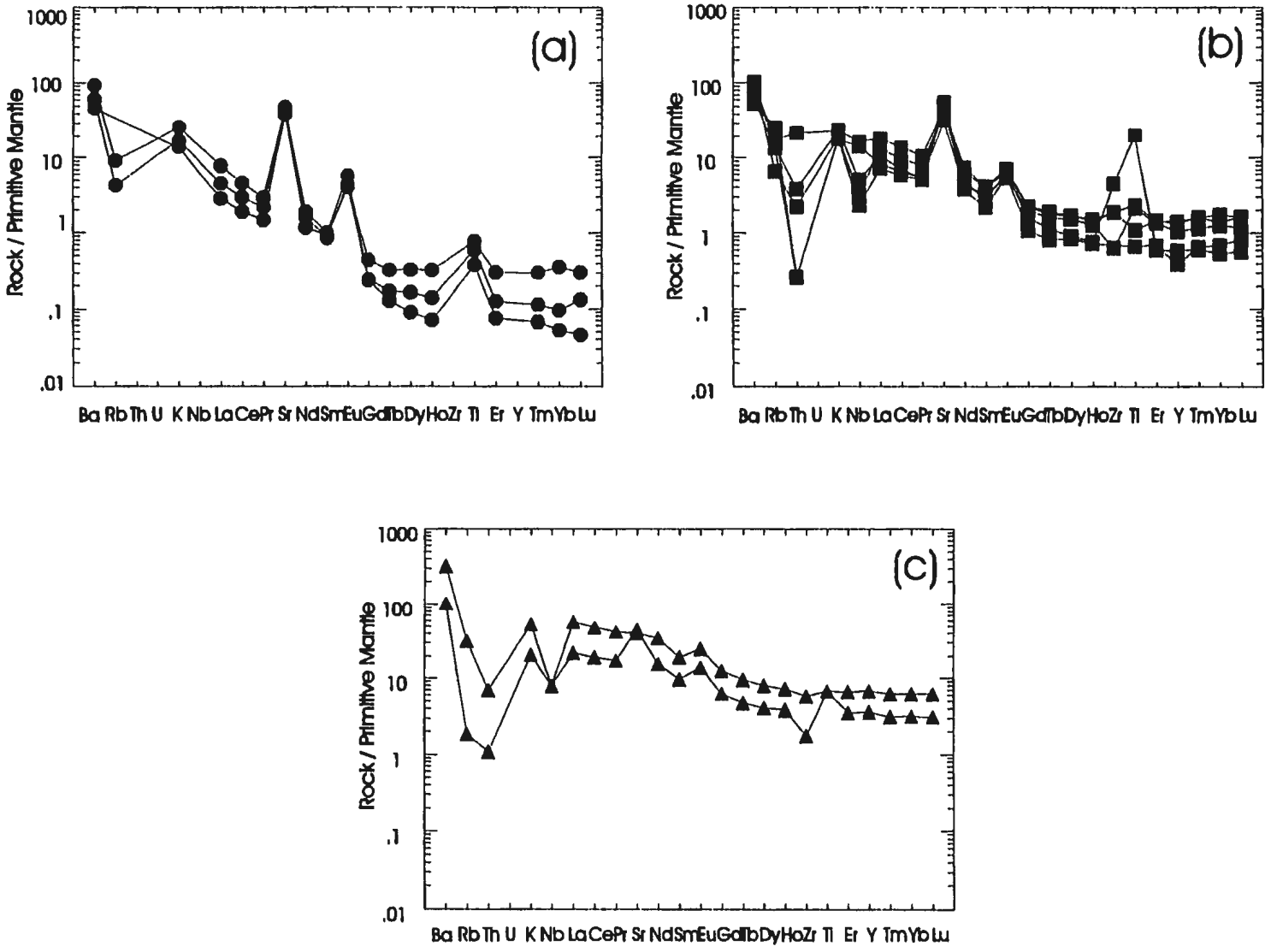

Figure 4.6. Primitive mantle normalized extended multi-element plots of the OKG (a) *an* group, (b) *In1* group, and (c) *In2* group. Normalization factors from Hofmann (1988).

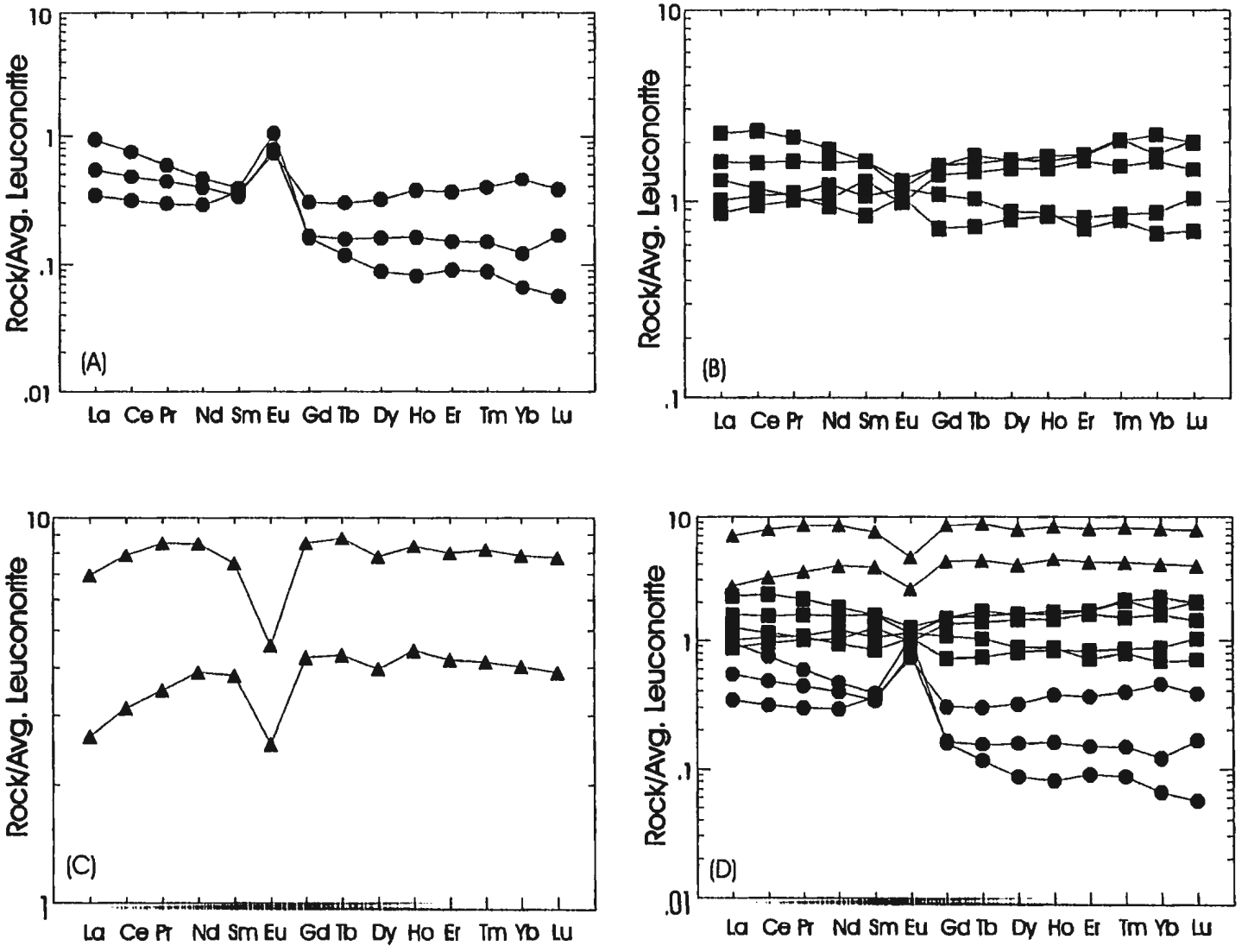

Figure 4.7. Average OKG leuconorite normalized REE plots of (a) *an* group, (b) *In1* group, (c) *In2* group, and (d) composite plot of anorthositic groups.

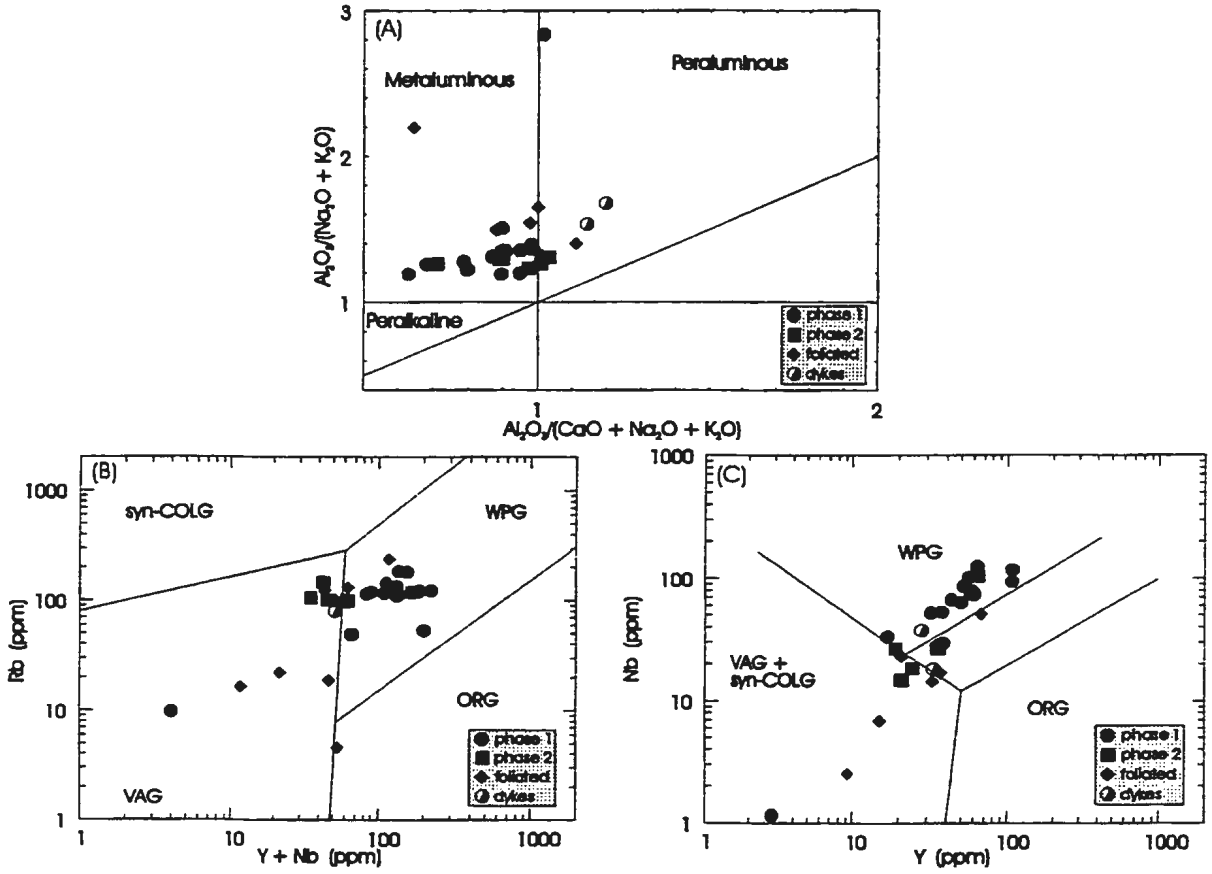

Figure 4.8. Discrimination diagrams of the OKG granitoids, including (a) Shand's Index of Maniar and Piccoli (1989), and the Rb-Y+Nb and Nb-Y diagrams of Pearce et al. (1984). Fields in (b) and (c) include: syn-COLG=syn collisional granitoids; WPG= within plate granitoid; ORG=orogenic granitoids; and VAG=volcanic arc granitoids.

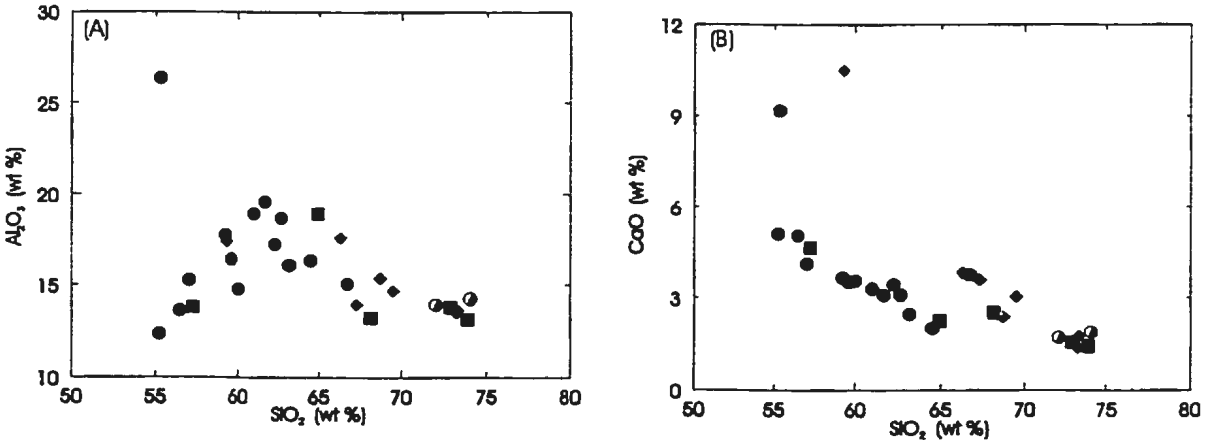

Figure 4.9. SiO_2 versus major element plots, including (a) Al_2O_3, (b) CaO, (c) K_2O, (d) Na_2O, (e) MgO, (f) FeO*, (g) MnO (h) TiO_2, and (i) P_2O_5. Symbols as in figure 4.8.

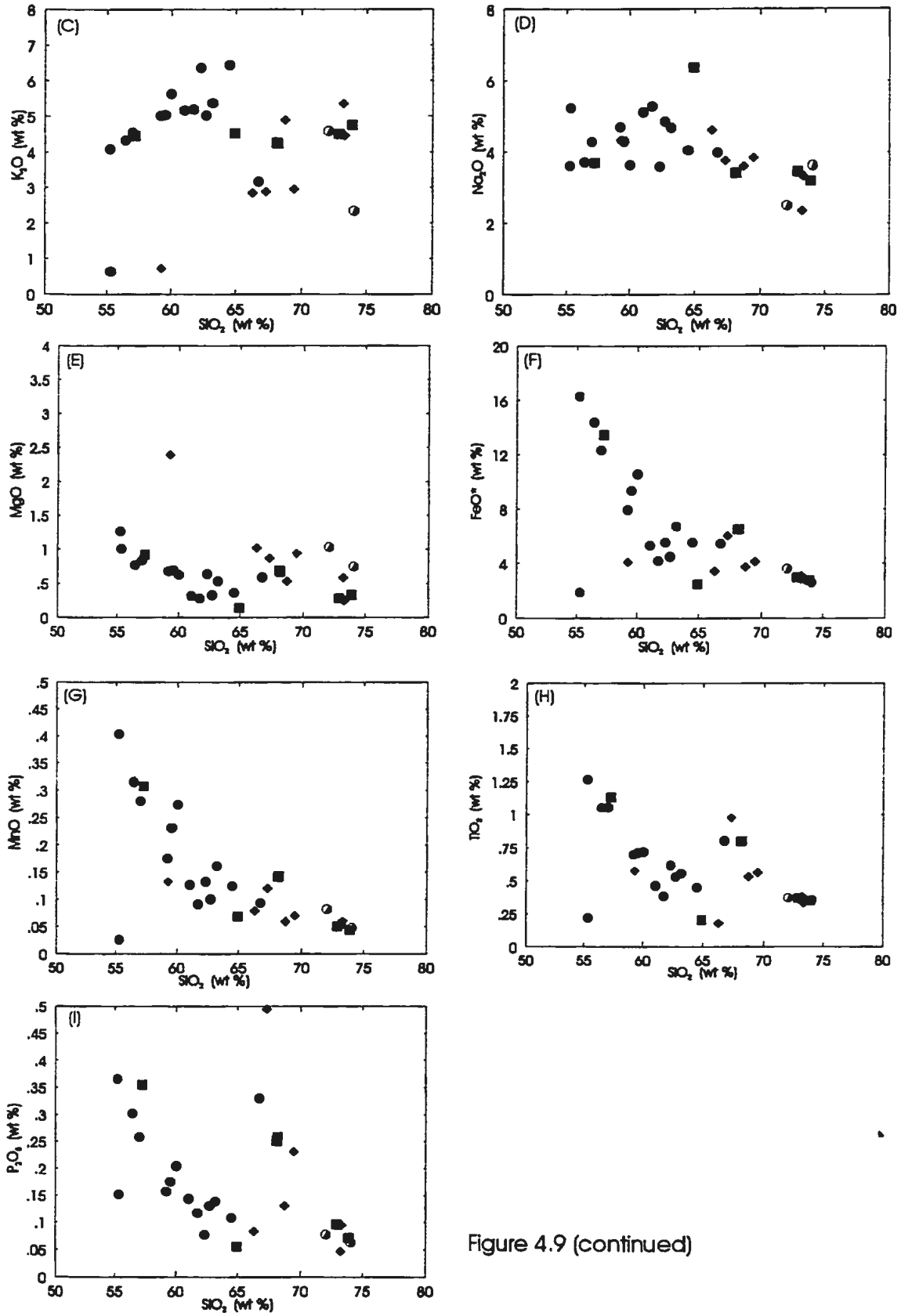

Figure 4.9 (continued)

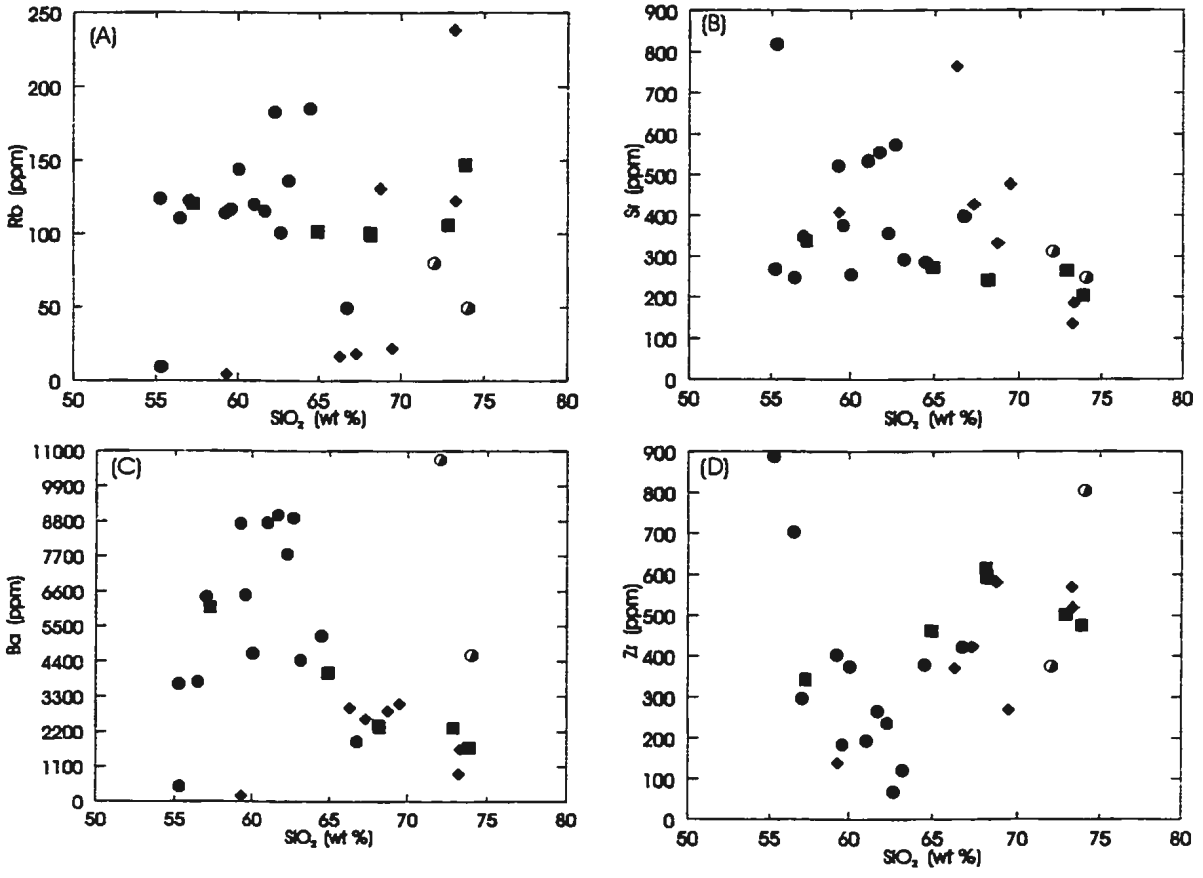

Figure 4.10. SiO_2 versus trace element plots, including (a) Rb, (b) Sr, (c) Ba, and (d) Zr.

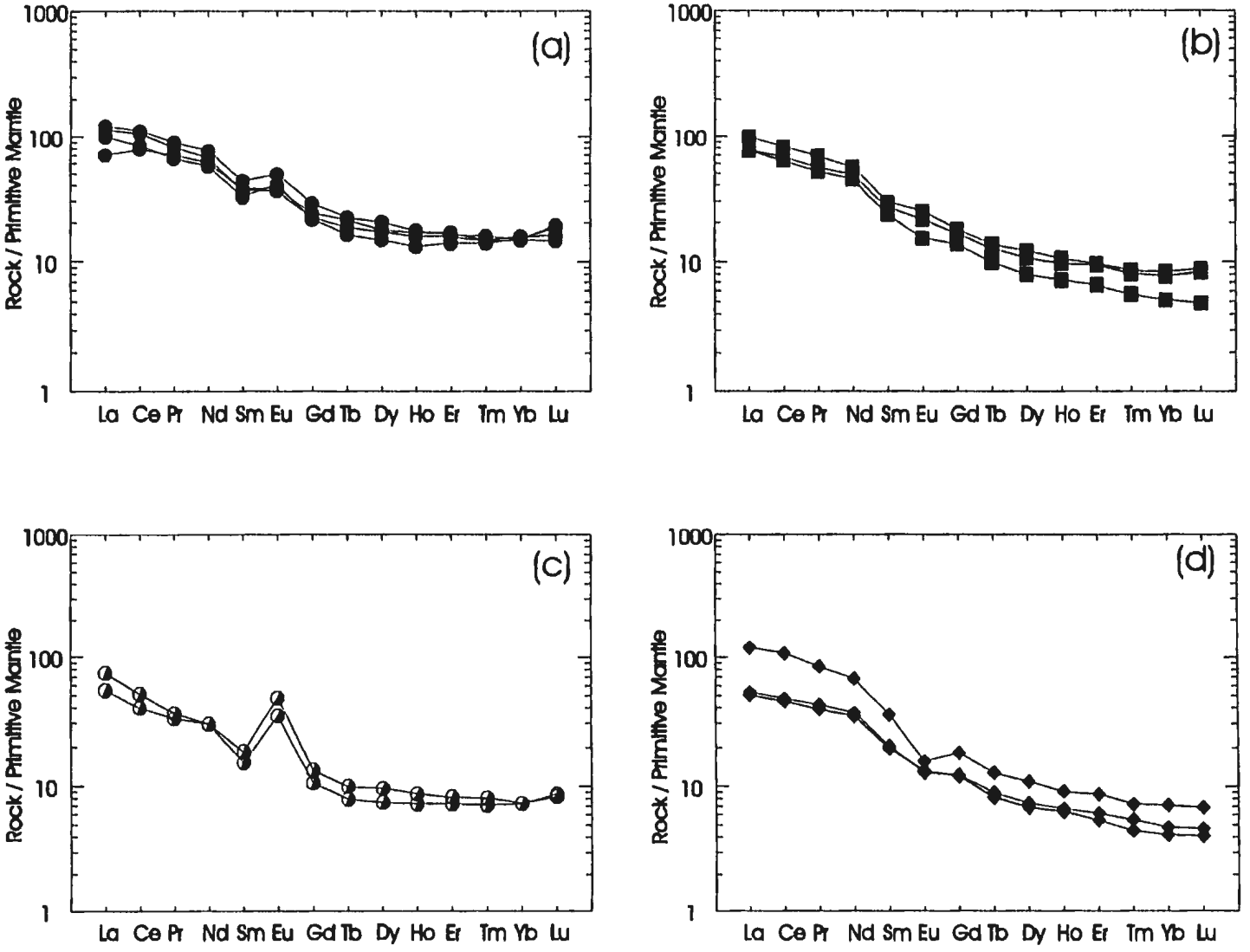

Figure 4.11. Primitive mantle normalized REE plots of the phase 1 granitoids (a), phase 2 granitoids (b), felsic dykes (c),and foliated granitoids (d). Primitive mantle normalization values from Hofmann (1988).

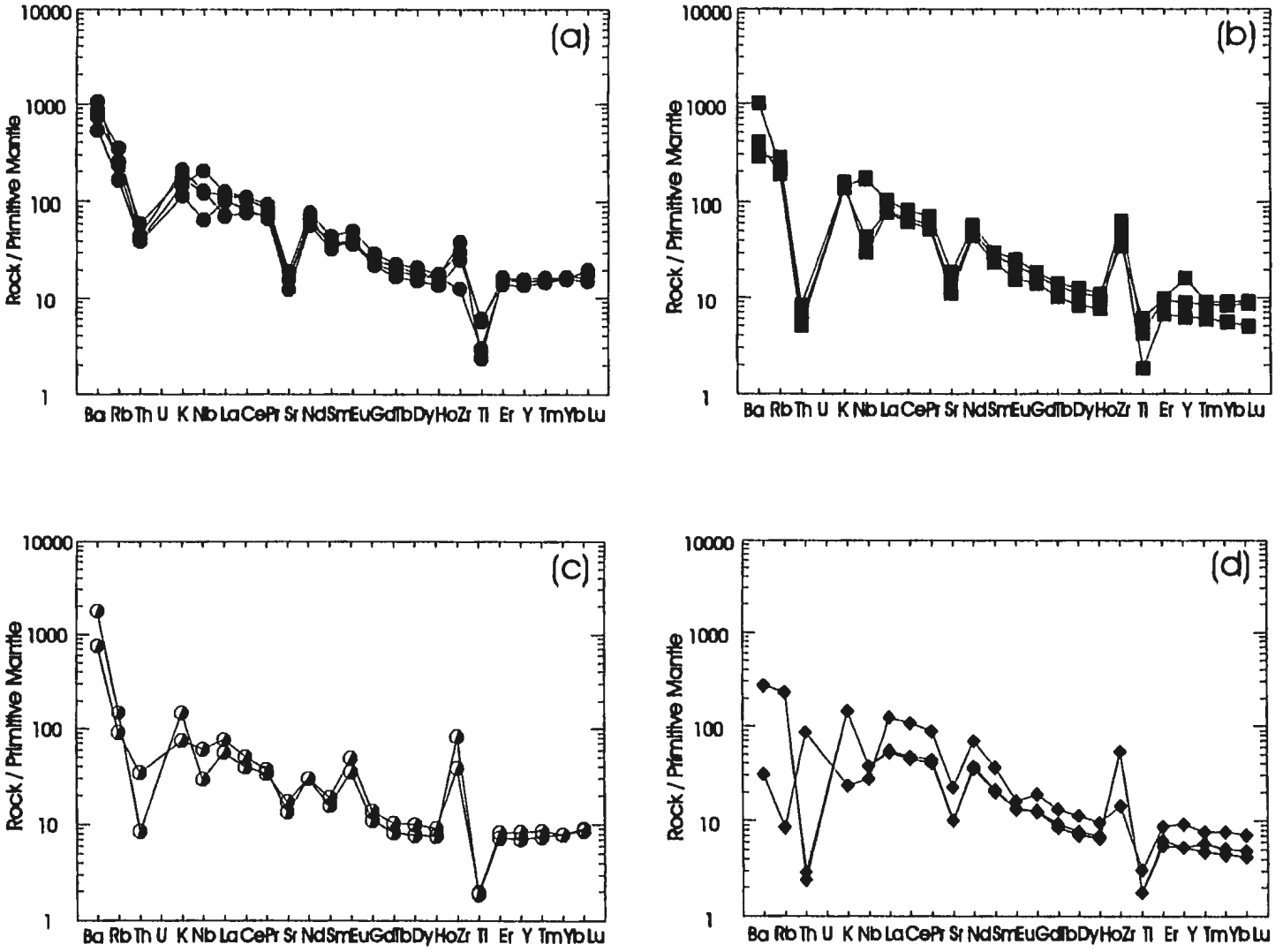

Figure 4.12. Extended primitive mantle normalized trace element plots of the phase 1 granitoids (a), phase 2 granitoids (b), felsic dykes (c), and foliated granitoids (d). Primitive mantle normalization values from Hofmann (1988).

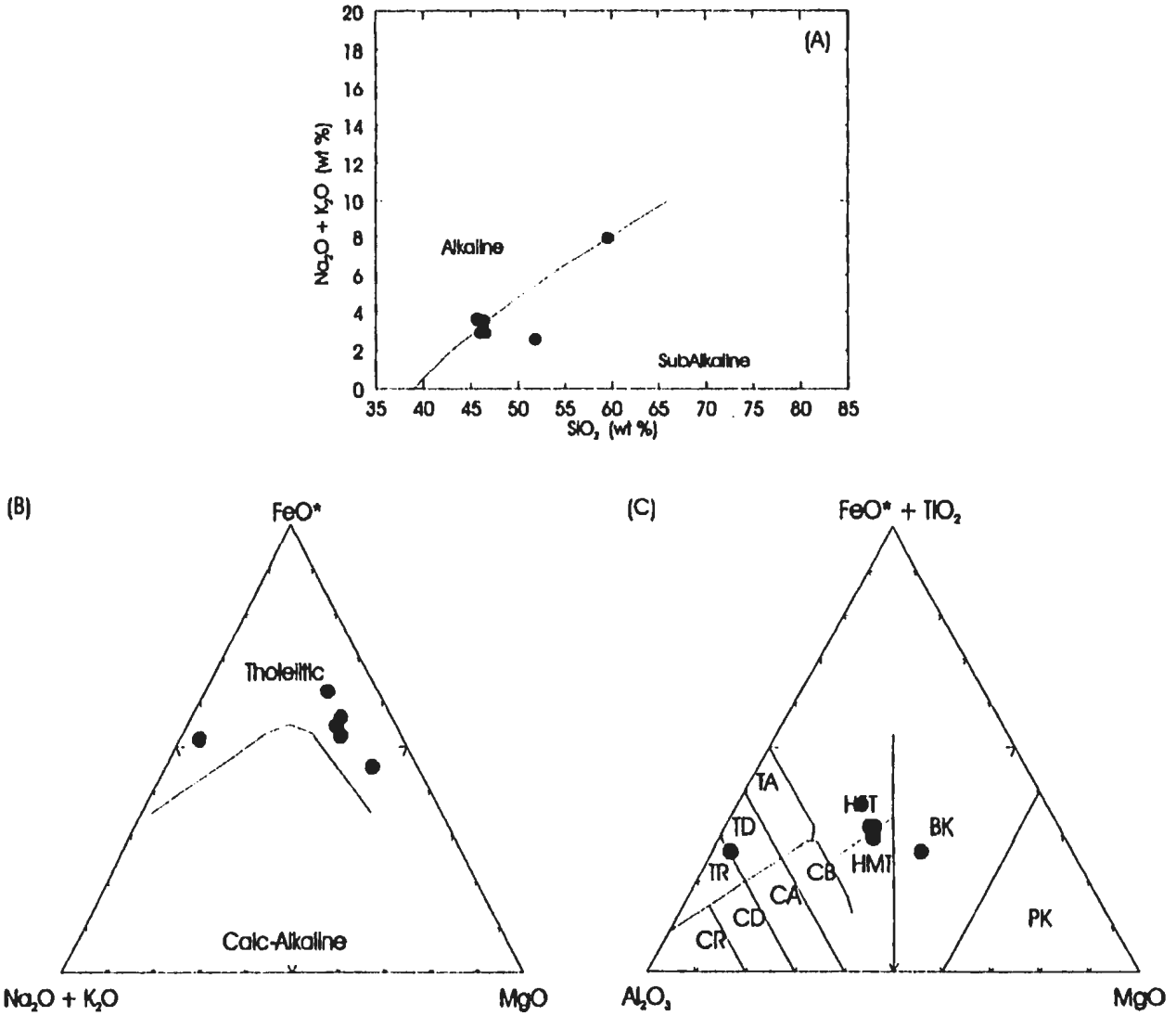

Figure 4.13. Irvine and Baragar's (1971) TAS (a) and AFM (b), and Jensen's (1976) cation plots (fields as in Figure 4.1) of the OKG mafic-felsic dykes.

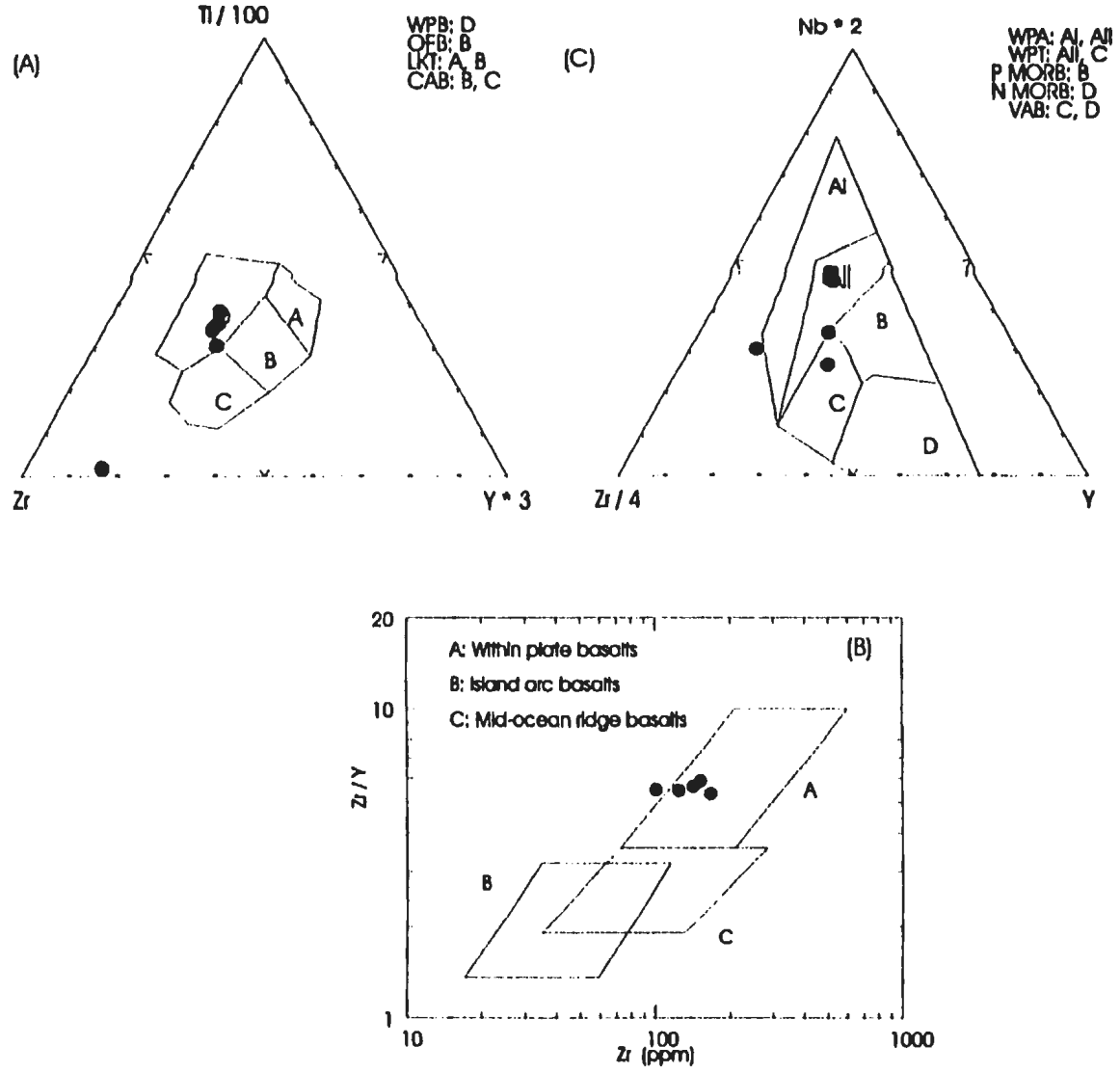

Figure 4.14. Pearce and Cann's (1973) Ti-Zr-Y (a), Pearce and Norry's (1979) Zr-Zr/Y (b), and Meschede's (1986) Zr-Nb-Y (c) discrimination plots of the OKG mafic-felsic dykes.

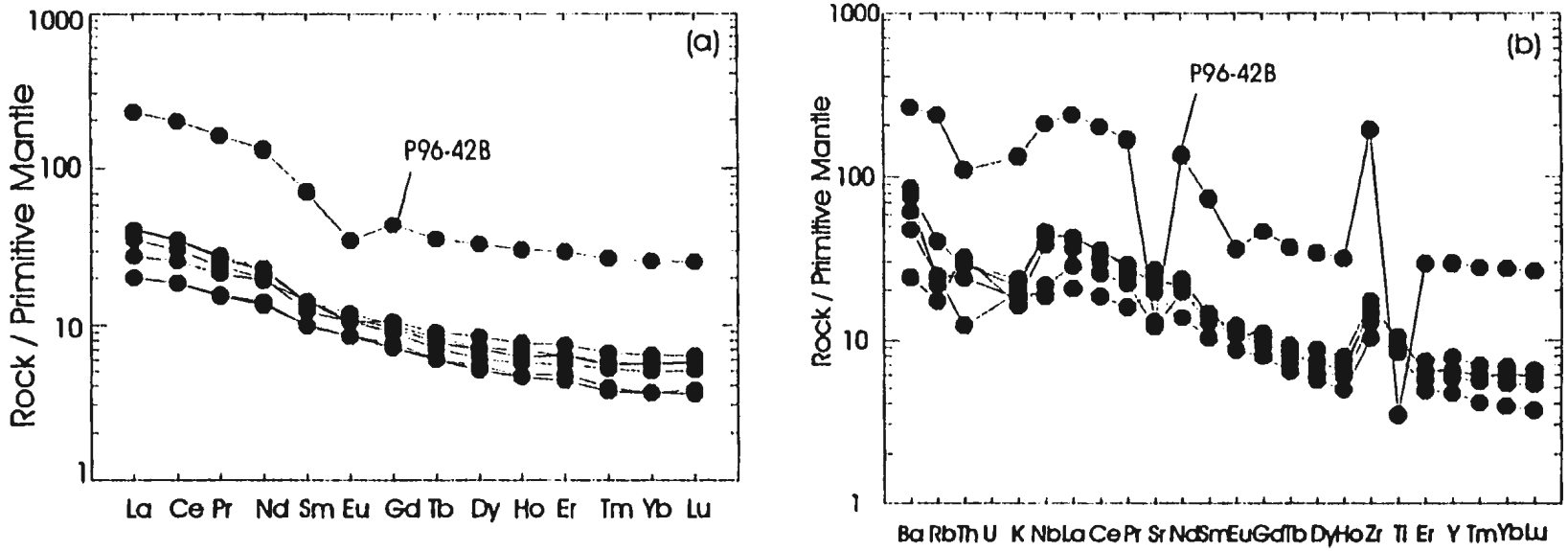

Figure 4.15. Primitive mantle normalized REE (a) and multi-element (b) plots of mafic and felsic dykes. Primitive mantle normalization values from Hofmann (1988).

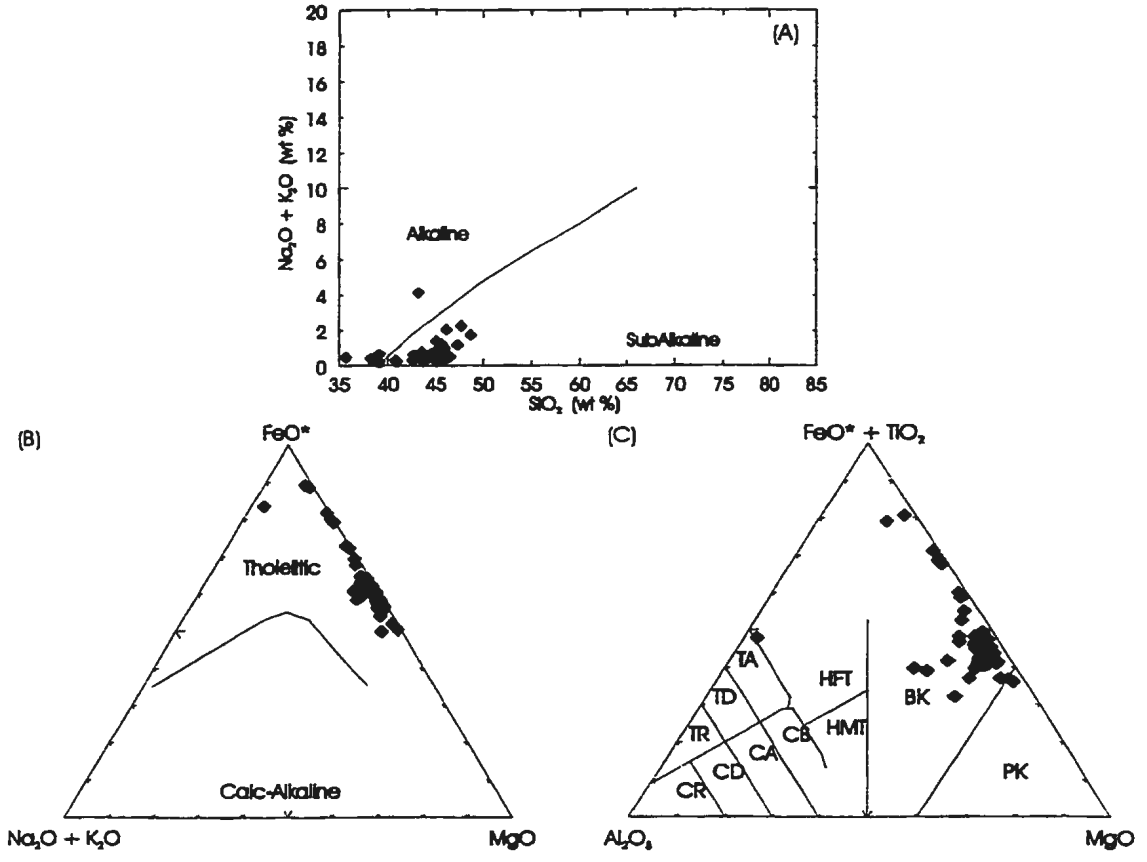

Figure 4.16. Irvine and Baragar's (1971) Total alkalis versus silica (TAS; a) and AFM plots (B), and Jensen (1976) cation plot (C; fields as in Figure 4.1) of the OKG pyroxenitic rocks.

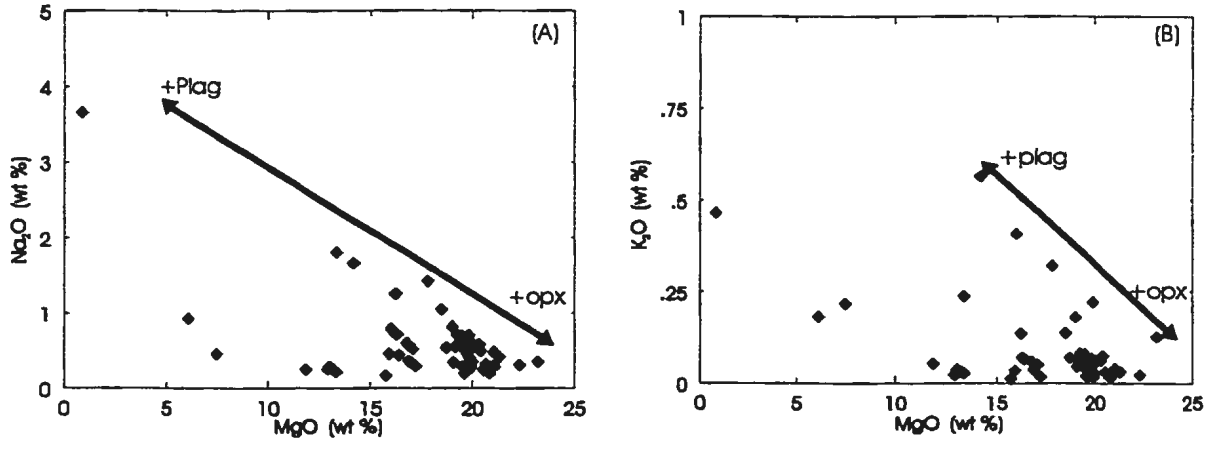

Figure 4.17. MgO versus major element plots of the OKG pyroxenites, including (a) Na_2O, (b) K_2O, (c) Al_2O_3, (d) CaO, (e) MnO, (f) TiO_2, (g) FeO*, and (h) P_2O_5.

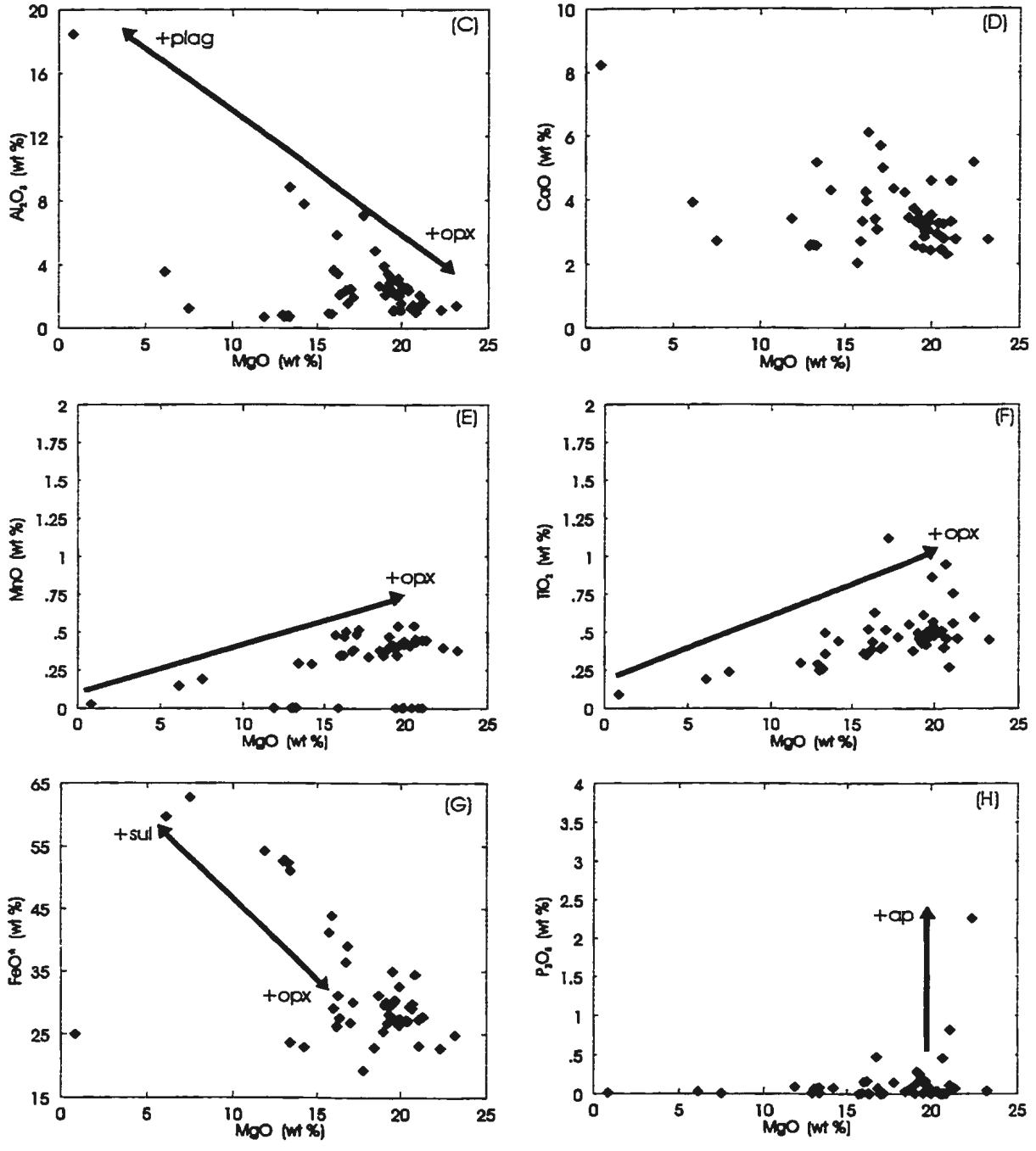

Figure 4.17. (Continued)

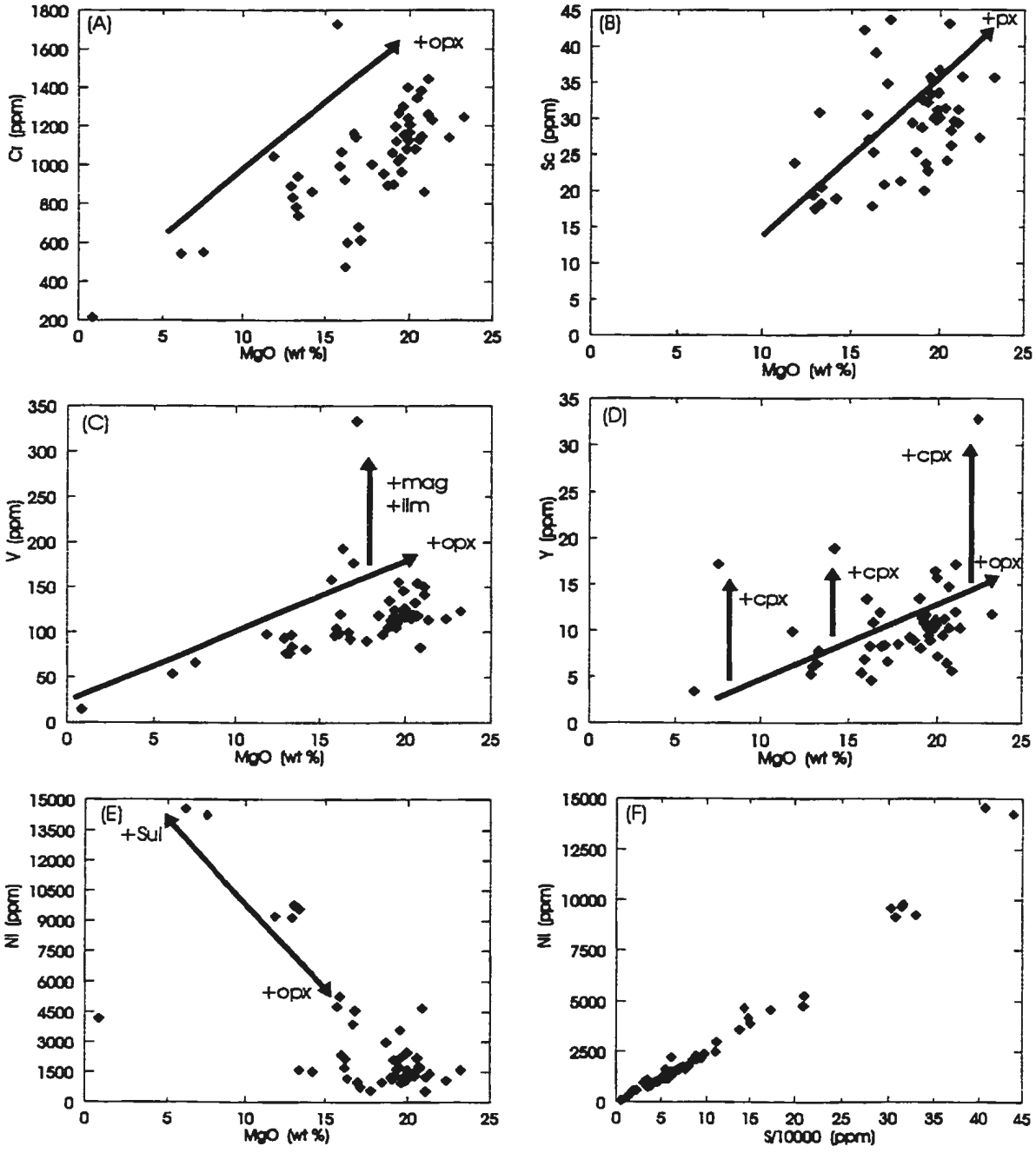

Figure 4.18. MgO versus (a) Cr, (b) Sc, (c) V, (d) Y, (e) Ni, (f) S versus Ni, (g) Mg# versus Ni, (h) MgO versus Cu, (i) S versus Ni, and MgO versus (j) Sr and (k) Ga.

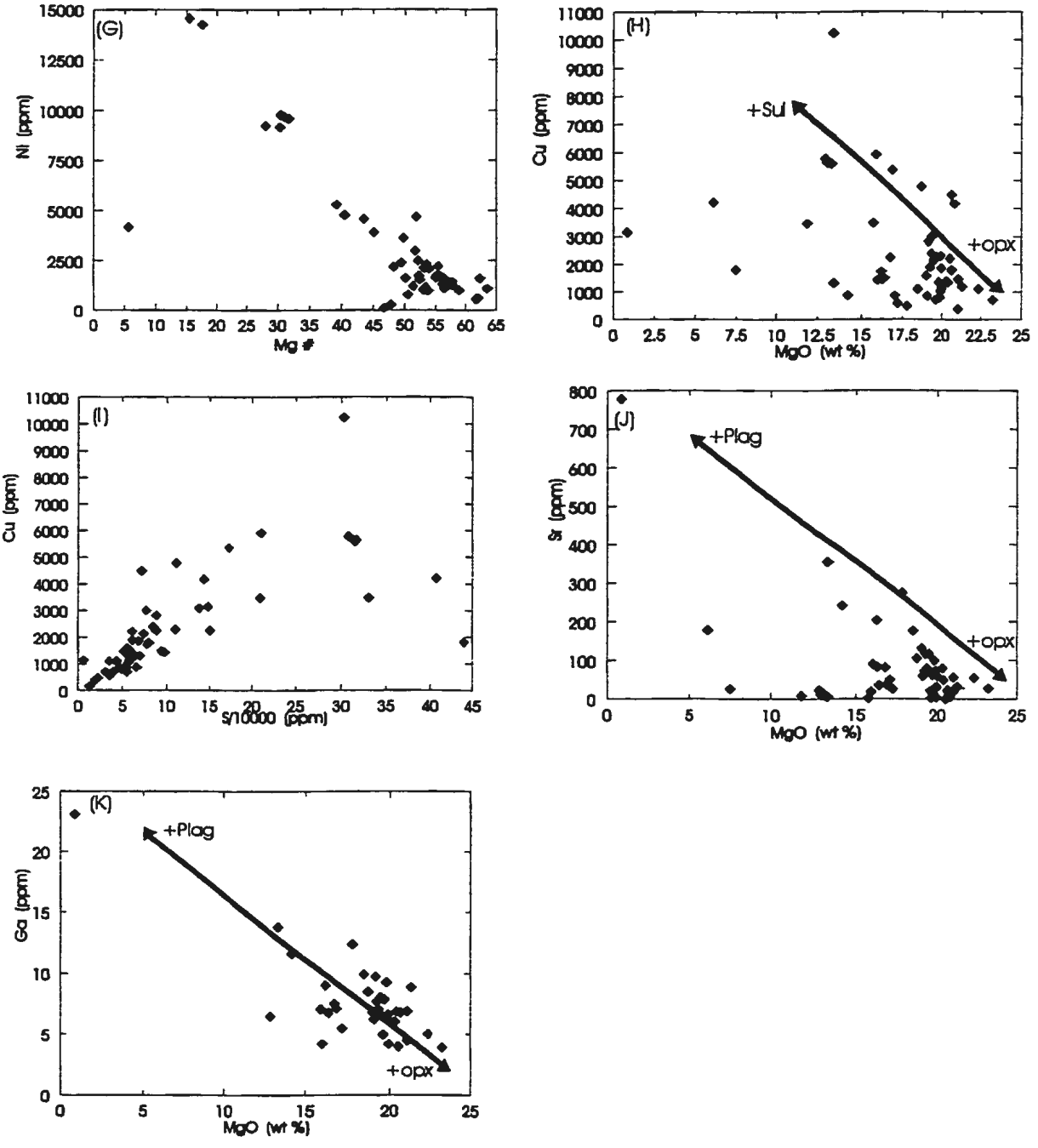

Figure 4.18. (Continued).

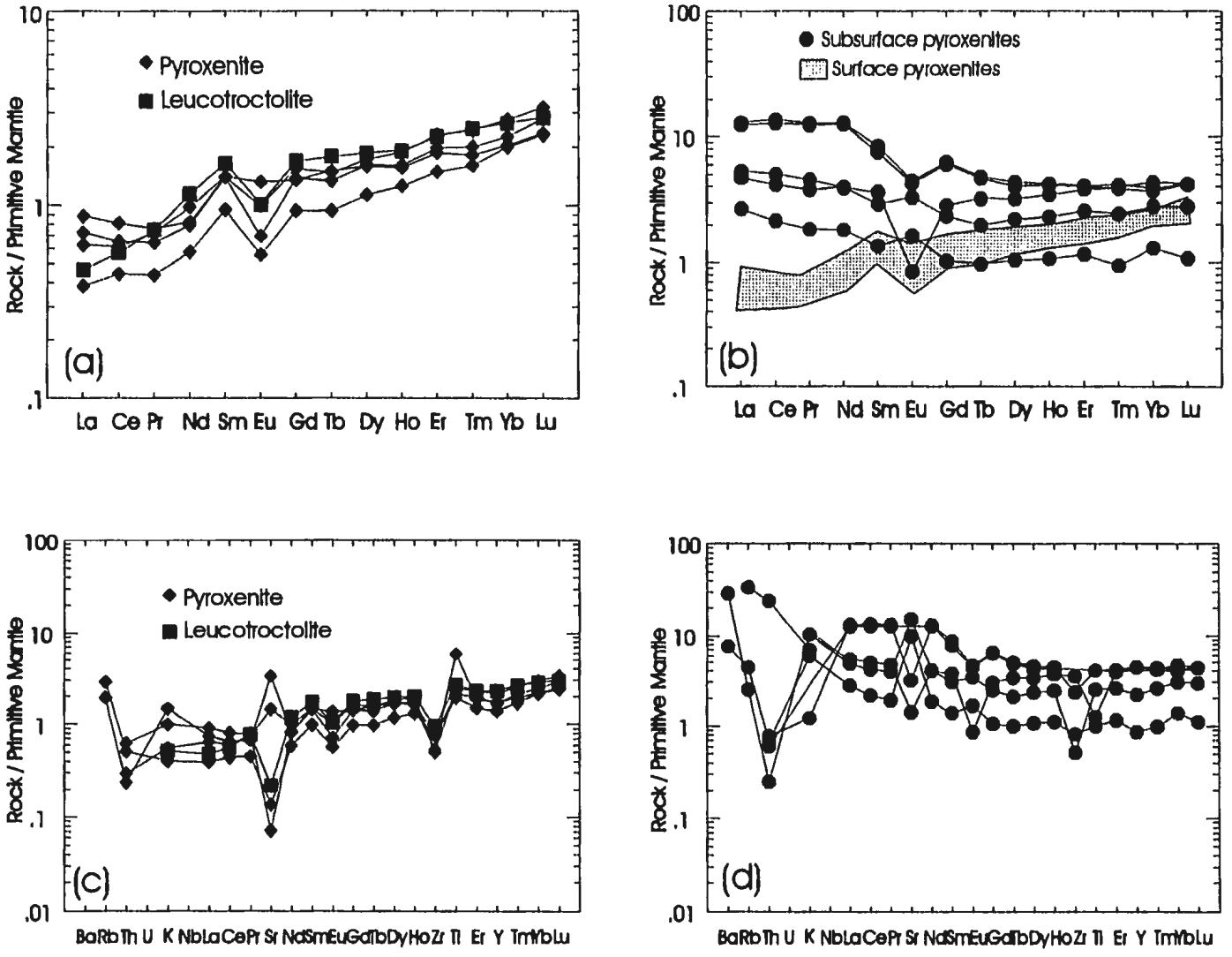

Figure 4.19. Primitive mantle normalized REE and extended trace element plots for (a) and (c) surface pyroxenites and leucotroctolites, and (b) and (d) subsurface pyroxenites. Primitive mantle normalization values from Hofmann (1988).

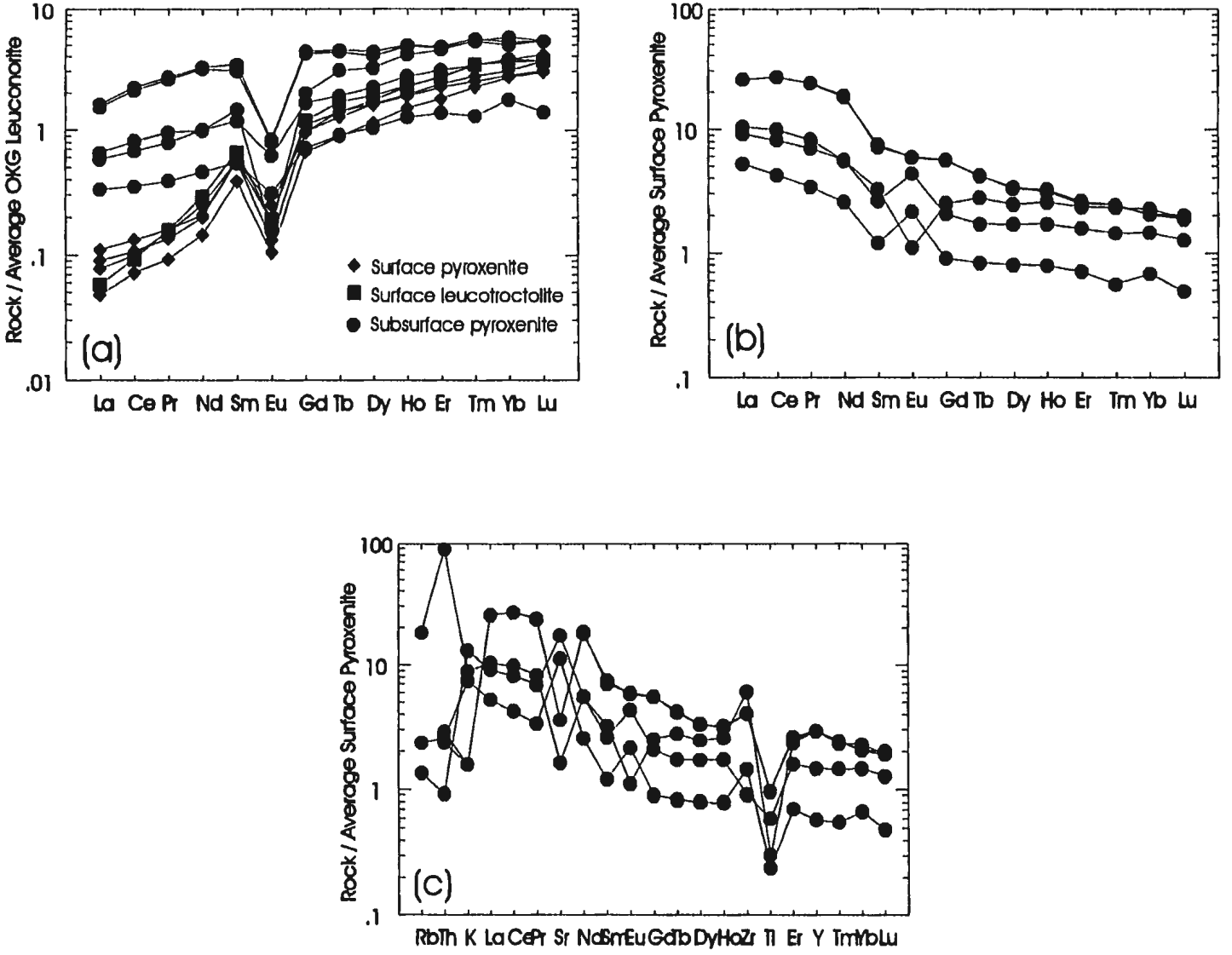

Figure 4.20. Average OKG leuconorite normalized plot for the mineralized pyroxenites (a), and surface pyroxenite normalized plots for the OKG subsurface dykes, (b) and (c).

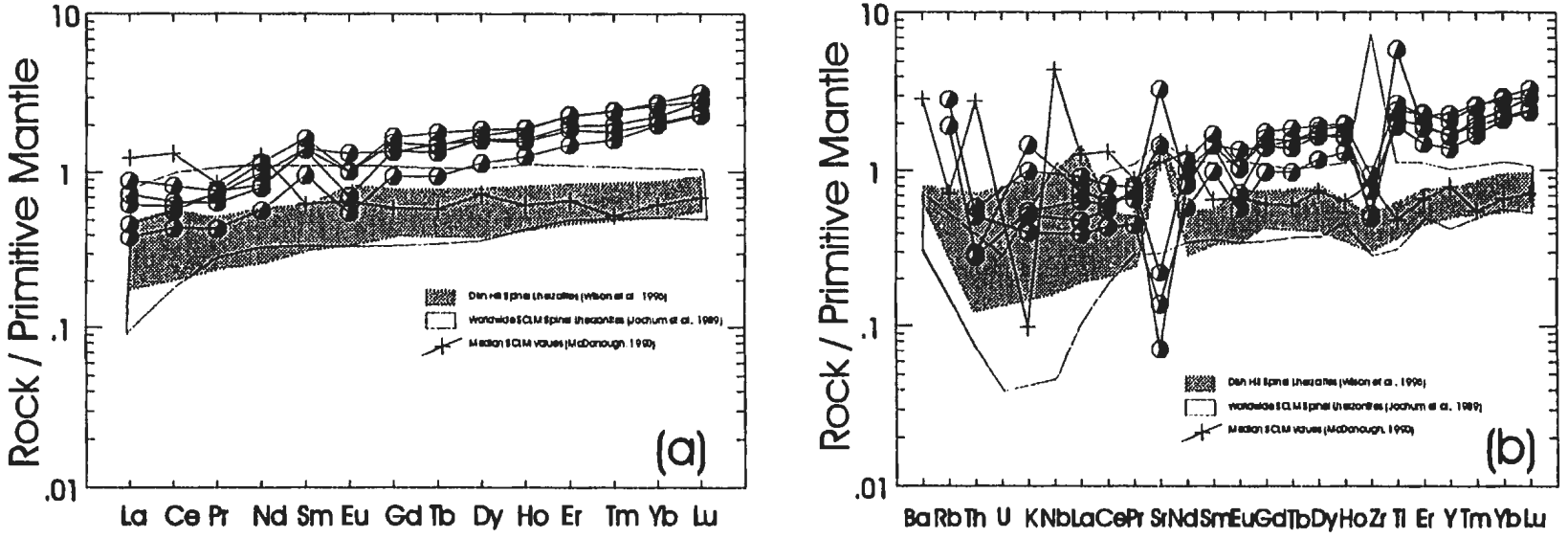

Figure 4.21. Primitive mantle normalized REE (a) and extended trace element plot (b) for the OKG surface pyroxenites and their relationship to the subcontinental lithospheric mantle (SCLM). Primitive mantle normalization values from Hofmann (1988), and SCLM data from Jochum et al. (1989), McDonough (1990), and Wilson et al. (1996).

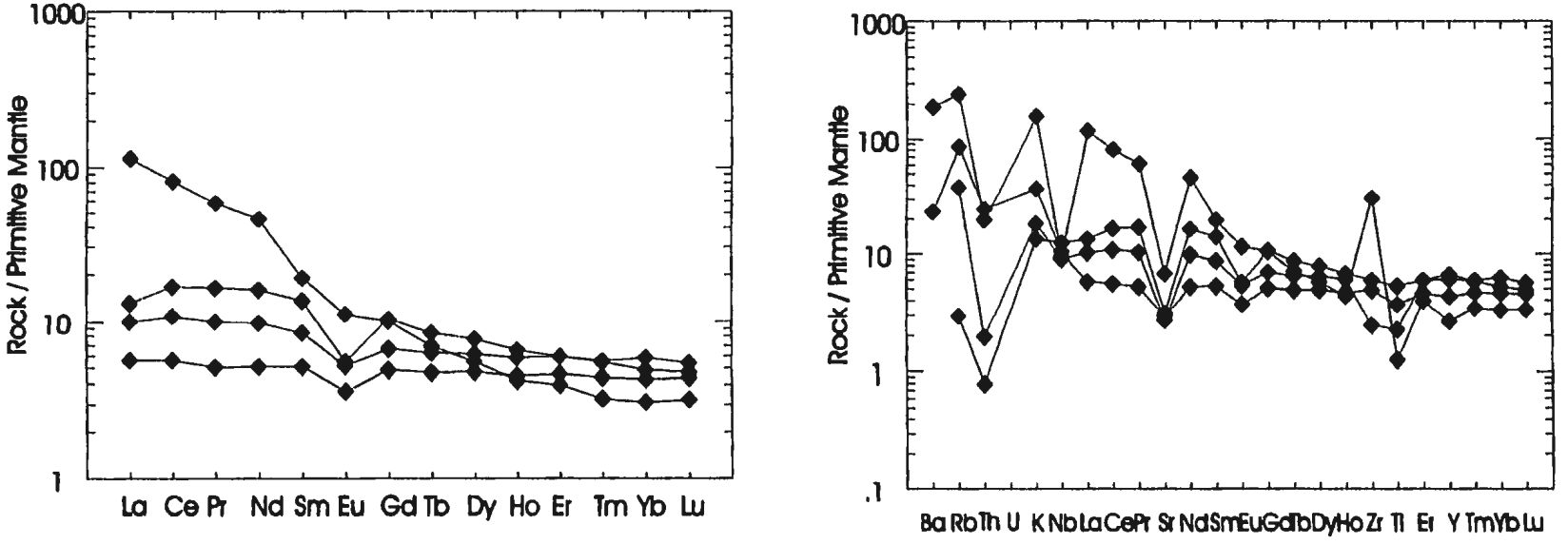

Figure 4.22. Primitive mantle normalized REE (a) and extended trace element (b) plots for Nain Province amphibolites and mafic granulites from the OKG prospect. Primitive mantle normalization factors from Hofmann (1988).

Table 4.1. Select trace element ratios for the anorthositic rocks groups of the OKG prospect. Normalization values after Hofmann (1988)

Group	$(La/Yb)_N$	$(Ce/Yb)_N$	$(La/Sm)_N$	$(Gd/Yb)_N$	Eu*	Eu/Eu*
an group (n=3)	8.17-155.12 (avg = 70.71)	5.69-94.61 (avg = 44.41)	3.08-7.96 (avg = 5.45)	1.27-4.61 (avg = 2.83)	0.41-0.57 (avg = 0.47)	6.27-12.06 (avg = 9.31)
ln1 group (n=5)	5.93-16.02 (avg = 11.81)	4.93-12.90 (avg = 9.02)	2.24-4.95 (avg = 3.62)	1.33-3.02 (avg = 1.85)	1.41-2.75 (avg = 2.16)	2.07-3.03 (avg = 2.66)
ln2 group (n=2)	7.20-9.65 (avg = 8.43)	6.49-8.34 (avg = 7.41)	2.26-3.02 (avg = 2.64)	2.03-2.08 (avg = 2.05)	6.84-13.51 (avg = 10.17)	1.62-1.79 (avg = 1.70)

Table 4.2. Select trace element ratios for the granitoid rocks groups of the OKG prospect. Normalization values after Hofmann (1988).

Group	$(La/Yb)_N$	$(Ce/Yb)_N$	$(La/Sm)_N$	$(Gd/Yb)_N$	Eu*	Eu/Eu*
ph1 group (n=4)	2.83-5.13 (avg = 4.25)	4.99-7.37 (avg = 6.30)	1.20-1.96 (avg = 1.72)	1.43-1.91 (avg = 1.59)	7.08-8.25 (avg = 7.71)	0.71-0.85 (avg = 0.77)
ph2 group (n=3)	6.20-9.28 (avg = 7.65)	8.74-12.23 (avg = 10.25)	1.81-2.15 (avg = 2.01)	2.21-2.65 (avg = 2.30)	5.96-6.71 (avg = 6.41)	0.37-0.53 (avg = 0.46)
Felsic dyke group (n=2)	4.69-6.43 (avg = 5.56)	5.38-6.94 (avg = 6.16)	1.88-3.11 (avg = 2.50)	1.44-1.79 (avg = 1.61)	5.05-5.57 (avg = 5.31)	1.00-1.26 (avg = 1.13)
Foliated Group (n=3)	7.02-10.51 (avg = 8.41)	9.91-15.01 (avg = 11.92)	1.63-2.14 (avg = 1.81)	2.53-2.87 (avg = 2.66)	5.51-7.00 (avg = 6.04)	0.31-0.34 (avg = 0.33)

Table 4.3. Select trace element ratios for the mafic dykes and a felsic dyke of the OKG prospect. Normalization values after Hofmann (1988)

Group	$(La/Yb)_N$	$(Ce/Yb)_N$	$(La/Sm)_N$	$(Gd/Yb)_N$	Eu*	Eu/Eu*
Mafic Dykes (n=6)	2.71-4.68 (avg = 3.92)	3.98-6.36 (avg = 6.30)	1.24-1.87 (avg = 1.55)	1.64-2.13 (avg = 1.85)	3.97-4.81 (avg = 4.42)	0.29-0.34 (avg = 0.32)
Felsic dyke P96-42B	5.49	7.57	1.97	1.72	10.41	0.63

Table 4.4. Select trace element ratios for the surface and subsurface mineralized pyroxenites from the OKG prospect. Normalization values after Hofmann (1988).

Group	$(La/Yb)_N$	$(Ce/Yb)_N$	$(La/Sm)_N$	$(Gd/Yb)_N$	Eu*	Eu/Eu*	Zr/Y	Th/Y
Surface dykes (n=5)	0.18-0.31 (avg = 0.27)	0.22-0.36 (avg = 0.27)	0.28-0.52 (avg = 0.46)	0.47-0.66 (avg = 0.59)	0.68-1.35 (avg = 1.13)	0.08-0.14 (avg = 0.10)	0.6-1.4 (avg = 1.0)	0.003-0.008 (avg = 0.004)
Subsurface dykes (OKG 96-09) (n=5)	1.23-3.33 (avg = 2.32)	1.16-3.50 (avg = 2.26)	1.47-1.99 (avg = 1.65)	0.65-1.62 (avg = 1.10)	0.77-6.90 (avg = 3.78)	0.04-0.21 (avg = 0.12)	0.6-2.3 (avg = 1.5)	0.002-0.114 (avg = 0.028)

Chapter 5. Metal and Platinum Group Element Geochemistry

5.1 Introduction

The use of PGE and metal ratios to study of magmatic Ni-Cu-PGE deposits has been ongoing for a significant period of time (e.g. Naldrett *et al.*, 1979; Naldrett, 1981; Naldrett and Duke, 1980; Barnes *et al.*, 1985,1988). The impetus of this chapter is to describe and assess the PGE and metal geochemistry of the OKG sulphides to better understand the controls on their metal chemistry. It must be noted all PGE analyses were carried out on surface samples and any inferences of subsurface PGE behaviour are speculative. All Ni and Cu determinations were carried out via XRF on pressed powder pellets following the method of Longerich (1995); PGE+Au determinations (Os, Ir, Ru, Rh, Pt, Pd, Au) were analyzed by ICP-MS following the Ni-S bead fire-assay preparation method of Jackson *et al.* (1990). All analytical methods, precision and accuracy are outlined in Appendix A.

5.2 Primitive Mantle Normalized PGE Plots

Chondrite and primitive mantle normalization of PGE data have been carried out for some time and provide an excellent tool in understanding the genesis of PGE in Ni-Cu and PGE sulphide environments. Early work in the field of PGE studies involved the

calculation of all PGE in a rock to 100% sulphides coupled with normalization to values of C1 chondrites (Naldrett *et al.*, 1979; Naldrett and Duke, 1980; Naldrett, 1981; Barnes *et al.*, 1985). However, in the last ten years most authors normalize PGE values to the primitive mantle (cf. Barnes *et al.*, 1988), and rarely are 100% sulphide calculations undertaken; hence, all plots in this section are normalized to the primitive mantle values of Barnes *et al.* (1988).

Samples from the OKG property are restricted to surface showing samples and are subdivided into four groups including: 1) massive sulphides; 2) disseminated pyroxenite, leucotroctolite and anorthosite hosted sulphides, with 5-50% disseminated sulphide; 3) other disseminated sulphides; and 4) Nain Province amphibolites to mafic granulites.

5.2.1 Massive Sulphides

The PGE patterns of the OKG massive sulphides are quite distinct and characterized by a roughly trough-shaped pattern containing elevated Ni and Cu with relatively flat PGE (Figure 5.1a,b). Elevated Au is common in most of the OKG massive sulphides, however, these values may be an analytical artifact due to the memory effect that Au shows via ICP-MS analysis (Jackson *et al.*, 1990); while Pt exhibits flat to distinctly negative anomalies relative to Rh and Pd. The overall trough shaped and low PGE contents (ca. 1-10 times primitive mantle; Figure 5.1a) relative to Ni and Cu are consistent with a prior removal of PGE at some point in the past, this will be discussed in further detail in section 5.4.

When this trough shaped pattern is compared to that for the pyroxenitic rocks (see section 5.2.2) there is a close similarity in shape. Both show distinctive trough shaped

patterns with depleted PGE relative to Ni and Cu with the exception of total concentration of the PGE and Ni and Cu. The presence of a negative Pt anomaly is the exception relative to the disseminated sulphides. Edwards (1990) noted from mantle rocks in the Bay of Islands ophiolite that as melts evolve Pt-Pd arsenides can be trapped in pyroxene and this may explain the Pt distribution. Barnes (1998) suggested that Pd and Rh appear to be higher in concentration relative to Pt in most sulphide ores associated with mafic and ultramafic rocks. Barnes (*op cit*) provided a number of reasons including: 1) during sulphide segregation Pd and Rh diffuse into the sulphide magma faster than Pt; 2) Pt is stabilized by ligands of As, Sb, or Te in the silicate magma; or 3) that sulphides may be sedimentary and only partially equilibrated with the magma. Factor 3 appears unlikely considering the S-isotope data presented in Chapter 7; however, it is possible that factors 1 and 2 may have controlled the Rh-Pd-Pt distribution in the massive sulphides.

5.2.2 Disseminated Sulphides in Pyroxenite-Leucotroctolite and Anorthosite

The disseminated sulphides of the OKG prospect occur predominantly within the pyroxenitic-leucotroctolitic dykes, with lesser sulphide occurrences in the anorthositic rocks; disseminated sulphides are between 5-50%. The PGE associated with the disseminated sulphides are typically 0.03-1x the primitive mantle, and have a similar, but slightly variable pattern when compared to the OKG massive sulphides; yet are insensitive to the rock type that is hosting them (Figure 5.1c-d).

The disseminated sulphides are characterized by a U-shaped pattern with elevated Ni, Cu, and Au and fairly depleted PGE (Figure 5.1c-d). Following Ni there is a decrease

to Os, an increase from Os to Ru and roughly straight from Rh to Pd with an increase in Au and Cu (Figure 5.1c-d). The U-shaped pattern is very similar to the massive sulphides, however, there is close to an order of magnitude difference in the PGE. The shape of the pattern, with the exception of the Pt anomaly associated with the massive sulphides, suggests a genetic link between the massive and disseminated sulphides; that is, the massive sulphides have segregated from the pyroxenitic-leucotroctolitic dykes.

5.2.3 Other Plots

Two rocks show extremely variable patterns when compared to the massive or disseminated sulphides and include samples P96-192 and P96-472 (disseminated sulphide in pyroxenite); neither of which are likely representative or provide much descriptive importance. The sample P96-192 is characterized by negligible Ni and Os, and a saw tooth pattern with negative Ir, Rh, Pd and Cu, accompanied by positive Ru, Pt, and Au (Figure 5.1e-f). The incomplete pattern does not allow easy correlations or genetic inferences; however, the detectable PGE (Figure 5.1f) have somewhat similar distributions as the other disseminated mineralization.

The sample P96-472 is not as problematic as sample P96-192 and is characterized by flat Ni to Os, depleted Ir and Rh, elevated Ru, and a progressive increase from Rh to Cu (Figure 5.1e-f). Although, Ir depletions could be explained by olivine or chromite fractional crystallization (Barnes *et al.*, 1985,1988; Barnes, 1990), the relative insensitivity of Ru and Os which should follow Ir in geochemical behaviour prevents such interpretation.

5.2.4 Amphibolites from the Nain Province Gneisses

Although there were no observed sulphides in the Nain Province Gneisses in proximity to the OKG sulphide occurrences, some have fairly high Ni concentrations and were analyzed for PGE content. On the primitive mantle normalized plots they have characteristics, which are very flat for all elements with the exception of a slight Cu, Os and Ir depletions (Figure 5.1g-h). The overall flat pattern is somewhat akin to komatiitic rocks (e.g. Barnes *et al.*, 1988) with the exception of nearly a 2-3 order of magnitude difference in PGE concentration.

5.3 Metal Ratio Plots of the OKG Rocks and Sulphides

The usage of metal ratio plots to assess the influence of sulphide and silicate crystallization and to discriminate between sulphides of different petro-tectonic settings is invaluable (e.g. Barnes, 1987, 1990; Barnes *et al.*, 1988). This section deals with the plots which have been constructed by Barnes (1987,1990) and Barnes *et al.* (1988), including the Ni/Cu versus Pd/Ir, Pd/Rh, and Pd/Pt; and the Ni/Pd versus Cu/Ir, Cu/Rh and Cu/Pt plots. Unlike the normalized plots, all of the respective OKG sulphide-groups are plotted together for comparative purposes.

The massive sulphides have fairly restricted Ni/Cu ratios, ranging from 1.51 to 29.98 (avg 6.82; which is elevated due to the upper limit value) and on Ni/Cu versus Pd/PGE plots lie either within or close to the field for layered intrusions (Figure 5.2a-c). Similarly, the pyroxenite hosted disseminated sulphides have Ni/Cu ratios of 0-1.37 (avg 0.94), and lie within or just outside of the fields for layered intrusions-PGE reefs; while the anorthosite hosted disseminated sulphides (Ni/Cu= 1.49-1.77) have similar affinities

as the pyroxenite-hosted sulphides (Figure 5.2a-c). The disseminated and massive sulphides have fairly restricted Ni/Cu ratios for the most part with minimal changes in the Pd/Ir and Pd/Rh ratios (Figure 5.2a-b; Table 1). In contrast, the massive sulphides have Pd/Pt ratios that exhibit much more variation leading to a vertical trend on the Ni/Cu-Pd/Pt plot (Figure 5.2c) and this reflects the magnitude of the Pt anomalies in Figure 5.1a-b). In contrast, the Pd/Pt ratios of the disseminated mineralized is much more tightly clustered (Figure 5.2c) reflecting the absence of a variation in Rh and Pd with Pt (e.g. Figure 5.1c-d).

Similar to the Ni/Cu-Pd/PGE plots, on the Ni/Pd versus Cu/PGE plots the sulphide groups plot close to field for layered intrusions with minor exceptions (Figure 5.2d-f). The massive sulphides have ratios of Ni/Pd = 413377-1712243; Cu/Ir = 96928-4584820; and Cu/Rh= 101329-4131942 and most lie in or close to the field for layered intrusions (Figure 5.2d-e; Table 5.1). Similar to the Pd/Pt ratios, the massive sulphides have Cu/Pt (209507-14603346) ratios that exhibit some scatter versus Ni/Pd but still lie within or close to the field for layered intrusions (Figure 5.2f)

The disseminated anorthosite- and pyroxenite-hosted sulphides exhibit similar characteristics to the massive sulphides and lie in or close to the fields for layered intrusions. They generally exhibit a similar range of Ni/Pd ratios, with averages higher than the massive sulphides, and have consistent Cu/Ir and Cu/Rh behaviour; while Cu/Pt ratios are much less variable than the massive sulphides (Figure 5.2d-f; Table 1)

5.4 Significance of PGE Patterns and Metal Ratios

The very low total PGE, trough-shaped PGE patterns, and restricted PGE and metal ratios of the OKG sulphides show marked depletions in the PGE relative to Ni and Cu. These variations are likely a function of PGE loss at some time in the past due to the higher partition coefficients of the PGE into sulphide liquids (ca. 10000 or higher Stone *et al.*, 1990; Crocket *et al.*, 1992; Bezman *et al.*, 1994; Peach *et al.*, 1994; Barnes *et al.*, 1997a) relative to Ni and Cu (ca. 250; Rajamani and Naldrett, 1978). Depletions in the PGE relative to Ni and Cu can be attributed to a number of factors including: 1) the mantle source region for the pyroxenitic magmas was depleted in PGE to begin with; 2) a previously segregated sulphide liquid depleted the sulphides in PGE relative to Ni and Cu before being emplaced into their current positions (e.g. Barnes 1987, 1990; Barnes *et al.*, 1993; Barnes and Francis, 1995); 3) the PGE were retained in the mantle source region in some silicate-oxide-sulphide phase during partial melting (e.g. Barnes *et al.*, 1985, 1988; Barnes, 1990); or 4) were removed by a silicate-oxide phase during fractionation of the pyroxenitic magmas prior to sulphide saturation (e.g. olivine, chromite, platinum-group-mineral; Barnes, 1987, 1990; Brügmann *et al.*, 1987; Barnes *et al.*, 1988; Barnes and Picard, 1993).

The fractionation of the PGE by a silicate or oxide phase prior to sulphide saturation appears to be unlikely considering the geochemical data for the pyroxenites and massive sulphides. Work by Barnes *et al.* (1985, 1988), Barnes (1987, 1990), Brügmann *et al.* (1987) and Barnes and Picard (1993) all show that olivine and chromite can fractionate the PGE if these silicate-oxide phases fractionate prior to sulphide

saturation. In Chapter 4 the role of olivine was shown not to be important in the Ni distribution associated with the OKG pyroxenitic rocks, and that sulphides controlled Ni distributions (Figure 4.18). Assuming that olivine would play a role in the PGE distribution also seems unlikely. Likewise if olivine (or chromite) crystallizes before sulphide saturation then it would preferentially deplete the melts in Ir-group PGE (IPGE=Os, Ir, Ru), at the expense of the Pd-group PGE (PPGE=Pt, Pd, Rh; Barnes *et al.*, 1985, 1988; Barnes, 1987, 1990; Brüghmann *et al.*, 1987; Barnes and Picard, 1993). The ratios of Pd to Ir (Pd/Ir) provide a measure of fractionation of IPGE from the PPGE. The OKG sulphides have mildly fractionated, but very restricted Pd/Ir ratios (avg MS = 4.73, avg. DS in pyroxenite = 3.07, avg. DS in anorthosite = 1.81; Table 5.1), and it is unlikely olivine or chromite have fractionated the PGE (e.g. Figure5.1b and 5.1d).

The argument for incomplete partial melting and retention of PGE within the mantle is also unlikely (ca. 20-25% partial melting; Barnes *et al.*, 1988, 1997a; Barnes and Picard, 1993). Firstly, the likely Mesoproterozoic age for the pyroxenitic magmas infers a cursory link to the heat source related to NPS (cf. Emslie *et al.*, 1994). Widespread plume-type magmatism related to NPS genesis likely resulted in large scale crust-mantle melting episodes (e.g. Emslie *et al.*, 1994), and likely associated with this would be complete melting of any mantle sulphides. Similar to above, the Pd/Ir ratios of the OKG sulphides argue against preferential retention within silicate-oxide phases during incomplete partial melting.

The argument for a prior sulphide segregation event appears to be very attractive, since there are numerous subsurface intersections of sulphide mineralization (e.g. Table

8.1) which could have depleted the surface dykes in PGE prior to their emplacement on surface. If an assumption is made that the pyroxenite-hosted mineralization had origins in an undepleted, primitive mantle, then sulphide segregation prior to emplacement on surface would be supported by the trough-shaped PGE patterns (e.g. Figure 5.1a,c), and by metal ratios (e.g. massive sulphides: $Pd/Ir_{avg} = 4.73$, $Cu/Pd_{avg} = 208441$, $Pd/Pt_{avg} = 20.52$, $Ni/Ir_{avg} = 3567877$; versus unfractionated primitive mantle: $Pd/Ir_{avg} = 1$, $Cu/Pd_{avg} = 63636$, $Pd/Pt_{avg} = 0.48$, $Ni/Ir_{avg} = 454545$; Tables 5.1 and 5.2). Furthermore, on the Cu/Pd-Pd plot (Figure 5.3a) of Barnes *et al.* (1993) all the OKG sulphides have depleted signatures; while mantle normalized Cu/Pd_{MN} and Ni/Ir_{MN} ratios of the massive sulphides (Cu/Pd_{MN} =0.5-17.9, Ni/Ir_{MN} = 4.6-15.2; Table 5.2), and disseminated sulphides (Cu/Pd_{MN} =0.3-18, Ni/Ir_{MN} = 1.6-17.8; Table 5.2) are fractionated in PGE relative to unfractionated sulphides (Cu/Pd_{MN} and Ni/Ir_{MN} = 1-3; Barnes *et al.*, 1988, 1993; Barnes and Francis, 1995).

The fractionated signatures of the PGE relative to the primitive mantle suggest that there has been a preferential loss of the PGE relative to Ni and Cu due to sulphide segregation, and is supported by the data presented in the prior paragraph. However, when the primitive mantle normalized patterns for the pyroxenite-hosted disseminated sulphides are compared to SCLM mantle xenoliths from Dish Hill, California (Wilson *et al.*, 1996), they bear a striking resemblance. They are quite similar in all respects with the exception of slightly lower Au and Cu (Figure 5.4a); while the pattern for just the noble metals (Figure 5.4b) is even more strikingly similar. Since the pyroxenitic rocks are not liquids this similarity to the SCLM xenoliths may be serendipitous; these sulphide

bearing xenoliths may also have underwent a previous sulphide segregation/differential melting event in their petrologic history.

In summary, two major conclusions can be drawn from the PGE data. These include: 1) the PGE patterns for the pyroxenite-hosted sulphides and massive sulphides have similar trough-shaped patterns, with the exception of Pt in the massive sulphides, and suggest that the massive sulphides have been derived from the pyroxenitic intrusives; and 2) that the depleted PGE relative to Ni and Cu in the pyroxenitic dykes may be a function of the mantle source region from which they were derived (e.g. refractory, PGE-depleted SCLM). However, it is highly likely that the PGE-depleted character of the OKG surface sulphides was due to a prior sulphide segregation event before emplacement onto surface.

5.5 Modeling of PGE Data

The OKG sulphides represent an entirely new suite of magmatic Ni-Cu-Co sulphide mineralization in Labrador that are relatively unknown from a PGE standpoint. Furthermore, although they may be derived from a SCLM source, finding a starting liquid from which to model the PGE data is also problematic since the pyroxenitic rocks are cumulates far removed from liquid compositions. In an attempt to model the PGE data of the sulphides a suitable analogue has been chosen and the reasons are outlined below. However, prior to any modeling of the PGE composition of the OKG sulphides, the theoretical aspects of modeling PGE data in magmatic Ni-Cu sulphide systems is discussed below, followed by the results and implications of PGE modeling.

5.5.1 Theoretical Aspects of PGE Modeling

The process whereby PGE, Ni, Cu and Co (chalcophile elements) become concentrated into a sulphide liquid from a mafic-ultramafic silicate liquid hinges on their inherent affinity for the sulphide phases over the silicate phases. The inherent affinity of a given element towards a sulphide liquid versus of a silicate liquid can be expressed by its partition coefficient, given by the following:

$\mathbf{D^{sulphide/silicate}}$ **= concentration in sulphide liquid/concentration in silicate liquid** (4-1).

Elements that have values of D greater than 1 (D>1) have a strong affinity for the sulphide liquid; while those with D values less than 1 (D<1) prefer the silicate liquid. Partition coefficients are highly variable and are dependent on the particular element. For instance, the partition coefficients for Cu range from 200-2000 (Rajamani and Naldrett, 1978; Peach *et al.*, 1994; Barnes *et al.*, 1997a), while partition coefficients for the PGE can range from 10^3-10^6 (Stone *et al.*, 1990; Crocket *et al.*, 1992; Bezman *et al.*, 1994; Peach *et al.*, 1994; Barnes *et al.*, 1997a). These variations in partition coefficients have fundamental effects on the behaviour of Ni-Cu-PGE during sulphide segregation.

The preference of the chalcophile elements for sulphide liquids leads to the question: What is the controlling factor on their tenor in Ni-Cu-PGE sulphide deposits? The early work of Campbell and Naldrett (1979) provided a series of equations that described the controls of chalcophile element tenor in sulphide bodies as a function of the mass of silicate liquid which the sulphide liquid equilibrated with (R-factor). The latter is given by the equation:

$\mathbf{C_C^E = C_L^E\ D\ (R+1)/(R+D)}$ (4-2);

where C_C^E represents the concentration of element E in the sulphide phase, C_L^E represents the concentration of element E in the silicate liquid which the sulphide liquid equilibrated with, D is the sulphide-silicate partition coefficient of element E, and R is the R-factor as described above. In Ni-Cu sulphide dominated deposits (e.g. Duluth and Kambalda) R-factors vary from 100-10000; while in most PGE dominated deposits (e.g. Bushveld and Stillwater) the R-factors are quite higher, in the range of 10000 to greater than 100000 (Campbell and Naldrett, 1979; Campbell *et al.*, 1983; Campbell and Barnes, 1984; Naldrett *et al.*, 1984b; Barnes and Naldrett, 1986; Naldrett, 1993; Barnes *et al.*, 1997a; and others).

Returning to equation 4-2 and the partition coefficients, equation 4-2 works quite well for all chalcophile elements; however, it can be simplified when partition coefficients are very high (Campbell and Barnes, 1984; Barnes *et al.*, 1993; Barnes and Francis, 1995; Barnes *et al.*, 1997a). In particular the PGE have very high partition coefficients and once D > 10R, then equation 4-2 can be rewritten to the following:

$$C_C^E/C_L^E = (R+1) \quad (4\text{-}3);$$

which can be further rewritten to the following:

$$C_C^E/C_L^E \approx R \quad (4\text{-}4);$$

hence, the use of equation 4-4 can be used to estimate the R-factor of the sulphides (Campbell and Barnes, 1984; Barnes *et al.*, 1993; Barnes and Francis, 1995; Barnes *et al.*, 1997a).

5.5.2 Modeling the OKG Ni-Cu-Co Sulphides

A number of inherent problems arise when trying to model the OKG sulphides. Firstly, when using equation 4-2 or 4-4 finding a suitable starting liquid from which to model the sulphides is problematic. This arises primarily from the inherent inability to find the "true" starting parental magma for the pyroxenitic intrusives, and the related problem that the pyroxenitic rocks are somewhat cumulate and do not represent liquid compositions.

A remedy to this problem can be found by choosing a possible analogous starting liquid. The data of Barnes et al. (1997a) for the Minnimax occurrences within the Duluth Complex have significant similarities in their PGE geochemistry when compared to the OKG massive sulphides (Figure 5.5). Furthermore, the host-rocks within the Duluth Complex that host the sulphides (troctolites-norites) are somewhat similar to those at the OKG prospect (e.g. Mainwaring and Naldrett, 1977; Ripley, 1981,1986; Thériault *et al.*, 1997), suggesting that the starting material of the OKG sulphides may be somewhat similar to that of the Duluth Complex.

Taking the partition coefficients and starting material (PGE depleted basalt) of the Duluth Complex from Barnes *et al.* (1997a) (Table 5.3), the R-factors for the OKG sulphides have been calculated. For the massive sulphides there is a close agreement between the model liquids for some elements (Ni, Os, Ir, Ru, Au, Cu), while there is poor agreement for other elements (Rh, Pt, Pd; Figure 5.6). The differences between the latter elements could arise from: 1) the pronounced Pt anomalies associated with the massive

sulphides which diluted the Rh and Pd signatures; 2) incorrect starting silicate liquid; and 3) or incorrect partition coefficients (e.g. Barnes *et al.*, 1997a).

Regardless of the inconsistencies between Rh, Pt and Pd, the other chalcophile elements provide an approximation of the R-factors associated with the OKG massive sulphides. Using equation 4-2, the R-factors of the model liquids have been calculated and are plotted against the massive sulphides (Figure 5.6a), these show that R-factors for Ni, Os, Ir and Ru range from 100-500; while those for Cu and Au range from less than 100 to approximately 500. Using equation 4-4 the R-factors of Os, Ir and Ru range from approximately 50 to 265, which are lower than those using equation 4-2, but within the range of those calculated from equation 4-2.

The disseminated mineralization associated with pyroxenite-leucotroctolite shows less agreement with the model liquids than the massive sulphides; however, there is fairly good agreement with Ni, Os, Ir, Ru, Au and Cu (Figure 5.6b). R-factors modeled using elements Ni, Os, Ir and Ru, and equation 4-2 range from approximately 5-50; while Cu and Au show a similar range (Figure 5.6b). Using equation 4-4 the R-factors for Os, Ir and Ru range from approximately 5-90; which is slightly over that of the model liquids using equation 4-2.

When compared to other Ni-Cu sulphide occurrences, the OKG sulphides show some overlap in R-factor values. The pyroxenite hosted sulphides are very metal-poor in terms of PGE, and likewise have very low R-factors which are within the range of the Pipe deposit in Manitoba (R=50; Campbell and Naldrett, 1979; Naldrett *et al.*, 1979).

However, with the exception of the Pipe, most other significant occurrences have much higher R-factors than the OKG disseminated sulphides.

In contrast, the R-factors for the OKG massive sulphides overlap with many significant Ni-Cu producers within the world. When compared to Archean komatiite-hosted Ni-Cu sulphides the R-factors of the massive sulphides (R=100-600) are similar to those at Kambalda and the Cape Smith Fold Belt (R=100-500, up to 2500; Campbell and Naldrett, 1979; Naldrett *et al.*, 1979; Barnes and Picard, 1993; Lesher and Campbell, 1993). Furthermore, when compared to other gabbro hosted sulphides such as those within the Belleterre-Angliers Belt of the Superior provinces (R=200-1000; Barnes *et al.*, 1993); the Muskox Intrusion (R=200-2000; Barnes and Francis, 1995; Barnes *et al.*, 1997a); and the Sudbury Complex (R=300-1300; Naldrett, 1981; Campbell and Barnes, 1984), there is significant overlap within the lower R-factor ranges of these deposits.

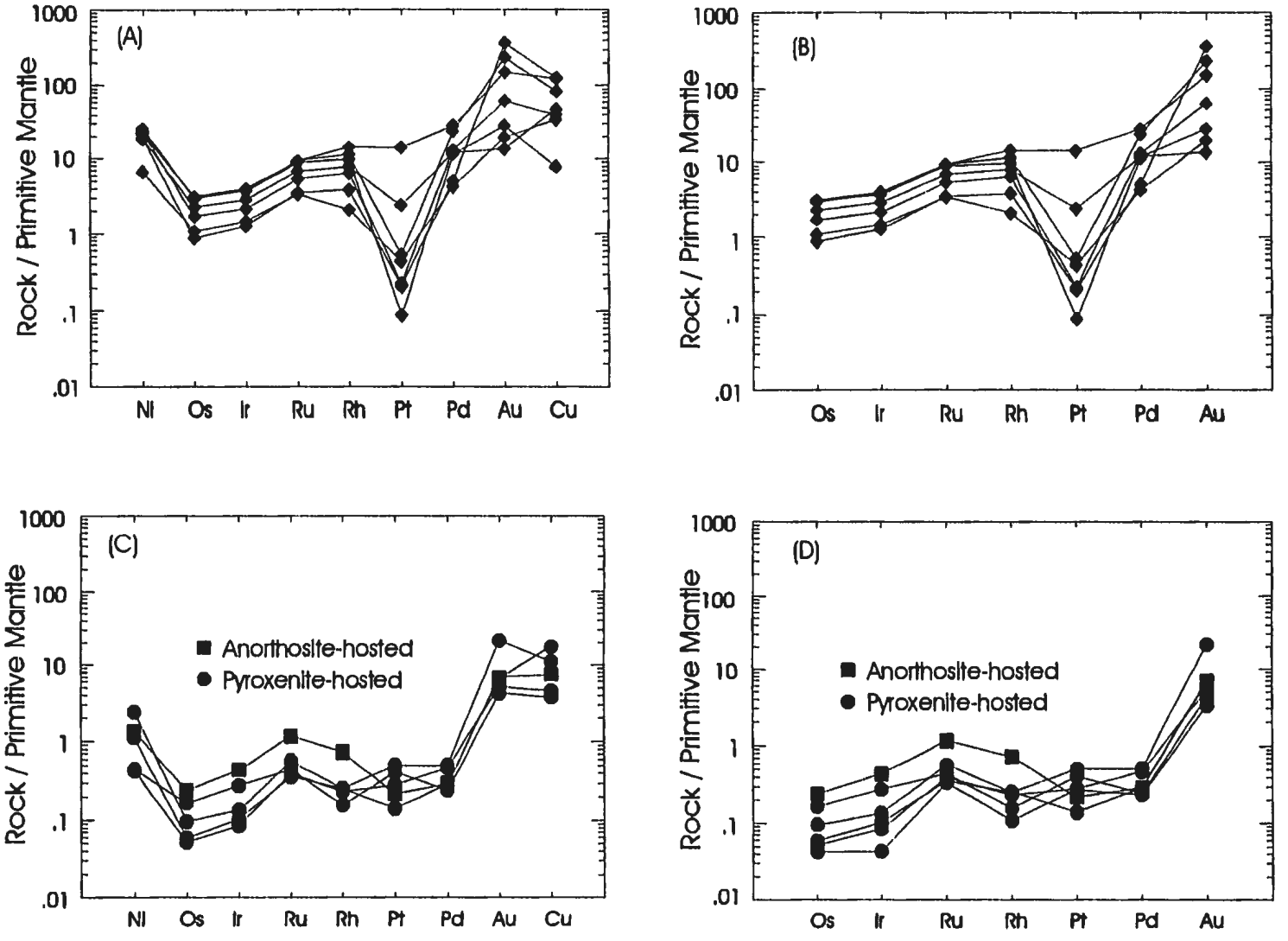

Figure 5.1. Primitive mantle-normalized PGE+Ni+Cu and PGE plots of the OKG massive sulphides (a-b), disseminated sulphides(c-d), other samples (e-f) and Nain Province amphibolites-mafic granulites (g-h). Primitive mantle normalized values from Barnes et al. (1988).

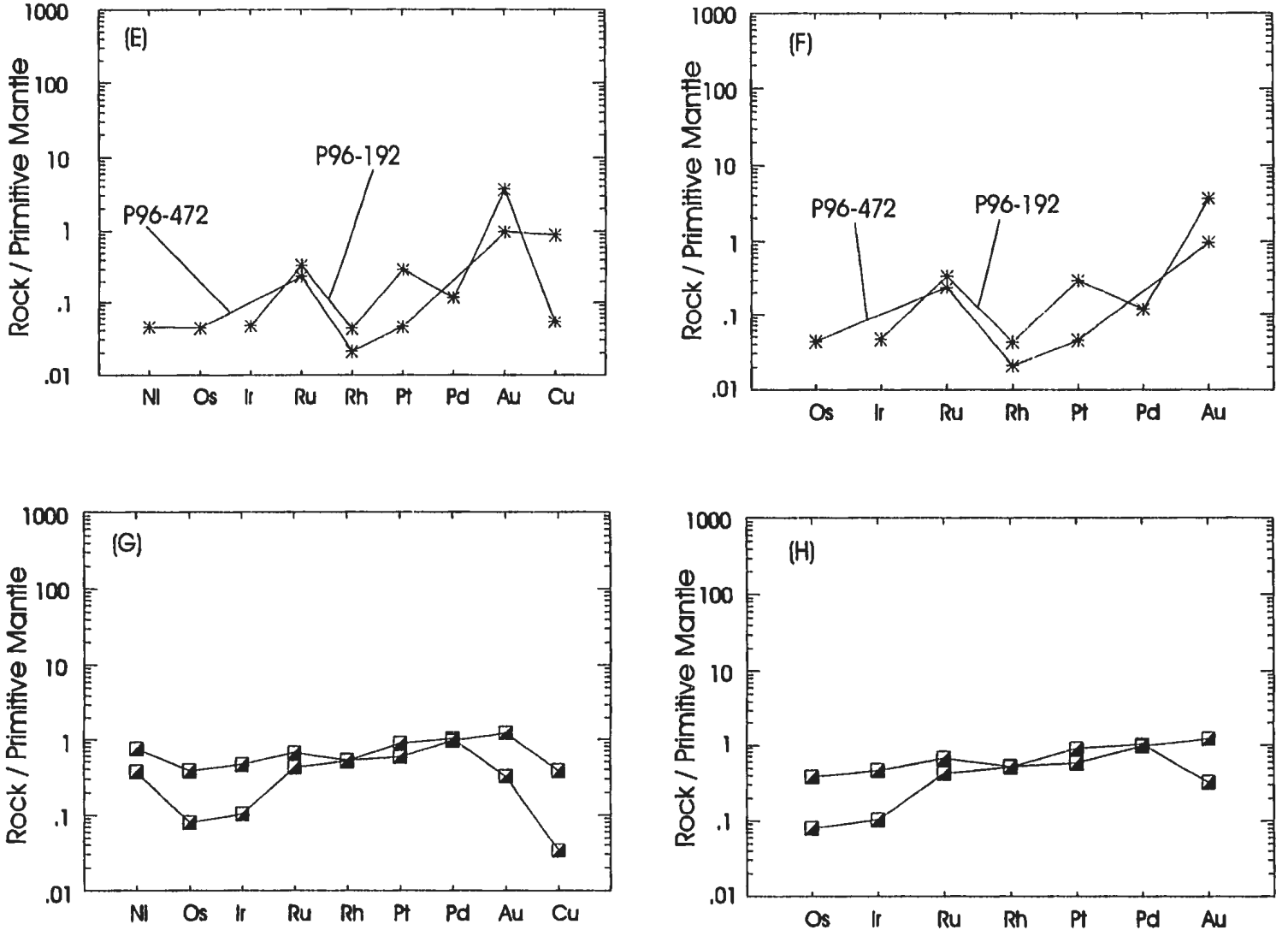

Figure 5.1 continued

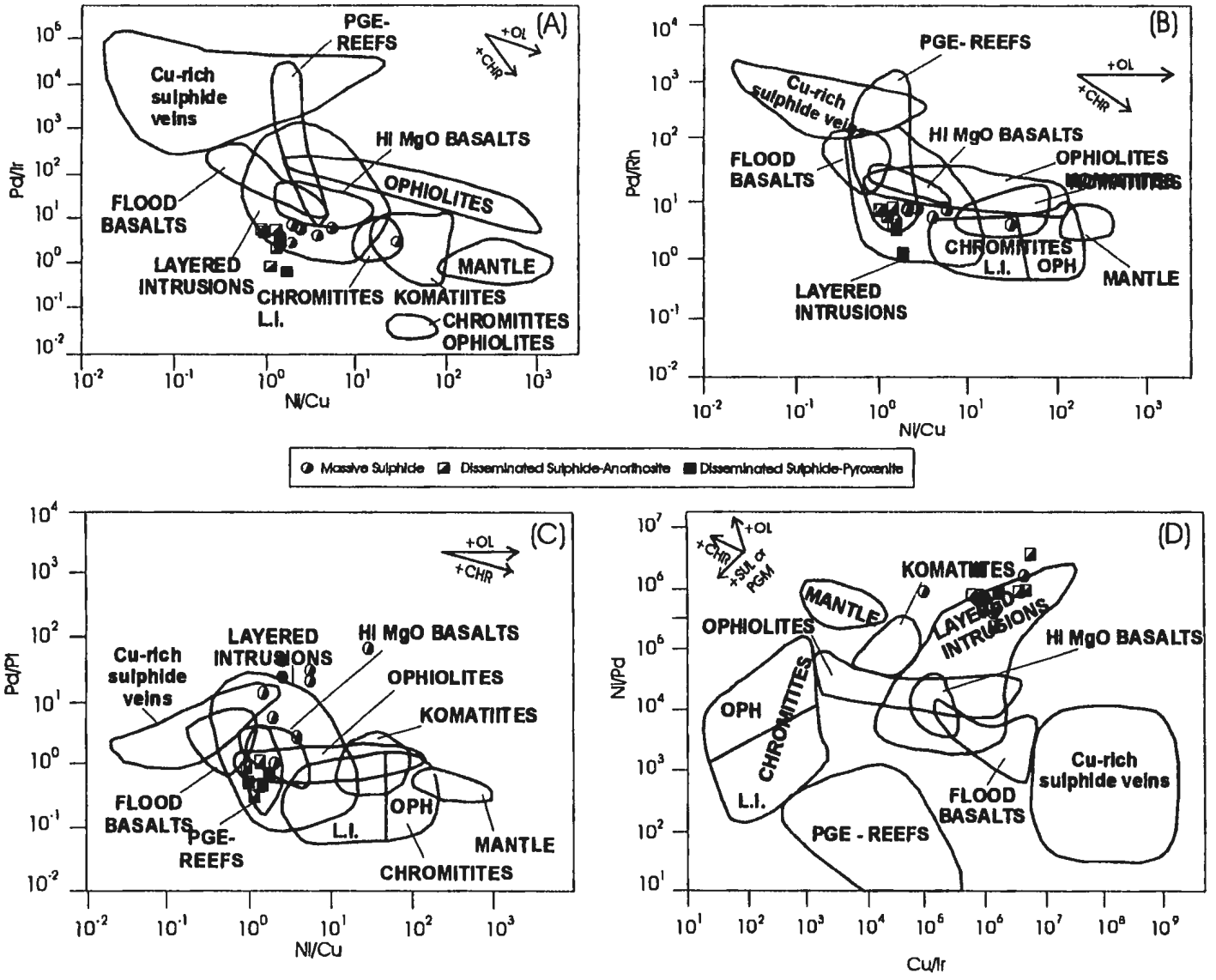

Figure 5.2. Metal ratio plots of the OKG sulphides, including Ni/Cu versus Pd/Ir (a), Pd/Rh (b) and Pd/Pt (c), and Ni/Pd versus Cu/Ir (d), Cu/Rh (e) and Cu/Pt (f). Fields after Barnes (1987, 1990) and Barnes et al. (1988).

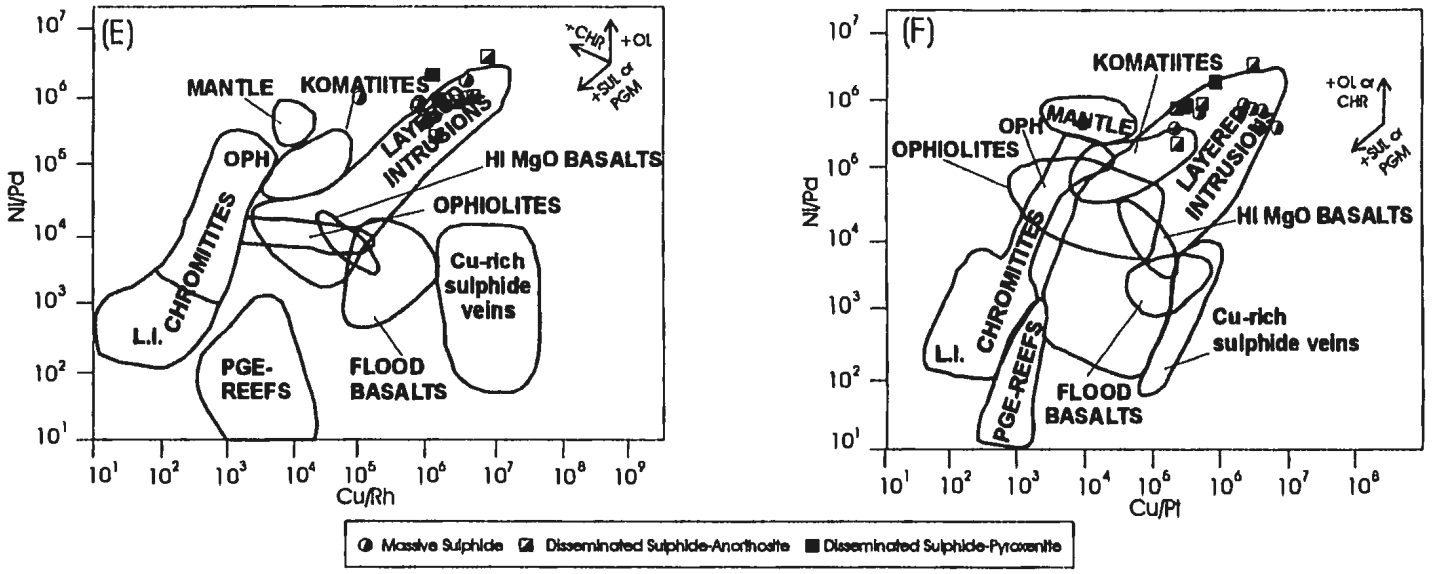

Figure 5.2. (Continued)

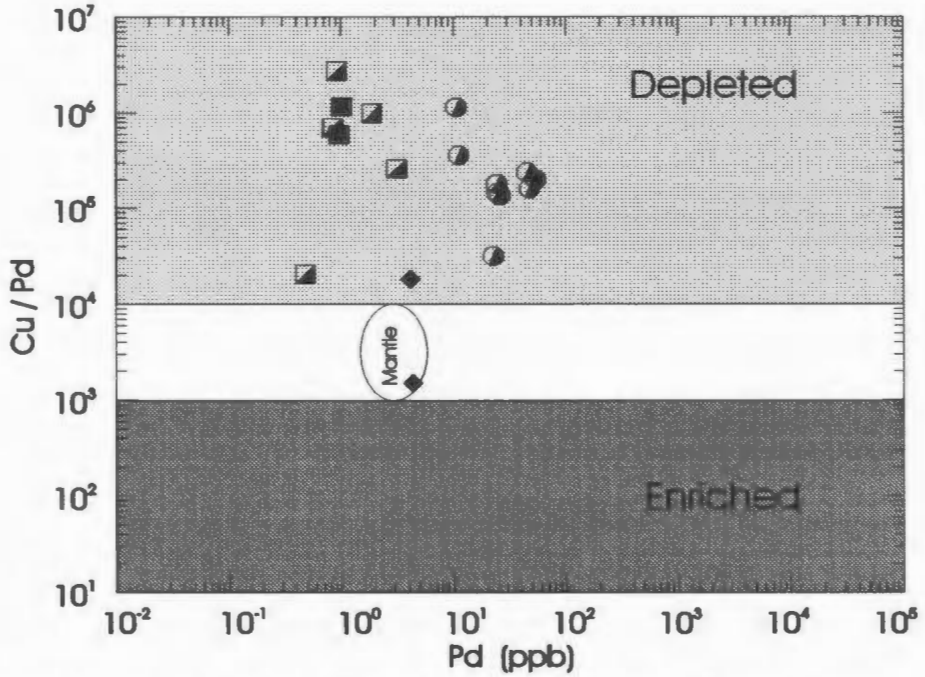

Figure 5.3. Cu/Pd-Pd plot of sulphides from the OKG prospect; symbols as in Figure 5.2 and fields after Barnes et al. (1993)

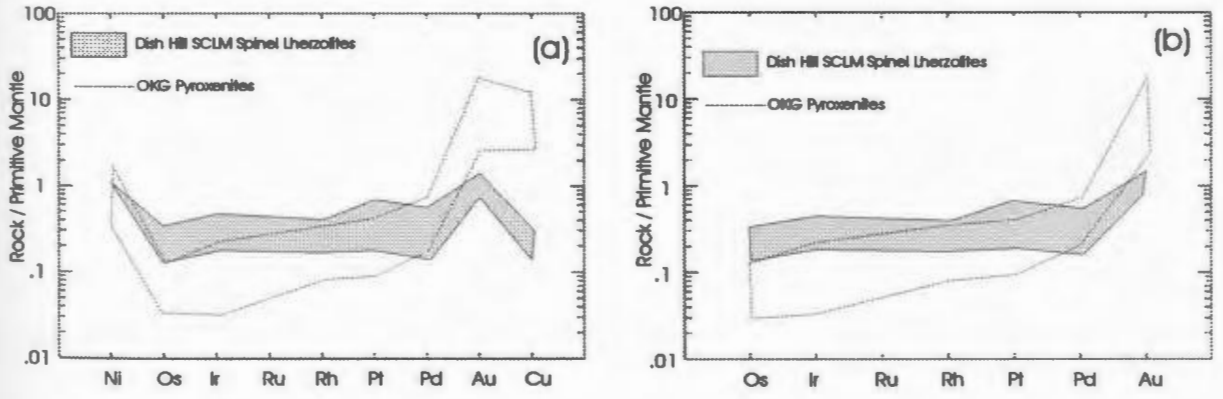

Figure 5.4. Comparitive PGE plots for the OKG pyroxenites relative to subcontinental lithospheric mantle (SCLM) spinel lherzolite xenoliths from Dish Hill, California. Primitive mantle normalization values from Barnes et al. (1988) and values for SCLM xenoliths from Wilson et al. (1996).

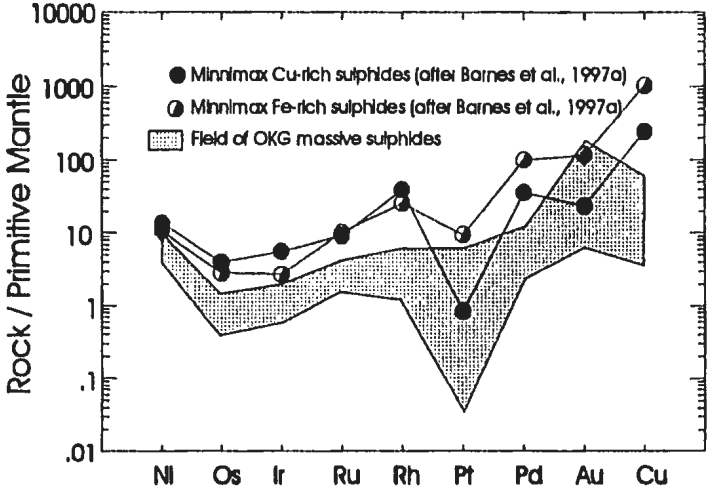

Figure 5.5. Primitive mantle normalized plots of the Minnimax Fe and Cu-rich sulphides in comparison to the OKG massive sulphides. All values are normalized to the primitive mantle values of Barnes et al. (1988).

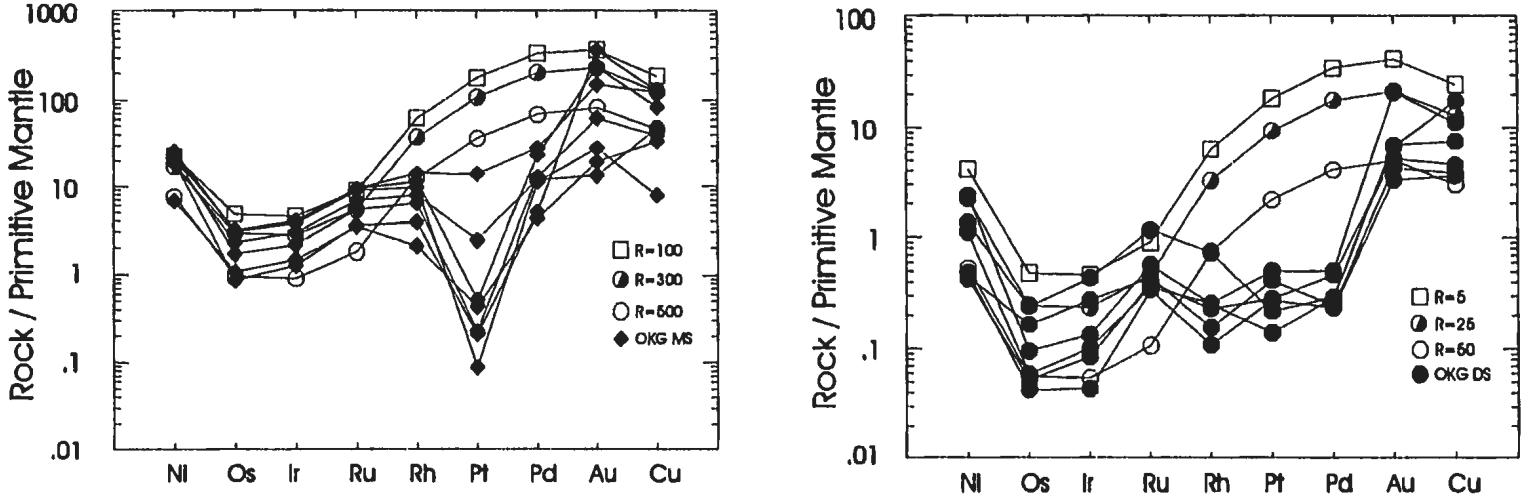

Figure 5.6. R-factor models for the OKG massive and disseminated sulphides. Starting liquids and partition coefficients from Barnes et al. (1997a).

Table 5.1 Metal ratios of respective sulphide bearing units and comparisons to the primitive mantle.

Type	Ni/Cu	Pd/Ir	Pd/Rh	Pd/Pt	Ni/Pd	Cu/Ir	Cu/Rh	Cu/Pt
OKG Massive Sulphides	1.51-29.98 avg = 6.82	2.90-7.04 avg = 4.73	3.19-5.69 avg = 4.76	1.05-68.13 avg = 20.52	413377-1712243 avg = 816405	96928-4584820 avg = 1381802	101529-4131942 avg = 1398422	209507-14603346 avg = 3901683
OKG Disseminated Sulphides (Pyroxenite)	0-1.36 avg = 0.91	0-5.54 avg = 3.07	0-5.95 avg = 7.57	0-1.10 avg = 0.50	0-3744155 avg = 1125599.63	51927-7069232 avg = 3390897	154805-8570363 avg = 4001097	4365-2999461 avg = 680675
OKG Disseminated Sulphides (Anorthosite)	1.49-1.77 avg = 1.63	0.67-2.94 avg = 1.81	1.10-2.72 avg = 1.91	0.48-0.71 avg = 0.60	877936-2062624 avg = 1470278	779921-1737051 avg = 1258486	1280356-1606238 avg = 1443297	280696-831137 avg = 555916
Primitive Mantle[1]	7.14	1	2.2	0.48	454545	63636	140000	30435

[1]Data from Barnes *et al.* (1988).

Table 5.2 Cu/Pd, Ni/Ir and mantle normalized Cu/Pd and Ni/Ir ratios. Normalization values from Barnes *et al.* (1988).

Type	Cu/Pd	Ni/Ir	Cu/Pd_{MN}	Ni/Ir_{MN}
OKG Massive Sulphides	31788-1135666 avg = 208441	2091505-6912528 avg = 3567877	0.50-17.85 avg = 4.96	4.60-15.21 avg = 7.85
OKG Disseminated Sulphides (Pyroxenite)	020442-2729928 avg = 898519	0-8083628 avg = 3396472	0.32-42.90 avg = 14.12	0-17.78 avg = 17.47
OKG Disseminated Sulphides (Anorthosite)	589955-1162677 avg = 876316	1383608-2584974 avg = 1984289	9.27-18.27 avg = 13.77	3.04-5.69 avg = 4.37
Primitive Mantle[1]	63636	454545	1	1

[1]Data from Barnes *et al.* (1988).

Table 5.3. Model liquid and partition coefficient parameters for R-factor modeling of the OKG sulphides. Liquid and partition coeffecient data from the Duluth Complex PGE-depleted basalt from Barnes *et al.* (1997a).

Element	C_L	$D^{sulphide/silicate}$
Ni (ppm)	180	500
Cu (ppm)	100	1500
Os (ppb)	0.04	100000
Ir (ppb)	0.04	100000
Ru (ppb)	0.1	100000
Rh (ppb)	0.2	100000
Pt (ppb)	3	100000
Pd (ppb)	3	100000
Au (ppb)	1	4000

Chapter 6. Radiogenic Isotope Geochemistry

6.1 Introduction

Radiogenic isotopes provide a valuable mechanism for studying igneous petrogenesis and the interrelationship between crust-mantle processes, crustal contamination and basement influence on the genesis of igneous rocks (DePaolo, 1981; Naldrett *et al.*, 1986; DePaolo, 1988; Emslie and Hegner, 1993; Emslie *et al.*, 1994; and others). In regions such as that of the OKG, sufficient age contrasts exist between the igneous units (e.g. anorthositic-granitoid-pyroxenitic) and the basement rocks (e.g. Nain Province) that the relative effects of contamination and basement influence should readily appear within the isotopic signatures of the units (e.g. Emslie *et al.*, 1994; Hamilton, 1997). This chapter provides Rb-Sr and Sm-Nd isotope data for the anorthositic, granitoid, amphibolite-mafic granulite, and pyroxenitic rocks from the OKG in an attempt to assess the following: 1) the role of basement influence and crustal contamination have on the anorthositic and granitoid rocks of the property; 2) to assess the role that crustal contamination has played in the genesis of the pyroxenite hosted mineralization; and 3) to isotopically fingerprint the possible crustal contaminant(s) associated with 1 and 2.

6.2 Theory: Rb-Sr and Sm-Nd Isotope Systematics

6.2.1 The Rb-Sr Isotopic System

The early usage of the Rb-Sr system was primarily studied for geologic dating purposes; however, since the 1970's the Rb-Sr system has been used extensively for assessing and fingerprinting crust-mantle influences in igneous rocks (e.g. Faure and Powell, 1972; Faure, 1986; Zindler and Hart, 1986; and others). The Rb-Sr system is based on the decay of ^{87}Rb to ^{87}Sr over geologic time, and in general Sr isotopes are measured relative to the unradiogenic Sr isotope, ^{86}Sr (Faure and Powell, 1972; Faure, 1986; Rollinson, 1993).

The use of the Rb-Sr system is closely allied to the crust-mantle evolution of the Earth from a uniform Sr-isotope reservoir (e.g. UR), generally believed to represent the Rb-Sr composition of meteoritic rocks (Faure and Powell, 1972; Faure, 1986). The aforementioned meteoritic reservoir was defined on the basis of numerous studies of achondritic meteorites, and a value for the bulk Earth was established, commonly referred to as the "basaltic achondrite best initial", or BABI (Faure and Powell, 1972; Faure, 1986; Rollinson, 1993). The value of BABI likely represents the "bulk Earth", or uniform reservoir (UR), and evolved from a $^{87}Sr/^{86}Sr$ value close to 0.699, while the present day value of the UR is likely between 0.7020 and 0.7045 (Faure, 1986; Rollinson, 1993).

The behaviour of the Rb-Sr system during the Earth's evolution is controlled by the fractionation of Rb and Sr during crust-mantle formation, and the effective Rb/Sr ratio of the reservoir in question (Faure and Powell, 1972; Faure, 1986; Rollinson, 1993).

The formation of continental crust and depleted mantle reservoirs from the UR has been argued to have occurred at different times (see section 6.2.2); however, for simplistic purposes an age of ca. 3.7 Ga is chosen to represent time when granitoids appeared in the earth's crust (Faure, 1986; Rollinson, 1993). At this time the appearance of granitoids would likely represent the formation of continental crust and depleted mantle; forming two distinct reservoirs with different Rb/Sr ratios.

The extreme partitioning of Rb from Sr in crustal rocks led to an irreversible loss of Rb from the mantle and exorbitant enrichment in the continental crust, resulting in lower and higher Rb/Sr ratios relative to the bulk earth, respectively (Figure, 6.1; Faure, 1986). The higher Rb/Sr ratios of the crustal reservoir led to a time integrated evolution towards higher $^{87}Sr/^{86}Sr$ ratios due to the pronounced increase in ^{87}Sr from the radioactive breakdown of ^{87}Rb through time (Figure 6.1; Faure, 1986). In contrast, the lower Rb/Sr values in the depleted mantle resulted in retarded growth of ^{87}Sr and a resultant curve depleted in $^{87}Sr/^{86}Sr$ relative to the bulk Earth (Figure 6.1; Faure, 1986). In Figure 6.1a, this is portrayed as a simple linear evolution, very similar to that for the Sm-Nd system (DePaolo, 1988; see section 6.2.2); however, the sharp contrasting geochemical behaviour between Rb and Sr is much different than the more geochemically coherent behaviour of Sm and Nd. Hence, the evolution of the mantle and crust is likely non-linear and likely is quite curvilinear due to the extreme depletions of Rb in the depleted mantle reservoir (Figure 6b; Faure and Powell, 1972; Faure, 1986).

Regardless, of the complexities in the Rb-Sr system, it provides a valuable tool in understanding petrogenesis, contamination, and basement influence associated with

AMCG suites, and nickeliferous mafic-ultramafic magmatism (e.g. Ashwal *et al.*, 1986; Naldrett *et al.*, 1986; Emslie and Hegner, 1993; Emslie *et al.*, 1994; and others); and in tandem with Nd isotopes, can be very valuable (*op cit*). A caveat to the Rb-Sr system lies in the inherent geochemical characteristics of Rb and Sr, and particularly Rb. Rubidium, being an alkali metal, is very mobile during hydrothermal alteration and metamorphism; while Sr is a little more robust, it must also be viewed with caution as it can also be mobile during alteration/metamorphism (Collerson, 1983; Collerson *et al.*, 1984, 1989; Rollinson, 1993; and others). Consideration of these characteristics must be taken into account when interpreting $^{87}Sr/^{86}Sr$ in old rocks, and like those in this thesis, must be viewed with caution as the effects of secondary processes must always be addressed.

6.2.2 The Sm-Nd Isotopic System

Similar to the Rb-Sr system, the Sm-Nd system is quite valuable as a petrogenetic tool, as it provides excellent information on petrogenesis, crustal contamination, fractional crystallization and other processes (DePaolo 1981, 1988; Ashwal and Wooden, 1985; Faure, 1986; Ashwal *et al.*, 1986; Emslie *et al.*, 1994; Hamilton, 1997; and others). The premise behind the Sm-Nd system is quite similar in context to that of the Rb-Sr system, that a radiogenic parent isotope (i.e. ^{147}Sm) decays to a daughter isotope (i.e.^{143}Nd; DePaolo, 1988). However, in contrast to the Rb-Sr system, the Sm-Nd system is much more robust and in most cases is resistant to secondary processes such as metamorphism and alteration (DePaolo, 1988; Faure, 1986; Rollinson, 1993). Bearing the latter in mind, there is evidence, however, for fractionation of the Sm and Nd during

high grade (granulite facies) metamorphism and possibly during crustal anatexis (Collerson *et al.*, 1989).

In the context of planetary evolution the Sm-Nd system begins with the "bulk earth", represented by the Sm-Nd composition of chondritic meteorites, and referred to as the "chondrite uniform reservoir", or CHUR (DePaolo and Wasserburg, 1976; DePaolo, 1981, 1988). The early evolution of the Earth from the solar nebula resulted in the coalescence of the bulk earth retaining the values approximated by CHUR (Figure 6.2; Faure, 1986; DePaolo, 1988; and others). From CHUR the subsequent evolution of the crust and mantle reservoirs is believed to have began when there was widespread partial melting of the bulk earth (primitive mantle) to form the crust and depleted mantle (DM; DePaolo, 1981, 1988). Conservative estimates on the timing of this event are placed at ca. 2.0 Ga (Patchett, 1989), at 2.9 Ga (Bell and Blenkinsop, 1987), at ca. 3.5 Ga or older (Chase and Patchett, 1988), while Collerson *et al.* (1991) provide evidence for LREE depletion in the mantle prior to 3.8 Ga, and possibly even before 4.0 Ga. Early Archean ages for mantle depletion do not likely represent widespread continental crust formation, and Nd depletions were likely due to the extraction of mafic/ultramafic oceanic crust (Collerson *et al.*, 1991), accompanied with temporary storage without recycling back into the mantle; allowing for time integrated positive εNd values (Chase and Patchett, 1988).

Like the Rb-Sr system, the variations in Nd isotope geochemistry, relative to CHUR, are dependant on the Sm/Nd ratios of the reservoir in question (DePaolo, 1988). The genesis of the crustal and DM reservoirs as described above resulted in 1) a crustal reservoir enriched in LREE and lower Sm/Nd relative to CHUR; and 2) a DM with

LREE depletion and higher Sm/Nd relative to CHUR (Figure 6.2; DePaolo, 1981, 1988). These variations have important consequences especially when using Nd for petrogenetic tracing. In time, the high Sm/Nd DM reservoir will show a marked increase in ^{143}Nd, due to the elevated ^{147}Sm in this reservoir (Figure 6.2), and consequently will evolve with a $^{143}Nd/^{144}Nd$ ratio greater than CHUR (Figure 6.2). In contrast, the crustal reservoir with low Sm/Nd will have a retarded time integrated ^{143}Nd growth because of the lower amount of radiogenic ^{147}Sm in this reservoir (Figure 6.2). Of course this is a simplified model and the geochemical dynamics of the crust-mantle reservoirs are likely not this simple (e.g. Zindler *et al.*, 1982; Hart, 1984, 1988; Zindler and Hart, 1986; DePaolo, 1988; Menzies 1989, 1990); however, they do provide a gauge and descriptive mechanism to discuss Nd isotope variations.

6.2.3 Notations Used for the Sm-Nd Isotopic System and Isotope Evolution

The notations used in much of the discussions hereafter are of significant importance and provide a coherent and dynamic means of presenting Nd isotope data. The most universal and key notations used with the Sm-Nd system are epsilon values, given by εNd (DePaolo and Wasserburg, 1976; DePaolo, 1981), and the equation:

$$\varepsilon Nd = \{[(^{143}Nd/^{144}Nd_{rock,\,t})/(^{143}Nd/^{144}Nd_{CHUR,\,t})]-1\}*10^4 \quad (6\text{-}1)$$

where $^{143}Nd/^{144}Nd_{rock,\,t}$ is the ratio of $^{143}Nd/^{144}Nd$ at time t, and $^{143}Nd/^{144}Nd_{CHUR,\,t}$ is the ratio of $^{143}Nd/^{144}Nd$ of CHUR at time t. This notation allows the comparison and coherent presentation of Nd isotopes relative to CHUR and provides a means of measuring variations relative to the standard CHUR reservoir. The calculation of εNd values at a given time is strongly dependant on the CHUR model, and the value at t must be calculated based on some

known age (e.g. U-Pb zircon age, Sm-Nd isochron age, or a realistic age assumption). For the purposes of this chapter discussions of the isotope chemistry will use three ages for respective εNd evaluations. The older Nain Province rocks of the property are likely of Mid-Archean age and similar to those in Okak Bay region (Schiøtte *et al.*, 1993), and are normalized to 3235 Ma, interpreted to be the precursor age of those in the Okak Bay region (*op cit*). The age of the anorthositic and granitoid rocks is subject to debate, however, geochronological and field mapping has shown that these rocks may be of Paleoproterozoic age (Hamilton, 1997; Emslie *et al.*, 1997; Ryan *et al.*, 1997, 1998; Hamilton *et al.*, 1998; see Chapter 3). The possible lower limit of this magmatic age is bracketed at ca. 2045 Ma (Hamilton 1997; Hamilton *et al.*, 1998) and εNd calculations are carried out using an age of 2050 Ma. For the purposes of mixing and evaluation of contamination in the pyroxenites an age of 1300 Ma is used, as the pyroxenitic rocks and associated mineralization at the OKG prospect are probably of Mesoproterozoic age (see Chapter 3).

Similar to $^{143}Nd/^{144}Nd$ variations, the evolution of εNd is closely tied to the time integrated evolution of the Sm-Nd system and related Sm/Nd ratios of a given reservoir (see section 6.2.2). By convention εNd values for CHUR are always 0, regardless of age (Figure 6.2; DePaolo and Wasserburg, 1976; DePaolo, 1981, 1988). However, considering equation 6-1, values for the DM reservoir will evolve in time to more positive epsilon values in time because of the higher Sm/Nd ratio relative CHUR (Figure 6.2; DePaolo, 1981, 1988). In contrast, the crustal reservoir will temporally evolve to more negative εNd values due to lower Sm/Nd ratios relative to CHUR (Figure 6.2;

DePaolo, 1981, 1988). In general, εNd variations can be summarized in the following manner (after Faure, 1986; DePaolo, 1981, 1988; Rollinson, 1993; and others):
a) εNd >0 infers derivation from LREE depleted sources (i.e. DM or mantle reservoirs); b) εNd <0 suggests derivation from LREE enriched sources (i.e. crustal sources), or contamination by such sources (i.e. crustal contamination); and c) εNd = 0 infers derivation from CHUR-like sources.

The use of "model ages" and "crustal residence age" (cf. DePaolo, 1981, 1988) generally refers to the time at which a given material has been derived from a given reservoir. In essence, the time at which the sample has an εNd value equivalent to the reservoir in question (Figure 6.3; DePaolo, 1981, 1988). Early workers concentrated on the use of model ages relative to CHUR, or T_{CHUR}; however, DePaolo (1981) suggested that many crustal rocks (mafic or felsic) are derived from a non-CHUR reservoir, and in many cases had come from a depleted mantle reservoir. Commonly model ages are given with respect to this depleted mantle (DM) and are referred to as "depleted mantle model ages", which can be calculated using the following equation:

$$T_{DM} = 1/\lambda\, ln\{[(^{143}Nd/^{144}Nd_{rock,today} - ^{143}Nd/^{144}Nd_{DM,\,today})/(^{147}Sm/^{144}Nd_{rock,today} - ^{147}Sm/^{144}Nd_{DM,today})]+1\} \quad (6\text{-}2)$$

where the $^{143}Nd/^{144}Nd$ and $^{147}Sm/^{144}Nd$ ratios are those of the rock and DM at the present day and λ is the decay constant of the Sm-Nd system (Lugmair and Marti, 1976; DePaolo, 1981, 1988; Rollinson, 1993).

The significance of model ages must be evaluated with considerable skepticism, as often they have no geochronological significance (Arndt and Goldstein, 1987). The T_{DM} age has geochronological significance only when the rock in question has evolved in

a single stage manner with an unchanged Sm/Nd ratio and has not mixed with isotopically different reservoirs (i.e. evolved as a closed system; Figure 6.3). However, this is usually not the case and often rocks are mixtures of different reservoirs (Figure 6.3; Arndt and Goldstein, 1987). Consider the case where a rock is a mixture of different reservoirs, in particular a rock with a juvenile component with a model age of T_x, and an older component at T_y (Figure 6.3; Arndt and Goldstein, 1987). The actual geochronological age of the rock is likely close to the value of the juvenile component at T_x ; however, mixing with an isotopically distinct crustal reservoir with a model age of T_y would yield a rock with a model age of T_{xy} that is a hybrid model age of both of these sources and is substantially different that the geochronological age! (Figure 6.3; Arndt and Goldstein, 1987).

The question that arises from the latter is: "What is the significance of model ages if they cannot provide one with information on geochronology?" The answer to this question has been partially answered by Patchett (1989). He stated that in areas where the basement (or crustal contributor) is greater than 500 Ma older than the magmatic event in question, deciphering of the crustal age can provide an idea of the nature of the contaminant/basement. Studies using T_{DM} ages to decipher the nature of the basement and their contributions to igneous rocks have been exemplified by the early works of DePaolo (1981), Farmer and DePaolo (1984), Bennett and DePaolo (1987) and Farmer *et al.* (1989) in the southwestern United States; while it's application in Labrador is illustrated by the work of Kerr and Fryer (1990), Emslie and Thériault (1991), Hamilton and Shirey (1992), Emslie and Loveridge (1992), and Emslie and Hegner (1993).

Closely allied with the usage of εNd and model ages is the "neodymium crustal index" or NCI (DePaolo *et al.*, 1992). This index measures the relative contributions of crust and mantle Nd in given igneous rocks, and provides a measure of contamination and basement contribution. The NCI is given by the following:

$\mathbf{NCI = [\varepsilon Nd_{rock} - \varepsilon Nd_{MC}]/[\varepsilon Nd_{CC} - \varepsilon Nd_{MC}]}$ (6-3); where εNd is as in equation 6-1, while the subscripts are for the rock, MC is the mantle component of the mixture, and CC is the crustal component of the mixture (DePaolo *et al.*, 1992). This works quite well if the crustal and mantle components are well constrained; however, this is often not the case and some assumptions must be made, and most certainly ambiguities exist. If a reasonable idea of the crustal domain of influence can be ascertained, as well as the mantle component, then application of the NCI can be quite powerful. The application of NCI to assess crust-mantle contributions in AMCG genesis in Labrador has been readily applied by Emslie *et al.* (1994).

Another notation often used with the Sm-Nd system is the "fractionation factor" of DePaolo (1988), given by the following equation:

$\mathbf{f_{Sm/Nd} = [(^{147}Sm/^{144}Nd_{rock})/(^{147}Sm/^{144}Nd_{CHUR})]-1}$ (6-4); where $^{147}Sm/^{144}Nd_{rock}$ and $^{147}Sm/^{144}Nd_{CHUR}$ are the $^{147}Sm/^{144}Nd$ ratios of the rock and CHUR, respectively. The fractionation factor provides an estimate of the Sm/Nd ratio of the reservoir/rock in question and generally reflects the degree of Sm and Nd fractionation (DePaolo, 1988). By convention values of $f_{Sm/Nd}$ for CHUR will always be 0 (see equation 6-4 and DePaolo, 1988). Depleted sources (e.g. DM) have Sm readily enriched relative to Nd, and consequently have $f_{Sm/Nd}$ values greater than CHUR (e.g. $f_{Sm/Nd} > 0$); while crustal

reservoirs are generally depleted in Sm relative to Nd and have $f_{Sm/Nd}$ values less than CHUR (i.e. $f_{Sm/Nd} < 0$). The typical depleted mantle model reservoir of DePaolo (1988) has an $f_{Sm/Nd}$ value of +0.09; while Collerson *et al.* (1991) have residual mantle and metakomatiitic rocks of ca. 3.8Ga with $f_{Sm/Nd}$ values ranging from +0.17 to +0.59. Typical continental crustal material, or depleted materials contaminated/enriched by such a source, should have $f_{Sm/Nd}$ values <0, and typical continental crust has an $f_{Sm/Nd} \approx -0.4$ (DePaolo, 1988).

Although this seems simplistic and quite similar to the εNd notation, it must be noted that the fractionation factor is not a time integrated variable and can be strongly controlled by partial melting or fractional crystallization processes (DePaolo, 1988; this chapter). Repeated melting events of a common source region, without subsequent recycling of Sm and Nd, can result in strong fractionations in Sm/Nd with time. Such repeated melt episodes in a given source tend to cause increases in Sm/Nd with time, and consequently the $f_{Sm/Nd}$ value of that region and subsequent rocks derived from it (DePaolo, 1988; see section 6.4.4). DePaolo (1988) suggested that Archean source materials that have experienced numerous intracrustal REE fractionation events may in fact evolve to greater $f_{Sm/Nd}$ with time; and this has also been observed in granitoids ranging in age from ca. 2100 to 1300 Ma in Labrador (Emslie and Loveridge, 1992).

What is obvious from the above discussions on notations is that the Rb-Sr and Sm-Nd system are simple three component systems (i.e. CHUR or UR, depleted mantle and crustal reservoirs). In many cases this is likely not the case and the geodynamic aspects of the crust and mantle are likely much more complex; summaries of the

complexities of these reservoirs are discussed in papers by Zindler *et al.* (1982), Hart (1984, 1988), Zindler and Hart (1986) and Menzies (1989).

6.3 Sr Isotope Geochemistry

6.3.1 Nain Province Gneisses

Only four samples have been analyzed for Sr isotopes, all of which are amphibolites/mafic granulites, and have initial ratios calculated at 3235 Ma. ISr (@3235Ma) values have a wide range for the gneisses from 0.6770 to 0.8399, with Rb/Sr ratios ranging from 0.0610 to 0.9234. Both the lower and upper bounds of these initial Sr ratios are unrealistic. For instance, the lower bound 0.6770 is lower than BABI (or the bulk earth; Faure, 1986) which is impossible; while the upper value appears to be from a source with an extremely long crustal residence time. It is possible that the age used for normalization is incorrect. However, considering the petrological history of these rocks it is more likely that these rocks have had considerable isotopic disturbance and putting considerable trust on the Sr isotope data is problematic. For instance if these rocks are actually ca. 3.2 Ga (Schiøtte *et al.*, 1993) then they would have experienced granulite facies metamorphism at 2.8-2.7 Ga (Schiøtte *et al.*, 1989a,b, 1990; Chapter 3), possible influence from the intrusion of ca. 2.1Ga foliated granitoids (Hamilton *et al.*, 1998; Chapter 3), and later Torngat Orogen related greenschist facies metamorphism (Ryan *et al.*, 1998; Chapter 3). These events would likely have resulted in extreme resetting of the Sr isotope system and the values of the gneisses cannot be used for any reasonable inferences on crustal influence and source tracing.

6.3.2 Anorthositic Rocks

Anorthositic rocks have initial Sr isotope ratios ($^{87}Sr/^{87}Sr$, or ISr) calculated at 2050Ma (ISr (@2050Ma)) for reasons provided in section 6.2.3. Values for the rocks have very restricted ISr (@2050Ma), ranging from 0.7048 to 0.7082, and Rb/Sr ratios ranging from 0.0013 to 0.0217 (Figure 6.4; Table 6.2). Within the subgroups there is a similar overlap and restricted isotopic characteristics with the *an* group having ISr (@2050Ma) from 0.7048-0.7082 (avg 0.7064), the *ln1* group having values from 0.7053 to 0.7061 (avg 0.7055), and the *ln2* group with values between 0.7057-0.7059 (Figure 4; Table 6.2). Epigenetically mineralized *an* group rocks are variable, and one sample could not be recalculated because the low Rb, and absent $^{87}Rb/^{86}Sr$; however, the close correlation between the initial ratios of the anorthosites at 2050 Ma and the present (Table 6.2) suggests that the present day $^{87}Sr/^{86}Sr$ in sample P96-468a likely approximates the value of ISr (@2050Ma). These samples then have values equivalent to 0.7062-0.7067, within the range of the other anorthositic subgroups (Table 6.2; Figure 6.4).

The relatively consistent ISr (@2050Ma) data for the anorthositic rocks is consistent with those of other workers (Ashwal *et al.*, 1986; Geist *et al.*, 1990; Emslie and Hegner, 1993; Emslie *et al.*, 1994). The low Rb, high Sr, and Rb/Sr of the anorthositic rocks effectively negates any large change in $^{87}Sr/^{86}Sr$ ratio with time (cf. Table 6.1), and the present day initial ratios closely approximate the values calculated at 2050Ma. It is also evident that although Rb and Sr can be mobile during greenschist facies metamorphism (Rollinson, 1993), the relatively coherent and restricted ISr (@2050

Ma) values have not been isotopically reset by Torngat Orogen metamorphism and deformation (Figure 6.5; cf. Bertrand et al., 1993; Van Kranendonk, 1996; and others). Furthermore, the high ISr (@2050Ma) values from 0.7048 to 0.7082 are consistent with crustal contamination of some sort, in particular a source with long Sr crustal residence time; further details on the role of crustal contamination will be discussed in section 6.4.2.

Some samples do not behave coherently and have elevated ISr (@2050Ma) relative to the main trend, in particular P96-19 (*an* group), and P96-469 (mineralized *an* group; Figure 6.5). It is likely that these rocks may have had radiogenic Sr addition related to either the mylonitic deformation and related carbonate alteration observed in the Main Showing area, or fluids related to the emplacement of the pyroxenitic dykes and related mineralization.

6.3.3 Granitoid Rocks

Initial $^{87}Sr/^{86}Sr$ are calculated for the granitoids at 2050 Ma similar to the anorthositic rocks. The variation in ISr (@2050Ma) is much more variable for the granitoids than the anorthositic rocks and ranges from 0.7036 to 0.7095, with Rb/Sr ratios ranging from 0.1716 to 0.7338 (Table 6.2). The felsic dykes have only one sample with detectable $^{87}Rb/^{87}Sr$, which has a recalculated ISr (@2050Ma) of 0.7058; however, unlike the anorthositic rocks there is substantial difference between $^{87}Sr/^{86}Sr$ today and ISr (@2050 Ma), therefore the second sample with undetectable $^{87}Rb/^{86}Sr$ is not included above. The phase 1 granitoids have ISr (@2050Ma) values that range from 0.7036 to

0.7049 (avg 0.7043), while the phase 2 granitoids have ISr (@2050Ma) ranging from 0.7094 to 0.7095 (avg 0.70945; Figure 6.4; Table 6.2).

The higher ISr (@2050Ma) of the granitoid rocks relative to the anorthositic rocks is expected to a certain extent, since they likely contain a greater crustal contribution, as well as variable Rb/Sr ratios proportional to the plagioclase/K-feldspar ratios. The samples ranging from 0.7036-0.7095 is consistent with variable amounts of crustal input; however, the lower values may represent input from a source with shorter Sr crustal residence time, possibly from a mantle source (e.g. Emslie *et al.*, 1994)
Most samples have ISr (@2050Ma) values that range from 0.7036 to 0.7095, consistent with generation from crustal materials with mantle input.

6.3.4 Pyroxenitic Rocks

The pyroxenitic rocks of the OKG prospect are characterized by extremely low Rb, and in most samples Rb was below detection limits, and consequently had non-detectable $^{87}Rb/^{86}Sr$. Due to this only two samples could be calculated at 1300 Ma with values that range from 0.7069 to 0.7091. Regardless, the low Rb in the samples suggests that the present day initial ratios are close, or approximately similar, to those at 1300 Ma and thus present day $^{87}Sr/^{86}Sr$ values can be used for descriptive purposes.

The surface pyroxenites have $^{87}Sr/^{86}Sr$ ratios which range from 0.7058 to 0.7329 (avg 0.7160), while subsurface samples have values ranging from 0.7069 to 0.7691 (avg 0.7197; Table 6.3; Figure 6.6). The average values of the subsurface pyroxenites are higher than the surface examples, which suggests a greater contribution of crustal material and radiogenic Sr. However, there is not a large difference between the average

$^{87}Sr/^{86}Sr$ for the two groups and there isn't as clear cut a crustal influence as there is with the Nd isotope geochemistry (section 6.4.4).

Alternative explanations for the variable $^{87}Sr/^{86}Sr$ ratios may be related to the Rb and Sr content of the rocks. Two surface samples have detectable Rb, however, it is less than 1 ppm (0.26-0.73ppm), and have lower average Sr values (avg 15.9ppm) than the subsurface examples which have no detectable Rb and higher average Sr (avg 123.2 ppm). On a plot of $^{87}Sr/^{86}Sr$ versus Sr for the two suites (Figure 6.7) two relatively distinctive trends arise, with minor exceptions. The surface samples, with the exception of one sample (P96-5B), have a relatively positive correlation with increasing Sr, showing an overall increase in $^{87}Sr/^{86}Sr$ with increasing Sr (Figure 6.7). In these samples the radiogenic ^{87}Sr was likely derived from the ^{87}Rb within the rocks at the time of formation, with less input from external assimilation of crustal ^{87}Sr. Sample P96-5B does not follow the trend discussed above, and contains very little Sr (1.1ppm) relative to other surface examples (Figure 6.7); however, the elevated $^{87}Sr/^{86}Sr$ likely follows the same logic, with any Sr present likely due to Rb breakdown and relatively minor crustal contribution.

The subsurface examples appear to contrast with the positive correlation observed in the surface pyroxenites. The relatively constant $^{87}Sr/^{86}Sr$ regardless of Sr content in the dykes, with the exception of sample 16715, suggests that the major controlling factor in the isotopic signatures was not likely the initial Rb in the samples, but rather assimilation of variable amounts of crustal Sr with elevated $^{87}Sr/^{86}Sr$ (Figure 6.7).

The elevated sample, 16715, with $^{87}Sr/^{86}Sr = 0.7691$, could be explained by the same mechanism responsible for the elevated surface samples with lesser contributions from crustal contamination.

6.4 Nd Isotope Geochemistry

6.4.1 Nain Gneissic Rocks

Four samples of Nain Province amphibolite and mafic granulite were analyzed for Nd isotopes and have εNd calculated at 3235Ma. Even with only four analyses, a two-fold subdivision exists with three samples having εNd (@3235Ma) ranging from +4.4 to +11.2, and $f_{Sm/Nd}$ from –0.22 to –0.58, and Sm/Nd ratios from 0.14 to 0.25; a fourth sample has εNd (@3235Ma) = -9.1, $f_{Sm/Nd}$ = +0.11, and Sm/Nd = 0.35. Isotopically evolving these two groups show two diverging trends with the first (crustal?) group evolving to progressively negative values with εNd (@0Ma) values ranging from –11.8 to –37.5; while the fractionated sample evolves to εNd (@0Ma)= -0.2 (Figure 6.8; Table 6.4).

Comparing the two groups with Collerson *et al.*'s (1989) Early-Archean Kiyuktok gneisses from the Saglek area, and Schiøtte *et al.*'s (1993) Mid-Archean Nain Province gneisses from Okak Bay shows some considerable overlap; at least in the case of the latter group (Figure 6.9). Epsilon values of Schiøtte *et al.*'s (*op cit*) gneisses from Okak Bay show a range that is smaller, but similar to those of the crustal group, (e.g. εNd(@3235Ma) = -4.3 to +6.5); while Collerson *et al.*'s (1989) Early-Archean gneisses are much more negative at 3235 Ma with εNd = -10.2 to –20.2. This suggests that the

crustal suite is more likely related to the Mid-Archean gneisses at Okak Bay, rather than the Late-Archean gneisses in the Saglek area.

In contrast to the crustal suite, the fractionated sample is characterized by negative εNd values that progressively increase with time (Figure 6.8), typical of mantle-type rocks (DePaolo, 1988). Collerson *et al.* (1991) have reported meta-komatiites from the Saglek area that show similar evolutionary trends towards positive values; however, to much greater εNd values at the present day (+16.37 to +56.43), with higher $f_{Sm/Nd}$ values (+0.16 to +0.59), than the fractionated sample. The observed isotopic evolution of the fractionated sample may be a result of: 1) the fractionation of Sm/Nd during partial melting events in the past; 2) the fractionated rocks could be meta-komatiitic in origin like Collerson *et al.*'s (1991) samples; or 3) it could be a function of REE mobility during granulite facies/fluid related metamorphism (e.g. Collerson *et al.*, 1984, 1989; Taylor and Fryer, 1982).

The third hypothesis is quite a distinct possibility since all samples have been subject to granulite facies metamorphism, followed by lower grade metamorphism associated with the Torngat Orogen (see Chapter 3); however, similar REE mobility would be expected in all of the samples, rather than just one sample. The other two hypothesis are interrelated and it is likely that these samples represent a mafic-ultramafic rock that was derived from a fractionated reservoir, much different than the conventional depleted mantle, and in fact may be meta-komatiitic.

6.4.2 Anorthositic Rocks

The anorthositic rocks as a whole, including two with epigenetic Ni-Cu sulphide mineralization, have εNd (@2050Ma) ranging –4.1 to –15.9 and $f_{Sm/Nd}$ ranging from –0.14 to –0.68. The *an* group of anorthositic rocks are characterized by a spread of εNd (@2050 Ma) values from –4.11 to –11.87, the *ln1* group with values ranging from –5.82 to –15.88, the *ln2* group with restricted values between –8.79 to –9.29, and the epigenetically mineralized *an* group with values from –6.57 to –8.51 (Figure 6.10-11; Table 6.5). Fractionation factors ($f_{Sm/Nd}$) closely mirror the εNd values and range from –0.30 to –0.63 for the *an* group, -0.36 to –0.52 for the *ln1* group, -0.38 to –0.44 for the *ln2* group, and –0.14 to –0.24 for the epigenetically mineralized *an* group (Figure 6.11; Table 6.5).

The anorthositic rocks have overlapping and similar εNd values and suggest a common origin or contaminant in their genesis. Although the *ln2* group could be considered a different intrusive based on field and petrographic evidence (Ryan *et al.*, 1998; this study), the overlapping εNd values and $f_{Sm/Nd}$ values with those of the western part of the property (e.g. *an* and *ln1* groups) attest to a similar basement (crustal) contributor in their genesis. The influence of basement rock on the genesis of massif anorthosite is consistent with the work of others in both the NPS, Wyoming and the Grenville Province (Ashwal and Wooden, 1985; Ashwal *et al.*, 1986; Geist *et al.*, 1990; Emslie and Hegner, 1993; Emslie *et al.*, 1994; Scoates and Frost, 1996; and others). A further discussion of basement contributions will be discussed in section 6.6

6.4.3 Granitoid Rocks

Only the felsic dykes in the Main Showing area, and phase 1 granitoids (ph1) and phase 2 (ph2) granitoids south of Umiakoviarusek Lake have been analyzed for radiogenic isotopes. The εNd (@2050 Ma) values for the granitoids range from –5.56 to –9.90, while $f_{Sm/Nd}$ values range from –0.34 to –0.50 (Figure 6.10-11; Table 6.5). Felsic dykes from the Main Showing region have εNd (@2050 Ma) values ranging from –5.57 to –6.81, phase 1 granitoids have values from –5.14 to –7.50, while the phase 2 granitoids have values from –5.92 to –9.70 (Figure 6.10-11; Table 6.5). Fractionation factors range from –0.35 to –0.45 in the felsic dykes, -0.34 to –0.43 in the phase 1 granitoids, and from –0.41 to –0.50 in the phase 2 granitoids (Figure 6.11; Table 6.5).

Epsilon values and fractionation factors overlap for all three granitoid groups and like the anorthosites have had similar basement influence. What remains perplexing is that one would expect the granitoid rocks to show a greater influence of crustal material, and related lower εNd and $f_{Sm/Nd}$ values, if they are derived from partial melting of a crustal domain by basaltic underplating (Kolker *et al.*, 1990; Emslie, 1991; Emslie and Stirling, 1993; Emslie and Hegner, 1993; Emslie *et al.*, 1994). This is consistent with the idea that the granitoids have a significant mantle component involved in their genesis (DePaolo *et al.*, 1992; Emslie and Hegner, 1993; Emslie *et al.*, 1994), and would be in accordance with the Sr isotope data.

6.4.4 Pyroxenitic Rocks

The pyroxenitic rocks have variable signatures and are normalized to 1300 Ma instead of 2050 Ma because they are likely of Mesoproterozoic, rather than Paleoproterozoic in age, for reasons cited in Chapter 2 and Kerr (1998). The dykes have been subdivided into two groupings including those 1) associated with surface exposures (Type 1 and Type 2 dykes) and 2) those in drill core section OKG96-09 (Type 1 dykes). The εNd (@1300Ma) values of the dykes range from relatively uncontaminated (-1.12), to significantly contaminated (-13.56) (Table 6.6; Figure 6.12). The surface examples of the pyroxenites have εNd (@1300Ma) values ranging from –1.12 to –4.80 (avg. –2.77) compared to those from drill core which have values that range from –3.94 to –13.56 (avg. –9.18; Figure 6.12-13; Table 6.6). The $f_{Sm/Nd}$ values of the pyroxenites are very interesting as all of the surface pyroxenites have positive values, ranging from 0.23 to 0.75 (avg. 0.47), while the drill core examples have very restricted values from -0.30 to -0.47 (avg -0.36; Figure 6.13; Table 6.6).

These data are quite interesting and perplexing from both a source characterization and contamination viewpoint. The surface examples are perplexing because they have positive $f_{Sm/Nd}$, higher Sm/Nd, and yet have negative εNd (@1300Ma) values (e.g. average εNd (@1300Ma)= -2.8, $f_{Sm/Nd}$ = 0.47, Sm/Nd = 0.39-0.55). The paradoxical behaviour of positive $f_{Sm/Nd}$, typical of depleted reservoirs, and negative εNd (@1300Ma), typical of crustal contamination or enriched reservoirs, can be explained by the extreme fractionation of Sm and Nd during mantle melting coupled with lesser crustal Nd input, relative to the subsurface examples. The refractory source characteristics

illustrated in Chapter 4 for the pyroxenites suggest a reservoir that has undergone multiple melting episodes, that would effectively increase $f_{Sm/Nd}$ and Sm/Nd in time, explaining the values observed in the surface dykes.

The refractory nature of the mantle source for the pyroxenites can explain the Sm/Nd and $f_{Sm/Nd}$ values of the pyroxenites; however, explaining the negative εNd values is somewhat problematic. The negative εNd (@1300Ma) values would suggest the influence of crustal material, which is likely, however, in time they evolve to more positive values (e.g. εNd (0) = +6.1 to +23.3, avg +12.5; Figure 6.14). This suggests that even though the rocks were contaminated close to their time of formation, in time the low Sm/Nd ratio of the surface dykes resulted in an effective swamping of the unradiogenic crustal ^{144}Nd, with radiogenic ^{143}Nd derived from the breakdown of ^{147}Sm.

In contrast to the surface pyroxenites, the subsurface pyroxenites show a greater degree of crustal influence and are characterized by lower εNd, negative crust-like $f_{Sm/Nd}$, and lower Sm/Nd ratios, while maintaining similar petrographic characteristics. This proposes the question of why the subsurface examples have greater crustal influence than the surface examples. Possible scenarios exist to explain this, including: 1) the surface examples are a later pulse that was chemically insulated to a greater extent than the subsurface samples (cf. Scoates and Frost, 1996); and/or 2) they were emplaced rapidly with lesser interaction with the surrounding wall rock.

6.4.5 Nd Model Ages

The model ages discussed in the following section follow that of the description provided in section 6.2.3, and the curves and calculations provided in the following subsections use the DM curve and equations of DePaolo (1981, 1988).

6.4.5.1 Nain Province Gneisses

The Nain Province gneisses have very strange depleted mantle model ages (T_{DM}) ranging from 2.34 to 3.06 Ga for the crustal suite, and a negative number for the fractionated sample. The fractionated sample is not considered further, as it is not derived from a DM reservoir (Figure 6.8) and gives an unrealistic model age.

The upper age bound for the NP gneisses within the OKG prospect overlaps with the lowest DM age of Schiøtte *et al.* (1993) (3.05 Ga); however, the other lower T_{DM} ages are not representative of the Nain Province on the whole (Collerson *et al.*, 1989; Schiøtte *et al.*, 1993) and require explanation (Table 6.4). The 2.84 and 2.34 Ga model ages for the gneisses either require a isotopic reequilibration of the Sm-Nd system, addition of more juvenile material at a later time, or both. There is documentation of major granulite to amphibolite facies metamorphism at ca. 2800-2700Ma in much of the Nain Province (Schiøtte *et al.*, 1989a,b, 1990) and this could possibly explain the ca. 2.84 Ga model age with partial reequilibration of the Sm-Nd system. However, the lower 2.34 Ga age cannot be easily explained solely by this mechanism. Alternatively, the ca. 2.1 Ga emplacement of the foliated granitoids (Hamilton *et al.*, 1998), in proximity to the Nain Province gneisses may have resulted in infiltration of fluids containing juvenile Nd-isotopic signatures, resulting in an effective lowering of the model ages. Although, this is

somewhat speculative, the close proximity of the gneisses and the ca. 2.1 Ga granitoids suggest that the latter may be a distinct possibility; however, isotopic reequilibration during granulite facies metamorphism at 2.7-2.8 Ga cannot be ruled out.

6.4.5.2 Anorthositic Rocks

The model ages for all the anorthositic subgroups overlap with T_{DM} values ranging from 2.54 to 3.84 Ga, with an average of 3.16 Ma (mineralized *an* subgroup not inclusive; Table 6.5). The *an* subgroup have T_{DM} ages ranging from 2.54 to 3.84 Ga, the *ln1* subgroup have ages from 2.82 to 3.64 Ga, and the *ln2* subgroup have values from 3.13 to 3.31 Ga (Table 6.5). The epigenetically mineralized *an* subgroup rocks have T_{DM} ages that range from 3.55 to 4.58 Ga (Table 6.5).

The wide range of values for the anorthositic rocks, particularly the *an*, *ln1* and *ln2* subgroups, suggest that they may have been influenced by crustal material that ranges in age from Early to Late Archean in age, with an average T_{DM} of Middle Archean age. This is consistent with the assimilation and incorporation of Middle Archean rocks of the Nain Province, similar to those in the Okak Bay region (Schiøtte *et al.*, 1993); however, contributions from a Late Archean Nain Province source cannot be ruled out (Collerson *et al.*, 1989). Furthermore, there is a possibility of variable contributions from rocks ranging from Late to Early Archean considering the complex Archean to Paleoproterozoic history of northern Labrador (e.g. Schiøtte *et al.*, 1990, 1993; and others).

The epigenetically mineralized anorthositic samples have values that are overlap with the upper limit of the *an* subgroup, but one sample (P96-468a) is much higher than

the *an* subgroup with T_{DM} = 4.58 Ga, considerably higher than any of the anorthositic rocks. Explaining this could be easily done if they had assimilated Late-Archean gneisses, which are known to have older than 4.0 Ga model ages (cf. Kiyuktok gneisses; Collerson *et al.*, 1989). However, this is hard to reconcile considering that all of the rocks in this area should have inherited this older Nd signature. Alternatively, the rocks could have their signature effectively diluted by the presence of sulphide mineralization, and their proximity to mylonitic ductile faults and fluid migration may have disrupted Nd-isotopes in the sample. This is speculative, but ductile (mylonitic) faults in the Main Showing region may have caused fluids to mix with the underlying basement, and particularly if they were Cl^- or F^- rich (Taylor and Fryer, 1982), could mobilize Sm and Nd and deposit them in the surrounding anorthosite leading to much older signatures. There is no conclusive answer to this extremely elevated model age and it is viewed with great caution.

6.4.5.3 Granitoid Rocks

Granitoid rocks of the property have model ages that lie within the range of the anorthositic rocks but have less spread, ranging from 2.82 to 3.26 Ga, with an average T_{DM} of 3.03 Ga (Table 6.5). Similar to the anorthositic rocks the model ages do not vary significantly within the different granitoid groups, the felsic dyke group have T_{DM} ages from 2.96 to 3.06 Ga, 2.90 to 3.25 Ga, and the phase 2 granitoids have T_{DM} ages between 2.82 to 3.26 Ga (Table 6.5).

The Archean model ages for the granitoids have an average value that lies within 125 Ma of the anorthositic rocks and suggest that they have had similar basement

contributors in their respective genesis. In particular, the consistent Mid-Archean age between both suites of rocks suggests that the Mid-Archean Nain Province gneisses, like those near Okak Bay (Schiøtte *et al.*, 1993), are the likely basement contributors.

6.4.5.4 Pyroxenitic Rocks

Similar to the εNd (@1300 Ma) characteristics of the pyroxenitic dykes, a similar T_{DM} distribution occurs between the subsurface and surface pyroxenites. The surface (relatively uncontaminated) pyroxenites yield incredibly inconsistent and unrealistic model ages ranging from –793 to 833 Ma (Table 6.6), which combined with the other Nd data suggest that they have not been derived from a DM reservoir, but rather a distinctive, possibly subcontinental lithospheric mantle source (e.g. Figure 6.14). As a result no further discussions of the surface model ages is warranted.

Even though it is likely, almost certainly, that the OKG pyroxenites do not represent melts from a conventional depleted mantle, the use of model ages can give some idea of the nature and relative age of the contaminant. Model ages for the subsurface pyroxenites range from Paleoproterozoic to Middle Archean, from 1.80 Ga to 3.05 Ga, but have a Late Archean average of 2.74 Ga (Table 6.6), suggesting the influence of crust with significantly older crustal residence time. Considering the rocks that temporally precede the pyroxenite dykes there are a number of possible contributors including the Middle Archean Nain gneisses (e.g. Schiøtte *et al.*, 1993), and possibly the Late Archean Nain Province gneisses (e.g. Collerson *et al.*, 1993), any of the Paleoproterozoic intrusives (e.g. Ryan *et al.*, 1998; Hamilton *et al.*, 1998), or even the Tasiuyak gneiss (e.g. Ryan *et al.*, 1995). Considering conventional models for Voisey's

Bay it has been advocated that the Nain and Tasiuyak gneisses have influenced the genesis of the Ni-Cu deposits there (Ryan *et al.*, 1995; Ripley *et al.*, 1997; Lambert *et al.*, 1997; Lightfoot, 1998), and this would be a suitable area to begin the following discussion.

The Tasiuyak gneiss as a possible contributor to the genesis of the contaminated pyroxenites is possible considering that the average εNd (@1300Ma) value of the Tasiuyak gneiss (εNd (@1300Ma) = -9.3) is virtually identical to that of the contaminated pyroxenites (εNd (@1300Ma) = -9.2). However, comparing the model ages of both the contaminated pyroxenites (avg. T_{DM} = 2.74 Ga), is much higher than those of the Tasiuyak gneiss (avg. T_{DM} = 2.42 Ga), and requires input from a source in which Nd has had a much longer crustal residence time. This points to a number of sources, firstly Paleoproterozoic anorthositic and granitoid rocks have very old model ages (T_{DM} = 3.16 and 3.03 Ga, respectively), and it is possible that these have contributed a crustal component to the pyroxenites. It is also likely that the older, Mid-Archean Nain Province gneisses, like those at Okak Bay (Schiøtte *et al.*, 1993), are a possible contributor. Their Mid-Archean age (ca. 3.2 Ga) coupled with their presence in the Umiakoviarusek Lake region provides these as a distinct contributor. Further discussion of these will be presented in the following section on neodymium crustal indexes.

6.4.6 Neodymium Crustal Index Calculations for the OKG Plutonic Rocks

The neodymium crustal indexes (NCI) for the OKG plutonic rocks are calculated using the equation of DePaolo *et al.* (1992) presented in section 6.2.3. When considering the anorthositic and granitoid rocks a value representative of the depleted mantle at that

time is chosen for the mantle component (MC), which at 2050 Ma had an εNd value of +2.6; while the crustal component is chosen to be the average Nain Province gneiss crust from the Okak Bay area of Schiøtte *et al.* (1993) (εNd (@2050Ma) = -14.6). For the pyroxenitic rocks, the εNd values for the mantle component are chosen to be the highest, relatively uncontaminated surface pyroxenite (ca. εNd (@1300Ma) = -1.0), and a variety of possible crustal contributors are chosen including the Nain Gneiss as above (εNd (@1300Ma)= -23.8), Tasiuyak Gneiss (εNd (@1300 Ma) = -9.3; Thériault and Ermanovics, 1997; Wilton, unpublished data), as well as the average Paleoproterozoic anorthositic and granitoid rocks (εNd(@1300Ma) = -17.7 and –14.8, respectively).

6.4.6.1 Anorthositic and Granitoid Rocks

Considering the depleted mantle reservoir as the source for anorthositic rocks (cf. Ashwal and Wooden, 1983, 1985; Ashwal *et al.*, 1986; Geist *et al.*, 1990; Emslie and Hegner, 1993) may be a simplified assumption when carrying out NCI determinations, as it may not be the true mantle component in AMCG genesis (e.g. Scoates and Frost, 1996). However, it does give a starting point from which to convey ideas about crustal contamination and relative influence of wall-rock assimilation involved in the anorthositic and granitoid rocks. In contrast to picking a mantle component, the crustal component involved is much easier to choose, as all of these rocks at 2050 Ma would have been emplaced within the Nain Province crust, likely similar to that of the Okak Bay region (Schiøtte *et al.*, 1993). Hence, the latter is chosen as the crustal component in the NCI calculations.

Neodymium crustal indexes for the anorthositic and granitoid rocks are relatively similar ranging from 0.47 to 0.72 for the granitoid rocks, and 0.39 to 0.84 for the anorthositic rocks (NCI averages = 0.55 and 0.62, respectively; Table 6.7; Figure 6.15). These values appear to be very similar for both suites, which is as observed in the εNd values. However, why the granitoids have a lower NCI than the anorthositic rocks is unknown, considering that they are likely a result of basaltic underplating and anatexis of crustal material combined with mantle material (Emslie and Loveridge, 1992; Emslie and Stirling, 1993; Emslie and Hegner, 1993; Emslie *et al.*, 1994; and others). The intrusive relationship of the phase 1 and 2 granitoids and felsic dykes into the anorthositic rocks (Ryan *et al.*, 1998) may provide an answer to this problem. Although the granitoids were likely derived from crustal anatexis, any subsequent contamination by wall rock upon emplacement may have been chemically sheltered by the preexisting anorthositic bodies; similar results have been observed in successive anorthositic plutons in the Laramie Complex in Wyoming (Scoates and Frost, 1996).

Explaining the NCI of the anorthositic rocks is much more straightforward. It has long been noticed that anorthositic rocks are a product of a mantle derived magma, coupled with crustal contamination of some sort (Ashwal and Wooden, 1983, 1985; Ashwal *et al.*, 1986; Geist *et al.*, 1990; Emslie and Hegner, 1993; Emslie *et al.*, 1994; Scoates and Frost, 1996; and others). Hence, the NCI values ranging from 0.39 to 0.84 (avg. 0.62, sample P96-44A excluded; Figure 6.16; Table 6.7) are in accordance with previous interpretations cited above. However, the considerable range of NCI values relative to the granitoids suggests that there were different degrees of crustal influence,

unlike the relatively consistent proportion involved in granitoid genesis (Figure 6.15; Table 6.7).

6.4.6.2 Pyroxenitic Rocks

Neodymium crustal index calculations for the surface and subsurface pyroxenitic rocks have variable NCI values that show a close correlation with the εNd values. If an assumption is made that the Tasiuyak gneiss was the major crustal contaminant in the OKG pyroxenites, then NCI values range from 0.03 to 0.17 in the surface examples (average 0.21), and from 0.35 to 1.51 (average 0.99) in the subsurface examples (Figure 6.16; Table 6.8). Although the NCI values for the surface pyroxenites seem geologically reasonable, most of the subsurface examples require over 100% contribution of crustal Nd from the Tasiuyak gneiss, with the exception of two samples. This is an impossible result from a heat and assimilation perspective, considering that it would require 100% melting and assimilation of the Tasiuyak gneiss by the pyroxenitic magmas.

The contribution of the anorthositic and granitoid rocks of the property must also be considered since both of these rock types are in abundance at the OKG prospect. NCI values using a sole anorthosite contaminant range from 0.04 to 0.23 (avg. 0.11) in the surface pyroxenites, and from 0.17 to 0.70 (avg 0.49) in the subsurface pyroxenites (Figure 6.16; Table 6.8) . Granitoids have a similar overlap with NCI values ranging from 0.04 to 0.28 (avg 0.13) in the surface examples, and from 0.21 to 0.85 (avg. 0.59) in the subsurface examples (Figure 6.16; Table 6.16). Although the latter two groups could be contaminants a number of lines of evidence suggest against them. Firstly the geological aspects of the granitoids from the property are that they represent a cap on the

anorthositic rocks (Ryan *et al.*, 1998), and are found in very low abundance in drill core with the exception of small dykes (Kerr, 1998; *this study*). This virtually negates the possibility of them acting as contaminants in the subsurface. In contrast, the anorthositic rocks are common in drill core and could be a likely contributor. However, the presence of the pyroxenites which are sulphide bearing before they have been emplaced into the anorthositic rocks, and the requirement for over half of the crustal Nd to be derived from the anorthosites presents fairly convincing arguments against an anorthositic contamination. Furthermore, as the anorthositic rocks would likely be quite cold upon emplacement of the dykes and would also require a large heat gradient to assimilate a significant quantity of anorthositic wall rock. Likewise if the pyroxenitic rocks did assimilate anorthositic material it would have resulted in hybrids of pyroxenite and anorthosite which are also not readily observed at the OKG prospect.

The Mid-Archean Nain Province gneisses also have a distinct possibility of being the source of crustal Nd and this is consistent with those of workers elsewhere (Lightfoot, 1998). NCI values calculated for a Nain Province contribution range from 0.01-0.17 (avg 0.08) for the surface dykes, and 0.13-0.55 (avg 0.36) for the subsurface dykes. Invoking a Nain Province crustal influence would require much lower contributions of crustal Nd to account for their contaminated nature. This seems likely to be the most geologically reasonable contaminant because the low required contribution of crustal Nd from the Nain Province would not likely require large heat fluxes, and contamination deeper in the crust by these basement gneisses could explain the sulphide-laden nature of the pyroxenites prior to emplacement into the anorthositic rocks.

6.5 Nd-Sr Isotope Covariance in the Anorthositic and Granitoid Rocks

Work on younger AMCG terrains in both the Laramie Complex of Wyoming (Geist *et al.*, 1990), and the Nain Plutonic Suite of Labrador (Emslie *et al.*, 1994) have shown that a distinctive ISr-εNd covariance exists between the compositional groupings of AMCG complex (e.g. anorthositic, granitoid, ferrodiorite). This covariant plot is employed within the section to see whether the Paleoproterozoic anorthositic and granitoid rocks have similar isotopic variation relative to other AMCG suites.

On the ISr(@2050Ma)-εNd(@2050Ma) covariant plot (Figure 6.17) the anorthositic and granitoid rocks form two distinctive trends. The anorthositic rocks show a distinctive vertical trend with varying εNd and relatively coherent ISr. In contrast, the granitoids show a horizontal trend with varying ISr and relatively lesser changes in eNd. This variations are consistent with both the isotopic characteristics of the NPS as well as the Laramie Complex in Wyoming (Geist *et al.*, 1990; Emslie *et al.*, 1994) and suggest from an isotopic perspective: 1) that the Paleoproterozoic anorthositic rocks from the OKG formed in a similar anorogenic petro-tectonic setting as the NPS and Laramie Complex; and 2) they have formed by similar petrogenetic processes.

6.6 Mixing, Contamination and Basement Contributions: Summary

6.6.1 Anorthositic and Granitoid Rocks

The anorthositic and granitoid rocks of the OKG prospect show very strong evidence, in particular from Nd isotopes, for the influence of crustal contamination and basement influence in their genesis. Their presumed Paleoproterozoic age (Ryan *et al.*, 1998; Hamilton *et al.*, 1998) suggests emplacement into the Nain craton, most likely

similar to the Nain Province gneissic rocks at Okak Bay (Schiøtte *et al.*, 1993). Several lines of evidence within this chapter also provide good evidence for influence of the Nain Province basement in their genesis.

Firstly, the Sr isotopes for the anorthositic rocks have a restricted ISr (@2050Ma) ranging from 0.7050 to 0.7082. Although the values are restricted, they are consistent with the assimilation and influence of older crustal material that had long residence times, and time integrated breakdown of ^{87}Rb to ^{87}Sr. The relatively restricted range of ISr (@2050Ma) is consistent with the assimilation of a high Sr/Nd magmas (e.g. anorthositic) by crustal material with low Sr/Nd, virtually negating any large variations in ISr (@2050Ma) (cf. Geist *et al.*, 1990; Emslie *et al.*, 1994). In contrast to the anorthositic rocks, the granitoids have show much greater variation in ISr (@2050Ma), ranging from those with less crustal influence (ISr(@2050Ma) = 0.7036), to that with good evidence of crustal input (ISr(@2050Ma)=7095). The upper bounds are consistent with a crustal influence in their genesis, while the lower bound may suggest the influence of a reservoir with shorter crustal residence time for Sr, possible input from a mantle source (Geist *et al.*, 1990; DePaolo *et al.*, 1992; Emslie *et al.*, 1994).

Neodymium isotopes are much more constrained than the Sr isotopes and provide very strong evidence for basement influence, regardless of compositional group. Epsilon values (εNd @ 2050Ma), range from –4.11 to –11.87 suggesting the influence of older crustal Nd in their genesis. Furthermore, this is supported by model age data which has a consistent average Mid-Archean age for both the anorthositic and granitoid rocks (3.16 Ga and 3.03 Ga, respectively). These Mid-Archean average model ages and eNd values,

attest to the influence of a crustal source with a long crustal residence time was involved in their genesis, most likely Nain Province rocks like those at Okak Bay (cf. Schiøtte *et al.*, 1993).

6.6.2 Pyroxenitic Rocks

The role of crustal contamination, or felsification, in the genesis of magmatic Ni-Cu sulphide deposits has been shown to be of critical importance in deposits such as Sudbury (e.g. Kuo and Crockett, 1979; Naldrett, 1984c; Naldrett et al., 1986; Lightfoot et al., 1997a,b,c); while recently Naldrett (1997), Lambert et al. (1997) and Lightfoot (1998) suggest that crustal contamination may have been important in the genesis of the Voisey's Bay deposits. The use of radiogenic isotopes to assess the role of contamination in particularly useful (DePaolo, 1981b) and the data presented in this chapter provide fairly convincing evidence that crustal contamination was a major contributor involved in the genesis of the OKG Ni-Cu sulphide occurrences. At least from an isotopic viewpoint, several lines of evidence support this hypothesis.

Although Sr isotopes can identify crustal influence, they were not as successful as Nd isotopes in fingerprinting the isotopic source of influence. The low Rb content of the pyroxenites presented problems in calculating ISr values at 1300Ma; however, two samples with detectable Rb yielded values of 0.7069 and 0.7091, consistent with influence of crustal material. Regardless, the low Rb contents suggest that present day $^{87}Sr/^{86}Sr$ provides an approximation of their Sr isotopic signature. Present day values range from 0.7058-0.7329 (avg 0.7160) in surface pyroxenites, and 0.7069-0.7691 (avg 0.7197) in the subsurface. Although both examples have values consistent with crustal Sr

input, the subsurface ones appear to have had greater influence, consistent with Nd data presented below.

In contrast to the Sr isotopes, the Nd isotopes have been particularly powerful petrogenetic indicators and provide significant evidence that points to a Nain Province crustal contaminant. Although this is the hypothesis, Paleoproterozoic anorthositic and granitoid rocks and the Tasiuyak gneiss are also possible contributors. However, several lines of evidence provide convincing arguments against the influence of the latter. Firstly, considering the anorthositic and granitoid rocks as possible contributors. The granitoid rocks not abundant in the subsurface, with exception of small dykes (Kerr, 1998), and have been interpreted as a cap on the anorthositic rocks of the OKG prospect (Ryan et al., 1998). This geological interpretation does not provide convincing evidence for their presence in significant quantities in the subsurface and they are likely not contributors to the Nd signature observed in the dykes. In contrast, the anorthositic rocks are in significant abundance in the subsurface; however, these can be negated based on the nature of the pyroxenite hosted mineralization. The ubiquitous presence of disseminated sulphide in pyroxenites suggests that they were sulphide saturated *prior to* emplacement into the anorthositic rocks and did not achieve sulphide saturation due to local assimilation of anorthositic wall rock.

This leaves the Tasiuyak gneiss and the Nain Province gneisses as possible crustal contributors in the genesis of the OKG sulphides. Choosing the Tasiuyak gneiss may explain the LREE and LFSE enrichments observed in the dykes (cf. Chapter 4). However, NCI determinations on the pyroxenites negates this possibility. Average NCI

values for the subsurface dykes would require almost a 100% contribution of Nd from the Tasiuyak gneiss to account for the subsurface signatures which not only seems improbable, but also seems geologically unreasonable. Furthermore, the average model age for the subsurface dykes (T_{DM} = 2.74 Ga) is nearly 320 Ma older than that of Thériault and Ermanovics' (1997) Tasiuyak gneiss data (T_{DM} = 2.42 Ga), requiring the input of Nd from a source with longer crustal residence time.

Such an older source could be readily accommodated by the Mid-Archean Nain Province rocks and could explain the model age values as well as the NCI values. NCI values for the OKG surface and subsurface rocks range from 0.01 to 0.55, and the average subsurface dykes have an average NCI of 0.36. These values suggest that even in the more contaminated subsurface examples only 35% of the crustal Nd needs to be derived from the Nain Province rocks, providing fairly conclusive evidence for Nain Province involvement in the genesis of the OKG sulphides. This is further supported by εNd – REE ratio plots (La/Yb, Ce/Yb, La/Sm, Sm/Yb; Figure 6.18). All of these plots show consistent mixing lines towards the Nain Province rocks, and have no inclination towards the Tasiuyak gneiss further supporting a Nain Province crustal contamination influence.

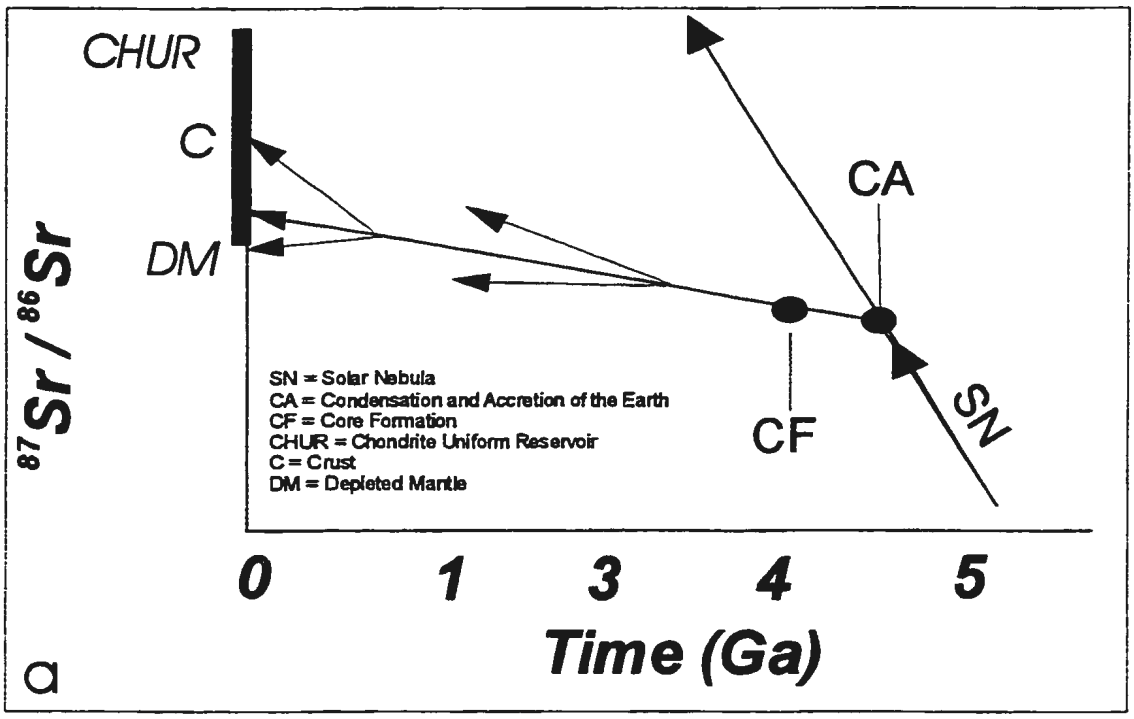

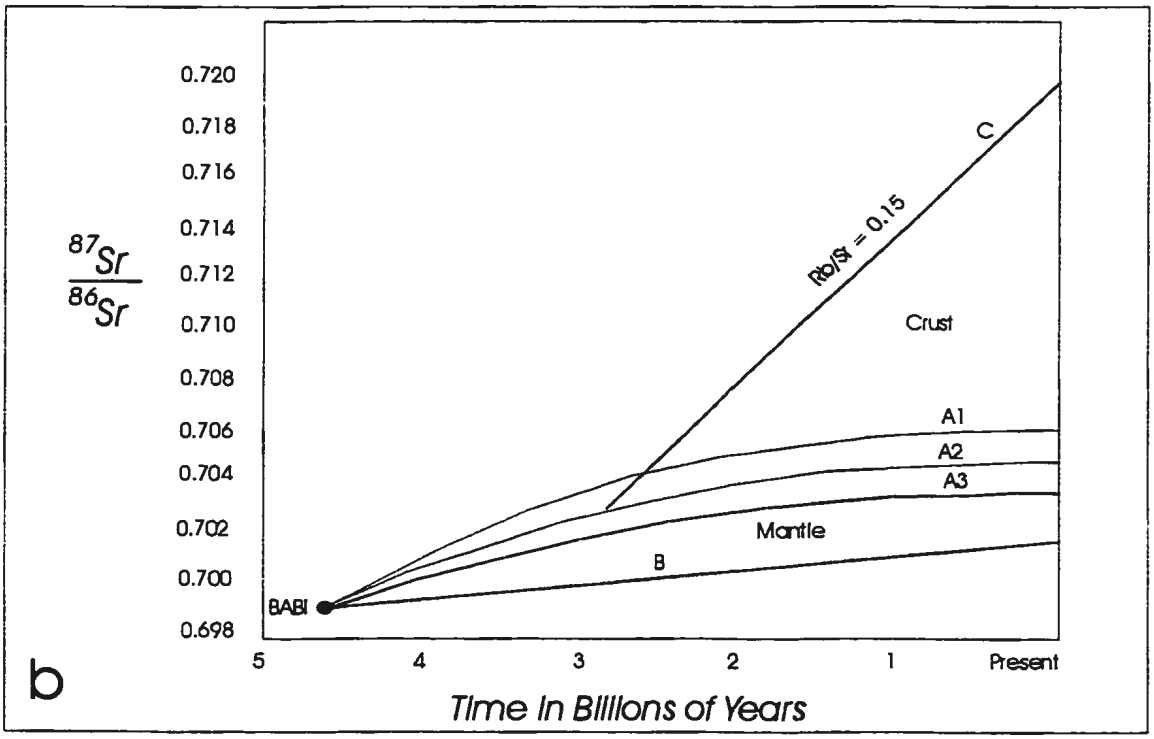

Figure 6.1. Schematic diagrams illustrating the evolution of Sr isotopes in time, including (a) a simple linear evolution (after DePaolo, 1988), and (b) a curvilinear evolution for the mantle domains (after Faure and Powell, 1972).

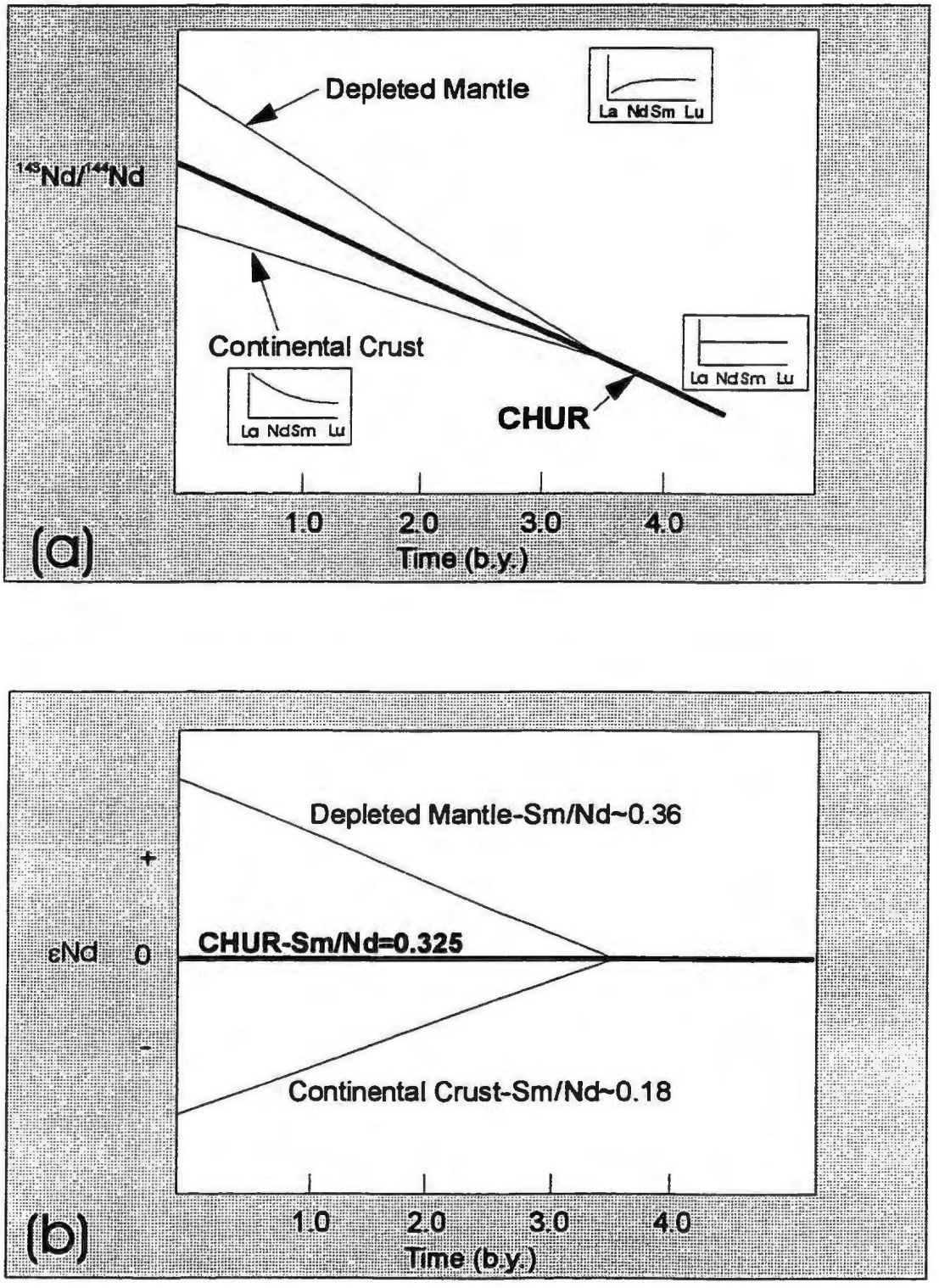

Figure 6.2. Schematic illustration of the evolution of the Nd isotopic system (a), and εNd with time (b). Modified after DePaolo (1988) and Swinden et al. (1997).

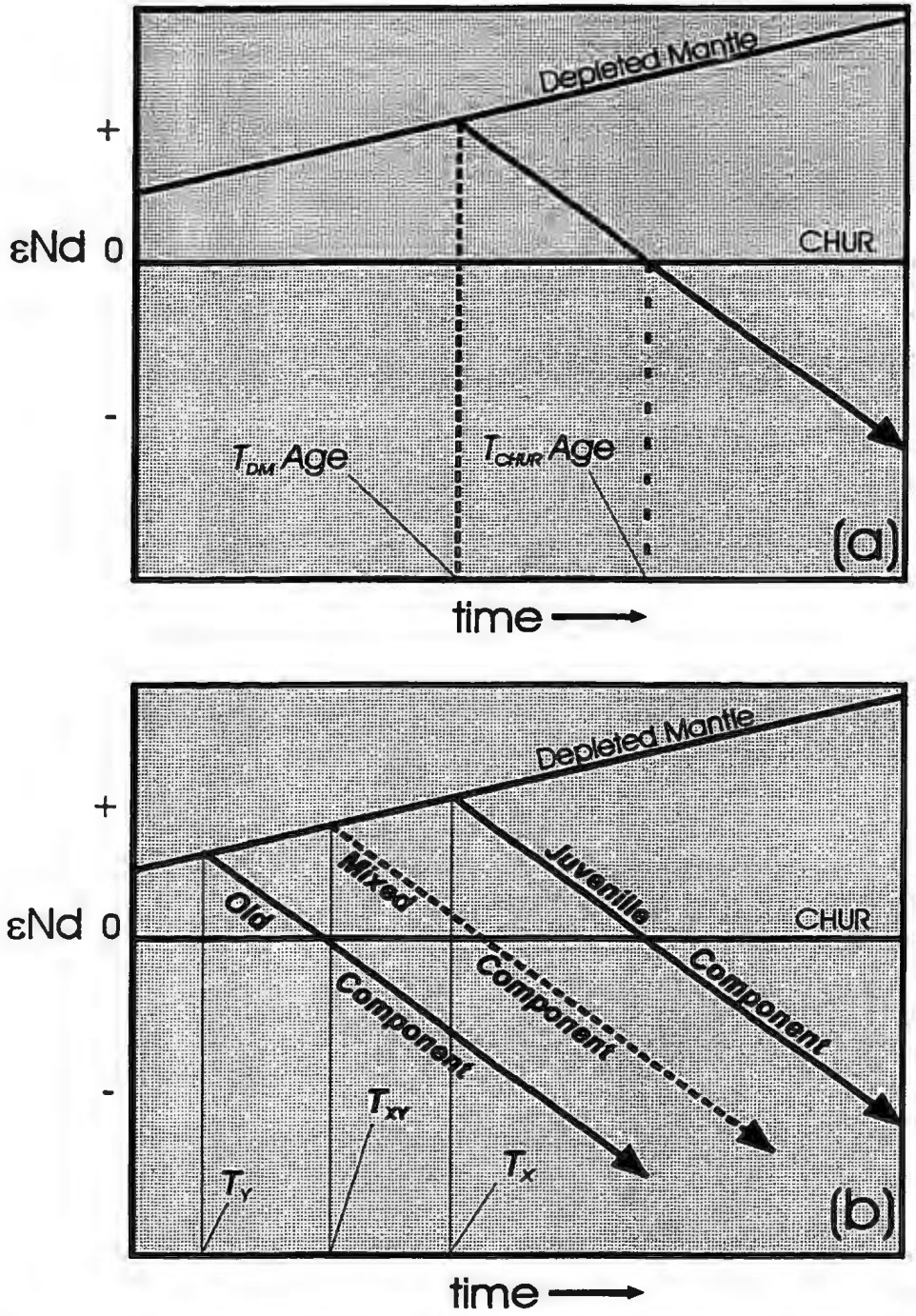

Figure 6.3. Schematic diagrams illustrating the concept of model age determinations. In (a) the model age represents a single stage evolution age, while in (b) the model age is a result of mixing a juvenile (T_x) component with an older component (T_y) yielding a hybrid model age (T_{xy}). Diagrams modified after DePaolo (1981) and Arndt and Goldstein (1987).

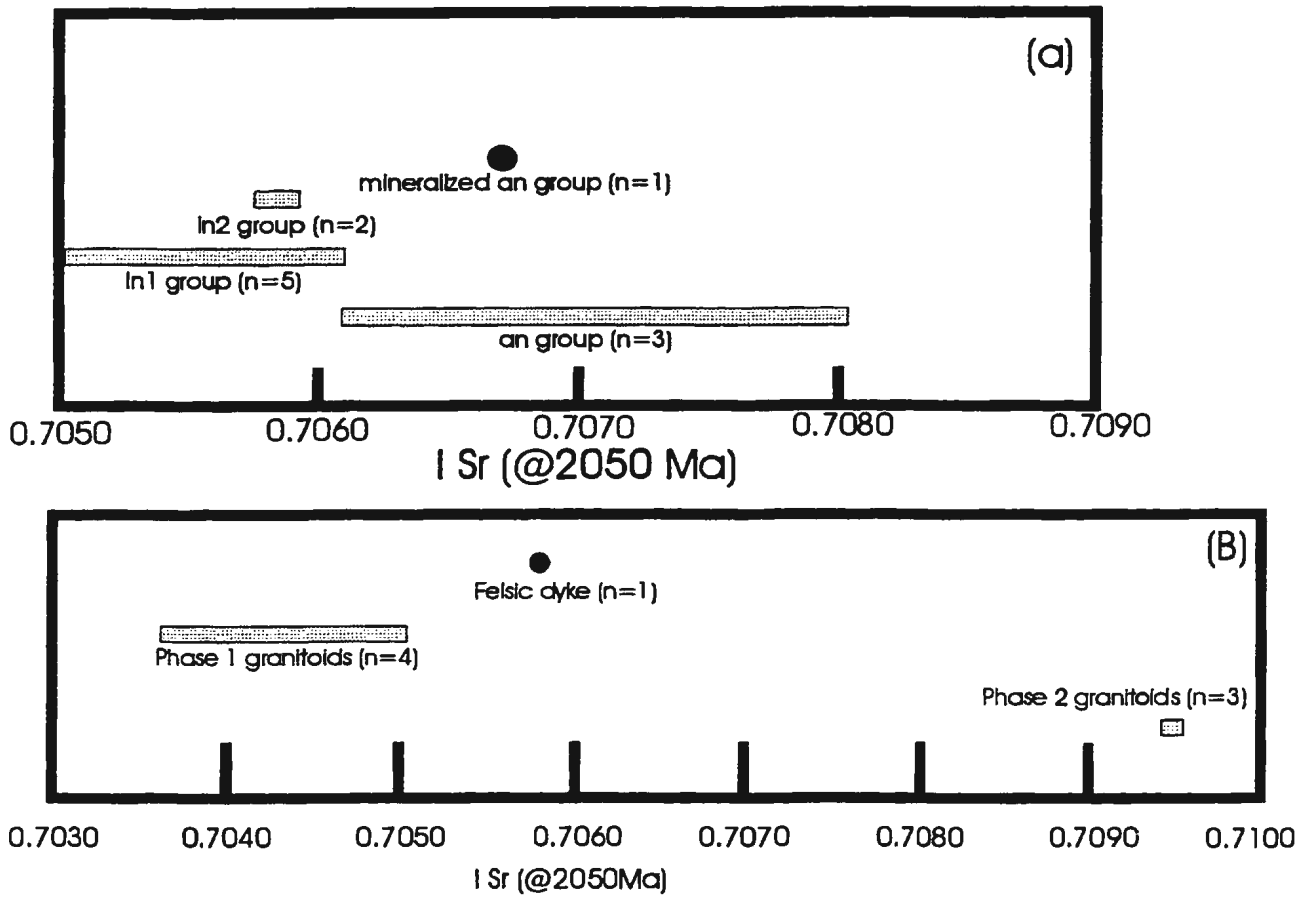

Figure 6.4. Initial Sr isotope ratios of the OKG anorthositic (a), and granitoid (b) rocks.

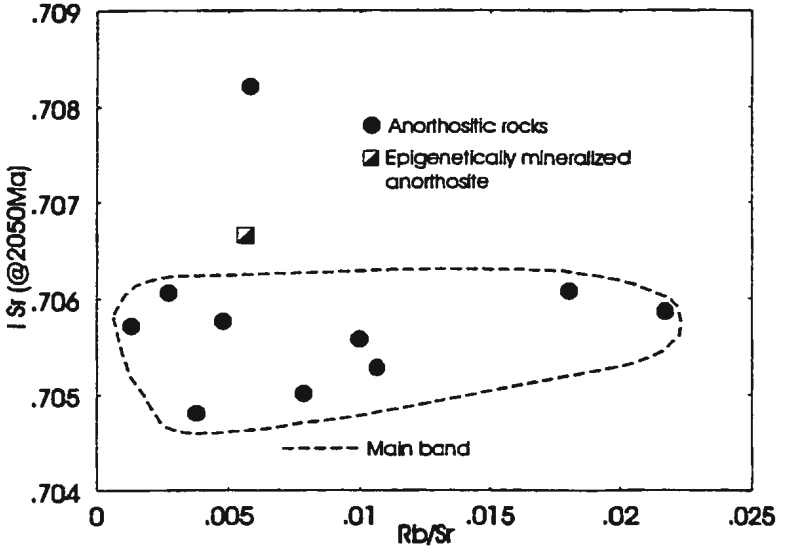

Figure 6.5. Plot of ISr (@2050Ma) versus Rb/Sr illustrates that the anorthositic rocks have very restricted Sr isotope signatures regardless of Rb/Sr ratio. There are only minor exceptions and are illustrated by those samples lying off the main band of anorthositic rocks.

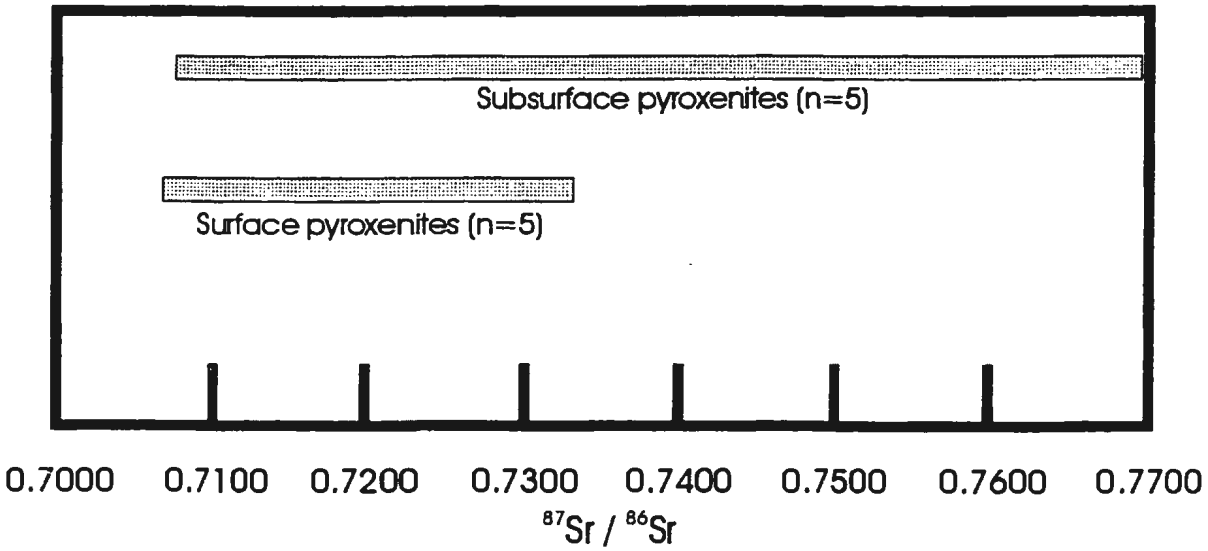

Figure 6.6. Present day Sr isotope distribution of the OKG surface and subsurface pyroxenitic rocks.

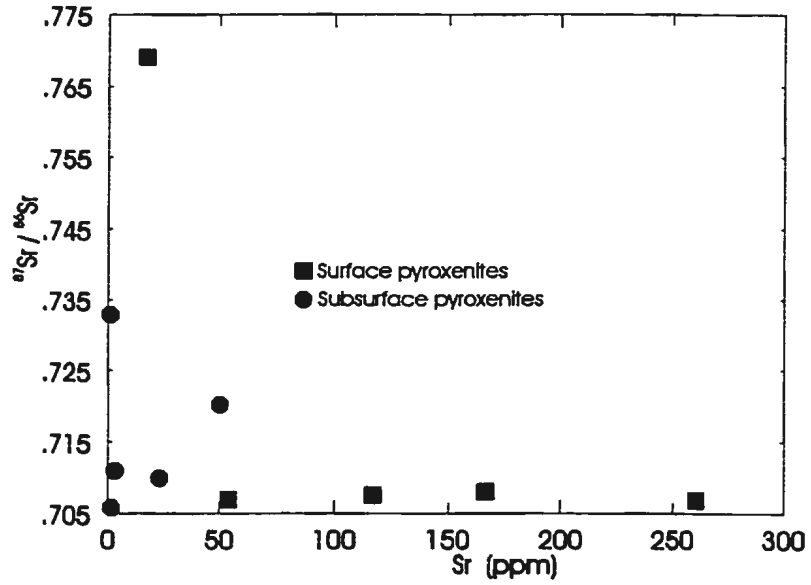

Figure 6.7. Initial Sr isotope ratios at the present day versus Sr (ppm) for pyroxenitic rocks of the OKG prospect. Details on the isotope systematics are discussed in the text.

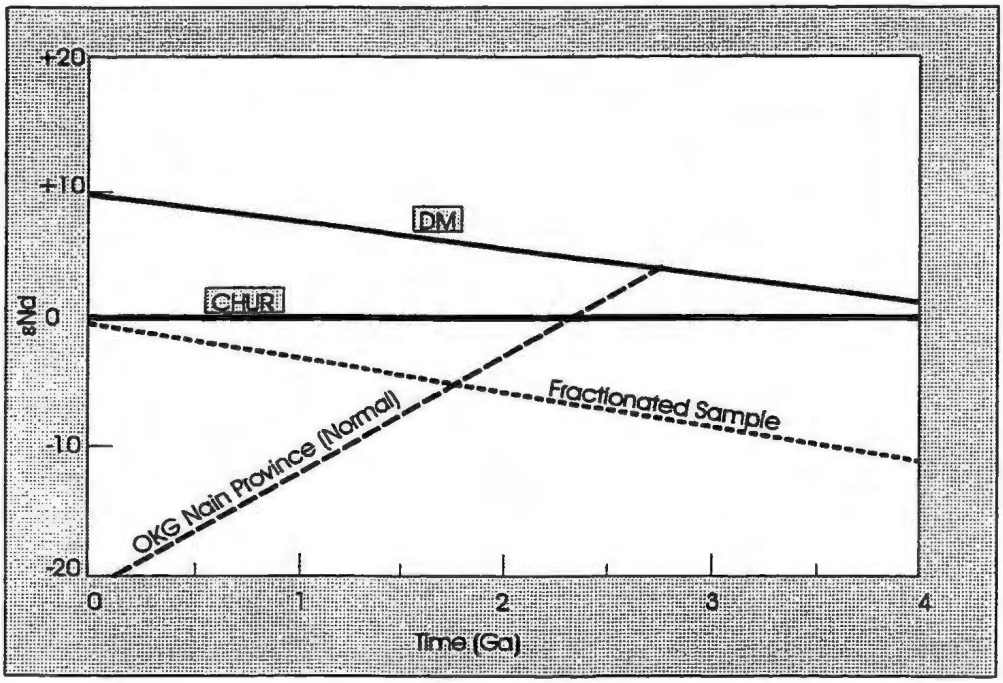

Figure 6.8. Neodymium isotope evolution curves for the Nain Province amphibolites and mafic granulites from the OKG prospect. DM and CHUR curves from DePaolo (1988).

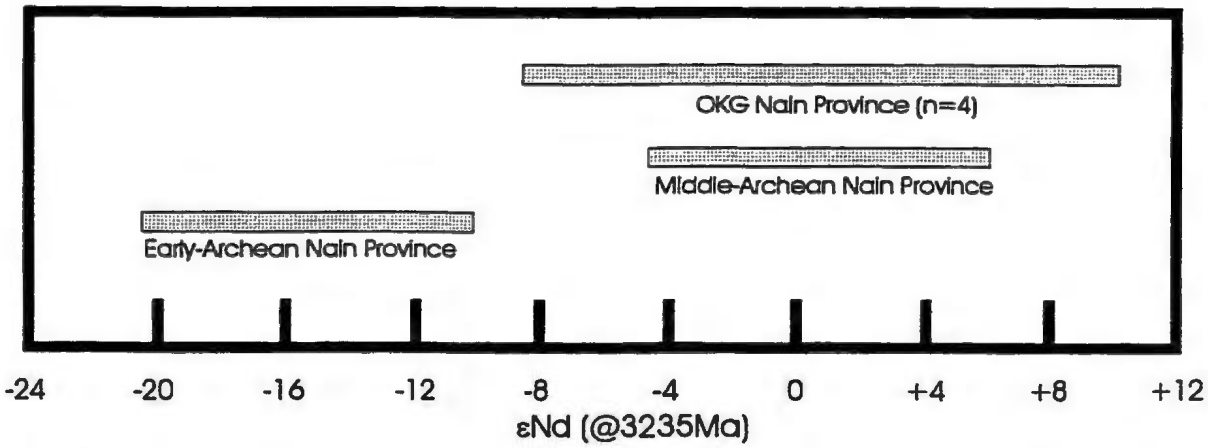

Figure 6.9. Epsilon Nd (εNd @3235Ma) for the OKG Nain Province rocks and their relationship to Mid-Archean and Early-Archean Nain Province rocks. Early Archean values are from Collerson et al. (1989) and Mid-Archean values from Schiøtte et al. (1993).

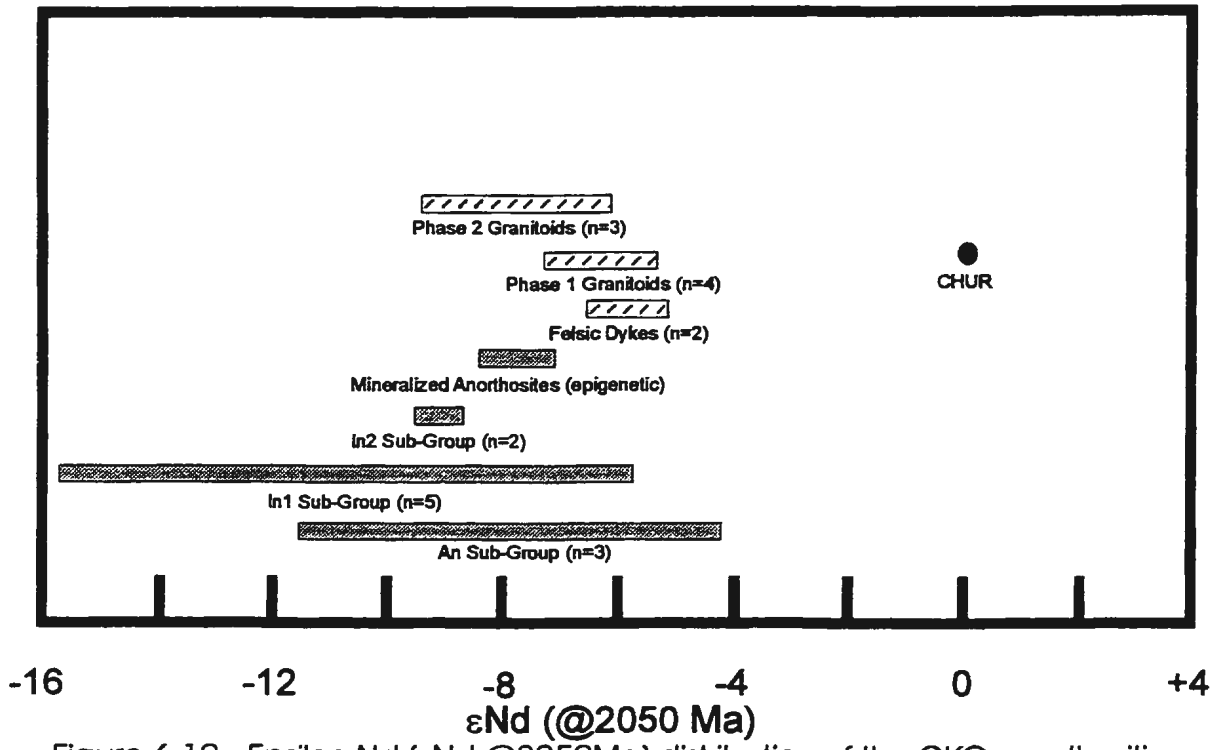

Figure 6.10. Epsilon Nd (εNd @2050Ma) distribution of the OKG anorthositic and granitoid rocks.

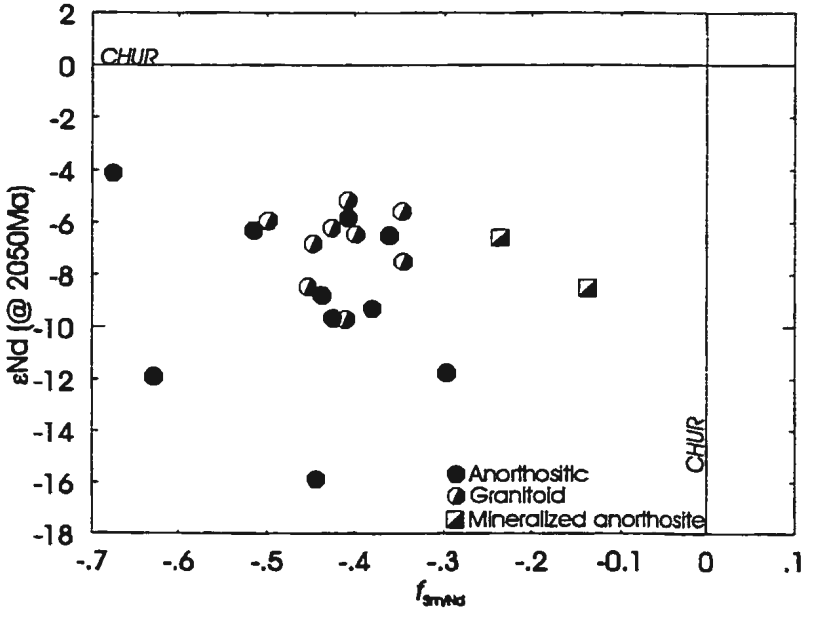

Figure 6.11. Epsilon Nd (εNd (@2050Ma)) versus $f_{Sm/Nd}$ covariance within the anorthostic and granitoid rocks of the OKG prospect.

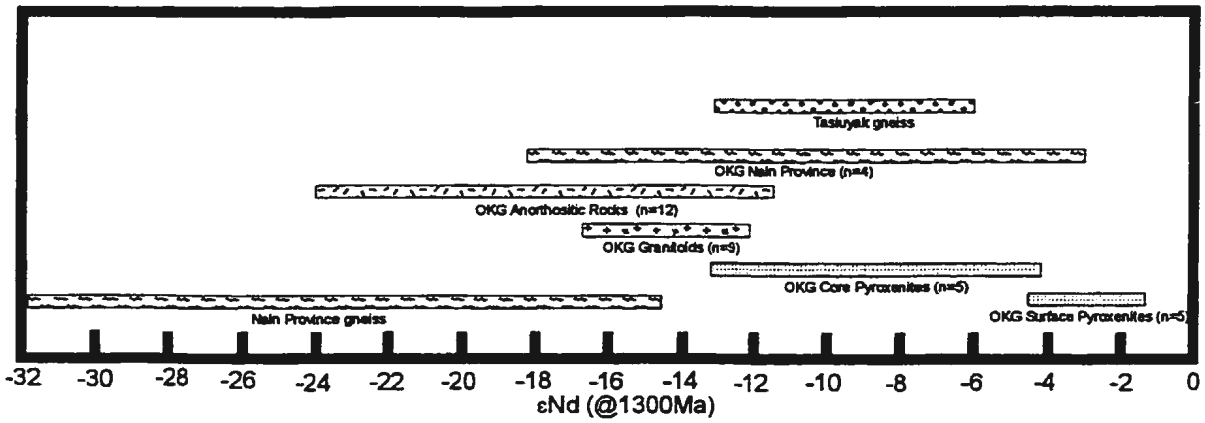

Figure 6.12. Epsilon Nd (εNd @1300Ma) distribution of the OKG pyroxenitic rocks in comparison to the ranges of possible contaminants involved in their genesis. Data from the Nain Province gneiss from Schiøtte et al. (1993), and the Tasiuyak gneiss from Theriault and Ermanovics (1997) and Wilton (unpublished data).

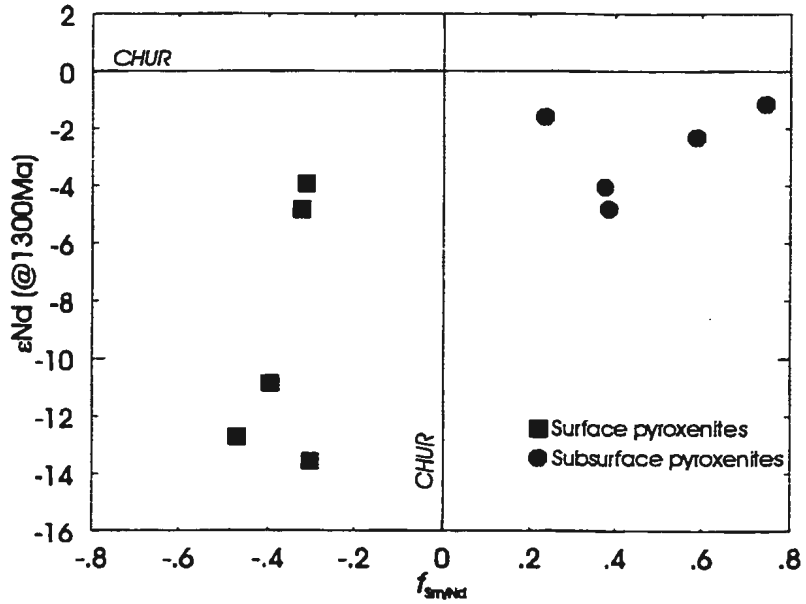

Figure 6.13. Epsilon Nd (εNd @1300Ma) versus fractionation factor ($f_{Sm/Nd}$) for the OKG pyroxenites. For details see text.

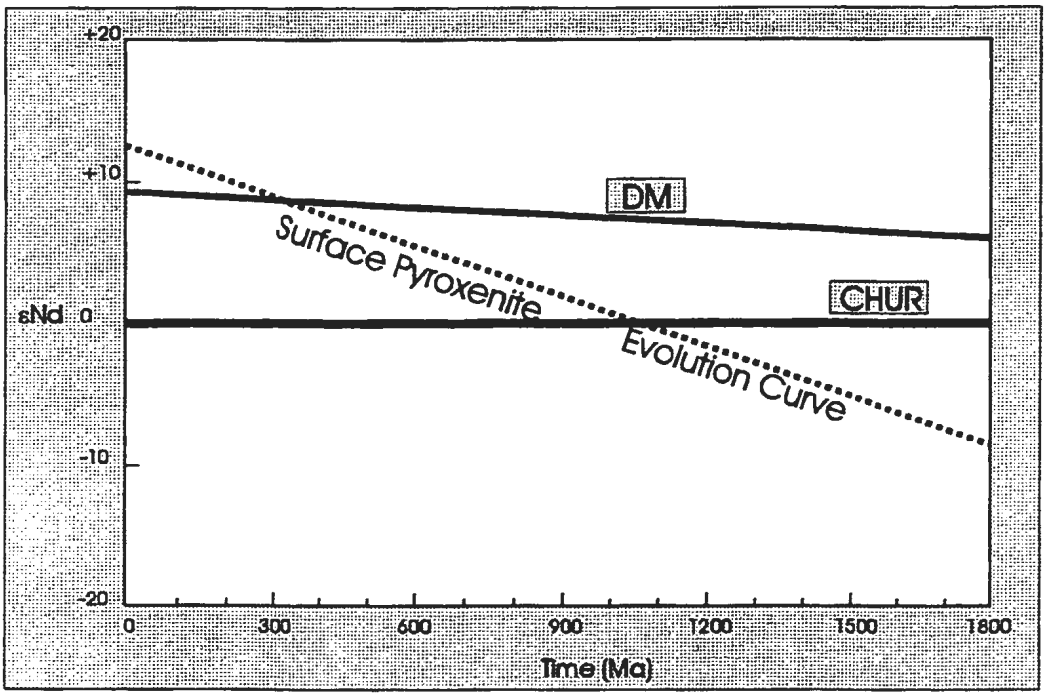

Figure 6.14. Neodymium isotope evolution curve for the OKG surface pyroxenites. The evolution towards positive εNd values in the present day points to a source fractionated in Nd with high Sm/Nd values, possibly a subcontinental lithospheric mantle source. CHUR and DM curves after DePaolo (1988).

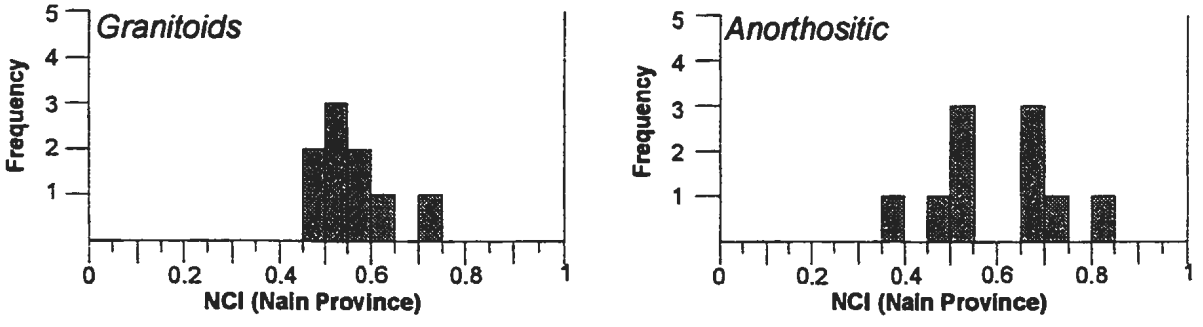

Figure 6.15. Frequency histograms of the Neodymium Crustal Index (NCI) of DePaolo et al. (1992) using the Nain Province as the crustal contributor. Details of the NCI are provided in Table 6.7 and the text.

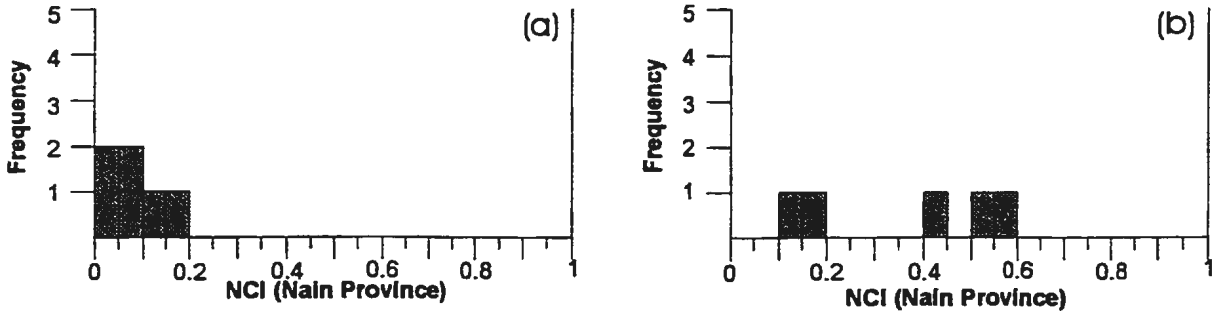

Figure 6.16. Frequency histograms of the Neodymium Crustal Index of DePaolo et al. (1992) using a Nain Province crustal contributor for (a) surface pyroxenites, and (b) subsurface pyroxenites. Details of the NCI are provided in Table 6.8 and the text.

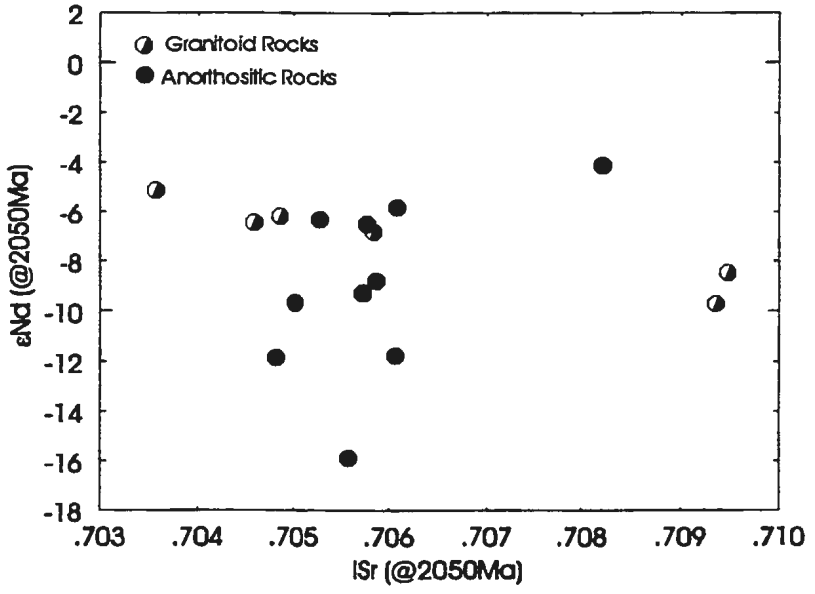

Figure 6.17. Epsilon Nd (εNd @2050Ma) versus initial Sr (I Sr @2050Ma) covariant plot for the OKG anorthositic and granitoid rocks. Although these samples are Paleoproterozoic the distinctive vertical trend of the anorthositic rocks and horizontal trend of the granitoid rocks is consistent with the isotopic distributions of similar rock types in the Mesoproterozoic NPS (Emslie et al., 1994) and the Laramie Complex (Geist et al., 1990).

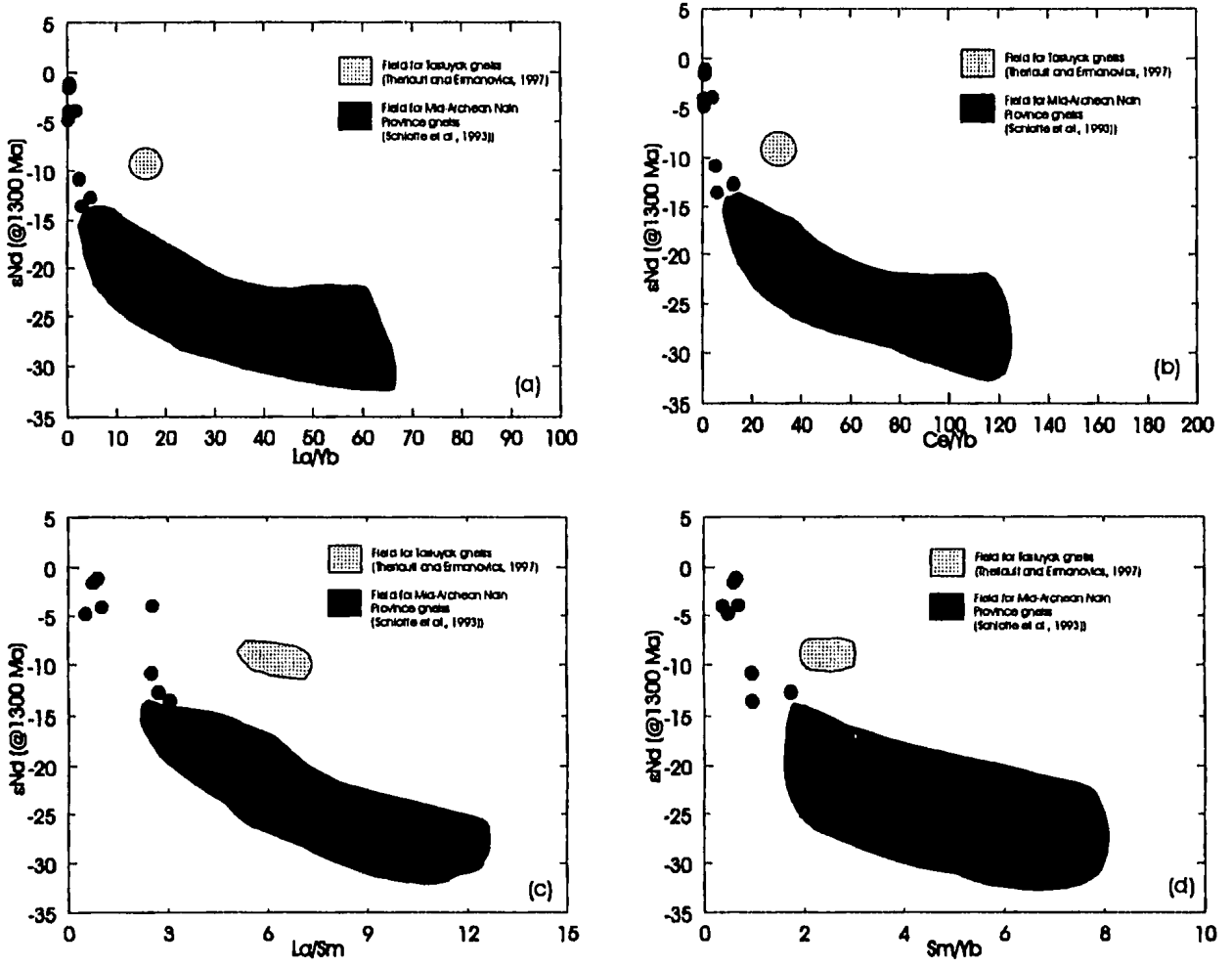

Figure 6.18. Epsilon Nd (εNd @1300Ma) against REE ratios including (a) La/Yb, (b) Ce/Yb, (c) La/Sm, (d) Sm/Yb. All of these plots show consistent mixing lines towards the Mid-Archean Nain Province gneisses of Schiøtte et al. (1993), and have no affinity for the Tasiuyak gneiss (Theriault and Ermanovics, 1997), suggesting that the Nain Province was the integral contaminant involved in the genesis of the OKG sulphide mineralization.

Table 6.1. Summary of Sr isotope geochemistry of the Nain Province gneisses from the OKG prospect.

Rock Types	**$^{87}Sr/^{86}Sr$**	**$^{87}Rb/^{86}Sr$**	**ISr (@3235Ma) Range**	**ISr (@3235Ma) Average**	**Rb/Sr**
Crustal Suite	0.7102-0.8949	0.1701-2.6331	.6771-.8399	0.7397	0.06-0.41
Refractory Sample	0.7972	2.1365	.6968	NA	0.75

NA = not applicable

Table 6.2. Summary of Sr isotope geochemistry for the anorthositic and granitoid rocks of the OKG prospect.

Rock Types	**$^{87}Sr/^{86}Sr$**	**$^{87}Rb/^{86}Sr$**	**ISr (@2050Ma) Range**	**ISr (@2050Ma) Average**	**Rb/Sr**
an group	0.7048-0.7082	0.7051-0.7087	0.7048-0.7082	0.7064	0.003-0.010
ln1 group	0.7056-0.7075	0.0133-0.0511	0.7050-0.7060	0.7055	0.005-0.018
ln2 group	0.7058-0.7076	0.0038 -0.0612	0.7057-0.7059	0.7058	0.001-0.022
Epi min an group	0.7062-0.7071	ND-0.0159	NC-0.7067	NA	0.75
Felsic dykes	0.7226-0.7285	ND-0.5661	NC-0.7058	NA	NA-0.200
Phase 1 granitoids	0.7189-0.7441	0.4854-1.3289	0.7036-0.7049	0.7043	0.172-0.469
Phase 2 granitoids	0.7168-0.7711	1.1625-2.0869	0.7094-0.7095	0.70945	0.414-0.734

ND = not detected, NC = not calculated, NA = not applicable

Table 6.3. Summary of Sr isotope geochemistry of the OKG pyroxenitic rocks.

Rock Types	**$^{87}Sr/^{86}Sr$**	**$^{87}Rb/^{86}Sr$**	**ISr (@1300Ma) Range**	**$^{87}Sr/^{86}Sr$ Average**	**Rb/Sr**
Surface pyroxenites	0.7057-0.7329	ND-0.4433	NC-0.7119[1]	0.7160	NC-0.159[1]
Drill Core pyroxenites (OKG96-09)	0.7069-0.7691	0.0133-0.0511	NA	0.7197	NA

[1]Due to low Rb and $^{87}Sr/^{86}Sr$, recalculation to these values was not possible.
ND = not detected, NC = not calculated, NA = not applicable

Table 6.4. Summary of Nd isotope geochemistry for the Nain Province rocks of the OKG prospect.

Rock Group	**$^{143}Nd/^{144}Nd$ (range)**	**$^{147}Sm/^{144}Nd$ (range)**	**εNd (@3235Ma)**	**εNd (@0Ma)**	**$f_{Sm/Nd}$**	**T_{DM} (Ma)**	**Sm/Nd**
Crustal Suite	0.510716-0.512023	0.08339-0.15324	+4.4 to +11.2 (avg +8.5)	-11.8 to -37.5 (avg –21)	-0.22 to –0.58 (avg –0.36)	2344 – 3064 (avg 2748)	0.14-0.25 (avg 0.21)
Fractionated Sample	0.512627	0.21779	-9.1	-0.2	+0.11	-12175	0.35

Table 6.5. Summary of Nd isotope geochemistry of anorthositic and granitoid rocks from the OKG prospect.

Rock Group	**$^{143}Nd/^{144}Nd$ (range)**	**$^{147}Sm/^{144}Nd$ (range)**	**εNd (@2050Ma)**	**εNd (@0Ma)**	**$f_{Sm/Nd}$**	**T_{DM} (Ma)**	**Sm/Nd**
an group	0.513364-0.511252	0.063650-0.138340	-4.1 to -11.8 (avg –9.25)	-27.0 to –44.4 (avg –36.8)	-0.30 to –0.68 (avg –0.53)	2544-3844 (avg 3131)	0.10-0.22 (avg 0.15)
ln1 group	0.510650-0.511350	0.095300-0.125720	-5.8 to –5.9 (avg –8.83)	-25.1 to –38.8 (avg –31.1)	-0.36 to –0.52 (avg –0.43)	2823-3644 (avg 3151)	0.15-0.20 (avg 0.18)
ln2 group	0.511029-0.511157	0.110590-0.121980	-8.8 to –9.3 (avg –9.04)	-28.9 to –31.4 (avg –30.1)	-0.38 to –0.44 (avg –0.41)	3127-3307 (avg 3217)	0.18-0.20 (avg 0.19)
Epi min an group	0.511677-0.511839	0.150230-0.169560	-6.5 to -8.5 (avg –7.5)	-15.6 to –18.8 (avg –17.2)	-0.14 to -0.24 (avg –0.19)	3546-4582 (avg 4064)	0.24-0.27 (avg 0.26)
Felsic dykes	0.511103-0.511437	0.108600-0.128650	-5.6 to –6.8 (avg –6.2)	-23.4 to –29.9 (avg –26.7)	-0.35 to -0.45 (avg –0.40)	2960-3064 (avg = 3012)	0.17-0.20 (avg=0.19)

Table 6.5. (Continued)

Rock Group	$^{143}Nd/^{144}Nd$ (range)	$^{147}Sm/^{144}Nd$ (range)	εNd (@2050Ma)	εNd (@0Ma)	$f_{Sm/Nd}$	T_{DM} (Ma)	Sm/Nd
Phase 1 granitoids	0.511191-0.511341	0.112800-0.128830	-5.1 to –7.5 (avg –6.3)	-25.3 to –28.23 (avg –26.7)	-0.34 to -0.43 (avg –0.39)	2900-3245 (avg 3030)	0.18-0.21 (avg 0.19)
Phase 2 granitoids	0.511002-0.511055	0.09858-0.11596	-5.9 to –9.7 (avg –8.3)	-30.8 to –31.7 (avg –31.3)	-0.41 to –0.50 (avg -0.45)	2819-3261 (avg 3050)	0.16-0.19 (avg 0.17)

Table 6.6. Summary of Nd isotope geochemistry of pyroxenitic rocks from the OKG prospect.

Rock Group	$^{143}Nd/^{144}Nd$ (range)	$^{147}Sm/^{144}Nd$ (range)	εNd (@1300Ma)	εNd (@0Ma)	$f_{Sm/Nd}$	T_{DM} (Ma)	Sm/Nd
Surface pyroxenites	0.512951-0.513833	0.242740-0.343260	-1.1 to –4.8 (avg –2.8)	+6.1 to +23.3 (avg +12.5)	+0.39 to +0.75 (avg +0.47)	NA	0.44-0.55 (avg 0.47)
Drill core pyroxenites (OKG06-09)	0.511199-0.511913	0.104140-0.135250	-3.9 to –13.6 (avg –9.2)	-14.1 to –28.1 (avg –21.0)	-0.30 to –0.47 (avg –0.36)	2390-3402 (avg 2744)	0.17-0.22 (avg 0.20)

NA = not applicable

Table 6.7a. Neodymium crustal indicies (NCI) for the OKG granitoid rocks.

Sample	Rock Type	εNd (@2050Ma)	NCI[1]
P96-3B	Felsic dyke	-5.6	0.47
P96-28B	Felsic dyke	-6.8	0.55
P96-39	Ph1	-5 .1	0.45
P96-66A	Ph1	-6 .5	0.53
P96-75B	Ph2	-5_9	0.50
P96-76	Ph2	-9_7	0.72
P96-85	Ph1	-7_5	0.59
P96-86B	Ph1	-6_2	0.51
P96-87	Ph2	-8. 5	0.64
Average			0.55

Table 6.7b. Neodymium crustal indicies (NCI) for the OKG anorthositic rocks.

Sample	Rock Type	εNd (@2050Ma)	NCI[1]
P96-3A	an	-11.8	0.83
P96-19	an	-4.1	0.39
P96-33	an	-11.9	0.84
P96-55B	ln1	-9.7	0.71
P96-83	ln1	-5.8	0.49
P96-174	ln1	-6.5	0.53
P96-182	ln1	-6.3	0.52
P96-199	ln2	-8.8	0.66
P96-203	ln2	-9.3	0.69
P96-468a	Min an	-8.5	0.65

Table 6.7b. (continued)

Sample	Rock Type	εNd (@2050Ma)	NCI[1]
P96-469	Min an	-6.6	0.53
Average			0.62

[1]All NCI determinations are carried out using MC from the DM reservoir of DePaolo (1998) with εNd (@2050Ma) = +2.6, and CC is the average Mid-Archean Nain Province rocks of Schiotte et al. (1993) with εNd (@2050Ma) = -14.6

Table 6.8. Neodymium crustal indicies (NCI) of the pyroxenitic rocks using average Nain Province gneiss, Tasiuyak gneiss, anorthositic and granitoid rocks of the OKG prospect. NCI values are determined using the equation of DePaolo *et al.* (1992).

Sample	Rock Type	εNd (@1300Ma)	NCI (Nain)[1]	NCI (Tasiuyak)[2]	NCI (Anorthositic)[3]	NCI (Granitoid)[4]
P96-5B	Px-sur	-1.1	0.01	0.01	0.01	0.01
P96-W1	Px-sur	-4.8	0.17	0.46	0.23	0.28
W96-50E	Px-sur	-2.3	0.06	0.16	0.08	0.09
P96-463	Px-sur	-4.0	0.13	0.37	0.18	0.22
P96-464	Px-sur	-1.6	0.03	0.07	0.04	0.04
Average	Px-sur	**-2.8**	**0.08**	**0.21**	**0.11**	**0.13**
16701	Px-core	-4.8	0.17	0.46	0.23	0.28
16715	Px-core	-3.9	0.13	0.35	0.18	0.21
16730	Px-core	-13.6	0.55	1.51	0.75	0.91
16737	Px-core	-10.9	0.43	1.19	0.59	0.71
16747	Px-core	-12.7	0.51	1.41	0.70	0.85
Average	Px-core	**-9.18**	**0.36**	**0.99**	**0.49**	**0.59**

All MC values use the least contaminated surface pyroxenite with εNd (@1300Ma) ≈ -1.0.

[1] CC is average Nain Province of Schiøtte *et al.* (1993) with εNd (@1300Ma) = -23.8

[2] CC is average Tasiuyak gneiss of Thériault and Ermanovics (1997) and Wilton (unpublished data), with εNd (@1300Ma) = -9.3

[3] CC is average anorthositic rock of this study with εNd (@1300Ma) = -17.7

[4] CC is average granitoid rock of this study with εNd (@1300Ma) = -14.8

Chapter 7. Sulphur Isotope Geochemistry

7.1 Introduction

The use of sulphur isotope geochemistry to decipher the origin of sulphur within magmatic sulphide deposits has been shown to be a valuable tool in many Ni-Cu sulphide deposits (e.g. Mainwaring and Naldrett, 1977; Naldrett and MacDonald, 1980; Ripley, 1981, 1986, 1990a,b). Similarly, the major goal of sulphur isotope analysis is to trace the source of sulphur found in the OKG sulphides, in particular, whether the sulphur is of magmatic origin, or has been assimilated from an external sulphur source (e.g. from the Tasiuyak, Nain Province, or Churchill Province gneisses). A total of 12 sulphide separates have been analyzed for their sulphur isotope characteristics, and details on sampling protocol and analytical methods are provided in Appendix A.

7.2 Notations and Theory

The sulphur isotope system has been studied for considerable time with respect to hydrothermal systems, the mantle, and mineral deposit studies (e.g. Ohmoto, 1972; Rye and Ohmoto, 1974; Mainwaring and Naldrett, 1977; Ohmoto and Rye, 1979; Hoefs, 1980; Ripley, 1981, 1986, 1990a,b; Ohmoto, 1986; Kyser, 1986, 1990; and others). Sulphur has four naturally occurring isotopes including ^{32}S (95.02%), ^{33}S (0.75%),

^{34}S(4.2%) and ^{36}S (0.017%) (Ohmoto and Rye, 1979; Hoefs, 1980; Faure, 1986; Rollinson, 1993). In terms of S-isotope studies the two most abundant isotopes are used ^{32}S and ^{34}S, and much of the interpretations of S-isotope geochemistry hinges on the geochemical behaviour of these two isotopes and their related $^{34}S/^{32}S$ ratio. Variations in $^{34}S/^{32}S$ ratios are generally measured relative to a known standard, the Canon Diablo Troilite (CDT), believed to represent the bulk undifferentiated earth (Ohmoto and Rye, 1979). Comparisons and variations are generally made in terms of the "delta" notation that measures the "per mil" deviation of the sample from the CDT, and is given by the following: $\delta^{34}S = [(^{34}S/^{32}S_{sample} / {}^{34}S/^{32}S_{CDT})-1]*1000$ (7-1), where $^{34}S/^{32}S_{sample}$ and $^{34}S/^{32}S_{CDT}$ are the $^{34}S/^{32}S$ values for the sample and Canon Diablo Troilite (0.0450045), respectively. Delta values are commonly subdivided into two groups: 1) those with $\delta^{34}S > 0$, are considered to be isotopically heavy, containing greater abundances of the isotopically heavier ^{34}S; and 2) those with $\delta^{34}S < 0$ are considered to be isotopically lighter, having lesser ^{34}S, and greater contents of the isotopically light ^{32}S (Ohmoto, 1972; Rye and Ohmoto, 1974; Ohmoto and Rye, 1979; Hoefs, 1980).

The subdivisions between isotopically heavy and light are generally controlled by the relative fractionation of ^{34}S and ^{32}S from one another in nature. However, unlike major and trace elements, and radiogenic isotopes, stable isotope fractionation is related to isotopic mass, rather than the chemical properties of the element in question (e.g. S, O, H, or C; Hoefs, 1980). Stable isotope fractionation is generally considered to be of two forms: 1) equilibrium fractionation and isotopic exchange (e.g. melt-crystal, crystal-crystal, fluid-rock); and 2) kinetic isotope fractionation controlled by some kinetic factor

(e.g. biotic-related metabolic fractionation, evaporation and condensation reactions) (Taylor, 1974; Ohmoto and Rye, 1979; Hoefs, 1980; Ohmoto, 1986; Faure, 1986; Rollinson, 1993).

Equilibrium fractionation is commonly the result of stable isotopic exchange reactions, such as the exchange of isotopes between sulphide-sulphide, sulphide-sulphate, and melt/fluid-sulphide/sulphate/silicate fractionation (Ohmoto and Rye, 1979; Hoefs, 1980; Ohmoto, 1986; Faure, 1986). In magmatic systems, like magmatic Ni-Cu sulphide systems, fractionation between sulphide species at high temperatures (750-1250°C) can be considered negligible, generally between tenths of a per mil to less than 0.5‰ (Ohmoto and Rye, 1979; Ohmoto, 1986; Kyser, 1990). Furthermore, primary sulphides in mantle derived rocks can be assumed to inherit the $\delta^{34}S$ characteristics of their parental mantle melt and mantle source region, and usually lie within $0 \pm 3‰$ (i.e. $\delta^{34}S_{sulphide} \approx \delta^{34}S_{mantle\ source}$; Ohmoto and Rye, 1979; Ohmoto, 1986; Kyser, 1986, 1990). Any values in mantle derived rocks that lie outside of this range have likely inherited a partial S-isotopic signature from an external sulphur source, or result heterogeneities in the mantle source region (Mainwaring and Naldrett, 1977; Ripley, 1981, 1986; Kyser, 1986, 1990; Chaussidon et al., 1987, 1989). However, it must be noted that variations in mantle derived rocks can exist. For example, the degassing of mafic lavas can deplete a melt in the oxidized SO_2 species, which can cause depletions in $\delta^{34}S$ due to the loss of ^{34}S with SO_2 gasses (Kyser, 1986, 1990). Conversely, high oxygen fugacities in melts can cause oxidation of the sulphide species to SO_2 gas, which when trapped in a melt can cause increases in the $\delta^{34}S$ values due to preferential enrichment of ^{34}S in the SO_2 gas (Ripley,

1983). Furthermore, mantle S-isotope heterogeneity, and mantle metasomatism with crustal fluids and sediments (+S) can lead to $\delta^{34}S$ shifts related to the sulphur isotopic nature of the metasomatic material (Chaussidon et al., 1987, 1989; Kyser, 1990; Wilson *et al.*, 1996). Evidently, blindly assuming values of $\delta^{34}S = 0 \pm 3$ for the mantle may not be wise, and although samples may have non-magmatic signatures, they may be derived from a metasomatized mantle source.

Equilibrium, fluid-rock interactions between hydrothermal fluids and rock, can also have considerable fractionation of S isotopes and are controlled by temperature of the fluid, pH, and total sulphur in the fluid-rock system (Ohmoto, 1972, 1986; Rye and Ohmoto, 1974; Ohmoto and Rye, 1979). However, this thesis concentrates on rocks of magmatic origin and hydrothermal alteration is not likely to be of significant importance; however, readers are forwarded to the papers of Ohmoto (1972), Rye and Ohmoto (1974), Ohmoto and Rye (1979), and Ohmoto (1986) for detailed discussions.

In contrast to equilibrium fractionation, kinetic fractionation is often controlled by bacterial/organism metabolic process, and processes such as evaporation and condensation (Taylor, 1974; Ohmoto and Rye, 1979; Hoefs, 1980; Ohmoto, 1986; and others). Kinetic isotope fractionation in oceanic and near-surface environments by seawater sulphate reducing bacteria can be quite significant and result in 15-60‰ (average 40‰) fractionations (*op cit*). Furthermore, the effectiveness of sulphate reducing bacteria and related $\delta^{34}S$ values of sedimentary sulphides are often closely linked to the $\delta^{34}S$ values of seawater sulphate (which has varied through time), the efficiency of kinetic isotope fractionation associated with sulphate reducing bacteria, and

whether a reservoir is open or closed to sulphide and sulphate (Ohmoto and Rye, 1979; Hoefs, 1989; Ohmoto, 1986; Strauss 1986, 1993). In general, sedimentary sulphides have a wide range from +70 to –70, with most isotopically lighter than seawater sulphate due to the efficiency of sulphate reduction by sulphate reducing bacteria (Ohmoto and Rye, 1979; Ohmoto, 1986; Rollinson, 1993).

In terms of kinetically controlled condensation and evaporation reactions, these primarily deal with O and H isotopes and readers are forwarded to the review paper of Taylor (1974).

7.3 Results

A total of twelve sulphide separates were analyzed for their sulphur isotope compositions including 8 pyrrhotite samples, 2 chalcopyrite samples and 1 pyrite sample from the massive sulphides, and 1 pyrrhotite sample from disseminated sulphide within the pyroxenites. All of the sulphides show considerable homogeneity with $\delta^{34}S$ values ranging from +1.0 to +1.8. Pyrrhotite separates show the greatest range in variability encompassing all of the range discussed above, while pyrrhotite from the pyroxenites has a $\delta^{34}S$ value of +1.2, chalcopyrite separates values ranging from +1.5 to +1.6, the pyrite separate has a value of +1.7 (Figure 7.1; Table 7.1).

The considerable homogeneity within the OKG sulphides attests to a common, homogeneous sulphur source, be that the magma, or an external sulphur source; this will be discussed in section 7.4. Pyrrhotite separates have the widest range in values; however, the range is only 0.8‰, which attests to similar sulphur origins. Furthermore, the pyrrhotite separate from the pyroxenites has an identical $\delta^{34}S$ ratio as the massive

sulphides, suggesting that the two are genetically related, and supports the PGE data presented in chapter five. Chalcopyrite and pyrite separates from the OKG massive sulphides are even further restricted, lying within 0.3‰, also supporting a similar homogeneous sulphur reservoir.

7.4 External or Magmatic Sulphur?

The considerable homogeneity in $\delta^{34}S$ values for the OKG sulphides suggests that they have been derived, or contaminated by, a reservoir with consistent and homogeneous sulphur isotope characteristics. The values for the sulphides lie well within the range for magmatic sulphur ($\delta^{34}S = 0\pm3$ ‰; Ohmoto and Rye, 1979; Ohmoto, 1986; Kyser, 1986, 1990; Chaussidon and Lorand, 1990), and that the source of sulphur in the OKG sulphides has been derived from the magma itself, rather than from an external source (e.g. Tasiuyak, Nain Province and Churchill Province, gneisses). An external sulphur source cannot be ruled out; however, several lines of evidence provide convincing arguments to support a magmatic, rather than external, sulphur origin.

Early models for the genesis of the Voisey's Bay deposit, and recent work, suggest that the sulphidic Tasiuyak gneiss may be important in the genesis of the Voisey's Bay sulphides (Ryan *et al.*, 1995; Ripley *et al.*, 1997; Lightfoot, 1998). In contrast to the OKG sulphides, $\delta^{34}S$ values for the Tasiuyak are very broad, and negative, ranging from -0.9‰ to -17‰ (avg -10‰; Figure 7.2; Table 7.1; Ripley *et al.*, 1997). The distinctly positive, and tightly clustered $\delta^{34}S$ values (+1.0 to +1.8‰) for the OKG sulphides are inconsistent with sulphur contamination from the Tasiuyak gneiss (Figure 7.2). Several lines of evidence suggest this, including: 1) mixing of a negative $\delta^{34}S$

source, with magmatic sulphur at ca. $\delta^{34}S = 0‰$ cannot easily produce negative $\delta^{34}S$ values in the sulphides; and 2) if the Tasiuyak gneiss was the S-contaminant, then the heterogeneous $\delta^{34}S$ distribution in the Tasiuyak gneiss should be partly inherited in the OKG sulphides, which is not the case.

Similar arguments for sulphur contamination from the Churchill Province can also be proposed. Although pyrite separates from the Churchill Province gneisses (Wilton, unpublished data) partly overlap with the OKG sulphides, they have a considerable range and heterogeneity in their $\delta^{34}S$ signatures ($\delta^{34}S = -9.4$ to $+10.7‰$; Figure 7.2). If the CP was the major sulphur contributor, then there should be some evidence of the sulphur isotope heterogeneity in the OKG sulphides. (Figure 7.2; Table 7.1).

Deciphering external input of S from the Nain Province, relative to the mantle is somewhat more problematic, since $\delta^{34}S$ values of the Nain Province overlap the OKG sulphides considerably (e.g. $\delta^{34}S = +0.2$ to $+3.3‰$; Figure 7.2; Table 7.1; Ripley *et al.*, 1997). The significant overlap suggests that the OKG sulphides may have in fact, inherited sulphur from the Nain Province gneisses. However, like the Churchill and Tasiuyak gneisses, the gneisses have a much broader range than the relatively restricted $\delta^{34}S$ range of the OKG sulphides. This does not provide as convincing an argument relative to the Tasiuyak or Churchill Province gneisses; however, the Nain Province is generally sulphur poor (Lightfoot, 1998). Furthermore, if an average value for mantle derived sulphur is taken at 0‰, and the midpoint of Ripley *et al.*'s (1997) data is taken at +1.6‰, it would require over 100% sulphur input from the Nain Province, which does not seem geologically reasonable.

A second argument against Nain Province, or external contamination, comes from comparisons with other magmatic Ni-Cu sulphide occurrences in this region of Labrador (Figure 7.2; Table, 7.1; Wilton and Piercey, unpublished data; Wells, 1997). The majority of NPS epigenetic and syngenetic occurrences, outside of Voisey's Bay, have positive $\delta^{34}S$ values, generally between +1 to +3‰, regardless of geographic position (Figure 7.2; Table 7.1). The disregard for geographic position has very important implications, for different regions are likely to have different external sources of sulphur, with different $\delta^{34}S$ values. The close similarity between all these occurrences could be easily fathomed if they had a common sulphur contaminant, like the Nain Province gneiss. However, assuming such for geographically separated occurrences would be quite unlikely, and the commonality between these occurrences ($\delta^{34}S$ between +1 to +3‰), provides very convincing support of a common magmatic sulphur origin, rather than derivation from an external sulphur source.

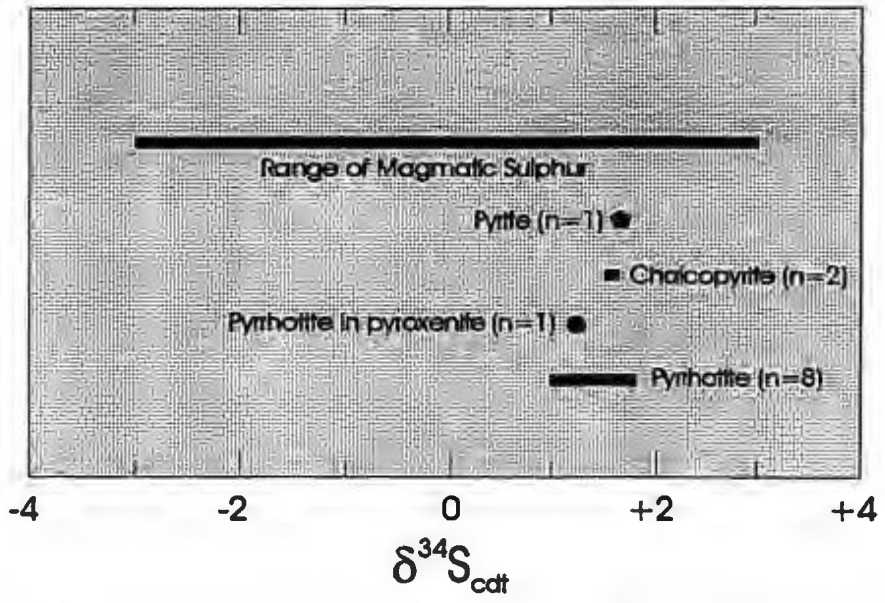

Figure 7.1. Sulphur isotope compositons of sulphide separates from the OKG prospect. Magmatic sulphur range from Ohmoto and Rye (1979), Ohmoto (1986), Kyser (1986, 1990), and Chaussidon and Lorand (1990).

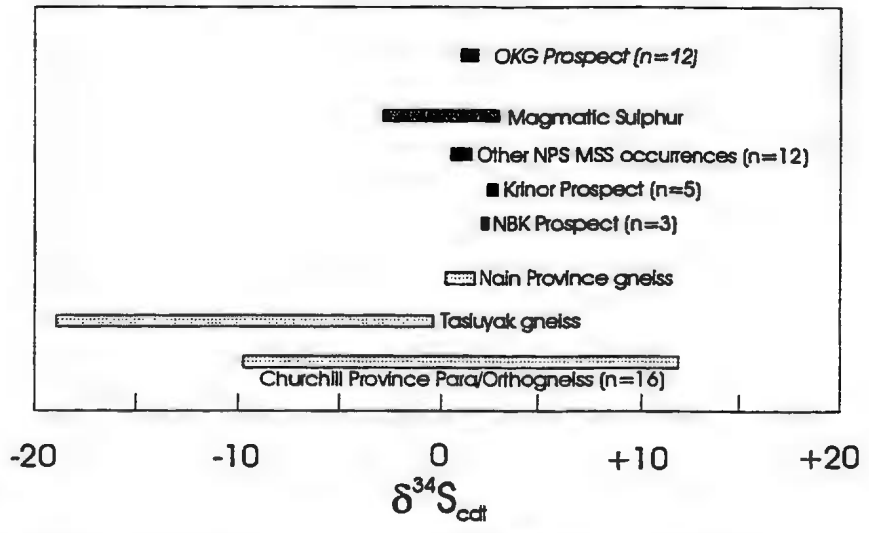

Figure 7.2. Sulphur isotope comparison of the OKG sulphides in comparison to possible contaminants, mantle sulphur and other Nain Plutonic Suite hosted Ni-Cu sulphide occurrences. Data from the Tasiuyak and Nain Province gneisses are from Ripley *et al.* (1997) and Lightfoot (1998); the NBK, Krinor, other MSS, and Churchill Province from Wilton and Piercey (unpublished data).

Table 7.1 Summary of sulphur isotopic characteristics of the OKG sulphides, other sulphides from other NPS sulphide occurrences, and potential sulphur contaminants.

Sample Type	Mineral Separate	Range of $\delta^{34}S$	Source
Massive Sulphides	Pyrrhotite (n=8)	+1.0 to +1.8	This Study
Pyroxenite-hosted	Pyrrhotite (n=1)	+1.2	This Study
Massive Sulphides	Chalcopyrite (n=2)	+1.5 to +1.6	This Study
Massive Sulphides	Pyrite (n=1)	+1.7	This study
NBK Prospect MS	Pyrite, Pyrrhotite, Chalcopyrite (n=3)	+2.1 to +2.2	Wilton and Piercey, Unpublished data
Krinor Prospect MS	Pyrrhotite, Chalcopyrite	+2.3 to +2.8	Wilton and Piercey, Unpublished data
Hettasch Intrusion (MS)	Pyrrhotite	+1.6 to +2.1	Wells (1997)
Voisey's Bay	Not quoted	-4.1 to +2.7	Ripley *et al.* (1997)
Tasiuyak gneiss	Pyrrhotite	-0.9 to –17.0	Ripley *et al.* (1997)
Nain Province gneiss	Not quoted	+0.2 to +3.3	Ripley *et al.* (1997)
Chuchill Province gneiss	Pyrite	-9.4 to +10.7	Wilton and Piercey, Unpublished data

Chapter 8. Discussion and Conclusions

8.1 Introduction

Throughout the previous seven chapters combined field, petrographical, geochemical and isotopic data has been provided in an attempt to provide a greater understanding of the nature of magmatism, magmatic Ni-Cu sulphide mineralization, and metallogeny in the Umiakoviarusek Lake region. This approach has answered many questions and has provided insight into the magmatic and metallogenic evolution of this region; however, as with any study numerous questions still remain unanswered. A logical start to this chapter is a return to the goals and aims of this thesis outlined in Chapter 1 to set the stage for the forthcoming discussions. The purpose and scope of this thesis as presented in Chapter 1 is as follows: 1) to provide detailed petrographic and descriptive documentation of the geology and mineralization of the OKG prospect; 2) to geochemically and isotopically characterize the likely Paleoproterozoic anorthositic-granitoid intrusives of the Umiakoviarusek Lake region to see if a relationship between magmatism, crustal contamination and petrogenesis exists and to see if they have formed in a similar manner to the younger Nain Plutonic Suite; 3) to used a combined geochemical and isotopic approach to decipher the relationships between mantle

magmatism, sulphide saturation and sulphide genesis; and 4) to provide a coherent and logical physio-chemical model for the genesis of the OKG Ni-Cu sulphide occurrences. This chapter provides a discussion of these goals and in addition provides directions for future study to help answer the questions that have not been possible to address in this work. The final section of this thesis provides an overview of the applications of the data presented in this thesis to the search for other Ni-Cu sulphide mineralization in this region.

8.2 Petrogenesis and Basement Control on the Genesis of the OKG Anorthositic and Granitoid Rocks

8.2.1 Descriptive Aspects of the OKG Anorthositic, Granitoid and Basic Dyke Rocks

Recent work in the area from Alliger Lake and Umiakoviarusek Lake regions has shown that some of the rocks originally assigned to the Mesoproterozoic Nain Plutonic Suite (NPS), are actually much older with Paleoproterozoic ages (Emslie and Loveridge, 1992; Ryan and Connelly, 1996; Ryan *et al.*, 1997, 1998; Emslie *et al.*, 1997; Hamilton, 1997; Hamilton *et al.*, 1998). Unlike the Mesoproterozoic NPS, the Paleoproterozoic suite of rocks have been variably effected by the Torngat Orogen (1.87-1.74 Ga; Bertrand *et al.*, 1993; Van Kranendonk and Wardle, 1994, 1997; Van Kranendonk, 1996), and these effects have been outlined in chapters 3 and 4. The OKG anorthositic, granitoid, and basic dyke rocks have features consistent with influence from the TO and are likely pre-TO, and Paleoproterozoic in age, a further discussion of this is put forth in section 8.2.2.

The OKG prospect contains representatives of at least three granitoid intrusives, and at least two separate anorthositic intrusives (Ryan *et al.*, 1998; this study). Granitoid

intrusives include the phase 1 and phase 2 granitoids south of Umiakoviarusek Lake (Owl River Valley pluton and ovoidal-feldspar quartz monzonite, respectively, of Ryan *et al.*, 1998); the foliated fayalite-orthopyroxene bearing granitoids in the eastern portion of the property (fayalite quartz-monzonite unit of Ryan *et al.*, 1998); and in lesser abundance, but present, felsic dykes located in the Main Zone region of the property. The anorthositic intrusives include anorthositic rocks (*an* group) and leuconoritic rocks (*ln1* group) group located both north and south of Umiakoviarusek Lake (Goudie Lake pluton of Ryan *et al.*, 1998); and buff weathering leuconoritic rocks in the eastern portion of the property (*ln2* group; Pripet Marshes pluton of Ryan *et al.*, 1998). Although they form only a minor proportion of the property, basic dykes are present south of Umiakoviarusek Lake and intrude the anorthositic rocks (*ln1* group).

The phase 1 granitoids south of Umiakoviarusek Lake consist predominantly of coarse to medium grained, variably foliated monzonite and lesser syenite. Petrographically, the granitoids are dominated by orthopyroxene, fayalite, and clinopyroxene, with lesser hornblende and biotite; while having relatively subequal percentages of K-feldspar and plagioclase. Towards the western edge of the property, south of Umiakoviarusek Lake, the phase 1 intrusives are intruded by a second phase of medium grained, granular quartz monzonite. Only a cursory examination of these intrusives was undertaken; however, further west, outside the property boundaries, they form a regional unit of ovoidal-feldspar quartz monzonite (Ryan *et al.*, 1998). In contrast to the granitoids south of Umiakoviarusek Lake, the granitoids of the eastern portion of the property exhibit a well-developed foliation, coincident with the Archean Nain

Province gneisses, and exhibit greater degrees of recrystallization. These observations suggest that they may be older than those south of Umiakoviarusek Lake and they range in petrographic composition from quartz-monzonite, monzonite, syenite to alkali feldspar granite; recently the latter intrusion has been dated at ca. 2124 Ma (Hamilton *et al.*, 1998). Felsic dykes form only a minor proportion of the granitoids, and are restricted to the region of the Main Showing. These dykes are aplitic to coarse grained, cut the anorthositic rocks, and are dominated by plagioclase, quartz, with lesser biotite, hornblende and magnetite and have widespread sericite-epidote replacement of feldspars.

The anorthositic rocks of the property are in subequal proportions to the granitoids and consist predominantly of anorthosite and leuconorite. North of Umiakoviarusek Lake the anorthositic rocks are predominantly dark black to grey anorthosite (*sensu stricto*) containing euhedral plagioclase and intercumulus mafic minerals; while leuconorite is lesser in abundance and contains 15-25% orthopyroxene which is replaced by chlorite-actinolite-tremolite assemblages. South of Umiakoviarusek Lake the anorthositic rocks are predominantly leuconoritic with lesser anorthosite and are predominantly grey to white, often have a distinctive bleaching, particularly near contacts with basic dykes, and show much greater evidence of secondary metamorphic mineral replacement. Mafic minerals in the *lnI* group are almost totally replaced by secondary chlorite, actinolite, and lesser tremolite; while plagioclase contains dustings of, or complete replacement by, sericite and epidote, and locally contain veinlets of calcite and dolomite. Some exceptions to the above include a few samples or leuconorite with pristine euhedral plagioclase and intercumulus orthopyroxene; however, this is rare. The

anorthositic rocks of the eastern portion of the property (*ln2* group; Pripet Marshes pluton of Ryan *et al.*, 1998), are predominantly buff weathering, and very crumbly, leuconorite that contains greater orthopyroxene and magnetite relative to those in the eastern portion of the property. Petrographically these rocks are dominated by plagioclase, intercumulus orthopyroxene, and lesser clinopyroxene and magnetite; typically the *ln2* group contain lesser secondary, metamorphic mineral assemblages relative to the *ln1* group.

The relationship of basic dykes to the entire granitoid-anorthosite suite in the Umiakoviarusek Lake region is not well constrained and is further discussed in section 8.2.2. Those observed as part of this study only intrude the anorthositic rocks south of Umiakoviarusek Lake and have no preferred orientation, ranging from northwest, east-northeast to north. Furthermore, they have variable contact relationships with the host anorthosite ranging from straight walled, tentacle-like, as well as rounded edges, and are typically fine to medium grained; no dykes exhibit any evidence of deformation. Petrographically, the dykes are dominated by a dark black to green matrix of mafic material containing numerous laths of fine plagioclase grains, as well as rounded grains of altered olivine-talc-serpentine assemblages. As evidenced by the dark green to black matrixes, all of the dykes show secondary metamorphic mineral assemblages dominated by chlorite, actinolite, sericite and epidote.

8.2.2. Contact Relationships and Structural Geology of Anorthositic, Granitoid and Basic Dyke rocks: A Paleoproterozoic Origin?

The contact relationships and structural geology of all plutonic rocks in this thesis are somewhat problematic due to the artificial limitations imposed by mineral prospect boundaries. Regardless, mapping inside the boundaries for this study define complete

structural and contact relationships. Within the eastern portion of the property, the anorthositic, granitoid and gneissic rocks have distinctive relationships. The gneissic rocks are certainly the oldest rocks and are in tectonic contact with the foliated granitoids, marked by a north-northwesterly striking sinistral strike slip fault, with both units exhibiting coincident, steeply dipping, northwesterly to southwesterly dipping foliations. The contact relationship between the anorthositic (i.e. *ln2* group) and granitoid rocks (i.e. foliated granitoids) is more problematic, and is not well exposed within the property boundaries. However, the anorthositic rocks do not show a defined foliation like the granitoids, are less altered and recrystallized, and hence, are likely younger than the foliated granitoids. This is supported by Ryan *et al.* (1998) who have documented the *ln2* group (Pripet Marshes pluton) intruding the foliated granitoids outside the property boundaries.

The relationship between the eastern rock units and the western rock units of property remains uncertain and contact relationships between these two regions are unable to be drawn. In contrast, the rocks south and north of Umiakoviarusek Lake have distinctive contact relationships, with minor exceptions. The older of the intrusive events in this area include the anorthositic and leuconoritic rocks both north and south of Umiakoviarusek Lake region (*an* and *ln1* groups; Goudie Lake Pluton; Ryan *et al.*, 1998). South of Umiakoviarusek Lake, the phase 1 granitoids intrude the anorthositic rocks and locally contain small 30-45cm granular anorthositic fragments, as well as 2-3m and 10-25m raft like occurrences of anorthosite, suggested post-anorthosite intrusive relationship. The phase 2 granitoids were only observed in a few locations but intrude

the phase 1 granitoids, and form a larger scale regional intrusive outside of property boundaries (Ryan *et al.*, 1998). Felsic dykes north of Umiakoviarusek Lake also post-date the anorthositic rocks, but their relationships to the other granitoid intrusives is unsure.

Mafic dykes appear to be the youngest Paleoproterozoic magmatic event in the Umiakoviarusek Lake region. The dykes have only been observed to intrude the anorthositic rocks of the property and may be post-granitoid emplacement; however, Ryan *et al.* (1998) have stated that mafic dykes intrude the boundary between the phase 1 and phase 2 granitoids further west, and add support to the dykes representing the latest Paleoproterozoic magmatic activity in the Umiakoviarusek Lake region.

Although these relationships in themselves do not imply a Paleoproterozoic origin, in tandem with structural aspects of the property and the nature of the silicate mineralogy a Paleoproterozoic age can be inferred. If the anorthositic and granitoid rocks were of Mesoproterozoic age, explaining the ductile (mylonitic) deformation within the Main Showing region and sinistral strike-slip faulting in the foliated granitoids-Nain Province gneisses would be quite problematic, since a major post-Mesoproterozoic regional deformation event has yet to be recognized in north-central Labrador.

Several other lines of evidence related to the OKG would also remain unexplained if the anorthositic, granitoid and basic dyke rocks are of Mesoproterozoic age. Although it is heterogeneous, the distinctive presence of low grade (greenschist facies) replacement of primary igneous minerals in the anorthositic, granitoid and basic dyke rocks cannot be easily explained without influence from a regional metamorphic event. Although it could

be argued that secondary, hydrous, mineral growth is due to late stage fluids in a magma chamber, the distribution in all rocks, regardless of composition, argues against this. Furthermore, in tandem with secondary mineral growth, the presence of localized mineral foliations, well developed annealing, and widespread subgrain formation of silicate grains in nearly all rocks, and is consistent with influence from the Torngat Orogen.

The lack of a post-Mesoproterozoic regional metamorphic/deformation event in this region, coupled with preliminary U-Pb geochronological dating in this region (Hamilton, 1997; Hamilton *et al.*, 1998), and the secondary metamorphic-deformation features outlined above are consistent with influence from the Torngat Orogen. The Paleoproterozoic age of this orogenic event (Bertrand *et al.*, 1993), and resulting influence thereof on the anorthositic-granitoid-basic dyke rocks of the OKG, suggest a pre-Torngat, and likely Paleoproterozoic (ca. 2135-2045 Ma) age for these rocks.

8.2.3 Geochemical and Isotopic Attributes of the Anorthositic and Granitoid Rocks

The geochemical attributes of the anorthositic and granitoid rocks of the property can be best exemplified by primitive mantle normalized REE and extended multi-element plots; while isotopic data can show the relative inputs of mantle versus crustal material, and assist in the trace element data fingerprinting of a contaminant source(s). Primitive mantle REE patterns for the OKG anorthositic rocks show a distinctive compositional variation in the total REE and shape of the Eu anomaly that are primarily controlled by the orthopyroxene (±clinopyroxene). The progression from the *an* and *ln1* groups (Goudie Lake Pluton) to the *ln2* group (Pripet Marshes pluton) shows progressive increases in total REE, and marked decreases in the size of the positive Eu anomaly,

related to the relative increase in orthopyroxene content from 0-10%, 15-25%, to 25-35%, respectively. In contrast, the REE chemistry of the granitoid rocks, regardless of pluton or style, is fairly consistent with minor exceptions. All of the granitoids have LREE enrichments with decreases relative to the HREE, and have Eu anomalies that are slightly positive (phase 1 rocks), relatively flat (phase 2 and foliated granitoids), or negative (1 of the foliated granitoids). The exception to this Eu anomaly behaviour are the felsic dykes of Main Showing region, that show positive Eu anomalies, even though they are quartz rich.

On the multi-element primitive mantle normalized plots, a number of consistencies arise in both the anorthositic and granitoid groups. Both suites are characterized by enrichments in the LREE and most LFSE; with the granitoids having greater abundance of the LREE and LFSE. Similarly, with the exception of the *an* group, where Nb was not detected, most of the granitoids and anorthositic rocks have negative Nb anomalies, with minor exceptions of flat to slightly positive Nb. Likewise, negative Th anomalies are pronounced in all the anorthositic and granitoid groups with only minor exceptions including one *ln1* sample, one foliated granitoid, and the *an* group (Th < detection limit). In contrast to the similarities, the granitoids have pronounced negative Sr and Ti anomalies, coupled with variably positive Zr anomalies and enrichments in Ba and Rb; while the anorthositic rocks have pronounced positive Sr anomalies (with one *ln2* outlier), have flat to very positive Ti anomalies, variably flat to negative Zr anomalies and lesser enrichments in Ba and Rb.

These geochemical similarities and differences between the anorthositic and granitoid rocks require explanation, in particular why both suites are characterized by relatively negative Th and Nb, as well as why the granitoids have depleted Sr and Ti, and Zr enrichments, and the anorthositic rocks exhibit the opposite behaviour. The inverse relationships of Sr, Ti and Zr between the anorthositic rocks and granitoids is common with anorthositic and granitoid rocks of the Nain Plutonic Suite (e.g. Emslie and Stirling, 1993; Emslie *et al.*, 1994). At least in terms of the Labrador AMCG complexes, it has been proposed that early melting of the lower crust by basaltic underplating would form granitoids enriched in REE (especially LREE), Zr, Rb Ba, K, K/Ti, and Fe/(Fe+Mg), leaving a residue depleted in these elements and enriched in Sr and Ti (Emslie, 1991; Emslie and Hegner, 1993; Emslie and Stirling, 1993; Emslie *et al.*, 1994). Contamination of this hot pyroxene-plagioclase residue by underplating basaltic magma plumes would in part lead to the formation of anorthositic magmas and related rocks with the opposite geochemical signature (*op cit*). Some of these characteristics hold true for the OKG anorthositic rocks, including: lower total REE and LREE, lesser Rb and Ba, flat to negative Zr, as well as positive Sr and Ti.

The geochemical data for the anorthositic and granitoid rocks from the Umiakoviarusek Lake region is very similar to other AMCG complex anorthositic and granitoid rocks; however whether they have similar radiogenic isotope systematics has not been fully addressed. Many workers have documented the importance of crustal contamination in the genesis of anorthositic and granitoid rocks worldwide (e.g. Ashwal and Wooden, 1983, 1985; Emslie, 1985; Ashwal *et al.*, 1986; Geist *et al.*, 1989, 1990;

Kolker *et al.*, 1990; Emslie and Thériault, 1991; Hamilton and Shirey, 1992; Emslie and Loveridge, 1992; Emslie and Hegner, 1993; Emslie *et al.*, 1994; Scoates and Frost, 1996; Hamilton, 1997). The data presented in this thesis also support these other workers. Initial strontium isotope values (ISr (@2050Ma)) for the granitoid rocks are variable (0.7036-0.7095) but consistent with variable amounts of crustal influence. Likewise, the ISr values for the anorthositic rocks (0.7048-0.7082) are also quite elevated and are consistent with influence from sources with significant crustal residence time. The latter interpretations are supported by the εNd (@2050Ma) and Nd depleted mantle model ages. The εNd (@1300Ma) values for both the granitoids and anorthositic rocks overlap significantly and range from –4.1 to –11.8, requiring input from a LREE enriched crustal source (e.g. Nain Province). Furthermore, T_{DM} model ages (cf. DePaolo, 1981, 1998) have averages of ca. 3.0-3.2 Ga for both the granitoid and anorthositic rocks requiring input from a source with long crustal residence time. This source would also have to have low Th and Nb, features that are prevalent in both the anorthositic rocks, and is likely similar to Mid-Archean Nain Province rocks of Schiøtte *et al.* (1993). This contaminant could provide the LREE-enrichment, source with significant crustal residence time, and is low in both Th and Nb. It is suggest that the Nain Province gneisses have had significant crustal influence in the genesis of the anorthositic and granitoid rocks of the Umiakoviarusek Lake region.

Quantification of the crustal influence of the Nain Province was attempted using DePaolo *et al.*'s (1992) neodymium crustal index (NCI). Assimilation of the average of Schiøtte *et al.*'s (1993) Mid-Archean Nain Province yielded NCI values between 0.47-

0.55, with an average of 0.55 for the granitoids; while NCI values for the anorthositic rocks cover a broader range from 0.39-0.84, with an average of 0.65. Furthermore, although the granitoid rocks exhibit slightly less contamination, on εNd-ISr correlation diagrams, the anorthositic-granitoid rocks of the OKG show similar distributions to those of the NPS (Emslie *et al.*, 1994) and the Laramie Complex in Wyoming (Geist *et al.*, 1989, 1990; Scoates and Frost, 1996). The similarities in geochemistry and radiogenic isotope systematics of the anorthositic and granitoid rocks from the Umiakoviarusek Lake region suggest that they have petrogenetic origins similar to the younger Nain Plutonic Suite and other AMCG complex anorthositic and granitoid rocks worldwide.

8.2.4 Petrogenesis and Paleoproterozoic Crustal Evolution

In this section an overview and crustal evolution model is proposed for the plutonic and metamorphic/structural evolution of the anorthositic, granitoid and basic dyke rocks of the OKG prospect. Any model for the petrogenetic and metamorphic evolution of the area must account for: 1) the high content of the orthopyroxene, clinopyroxene, and lesser fayalite in the granitoid rocks; 2) the observed geochemical and isotopic attributes of the anorthositic and granitoid rocks; 3) the presence of secondary, greenschist facies, metamorphic mineral assemblages in many of the granitoids, anorthositic and basic dyke rocks; 4) the presence of sinistral strike-slip faulting and ductile (mylonitic) faulting present on the property.

The Paleoproterozoic age of the entire suite of the anorthositic and granitoid rocks within the OKG prospect remains equivocal at best, since most of the rocks from this region have yet to be dated, and dating is still in the preliminary stages (Emslie and

Loveridge, 1992; Ryan and Connelly, 1996; Hamilton, 1997; Hamilton *et al.*, 1998). However, even though dating is in the early stages, there is good evidence for Paleoproterozoic plutonism at ca. 2.1 Ga, possibly extending to ca. 2.0 Ga (Emslie and Loveridge, 1992; Ryan and Connelly, 1996; Hamilton, 1997; Hamilton *et al.*, 1998), and it is highly likely that the anorthositic and granitoid rocks of the OKG are members of this Paleoproterozoic suite.

Although these ages do not prove that the anorthositic, granitoid rocks and basic dykes of the OKG prospect are of Paleoproterozoic age, the OKG has a number of characteristics that are similar to these rocks. Features such as secondary, low grade, greenschist facies metamorphic mineral assemblages, and localized ductile and sinistral strike-slip faulting are features consistent with the Paleoproterozoic rocks. Since there is no major regional deformation/metamorphic event in post-Mesoproterozoic time in this region of Labrador, the features observed above likely reflect the effects of the Torngat Orogen (ca. 1.86-1.74Ga; Bertrand *et al.*, 1993;Van Kranendonk and Wardle, 1994, 1997; Van Kranendonk, 1996); satisfying criteria 3 and 4 outlined above.

Even though the anorthositic and granitoid rocks of the OKG prospect are likely of Paleoproterozoic age, do they truly represent "anorogenic" AMCG magmatism, and have they formed similarly to those of the NPS? The AMCG intrusions dated thus far indicate a minimum intrusion interval from 2135-2045 Ma (Emslie and Loveridge, 1992; Ryan and Connelly, 1996; Hamilton, 1997; Hamilton *et al.*, 1998). The closest preceding orogenic event occurred at ca. 2.6-2.5 Ga marked by the collision of the Hopedale and Saglek blocks of the Nain Province (Connelly and Ryan, 1992, 1994); while the Torngat

Orogen is the closest post-emplacement orogenic event at ca. 1.86-1.74 Ga (Bertrand *et al.*, 1993). If the definition of Emslie (1991) is invoked, that being anorogenic magmatism occurs generally between 100 Ma and 600 Ma after orogenic activity, then the rocks of the OKG prospect are likely "anorogenic" in the strictest sense.

Even if these rocks are "anorogenic" in the strictest sense have they formed in a petrogenetic manner similar to the NPS, and by the same mechanisms? The geochemical and isotopic data presented in this thesis would be in accordance with petrogenesis in a manner similar to anorthositic and granitoid rocks in other AMCG complexes. In particular, they likely have formed in a petrogenetically similar manner as the model proposed by Emslie *et al.* (1994). In their model mantle plume (hot spot) activity results in high temperature, low fH_2O partial melting and anatexis of a fairly undepleted lower crustal reservoir forming granitoid melts that rise into the crust. This early partial melting event would result in granitoid magmas enriched in total REE, LREE, Rb, Ba, and Zr, and depleted in Ti and Sr; while the residue would inherit the opposite attributes (Emslie and Hegner, 1993; Emslie and Stirling, 1993; Emslie *et al.*, 1994). The high content of orthopyroxene, clinopyroxene and lesser fayalite in the granitoids from the OKG prospect would be in accordance with high temperature-low fH_2O melting; while the geochemical signatures would also be in accordance with genesis in this manner. In contrast, hornblende and biotite rims on the higher temperature mafic minerals may reflect late stage buildup of water in the magma upon emplacement or en-route to higher levels in the crust.

The crustal residue remaining after granitoid genesis would be a hot plagioclase-pyroxene rich residue that was depleted in total REE, especially the LREE, Zr, to a lesser extent Rb and Ba, and enriched in Sr and Ti (Emslie, 1991; Emslie and Hegner, 1993; Emslie and Stirling, 1993; Emslie *et al.*, 1994). This residue would likely be close to its liquidus temperature and be a prime candidate for crustal assimilation by underplated basaltic magmas (Emslie, 1991; Emslie and Hegner, 1993; Emslie and Stirling, 1993; Emslie *et al.*, 1994). Crustal assimilation by this magma would put plagioclase on the liquidus and generate Sr and Ti rich anorthositic magmas which would float to higher levels in the crust due to gravitational instability (Emslie *et al.*, 1994). The overwhelming adherence of the geochemical data for the anorthositic rocks to the above suggests that the OKG anorthositic rocks likely formed in a similar petrogenetic manner to the anorthositic rocks of the NPS. Furthermore, the strong crustal influence involved in the genesis of anorthositic and granitoid rocks that is inferred from the above discussions is also in accordance with the discussion of the Nd and Sr isotopic data presented in the previous section (see section 8.2.3)

The major problem that remains unresolved and not readily discussed is the relative timing of the anorthositic and granitoid pulses. Based on field relationships there are granitoid pulses that are both older (e.g. foliated granitoids), and younger (*ph1*, *ph2*, and felsic dykes) that the anorthositic rocks. In the case of the foliated granitoids, the timing requirements for the model of Emslie *et al.* (1994) would hold true; however, the model is less constrained for the younger pulses. However, this problem has also been addressed in the younger NPS. For instance, even though some of the granitoids intrude

the anorthositic rocks, based on U-Pb geochronology, most of the earlier members of the NPS are actually the granitoids (see Chapter 2; Ryan *et al.*, 1991; Emslie and Loveridge, 1992; Connelly and Ryan, 1994; Hamilton *et al.*, 1994, 1998; Hamilton, 1997). Furthermore, Emslie *et al.* (1994) state that in most cases granitoids and anorthositic rocks have closely overlapping ages. If the latter assumption is made with respect to the Umiakoviarusek Lake intrusives, then the model for the anorthositic and granitoid rocks genesis provided would be valid when compared to the NPS.

In summary, the OKG anorthositic and granitoid rocks have field, geochemical and isotopic characteristics that have cursory similarities to the NPS and have likely formed in a similar petrogenetic manner. Furthermore, Archean source materials like those of the Nain Province have been integral in the genesis of the OKG anorthositic and granitoid rocks.

8.3 Nature and Style of Mineralization: Summary

The OKG prospect provides a unique opportunity to study magmatic Ni-Cu sulphide mineralization in a region that has been poorly explored at best (cf. Kerr and Smith, 1997; Kerr, 1998). Mineralization at the OKG prospect is characterized by massive to disseminated Ni-Cu sulphide mineralization that is both spatially and genetically associated with pyroxenitic and leucotroctolitic dykes (Wilton and Baker, 1996; Kerr and Smith, 1997; Piercey, 1997; Piercey and Wilton, 1998; Kerr, 1998). Surface samples from the OKG have yielded a best assay value of 1.78% Ni, 1.44% Cu and 0.21% Co (Castle Rock Exploration Press Release (CTP-PR), September 21, 1995; Kerr and Smith, 1997). Diamond drilling of the OKG prospect has yet to yield a "second

Voisey's Bay"; however, numerous interesting intersections have been encountered with only twenty-one drill holes completed to date. A summary of representative intersections and grades are listed in Table 8.1; other information can be found in Kerr and Smith (1997).

The style of mineralization in both the surface and drill core is both very similar and associated with predominantly pyroxenitic intrusives, with one location on surface containing leucotroctolite. The mineralization is truly syngenetic in origin (Wilton and Baker, 1996; Kerr and Smith, 1997; Piercey, 1997; Piercey and Wilton, 1998; Kerr, 1998) containing superb magmatic sulphide textures. On surface, massive sulphide mineralization is podiform in nature and in proximity to small-scale pyroxenitic intrusives which generally contain disseminated "net textured" sulphides and appear to grade into the massive sulphides. A less common variant is disseminated sulphides within the anorthositic rocks that are epigenetic and likely have been derived from a sulphide liquid emplaced into the anorthositic rocks. Unlike the anorthositic rocks that bound the pyroxenites, the pyroxenites have primary igneous mineralogy and do not contain widespread secondary metamorphic mineral assemblages typical of the anorthositic rocks in the Main Showing region.

In drill core there is a spatial distribution of the pyroxenitic rocks and sulphide mineralization. The pyroxenitic dykes have sharp contacts with the surrounding anorthositic rocks at both their upper and lower contacts and have a gradational distribution of sulphides from disseminated near the top, to semi-massive, through massive near their bases (cf. Wilton and Baker, 1996; Kerr, 1998). In some dykes the

lower basal sulphides contain centimeter scale fragments of the wall rock anorthositic material. These fragments generally have rounded edges indicative of thermal erosion by the sulphide liquid, and in some examples have chalcopyrite along the fractures of the anorthositic material. Sulphide liquid rarely migrates from the basal section into the host rock anorthositic material for more than a few centimeters (Kerr, 1998); however, where it does migrate it occurs as fine disseminations of pyrrhotite and lesser chalcopyrite.

Silicate and sulphide petrography of the pyroxenites (*sensu lato*) and sulphides show very interesting descriptive and genetic subdivisions. The pyroxenitic rocks (*s.l.*) occur in two types: Type 1 dykes and Type 2 dykes. Type 1 dykes are orthopyroxenitic in nature and have two variants including the Type 1 proper which contains orthopyroxene with predominantly rutile exsolution lamellae; and Type 1A dykes which contain orthopyroxene with both clinopyroxene exsolution lamellae and intercumulus clinopyroxene. The Type 1 dykes and their subdivisions occur both in drill core and on surface. The Type 2 dykes are petrographically distinct and are leucotroctolitic to olivine gabbroic in composition and restricted to one location on surface. These divisions are descriptive, rather than genetic and are not correlable with variations in geochemical or isotopic signatures.

Petrography of both the disseminated mineralization in the dykes and massive sulphides indicate that they have similar sulphide assemblages dominated by pyrrhotite that is host or is in proximity to all other sulphide phases (e.g. Piercey, 1997). The pyrrhotite and associated magnetite are interpreted to represent a high temperature sulphide-oxide assemblage, followed by successively lower pyrite, chalcopyrite and

pentlandite exsolved within the pyrrhotite. The predominant euhedral nature of magnetite, inclusion within pyrrhotite, and the pseudo-sub-ophitic relationship of magnetite to pyrrhotite in some cases, suggests that magnetite was the earliest crystallizing phase and was accompanied by possible co-crystallization with pyrrhotite at lower temperatures. Pyrite appears to be the highest temperature exsolved mineral of the low temperature assemblage and always occurs as resorbed grains that are surrounded by chalcopyrite. This relationship suggests that chalcopyrite is the next exsolving phase, following pyrite, and chalcopyrite is also present in a variety of exsolved blebs and flames, as well as coronas on pyrite and silicate grains. Pentlandite is often found on the edges of chalcopyrite and in a variety of exsolved forms. Exsolved flames, blebs and worm-like forms are common; while partial to full enclosure of pyrrhotite by pentlandite is lesser common, but still present in many sections. All of these sulphide petrographic features are common to magmatically derived Ni-Cu sulphide occurrences (e.g. Naldrett, 1984b).

8.3.1 Nature of the Mantle Source Region

As outlined in Chapter 1, the genesis of magmatic Ni-Cu sulphide mineralization involves the segregation of an immiscible sulphide liquid from a mafic-ultramafic silicate melt due to sulphur saturation in the silicate melt (e.g. Naldrett, 1973; Rajamani and Naldrett, 1978; Naldrett and MacDonald, 1980; Naldrett, 1989a; and others). The first ingredient necessary for forming a Ni-Cu sulphide deposit is the recognition of a metal-rich mafic-ultramafic melt derived from a mantle domain. This subsection discusses the

nature of the OKG mafic-ultramafic rocks and their probable origins from a mantle domain using a combined petrographic and geochemical approach.

The first indication of mantle parentage for the sulphide bearing OKG dykes is their inherent petrographic characteristics. The predominance of orthopyroxene and orthopyroxenitic rocks with minor leucotroctolite attests to a mafic-ultramafic parentage and likely origin in the mantle. These rocks are cumulates and likely do not represent liquid compositions; however, their parental liquids from which they were derived and partially equilibrated must have been of mafic to ultramafic and mantle-derived parentage for reasons outlined below.

The surface dykes at the OKG provide the best inference into the nature of the source region since they exhibit only minor crustal contamination (e.g. Chapters 4 and 6), in particular the leucotroctolitic rocks. The leucotroctolitic rocks from the OKG have abundant plagioclase (60-70%), which should strongly control the dyke chemistry resulting in elevated Eu and LREE, similar to other plagioclase cumulates and troctolitic rocks (e.g. this study; NPS-Emslie *et al.*, 1994; Hettasch Intrusion-Emslie *et al.*, 1997; Reid Brook Intrusion-Emslie, 1996). However, this is obviously not the case and the Eu and LREE depletions suggest that the plagioclase (and other minerals) equilibrated with a source liquid that was depleted in Eu and LREE. Furthermore, the geochemical similarities between the leucotroctolitic and pyroxenite dykes suggest a genetic relationship between the two and derivation of cumulates from a similar source liquid (Figure 4.19).

When these dykes are compared to compiled values for subcontinental lithospheric mantle spinel lherzolites and peridotites (e.g. Figure 4.21; cf. Jochum *et al.*, 1989; McDonough, 1990; Wilson *et al.*, 1996) there is a strong similarity and it is possible that the source magmas that the pyroxenitic rocks equilibrated with were partial melts from such a source. Similarly, the Nd isotopic signatures of the surface dykes have some evidence of crustal influence; however, they temporally evolve in a "mantle-like" manner, akin to the way MORB-like magmas evolved in time. This "mantle-like" time integrated evolution suggests that the OKG pyroxenitic and leucotroctolitic rocks have ties to a mantle source, and possibly a SCLM origin.

It is also likely that the OKG mineralized dykes were also metal rich, at least in the terms of Ni and Cu. Although the liquid compositions from which the dykes were derived cannot be determined directly, the ubiquitous presence of sulphides in the dykes with anomalous metal (Ni and Cu) contents suggests that the magma source from which the dykes were derived had elevated metal contents. In essence, the dykes at the OKG prospect had origins in a mantle source region, and likely had elevated metal contents.

8.3.2 Crustal Contamination and the Genesis of the OKG Ni-Cu Sulphides

As outlined in section 8.3.2 the key to forming a Ni-Cu sulphide occurrence/deposit requires the segregation of sulphide liquid from a silicate melt due to sulphur saturation. Although there were a number of mechanisms suggested in chapter 1 to induce sulphur saturation, the two most common include: 1) sulphur addition or sulphurization (e.g. Mainwaring and Naldrett, 1977; Naldrett and MacDonald, 1980; Ripley, 1981, 1986); and 2) silica addition or felsification (e.g. Kuo and Crockett, 1979;

Naldrett *et al.*, 1986; Lightfoot *et al.*, 1990, 1994; Lightfoot *et al.*, 1997a,b,c; Zhou *et al.*, 1997; Lightfoot, 1998). In this section fairly conclusive evidence is provided for a crustal, felsification origin for the OKG sulphide occurrences using combined S-isotopic, radiogenic isotope and trace element-REE arguments.

To provide evidence against a sulphur assimilation origin a return to chapter 7 must be made, where the results of sulphur isotope data were discussed. Sulphur isotope ratios have worked considerably well in regions such as Duluth (Ripley, 1981, 1986, 1990a,b) and Noril'sk-Talnakh (Naldrett and MacDonald, 1980), to delineate an external sulphur source and sulphurization as a mechanism for inducing sulphide segregation. A number of possible sulphur reservoirs exist in Labrador to act as external contaminants. Early models for the Voisey's Bay deposit suggested the importance of sulphur contamination from the sulphur bearing Tasiuyak gneiss (Ryan *et al.*, 1997); while recently it has been shown that it has influence, but to a lesser extent than proposed by Ryan *et al.* (*op cit*) (Ripley *et al.*, 1997; Lightfoot, 1998). Furthermore, other possible sulphur reservoirs include the Nain Province gneiss, which is generally sulphur poor (Lightfoot, 1998), and the Churchill gneiss.

The data for sulphides from the OKG prospect are inherently restricted in their sulphur isotopic composition, having $\delta^{34}S$ values that range from +1.0 to +1.8‰, within the range for magmatic sulphur defined as $\delta^{34}S = 0 \pm 3‰$ (Ohmoto and Rye, 1979; Ohmoto, 1986; Kyser, 1986, 1990). There are also a number of arguments to point against an external sulphur source, and point to a magmatic source. Sulphur isotope ratios for the Tasiuyak gneiss are different than those from the OKG sulphides, with

strongly negative values ranging from $\delta^{34}S$ = -0.9 to –17.0‰ (avg –10‰; Ripley *et al.*, 1997). Such strongly negative values, coupled with considerable heterogeneity cannot explain the very homogenous and distinctly positive $\delta^{34}S$ values in the OKG sulphides and points against a Tasiuyak sulphur source.

The Churchill Province has a very heterogeneous signature that has $\delta^{34}S$ values that range from –9.7 to +10.7‰ (Wilton and Piercey, unpublished data). Although the positive values of the CP could explain the shift of the OKG sulphides from 0‰ to a more positive number, the heterogeneity of the sulphides in the Churchill Province should be at least partly inherited within the sulphur isotopic signatures of the OKG sulphides. This is not the case, and the homogenous signatures point to a source unrelated to the Churchill Province gneisses. The Nain Province is much more problematic, values for the Nain Province overlap considerably with the OKG sulphides ($\delta^{34}S$ = +0.3 to +3.3‰; Ripley *et al.*, 1997); and are relatively homogeneous. The Nain Province could be a possible sulphur contributor, but the Nain Province is generally sulphur poor (Lightfoot, 1998), and is somewhat more heterogeneous relative to the OKG sulphides. This in itself does not preclude input from the gneiss; however, regional $\delta^{34}S$ ratios in numerous Ni-Cu sulphide occurrences with variable styles and host rocks in the region from Nain to Okak Bay region all have a restricted range from +1.0 to +2.8‰ (Wilton and Piercey, unpublished data; Wells, 1997). Although this does not prove a magmatic origin, the overwhelming similarities in $\delta^{34}S$ values over this broad geographic area suggests either a common contaminant or common magmatic source. It is possible that the Nain Province could have influenced all of these occurrences; however, the Nain

Province as the sole sulphur contaminant over such geographically and variably styled Ni-Cu occurrences points against the NP and towards a common magmatic source.

With this in mind, another mechanism for inducing sulphide segregation is required, and this leaves felsification as the only viable alternative. A number of possible contaminants could have felsified the pyroxenitic magmas associated with the OKG Ni-Cu occurrences including: 1) Tasiuyak gneiss; 2) Churchill Province gneiss; 3) Nain Province gneiss; and even 4) the Paleoproterozoic granitoid and anorthositic rocks of the property. These anorthositic and granitoids can be virtually negated as contaminants based on field and drill core characteristics of these rocks and mineralization. Granitoid rocks form only a minor proportion of the drill core material and are typically restricted to small dykes in drill core (Kerr, 1998). Furthermore, geologic evidence suggests that the granitoids form a cap on the anorthositic rocks (Ryan *et al.*, 1998), and assuming they form a significant portion of the subsurface does not seem reasonable.

The anorthositic rocks are not as easily nullified as a possible crustal contributor. However, the nature of the sulphide mineralization, and pyroxenite-anorthosite relationship can point against such a source. The sharp contacts observed with the anorthositic rocks, the lack of chilled anorthositic inclusions within the dykes, and the ubiquitous presence of sulphides in the pyroxenites suggest that sulphide saturation was achieved *prior to emplacement* into the anorthositic rocks; likely by some contaminant at depth.

This leaves the possible Churchill Province gneisses, Tasiuyak gneiss, and the Nain Province gneisses as possible contaminants. Using primarily Nd isotopes an

argument against a Churchill Province origin can be put forth. Average εNd (@1300Ma) values (-14.6) and model age for the Churchill Province (2.7 Ga) from Emslie *et al.* (1994) suggest that this source cannot be the source of contamination for the subsurface dykes at the OKG. Firstly, the average model age of 2.7 Ga for the CP is lower than the average Nd model age for the subsurface pyroxenites (2.74 Ga) and requires input from a crustal reservoir with longer Nd crustal residence time. Furthermore, NCI determinations on the CP require up to 92% Nd input to account for the most contaminated signature in the subsurface pyroxenites requiring an impossible degree of Nd input.

The Nain Province and Tasiuyak gneisses are also possible contaminants. Both of these sources are LREE and LFSE enriched and could act as potential contaminants explaining the LREE enrichments in the dykes. However, on primitive mantle normalized plots the dykes are characterized by a distinctly negative Th anomaly in both the surface and subsurface dykes. The retention of such anomaly from a mantle source region is unlikely, and it probably has a crustal origin; however, if the negative Th anomaly is a function of the mantle source region, any subsequent crustal contaminant must be Th-poor to explain the retention of the negative Th anomaly regardless of the degree of contamination (e.g. retention in the surface and subsurface examples). The Tasiuyak gneiss of Thériault and Ermanovics (1997) and that of Lightfoot (1998) *do not* show pronounced negative Th anomalies. Furthermore, depleted mantle model ages for the Tasiuyak gneiss of Thériault and Ermanovics (1997) are over 300 Ma younger than the average model ages for the subsurface contaminated dykes; while NCI values for the subsurface dykes require nearly 100% crustal Nd input from the Tasiuyak gneiss to

account for their εNd (@1300Ma) signatures. This is geologically unreasonable and would require complete assimilation of a Tasiuyak gneiss source.

The Nain Province provides the most coherent and most probable crustal contaminant involved in the genesis of the OKG sulphides. The Nain Province can provide a source of LREE and LFSE exemplified in the subsurface dykes; and to a lesser extent in the surface dykes. The Nain Province can also explain the well developed negative Th anomaly, as the Nain Province is also Th-poor and shows a well pronounced negative Th anomaly (e.g. Chapter 4; cf. Lightfoot, 1998; Schiøtte *et al.*, 1993). The Nain Province also can explain the observed Nd isotope signatures within the dykes. The Nain Province gneisses are typically very old and have considerably older Nd isotopic signatures which can explain the model ages and the εNd (@1300Ma) signatures of the dykes. Furthermore, NCI determinations only require an average of 35% crustal Nd input into the subsurface pyroxenites, and only an average of 8% input into the surface dykes; which seems much more reasonable than any other possible contaminant. Thus, the Nain Province is likely the contaminant, and provided a mechanism to induce sulphur saturation in the pyroxenitic rocks and the formation of the observed sulphides.

8.4 Metallogenic Model for the OKG Ni-Cu Sulphides

A metallogenic model for the OKG Ni-Cu sulphide occurrences must be able to account for: 1) the field characteristics and nature of the pyroxenite-leucotroctolite hosted mineralization; 2) the relatively primitive nature of the dykes and their origin; 3) the homogeneity in sulphur isotopic composition of the sulphides; 4) the varying degrees and effects of crustal influence. The field characteristics of the OKG mineralization show a

spatial and genetic relationship between the pyroxenitic rocks and magmatic Ni-Cu sulphide mineralization. Furthermore, they intrude the anorthositic rocks that bound them, are all sulphide bearing, and by association suggest that they were sulphide saturated *prior to emplacement*. In surface examples they also have a spatial association to ductile, mylonite zones; however, unlike the anorthositic rocks in this region, they do not exhibit secondary metamorphic mineralogy and are post-ductile deformation. This relationship coupled with the lack of deformation associated with their margins in drill core (cf. Kerr, 1998), a feature common to many mafic and felsic dykes in core, suggest that they are in fact Mesoproterozoic, rather than Paleoproterozoic like the bounding anorthositic rocks.

The likely Mesoproterozoic age for the pyroxenitic intrusives suggests that they may be somewhat related to the NPS (cf. Emslie *et al.*, 1994). Plume-related magmatism associated with the Mesoproterozoic NPS would likely have provided a heat source required to induce partial melting of a depleted (SCLM?) mantle reservoir. This melting of this source resulted in the generation of a refractory, depleted magma that began to rise upward into the crust, likely along crustal-scale faults associated with the later stages of uplift during the Torngat Orogen (cf. Ryan *et al.*, 1995) and extension related to NPS genesis (cf. Emslie *et al.*, 1994; Figure 8.1a). Upon rising into the crust this magma began to crystallize orthopyroxene (± plagioclase ± olivine) resulting in an orthopyroxene-charged crystal-liquid mush that assimilated Nain Province crustal material. This interaction with the Nain Province resulted in enrichments in LREE, Ba, Rb, K, unradiogenic Nd (low negative εNd values), likely SiO_2 and possibly S (Figure

8.1b). This assimilation resulted in the effective felsification of the pyroxenitic melts and coupled with silicate fractionation induced sulphur saturation and the commencement of sulphide droplet formation (Figure 8.1b). The emplacement of these sulphide-bearing magmas into favourable traps (fractures?) within the subsurface anorthositic rocks resulted in the settling out of the sulphide droplets forming massive sulphides at the bases of the dykes. Upon emplacement the dykes and related sulphide liquids likely entrained anorthositic fragments and accompanied with the above resulted in the geological relationships shown in Figure 3.4c.

Continued underplating and melting of this reservoir likely created multiple melts from the refractory, depleted mantle reservoir. Subsequent later pulses likely underwent crystallization and formation of pyroxene-(±olivine ± plagioclase)-rich crystal-liquid mushes that rose into the crust. However, the subsequent pulses that likely formed the surface showings followed paths and conduits that were previously used by the subsurface pulses (Figure 8.1c). By using these pathways the younger pulses were sheltered from the Nain Province wall rock and underwent less crustal contamination (Figure 8.1c). However, there was some crustal influence (felsification) resulting in the incorporation of unradiogenic Nd (negative εNd (@2050 Ma) values) but very little LREE or LFSE enrichments. The felsification coupled with silicate fractionation resulted in sulphur saturation and the formation of sulphide droplets within the crystal-liquid mushes (Figure 8.1c). With continued rising to the surface there was a partial loss of sulphides en-route and losses of PGE at the expense of Ni and Cu (e.g. Chapter 5), and

upon reaching the surface segregated sulphides within the anorthositic rocks forming the observed surface mineralization characteristics (e.g. Figure 3.4a).

8.5 Conclusions

The OKG prospect in the Umiakoviarusek Lake region of Labrador provides an excellent laboratory for the study of AMCG-related anorthositic-granitoid petrogenesis, and magmatic Ni-Cu sulphide mineralization. This study has attempted to provide a greater database on the nature of AMCG genesis and magmatic Ni-Cu sulphide mineralization in a region that has been relatively unexplored and at best poorly understood. The major conclusions of this study can be summarized as follows:

1) the anorthositic, granitoid and basic rocks of the OKG are likely of Paleoproterozoic age and contain a number of features consistent with other dated Paleoproterozoic anorthositic and granitoid rocks including: a) the presence of secondary, greenschist facies, metamorphic replacement of primary igneous assemblages; b) intrusion of anorthositic rocks by mafic dykes with secondary metamorphic mineral assemblages; c) presence of widespread metamorphic recrystallization of primary igneous mineralogy; d) evidence of ductile and sinistral strike-slip faulting likely related to the Torngat Orogen;
2) even though the anorthositic and granitoid rocks are of Paleoproterozoic age, they likely represent truly "anorogenic" AMCG magmatism;
3) geochemical and isotopic characteristics of the anorthositic and granitoid rocks are very consistent with other AMCG complexes including the NPS and Laramie Complex in Wyoming;

4) the geochemical and isotopic characteristics of the anorthositic and granitoid rocks are consistent with genesis in a manner similar to NPS as provided in the model of Emslie *et al.* (1994) and have had significant basement influence from the Nain Province;

5) magmatic Ni-Cu sulphide mineralization associated with the OKG prospect is truly syngenetic and is both spatially and genetically associated with Mesoproterozoic pyroxenitic and leucotroctolitic intrusives and have magmatic sulphide textures and sulphide petrographic features consistent with other magmatic Ni-Cu sulphide occurrences;

6) petrography and geochemical attributes of the dykes suggest that they are mantle-derived and metal-rich mafic-ultramafic magmas required as a metal source for magmatic Ni-Cu sulphide mineralization;

7) PGE, REE and trace element geochemistry of the relatively uncontaminated pyroxenitic dykes suggest a relationship to refractory, depleted mantle sources, possibly similar to subcontinental lithospheric mantle (SCLM) spinel peridotites and lherzolites;

8) the genesis of the sulphide mineralization at the OKG prospect was not influenced by external sulphur input and involved crustal contamination rather than sulphurization; REE, trace element and Nd isotope geochemistry provide good evidence for a Nain Province crustal influence in the genesis of the OKG Ni-Cu sulphide occurrences

8.6 Directions for Further Study

Although a variety of data have been presented in this thesis, there is considerable room for future study, research and exploration. From a research and crustal evolution perspective a number of distinctive studies should be carried out. Firstly, detailed U-Pb geochronology of the granitoid, anorthositic and basic dykes should be carried out to put the temporal constraints required to decipher and "shore up" the Paleoproterozoic versus Mesoproterozoic question. Likewise, Re-Os isotope systematics on the sulphides and pyroxenitic rocks of the OKG could possibly provide an age for the sulphide mineralization. If not, the crustal influence of the Nain Province may be further proven/disproven by using the Os isotope system. These age questions are very important and this is likely one of most important scientific questions remaining in this area.

From a metallogenic and mineral exploration viewpoint a number of things remain to be undertaken in this region. Detailed probe work on mineral phases within the anorthositic rocks in drill core may provide a "ghost" stratigraphy, which may foster correlations often unobservable by rock identification along. Likewise detailed mineral chemical work on the pyroxene, olivine and plagioclase in the pyroxenitic-leucotroctolitic rocks may provide a greater understanding of the nature of their source magmas and petrogenetic histories. Further detailed sampling of the anorthositic and pyroxenitic rocks accompanied by REE, trace element, and isotopic studies may provide further clues to the source and causes of mineralization. In essence, to either support or disprove the crustal influence involved in the genesis of the OKG sulphides.

From a purely explorationist viewpoint, only 21 drill holes have been completed on the OKG property and it clearly in the early stages of exploration. The OKG has the ingredients to host significant quantities of Ni-Cu sulphide mineralization, including: 1) metal-rich mafic-ultramafic dykes that likely have source magmas that are rich in metals; and 2) conclusive evidence of a crustal contamination mechanism required to induce sulphur saturation. Only further drilling, exploration, and academic study will show if the OKG prospect has significant quantities of Ni-Cu sulphide mineralization that have graced better explored terrains elsewhere in Canada and the world.

8.7 Exploration Directives and Tools for Exploration

Much of the data presented herein appear to be of academic character, rather than having a direct exploration application; however, much of the data presented when viewed with an open mind, can be of direct application to finding other Ni-Cu sulphide occurrences in Labrador. From a field perspective favourable hosts to mineralization would include those rocks which are of mafic-ultramafic parentage (e.g. pyroxenite, olivine gabbro, troctolite), and have a definite syngenetic relationship with sulphide mineralization (e.g. OKG prospect, South Voisey's Bay project, Voisey's Bay; cf. Kerr, 1998). This search can also be readily aided by the usage of detailed thin section silicate petrography, which can identify prospective hosts; while sulphide petrography can show if the sulphides have similar sulphide assemblages and paragenesis commonly associated with magmatic Ni-Cu sulphide mineralization. The *correct* identification of mafic-ultramafic rocks with associated syngenetic magmatic Ni-Cu sulphide mineralization is of utmost importance because it can provide a relatively cheap means of identifying one

essential ingredient for forming a deposit, a metal-rich source magma. The further establishment of the mafic-ultramafic parentage suitable for a source rock can be achieved using major and trace elements. Ideal parental rocks should have high MgO contents, high Mg#'s (Mg# = (MgO/MgO+FeO*)), and should also have elevated Ni and Cu contents metal contents (e.g. OKG pyroxenites as outlined above). It should also be noted, however, that cumulate rocks may not be truly representative of liquid compositions and ideal source magmas would exhibit finer grained textures with the above characteristics (e.g. chilled margins in the Reid Brook Intrusion, Lightfoot, 1998; fine grained gabbros at South Voisey's Bay-Kerr, 1998).

Successful identification of a primitive, metal-rich magma suitable as a source is relatively easy using the above petrographic techniques with relatively minor amounts of geochemical data. In contrast, deciphering the mechanism of inducing sulphur saturation is somewhat more problematic. From a field perspective any mafic-ultramafic intrusive that intrudes a sulphide-bearing unit has potential for magmatic Ni-Cu sulphide mineralization. For example, the Duluth Complex intrudes the sulphur-rich metasedimentary rocks of the Virginia Formation (cf. Ripley, 1981, 1986); or the Kiglapait intrusion intrudes the sulphide-bearing rocks of the Snyder Group (cf. Morse, 1969; Emslie *et al.*, 1997). In both of these cases there is often a significant difference in sulphur isotope composition of the magma ($\delta^{34}S \approx 0$) and the host wall rock (e.g. $\delta^{34}S \approx +15$ in the Virginia Formation at Duluth), and if the magmatic sulphides interacted with sulphidic wall rock they should show the sulphur isotopic influence of the wall rock.

Although intrusion into sulphide bearing country rocks works as an exploration tool in some cases, as above, it does not always hold true (e.g. Voisey's Bay), and oftentimes the sulphur isotope data are not diagnostic and do not point to sulphurization. In these cases an alternative mechanism (e.g. felsification), and the means of identifying them, are required. From field identifications, chilled inclusions within the mafic-ultramafic sulphide-bearing magma can illustrate the possibility of contamination; however, this is not always the case and alternative mechanisms to identify felsification are required. The most prospective and useful tools for identifying felsification include the use of trace elements and isotopes. Mafic and ultramafic magmas with mafic to ultramafic mineralogy, accompanied by high MgO and Mg# can be often contaminated with crustal material, accompanied by effectively little change in MgO, Mg# or the mineralogy. In these crustally contaminated, or felsified rocks, they should inherit the signature of the crustal contaminant. In particular, felsic contaminants should cause LREE enrichments (e.g. La/Yb, Ce/Yb), and LFSE enrichments (e.g. Th/Y), and should also create elevated $^{87}Sr/^{86}Sr$ values, and strongly negative εNd values (at a given age). Specifics of the crustal source can also be used to fingerprint the source contamination. For instance, the negative Th and Nb, coupled with old Nd model ages, low εNd, and high $^{87}Sr/^{86}Sr$ of the Nain Province provide a fingerprint that differs from that of the Tasiuyak gneiss.

In conclusion, prospective Ni-Cu sulphide prospects, terrains, occurrences and deposits should have: 1) mafic to ultramafic host rocks with distinctive mafic-ultramafic mineralogy that should be accompanied with high MgO and Mg#, as well as trace metals

such as Ni and Cu; 2) evidence for sulphurization, when the difference between the magma and sulphur contaminant can be indicated by $\delta^{34}S$ values; and/or 3) evidence for crustal input (or felsification), rocks contaminated in this manner should show evidence of LREE enrichments (e.g. elevated La/Yb, Ce/Yb), LFSE enrichment (e.g. Th/Y), and should have high $^{87}Sr/^{86}Sr$ (high ISr values) and low εNd values. Prospects and occurrences which have evidence of criteria 1 and either criteria 2 or 3 (or both) are quite prospective and have the potential to host significant quantities of Ni-Cu sulphide mineralization and these are the occurrences for which explorationists should search.

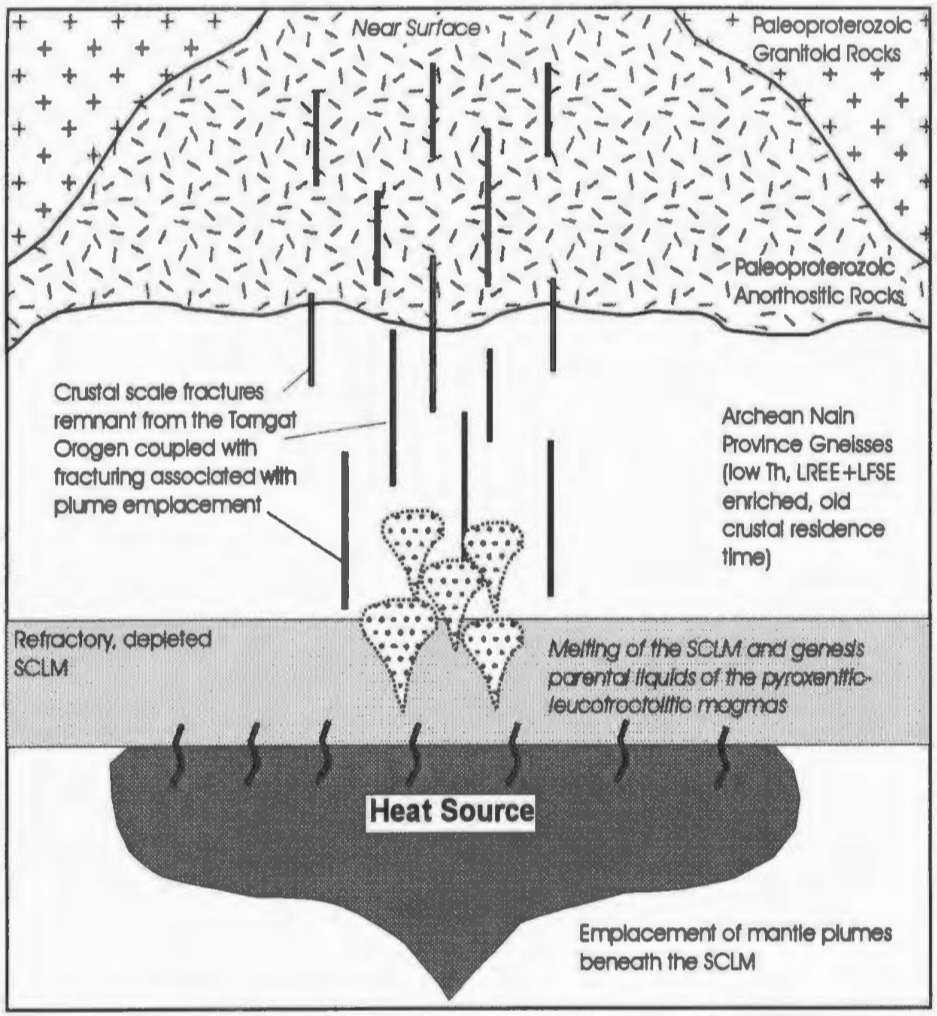

a) Emplacement of mantle plumes associated with the Nain Plutonic Suite below the SCLM during Mesoproterozoic AMCG magmatism. Partial melting of the SCLM by the mantle plume resulted in the genesis of the depleted parental magmas that formed the pyroxenitic-leucotroctolitic magmas. These magmas rose along previously existing crustal faults related to the Torngat Orogen, and those likely associated with plume emplacement.

Figure 8.1. Metallogenic model for the OKG Ni-Cu sulphide occurrences.

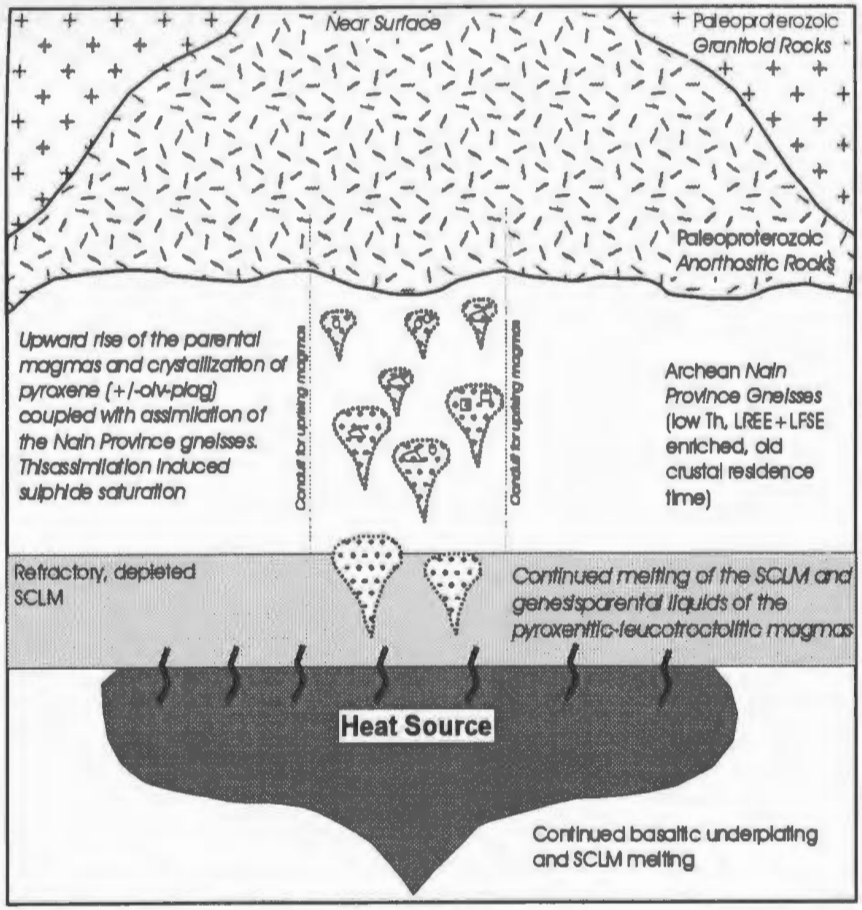

Figure 8.1. (continued)

b) Upward rise of early pulses of the parental liquids and the crystallization of pyroxene (+/- olivine and plagioclase) forming pyroxene-charged crystal-liquid mushes. This upward rising "pyroxenitic" magmas assimilated Nain Province gneisses resulting in LREE Ba, Rb, K enrichments and low εNd (@1300Ma) signatures. .

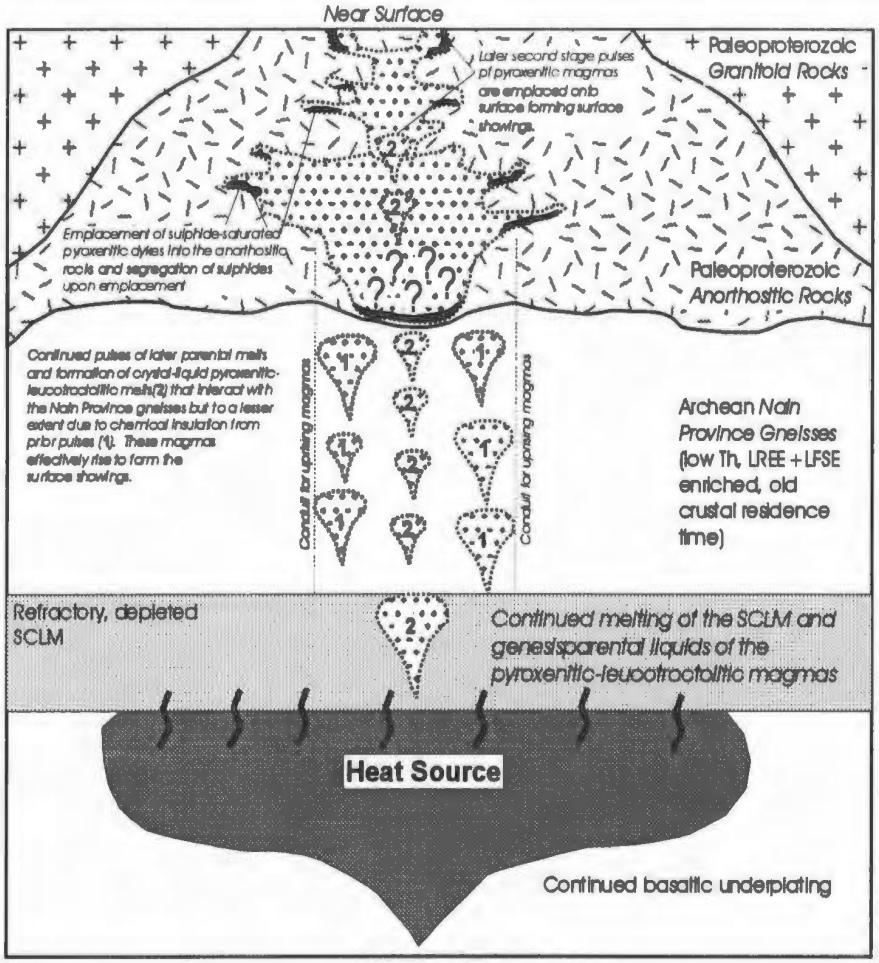

Figure 8.1. (continued)

c) Emplacement of early phases of sulphide-saturated pyroxenitic magmas that are intruded into the anorthositic rocks. Upon emplacement these segregate Ni-Cu sulphides forming the subsurface dykes. Later pulses of pyroxenitic magmas rise upwards and interact with the Nain Province gneisses but to a lesser extent due to chemical insulation by prior pulses. These later pulses continue upward and form the surface showings of Ni-Cu sulphide.

Table 8.1 Summary of representative intersections and grades from the OKG prospect. Data compiled from Castle Rock Exploration Press Releases and Kerr and Smith (1997).

Drill Hole	Intersection	Grade	Notes
Surface showing	NA[1]	Best assay 1.78% Ni, 1.44% Cu, 0.21% Co	Massive sulphide pods in anorthosite, associated with pyroxenites
OKG-1, 2, 3	Four intersections over 5m.	Not quoted	Associated with pyroxenites
OKG-3	3.2m wide intersection	1.10% Ni, 0.93% Cu, 0.104% Co	Associated with pyroxenites
OKG-4	3m wide 30-50% po+cp in pyroxenites	1.10% Ni, 0.37%Cu, 0.06% Co	Associated with pyroxenites
OKG-5	Four intersections, 1.1-7.5m	0.86-1.07% Ni, 0.45-0.72% Cu, 0.04-0.09% Co	Pyroxenite layers, basal massive sulphide grading upward into semi-massive and disseminated (CTP-PR Dec. 18, 1995).
OKG-96-09	Four 1m intersections over 14m interval.	0.26-0.87% Ni, 0.09-0.43% Cu, 0.04-0.11% Co	Associated with pyroxenitic "layers" and had four intervals over apparent 14m

Drill Hole	Intersection	Grade	Notes
OKG-96-10	2 intersections 0.5-1.0m	0.34-0.67% Ni, 0.26-0.71% Cu, 0.04-0.08% Co	Associated with pyroxenites
OKG-96-16	6.10m intersection	0.6% Ni, 0.32% Cu, 0.10% Co	Ten pyroxenite lenses over interval
OKG-97-20	NA[1]	subeconomic grades	Pyroxenite hosted, magnetite rich with disseminated sulphide
OKG-97-21	NA[1]	subeconomic grades	Intrusive "gabbroic" textured ultramafic; 20% magnetite and disseminated sulphide

[1]NA = not applicable

References

Abrajano, T.A., and Pasteris, J.D., 1989. Zambaldes ophiolite, Philippines II. Sulfide petrology of the critical zone of the Acoje Massif. Contributions to Mineralogy and Petrology, **103**: 64-77.

Abrajano, T.A., Pasteris, J.D., and Bacuta, G.C., 1989. Zambaldes ophiolite, Philippines, I. Geology and petrology of the critical zone of the Acoje massif. Tectonophysics, **168**: 65-100.

Amelin, Y., Li, C., Naldrett, A.J., 1997. Multistage evolution of the Voisey's Bay Complex, Labrador, Canada, revealed by U-Pb systematics of zircon, baddelleyite, and apatite. American Geophysical Union (AGU) Fall Meeting 1997, Electronic Program with Abstracts.

Archibald, S.M., 1995. The Geology, Mineralization, Geochemistry, and Metallogeny of the Paleoproterozoic Ramah Group, Northern Labrador. Unpublished M.Sc. thesis, Memorial University of Newfoundland, St. John's, Newfoundland, 243 pages.

Arndt, N.T., and Jenner, G.A., 1986. Crustally contaminated komatiites and basalts from Kambalda, Western Australia. Chemical Geology, **56**: 229-255.

Arndt, N.T., and Goldstein, S.L., 1987. Use and abuse of crust-formation ages. Geology, **15**: 893-895.

Ashwal, L.D., 1993. Anorthosites. Springer-Verlag, Berlin. 422 pages.

Ashwal, L.D., and Wooden, J.L., 1983. Isotopic evidence from the eastern Canadian Shield for geochemical discontinuity in the Proterozoic mantle. Nature, **306**: 679-680.

Ashwal, L.D., and Wooden, J.L., 1985. Sm-Nd isotopic studies of Proterozoic anorthosite: systematics and implications. *In* The Deep Proterozoic Crust in the North Atlantic Provinces. *Edited by* A.C. Tobi and J.L.R. Touret. D. Reidel Publishing Company, pp. 61-73.

Ashwal, L.D., Wooden, J.L., and Emslie, R.F., 1986. Sr, Nd, and Pb isotopes in Proterozoic intrusives astride the Grenville Front in Labrador: Implications for crustal contamination and basement mapping. Geochemica et Cosmochimica Acta, **50**: 2571-2585.

Barley, M.E., and Groves, D.I., 1992. Supercontinent cycles and the distribution of metal deposits through time. Geology, **20**: 291-294.

Barnes, S.-J., 1987. Unusual nickel and copper to noble-metal ratios from the Råna Layered Intrusion, northern Norway. Norsk Geologisk Tidsskrivt, **67**: 215-231.

Barnes, S.-J., 1990. The use of metal ratios in prospecting for platinum-group element deposits in mafic and ultramafic intrusions. Journal of Geochemical Exploration, **37**: 91-99.

Barnes, S.-J, 1998. Possible causes of high Pd/Pt, Pd/Ir, Rh/Ir, Pd/Os ratios in sulphide ores. GAC/MAC Annual Meeting, Quebec City, 1998, Program with Abstracts, p. A-9.

Barnes, S.J., and Naldrett, A.J., 1985. Geochemistry of the J-M (Howland) Reef of the Stillwater Complex, Minneapolis adit area-I. Sulfide chemistry and sulfide-olivine equilibrium. Economic Geology, **80**: 627-645

Barnes, S.J., and Naldrett, A.J., 1986. Geochemistry of the J-M (Howland) Reef of the Stillwater Complex, Minneapolis adit area-II. Silicate mineral chemistry and petrogenesis. Journal of Petrology, **27**: 791-825.

Barnes, S.-J., and Picard, C.P., 1993. The behaviour of platinum-group elements during partial melting, crystal fractionation, and sulphide segregation: An example from the Cape Smith Fold Belt, northern Quebec. Geochemica et Cosmochimica Acta, **57**: 79-87.

Barnes, S-J., and Francis, D., 1995. The distribution of platinum-group elements, nickel, copper, and gold in the Muskox layered intrusion, Northwest Territories, Canada. Economic Geology, **90**: 135-154.

Barnes, S.-J., Naldrett, A.J., and Gorton, M.P., 1985. The origin of the fractionation of platinum-group elements in terrestrial magmas. Chemical Geology, **53**: 303-323.

Barnes, S.-J., Boyd, R., Korneliussen, A., Nilsson, L.P., Often, M., Pedersen, R.B., and Robins, B., 1988. The use of mantle normalization and metal ratios in discriminating between the effects of partial melting, crystal fractionation and sulphide segregation of platinum-group elements, gold, nickel and copper: examples from Norway. *In* Geoplatinum 87. *Edited by* H.M. Prichard, P.J. Potts, J.F.W. Bowles, and S. Cribb. Elsevier, Amsterdam, pp. 113-143.

Barnes, S.-J., Picard, C., Giovenazzo, D., and Tremblay, C., 1992. The composition of nickel-copper sulphide deposits and their host rocks from the Cape Smith Fold Belt, Northern Quebec. Australian Journal of Earth Sciences, **39**: 335-347.

Barnes, S.-J., Coutre, J.-F., Sawyer, E.W., and Bouchaib, C., 1993. Nickel-copper occurrences in the Belleterre-Angliers Belt of the Pontiac Subprovince and the use of Cu-Pd ratios in interpreting platinum-group element distribution. Economic Geology, **88**: 1402-1418.

Barnes, S.-J., Zientek, M.L., and Severson, M.J., 1997a. Ni, Cu, Au, and platinum-group element contents of sulphides associated with intraplate magmatism: a synthesis. Canadian Journal of Earth Sciences, **34**: 337-351.

Barnes, S.-J., Makovicky, E., Makovicky, M., Rose-Hansen, J., and Karup-Moller, S., 1997b. Partition coefficients for Ni, Cu, Pd, Pt, Rh, and Ir between monosulfide solid solution and sulfide liquid and the formation of compositionally zoned Ni-Cu sulfide bodies by fractional crystallization of sulfide liquid. Canadian Journal of Earth Sciences, **34**: 366-374.

Barrie, C.T., and Naldrett, A.J., 1988. The geology and tectonic setting of the Montcalm Gabbroic Complex and Ni-Cu deposit, Western Abitibi Subprovince, Ontario, Canada. *In* Proceedings of the 5th Magmatic Sulfides Conference, Harare, Zimbabwe. Institution of Mining and Metallurgy of London, pp. 151-164.

Bell, K., and Blenkinsop, J., 1987. Archean depleted mantle: Evidence from Nd and Sr initial isotopic ratios of carbonatites. Geochemica et Cosmochimica Acta, **51**: 291-298.

Bennett, V.C., and DePaolo, D.J., 1987. Proterozoic crustal history of the western United States as determined by neodymium isotopic mapping. Geological Society of America Bulletin, **99**: 674-685.

Bezemen, N.L, Asif, M., Brugmann, G.E., Romanenko, I.M, and Naldrett, A.J., 1994. Distribution of Pd, Ru, Rh, Ir, Os, and Au between sulfide and silicate melts. Geochemica et Cosmochimica Acta, **58**: 1251-1260.

Berg, J.H., Emslie, R.F., Hamilton, M.A., Morse, S.A., Ryan, A.B., and Wiebe, R.A., 1994. Anorthositic, granitoid and related rocks of the Nain Plutonic Suite. IGCP Correlation Program, IGCP Projects #290 and #315, Field Trip Guidebook. 69 pages.

Bertrand, J.-M., Van Kranendonk, M.J., Hamner, S., Roddick, J.C., and Ermanovics, I., 1990. Structural and metamorphic geochronology of the Torngat Orogen in the North River-Nutak transect area, Labrador: Preliminary results of U-Pb dating. Geoscience Canada, **17**: 297-301

Bertrand, J.-M., Roddick, J.C., Van Kranendonk, M.J., and Ermanovics, I., 1993. U-Pb geochronology of deformation and metamorphism across a central transect of the Early Proterozoic Torngat Orogen, North River map area, Labrador. Canadian Journal of Earth Sciences, **30**: 1470-1489.

Brace, T.D., 1991. Geology, geochemistry and metallogeny of the Archean Florence Lake Group and associated trondhjemitic rocks, Nain Province, Labrador. Unpublished M.Sc. thesis, Memorial Univeristy of Newfoundland, St. John's, Newfoundland, 256 pages.

Brace, T.D., and Wilton, D.H.C., 1989. Preliminary lithological, petrological, and geochemical investigations of the Archean Florence Lake Group, central Labrador. *In* Current Research, Part C. Geological Survey of Canada, Paper 89-1C, pp. 333-334

Brüghman, G.E., Arndt, N.T., Hofmann, A.W., and Tobschall, H.J., 1987. Noble metal abundances in komatiites suites from Alexo, Ontario, and Gorgona Island, Colombia. Geochemica et Cosmochimica Acta, **51**: 2159-2169.

Brüghman, G.E., Naldrett, A.J., Asif, M., Lightfoot, P.C., Gorbachev, N.S., and Federenko, V.A., 1993. Siderophile and chalcophile metals as tracers of the evolution of the Siberian trap in the Noril'sk region, Russia. Geochemica et Cosmochimica Acta, **57**: 2001-2018.

Bucher, K., and Frey, M., 1994. Petrogenesis of Metamorphic Rocks, 6th Edition. Springer-Verlag, 318 pages.

Cadman, A.C., Heaman, L., Tarney, J., Wardle, R., and Krogh, T.E., 1993. U-Pb geochronology and geochemical variation within two Proterozoic mafic dyke swarms, Labrador. Canadian Journal of Earth Sciences, **30**: 1490-1504.

Calon, T.J., and Jamison, W., 1992. Structural evolution of the Eastern Borderland of the Torngat Orogen, Kiki Lake transect, Saglek Fiord area, northern Labrador. Eastern Canadian Shield Onshore-Offshore Transect (ECSOOT) transect meeting, LITHOPROBE Report 32, pp. 90-112.

Calon, T.J., and Jamison, W., 1994. Structural evolution of the Eastern Borderland of the Torngat Orogen, Kiki Lake transect, Saglek Fiord area, northern Labrador. Eastern Canadian Shield Onshore-Offshore Transect (ECSOOT) transect meeting, LITHOPROBE Report 36, pp. 89-99.

Campbell, I.H., and Naldrett, A.J., 1979. The influence of silicate : sulphide ratios on the geochemistry of magmatic sulphides. Economic Geology, **74**: 1503-1505.

Campbell, I.H., and Barnes, S.-J., 1984. A model for the geochemistry of platinum-group elements in magmatic sulphide deposits. Canadian Mineralogist, **22**: 151-160

Campbell, I.H., Naldrett, A.J., and Barnes, S.J., 1983. A model for the origin of platinum-rich horizons in the Bushveld and Stillwater Complexes. Journal of Petrology, **24**: 133-165.

Chai, G., and Naldrett, A.J., 1992a. Petrology and geochemistry of the Jinchuan ultramafic intrusion: cumulate of a high-Mg basaltic magma. Journal of Petrology, **33**: 1-27.

Chai, G., and Naldrett, A.J., 1992b. PGE mineralization of the Jinchuan Ni-Cu sulfide deposit, N.W. China. Economic Geology, **87**: 1475-1495.

Chai, G., and Eckstrand, O.R., 1994. Origin of the Sudbury Igneous Complex, Ontario-differentiation of two separate magmas. *In* Current Research, Part C. Geological Survey of Canada, Paper 93-1C, 219-230.

Chai, G., Eckstrand, O.R., and Grégoire, C., 1993. Platinum group element concentrations in the Sudbury rocks, Ontario-an indicator of petrogenesis. *In* Current Research, Part C. Geological Survey of Canada, Paper 93-1C, pp. 287-293.

Chase, C.G., and Patchett, P.J., 1988. Stored mafic/ultramafic crust and early Archean mantle depletion. Earth and Planetary Science Letters, **91**: 66-72.

Chaussidon, M., and Lorand, J.P., 1990. Sulphur isotope composition of orogenic spinel lherzolite massifs from Ariege, northeastern Pyrenees, France: An ion microprobe study. Geochemica et Cosmochimica Acta, **54**: 2835-2846.

Chaussidon, M., Albarede, F., and Sheppard, S.M.F., 1987. Sulphur isotope heterogeneity in the mantle from ion microprobe measurements of sulphide inclusions in diamond. Nature, **330**: 242-244.

Chaussidon, M., Albarede, F., and Sheppard, S.M.F., 1987. Sulphur isotope heterogeneity in the mantle from ion microprobe analyses of micro-sulfide inclusions. Earth and Planetary Science Letters, **92**: 144-156.

Collerson, K.D., 1983. The Archean gneiss complex of northern Labrador. 2. Mineral ages, secondary isochrons, and diffusion of strontium during polymetamorphism of the Uivak gneiss. Canadian Journal of Earth Sciences, **20**: 707-718.

Collerson, K., 1991. New field and isotopic constraints on the evolution of early Archean gneisses in Northern Labrador. Eastern Canadian Shield Onshore-Offshore Transect (ECSOOT) Transect Meeting, LITHOPROBE Report 27, pp. 96-101.

Collerson, K.D., McCulloch, M.T., and Bridgwater, D., 1984. Nd and Sr isotopic crustal contamination patterns in an Archean meta-basic dyke from northern Labrador. Geochemica et Cosmochimica Acta, **48**: 71-83.

Collerson, K.D., McCulloch, M.T., and Nutman, A.P., 1989. Sr and Nd isotope systematics of polymetamorphic Archean gneisses from southern West Greenland and northern Labrador. Canadian Journal of Earth Sciences, **26**: 446-466.

Collerson, K.D., Campbell, L.M., Weaver, B.L., and Palacz, Z.A., 1991. Evidence for extreme mantle fractionation in early Archean ultramafic rocks from northern Labrador. Nature, **349**: 209-214.

Connelly, J.N., and Ryan, B., 1992. U-Pb constraints on the thermotectonic history of the Nain area. Eastern Canadian Shield Onshore-Offshore Transect (ECSOOT) Transect Meeting, LITHOPROBE Report 32, pp. 137-144.

Connelly, J.N., and Ryan, B., 1994. Late Archean and Paleoproterozoic events in the central Nain craton. Eastern Canadian Shield Onshore-Offshore Transect (ECSOOT) Transect Meeting, LITHOPROBE Report 36, pp. 53-61.

Corfu, F., and Lightfoot, P.C., 1996. U-Pb geochronology of the Sublayer environment, Sudbury Igneous Complex, Ontario. Economic Geology, **91**: 1263-1269

Crocket, J.H., Fleet, M.F., and Stone, W.E., 1992. Experimental partitioning of osmium, iridium, and gold between basalt melt and sulfide liquid at 1300°C. Australian Journal of Earth Sciences, **39**: 427-432.

DePaolo, D.J., 1981. Neodymium isotopes in the Colorado Front Range and crust-mantle evolution in the Proterozoic. Nature, **291**: 193-196.

DePaolo, D.J., 1985. Isotopic studies in mafic magma chambers: I. The Kiglapait Intrusion, Labrador. Journal of Petrology, **26**: 925-951.

DePaolo, D.J., 1988. Neodymium Isotope Geochemistry: An Introduction. Springer-Verlag, 187 pages.

DePaolo, D.J., and Wasserburg, G.J., 1976. Nd isotopic variations and petrogenetic models. Geophysical Research Letters, **3**: 249-252.

DePaolo, D.J., Perry, F.V., and Baldridge, W.S., 1992. Crustal versus mantle sources of granitic magma: a two parameter model based on Nd isotopic studies. Transactions of the Royal Society (Edinburgh), Earth Sciences, **83**: 435-446

Eckstrand, O.R., 1996. Nickel-copper sulphide. *In* Geology of Canadian Mineral Deposit Types. *Edited by* O.R. Eckstrand, W.D. Sinclair, and R.I. Thorpe. Geological Survey of Canada, Geology of Canada, number 8, pages 584-605.

Edwards, S.J., 1990. Harzburgites and refractory melts in the Lewis Hills Massif, Bay of Islands Ophiolite Complex: The base and precious metals story. Canadian Mineralogist, **28**: 537-552.

Ellis, S., Beaumont, C., and Wardle, R.J., 1997. Comparisons between process-based models and the inferred evolution of the Torngat and New Quebec Orogens. Eastern Canadian Shield Onshore-Offshore Transect (ECSOOT) Transect Meeting, LITHOPROBE Report 61, pp. 64-76.

Emslie, R.F., 1978. Elsonian magmatism in Labrador: age, characteristics and tectonic setting. Canadian Journal of Earth Sciences, **15**: 438-453.

Emslie, R.F., 1980. Geology and petrology of the Harp Lake Complex, central Labrador: An example of Elsonian magmatism. Geological Survey of Canada, Bulletin 293, 136 pages.

Emslie, R.F., 1985. Proterozoic anorthosite massifs. *In* The Deep Crust in the North Atlantic Provinces. *Edited by* A.C. Tobi and J.L.R. Touret. D. Reidel Publishing Company, pp. 39-60.

Emslie, R.F., 1991. Granitoids of rapakivi-anorthosite and related associations. Precambrian Research, **51**: 173-192.

Emslie, R.F., 1996. Troctolitic rocks of the Reid Brook Intrusion, Nain Plutonic Suite, Voisey Bay area, Labrador. *In* Current Research, Part C. Geological Survey of Canada, Paper 96-1, pp. 183-196.

Emslie, R.F., and Russell, W.J., 1988. Umiakovik Lake batholith and other felsic intrusions, Okakh Bay area, Labrador. *In* Current Research, Part C. Geological Survey of Canada, Paper 88-1C, pp. 27-35.

Emslie, R.F., and Thériault, R.J., 1991. Sm-Nd and Rb-Sr isotopic characteristics of ferrodiorites and related rocks associated with anorthosite complexes, central Labrador. GAC/MAC Annual Meeting, Toronto, May 1991. Program with Abstracts, **16**: A34.

Emslie, R.F., and Loveridge, W.D., 1992. Flourite bearing early and middle Proterozoic granites, Okak Bay area, Labrador: geochronology, geochemistry and petrogenesis. Lithos, **28**: 87-109.

Emslie, R.F., and Hegner, E., 1993. Reconnaissance isotopic geochemistry of anorthosite-mangerite-charnockite-granite (AMCG) complexes, Grenville Province, Canada. Chemical Geology, **106**: 279-298.

Emslie, R.F., and Stirling, J.A.R., 1993. Rapakivi and related granitoids of the Nain Plutonic Suite: geochemistry, mineral assemblages and fluid equilibria. Canadian Mineralogist, **31**: 821-847.

Emslie, R.F., Hamilton, M.A., and Thériault, R.J., 1994. Petrogenesis of a Mid-Proterozoic anorthosite-mangerite-charnockite-granite (AMCG) complex: Isotopic and chemical evidence from the Nain Plutonic Suite. Journal of Geology, **102**: 539-558.

Emslie, R.F., Ermanovics, I., and Ryan, B., 1997. Geology of the northern Nain Plutonic Suite and its envelope rocks, Labrador. *In* Current Research, Part C. Geological Survey of Canada, Paper 97-1C, pp. 223-234.

Ermanovics, I., 1993. Geology of the Hopedale Block, southern Nain Province, and the adjacent Proterozoic terranes, Labrador, Newfoundland. Geological Survey of Canada, Memoir 431, 161 pages.

Ermanovics, I., and Raudsepp, M., 1979. Geology of the Hopedale block of the eastern Nain Province, Labrador. *In* Current Research, Part B . Geological Survey of Canada Paper, 79-1B, pp. 341-348.

Ermanovics, I., and Ryan, B., 1990. Early Proterozoic orogenic activity adjacent to the Hopedale block of southern Nain Province. Geoscience Canada, **17**: 397-301.

Ermanovics, I., and Van Kranendonk, M.J., 1990. The Torngat Orogen in the North River-Nutak transect area of the Nain and Churchill provinces. Geoscience Canada, **17**: 279-283.

Ermanovics, I.F., Van Kranendonk, M., Corriveau, L., Mengel, F., Bridgwater, D., Sherlock, R., 1989. The Boundary zone of the Nain-Churchill provinces in the North-River-Nutak map areas, Labrador. *In* Current Research, Part C. Geological Survey of Canada, Paper 89-1C, pp. 385-394.

Farmer, G.L., and DePaolo, D.J., 1984. Origin of Mesozoic and Tertiary granite in the western United States and implications for Pre-Mesozoic crustal structure 2. Nd and Sr isotopic studies of unmineralized and Cu- and Mo-mineralized granites in the Precambrian craton. Journal of Geophysical Research, **89, #B12**: 10141-10160.

Farmer, G.L., Perry, F.V., Semken, S., Crowe, B., Curtis, D., and DePaolo, D.J., 1989. Isotopic evidence on the structure and origin of subcontinental lithospheric mantle in southern Nevada. Journal of Geophysical Research, **94, #B6**: 7885-7898.

Faure, G., 1986. Principles of Isotope Geology, 2nd edition. John Wiley and Sons, 589 pages.

Faure, G., and Powell, J.L., 1972. Strontium Isotope Geology. Springer-Verlag, 188p.

Federenko, V.A., 1994. Evolution of magmatism as reflected in the volcanic sequence of the Noril'sk region. *In* Proceedings of the Sudbury-Noril'sk Symposium. *Edited by* P.C. Lightfoot and A.J. Naldrett. Ontario Geological Survey Special Volume 5, pp. 171-183.

Feininger, T., and Ermanovics, I., 1994. Geophysical interpretation of the Torngat Orogen along the North River-Nutak transect, Labrador. Canadian Journal of Earth Sciences, **31**: 722-727.

Finn, G.C., 1989. Rb-Sr geochronology of the Archean Maggo gneiss from the Hopedale block, Nain Province, Labrador. Canadian Journal of Earth Sciences, **26**: 2512-2522.

Geist, D.J., Frost, C.D., Kolker, A., and Frost, B.R., 1989. A geochemical study of magmatism across a major terrane boundary: Sr and Nd isotopes in Proterozoic granitoids of the southern Laramie Range, Wyoming. Journal of Geology, **97**: 331-342.

Geist, D.J. Frost, C.D., and Kolker, A., 1990. Sr and Nd isotopic constraints on the origin of the Laramie Anorthosite Complex, Wyoming. American Mineralogist, **75**: 13-20.

Godlevsky, M.N., and Grinecko, L., 1968. Some data on the isotopic composition of sulfur in the sulfides of the Noril'sk deposit. Geochemistry, **1**: 335-341.

Gower, C.F., and Ryan, A.B., 1986. Proterozoic evolution of the Grenville Province and adjacent Makkovik Province in eastern-central Labrador. *In* The Grenville Province. *Edited by* J.M. Moore, A. Davidson and A.J. Baer. Geological Association of Canada, Special Paper 31, pages 281-296.

Gower, C.F., Flanagan, M.J., Kerr, A., and Bailey, D.G., 1982. The geology of the Kaipokok-Big River area, Central Mineral Belt, Labrador. Newfoundland Department of Mines and Energy, Mineral Development Division, Report 82-7, 77 pages.

Gower, C.F., James, D.T., Nunn, G.A.G., and Wardle, R.J., 1995. The Eastern Grenville Province. *In* The Geology and Mineral Deposits of Labrador: A guide for the Exploration Geologist (Compiled by R.J. Wardle). Newfoundland Department of Natural Resources-Center for Earth Resources Research Report, pp. 73-101.

Grant, R.W., and Bite, A., 1984. Sudbury quartz diorite Offset dikes. *In* The Geology and Ore Deposits of the Sudbury Structure. *Edited by* E.G. Pye, A.J. Naldrett and P.E. Giblin. Ontario Geological Survey Special Volume 1, pages 275-300.

Greene, B.A., 1972. Geological map of Labrador. Newfoundland Department of Mines, Agriculture and Resources, Mineral Resources Division.

Gresham, J.J., and Loftus-Hills, G.D., 1981. The geology of the Kambalda nickel field, Western Australia. Economic Geology, **76**: 1373-1416.

Grineko, L.N., 1985. Sources of sulfur of the nickeliferous and barren gabbro-dolerite intrusions of the northwest Siberian platform. International Geology Review, **27**: 695-708.

Groves, D.I., Barrett, F.M., and McQueen, K.G., 1979. The relative roles of magmatic segregation, volcanic exhalation and regional metamorphism in the generation of volcanic-associated nickel ores of Western Australia. Canadian Mineralogist, **17**: 319-336.

Groves, D.I., Korkiakoski, E.A., McNaughton, N.J., Lesher, C.M., and Cowden, A., 1986. Thermal erosion by komatiites at Kambalda, Western Australia and the genesis of nickel ores. Nature, **319**: 136-139.

Hamilton, M.A., 1994. Tholeiitic and weakly alkalic basaltic volcanism of the Mugford Group, northern Labrador: preliminary geochemical results. *In* Current Research, Part C. Geological Survey of Canada, Report 1994-1C, pp. 333-342.

Hamilton, M.A.,1997. New U–Pb geochronological results from the Mesoproterozoic Nain Plutonic Suite, Labrador, and implications for the origin and emplacement of massif anorthosites and related rocks. COPENA conference Abstracts and proceedings, Trondheim, Norway, 2 pages.

Hamilton, M.A., and Shirey, S.B., 1992. Nd and Sr isotopic variations in anorthositic rocks of the Nain Plutonic Suite, Labrador. American Geophysical Union, 1992 Spring Meeting Abstracts, EOS Supplement, **74**: 355.

Hamilton, M.A., Emslie, R.F., and Roddick, J.C., 1994. Detailed emplacement chronology of the Mid-Proterozoic Nain Plutonic Suite, Labrador: insights from U-Pb systematics in zircon and badelleyite. Eighth International Conference on Cosmochronology and Isotope Geology. United States Geological Survey Circular 1107, p. 124.

Hamilton, M.A., Emslie, R.F., and Ryan, B., 1998. U-Pb evidence for Paleoproterozoic anorthositic and granitoid magmatism predating the emplacement of the Mesoproterozoic Nain Plutonic Suite, Labrador. GAC/MAC Annual Meeting, Quebec City, 1998, Program with Abstracts, p. A-71.

Hart, S.R., 1984. A large-scale isotope anomaly in the Southern Hemisphere mantle. Nature, **309**: 753-757.

Hart, S.R., 1988. Heterogeneous mantle domains: signatures, genesis and mixing chronologies. Earth and Planetary Science Letters, **90**: 273-296.

Hill, R.E.T., Barnes, S.J., Gole, M.J., and Dowling, S.E., 1995. The volcanology of komatiites as deduced from field relationships in the Norseman-Wiluna greenstone belt, Western Australia. Lithos, **34**: 159-188.

Hoatson, D.M., and Keays, R.R., 1989. Formation of platiniferous horizons by crystal fractionation and magma mixing in the Munni Munni layered intrusion, West Pilbara Block, Western Australia. Economic Geology, **84**: 1775-1804.

Hoefs, J., 1980. Stable Isotope Geochemistry, 2nd edition. Springer-Verlag, 208 pages.

Hoffman, P.F., 1988. United plates of America, the birth of a craton: Early Proterozoic assembly and growth of Laurentia. Annual Reviews in Earth and Planetary Science, **16**: 543-603.

Hofmann, A.W., 1988. Chemical differentiation of the Earth: the relationship between mantle, continental crust, and oceanic crust. Earth and Planetary Science Letters, **90**: 297-314.

Huang, W.L., and Williams, R.J., 1980. Melting relations portions of the system Fe-S-Si-O to 32kb with to the nature of the mantle core boundary (abs.). Lunar and Planetary Science XI, Lunar and Planetary Institute, Houston: 486-488.

Huppert, H.E., and Sparks, R.S.J., 1985. Cooling and contamination of mafic and ultramafic magmas during ascent through continental crust. Earth and Planetary Science Letters, **74**: 371-386.

Huppert, H.E., Sparks, R.S.J., Turner, J.S., and Arndt, N.T., 1984. Emplacement and cooling of komatiite lavas. Nature, **309**: 19-22.

Irvine, T.N., 1975. Crystallization sequences in the Muskox intrusion and other layered intrusions-II. Origin of chromitite layers and similar deposits of other magmatic ores. Geochemica et Cosmochimica Acta, **39**: 991-1020.

Irvine, T.N., and Baragar, W.R.A., 1971. A guide to the chemical classification of the common volcanic rocks. Canadian Journal of Earth Sciences, **8**: 523-548.

Jackson, S.L., Fryer, B.J., Gosse, W., Healey, D.C., Longerich, H.P., and Strong, D.F., 1990. Determination of the precious metals by inductively coupled plasma-mass spectrometry (ICP-MS) with nickel sulphide fire-assay collection and tellurium coprecipitation. Chemical Geology, **83**: 119-132.

James, D.T., 1993. Geology of the Ashuanipi Complex in western Labrador. Newfoundland Department of Mines and Energy, Open File Maps 93-17 and 93-18.

James, D.T., 1995. The Superior Province. *In* The Geology and Mineral Deposits of Labrador: A guide for the Exploration Geologist (Compiled by R.J. Wardle). Newfoundland Department of Natural Resources-Center for Earth Resources Research Report, pp. 24-25.

James, D.T., 1997. The Archean Hunt River greeenstone belt, Hopedale Block, eastern Labrador (NTS 13/7 and 13N/10): Geology and exploration potential. *In* Current Research. Newfoundland Department of Mines and Energy, Geological Survey Branch, Report 97-1, pp. 9-27.

James, D.T., and Mahoney, K.L., 1993. Structural, metamorphic and intrusive relationships in the hinterland of the eastern Churchill Province, western Labrador. *In* Current Research. Newfoundland Department of Mines and Energy, Geological Survey Branch, Report 93-1, pp. 371-385.

James, D.T., Connelly, J.N., Wasteneys, H.A., and Kilfoil, G.J., 1996a. Paleoproterozoic lithotectonic divisions of the southeastern Churchill Province, western Labrador. Canadian Journal of Earth Sciences, **33**: 216-230.

James, D.T., Miller, R.R., Patey, R.P., and Thibodeau, S., 1996b. Geology and mineral potential of the Archean Florence Lake greenstone belt, Hopedale Block (Nain Province), eastern Labrador. *In* Current Research. Newfoundland Department of Natural Resources, Geological Survey Branch, Report, 96-1, pp. 85-107.

James, D.T., Krogh, T., and Kamo, S., 1997. Evolution of Archean supracrustal sequences in the Hopedale Block, southern Nain Province (Labrador): Preliminary U-Pb geochronological data. Eastern Canadian Shield Onshore-Offshore Transect (ECSOOT) Transect Meeting, LITHOPROBE Report 61, pp. 135-156.

Jamison, W., and Calon, T.J., 1995. Structural geology of the Ramah Disturbed Belt, Torngat Orogen, Labrador. Eastern Canadian Shield Onshore-Offshore Transect (ECSOOT) transect meeting, LITHOPROBE Report 45, pp. 90-109.

Jenner, G.A., Longerich, H.P., Jackson, S.E., Fryer, B.J. 1990. ICP-MS- A powerful tool for high-precision trace-element analysis in Earth Sciences: Evidence from analysis of selected U.S.G.S. reference samples. Chemical Geology, **83**: 133-148.

Jensen, L.S., 1976. A new cation plot for classifying subalkalic volcanic rocks. Ontario Division of Mines, Miscellaneous Paper 66.

Jochum, K.P., McDonough, W.F., Palme, H., and Spettel, B., 1989. Compositional constraints on the continental lithospheric mantle from trace elements in spinel peridotite xenoliths. Nature, **340**: 548-550.

Kamo, S.J., Gower, C.F., and Krogh, T.E., 1989. Birthdate for the Iapetus Ocean? A precise U-Pb badelleyite age for the Long Range dykes, southeast Labrador. Geology, 17: 602-605

Kerr, A., 1994. Early Proterozoic magmatic suites of the eastern Central Mineral Belt (Makkovik Province, Labrador: Geology, geochemistry and mineral potential. Newfoundland Department of Natural Resources, Geological Survey Branch, Report 94-3, 149 pages.

Kerr, A., 1998. Petrology of magmatic sulphide mineralization in northern Labrador: Preliminary results. *In* Current Research. Newfoundland Department of Mines and Energy, Geological Survey Branch, Report 98-1, pp. 53-75.

Kerr, A., and Fryer, B.J., 1990. Sources of Early and Middle Proterozoic magmas in the Makkovik Province, Labrador: Evidence from Nd isotope data. *In* Mid-Proterozoic Laurentia-Baltica. *Edited by* C.F. Gower, T. Rivers and B. Ryan. Geological Association of Canada, Special Paper 38, pp. 53-64.

Kerr, A., and Smith, J.L., 1997. The search for magmatic Ni-Cu-Co mineralization in northern Labrador: A summary of active exploration programs. *In* Current Research, Newfoundland Department of Mines and Energy, Geological Survey, Report 97-1, pp. 73-91.

Knight, I., and Morgan, W.C., 1981. The Aphebian Ramah Group, Northern Labrador. *In* Proterozoic Basins of Canada. *Edited by* F.H.A. Campbell. Geological Survey of Canada, Paper 81-10, pages 313-330.

Kolker, A., Lindsley, D.H., and Hanson, G.N., 1990. Geochemical evolution of the Maloin Ranch pluton, Laramie Anorthosite Complex, Wyoming: Trace elements and petrogenetic models. American Mineralogist, **75**: 572-588.

Krogh, T.E., and Davis, G.L, 1973. The significance of inherited zircons on the age and origin of igneous rocks-an investigation of the Labrador adamellites. Carnegie Institution of Washington Yearbook, **72**: 610-613.

Krogh, T.E., McNutt, R.H., and Davis, G.L., 1982. Two high precision U-Pb zircon ages for the Sudbury Nickel Irruptive. Canadian Journal of Earth Sciences, **19**: 723-728.

Krogh, T.E., Davis, D.W., and Corfu, F., 1984. Precise U-Pb zircon and baddelleyite ages for the Sudbury Area. *In* The Geology and Ore Deposits of the Sudbury Structure. *Edited by* E.G. Pye, A.J. Naldrett and P.E. Giblin. Ontario Geological Survey Special Volume 1, pages 431-446..

Kuo, H-Y., and Crocket, J.H., 1979. Rare earth elements in the Sudbury Nickel Irruptive: comparison with layered gabbros and implications for nickel irruptive petrogenesis. Economic Geology, **79**: 590-605.

Kyser, T.K., 1986. Stable isotope variations in the mantle. *In* Stable Isotope Geochemistry in High Temperature Geological Processes. *Edited by* J.W. Valley, H.P. Taylor, Jr., and J.R. O'Neil. Mineralogical Society of America, Reviews in Mineralogy, Volume 16, pp. 141-164.

Kyser, T.K., 1990. Stable isotopes in the continental lithospheric mantle. *In* Continental Mantle. *Edited by* M.A. Menzies. Oxford Mongraphs on Geology and Geophysics, Oxford Press, Oxford, pp. 127-156.

Lambert, D.D., Foster, J.G., Frick, L.R., Li, C., and Naldrett, A.J., 1997. Re-Os isotopic systematics of the Voisey's Bay Ni-Cu-Co magmatic ore system, Labrador, Canada. American Geophysical Union, Fall Meeting, San Francisco, Electronic Program with Abstracts.

Lesher, C.M., 1989. Komatiite-associated nickel sulfide deposits. *In* Ore Deposition Associated with Magmas. *Edited by* J.A. Whitney and A.J. Naldrett. Society of Economic Geologists, Reviews in Economic Geology Volume 4, pp. 45-102.

Lesher, C.M., and Groves, D.I., 1986. Controls on the formation of komatiite-associated nickel-copper sulfide deposits. *In* Geology and Metallogeny of Copper Deposits. *Edited By* G.H. Friedrich, A.D. Genkin, A.J. Naldrett, J.D. Ridge and R.H. Sillitoe. Society for Geology Applied to Ore Deposits Special Publication 4. Springer-Verlag, Heidelberg, pp. 43-62.

Lesher, C.M., and Campbell, I.H., 1993. Geochemical and fluid dynamic modeling of compositional variations in Archean komatiite-hosted nickel sulfide ores in western Australia. Economic Geology, **88**: 804-816.

Lesher, C.M., and Arndt, N.T., 1995. REE and Nd isotope geochemistry, petrogenesis and volcanic evolution of contaminated komatiites at Kambalda, Western Australia. Lithos, **34**: 127-157.

Lesher, C.M., Arndt, N.T., and Groves, D.I., 1984. Genesis of komatiite-associated nickel sulphide deposits at Kambalda, Western Australia: a distal volcanic model. *In* Sulphide Deposits in Mafic and Ultramafic Rocks. *Edited by* D.L. Buchanan and M.J. Jones, Institution of Mining and Metallurgy, London, pages 70-80.

Li, C., and Naldrett, A.J., 1998. Melting reaction of gneiss xenoliths in the Voisey's Bay Complex: Evidence for crustal assimilation. GAC/MAC Annual Meeting, Quebec City, May 1998. Electronic Program with Abstracts.

Li, C., Naldrett, A.J., Coats, C.J.A., and Johannessen, P., 1992. Platinum, palladium, gold, and copper-rich stringers at the Stratchona mine, Sudbury: Their enrichment by fractionation of a sulfide liquid. Economic Geology, **87**: 1584-1598.

Likhachev, A.P., 1994. Ore-bearing intrusions of the Noril'sk region. *In* Proceedings of the Sudbury-Noril'sk Symposium. *Edited by* P.C. Lightfoot and A.J. Naldrett. Ontario Geological Survey Special Volume 5, pp. 185-201.

Lightfoot, P.C., 1996. The giant nickel deposits at Sudbury and Noril'sk. Program with Abstracts, Prospectors and Developers Association of Canada, 64th Annual Meeting, Sudbury, pp. 57-58.

Lightfoot, P.C., 1998. Geological and geochemical relationships in the Reid Brook Intrusive Complex, Labrador: Exploration strategies for Magmatic Ni-Cu-Co ores at Voisey's Bay. Pathways to Discovery 98, Extended Abstracts Volume, pp. 26-29.

Lightfoot, P.C., Naldrett, A.J., Gorbachev, N.S., Doherty, W., and Federenko, V.A., 1990. Geochemistry of the Siberian Trap of the Noril'sk area, USSR, with implications for the relative contributions of crust and mantle to flood basalt magmatism. Contributions to Mineralogy and Petrology, **104**: 631-644.

Lightfoot, P.C., Naldrett, A.J., Gorbachev, N.S., Federenko, V.A., Hawkesworth, C.J., Hergt, J., and Doherty, W., 1994. Chemostratigraphy of Siberian Trap lavas, Noril'sk district, Russia: Implications for the source of flood basalt magmas and their associated Ni-Cu Mineralization. *In* Proceedings of the Sudbury-Noril'sk Symposium. *Edited by* P.C. Lightfoot and A.J. Naldrett. Ontario Geological Survey Special Volume 5, pp. 283-312.

Lightfoot, P.C., Doherty, W., Farrell, K., Keays, R.R., Moore, M., and Pekeski, D., 1997a. Geochemistry of the Main Mass, Sublayer, Offsets, and Inclusions from the Sudbury Igneous Complex, Ontario. Ontario Geological Survey, Open File Report 5959, 231 pages.

Lightfoot, P.C., Keays, R.R., Morrison, G.G., Bite, A., and Farrell, K., 1997b. Geochemical relationships in the Sudbury Igneous Complex: Origin of the Main Mass and Offset Dikes. Economic Geology, **92**: 289-307.

Lightfoot, P.C., Keays, R.R., Morrison, G.G., Bite, A., and Farrell, K., 1997c. Geological and geochemical relationships between the Contact Sublayer, inclusions, and the Main Mass of the Sudbury Igneous Complex: A case study of the Whistle Mine Embayment. Economic Geology, **92**: 647-673.

Listerud, W.H., and Meineke, D.G., 1977. Mineral resources of a portion of the Duluth complex and adjacent rocks in St. Louis and Lake counties, northeastern Minnesota. Minnesota Department of Natural Resources, Division of Minerals, Minerals Exploration section, Report 93.

Loney, R.A., and Himmelberg, G.R., 1992. Petrogenesis of the Pd-rich intrusion at Salt Chuck, Prince of Wales Island: An Early Proterozoic Alaskan-type ultramafic body. Canadian Mineralogist, **30**: 1005-1022.

Longerich, H.P. 1995. Analysis of pressed pellets of geological samples using wavelength-dispersive X-ray fluorescence Spectrometry. X-Ray Spectrometry, **24**: 123-136.

Longerich, H.P., Jenner, G.A., Fryer, B.J., and Jackson, S.E., 1990. Inductively coupled plasma-mass spectrometric analysis of geological samples: A critical evaluation base on case studies. Chemical Geology, **83**: 105-118.

Loveridge, W.D., Ermanovics, I.F., and Sullivan, R.W., 1987. U-Pb ages on zircon from the Maggo Gneiss, the Kanairiktok Plutonic suite and the Island Harbour Plutonic Suite, coastal of Labrador, Newfoundland. *In* Radiogenic Age and Isotopic Studies, Report 1. Geological Survey of Canada, Paper 87-2, pp. 59-65.

Lugmair, G.W., and Marti, K., 1978. Lunar initial $^{143}Nd/^{144}Nd$: differential evolution of the lunar crust and mantle. Earth and Planetary Science Letters, **27**: 79-84.

MacLean, W.H., 1969. Liquidus phase relations in the FeS-FeO-Fe_3O_4-SiO_2 systems and their application in geology. Economic Geology, **64**: 865-884.

Mainwaring, P.R., and Naldrett, A.J., 1977. Country-rock assimilation and the genesis of Cu-Ni sulfides in the Waterhen intrusion, Duluth Complex, Minnesota. Economic Geology, **72**: 1269-1284.

Maniar, P.D., and Piccoli, P.M., 1989. Tectonic discrimination of granitoids. Geological Society of America Bulletin, **101**: 635-643.

McDonough, W.F., 1990. Constraints on the composition of the continental lithospheric mantle. Earth and Planetary Science Letters, **101**: 1-18.

Mengel, F., Rivers, T., and Reynolds, P., 1991. Lithotectonic elements and tectonic evolution of the Torngat Orogen, Saglek Fiord, northern Labrador. Canadian Journal of Earth Sciences, **28**: 1407-1423.

Menzies, M.A., 1989. Cratonic, circumcratonic and oceanic mantle domains beneath the western United States. Journal of Geophysical Research, **94, #B6**: 7899-7915.

Menzies, M.A., 1990. Archean, Proterozoic and Phanerozoic lithospheres. *In* Continental Mantle. *Edited by* M.A. Menzies. Oxford Mongraphs on Geology and Geophysics, Oxford Press, Oxford, pp. 67-86.

Meschede, M., 1986. A method of discriminating between different types of mid-ocean ridge basalts and continental tholeiites with the Nb-Zr-Y diagram. Chemical Geology, **56**: 207-218.

Morgan, W.C., 1975. Geology of the Precambrian Ramah Group and basement rocks in the Nachvak Fiord-Saglek Fiord area, north Labrador. Geological Survey of Canada, Paper 74-54, 42 pages.

Morse, S.A., 1969. The Kiglapait Layered Intrusion, Labrador. Geological Society of America Memoir 112, 204 pages.

Morse, S.A., 1983. Reconnaissance geology of the Bird Lake massif, Labrador. *In* Nain Anorthosite Project, Labrador: Field Report, 1981. *Edited by* S.A. Morse. Department of Geology and Geography, University of Massachusetts, Contribution No. 40: pp. 37-41.

Muir, T.L., 1984. The Sudbury Structure: Considerations and models for an endogenic origin. *In* The Geology and Ore Deposits of the Sudbury Structure. *Edited by* E.G. Pye, A.J. Naldrett and P.E. Giblin. Ontario Geological Survey Special Volume 1, pages 449-489.

Muir, T.L, and Peredery, W.V., 1984. The Onaping Formation. *In* The Geology and Ore Deposits of the Sudbury Structure. *Edited by* E.G. Pye, A.J. Naldrett and P.E. Giblin. Ontario Geological Survey Special Volume 1, pages 139-210.

Naldrett, A.J., 1973. Nickel sulphide deposit-their classification and genesis with special emphasis on deposits of volcanic association. Transactions of the Canadian Institute of Mining and Metallurgy, 76: 183-201.

Naldrett, A.J., 1981. Nickel sulfide deposits: Classification, composition and genesis. Economic Geology 75th Anniversary Volume, pp. 628-685.

Naldrett, A.J., 1984a. Ni-Cu ores of the Sudbury Igneous Complex-Introduction. *In* The Geology and Ore Deposits of the Sudbury Structure. *Edited by* E.G. Pye, A.J. Naldrett and P.E. Giblin. Ontario Geological Survey Special Volume 1, pages 302-306.

Naldrett, A.J., 1984b. Mineralogy and composition of the Sudbury ores. *In* The Geology and Ore Deposits of the Sudbury Structure. *Edited by* E.G. Pye, A.J. Naldrett and P.E. Giblin. Ontario Geological Survey Special Volume 1, pages 309-325.

Naldrett, A.J., 1984c. Summary, discussion and synthesis. *In* The Geology and Ore Deposits of the Sudbury Structure. *Edited by* E.G. Pye, A.J. Naldrett and P.E. Giblin. Ontario Geological Survey Special Volume 1, pages 523-569.

Naldrett, A.J., 1989a. Introduction: Magmatic deposits associated with mafic rocks. *In* Ore Deposition Associated with Magmas. *Edited by* J.A. Whitney and A.J. Naldrett. Society of Economic Geologist, Reviews in Economic Geology Volume 4, pp. 1-3.

Naldrett, A.J., 1989b. Sulfide melts: crystallization temperatures, solubilities in silicate melts, and Fe, Ni, and Cu partitioning between basaltic magmas and olivine. *In* Ore Deposition Associated with Magmas. *Edited by* J.A. Whitney and A.J. Naldrett. Society of Economic Geologist, Reviews in Economic Geology Volume 4, pp. 5-20.

Naldrett, A.J., 1989c. Ores associated with flood basalts. *In* Ore Deposition Associated with Magmas. *Edited by* J.A. Whitney and A.J. Naldrett. Society of Economic Geologist, Reviews in Economic Geology Volume 4, pp. 103-118.

Naldrett, A.J., 1989d. Contamination and the origin of the Sudbury structure and its ores. *In* Ore Deposition Associated with Magmas. *Edited by* J.A. Whitney and A.J. Naldrett. Society of Economic Geologist, Reviews in Economic Geology Volume 4, pp. 119-134.

Naldrett, A.J., 1989e. Stratiform PGE deposits in layered intrusions. *In* Ore Deposition Associated with Magmas. *Edited by* J.A. Whitney and A.J. Naldrett. Society of Economic Geologist, Reviews in Economic Geology Volume 4, pp. 135-165.

Naldrett, A.J., 1993. Models for the formation of strata-bound concentrations of platinum group elements in layered intrusions. *In* Mineral Deposit Modeling, Geological Association of Canada Special Paper 40. *Edited by* R.V. Kirkham, W.D. Sinclair, R.I. Thorpe, and J.M. Duke. Pp. 373-387.

Naldrett, A.J., 1997. Key factors in the genesis of Noril'sk, Sudbury, Jinchuan, Voisey's Bay and other world-class Ni-Cu-PGE deposits: implications for Exploration. Australian Journal of Earth Sciences, 44: 283-315.

Naldrett, A.J., and Duke, J.M., 1980. Platinum metals in magmatic sulfide ores. Science, 208: 1417-1424.

Naldrett, A.J., and MacDonald, A.J., 1980. Tectonic settings of Ni-Cu sulphide ores: their importance in genesis and exploration. *In* The Continental Crust and Its Mineral Deposits. *Edited by* D.W. Strangway. Geological Association of Canada Special Paper 20: pp. 633-657.

Naldrett, A.J., and Hewins, R.H., 1984. The Main Mass of the Sudbury Igneous Complex. *In* The Geology and Ore Deposits of the Sudbury Structure. *Edited by* E.G. Pye, A.J. Naldrett and P.E. Giblin. Ontario Geological Survey Special Volume 1, pages 235-251.

Naldrett, A.J., and von Gruenewaldt, G.,1989. Association of platinum-group elements with chromitite in layered intrusions and ophiolite complexes. Economic Geology, **84**: 180-187.

Naldrett, A.J., Hoffman, E.L., Green, A.H., Chien-Lin, C., and Naldrett, S.R., (1979). The composition of Ni-sulphide ores, with particular reference to their content of PGE and Au. Canadian Mineralogist, **17**: 403-415.

Naldrett, A.J., Hewins, R.H., Dressler, B.O., and Rao, B.V., 1984a. The Contact Sublayer of the Sudbury Igneous Complex. *In* The Geology and Ore Deposits of the Sudbury Structure. *Edited by* E.G. Pye, A.J. Naldrett and P.E. Giblin. Ontario Geological Survey Special Volume 1, pages 253-274.

Naldrett, A.J., Duke, J.M., Lightfoot, P.C., and Thompson, J.F.H., 1984b. Quantitative modeling of segregation of magmatic sulphides: an exploration guide. CIM Bulletin, 77, **#864**: 46-56.

Naldrett, A.J., Rao, B.V., and Evensen, N.M., 1986. Contamination at Sudbury and its role in ore formation. *In* Metallogeny of Basic and Ultrabasic Rocks. *Edited by* M.J. Gallagher, R.A. Ixer, C.R. Neary and H.M. Pritchard. Institution of Mining and Metallurgy, London, Special Publication, pp. 75-92.

Naldrett, A.J., Brügmann, G.E., and Wilson, A.H., 1990. Models for the concentration of PGE in layered intrusions. Canadian Mineralogist, **28**: 389-408.

Naldrett, A.J., Lightfoot, P.C., Federenko, V.A., Gorbachev, N.S., and Doherty, W., 1992. Geology and geochemistry of intrusives and flood basalts of the Noril'sk region, USSR with implications for the origin of Ni-Cu ores. Economic Geology, **87**: 975-1004.

Naldrett, A.J., Federenko, V.A., Lightfoot, P.C., Kunilov, V.A., Gorbachev, N.S., Doherty, W., and Johan, Z., 1995. Ni-Cu-PGE deposits of the Noril'sk region, Siberia: Their formation as conduits for flood basalt volcanism. Institute of Mining and Metallurgy Transactions, **104**: B18-B36.

Naldrett, A.J., Keats, H., Sparkes, K., and Moore, R., 1996a. Geology of the Voisey's Bay Ni-Cu-Co Deposit, Labrador, Canada. Exploration and Mining Geology, **5**: 169-179.

Naldrett, A.J., Federenko, V.A., Mohammed, A., Lin, S., Kunilov, V.E., Stekhin, A.I., Lightfoot, P.C., and Gorbachev, N.S., 1996b. Controls on the composition of Ni-Cu sulfide deposits as illustrated by those at Noril'sk, Siberia. Economic Geology, **91**: 751-773.

Naldrett, A.J., Li, C., Krstic, S., Asif, M., and Amelin, Y., 1998. The Voisey's Bay Ni-Cu-Co deposit, Labrador, Canada. GAC/MAC Annual Meeting, Quebec City, 1998, Program with Abstracts, p. A-133.

Nutman, A.P., and Collerson, K.D., 1991. Very early Archean crustal-accretion complexes preserved in North Atlantic craton. Geology, **19**: 791-794.

Nutman, A.P., Fryer, B.J., and Bridgwater, D., 1989. The early Archaean Nulliak (supracrustal) assemblage, northern Labrador. Canadian Journal of Earth Sciences, **26**: 2159-2168.

Ohmoto, H., 1972. Systematics of sulfur and carbon isotopes in hydrothermal ore deposits. Economic Geology, **67**: 551-578.

Ohmoto, H., 1986. Stable isotope geochemistry of ore deposits. *In* Stable Isotope Geochemistry in High Temperature Geological Processes. *Edited by* J.W. Valley, H.P. Taylor, Jr., and J.R. O'Neil. Mineralogical Society of America, Reviews in Mineralogy, Volume 16, pp. 491-559.

Ohmoto, H., and Rye, R.O., 1979. Isotopes of sulfur and carbon. *In* Geochemistry of Hydrothermal Ore Deposits, 2nd edition. *Edited by* H.L. Barnes. J. Wiley and Sons, pp. 509-567.

Patchett, P.J., 1989. Radiogenic isotope geochemistry of the rare earth elements. *In* Geochemistry and Mineralogy of Rare Earth Elements. *Edited by* B.R. Lipin and G.A. McKay. Mineralogical Society of America, Reviews in Mineralogy, Volume 21, pp. 25-44.

Peach, C.L., Mathez, E.A., Keays, R.R., and Reeves, S.J., 1994. Experimentally determined sulfide melt-silicate partition coefficients for iridium and palladium. Chemical Geology, **117**: 361-377.

Pearce, J.A., and Cann, J.R. 1973. Tectonic setting of basic volcanic rocks determined using trace element analyses. Earth and Planetary Science Letters, **19**: 290-300.

Pearce, J.A., and Norry, M.J., 1979. Petrogenetic implications of Ti, Zr, Y, and Nb variations in volcanic rocks. Contributions to Mineralogy and Petrology, **69**: 33-47.

Pearce, J.A., Harris, N.B.W., and Tindle, A.G., 1984. Trace element discrimination diagrams for the tectonic interpretation of granitic rocks. Journal of Petrology, **25**: 956-983.

Peredery, W.V., and geological staff, 1982. Geology and nickel sulfide deposits of the Thompson belt, Manitoba. *In* Precambrian Sulphide Deposits, H.S. Robinson Memorial Volume. *Edited by* R.W. Hutchinson, C.D. Spence, and J.M. Franklin. Geological Association of Canada, Special Paper 25, pp. 165-209.

Peredery, W.V., and Morrison, G.G., 1984. Discussion on the origin of the Sudbury. *In* The Geology and Ore Deposits of the Sudbury Structure. *Edited by* E.G. Pye, A.J. Naldrett and P.E. Giblin. Ontario Geological Survey Special Volume 1, pages 491-511.

Piercey, S.J., 1997. The OKG Ni-Cu-Co prospect, Umiakoviarusek Lake Region of Labrador: A possible analogue to the Voisey's Bay deposit? Fifth National Students' Conference on Northern Studies, Program with Abstracts, p. 80.

Piercey, S.J., and Wilton, D.H.C., 1998. Application of REE, isotopic and PGE geochemistry in the search for Voisey's Bay-type Ni-Cu-Co sulfide deposits: A case study from the OKG prospect, Umiakoviarusek Lake Region, Labrador. Pathways to Discovery 98, Extended Abstracts Volume, p. 241.

Potts, P.J., Tindle, A.G., and Webb, P.J. 1992. Geochemical Reference Material Compositions. CRC Press Inc., Boca Raton, 313 pages.

Rafter, T.A., 1965. Recent sulphur isotope measurements on a variety of specimens examined in New Zealand. Bulletin of Volcanology, **28**: 3-20.

Rajamani, V. and Naldrett, A.J., 1978. Partitioning of Fe, Co, Ni and Cu between sulphide liquid and basaltic melts and the composition of Ni-Cu sulphide deposits. Economic Geology: **73**: 82-93.

Ripley, E.M., 1981. Sulfur isotopic abundances of the Dunka Road Cu-Ni deposit, Duluth Complex, Minnesota. Economic Geology, **76**: 610-620.

Ripley, E.M., 1983. Sulfide mineralogy and sulfur isotope geochemistry of layered sills in the Deer Lake Complex, Minnesota. Mineralium Deposita, **18**: 3-15.

Ripley, E.M., 1986. Applications of stable isotope studies to problems of magmatic sulfide ore genesis with special reference to the Duluth Complex, Minnesota. *In* Geology and Metallogeny of Copper Deposits. *Edited By* G.H. Friedrich, A.D. Genkin, A.J. Naldrett, J.D. Ridge and R.H. Sillitoe. Society for Geology Applied to Ore Deposits Special Publication 4. Springer-Verlag, Heidelberg, pp. 25-42.

Ripley, E.M., 1990a. Platinum-group element geochemistry of Cu-Ni mineralization in the Basal Zone of the Babbitt deposit, Duluth Complex, Minnesota. Economic Geology, **85**: 830-841.

Ripley, E.M., 1990b. Se/S ratios of the Virginia Formation and Cu-Ni sulfide mineralization in the Babbitt area, Duluth Complex, Minnesota. Economic Geology, **85**: 1935-1940.

Ripley, E.M., Young-Rok, P., Li, C., and Naldrett, A.J., 1997. Sulfur and oxygen isotopic studies of the Voisey's Bay Ni-Cu-Co deposit, Labrador, Canada. American Geophysical Union, Fall Meeting, San Francisco, Electronic Program with Abstracts.

Rivers, T., 1997. Lithotectonic elements of the Grenville Province: review and tectonic implications. Precambrian Research, **86**: 117-154.

Rivers, T., Martingnole, J., Gower, C.F., and Davidson, A., 1989. New tectonic divisions of the Grenville Province, southeast Canadian Shield. Tectonics, **8**: 63-84.

Rollinson, H.R., 1993. Using Geochemical Data: evaluation, presentation, interpretation. Longman Scientific and Technical, John Wiley and Sons, 352 pages.

Rousell, D.H., 1984a. Onwatin and Chelmsford Formations. *In* The Geology and Ore Deposits of the Sudbury Structure. *Edited by* E.G. Pye, A.J. Naldrett and P.E. Giblin. Ontario Geological Survey Special Volume 1, pages 211-218.

Rousell, D.H., 1984b. Mineralization in the Whitewater Group. *In* The Geology and Ore Deposits of the Sudbury Structure. *Edited by* E.G. Pye, A.J. Naldrett and P.E. Giblin. Ontario Geological Survey Special Volume 1, pages 219-232.

Ryan, A.B., 1984. Regional geology of the central part of the Central Mineral Belt, Labrador. Newfoundland Department of Mines and Energy, Mineral Development Division, Memoir 3, 185 pages.

Ryan, B., 1990a. Preliminary geological map of the Nain Plutonic Suite and surrounding rocks (Nain-Nutak, NTS 14SW). Newfoundland Department of Mines and Energy, Map 90-44.

Ryan, B., 1990b. Does the Labrador-Québec border area of the Rae (Churchill) Province preserve vestiges of an Archean history? Geoscience Canada, **17**: 255-259

Ryan, B., 1991a. New perspectives on the Nain Plutonic Suite and its country rocks. *In* Current Research. Newfoundland Department of Mines and Energy, Geological Survey Branch, Report 91-1, pp. 231-255.

Ryan, B., 1991b. Makhavinekh Lake pluton, Labrador, Canada: geological setting, subdivisions, mode of emplacement and comparison with Finnish rapakivi granites. Precambrian Research, **51**: 193-225.

Ryan, B., 1993. Further Results of mapping gneissic and plutonic rocks of the Nain Bay area, Labrador. *In* Current Research. Newfoundland Department of Mines and Energy, Geological Survey Branch, Report 93-1, pp. 61-75.

Ryan, B., 1995. Anorthosite-granite (AMCG) suites. *In* The Geology and Mineral Deposits of Labrador: A guide for the Exploration Geologist (Compiled by R.J. Wardle). Newfoundland Department of Natural Resources-Center for Earth Resources Research Report, pp. 53-67.

Ryan, B., 1996. The Voisey's Bay nickel-copper-cobalt deposit, Labrador, Canada: magmatic sulphide in anorogenic troctolitic rocks. Chronique de la Recherche Minére, **#525**: 3-11.

Ryan, B., 1996a. Commentary on the location of the Nain-Churchill boundary in the Nain area. *In* Current Research. Newfoundland Department of Natural Resources, Geological Survey Branch, Report 96-1, pp. 109-129.

Ryan, B., 1997. The Mesoproterozoic Nain Plutonic Suite in eastern Canada, and the setting of the Voisey's Bay Ni-Cu-Co sulphide deposit. Geoscience Canada, **24**: 173-188.

Ryan, T.P., 1996. Final Report on mineral licences 1446M, 1539M and 1582M (OKG Property). Assessment file, Newfoundland Department of Mines and Energy.

Ryan, B., and Lee, D., 1989. Geological map of the Reid Brook area (14D/8), 1: 50000. Newfoundland Department of Mines and Energy, Geological Survey Branch, Open File 89-18.

Ryan, B., and Emslie, R.F., 1994. Pre-Elsonian mafic magmatism in the Nain igneous complex, Labrador: the Bridges layered intrusion-comment. Precambrian Research, **68**: 179-181.

Ryan, B. and Connelly, J.N., 1996: Paleoproterozoic plutonism in the Nain area: similar rocks (but differing origins?) to the Mesoproterozoic Nain Plutonic Suite. *In* Proterozoic Evolution in the North Atlantic Realm. *Complied by* C.F. Gower. COPENA-ECSOOT-IBTA conference, Goose Bay, Labrador, Program and Abstracts, pages 156-157.

Ryan, B., Krogh, T.E., Heaman, L., Scharer, U., Philippe, S., and Oliver, G., 1991. On recent geochronological studies in the Nain Province, Churchill Province, and Nain Plutonic Suite. *In* Current Research. Newfoundland Department of Mines and Energy, Geological Survey Branch, Report 91-1, pp. 257-261.

Ryan, B., Wardle, R., Gower, C., and Nunn, G., 1995. Nickel-copper-sulphide mineralization in Labrador: The Voisey Bay discovery and its exploration implications. *In* Current Research, Newfoundland Department of Mines and Energy, Geological Survey, Report 95-1, pp. 177-204.

Ryan, B., Hynes, A., and Ermanovics, I., 1997. Geology of the Nain Plutonic Suite and its country-rock envelope, Alliger Lake area (NTS 14E/1), Labrador. *In* Current Research. Newfoundland Department of Mines and Energy, Geological Survey Branch, Report 97-1, pp. 29-47.

Ryan, B., Phillips, E., Shwetz, J., and Machado, G., 1998. A tale of more than ten plutons [Geology of the region between Okak Bay and Staghorn Lake, Labrador (parts of NTS Maps 14E/2,7,8)]. *In* Current Research. Newfoundland Department of Mines and Energy, Geological Survey Branch, Report 98-1, pp. 143-171.

Rye, R.O., and Ohmoto, H., 1974. Sulfur and carbons isotopes and ore genesis: A review. Economic Geology, **69**: 826-842.

Schiøtte, L., Compston, W., and Bridgwater, D., 1989a. U-Th-Pb ages of single zircons in Archean supracrustals from Nain Province, Labrador, Canada. Canadian Journal of Earth Sciences, **26**: 2636-2644.

Schiøtte, L., Compston, W., Bridgwater, D., 1989b. Ion probe U-Th-Pb zircon dating of polymetamorphic orthogneiss from northern Labrador, Canada. Canadian Journal of Earth Sciences, **26**: 1533-1556.

Schiøtte, L., Noble, S., and Bridgwater, D., 1990. U-Pb mineral ages from northern Labrador: Possible evidence for interlayering of Early and Middle Archean tectonic slices. Geoscience Canada, **17**: 227-231.

Schiøtte, L., Hansen, B.T., Shirey, S.B., and Bridgwater, D., 1993. Petrological and whole rock isotopic characteristics of tectonically juxtaposed Archean gneisses in the Okak area of the Nain Province, Labrador: relevance for terrane models. Precambrian Research, **63**: 293-323.

Scoates, J.S., and Frost, C.D., 1996. A strontium and neodymium isotopic study of the Laramie anorthosites, Wyoming, USA: Implications for magma chamber processes and the evolution of magma conduits in Proterozoic anorthosites. Geochemica et. Cosmochimica Acta, **60**: 95-107.

Scott, D.J., and Machado, N., 1994. U-Pb geochronology of the Northern Torngat Orogen: Results from work in 1993. Eastern Canadian Shield Onshore-Offshore Transect (ECSOOT)Transect Meeting, LITHOPROBE Report 36, pp. 141-155.

Scott, D.J., and Machado, N., 1995. U-Pb geochronology of the northern Torngat Orogen, Labrador, Canada: A record of Paleoproterozoic magmatism and deformation. Precambrian Research, **70**: 169-190.

Scribbins, B.T., Rae, D.R., and Naldrett, A.J., 1984.Mafic and ultramafic inclusions in the Sublayer of the Sudbury Igneous Complex. Canadian Mineralogist, **22**: 67-75.

Simmons, K.R., Wiebe, R.A., Snyder, G.A., and Simmons, E.C., 1986. U-Pb zircon ages of the Newark Island layered intrusion, Nain Anorthosite Complex, Labrador. Geological Society of America, Abstracts with Program, **18**: 751.

Smyth, W.R., 1976. Geology of the Mugford Group, Northern Labrador. Newfoundland Department of Mines and Energy, Report 76-1, pp. 72-79.

Smyth, W.R., and Knight, I., 1978. Correlation of Aphebian supracrustal sequence, Nain Province, Northern Labrador. *In* Report of Activities for 1977. Newfoundland Department of Mines and Energy, Mineral Development Division, pp. 59-64.

Smyth, W.R., Marten, B.E., and Ryan, A.B., 1978. A major Aphebian-Helikian unconformity within the Central Mineral Belt of Labrador: definition of a new group and metallogenic implications. Canadian Journal of Earth Sciences, **15**: 1954-1966.

Speer, J.A., 1978. The stratigraphy and depositional environment of the Aphebian Snyder Group, Labrador. Canadian Journal of Earth Sciences, **15**: 52-68.

St. Louis, R.M., Nesbitt, B.E., and Morton, R.D., 1986. Geochemistry of platinum-group elements in the Tulameen ultramafic complex, southern British Columbia. Economic Geology, **81**: 961-973.

Steele, T.M., Levin, J., and Copelowitz, I., 1975. The preparation and certification of a reference sample of precious metal ore. National Institute of Metallurgy, South Africa Report 1696, 4 pages.

Stone, W.E., Crocket, J.H, and Fleet, M.E., 1990. Partitioning of palladium, iridium, platinum, and gold between sulfide liquid and basalt melt at 1200°C. Geochemica et Cosmochimica Acta, **54**: 2341-2344.

Strauss, H., 1986. Carbon and sulfur isotopes in Precambrian sediments from the Canadian Shield. Geochemica et Cosmochimica Acta, **50**: 2653-2662.

Strauss, H., 1993. The sulfur isotopic record of Precambrian sulfates: new data and a critical evaluation of the existing record. Precambrian Research, **63**: 225-246.

Streckeisen, A.L., 1975. To each plutonic rocks its proper name. Earth Science Reviews, **12**: 1-33.

Swinden, H.S., Wardle, R.J., Davenport, P.H., Gower, C.F., Kerr, A., Meyer, J.R., Miller, R.R., Nolan, L., Ryan, A.B., and Wilton, D.H.C., 1991. Mineral exploration opportunities in Labrador: A perspective for the 1990's. *In* Current Research. Newfoundland Department of Mines and Energy, Geological Survey Branch, Report 91-1, pp. 349-390.

Swinden, H.S., Jenner, G.A., and Szybinski, Z.A., 1997. Magmatic and tectonic evolution of the Cambrian-Ordovician Laurentian margin of Iapetus: Geochemical and isotopic constraints from the Notre Dame subzone, Newfoundland. *In* The Nature of Magmatism in the Appalachian Orogen. *Edited by* A.K. Sinha, J.B. Whalen, and J.P. Hogan. Geological Society of America Memoir 191, Boulder, Colorado, pp. 337-365.

Taylor, F.C., 1971. A revision of Precambrian structural provinces in northeastern Quebec and northern Labrador. Canadian Journal of Earth Sciences, **8**: 579-584.

Taylor, H.P., 1974. The application of oxygen and hydrogen isotope studies to problems of hydrothermal alteration and ore deposition. Economic Geology, **69**: 843-883.

Taylor, R.P., and Fryer, B.J., 1982. Rare earth element lithogeochemistry of granitoid mineral deposits. CIM Bulletin, **77, #861**: 1-9.

Taylor, S.R., Campbell, I.H., McCulloch, M.T., and McLennan, S.M., 1984. A lower crustal origin for massif type anorthosites. Science, **311**: 372-374.

Thériault, R.J., and Ermanovics, I., 1997. Sm-Nd isotopic and geochemical characterization of the Paleoproterozoic Torngat Orogen, Labrador, Canada. Precambrian Research, **81**: 15-35.

Thériault, R.J., Hamilton, M.A., and Ermanovics, I., 1994. Nd isotopic and geochemical investigations in the Torngat Orogen, North River-Nutak Area. Eastern Canadian Shield Onshore-Offshore Transect (ECSOOT) Transect Meeting, LITHOPROBE Report 45, pp. 83-89.

Thériault, R.D., Barnes, S.-J., and Severson, M.J., 1997. The influence of country-rock assimilation and silicate to sulfide ratios (R factor) on the genesis of the Dunka Road Cu-Ni-platinum-group element deposit, Duluth Complex, Minnesota. Canadian Journal of Earth Sciences, **34**: 375-389.

Thompson, J.F.H., and Naldrett, A.J., 1984. Sulfide-silicate reactions as a guide to Ni-Cu-Co mineralization in central Main. *In* Sulphide Deposits in Mafic and Ultramafic Rocks. *Edited by* D.L. Buchanan and M.J. Jones, Institution of Mining and Metallurgy, London, pages 103-113.

Van Kranendonk, M.J., 1996. Tectonic evolution of the Paleoproterozoic Torngat Orogen: evidence from pressure-temperature-time-deformation paths in the North River area. Tectonics, **15**: 843-869.

Van Kranendonk, M.J., and Ermanovics, I., 1990. Structural evolution of the Hudsonian Torngat Orogen in the North River map area, Labrador: Evidence for east-west transpressive collision of Nain and Rae continental blocks. Geoscience Canada, 17: 283-288.

Van Kranendonk, M.J., and Wardle, R.J., 1994. Geological synthesis and musings on possible subduction-accretion models in the formation of the northern Torngat Orogen. Eastern Canadian Shield Onshore-Offshore Transect (ECSOOT) Transect Meeting, LITHOPROBE Report 36. pp. 32-80.

Van Kranendonk, M.J., and Wardle, R.J., 1997. Crustal-scale flexural slip folding during late tectonic amplification of an orogenic boundary peturbation in the Paleoproterozoic Torngat Orogen, northeastern Canada. Canadian Journal of Earth Sciences, **34**: 1545-1565.

Van Kranendonk, M.J., Wardle, R.J., Mengel, F.C., Ryan, B., and Rivers, T., 1992. Lithotectonic divisions of the northern part of the Torngat Orogen, Labrador, Quebec and N.W.T. Eastern Canadian Shield Onshore-Offshore Transect (ECSOOT) Transect Meeting, LITHOPROBE Report 32, pp. 21-31.

Walker, R.J., Morgan, J.W., Naldrett, A.J., Li, C., and Fassett, J., 1991. Re-Os isotopic systematics of the Ni-Cu sulfide ores, Sudbury Igneous Complex, Ontario: evidence for a major crustal component. Earth and Planetary Science Letters, **105**: 416-429.

Walker, R.J., Morgan, J.W., Hanski, E., and Smolkin, V.K., 1994. The role of the Re-Os isotope system in deciphering the origin of magmatic sulfide ores: a tale of three ores. *In* Proceedings of the Sudbury-Noril'sk Symposium. *Edited by* P.C. Lightfoot and A.J. Naldrett. Ontario Geological Survey Special Volume 5, pp. 343-356.

Wardle, R.J., 1983. Nain-Churchill Province cross-section, Nachvak Fiord, northern Labrador. *In* Current Research. Newfoundland Department of Mines and Energy, Mineral Development Division, Report 83-1, pp. 68-69.

Wardle, R.J., 1995. Introduction. *In* The Geology and Mineral Deposits of Labrador: A guide for the Exploration Geologist (Compiled by R.J. Wardle). Newfoundland Department of Natural Resources-Center for Earth Resources Research Report, pp. 2-14.

Wardle, R.J., and Bailey, D.G., 1981. Early Proterozoic sequences in Labrador. *In* Proterozoic Basins of Canada. *Edited by* F.H.A. Campbell. Geological Survey of Canada, Paper 81-10, pp. 331-358.

Wardle, R.J., and Wilton, D.H.C., 1995. The Nain Province. *In* The Geology and Mineral Deposits of Labrador: A guide for the Exploration Geologist (Compiled by R.J. Wardle). Newfoundland Department of Natural Resources-Center for Earth Resources Research Report, pp. 14-24.

Wardle, R.J., Rivers, T., Gower, C.F., Nunn, G.A.G., and Thomas, A., 1986. The northeastern Grenville Province: new insights. *In* The Grenville Province. *Edited by* J.M. Moore, A. Davidson, and A.J. Baer. Geological Association of Canada, Special Paper 31, pp. 13-29.

Wardle, R.J., Ryan, B., and Ermanovics, I., 1990a. The eastern Churchill Province, Torngat and New Québec orogens: An overview. Geoscience Canada, **17**: 217-222.

Wardle, R.J., Ryan, B., Nunn, G.A.G., and Mengel, F., 1990b. Labrador segment of the Trans-Hudson Orogen: crustal development through oblique convergence and collision. *In* The Trans-Hudson Orogen of North America: Lithotectonic Correlations and Evolution. *Edited by* J. Lewry and M. Stauffer. Geological Association of Canada, Special Paper 37, pp. 353-370

Wardle, R.J., Swinden, S., and James, D.T., 1995a. The Southeastern Churchill Province. *In* The Geology and Mineral Deposits of Labrador: A guide for the Exploration Geologist (Compiled by R.J. Wardle). Newfoundland Department of Natural Resources-Center for Earth Resources Research Report, pp. 26-42.

Wardle, R.J., Wilton, D.H.C., and Kerr, A., 1995b. The Makkovik Province. *In* The Geology and Mineral Deposits of Labrador: A guide for the Exploration Geologist (Compiled by R.J. Wardle). Newfoundland Department of Natural Resources-Center for Earth Resources Research Report, pp. 42-50.

Wasteneys, H., Wardle, R., Krogh, T., and Ermanovics, I., 1995. Preliminary U-Pb geochronology of the Ingrid Group and basement rocks in the Hopedale Block in the vicinity of the southern Nain craton/Torngat Orogen boundary. Eastern Canadian Shield Onshore-Offshore Transect (ECSOOT) transect Meeting, LITHOPROBE Report 45, pp. 206-216.

Wells, C.S., 1997. A Documentation and Study of Sulphide Mineralization in the Hettasch Intrusion, Labrador. Unpublished B.Sc. (Hons.) thesis, Memorial University of Newfoundland, St. John's, Newfoundland, 89 pages.

Wheeler, E.P., 1942. Anorthosite and associated rocks about Nain, Labrador. Journal of Geology, **50**: 611-642.

Wheeler, E.P., 1960. Anorthosite-adamellite complex of Nain, Labrador. Geological Society of America Bulletin, **71**: 1755-1762.

Wiebe, R.A., 1980. Commingling of contrasted magmas in the plutonic environment: examples from the Nain anorthosite complex. Journal of Geology, **88**: 197-209.

Wiebe, R.A., 1988. Structural and magmatic evolution of a magma chamber: the Newark Island layered intrusion, Nain, Labrador. Journal of Petrology, **29**: 311-411.

Wiebe, R.A., 1990. Dioritic rocks in the Nain Complex, Labrador. Schweizerische Mineralogische und Petrographische Mitteilungen, **70**: 199-208.

Wilson, M.R., Kyser, T.K., and Fagan, R., 1996. Sulfur isotope systematics and platinum group element behaviour in REE-enriched metasomatic fluids: A study of mantle xenoliths from Dish Hill, California, USA. Geochemica et Cosmochimica Acta, **60**: 1933-1942.

Wilton, D.H.C., 1994. The Mugford Group, northern Labrador, revisited: Notes from a Continuing study. *In* Current Research. Newfoundland Department of Mines and Energy, Geological Survey Branch, Report 94-1, pp. 409-414.

Wilton, D.H.C., 1996a. Metallogenic overview of the Nain Province, northern Labrador. CIM Bulletin, **89**: 43-52.

Wilton, D.H.C., 1996b. Metallogeny of the Central Mineral Belt and adjacent Archean basement, Labrador. Department of Mines and Energy, Geological Survey Branch, Mineral Resource Report 8, 178 pages.

Wilton, D.H.C., 1996c. Palaeoproterozoic, ~1.88-2.0Ga, organic matter from the Mugford/Kaumajet Mountain Group, northern Labrador. Precambrian Research, 77: 131-141.

Wilton, D.H.C., and Baker, N.W., 1996. The OKG Ni-Cu-Co showing: A new discovery in the Nain Plutonic Suite of northern Labrador. Geological Association of Canada, Program with Abstracts, **21**: A-102.

Wilton, D.H.C., Churchill, R.A., and Saunders, J.K., 1993. Stratigraphy and metallogeny of the Cod Island and Calm Cove formations, Mugford Group, northern Labrador. *In* Current Research. Newfoundland Department of Mines and Energy, Geological Survey Branch, Report 93-1, pp. 91-102.

Wilton, D.H.C., Archibald, S.M., Hussey, A.M., and Butler, Jr., R.W., 1994. Metallogeny of the Ramah Group: Discovery of a new Pb-Zn exploration target, northern Labrador. *In* Current Research. Newfoundland Department of Mines and Energy, Geological Survey Branch, Report 94-1, pp. 415-428.

Xue, S., and Morse, S.A., 1993. Geochemistry of the Nain massif anorthosite, Labrador: magma diversity in five intrusions. Geochemica et Cosmochimica Acta, **57**: 3925-3948.

Yu, Y., and Morse, S.A., 1993. $^{40}Ar/^{39}Ar$ chronology of the Nain anorthosites, Canada. Canadian Journal of Earth Sciences, **30**: 1166-1178.

Zhou, M.F., Lightfoot, P.C., Keays, R.R., Moore, M.L., and Morrison, G.G., 1997. Petrogenetic significance of chromian spinels from the Sudbury Igneous Complex, Ontario, Canada. Canadian Journal of Earth Sciences, **34**: 1405-1419.

Zientek, M.L., Likhachev, A.P., Kunilov, V.E., Barnes, S.-J., Meier, A.L., Carlson, R.R., Briggs, P.H., Fries, T.L., and Adrian, B.M., 1994. Cumulus processes and the composition of magmatic ore deposits: Examples from the Talnakh district, Russia. *In* Proceedings of the Sudbury-Noril'sk Symposium. *Edited by* P.C. Lightfoot and A.J. Naldrett. Ontario Geological Survey Special Volume 5, pp. 373-392.

Zindler, A., and Hart, S.R., 1986. Chemical geodynamics. Annual Reviews in Earth and Planetary Science, **14**: 493-571.

Zindler, A., Jagoutz, E., and Goldstein, S., 1982. Nd, Sr, and Pb isotopic systematics in a three-component mantle: a new perspective. Nature, **298**: 519-523.

Appendix A: Analytical Methods

A.1 Lithogeochemical and Sulphide Sampling Protocol

A key to understanding the geology, petrography and geochemistry of any geologic terrain is adequate sampling to provide a representatives of that given geologic terrain. This study primarily involved bulk sampling of the surface units during field mapping, and augmentation of the data set by subsurface samples and assay pulps, particularly for the mineralized units and the pyroxenitic rocks. The purpose of sampling in this manner was two fold, to provide an adequate spatial representation of the surface petrography and geochemistry (1); and subsurface examples from diamond drill-hole OKG 96-09 to correlate chemistry, petrology and mineralization styles relative to the style of surface mineralization (2). Unlike many hydrothermal deposit types (e.g. VMS, porphyry-Cu), alteration is not that significant in magmatic Ni–Cu sulphide mineralization and the mineralized rocks are relatively unaltered. In contrast, the Paleoproterozoic plutonic rocks exhibit fresh to minor greenschist facies assemblages (cf. Chapter 3); however, the effects of this alteration on chemistry appear minimal (cf. Chapter 4). On the other hand, the granulite-amphibolite assemblages of the Nain

Province gneisses are particularly sensitive to mobile elements, but unlikely disturbed with respect to the immobile elements.

Sulphide bearing samples were collected from rusty gossanous zones on surface, and augmented by assay pulps and samples in the subsurface. Very little petrographic variation exists on the microscopic scale between the subsurface and surface examples, and the style of mineralization is likely coherent between the two settings. Sampling was carried out to provide *representative samples*, and "high grading", typical of prospecting-type sampling, was not carried done to avoid biasing of the data set towards non-representative values.

Lithogeochemical and sulphide samples collected were approximately two fist sizes in diameter (e.g. 15-40cm), and were used for petrographic and geochemical analyses.

Samples were cut using a diamond-clad saw to remove weathered edges, and the resultant sample core was cut into a series of 2x2cm tall by 4-5cm long blocks which were used for thin sections and formation of rock powders. Samples of similar lithologic character (i.e. anorthositic, granitoid, pyroxenitic, sulphides) were cut and crushed together to minimize intergroup contamination between samples. For instance, all samples of anorthositic to noritic character were cut/crushed together, while all other sample groups were cut/crushed at a different time and together.

The cut blocks were crushed in a steel-jaw crusher forming numerous 0.5-1cm chips, which were subsequently crushed in a tungsten-carbide bowl and puck assembly to

produce powders of 200 mesh/74 μ size. All such powders were used in all the whole-rock geochemical techniques (e.g. XRF, ICP-MS (REE and PGE), and radiogenic isotopes). Chips from the steel-jaw crusher stage were used to hand pick sulphide separates for sulphur isotope analyses. The following subsections provide details for the analytical techniques employed in this thesis.

A.2 Trace Element Analyses

A.2.1 X-Ray Fluorescence

Selected trace element analyses were carried out at Memorial University of Newfoundland, Department of Earth Sciences, X-Ray Fluorescence (XRF) Lab using a Fisons/ARL (Mississauga, Ontario, Canada) model 8420+ sequential wavelength-dispersive X-ray spectrometer on pressed powder pellets. Quantitative determinations by this XRF pressed powder pellet method include the following elements: P_2O_5, S, Cl, K_2O, CaO, Sc, TiO_2, V, Cr, MnO, Fe_2O_3, Ni, Cu, Zn, Ga, As, Rb, Sr, Y, Zr, Nb, Ba, Ce, Pb, Th, and U (Figure A1-1; cf. Longerich, 1995). Semi-quantitative determinations include the following: Na_2O, MgO Al_2O_3, and SiO_2 (Figure A1-1; cf. Longerich, 1995). Although semi-quantitative the major element analyses provide a good approximation of the major element compositions, and can be quite useful.

Pressed powder pellet preparation is outlined by Longerich (1995) and is as follows:

- 5.00 g of rock powder and 0.70 g of BRP-5933 Bakelite™ phenolic resin (Bakelite Thermosets, Brampton, Ontario, Canada) were placed in a 100 ml glass jar.

- Two 0.5 inch diameter stainless steel ball bearings are added to this mixture and a plastic lid attached. This jar was then placed on a roller mixer for ten minutes so that the resin and powder were thoroughly mixed.
- The resulting mixture was then placed in a Herzog™ (Germany) pellet press (29mm diameter mould) and pressed for 5 seconds at a pressure of 20 tonnes.
- These pellets were placed in an oven for 15 minutes at 200° C and then labeled on the side, which was in contact with the oven tray.

Collection of data was done by automated computer system attached to the XRF. Four quality control reference materials (AGV-1, DNC-1, JG-2, BCR-1), and four internal standards were analyzed with the pressed pellet samples (Longerich, 1995). Reference materials used were (published values for these standards can be found in Potts *et al.* (1992), Jenner *et al.* (1990) and Longerich *et al.* (1990)), include: 1) BHVO-1, DTS-1, United States Geological Survey (USGS) reference standards (basalt and dunite respectively); 2) SY-2 and SY-3, syenite from the Canadian Certified Reference Materials Project (CCRMP); and 3) PACS-1, National Research Council of Canada reference material.

Raw data obtained from the XRF were translated into worksheet format using an in-house written program and data reduction was carried out using commercial spreadsheet software on a personal computer (Longerich, 1995).

Limits of detection vary depending on the elemental group in consideration. For pressed powder pellets Longerich (1995) quotes detection limits ranging from 0.6-0.7

ppm for Rb, Y, and Nb up to *ca.* 100ppm for Na_2O and MgO; detection limits for other elements in the trace package are given in Longerich (1995).

A.2.1.1 Test for Precision and Accuracy

Ten replicate analyses were performed on standard DNC-1 (diabase) from the period of September 1997 to February 1998. Precision is generally good (3-7% RSD) to excellent (0-3% RSD) with minor exceptions. Replicate determinations have yielded excellent precision for all elements with the exception of V, Ba and Rb, which have good precision (Table A.1). Other exceptions include Nb which has a high RSD = 9.74%; however, the average concentration of Nb in DNC-1 (1.9ppm), lies below the limit of quantification (2.3ppm; Table A.1); Longerich (1995) has quoted an RSD = 0.16% for Nb determinations over the long term via XRF analysis at MUN. Problematic elements include Sc and V which have high RSD values (Table A.1); however, Longerich (1995) quotes RSD values for these elements at 4.11% and 1.44%, respectively, and these should be better representatives than those quoted in this thesis.

Accuracy of the ten replicate analyses of DNC-1 are reported relative to Longerich's (1995) long term average for this standard at the MUN XRF lab. Excellent accuracy was returned for MgO, SiO_2, P_2O_5, K_2O, CaO, TiO_2, MnO, Fe_2O_3, V, C, Cr, Ga, Sr, and Zr (0-3% relative difference); while good accuracy was returned for Na_2O, Al_2O_3, S, Sc, Ni, Rb, Y, and Nb (3-7% relative difference; Table A.1). Although determinations

for the light major elements (Na_2O, MgO, Al_2O_3, and SiO_2) show good to excellent accuracy relative to Longerich (1995), it must be noted that these determinations are semi-quantitative (Longerich, 1995); however, for the descriptive purposes that they are used for in this thesis, the semi-quantitative determinations are valid for the interpretations provided.

A.2.2 Inductively Coupled Plasma Mass Spectrometry (ICP-MS)

The trace elements (Y, Zr, Nb, Hf, Ta, Th) and REE (La, Ce, Pr, Nd, Pr, Nd, Sm, Eu, Tb, Dy, Ho, Er, Tm, Yb, Lu,) were prepared by the sodium peroxide (Na_2O_2) sinter method of Longerich *et al.* (1990), followed by subsequent analysis on a SCIEX Elan (now Perkin-Elmer) model 250 inductively coupled plasma mass-spectrometer (ICP-MS). The Na_2O_2 sinter method was chosen because it provided an excellent means of breaking down many silicate minerals that are difficult to digest using the HF-nitric method (Longerich *et al.*, 1990). The Na_2O_2 sample preparation procedure (after Longerich *et al.* 1990) involves initial addition of 0.2 g of powdered rock sample and 0.8 g of Na_2O_2 into a Ni crucible which is mixed well and sintered in a muffle furnace at 480^{0}C for 1.5 hours. The crucibles are removed from the furnace, covered, and cooled for approximately 20 minutes while 10 ml of distilled water is added carefully, a few drops at a time. The cover is then rinsed into the crucible and the mixture was quantitatively transferred to a centrifuge tube where distilled water is added to make the total volume 30 ml. This mixture is then centrifuged for 15 minutes.

The residue remaining in the crucible is dissolved in 2.5 ml of 8 N HNO_3 and 1ml of 2% oxalic acid. The crucible was then rinsed with 0.2 N HNO_3 and this is added to the centrifuge tube. The solution is then transferred to a clean centrifuge tube and diluted with distilled water to a final volume of 50 g.

The solutions are further diluted prior to ICP-MS analysis, and 2 g of sample solution and 8g of 0.2 N HNO_3 are accurately weighted into a 12 ml (16mm) test tube. This produces a final solution with a rock concentration of approximately 0.7g/kg. The solution is mixed with an on-line standard addition spike at approximately 1 part spike to 2 parts sample giving a solution which reaches the nebulizer that has concentration of 0.5 g rock/kg solution. This results in a solution, for a typical continental crustal silicate rock, which has < 200 ppm total dissolved solids.

Detection limits for the Na_2O_2 sinter method are provided by Longerich *et al.* (1990), and are quoted in two forms: the calibration blank limit of detection (CLD) and the mean limit of detection of the reagent blanks (MLD). The prior of these, the CLD is a measure of instrument performance and often does not account for possible contamination by reagents and sample preparation equipment; thus, the MLD is generally a better measure of the detection limit because it does account for the latter (Longerich *et al.*, 1990). Using either the MLD or CLD, good to excellent detection limits exist, generally ranging from 0.009 ppm (CLD) and 0.006 ppm (MLD) for Lu to 0.07 ppm (CLD) and 0.14 ppm (MLD) for Nd; other CLD and MLD for the sinter method are provided in Longerich *et al.* (1990).

A.2.2.1 Test for Precision and Accuracy

Over the period of October 1996 to March 1998 seven analyses were carried out by the sinter method and analyzed by ICP-MS on standard MRG-1 (gabbro). Precision for all REE and Th range from good (0-3% RSD) to excellent (3-7% RSD). Excellent precision was shown for La, Ce, Pr, Gd, Tb Dy; while good precision was shown for Nd, Sm, Eu, Ho, Er, Tm, Yb, Lu, and Th (Table A.2). When compared to the long term average determinations over thirty runs from June 1992 to March 1993, the average values have relative differences (RD) that range from good (3-7% RD) to excellent (0-3% RD). Excellent accuracy was returned for La, Nd, Sm, Eu, Gd, Tb, Ho, Er, Tm, Yb, Lu; while good accuracy was returned for Ce, Pr, Dy, and Th (Table A.2).

A.3 Platinum Group Elements (PGE)

All sulphide samples and certain silicate samples (pyroxenites, amphibolites, mineralized anorthosites) were analyzed for PGE (Os, Ir, Ru, Rh, Pt, Pd) and Au contents as a means of comparing their possible descriptive and genetic origins. Determinations of the PGE were carried out using ICP-MS following the Ni-S fire assay pre-preparation method of Jackson *et al.* (1990).

The preparation technique for the Ni-S fire assay of Jackson *et al.* (1990) is outlined below. Ten grams of 74μ/200 mesh rock powder along with 6.70g of Na_2CO_3, 13.30g of $Na_2B_4O_7$, 5.00g of SiO_2, 1.00g of Ni, and 0.6g S are placed in a clay crucible,

mixed thoroughly, and then fused in a preheated oven at 1050°C for 1.25 hours. Following heating the crucible is removed and cooled at room temperature, when cool the clay crucible is then broken open and the Ni-S bead is retrieved.

The Ni-S bead is then transferred to a 30ml Oak Ridge screw-top Teflon centrifuge tube and 15ml of concentrated hydrochloric acid is added. This mixture is placed on an aluminum block holder and heated on a hot plate at ca. 150°C to dissolve the bead. Following dissolution, the top of the Teflon tube is removed and the solution is warmed for 1 hour and then allowed to cool until warm. Following this 2.5ml of 200ppm Te solution and 1ml $SnCl_2$ is added and the solution is diluted with 8-10ml of nanopure water. The solution is then boiled for 30 minutes to coagulate the PGE bearing precipitate.

The remaining solution is filtered through a Millipore filter system using a Whatman 0.4μ/243 mesh cellulose nitrate membrane filter paper and the filtered precipitate is washed with nanopure water. The filter paper and precipitate are transferred to a Teflon tube and 1ml of concentrated nitric acid and 0.5ml hydrochloric acid are added. The tube is then capped and warmed slowly to dissolve the filter paper and the precipitate contents. Following dissolution the Teflon tube is cooled and the solution is transferred to a 50ml polypropylene bottle and diluted with 20g of nanopure water. The remaining solution is then analyzed by the ICP-MS.

Detection limits for the PGE are quoted in Jackson *et al.* (1990) and range from 0.10 ppb for Ir to 8.75 ppb for Au; other detection limits for the PGE include (all in ppb):

Ru = 0.57, Rh = 0.14, Pd = 1.68, Os = 0.26, and Pt = 1.48. Determinations of precision were not undertaken as part of this study since only one run of PGE analyses were carried out. However, long term data collected by Jackson et al. (1990) quote RSD values for all the PGE and Au that are excellent (1.3-2.1% RSD) with the exception of Os (RSD = 11.4%); which is due to the volatility of Os via ICP-MS analysis (Jackson *et al.*, 1990). Accuracy has been determined in this study on one analysis of SARM-7 and shows RD values, relative to Steele *et al.*'s (1975) values for SARM-7, that range from 1.14 - 7.92% for Ru, Rh, Pd, Ir, and Pt; with high values for Os (RD = 27.97%) and Au (RD = 28.54%; Table A.3). Comparisons to average values quoted by Wilson *et al.* (1996) show higher RD variations ranging from 0.76% for Pt to 14.38% for Os (Table A.3). Further details on precision, accuracy and detection limits can be found in Jackson *et al.* (1990).

A.4 Radiogenic Isotopes

Rubidum-strontium and samarium-neodymium isotopic determinations were all carried out at the Atlantic Universities Radiogenic Isotope Facility (AURIF) at Memorial University of Newfoundland. Sample preparation and analytical methods are after Horan (internal report, AURIF, 1997) and are presented below.

Powdered rock samples as outlined above are accurately weighed to the fifth decimal place and dissolved with 1ml each of 8N nitric and 2X hydrofluoric acids and let to rest and reflux for a period of 2 to 7 days. Over this time period the samples that are high in aluminum and magnesium are checked for fluoride precipitates, and if present are redissolved prior to ion exchange chemistry. Following the above, the samples are split

and accurately weighed into isotopic concentration and isotopic dilution fractions. Isotopic dilution fractions are spiked with an accurately weighed Oak Ridge National Labs ^{150}Nd-^{147}Sm mixed spike based on the whole rock Nd concentration; while Rb and Sr spikes and spike weights are based on Sr whole rock concentration.

Following spiking the samples are loaded onto EICHROM TRU-Spec resin for initial Rb/Sr and REE group separations. If Rb and Sr separates are needed, they are collected immediately using 2B 3N HNO_3, the REE are collected after using 2B (double Teflon bottle distilled) H_2O. All collected fractions are evaporated to dryness. The Rb/Sr fractions are then loaded onto EICHROM SR-Spec resins, which retain Sr and remove all other trace elements. Rb is collected immediately after loading the sample with 2B 3N HNO_3 and the Sr is collected using 2B H_2O. The REE fractions are then placed in Teflon columns, which separate Nd and Sm; while the Rb-Sr sample fractions are ready for thermal-ionization mass spectrometry (TI-MS) measurements.

The Sm and Nd separations are carried out by taking the isotope concentration and dilution fractions and carefully pipetting them onto Teflon columns using 2X 0.15N HCl. The first of the LREE (e.g. La, Ce) are stripped using 2X 0.15N HCl. The isotopic concentration and dilution Nd fractions are collected next using 2X 0.17N HCl; while the isotope dilution Sm fraction is collected using 2X 0.50N HCl. Two drops of 1N phosphoric acid are added to each of the three collected fractions. All three fractions are then evaporated down to a single drop ready for thermal-ionization mass-spectrometry (TI-MS).

Isotopic determinations were carried out using VG MM30B and Finnigan MAT 262V thermal-ionization mass spectrometers. Rubidum fractions were analyzed using the VG MM30B TI-MS using a single peak jumping routine on either Daly or Faraday detectors to collect the $^{87}Rb/^{85}Rb$ ratio. The Sr fraction was loaded on outgassed Re double filaments for the Finnigan MAT 262V TIMS. The isotopic composition of the $^{87}Sr/^{86}Sr$ fraction was analyzed using a static Faraday multicollector routine. The isotope dilution Sr fraction is analyzed using a static Faraday multicollector routine to collect both the $^{84}Sr/^{86}Sr$ and $^{87}Sr/^{86}Sr$ ratios with each routine analyzing 5 blocks of data containing 20 scans for a total of 100 scans with on line drift and mass fractionation correction and statistical analysis. The $^{87}Sr/^{86}Sr$ errors are reported to 95% confidence levels (2σ) and are based solely on mass spectrometer measurements. The $^{87}Rb/^{86}Sr$ ratios are calculated with data reduction software created at Memorial University of Newfoundland using commercial spreadsheet software based on measured $^{87}Rb/^{85}Rb$ and $^{84}Sr/^{86}Sr$ spiked ratios.

The $^{87}Rb/^{86}Sr$ reported errors are absolute 2σ and are quadratically added using the 2σ errors for $^{87}Rb/^{85}Rb$ and $^{84}Sr/^{86}Sr$ measured isotopic ratios.

The Nd and Sm fractions were loaded on outgassed Re double filaments for the Finnigan MAT 262V TIMS. The isotopic composition fractions were analyzed using a static Faraday multicollector routine using 5 blocks of 20 scans for a total of 100 scans with on line drift and mass fractionation correction and statistical analysis. The $^{143}Nd/^{144}Nd$ errors are reported to 95% confidence levels (2σ) and are based solely on

mass spectrometer measurements. The $^{147}Sm/^{144}Nd$ ratios are calculated with data reduction software created at Memorial University of Newfoundland using commercial spreadsheet software based on measured $^{147}Sm/^{149}Sm$ and $^{150}Nd/^{144}Nd$ spiked ratios. The $^{147}Sm/^{144}Nd$ reported errors are absolute 2σ and are quadratically added using the 2σ errors for $^{147}Sm/^{149}Sm$ and $^{150}Nd/^{144}Nd$ measured isotopic ratios.

A.5 Sulphur Isotopes

Sulphur isotope determinations were carried out on SO_2 gas extractions from single crystals of sulphide material. The single crystals (pyrrhotite, chalcopyrite, pyrite) were picked from the chips left after crushing of the samples within the steel-jaw crusher. Individual crystals were picked and transferred into glass vials, and where possible duplicates of the samples were collected as well to see if there are in sample variations in the isotopic character of the sulphides.

Sample preparation for gas extraction was carried out at Memorial University of Newfoundland (MUN) and the Ottawa-Carleton Geoscience Centre. At MUN gas sample extractions and $\delta^{34}S$ determinations were carried out following the method outlined by Rafter (1965) and all analyses were carried out on a Finnigan MAT 252 isotope ratio mass spectrometer (IR-MS). Single crystal preparation methods at MUN are as follows: (1) Single crystals are crushed in a ceramic mortar and pestal assembly and the powder returned to their respective glass vials.

(2) The powder from (1), (6-9mg for chalcopyrite, 5-9mg for pyrrhotite, 4-6 mg), is weighed out an transferred to a ceramic mortar and pestal assembly (as above) and mixed with 140-150mg of fired CuO material.

(3) The mixture in (2) is then crushed as was done in step (1)

(4) The resultant crushed mixture of (3) is transferred to a fired, 1.5cm piece of quartz glass tubing ("boat") and each end of the boat is capped with pure quartz wool.

(5) The glass boat along with sulphide is place in a larger quartz glass tube with a piece of quartz wool and copper wire placed in the upper part of the tube assembly.

(6) This combination in (5) is then covered with wax paper to prevent any contamination until ready for combustion on the cryogenic separation line.

The glass tube assemblies with sulphide and CuO were combusted at 1000°C on a cryogenic separation line to remove SO_2 gas following the method of Rafter (1965) Extracted SO_2 gas was analyzed for $^{34}S/^{32}S$ ratios on a Finnigan MAT 252 isotope-ratio mass spectrometer (IR-MS) followed by data processing using a personal computer. Estimated uncertainties of $\delta^{34}S$ using this method are ±0.2‰.

At the Ottawa-Carleton Geoscience Center crushed powders were used to measure $^{34}S/^{32}S$ ratios from SO_2 gasses, by continuous flow elemental-analyzer (EA) IR-MS. Powders from the outlined procedure above, were combusted with vanadium pentoxide on an elemental analyzer followed by gas chromatography separation and subsequent analyses on a Finnigan MAT Delta plus IR-MS though a Conflo split interface. Estimated uncertainties in the $\delta^{34}S$ values by this method are ±0.2‰.

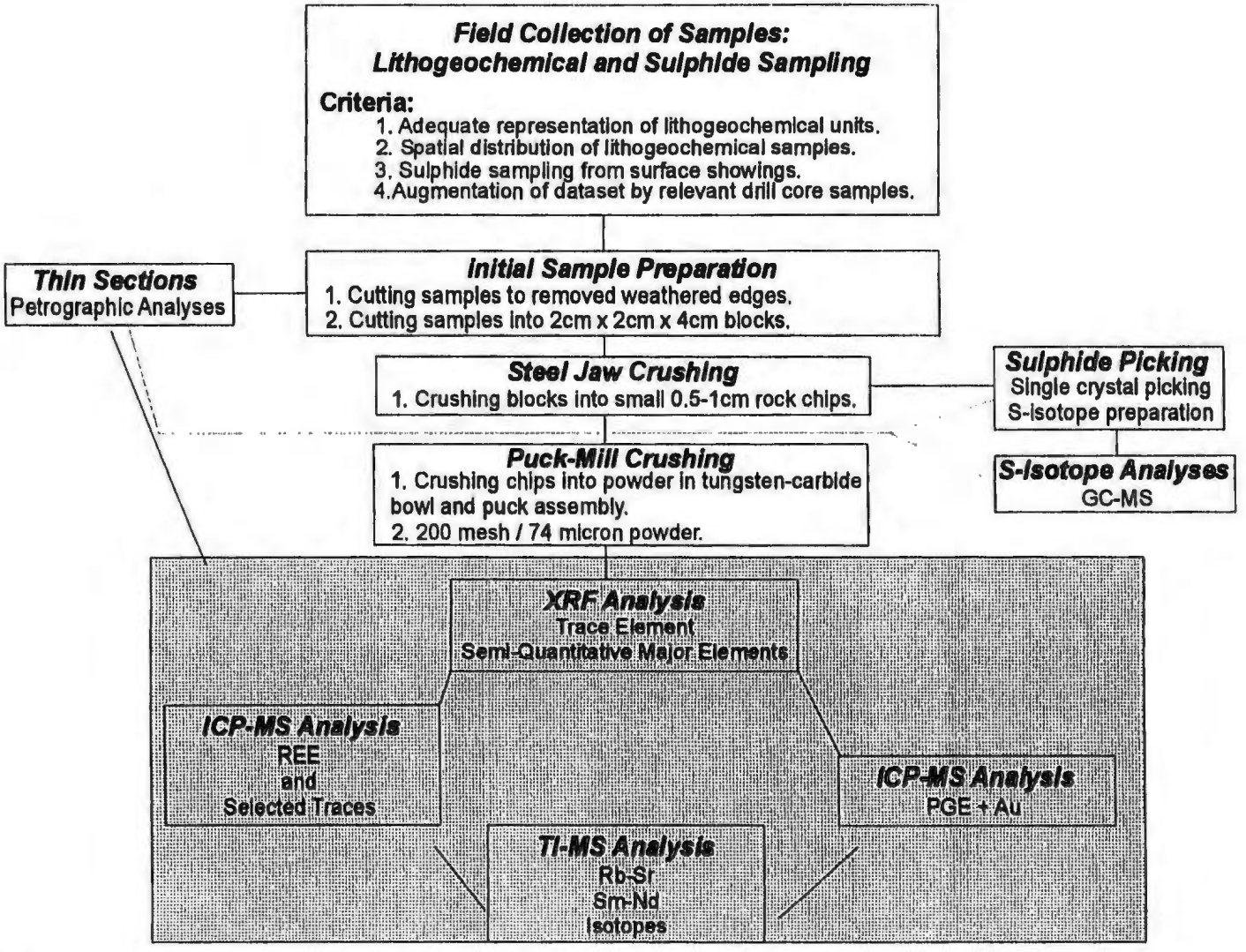

Figure A.1. Schematic illustration of sampling protocol and general overview of methodology of sample selection and geochemical analysis. The downward trend of the plot of this figure is a consistent and logical method of deciding analytical protocol and methodology.

Table A.1 Precision and accuracy for standard DNC-1 calculated from ten determinations over the period of September 1996 to February 1997. Good and excellent precision and accuracy are defined as 3-7% and 0-3%, respectively (Longerich, 1995; Jenner *et al.*, 1990).

Element [1]	**Average Value (n=10)**	**RSD (%)**[3]	**Quoted MUN**[1,2] **Values**	**RD (%)**[3]
Na_2O	2.05	0.39	1.94	5.76
MgO	9.94	0.25	9.90	0.37
Al_2O_3	18.44	0.57	17.67	4.37
SiO_2	43.72	2.68	43.56	0.36
P_2O_5	0.09	2.44	0.09	0.00
K_2O	0.26	1.81	0.26	0.93
CaO	10.97	0.44	11.02	0.45
TiO_2	0.45	1.16	0.45	1.00
MnO	0.15	1.35	0.15	1.31
Fe_2O_3(T)	10.11	0.27	10.12	0.09
S	1097	1.37	1032	6.26
Sc	32	13.24	31	3.64
V	144	3.66	148	2.87
Cr	300	2.19	307	2.39
Ba	113	5.00	115	1.41
Ni	242	1.32	252	4.00
Cu	86	1.34	87	1.44
Ga	14	10.44	14	0.81
Rb	3.5	4.27	3.4	3.20
Sr	144.3	0.63	142.2	1.46
Y	16.4	1.62	15.9	3.02
Zr	35.1	1.57	36	2.57
Nb	1.8	9.74[4]	1.9	6.16

[1] All major element oxides reported as weight percent (%) and traces reported to parts per million (ppm); [2] Data are long term averages of Longerich (1995); [3] RSD = relative standard deviation which is the standard deviation divided by the mean of the ten runs; RD = relative difference relative to the standard value given by: [(mean determination – quoted value)/(quoted value)]*100%; [4] Nb values are low in concentration and below the limit of quantification (Nb =2.3 ppm), typical RSD from Longerich (1995) for Nb is 0.16%.

Table A.2 Precision and accuracy for standard MRG-1 calculated from seven determinations over the period of October 1996 to March 1998. Good and excellent precision and accuracy are defined as 3-7% and 0-3%, respectively (Jenner *et al.*, 1990).

Element	**Average Value (n=7)**	**RSD (%)[1]**	**Quoted MUN Values**	**RD (%)[1]**
La	8.67	2.35	8.83	1.84
Ce	24.92	2.67	25.8	3.40
Pr	3.54	2.68	3.71	4.52
Nd	17.16	3.25	17.6	2.49
Sm	4.39	3.54	4.34	1.20
Eu	1.36	3.84	1.38	1.25
Gd	4.99	1.80	3.97	0.64
Tb	0.53	2.10	0.52	2.37
Dy	2.86	2.22	3.00	4.67
Ho	0.49	4.94	0.49	0.99
Er	1.15	4.04	1.16	0.86
Tm	0.14	4.91	0.14	0.16
Yb	0.77	6.13	0.79	2.07
Lu	0.11	5.18	0.11	2.79
Th	0.76	5.37	0.82	6.84

[1] RSD = relative standard deviation which is the standard deviation divided by the mean of the seven runs; RD = relative difference relative to the standard value given by: [(mean determination – quoted value)/(quoted value)]*100%.

Table A.3. Accuracy of SARM-7 determination for this study based on one run.

Element	**Reported[1]**	**Detected**	**RD[2] (%)**	**MUN Average[3]**	**RD[2] (%)**
Ru	430	425.11	1.14	397[4]	7.08
Rh	240±13	229.50	4.37	212	7.75
Pd	1530±32	1454.62	4.93	1353	6.49
Os	63±7	45.35	27.97	53	14.38
Ir	74±12	79.49	7.42	71	11.96
Pt	3740±45	3443.97	7.92	3395	0.76
Au	310±15	221.53	28.54	253	8.83

[1]Data from Steele *et al.* (1975); [2] RD = relative difference relative to the standard valu e given by: [(mean determination – quoted value)/(quoted value)]*100%; [3] Data from Wilson *et al.* (1996); [4]Quoted from long term average quoted in Wilson *et al.* (1996).

Appendix B: Data Tables

Table B.1a. Pressed powder X-ray fluorescence (XRF) data for the anorthostic rocks of the OKG prospect.

Sample Name	**P96-3A**	**P96-8A**	**P96-8C**	**P96-19**	**P96-21C**	**P96-22A**
Rock Type	an	an	an	an	an	an
Location 1	N Umiak	N Umiak	N Umiak	N Umiak	N Umiak	N Umiak
Location 2						
Na_2O	3.88	4.37	4.39	4.23	4.00	3.90
MgO	3.03	1.83	0.71	1.06	0.31	1.85
Al_2O_3	21.79	22.88	25.79	25.07	26.29	23.39
SiO_2	50.29	50.33	52.73	51.23	51.31	51.50
P_2O_5	0.0126	0.0108	0.0116	0.0089	0.0105	0.0096
K_2O	0.41	0.40	0.73	0.77	1.19	0.40
CaO	9.13	9.15	9.33	9.31	9.36	9.72
TiO_2	0.14	0.10	0.08	0.07	0.06	0.25
MnO	0.061	0.029	0.010	0.015	0.018	0.039
Fe_2O_3T	4.06	2.26	0.99	1.46	1.04	3.27
FeO*[1]	3.65	2.03	0.89	1.32	0.93	2.94
total	93.10	91.67	95.00	93.51	93.87	94.65
S	649	628	370	454	508	652
Sc	8	7	8	5	12	12
V	27	12	<LD	<LD	<LD	45
Cr	56	19	<LD	28	<LD	40
Ni	15	<LD	8	<LD	64	29
Cu	8	7	17	10	23	33
Ga	21	22	23	24	25	22
Rb	<LD	1.5	2.4	4.6	5.5	1.2
Sr	664.4	765.4	755.6	812.5	803.6	789.9
Y	<LD	<LD	<LD	<LD	<LD	<LD
Zr	<LD	<LD	<LD	<LD	<LD	<LD
Nb	<LD	<LD	<LD	<LD	<LD	<LD
Ba	266	287	345	529	486	248
Pb	4	4	<LD	5	6	4
U	<LD	<LD	<LD	<LD	<LD	<LD

Table B.1a. (continued): Pressed powder X-ray fluorescence (XRF) data for the anorthostic rocks of the OKG prospect.

Sample Name	**P96-24**	**P96-27A**	**P96-28A**	**P96-31**	**P96-32**
Rock Type	an	an	an	an	an
Location 1	N Umiak	N Umiak	N Umiak	N Umiak	N Umiak
Location 2					
Na_2O	4.58	4.07	4.12	4.13	4.03
MgO	1.15	3.77	4.98	1.23	1.80
Al_2O_3	25.97	21.82	21.16	25.24	25.47
SiO_2	53.44	51.95	52.60	50.66	52.72
P_2O_5	0.0108	0.0089	0.0112	0.0177	0.0118
K_2O	0.48	0.34	0.40	0.35	0.73
CaO	8.99	8.79	8.63	9.44	8.80
TiO_2	0.17	0.13	0.17	0.12	0.09
MnO	0.011	0.060	0.094	0.012	0.021
Fe_2O_3T	1.97	3.67	5.11	1.82	1.83
FeO*[1]	1.77	3.31	4.60	1.63	1.64
total	97.07	94.86	97.52	93.40	95.80
S	637	416	347	953	604
Sc	8	11	11	5	4
V	11	26	38	11	7
Cr	13	54	74	8	<LD
Ni	<LD	20	26	51	<LD
Cu	18	9	6	49	10
Ga	25	22	21	18	21
Rb	0.9	2.4	1.3	1.2	6.1
Sr	780.9	676.5	642.8	699.5	733.6
Y	<LD	<LD	1.2	<LD	<LD
Zr	<LD	<LD	<LD	<LD	<LD
Nb	<LD	<LD	<LD	<LD	<LD
Ba	316	249	247	238	324
Pb	5	<LD	<LD	4	4
U	<LD	<LD	<LD	<LD	<LD

Table B.1a. (continued): Pressed powder X-ray fluorescence (XRF) data for the anorthostic rocks of the OKG prospect.

Sample Name	**P96-33**	**P96-187**	**P97-188A**	**P96-36**	**P96-42A**
Rock Type	an	ln	ln	lnl	lnl
Location 1	N Umiak	NSSZ	NSSZ	S Umiak	S Umiak
Location 2					
Na_2O	4.23	3.39	2.95	4.19	3.26
MgO	1.65	1.95	6.43	1.03	5.76
Al_2O_3	24.18	19.62	16.56	24.80	16.19
SiO_2	51.49	45.71	44.89	50.90	47.66
P_2O_5	0.0103	0.0119	0.0093	0.0659	0.0152
K_2O	0.51	0.42	0.26	0.45	0.49
CaO	9.19	7.85	7.32	9.88	8.45
TiO_2	0.11	0.13	0.13	0.14	0.23
MnO	0.023	0.037	0.116	0.022	0.105
Fe_2O_3T	1.95	7.90	6.76	1.83	6.80
FeO*[1]	1.75	7.11	6.08	1.65	6.12
total	93.65	95.09	85.80	93.55	89.27
S	692	31063	755	327	413
Sc	5	6	10	10	18
V	10	27	29	16	69
Cr	27	46	171	<LD	182
Ni	10	844.72	110.68	<LD	27
Cu	11	567.63	36.60	<LD	11
Ga	23	19.83	21.68	22	20
Rb	2.1	1.40	1.21	2.1	2.7
Sr	735.1	683.31	677.98	776.3	643.8
Y	<LD	<LD	<LD	1.8	2.3
Zr	<LD	<LD	<LD	<LD	<LD
Nb	<LD	<LD	0.41	<LD	<LD
Ba	344	262.34	287.67	319	362
Pb	5	7.93	5.42	<LD	6
U	<LD	<LD	<LD	<LD	<LD

Table B.1a. (continued): Pressed powder X-ray fluorescence (XRF) data for the anorthostic rocks of the OKG prospect.

Sample Name	**P96-44A**	**P96-49A**	**P96-49B**	**P96-55B**	**P96-66C**
Rock Type	Inl	Inl	Inl	Inl	Inl
Location 1	S Umiak	S Umiak	S Umiak	S Umiak	S Umiak
Location 2					
Na_2O	4.17	4.58	4.08	5.34	4.18
MgO	1.51	0.48	3.26	0.29	4.54
Al_2O_3	20.60	15.77	13.53	25.87	19.96
SiO_2	48.13	56.98	66.29	53.53	55.07
P_2O_5	0.1712	0.1476	0.0430	0.0187	0.0805
K_2O	0.53	4.56	1.13	0.71	0.50
CaO	8.42	3.15	5.96	9.12	7.93
TiO_2	3.64	0.55	0.47	0.12	0.26
MnO	0.060	0.169	0.101	0.016	0.105
Fe_2O_3T	7.03	8.92	5.29	1.23	6.75
FeO*[1]	6.33	8.03	4.76	1.10	6.07
total	94.69	96.10	100.36	96.67	99.55
S	701	204	154	855	115
Sc	13	19	16	<LD	15
V	341	<LD	67	8	43
Cr	40	<LD	<LD	<LD	84
Ni	18	<LD	<LD	<LD	22
Cu	30	10	10	18	8.60
Ga	24	20	18	23	19.09
Rb	6.8	109.2	19.2	7.2	1.95
Sr	754.6	342.2	518.6	987.0	675.56
Y	2.2	30.5	5.9	1.5	2.99
Zr	41.2	92.0	23.3	<LD	<LD
Nb	8.2	29.0	2.7	3.0	<LD
Ba	358	5298	316	540	350.10
Pb	<LD	13	5	19	5.25
U	<LD	<LD	<LD	<LD	<LD

Table B.1a. (continued): Pressed powder X-ray fluorescence (XRF) data for the anorthostic rocks of the OKG prospect.

Sample Name	**P96-67**	**P96-83**	**P96-155A**	**P96-55B**	**P96-66C**
Rock Type	Inl	Inl	Inl	Inl	Inl
Location 1	S Umiak	S Umiak	S Umiak	S Umiak	S Umiak
Location 2					
Na_2O	4.12	2.97	3.10	5.34	4.18
MgO	4.11	6.31	4.25	0.29	4.54
Al_2O_3	20.15	15.39	15.80	25.87	19.96
SiO_2	56.34	52.20	45.44	53.53	55.07
P_2O_5	0.0222	0.0613	0.0147	0.0187	0.0805
K_2O	0.52	0.54	0.37	0.71	0.50
CaO	7.86	8.48	8.55	9.12	7.93
TiO_2	0.30	0.38	0.24	0.12	0.26
MnO	0.088	0.133	0.101	0.016	0.105
Fe_2O_3T	6.21	9.34	6.66	1.23	6.75
FeO*[1]	5.58	8.40	5.99	1.10	6.07
total	99.95	96.03	84.75	96.67	99.55
S	272	75	183	855	115
Sc	9	21	20	<LD	15
V	38	71	59	8	43
Cr	43	105	53	<LD	84
Ni	21	21	10.57	<LD	22
Cu	15.20	8.23	4.80	18	8.60
Ga	20.78	18.23	17.58	23	19.09
Rb	3.41	13.10	4.00	7.2	1.95
Sr	698.23	564.27	662.03	987.0	675.56
Y	3.29	3.95	5.52	1.5	2.99
Zr	4.20	5.96	<LD	<LD	<LD
Nb	0.95	1.34	<LD	3.0	<LD
Ba	400.59	313.65	356.83	540	350.10
Pb	5.30	5.97	7.57	19	5.25
U	<LD	<LD	<LD	<LD	<LD

Table B.1a. (continued): Pressed powder X-ray fluorescence (XRF) data for the anorthostic rocks of the OKG prospect.

Sample Name	**P96-67**	**P96-83**	**P96-155A**	**P96-182**	**P96-141**
Rock Type	ln1	ln1	ln1	ln1	ln
Location 1	S Umiak	S Umiak	S Umiak	S Umiak	Bluff above
Location 2					Main Show
Na_2O	4.12	2.97	3.10	4.64	3.73
MgO	4.11	6.31	4.25	1.41	5.25
Al_2O_3	20.15	15.39	15.80	23.74	19.67
SiO_2	56.34	52.20	45.44	52.54	50.45
P_2O_5	0.0222	0.0613	0.0147	0.0872	0.0075
K_2O	0.52	0.54	0.37	0.70	0.27
CaO	7.86	8.48	8.55	8.66	8.16
TiO_2	0.30	0.38	0.24	0.19	0.17
MnO	0.088	0.133	0.101	0.029	0.140
Fe_2O_3T	6.21	9.34	6.66	2.08	7.60
FeO*[1]	5.58	8.40	5.99	1.87	6.84
total	99.95	96.03	84.75	94.28	95.61
S	272	75	183	38	55
Sc	9	21	20	1	10
V	38	71	59	9	50
Cr	43	105	53	17	156
Ni	21	21	10.57	<LD	52.44
Cu	15.20	8.23	4.80	<LD	<LD
Ga	20.78	18.23	17.58	20.42	18.57
Rb	3.41	13.10	4.00	9.09	<LD
Sr	698.23	564.27	662.03	820.46	557.49
Y	3.29	3.95	5.52	5.14	1.11
Zr	4.20	5.96	<LD	16.81	<LD
Nb	0.95	1.34	<LD	9.73	<LD
Ba	400.59	313.65	356.83	538.21	183.06
Pb	5.30	5.97	7.57	6.09	<LD
U	<LD	<LD	<LD	<LD	<LD

Table B.1a. (continued): Pressed powder X-ray fluorescence (XRF) data for the anorthostic rocks of the OKG prospect.

Sample Name	**P96-149**	**P96-199**	**P96-201A**	**P96-203**
Rock Type	ln	ln2	ln2	ln2
Location 1	Bluff above	NE End	NE End	NE End
Location 2	Main Show			
Na_2O	4.05	3.90	4.03	3.73
MgO	0.72	1.35	0.61	2.06
Al_2O_3	24.78	17.09	25.17	18.98
SiO_2	49.49	49.48	49.77	48.45
P_2O_5	0.0068	0.4698	0.0263	0.5434
K_2O	0.38	1.50	0.75	0.59
CaO	9.29	6.45	9.46	8.11
TiO_2	0.09	1.14	0.09	1.15
MnO	0.017	0.122	0.012	0.111
Fe_2O_3T	1.38	9.42	0.94	7.53
FeO*[1]	1.24	8.47	0.84	6.77
total	90.35	91.30	91.02	91.49
S	71	84	51	165
Sc	2	16	6	11
V	<LD	113	6	94
Cr	19	22	13	23
Ni	<LD	<LD	<LD	<LD
Cu	<LD	12.64	7.10	10.28
Ga	22.25	25.03	20.22	24.27
Rb	1.23	15.16	5.40	0.89
Sr	718.49	660.33	719.64	746.23
Y	<LD	24.13	<LD	12.81
Zr	<LD	50.44	<LD	15.42
Nb	<LD	4.43	0.43	4.40
Ba	295.33	1765.70	316.32	560.90
Pb	<LD	11.71	4.19	4.72
U	<LD	<LD	<LD	<LD

[1]Recalculated using Fe_2O_3T

Table B.1b. Pressed powder X-ray fluorescence (XRF) data for the granitoid rocks of the OKG prospect.

Sample Name	**P96-3B**	**P96-28B**	**P96-47A**	**P96-48**	**P96-48A**
Rock Type	Qtz Monz	Qtz Monz	Monzonite	Monzonite	Monzonite
Location 1	Dykes	Dykes	Phl	Phl	Phl
Location 2	Main Show	Main Show	S Umiak	S Umiak	S Umiak
Na_2O	2.46	3.59	5.08	3.52	3.98
MgO	1.02	0.74	0.27	0.73	0.65
Al_2O_3	13.69	14.12	18.83	12.88	15.21
SiO_2	70.83	73.27	59.30	53.33	55.18
P_2O_5	0.0768	0.0634	0.1128	0.2864	0.1634
K_2O	4.51	2.32	5.00	4.09	4.67
CaO	1.69	1.87	2.98	4.76	3.26
TiO_2	0.37	0.35	0.37	1.00	0.66
MnO	0.081	0.048	0.088	0.298	0.215
Fe_2O_3T	3.97	2.89	4.50	15.10	9.64
FeO*[1]	3.57	2.60	4.05	13.59	8.68
total	100.11	100.26	97.74	96.73	94.59
S	360	1244	245	333	398
Sc	14	4	10	21	16
V	<LD	<LD	<LD	<LD	<LD
Cr	14	<LD	<LD	<LD	<LD
Ni	<LD	<LD	<LD	<LD	<LD
Cu	<LD	22	8	25	15
Ga	8	13	22	21	18
Rb	78.6	48.8	111.0	104.5	108.3
Sr	306.4	243.8	534.0	232.6	348.6
Y	32.3	27.5	30.6	56.8	39.7
Zr	369.4	795.9	255.8	664.1	171.1
Nb	17.8	37.2	50.0	69.7	61.9
Ba	10554	4558	8643	3559	6002
Pb	<LD	5	11	14	13
U	<LD	<LD	<LD	<LD	<LD

Table B.1b. (continued): Pressed powder X-ray fluorescence (XRF) data for the granitoid rocks of the OKG prospect.

Sample Name	**P96-56**	**P96-60**	**P96-61A**	**P96-66A**	**P96-66B**
Rock Type	Monzonite	Monzonite	Monzonite	Monzonite	Monzonite
Location 1	Phl	Phl	Phl	Phl	Phl
Location 2	S Umiak	S Umiak	S Umiak	S Umiak	S Umiak
Na_2O	4.48	4.05	5.01	4.74	3.67
MgO	0.65	0.79	0.97	0.32	0.65
Al_2O_3	16.96	14.44	25.27	18.26	17.66
SiO_2	56.46	53.88	53.03	61.27	63.78
P_2O_5	0.1499	0.2450	0.1464	0.1277	0.0803
K_2O	4.78	4.30	0.61	4.91	6.52
CaO	3.49	3.89	8.80	3.03	3.52
TiO_2	0.67	1.00	0.21	0.52	0.63
MnO	0.167	0.266	0.026	0.099	0.136
Fe_2O_3T	8.41	12.95	2.01	4.91	6.34
FeO*[1]	7.56	11.65	1.81	4.41	5.70
total	97.49	96.78	96.33	99.34	104.14
S	217	178	218	228	126
Sc	16	19	9	8	8
V	<LD	<LD	29	<LD	<LD
Cr	<LD	<LD	<LD	<LD	<LD
Ni	<LD	<LD	<LD	<LD	<LD
Cu	16	16	<LD	11.30	5.66
Ga	19	23	20	19.85	18.77
Rb	109.0	115.9	9.4	98.37	187.47
Sr	499.6	329.4	784.6	561.01	365.66
Y	49.2	59.7	2.7	16.56	57.02
Zr	385.6	280.7	<LD	66.69	243.15
Nb	82.4	118.5	1.1	32.70	104.20
Ba	8309	6070	460	8695.08	7947.30
Pb	20	20	12	10.01	17.81
U	<LD	<LD	<LD	<LD	<LD

Table B.1b. (continued): Pressed powder X-ray fluorescence (XRF) data for the granitoid rocks of the OKG prospect.

Sample Name	**P96-72**	**P96-85**	**P96-86B**	**P96-152**	**P96-155B**
Rock Type	Syenite	Syenite	Monzonite	Monzonite	Monzonite
Location 1	Phl	Phl	Phl	Phl	Phl
Location 2	S Umiak	S Umiak	S Umiak	S Umiak	S Umiak
Na_2O	4.10	4.11	4.70	4.78	3.17
MgO	0.61	0.37	0.54	0.30	0.54
Al_2O_3	15.51	16.58	16.18	17.74	12.84
SiO_2	68.70	65.37	63.45	57.05	52.21
P_2O_5	0.3404	0.1108	0.1403	0.1350	0.1776
K_2O	3.28	6.54	5.40	4.84	4.91
CaO	3.86	2.03	2.48	3.09	3.10
TiO_2	0.83	0.45	0.56	0.43	0.63
MnO	0.097	0.127	0.162	0.119	0.238
Fe_2O_3T	6.23	6.28	7.53	5.57	10.21
FeO*[1]	5.61	5.65	6.78	5.01	9.18
total	103.97	102.83	101.89	95.19	88.75
S	116	98	81	106	306
Sc	12	7	17	11	8
V	16	<LD	<LD	<LD	<LD
Cr	<LD	<LD	<LD	<LD	3
Ni	<LD	<LD	<LD	<LD	<LD
Cu	6.72	6.33	4.71	6.43	10.08
Ga	21.84	20.54	22.25	20.61	21.65
Rb	51.08	187.93	136.63	112.42	125.24
Sr	409.59	289.37	294.69	500.16	222.41
Y	38.99	60.16	57.98	34.79	43.50
Zr	433.91	384.57	122.70	182.21	326.36
Nb	30.41	79.07	75.80	49.69	55.21
Ba	1953.43	5285.31	4465.57	8178.73	4036.95
Pb	18.89	19.36	15.56	9.19	20.83
U	<LD	<LD	<LD	<LD	<LD

Table B.1b. (continued): Pressed powder X-ray fluorescence (XRF) data for the granitoid rocks of the OKG prospect.

Sample Name	**P96-163**	**P96-75A**	**P96-75B**	**P96-76**	**P96-87**
Rock Type	Monzonite	Qtz Monz	Monzonite	Qtz Syenite	Qtz Monz
Location 1	Ph1	Ph2	Ph2	Ph2	Ph2
Location 2	S Umiak	S Umiak	S Umiak	S Umiak	S Umiak
Na_2O	6.01	3.42	3.54	3.44	3.10
MgO	0.14	0.67	0.88	0.69	0.32
Al_2O_3	17.85	13.28	13.18	13.28	12.70
SiO_2	61.17	68.33	54.71	68.28	71.36
P_2O_5	0.0528	0.2600	0.3403	0.2521	0.0689
K_2O	4.26	4.25	4.26	4.26	4.59
CaO	2.12	2.51	4.45	2.55	1.39
TiO_2	0.19	0.81	1.08	0.80	0.34
MnO	0.065	0.144	0.294	0.142	0.042
Fe_2O_3T	2.61	7.28	14.29	7.27	2.99
FeO*[1]	2.35	6.55	12.85	6.54	2.69
total	95.07	101.53	98.07	101.56	97.24
S	83	112	515	119	53
Sc	<LD	9	26	15	<LD
V	<LD	<LD	<LD	10	11
Cr	<LD	<LD	<LD	<LD	26
Ni	<LD	<LD	<LD	<LD	<LD
Cu	<LD	5.83	14.75	6.89	4.02
Ga	22.03	19.85	18.40	19.08	22.54
Rb	95.53	99.55	115.05	100.89	142.11
Sr	257.20	240.60	323.95	242.84	196.67
Y	18.08	36.01	61.20	34.95	23.53
Zr	435.80	593.76	328.50	615.38	459.16
Nb	25.08	27.09	99.84	26.72	17.91
Ba	3811.61	2358.70	5830.35	2426.00	1636.44
Pb	8.77	23.61	15.39	25.14	18.19
U	<LD	<LD	<LD	<LD	<LD

Table B.1b. (continued): Pressed powder X-ray fluorescence (XRF) data for the granitoid rocks of the OKG prospect.

Sample Name	**P96-93**	**P96-179**	**P96-131A**	**P96-131B**	**P96-135**
Rock Type	Qtz Monz	Diorite	Monzonite	K-fsp granite	Monzonite
Location 1	Ph2	Ph2	Foliated	Foliated	Foliated
Location 2	S Umiak	S Umiak	E Property	E Property	E Property
Na_2O	3.40	3.26	3.97	3.22	3.44
MgO	0.28	1.14	2.20	0.24	0.50
Al_2O_3	13.56	11.15	15.94	13.13	14.64
SiO_2	71.55	49.76	54.38	70.70	65.47
P_2O_5	0.0952	0.3297	0.5578	0.0923	0.1251
K_2O	4.41	3.68	0.66	4.30	4.65
CaO	1.53	4.60	9.62	1.69	2.27
TiO_2	0.36	1.14	0.53	0.32	0.51
MnO	0.050	0.364	0.122	0.058	0.057
Fe_2O_3T	3.25	16.31	4.17	2.98	3.98
FeO*[1]	2.93	14.68	3.75	2.69	3.58
total	98.91	92.57	92.38	97.08	96.18
S	92	116	78	97	78
Sc	7	18	16	10	7
V	<LD	<LD	83	<LD	<LD
Cr	16	12	270	27	9
Ni	<LD	<LD	28.65	<LD	<LD
Cu	4.34	11.02	8.86	<LD	5.48
Ga	20.20	21.49	24.95	19.00	23.52
Rb	104.15	111.65	4.20	118.56	124.99
Sr	258.41	241.24	374.56	177.72	316.99
Y	20.48	96.74	33.39	20.15	32.78
Zr	491.45	800.15	127.64	500.64	553.47
Nb	14.56	105.76	15.52	22.38	27.29
Ba	2285.25	3320.06	170.74	1586.69	2713.79
Pb	17.60	20.81	13.54	14.86	20.16
U	<LD	<LD	<LD	<LD	<LD

Table B.1b. (continued): Pressed powder X-ray fluorescence (XRF) data for the granitoid rocks of the OKG prospect.

Sample Name	**P96-194**	**P96-197**	**P96-201B**	**P96-195**
Rock Type	Qtz Syenite	Qtz Monz?	Syenite	Qtz Monz
Location 1	Foliated	Foliated	Foliated	Foliated
Location 2	E Property	E Property	E Property	E Property
Na_2O	3.56	4.36	2.21	3.58
MgO	0.83	0.96	0.55	0.88
Al_2O_3	13.20	16.62	12.74	13.70
SiO_2	63.79	62.57	69.02	64.73
P_2O_5	0.4694	0.0785	0.0438	0.2163
K_2O	2.74	2.68	5.04	2.76
CaO	3.41	3.61	1.31	2.84
TiO_2	0.93	0.17	0.36	0.52
MnO	0.114	0.075	0.050	0.065
Fe_2O_3T	6.38	3.62	3.25	4.31
FeO*[1]	5.74	3.26	2.93	3.88
total	95.87	95.22	95.07	94.10
S	96	37	49	176
Sc	10	<LD	<LD	9
V	25	<LD	<LD	18
Cr	24	15	62	27
Ni	<LD	<LD	<LD	<LD
Cu	7.92	<LD	<LD	<LD
Ga	20.94	24.94	20.57	21.32
Rb	17.86	15.60	225.00	20.67
Sr	405.05	722.29	127.40	444.68
Y	30.81	8.71	62.95	14.05
Zr	400.78	350.87	537.16	251.36
Nb	13.69	2.41	48.16	6.47
Ba	2470.94	2783.45	828.14	2867.35
Pb	11.57	14.35	23.85	10.82
U	<LD	<LD	<LD	<LD

[1]Recalculated using Fe_2O_3T

Table B.1c. Pressed powder X-ray fluorescence (XRF) data for the mafic and felsic dyke rocks of the OKG prospect.

Sample Name	**P96-42B**	**P96-44B**	**P96-154**	**P96-158B**	**P96-160**	**P96-170**
Rock Type	Felsic Dyke	Mafic Dyke	Mafic Dyke	Mafic Dyke	Mafic Dyke	Mafic Dyke
Location 1	S Umiak	S Umiak	S Umiak	S Umiak	S Umiak	S Umiak
Na_2O	3.56	1.94	2.06	2.55	2.72	2.12
MgO	0.72	5.94	7.93	8.00	8.51	12.36
Al_2O_3	16.99	11.36	13.35	12.75	13.64	11.43
SiO_2	55.38	48.52	42.71	40.69	42.80	42.52
P_2O_5	0.1341	0.1319	0.2508	0.3176	0.3021	0.2000
K_2O	3.79	0.47	0.60	0.65	0.51	0.56
CaO	2.95	9.23	9.01	8.64	8.99	8.83
TiO_2	0.60	1.79	1.81	1.74	1.63	1.48
MnO	0.121	0.215	0.203	0.188	0.190	0.180
Fe_2O_3T	9.59	15.54	15.40	15.03	14.44	13.99
FeO*[1]	8.63	13.98	13.86	13.52	12.99	12.59
total	95.79	95.81	93.93	91.02	94.26	94.44
S	5613	1521	1272	723	1031	1483
Sc	12	30	18	29	29	31
V	<LD	389	226	218	216	245
Cr	<LD	96	93	60	88	786
Ni	<LD	57	113.89	122.87	131.40	331
Cu	32	170	70.69	48.95	56.62	92
Ga	39	22	21.13	21.09	21.53	17
Rb	115.3	8.6	10.63	19.17	12.29	12.1
Sr	219.5	205.4	367.23	437.10	415.30	328.4
Y	108.6	29.2	23.71	22.38	20.88	16.8
Zr	1686.3	156.7	139.79	126.41	114.89	92.9
Nb	116.6	12.4	26.29	23.92	21.87	10.5
Ba	1445	137	430.50	458.24	347.37	265
Pb	12	7	9.30	12.54	8.18	6
U	<LD	<LD	<LD	<LD	<LD	<LD

[1]Recalculated using Fe_2O_3T

Table B.1d. Pressed powder X-ray fluorescence (XRF) data for the pyroxenitic and leucotroctolitic dykes of the OKG prospect.

Sample Name	**P96-5B**	**P96-25**	**P96-463**	**P95-464**	**P96-W1**
Rock Type	Opxnite	Opxnite	Opxnite	Opxnite	Leucotroct
Location 1	MZ	MZ	NSSZ	NSSZ	MZ
Na_2O	0.21	0.12	0.28	0.26	0.16
MgO	17.31	11.31	15.97	15.04	15.87
Al_2O_3	1.09	0.68	1.75	1.71	0.92
SiO_2	37.93	28.09	37.96	38.40	36.46
P_2O_5	0.0018	0.0020	0.0061	0.0045	0.0152
K_2O	0.03	0.01	0.04	0.02	0.01
CaO	2.08	1.47	2.17	4.38	2.32
TiO_2	0.33	0.26	0.38	0.98	0.41
MnO	0.456	0.347	0.395	0.454	0.438
Fe_2O_3T	27.57	32.95	27.63	29.21	27.05
FeO*[1]	24.81	29.65	24.86	26.28	24.34
Total	100.57	113.81	90.25	98.42	98.44
S	51474	150470	45782	30701	24836
Sc	36	30	27	38	28
V	112	114	113	292	126
Cr	952	1243	755	536	1054
Ni	1875	3448	975	670	794.06
Cu	1869	2514	721	507	582.38
Ga	3	<LD	5	5	4.02
Rb	<LD	1.1	0.9	<LD	<LD
Sr	1.1	1.8	50.4	23.1	3.23
Y	5.5	3.9	6.8	5.9	7.25
Zr	6.1	5.4	4.1	4.5	7.41
Nb	<LD	<LD	<LD	<LD	<LD
Ba	<LD	<LD	<LD	<LD	<LD
Pb	13	11	9	10	4.55
U	<LD	<LD	<LD	<LD	<LD

Table B.1d. (continued): Pressed powder X-ray fluorescence (XRF) data for the pyroxenitic and leucotroctolitic dykes of the OKG prospect.

Sample Name	**16715**	**16730**	**16737**	**16747**
Rock Type	Opxnite	Opxnite	Opxnite	Opxnite
Location	Core	Core	Core	Core
Na_2O	0.29	0.61	1.35	0.46
MgO	4.81	3.98	16.85	19.93
Al_2O_3	0.79	2.32	6.73	1.95
SiO_2	15.82	16.47	46.12	43.97
P_2O_5	0.01	0.02	0.14	0.78
K_2O	0.14	0.12	0.30	0.04
CaO	1.75	2.56	4.13	4.34
TiO_2	0.15	0.12	0.44	0.71
MnO	0.12	0.10	0.32	0.42
Fe_2O_3T	44.79	27.02	20.37	24.42
FeO*[1]	40.30	38.91	18.33	21.97
Total	140.58	107.03	102.46	97.01
S	282276	265359	21225	17542
Sc	<LD	<LD	20	29
V	43	35	86	142
Cr	353	353	951	1365
Ni	9147	9494	577	533
Cu	1166	2752	462	375
Ga	<LD	<LD	12	7
Rb	12	2	1	<LD
Sr	17	117	261	54
Y	11	2	8	16
Zr	22	5	5	21
Nb	<LD	<LD	<LD	<LD
Ba	<LD	30	167	<LD
Pb	21	21	6	6
U	<LD	<LD	<LD	<LD

[1]Recalculated from Fe_2O_3T

Table B.1e. Pressed powder X-ray fluorescence (XRF) data for the Nain Province gneisses of the OKG prospect.

Sample Name	**P96-95**	**P96-103A**	**P96-125**	**P96-126**
Rock Type	Amphibolite	Amphibolite	Amphibolite	Metatonalite
Location	Eastern Sector	Eastern Sector	Eastern Sector	Eastern Sector
Na_2O	1.83	1.14	1.90	2.82
MgO	14.38	12.86	11.95	0.27
Al_2O_3	9.11	5.50	10.87	12.26
SiO_2	42.93	42.78	40.39	68.64
P_2O_5	0.0094	0.0593	0.0454	0.0307
K_2O	0.52	0.37	1.04	4.50
CaO	10.21	12.40	10.32	1.19
TiO_2	0.39	0.90	0.62	0.22
MnO	0.22	0.25	0.22	0.04
Fe_2O_3T	13.03	15.58	13.47	2.41
FeO	11.73	14.02	12.12	2.17
total	92.95	92.23	91.12	92.62
S	61	87	74	43
Sc	44	51	32	4
V	215	251	246	<LD
Cr	1186	1381	868	37
Ni	231	350	221	<LD
Cu	4	17	8	<LD
Ga	13	15	17	21
Rb	18.52	1.42	40.83	119.04
Sr	44.98	51.41	47.95	114.18
Y	21.56	23.6	15.32	9.52
Zr	21.69	51.91	42.53	273.46
Nb	5.12	6.93	5.69	5.42
Ba	<LD	<LD	125.86	1052.53
Pb	<LD	13.17	5.02	13.64
U	<LD	<LD	<LD	<LD

Table B.1f. Pressed powder X-ray fluorescence (XRF) data for sulphide bearing units used for PGE analyses not quoted in prior tables.

Sample Name	**P96-5A**	**P96-11A**	**P96-21A**	**P96-21B**	**P96-188B**	**P96-475**
Rock Type	MS	MS	MS	MS	MS (OKG)	MS (OKG)
Location	MZ	MZ	MZ	MZ	NSSZ	NSSZ
Na_2O	0.12	0.12	0.16	0.14	0.66	0.16
MgO	0.00	0.00	0.00	0.00	1.37	0.00
Al_2O_3	0.24	0.79	1.22	1.02	4.95	0.93
SiO_2	0.77	2.55	2.38	1.93	15.91	1.97
P_2O_5	0.0000	0.0000	0.0000	0.0000	0.0000	0.0000
K_2O	0.02	0.02	0.06	0.03	0.08	0.03
CaO	0.06	0.51	0.40	0.27	2.75	0.15
TiO_2	0.01	0.02	0.00	0.00	0.06	0.00
MnO	0.000	0.020	0.000	0.000	0.060	0.010
Fe_2O_3T	49.92	47.96	44.15	47.36	37.00	46.73
FeO*[1]	44.92	43.15	39.73	42.62	33.29	42.05
total	128.15	133.15	129.11	129.17	114.37	134.16
S	302028	312792	310999	304767	199921	330305
Sc	<LD	<LD	<LD	<LD	<LD	<LD
V	20	14	<LD	<LD	28	<LD
Cr	480	36	139	163	134	149
Ni	17177	18115	22340	20024	7990	21529
Cu	4374	12015	10806	7713	3996	718
Ga	<LD	<LD	<LD	<LD	10	<LD
Rb	<LD	<LD	1.2	<LD	<LD	<LD
Sr	14.1	46.1	58.2	34.1	294.1	21.8
Y	1.2	<LD	<LD	1.4	2.2	<LD
Zr	3	<LD	<LD	3.2	2.3	8.3
Nb	1.3	1.3	<LD	<LD	<LD	2.2
Ba	<LD	<LD	<LD	<LD	70	<LD
Pb	27	29	22	21	14	22
U	<LD	<LD	<LD	<LD	<LD	<LD

Table B.1f. (continued): Pressed powder X-ray fluorescence (XRF) data for sulphide bearing units used for PGE analyses not quoted in prior tables.

Sample Name	**P96-11B**	**P96-191**	**P96-192**	**P96-472**	**P96-187**	**P96-190**
Rock Type	DS-Pyroxenite	DS-Pyroxenite	DS-Pyroxenite	DS (OKG)	DS-Anorthosite	DS-Anorthosite
Location	MZ	NSSZ	NSSZ	DS-Pyroxenite	NSSZ	NSSZ
Na_2O	1.11	0.19	4.48	2.03	3.39	1.05
MgO	9.45	13.28	0.93	8.27	1.95	9.15
Al_2O_3	7.11	0.90	24.44	12.06	19.62	6.56
SiO_2	46.21	33.70	51.63	44.51	45.71	35.08
P_2O_5	0.0100	0.0000	0.0105	0.0100	0.0119	0.0100
K_2O	1.29	0.01	0.46	0.19	0.42	0.15
CaO	4.87	4.39	8.81	8.80	7.85	5.27
TiO_2	0.38	0.71	0.10	0.83	0.13	0.34
MnO	0.320	0.460	0.018	0.170	0.037	0.260
Fe_2O_3T	20.20	28.10	1.49	13.92	7.90	23.20
FeO*[1]	18.18	25.28	1.34	12.53	7.11	20.88
total	98.31	91.25	92.67	92.67	95.09	100.10
S	27661	36536	656	6492	31063	73655
Sc	33	36	4	34	6	24
V	94	240	6	369	27	119
Cr	360	615	10	139	46	627
Ni	765	710	<LD	80	844.72	2104
Cu	812	601	9.82	159	567.63	1186
Ga	11	5	24.24	19	19.83	10
Rb	36.5	<LD	1.04	<LD	1.40	2.9
Sr	171.3	6.3	754.00	411.6	683.31	267.5
Y	22.3	9.2	<LD	4.7	<LD	4.6
Zr	23.9	11.4	<LD	<LD	<LD	2.6
Nb	28.4	<LD	<LD	<LD	<LD	<LD
Ba	254	<LD	297.56	271	262.34	101
Pb	11	7	<LD	<LD	7.93	7
U	<LD	<LD	<LD	<LD	<LD	<LD

Table B.1f. (continued): Pressed powder X-ray fluorescence (XRF) data for sulphide bearing units used for PGE analyses not quoted in prior tables.

Sample Name	**P96-476**
Rock Type	MS (OKG)
Location	MZ
Na_2O	0.16
MgO	0.00
Al_2O_3	0.46
SiO_2	1.54
P_2O_5	0.0000
K_2O	0.02
CaO	0.23
TiO_2	0.01
MnO	0.010
Fe_2O_3T	47.64
FeO*[1]	42.87
total	134.68
S	331778
Sc	<LD
V	<LD
Cr	173
Ni	20243
Cu	3558
Ga	<LD
Rb	<LD
Sr	34.2
Y	<LD
Zr	2.6
Nb	1.7
Ba	33
Pb	21
U	<LD

[1]Recalculated from Fe_2O_3T

Table B.2a. ICP-MS REE and Th data for the OKG anorthostic rocks.

Sample Name	**P96-3A**	**P96-19**	**P96-33**	**P96-44A**	**P96-55B**
Rock Type	an	an	an	in1	in1
La	1.601	4.469	2.579	4.798	6.249
Ce	2.814	6.879	4.388	9.752	10.832
Pr	0.324	0.656	0.487	1.217	1.218
Nd	1.286	2.092	1.753	5.421	4.317
Sm	0.329	0.355	0.308	0.982	0.799
Eu	0.536	0.784	0.591	0.855	0.797
Gd	0.210	0.112	0.116	0.766	0.529
Tb	0.028	0.011	0.015	0.099	0.074
Dy	0.193	0.054	0.097	0.546	0.512
Ho	0.043	0.009	0.019	0.101	0.100
Er	0.121	0.031	0.050	0.244	0.288
Tm	0.018	0.004	0.007	0.037	0.040
Yb	0.137	0.020	0.037	0.210	0.274
Lu	0.018	0.003	0.008	0.034	0.051
Th	<LD	<LD	<LD	0.020	0.300
Sample Name	**P96-83**	**P96-174**	**P96-182**	**P96-199**	**P96-203**
Rock Type	in1	in1	in1	in2	in2
La	4.193	6.769	10.721	31.850	12.218
Ce	8.803	12.942	21.180	69.428	27.797
Pr	1.137	1.596	2.382	9.127	3.770
Nd	4.668	6.303	8.315	36.729	16.917
Sm	1.185	1.332	1.484	6.686	3.418
Eu	0.736	0.855	0.853	3.275	1.835
Gd	0.976	0.957	1.085	5.801	2.913
Tb	0.138	0.149	0.151	0.815	0.401
Dy	0.915	0.894	1.012	4.619	2.365
Ho	0.172	0.177	0.187	0.931	0.497
Er	0.554	0.528	0.584	2.603	1.374
Tm	0.070	0.086	0.094	0.360	0.183
Yb	0.496	0.477	0.675	2.315	1.191
Lu	0.070	0.086	0.095	0.356	0.179
Th	0.020	0.150	1.690	0.510	0.080

Table B.2b. ICP-MS REE and Th data for the OKG granitoid rocks.

Sample Name	**P96-85**	**P96-86B**	**P96-75B**	**P96-76**	**P96-87**
Rock Type	Ph1	Ph1	Ph2	Ph2	Ph2
La	44.924	71.626	60.019	48.021	46.101
Ce	126.138	168.832	124.686	107.661	96.618
Pr	17.771	20.680	16.449	13.936	12.432
Nd	74.674	80.721	64.923	58.537	51.677
Sm	14.895	14.563	11.157	10.602	8.904
Eu	5.786	5.407	3.543	3.204	2.203
Gd	12.937	11.772	9.116	8.758	7.010
Tb	2.098	1.809	1.273	1.226	0.926
Dy	11.785	11.197	7.672	7.062	5.098
Ho	2.515	2.351	1.497	1.440	1.040
Er	7.340	6.808	4.007	4.069	2.774
Tm	1.006	0.972	0.552	0.546	0.369
Yb	7.028	6.529	3.548	3.425	2.197
Lu	1.062	0.961	0.555	0.549	0.308
Th	3.750	4.880	0.470	0.410	0.650
Sample Name	**P96-3B**	**P96-28B**	**P96-39**	**P96-60**	**P96-66A**
Rock Type	Dyke	Dyke	Ph1	Ph1	Ph1
La	33.945	46.734	58.874	72.641	4.387
Ce	62.003	80.232	125.733	166.016	8.352
Pr	8.016	8.916	15.435	21.329	1.045
Nd	35.138	35.184	64.477	87.578	4.180
Sm	7.188	6.002	12.023	16.319	0.897
Eu	7.036	5.061	5.646	6.969	0.717
Gd	6.922	5.562	10.667	14.440	0.778
Tb	0.954	0.763	1.479	2.028	0.101
Dy	6.244	4.879	9.097	12.648	0.673
Ho	1.271	1.067	1.809	2.426	0.131
Er	3.494	3.108	5.587	6.617	0.376
Tm	0.538	0.477	0.881	1.005	0.058
Yb	3.202	3.212	6.197	6.261	0.366
Lu	0.541	0.568	1.180	1.151	0.057
Th	0.680	2.770	3.000	3.140	3.160

Table B.2b. (continued): ICP-MS REE and Th data for the OKG granitoid rocks.

Sample Name	**P96-131A**	**P96-131B**	**P96-131B D**
Rock Type	Fol	Fol	Fol
La	69.182	30.809	32.300
Ce	157.203	68.953	72.470
Pr	19.523	9.423	10.226
Nd	75.507	39.845	42.329
Sm	12.875	7.534	7.844
Eu	2.139	1.901	1.853
Gd	8.890	6.123	6.294
Tb	1.142	0.769	0.840
Dy	6.624	4.372	4.709
Ho	1.244	0.905	0.955
Er	3.462	2.269	2.583
Tm	0.451	0.292	0.359
Yb	2.911	1.768	2.032
Lu	0.416	0.259	0.297
Th	6.400	0.187	0.227

Table B.2c. ICP-MS REE and Th data for the OKG mafic and felsic dyke rocks.

Sample Name	**P96-42B**	**P96-44B**	**P96-154**	**P96-158B**	**P96-160**	**P96-170**	**P96-170 DUP**
Rock Type	Felsic Dyke	Mafic Dyke	Mafic Dyke	Mafic Dyke	Mafic Dyke	Mafic Dyke	Mafic Dyke
La	132	16.37	23.59	23.304	20.693	11.688	11.696
Ce	289.288	38.276	51.338	50.404	44.911	27.095	27.277
Pr	36.934	5	6.238	6.251	5.571	3.535	3.613
Nd	147.469	21.773	24.546	24.95	22.048	15.074	15.637
Sm	26.779	5.28	5.078	4.976	4.533	3.689	3.642
Eu	4.882	1.469	1.524	1.587	1.461	1.178	1.177
Gd	22.022	5.268	4.665	4.804	4.415	3.776	3.539
Tb	3.231	0.824	0.692	0.711	0.636	0.551	0.538
Dy	20.312	5.245	4.255	4.263	3.74	3.298	3.105
Ho	4.194	1.063	0.848	0.904	0.78	0.641	0.623
Er	11.863	3.029	2.538	2.464	2.248	1.916	1.731
Tm	1.679	0.422	0.344	0.347	0.324	0.242	0.23
Yb	10.629	2.672	2.304	2.202	2.023	1.474	1.453
Lu	1.567	0.393	0.353	0.335	0.307	0.214	0.23
Th	8.26	2.44	2.16	2.09	1.79	0.92	0.95

Table B.2d. ICP-MS REE and Th data for the OKG pyroxenitic rocks.

Sample Name	**P96-25**	**P96-463**	**P95-464**	**P96-W1**	
Rock Type	Opxnite	Opxnite	Opxnite	Leucotroct	
La	0.174	0.384	0.345	0.238	
Ce	0.506	0.873	0.853	0.732	
Pr	0.079	0.135	0.159	0.152	
Nd	0.501	0.805	1.041	1.128	
Sm	0.274	0.469	0.491	0.533	
Eu	0.06	0.126	0.174	0.123	
Gd	0.361	0.692	0.629	0.729	
Tb	0.066	0.121	0.128	0.141	
Dy	0.539	0.952	0.923	0.995	
Ho	0.134	0.232	0.203	0.229	
Er	0.463	0.835	0.705	0.791	
Tm	0.078	0.137	0.107	0.135	
Yb	0.634	1.024	0.792	0.947	
Lu	0.109	0.177	0.135	0.151	
Th	0.03	0.02	0.02	<LD	
Sample Name	**16715**	**16730**	**16737**	**16747**	**16747D**
Rock Type	Opxnite	Opxnite	Opxnite	Opxnite	Opxnite
La	2.156	1.097	2.807	7.689	7.755
Ce	5.147	2.233	6.278	20.493	20.356
Pr	0.728	0.302	0.900	3.028	3.077
Nd	3.044	1.432	4.554	14.685	15.138
Sm	0.927	0.349	1.105	3.190	2.997
Eu	0.081	0.159	0.468	0.630	0.639
Gd	0.969	0.356	1.182	3.170	3.194
Tb	0.202	0.061	0.184	0.442	0.450
Dy	1.354	0.447	1.389	2.723	2.664
Ho	0.329	0.103	0.324	0.589	0.607
Er	1.061	0.325	1.051	1.663	1.723
Tm	0.170	0.041	0.156	0.262	0.262
Yb	1.232	0.374	1.168	1.628	1.635
Lu	0.178	0.046	0.175	0.259	0.276
Th	1.260	0.036	0.019	0.060	0.049

Table B.2e. ICP-MS REE and Th data for the OKG Nain Province gneissic rocks.

Sample Name	**P96-95**	**P96-103A**	**P96-125**	**P96-126**	P96-126D
Rock Type	Amphibolite	Amphibolite	Amphibolite	Metatonalite	Metatonalite
La	5.730	7.432	3.168	66.109	67.535
Ce	15.766	23.875	7.984	119.307	126.619
Pr	2.276	3.711	1.132	13.571	14.548
Nd	10.767	17.390	5.539	50.624	54.791
Sm	3.077	4.869	1.830	6.966	7.927
Eu	0.708	0.747	0.487	1.538	1.487
Gd	3.236	4.944	2.327	4.954	5.314
Tb	0.558	0.743	0.411	0.618	0.664
Dy	3.723	4.553	2.796	3.370	3.318
Ho	0.787	0.869	0.595	0.575	0.609
Er	2.345	2.314	1.789	1.578	1.592
Tm	0.345	0.335	0.267	0.204	0.206
Yb	2.358	1.955	1.698	1.263	1.269
Lu	0.327	0.282	0.259	0.196	0.184
Th	0.144	0.058	1.760	1.479	1.821

Table B.3. ICP-MS platinum-group element and gold geochemistry of the OKG sulphide bearing units.

Sample Name	**P96-5A**	**P96-11A**	**P96-21A**	**P96-21B**	**P96-21B DUP**
Rock Type	Mass Sulph	Mass Sulph	Mass Sulph	Mass Sulph	Mass Sulph
Location 1	MZ	MZ	MZ	MZ	MZ
Location 2					
Ru	19.63	10.18	25.22	26.38	23.76
Rh	6.37	3.20	10.98	9.18	9.06
Pd	26.58	11.64	59.45	52.24	52.52
Os	4.84	1.89	5.98	6.65	6.03
Ir	6.46	2.88	8.45	8.84	8.76
Pt	10.16	0.91	56.74	2.21	1.20
Au	8.22	229.36	88.03	143.37	9.74

Sample Name	**P96-188B**	**P96-475**	**P96-476**	**P96-476 DUP**	**P96-5B**
Rock Type	Mass Sulph	Mass Sulph	Mass Sulph	Mass Sulph	DS-Pyroxenite
Location 1	NSSZ	NSSZ	MZ	MZ	MZ
Location 2					
Ru	12.41	24.91	14.98	14.03	2.97
Rh	2.17	7.78	5.10	4.89	0.61
Pd	12.19	24.85	28.44	26.89	3.30
Os	2.94	6.32	3.56	3.41	0.37
Ir	4.20	8.15	4.70	4.58	0.66
Pt	2.35	0.36	0.95	1.33	6.19
Au	15.13	16.81	37.16	22.53	37.57

Table B.3. (continued): ICP-MS platinum-group element and gold geochemistry of the OKG sulphide bearing units.

Sample Name	**P96-11B**	**P96-25**	**P96-W1**	**P96-191**	**P96-192**
Rock Type	DS-Pyroxenite	DS-Pyroxenite	DS-Pyroxenite	DS-Pyroxenite	DS-Pyroxenite
Location 1	MZ	MZ	MZ	NSSZ	NSSZ
Location 2					
Ru	3.46	4.07	2.71	3.42	3.03
Rh	0.58	0.51	0.25	0.35	0.11
Pd	3.21	1.61	1.47	1.50	0.84
Os	0.34	0.51	0.25	0.96	<LD
Ir	0.58	0.75	0.27	1.69	0.33
Pt	3.67	1.47	3.22	4.74	3.94
Au	9.69	10.12	5.61	7.04	7.03

Sample Name	**P96-472**	**P96-187**	**P96-190**	**P96-100A**	**P96-101**
Rock Type	DS-Pyroxenite	DS-Anorthosite	DS-Anorthosite	Amphibolite	Amphibolite
Location 1	NSSZ	NSSZ	NSSZ		
Location 2					
Ru	2.05	3.47	8.93	4.04	6.42
Rh	0.05	0.62	1.62	1.38	1.44
Pd	0.22	1.68	1.79	7.54	7.27
Os	0.29	0.36	1.40	0.57	2.78
Ir	0.04	0.57	2.66	0.77	3.51
Pt	0.59	3.54	2.50	12.53	8.34
Au	1.84	5.29	11.44	0.66	2.52

Table B.4a. Sr isotope geochemistry of the Nain Province gneisses from the OKG prospect

Sample	Rock	$^{87}Sr/^{86}Sr$ measured	2 σ	$^{87}Rb/^{86}Sr$	ISr (@3235Ma)	Rb	Sr	Rb/Sr
P96-95	Nain	0.894857	0.000044	1.16897	0.839906	16.67	41.05	0.41
P96-103A	Nain	0.710161	0.000053	0.17008	0.702166	2.42	39.65	0.06
P96-125	Nain	0.797233	0.000073	2.13645	0.696802	39.41	52.28	0.75
P96-126	Nain	0.800837	0.000055	2.63309	0.677060	110	119.13	0.92

Table B.4b. Sr isotope geochemistry of anorthositic rocks from the OKG prospect

Sample	Rock	$^{87}Sr/^{86}Sr$ measured	2 σ	$^{87}Rb/^{86}Sr$	ISr (@2050Ma)	Rb	Sr	Rb/Sr
P96-3A	An	0.706288	0.000026	0.00762	0.706063	1.78	660.02	0.003
P96-19	An	0.708690	0.000038	0.16200	0.708211	4.75	818.45	0.006
P96-33	An	0.705123	0.000046	0.01060	0.704810	2.77	737.81	0.004
P96-44A	ln1	0.706413	0.000036	0.02818	0.705581	7.51	753.39	0.010
P96-55B	ln1	0.705670	0.000041	0.02219	0.705015	7.75	986.82	0.008
P96-83	ln1	0.707590	0.000023	0.05108	0.706081	9.85	544.93	0.018
P96-174	ln1	0.706161	0.000034	0.01335	0.705767	3.14	655.06	0.005
P96-182	ln1	0.706175	0.000032	0.03009	0.705286	8.75	821.86	0.011
P96-199	ln2	0.707674	0.00004	0.06122	0.705866	14.18	654.79	0.022
P96-203	ln2	0.705837	0.000034	0.00381	0.705724	0.99	737.99	0.001
P96-468A	Min An	0.706187	0.000023	ND	0.706187	0.8	514.1[1]	0.002
P96-469	Min An	0.707124	0.000084	0.01588	0.706655	3.05	540.5[1]	0.006

[1]determined by XRF, ND = not detected

Table B.4c. Sr isotope geochemistry of granitoid rocks from the OKG prospect.

Sample	Rock	$^{87}Sr/^{86}Sr$ measured	2 σ	$^{87}Rb/^{86}Sr$	ISr (@2050Ma)	Rb	Sr	Rb/Sr
P96-3B	Fels	0.728491	0.000057	ND	NC	ND	306[1]	NA
P96-28B	Fels	0.722555	0.000047	0.56612	0.705833	51.15	255.69	0.200
P96-39	Ph1	0.737980	0.000044	1.16503	0.703568	82.6	200.99	0.411
P96-66A	Ph1	0.718921	0.000025	0.48537	0.704584	96.42	562.01	0.172
P96-76	Ph2	0.743695	0.000014	1.16246	0.709358	135.91	243.68	0.558
P96-86B	Ph1	0.744105	0.000034	1.32888	0.704853	100.75	290.11	0.347
P96-87	Ph2	0.771128	0.000026	2.08693	0.709485	144.63	197.11	0.734

[1]Determined by XRF, ND = not detected, NC = not calculated, NA = not applicable

Table B.4d. Sr isotope geochemistry of pyroxenitic rocks from the OKG prospect.

Sample	Rock	$^{87}Sr/^{86}Sr$ measured	2 σ	$^{87}Rb/^{86}Sr$	ISr (@1300Ma)	Rb	Sr	Rb/Sr
P96-5B	Px-sur	0.732918	0.000066	ND	NC	<LD	1.1	NA
P96-W1	Px-sur	0.711037	0.000083	ND	NC	<LD	3.23	NA
P96-463	Px-sur	0.709997	0.000067	0.05045	0.709997	0.73	50.4	0.014
P96-464	Px-sur	0.705798	0.000032	ND	NC	<LD	23.1	NA
W95-50E	Px-sur	0.720185	0.000049	0.44337	0.711924	0.26	1.64	0.159
16701	Px-core	0.708105	0.000030	ND	NC	<LD	167	NA
16715	Px-core	0.769089	0.000021	ND	NC	<LD	17	NA
16730	Px-core	0.707606	0.000057	ND	NC	<LD	117	NA
16737	Px-core	0.706929	0.000070	ND	NC	<LD	261	NA
16747	Px-core	0.706937	0.000037	ND	NC	<LD	54	NA

ND = not detected, NC = not calculated, NA = not applicable

Table B.5a. Nd isotope geochemistry of the OKG Nain Province gneissic rocks.

Sample	Rock	$^{143}Nd/^{144}Nd$ measured	2 σ	$^{147}Sm/^{144}Nd$	$^{143}Nd/^{144}Nd$ (@3235Ma)	εNd (@3235Ma)	εNd (@0)	$f_{Sm/Nd}$	T_{DM} (Ma)	Sm	Nd	Sm/Nd
P96-95	Nain	0.511935	0.000044	0.15324	0.508658	4.4	-13.7	-0.22	2084	1.45	5.83	0.25
P96-103A	Nain	0.512034	0.000053	0.1416	0.509006	11.2	-11.8	-0.28	1754	2.4	10.47	0.23
P96-125	Nain	0.512627	0.000073	0.21779	0.507970	-9.1	-0.2	0.11	2775	1.39	3.94	0.35
P96-126	Nain	0.510716	0.000011	0.08339	0.508933	9.8	-37.5	-0.58	2306	4.58	33.88	0.14

Table B.5b. Nd isotope geochemistry of the OKG anorthostic rocks.

Sample	Rock	$^{143}Nd/^{144}Nd$ measured	2 σ	$^{147}Sm/^{144}Nd$	$^{143}Nd/^{144}Nd$ (@2050Ma)	εNd (@2050Ma)	εNd (@0)	$f_{Sm/Nd}$	T_{DM} (Ma)	Sm	Nd	Sm/Nd
P96-3A	An1	0.511252	0.000040	0.13834	0.509385	-11.76	-27.04	-0.30	3844	1.25	0.28	4.48
P96-19	An1	0.510634	0.000009	0.06365	0.509775	-4.11	-39.09	-0.68	2544	2.35	0.24	9.69
P96-33	An1	0.510364	0.000008	0.07297	0.509379	-11.87	-44.36	-0.63	3006	1.44	0.17	8.44
P96-44A	In1	0.510650	0.000009	0.10931	0.509175	-15.88	-38.788	-0.44	3644	3.55	0.63	5.65
P96-55B	In1	0.511018	0.000008	0.11307	0.509492	-9.66	-31.60	-0.42	3222	3.162	0.58	5.46
P96-83	In1	0.511260	0.000009	0.11649	0.509688	-5.82	-26.88	-0.41	2955	4.76	0.90	5.29
P96-174	In1	0.511350	0.000014	0.12572	0.509653	-6.50	-25.12	-0.36	3113	6.39	1.3	4.92
P96-182	In1	0.510949	0.000009	0.09530	0.509663	-6.31	-32.95	-0.52	2823	8.33	1.29	6.46
P96-199	In2	0.511029	0.000006	0.11059	0.509536	-8.79	-31.39	-0.44	3127	36.20	6.48	5.59
P96-203	In2	0.511157	0.000011	0.121987	0.509511	-9.29	-28.89	-0.38	3307	16.64	3.29	5.06
P96-468a	Min An (An1)	0.511839	0.000009	0.16956	0.509550	-8.51	-15.59	-0.14	4582	2.24	0.61	3.67
P96-469	Min An (An1)	0.511677	0.000008	0.15023	0.509649	-6.57	-18.75	-0.24	3546	2.03	0.49	4.14

Table B.5c. Nd isotope geochemistry for the OKG granitoid rocks.

Sample	Rock	$^{143}Nd/^{144}Nd$ measured	2 σ	$^{147}Sm/^{144}Nd$	$^{143}Nd/^{144}Nd$ (@2050Ma)	εNd (@2050Ma)	εNd (@0)	$f_{Sm/Nd}$	T_{DM} (Ma)	Sm	Nd	Sm/Nd
P96-3B	Felsic Dyke	0.511437	0.000008	0.12865	0.509701	-5.57	-23.43	-0.35	3064	37.51	7.82	4.80
P96-28B	Felsic Dyke	0.511103	0.000033	0.10860	0.509637	-6.81	-29.94	-0.45	2960	35.6	6.26	5.69
P96-39	Ph1	0.511293	0.000010	0.11638	0.509722	-5.14	-26.23	-0.41	2900	66.61	12.56	5.30
P96-66A	Ph1	0.511250	0.000016	0.11813	0.509656	-6.45	-27.08	-0.40	3023	23.76	4.55	5.22
P96-75B	Ph2	0.511013	0.000021	0.09858	0.509682	-5.92	-31.70	-0.50	2819	71.27	11.38	6.26
P96-76	Ph2	0.511055	0.000008	0.11596	0.509490	-9.70	-30.88	-0.41	3261	57.91	10.88	5.32
P96-85	Ph1	0.511341	0.000008	0.12883	0.509602	-7.50	-25.30	-0.34	3245	66.37	13.85	4.79
P96-86B	Ph1	0.511191	0.000008	0.11280	0.509669	-6.20	-28.23	-0.43	2951	79.52	14.53	5.47
P96-87	Ph2	0.511002	0.000007	0.10735	0.509553	-8.46	-31.91	-0.45	3070	54.39	9.46	5.75

Table B.4d. Nd isotope geochemistry of the OKG pyroxenitic rocks.

Sample	Rock	$^{143}Nd/^{144}Nd$ measured	2 σ	$^{147}Sm/^{144}Nd$	$^{143}Nd/^{144}Nd$ (@1300Ma)	εNd (@1300Ma)	εNd (@0)	$f_{Sm/Nd}$	T_{DM} (Ma)	Sm	Nd	Sm/Nd
P96-5B	Px-sur	0.513833	0.000066	0.34326	0.510902	-1.12	23.31	0.75	833	0.54	0.98	0.55
P96-W1	Px-sur	0.513040	0.000083	0.27242	0.510714	-4.80	7.84	0.39	-183	0.46	1.05	0.44
W95-50E	Px-sur	0.513509	0.000024	0.31241	0.510842	-2.31	16.99	0.59	599	0.21	0.42	0.50
P96-463	Px-sur	0.513063	0.000009	0.27049	0.510753	-4.03	8.29	0.38	-130	0.38	0.86	0.44
P96-464	Px-sur	0.512951	0.00001	0.24274	0.510878	-1.59	6.11	0.23	-793	0.47	1.19	0.39
16701	Px-core	0.511848	0.000009	0.13309	0.510712	-4.85	-15.41	-0.32	2449	0.97	4.48	0.22
16715	Px-core	0.511913	0.000009	0.13525	0.510758	-3.94	-14.14	-0.31	2390	0.85	3.89	0.22
16730	Px-core	0.511435	0.000015	0.13685	0.510267	-13.56	-23.47	-0.30	3402	0.36	1.6	0.23
16737	Px-core	0.511421	0.000007	0.11902	0.510405	-10.86	-23.74	-0.39	2774	1.12	5.82	0.19
16747	Px-core	0.511199	0.000009	0.10414	0.510310	-12.71	-28.07	-0.47	2703	2.83	16.79	0.17

Table B.6. Sulphur isotope geochemistry of the sulphide separates from the OKG prospect.

Sample	Separate	Host	$\delta^{34}S$
W95-50B	po	ms	1.45
W95-50C	po	ms	1.42
W95-50C	cpy	ms	1.5
W95-50E	cpy	ms	1.64
W95-50E	py	ms	1.66
W95-50E	po	ms	1.78
P96-21B	po	ms	1
P96-21B (Dup)	po	ms	1.2
P96-25	po	pxnite	1.2
P96-188B	po	ms	1.5
P96-188B (Dup)	po	ms	1.5
P96-190	po	ms	1

po = pyrrhotite, cpy = chalcopyrite, py = pyrite, ms = massive sulphide, pxnite = pyroxenite.